VASCULAR HEALTH: THE ENDOTHELIAL PERSPECTIVE IN REGULATION OF INFLAMMATION AND INJURY

EDITED BY: Shampa Chatterjee, Silvia Lacchini, Wolfgang Jungraithmayr and Felix W. Wehrli

PUBLISHED IN: Frontiers in Physiology

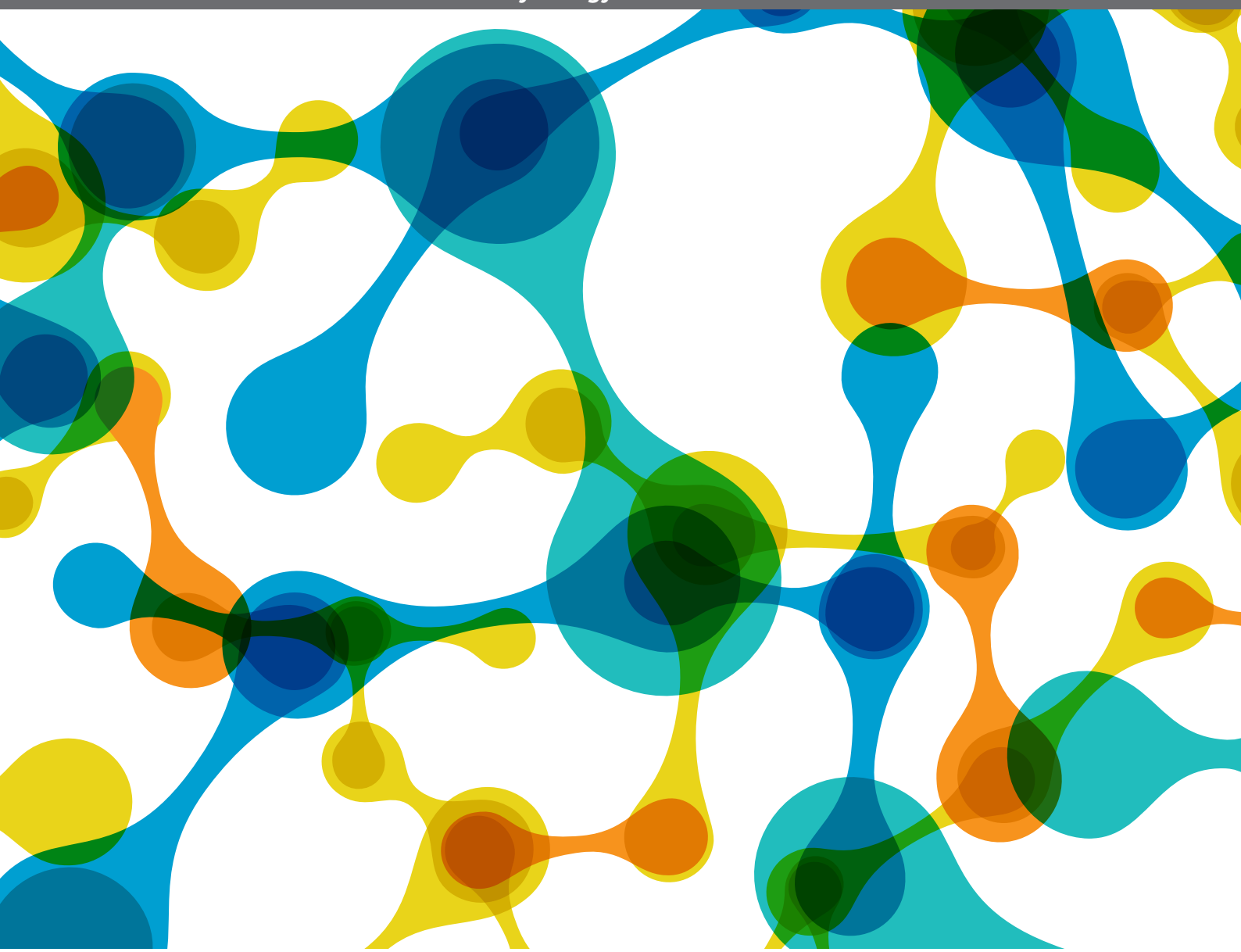

frontiers Research Topics

ISSN 1664-8714
ISBN 978-2-88971-418-6
DOI 10.3389/978-2-88971-418-6

About Frontiers

Frontiers is more than just an open-access publisher of scholarly articles: it is a pioneering approach to the world of academia, radically improving the way scholarly research is managed. The grand vision of Frontiers is a world where all people have an equal opportunity to seek, share and generate knowledge. Frontiers provides immediate and permanent online open access to all its publications, but this alone is not enough to realize our grand goals.

Frontiers Journal Series

The Frontiers Journal Series is a multi-tier and interdisciplinary set of open-access, online journals, promising a paradigm shift from the current review, selection and dissemination processes in academic publishing. All Frontiers journals are driven by researchers for researchers; therefore, they constitute a service to the scholarly community. At the same time, the Frontiers Journal Series operates on a revolutionary invention, the tiered publishing system, initially addressing specific communities of scholars, and gradually climbing up to broader public understanding, thus serving the interests of the lay society, too.

Dedication to Quality

Each Frontiers article is a landmark of the highest quality, thanks to genuinely collaborative interactions between authors and review editors, who include some of the world's best academicians. Research must be certified by peers before entering a stream of knowledge that may eventually reach the public - and shape society; therefore, Frontiers only applies the most rigorous and unbiased reviews.
Frontiers revolutionizes research publishing by freely delivering the most outstanding research, evaluated with no bias from both the academic and social point of view. By applying the most advanced information technologies, Frontiers is catapulting scholarly publishing into a new generation.

What are Frontiers Research Topics?

Frontiers Research Topics are very popular trademarks of the Frontiers Journals Series: they are collections of at least ten articles, all centered on a particular subject. With their unique mix of varied contributions from Original Research to Review Articles, Frontiers Research Topics unify the most influential researchers, the latest key findings and historical advances in a hot research area! Find out more on how to host your own Frontiers Research Topic or contribute to one as an author by contacting the Frontiers Editorial Office: frontiersin.org/about/contact

VASCULAR HEALTH: THE ENDOTHELIAL PERSPECTIVE IN REGULATION OF INFLAMMATION AND INJURY

Topic Editors:
Shampa Chatterjee, University of Pennsylvania, United States
Silvia Lacchini, University of São Paulo, Brazil
Wolfgang Jungraithmayr, University Hospital Zürich, Switzerland
Felix W. Wehrli, University of Pennsylvania, United States

Citation: Chatterjee, S., Lacchini, S., Jungraithmayr, W., Wehrli, F. W., eds. (2021). Vascular Health: The Endothelial Perspective in Regulation of Inflammation and Injury. Lausanne: Frontiers Media SA. doi: 10.3389/978-2-88971-418-6

Table of Contents

05 ***Editorial: Vascular Health: The Endothelial Perspective in Regulation of Inflammation and Injury***
Shampa Chatterjee, Silvia Lacchini, Wolfgang Jungraithmayr and Felix W. Wehrli

08 ***Mitochondrial DNA Promotes NLRP3 Inflammasome Activation and Contributes to Endothelial Dysfunction and Inflammation in Type 1 Diabetes***
Camila A. Pereira, Daniela Carlos, Nathanne S. Ferreira, Josiane F. Silva, Camila Z. Zanotto, Dario S. Zamboni, Valéria D. Garcia, Dora Fix Ventura, João S. Silva and Rita C. Tostes

23 ***Acute Increase in O-GlcNAc Improves Survival in Mice With LPS-Induced Systemic Inflammatory Response Syndrome***
Josiane Fernandes Silva, Vania C. Olivon, Fabiola Leslie A. C. Mestriner, Camila Ziliotto Zanotto, Raphael Gomes Ferreira, Nathanne Santos Ferreira, Carlos Alberto Aguiar Silva, João Paulo Mesquita Luiz, Juliano Vilela Alves, Rubens Fazan, Fernando Queiróz Cunha, Jose Carlos Alves-Filho and Rita C. Tostes

38 ***Vascular Integrity and Signaling Determining Brain Development, Network Excitability, and Epileptogenesis***
Jugajyoti Baruah, Anju Vasudevan and Rüdiger Köhling

50 ***Immune and Apoptosis Mechanisms Regulating Placental Development and Vascularization in Preeclampsia***
Nozha Raguema, Sarah Moustadraf and Mariane Bertagnolli

58 ***Quantitative and Dynamic MRI Measures of Peripheral Vascular Function***
Erin K. Englund and Michael C. Langham

67 ***Vascular Signaling in Allogenic Solid Organ Transplantation – The Role of Endothelial Cells***
Laura Kummer, Marcin Zaradzki, Vijith Vijayan, Rawa Arif, Markus A. Weigand, Stephan Immenschuh, Andreas H. Wagner and Jan Larmann

86 ***New Insights From MRI and Cell Biology Into the Acute Vascular-Metabolic Implications of Electronic Cigarette Vaping***
Felix W. Wehrli, Alessandra Caporale, Michael C. Langham and Shampa Chatterjee

94 ***Cystic Fibrosis Transmembrane Conductance Regulator (CFTR) in Human Lung Microvascular Endothelial Cells Controls Oxidative Stress, Reactive Oxygen-Mediated Cell Signaling and Inflammatory Responses***
Maha Khalaf, Toby Scott-Ward, Adam Causer, Zoe Saynor, Anthony Shepherd, Dariusz Górecki, Anthony Lewis, David Laight and Janis Shute

114 ***Additional Improvement of Respiratory Technique on Vascular Function in Hypertensive Postmenopausal Women Following Yoga or Stretching Video Classes: The YOGINI Study***
Cláudia Fetter, Juliana Romeu Marques, Liliane Appratto de Souza, Daniela Ravizzoni Dartora, Bruna Eibel, Liliana Fortini Cavalheiro Boll, Sílvia Noll Goldmeier, Danielle Dias, Katia De Angelis and Maria Cláudia Irigoyen

125 ***Metabolic Imaging and Biological Assessment: Platforms to Evaluate Acute Lung Injury and Inflammation***
Mehrdad Pourfathi, Stephen J. Kadlecek, Shampa Chatterjee and Rahim R. Rizi

139 ***Oxygen Glucose Deprivation Induced Prosurvival Autophagy Is Insufficient to Rescue Endothelial Function***
Venkateswaran Natarajan, Tania Mah, Chen Peishi, Shu Yi Tan, Ritu Chawla, Thiruma Valavan Arumugam, Adaikalavan Ramasamy and Karthik Mallilankaraman

153 ***Imaging Atherosclerosis by PET, With Emphasis on the Role of FDG and NaF as Potential Biomarkers for This Disorder***
Michael Mayer, Austin J. Borja, Emily C. Hancin, Thomas Auslander, Mona-Elisabeth Revheim, Mateen C. Moghbel, Thomas J. Werner, Abass Alavi and Chamith S. Rajapakse

166 ***Novel Strategies for Endothelial Preservation in Lung Transplant Ischemia-Reperfusion Injury***
Wolfgang Jungraithmayr

173 ***The Effect of Inflammation on Bone***
Scott Epsley, Samuel Tadros, Alexander Farid, Daniel Kargilis, Sameer Mehta and Chamith S. Rajapakse

187 ***Inflammation in Periodontal Disease: Possible Link to Vascular Disease***
Oindrila Paul, Payal Arora, Michael Mayer and Shampa Chatterjee

198 ***Osthole Alleviates Neointimal Hyperplasia in Balloon-Induced Arterial Wall Injury by Suppressing Vascular Smooth Muscle Cell Proliferation and Downregulating Cyclin D1/CDK4 and Cyclin E1/CDK2 Expression***
Yi-Qi Li, Ye-Li Li, Xiao-Tong Li, Jun-Yuan Lv, Yang Gao, Wen-Na Li, Qi-Hai Gong and Dan-Li Yang

frontiers in Physiology

EDITORIAL
published: 06 August 2021
doi: 10.3389/fphys.2021.732234

Editorial: Vascular Health: The Endothelial Perspective in Regulation of Inflammation and Injury

Shampa Chatterjee[1]*, *Silvia Lacchini*[2], *Wolfgang Jungraithmayr*[3] and *Felix W. Wehrli*[4]

[1] Department of Physiology, Institute for Environmental Medicine, University of Pennsylvania Perelman School of Medicine, Philadelphia, PA, United States, [2] Department of Anatomy, Institute of Biomedical Sciences, University of São Paulo, São Paulo, Brazil, [3] Department of Thoracic Surgery, Faculty of Medicine, Medical Center - University of Freiburg, Freiburg, Germany, [4] Radiologic Science, Biochemistry and Biophysics, University of Pennsylvania Perelman School of Medicine, Philadelphia, PA, United States

Keywords: endothelium, oxidative stress, inflammation, vascular dysfunction, hyperproliferation, autophagy, transplant signaling, imaging–radiology

Editorial on the Research Topic

Vascular Health: The Endothelial Perspective in Regulation of Inflammation and Injury

OPEN ACCESS

Edited by:
Irena Levitan,
University of Illinois at Chicago, United States

Reviewed by:
Ibra S. Fancher,
University of Delaware, United States
Cor de Wit,
University of Lübeck, Germany

***Correspondence:**
Shampa Chatterjee
shampac@pennmedicine.upenn.edu

Specialty section:
This article was submitted to Vascular Physiology, a section of the journal Frontiers in Physiology

Received: *28 June 2021*
Accepted: *13 July 2021*
Published: *06 August 2021*

Citation:
Chatterjee S, Lacchini S, Jungraithmayr W and Wehrli FW (2021) Editorial: Vascular Health: The Endothelial Perspective in Regulation of Inflammation and Injury. Front. Physiol. 12:732234. doi: 10.3389/fphys.2021.732234

This special Research Topic of Frontiers in Physiology collates 16 (review and original research) articles on the endothelium (the cell layer that lines blood vessels) and other components of the vascular system. Over the past decade, it has become increasingly clear that the vascular network is not a mere conduit for blood and the endothelium is not a "wallpaper" of the vascular network; rather both are dynamic entities that sense and respond to mechanical and chemical stimulation from the microenvironment. Both endothelial cells and vascular tissue (comprising of endothelial and smooth muscle layer and other cells such as inflammatory/immune cells) are equipped with complex molecular machinery that initiate and amplify signaling processes leading to physiological and pathophysiological changes. These changes range from vasodilation, vasoconstriction and angiogenesis to inflammation, leakage, injury, and vascular remodeling and form the basis of vascular health, disease and other etiologies.

Endothelial signaling initiated by various stimuli involve reactive oxygen species (ROS) induced signaling events, calcium influx (via various Ca^{2+} channels), activation of mitogen-activated protein (MAP) kinases, induction of cellular adhesion molecules (CAMs) which lead either to activation of downstream inflammation moieties (such as the NLRP3 inflammasome) or to modification of proteins that facilitate endothelial cell function. Collectively, these changes can alter vascular cell-cell junctions, vessel structure, and function. For instance, endothelial cells of a donor organ as the interface between the transplanted organ (graft) and the immune cells of the host, serve as the first target for host (recipient) immune cells post-transplant. Kummer et al. review how the sensing of a "foreign" entity by the human leukocyte antigen (HLA) I and II-recognizing natural killer (NK) cells, macrophages, and T-cells lead these cells to attack the endothelial layer. The damaged endothelial cells produce chemokines, express CAMs and drive a pro-inflammatory microenvironment. Inflammatory cells (macrophages, leukocytes, T-cells etc.) are recruited into this environment and transmigrate from the bloodstream across the endothelial monolayer into the vessel wall, causing vascular damage. Vascular damage initiates repair mechanisms whereby migration and continued proliferation of vascular smooth muscle cells occur in the vascular structures causing fibrous intimal hyperplasia, which ultimately leads to transplant failure. Thus, endothelial preservation, as proposed by Jungraithmayr can be a promising therapeutic strategy for the protection of the endothelium against ischemia and

reperfusion (i.e. maneuvers associated with transplant). Therefore, various receptors and signaling pathways that are well-recognized to be activated upon transplantation (ROS, MAP kinases, CAMs, angiotensin-converting enzyme) can be blocked in order to facilitate endothelial preservation against injury.

ROS production and calcium influx are pivotal cellular events that drive inflammation signaling. ROS production in endothelial cells is tightly regulated by certain receptors including the Cystic Fibrosis Transmembrane Conductance Regulator (CFTR). As reported by Khalaf et al., CFTR plays a role in endothelial oxidative damage by controlling ROS production. In naïve endothelial cells, ROS production is low but increases following inhibition of CFTR activity. ROS has been proposed as an upstream inducer of the NLRP3 inflammasome, a well-characterized platform of multiple subunits (NLRP3, ASC, pro-caspase) that cause caspase and interleukin (IL)-1β, IL-18 release, leading to inflammation induced cell death (pyroptosis). Thus, various pathologies or agents that drive NLRP3 activation can also lead to endothelial inflammation and injury. As reported by Pereira et al. in a murine model of diabetes, wild-type mice showed reduction in endothelium-dependent vasodilation, increased vascular ROS generation, caspase-1, and IL-1β activation. These changes were not observed in $Nlrp3^{-/-}$ mice, which appear to be protected. Paul et al. review the mechanisms underpinning the links between periodontal disease (PD) and diabetes and cardiovascular disease. ROS and oxidative stress may also play a role in amplification of bacterial driven inflammation by triggering pathological processes in distant organs. A two-way association between PD and other health conditions presumably arises via ROS and intermediate inflammation signaling. Thus, blocking these intermediate inflammation-signaling events (such as activation of the NLRP3 inflammasome, cytokines, chemokines) can facilitate endothelial preservation. Modification of proteins also serve as intermediate signals that can alter inflammatory mediators/response. Silva et al. show that in a murine model of sepsis (which results in a systemic inflammatory state that accompanies endothelial dysfunction), inflammation is reduced by acylation of proteins by O-linked N-acetylglucosamine (O-GlcNAcylation); indeed, increase in O-GlcNAc reduces systemic inflammation and cardiovascular dysfunction, indicating the therapeutic potential of this pathway.

Like ROS, calcium ions (Ca^{2+}) are prominent signaling molecules that participate in various physiological functions, such as vasodilation, cell migration, growth and apoptosis. In naïve cells, mitochondria sequester and release Ca^{2+} via mitochondrial calcium uniporter complexes. While oxidative stress or other deterrent stimuli, increase mitochondrial calcium overload leading to apoptotic cell death, the calcium uniporter complexes regulate prosurvival mechanisms such as autophagy for endothelial protection. Natarajan et al. report that with *in vitro* ischemia (achieved by oxygen-glucose deprivation) endothelial cells downregulate the mitochondrial calcium uniporter complex 1 (MCUR1), but that the resultant autophagic flux is insufficient to protect ischemic endothelial cells and an additional autophagic flux (by serum starvation of endothelial cells) is required for cell protection indicating that therapeutic strategies can involve targeting multiple mechanisms of endothelial protection.

How does the vasculature respond to inflammation, oxidative damage and injury? A major response to vascular injury is a hyperproliferative response of vascular smooth muscle cells (VSMC). This gives rise of hyperplasia which leads to vessel remodeling. This is detrimental specifically in the context of maneuvers such as percutaneous coronary intervention where balloon angioplasty to remove arterial blockage is followed by hyperplasia (VSMC proliferation) that reinstates the blockage (restenosis). Restenosis can potentially be alleviated by blockade of vascular signaling that drives hyperproliferation. Toward that goal, Li et al. use osthole (7-methoxy-8-isopentenoxy-coumarin) a pharmacologically active component of *Cnidium monnieri* (L.) Cusson and report that it alleviates hyperplasia in a rat model of balloon angioplasty by targeting the NF-κB and TGF-β1/Smad2 signaling pathways that play a role in facilitating VSMC proliferation. Vascularization also has implications in preeclampsia, as reviewed by Raguema et al. Abnormal placental vascularization presumably arises from chronic hypoxia due to reduced placental blood flow leading to fetal growth retardation and later to pre-eclampsia.

Another response is the disruption of the endothelial cell barrier. Indeed, as Baruah et al. review intrinsic defects within endothelial cells from the earliest developmental time points, the disruption of the blood-brain barrier (BBB) can be the cause for posttraumatic epilepsy and other similar etiologies. Under control conditions, the BBB is maintained via tight endothelial cell-cell junctions, but these can be loosened by inflammation and oxidative damage. These changes lead to vascular abnormalities and autonomously support the development of hyperexcitability and epileptiform activity. Thus, BBB protection by alleviation in inflammation or by repair of junctional proteins can be a potential therapeutic strategy in epilepsy control.

Vascular inflammation also affects cellular signaling of bone. Epsley et al. review the effect of inflammation on bone modeling, which is a continual process to renew the adult skeleton through the sequential growth and resorption processes of bone cells (osteoblasts and osteoclasts). Nuclear factor RANK, an osteoclast receptor, and its ligand RANKL, expressed on the surface of osteoblasts, result in coordinated control of bone remodeling. Inflammation skews this process toward resorption via the interaction of inflammatory mediators and their related peptides with osteoblasts and osteoclasts, as well as other immune cells, to alter the expression of RANK and RANKL.

Changes in endothelial cell signaling that transiently or chronically impair endothelial function, vascular reactivity, and oxygen metabolism can be evaluated non-invasively by quantitative magnetic resonance imaging (MRI). Englund and Langham review the use of MRI for vascular parameters via dynamic quantification of blood flow and oxygenation under conditions of ischemia or exercise and showcase this application for detection of endothelial dysfunction in clinical (cardiovascular disease) and sub-clinical settings (chronic smokers, non-smokers exposed to e-cigarette aerosol etc.).

Wehrli et al. review the ability of MRI to detect vascular function. When paired with endothelial cell signaling assays, these "MRI-biochemical pairing" methods highlight the fact that changes at the cellular level (i.e. microvascular endothelial signals) translate into altered vascular function at the macro level. Thus, MRI measures of vascular function may ultimately be used to complement the standard clinical metrics of vascular function and provide additional insight into efficacy of drugs for improvement of vascular function. Similarly, as reviewed by Mayer et al. endothelial signaling at cellular and molecular level, that contribute to atherosclerosis can be detected by non-invasive monitoring of calcification, a complex process facilitated by endothelial signaling that leads to transition of endothelial cells to osteoblast-like cells. Mayer et al. review existing literature on 18F-fluorodeoxyglucose (FDG) and 18F-sodium fluoride (NaF) positron emission tomography (PET) in assessing atherosclerosis via microcalcification and characteristic plaque buildup. Since the initiating event of atherogenesis is inflammation, the pathogenesis manifests in increased metabolic activity, detectable by FDG. At a later stage, atherosclerotic plaques become calcified. Calcification entails incorporation of calcium hydroxy apatite into the vascular walls. Injection of NaF as a tracer leads to partial exchange of hydroxyl ions by fluoride, therefore allowing direct detection of plaque constituents. Pourfathi et al. review the role of PET and hyperpolarized ^{13}C MRI imaging to detect the various stages of pulmonary inflammation. The most common PET tracer for metabolic imaging is FDG. A hallmark of inflammatory lung disease is increased glycolysis manifesting in enhanced FDG PET activity. An alternative strategy, which is at an early stage of development, is to quantify the formation of lactic acid by means of hyperpolarized carbon-13 spectroscopic imaging. The carbonyl carbons of lactic acid and its exogenously administered metabolic precursor (pyruvate) have characteristic chemical shifts allowing their distinction.

In conclusion, endothelial signaling has an impact on overall health. Under conditions where these signals lead to remodeling that affects homeostasis, interventions (such as employing respiratory techniques as reported by Fetter et al. can alter blood flow and improve vascular function) or inhibition/blockade of ROS or NLRP3 or inflammatory and metabolic pathways may be beneficial to restore vascular function.

AUTHOR CONTRIBUTIONS

SC drafted the editorial. All authors edited the article and approved the submitted version.

FUNDING

SC was supported by NIH-NHLBI grant R56 HL139559-01A1, SL by the São Paulo Research Foundation–FAPESP, WJ by the Swiss foundation of applied cancer research, and FW was supported by NIH-NHLBI grant R01 HL139358.

Conflict of Interest: The authors declare that the research was conducted in the absence of any commercial or financial relationships that could be construed as a potential conflict of interest.

Publisher's Note: All claims expressed in this article are solely those of the authors and do not necessarily represent those of their affiliated organizations, or those of the publisher, the editors and the reviewers. Any product that may be evaluated in this article, or claim that may be made by its manufacturer, is not guaranteed or endorsed by the publisher.

frontiers in Physiology

ORIGINAL RESEARCH
published: 17 January 2020
doi: 10.3389/fphys.2019.01557

Mitochondrial DNA Promotes NLRP3 Inflammasome Activation and Contributes to Endothelial Dysfunction and Inflammation in Type 1 Diabetes

Camila A. Pereira[1], Daniela Carlos[2], Nathanne S. Ferreira[1], Josiane F. Silva[1], Camila Z. Zanotto[1], Dario S. Zamboni[3], Valéria D. Garcia[4], Dora Fix Ventura[4], João S. Silva[2] and Rita C. Tostes[1]**

[1] Department of Pharmacology, Ribeirão Preto Medical School, University of São Paulo, Ribeirão Preto, Brazil, [2] Department of Biochemistry and Immunology, Ribeirão Preto Medical School, University of São Paulo, Ribeirão Preto, Brazil, [3] Cell and Molecular Biology and Pathogenic Bioagents, Ribeirão Preto Medical School, University of São Paulo, Ribeirão Preto, Brazil, [4] Department of Experimental Psychology, Institute of Psychology, University of São Paulo, São Paulo, Brazil

OPEN ACCESS

Edited by:
Shampa Chatterjee, University of Pennsylvania, United States

Reviewed by:
Owen Llewellyn Woodman, Monash University, Australia
Ennio Avolio, University of Calabria, Italy

***Correspondence:**
Camila A. Pereira
mila_cap@yahoo.com.br
Rita C. Tostes
rtostes@usp.br

Specialty section:
This article was submitted to Vascular Physiology, a section of the journal Frontiers in Physiology

Received: *13 August 2019*
Accepted: *11 December 2019*
Published: *17 January 2020*

Citation:
Pereira CA, Carlos D, Ferreira NS, Silva JF, Zanotto CZ, Zamboni DS, Garcia VD, Ventura DF, Silva JS and Tostes RC (2020) Mitochondrial DNA Promotes NLRP3 Inflammasome Activation and Contributes to Endothelial Dysfunction and Inflammation in Type 1 Diabetes. Front. Physiol. 10:1557. doi: 10.3389/fphys.2019.01557

Background: NLRP3 inflammasome activation in response to several signals, including mitochondrial DNA (mDNA), regulates inflammatory responses by caspase-1 activation and interleukin-1β (IL-1β) release. Circulating mDNA is linked to micro and macrovascular complications in diabetes. However, a role for mDNA in endothelial dysfunction is not clear. We tested the hypothesis that mDNA contributes to diabetes-associated endothelial dysfunction and vascular inflammation via NLRP3 activation.

Methods: Vascular reactivity, reactive oxygen species (ROS) generation, calcium (Ca^{2+}) influx and caspase-1 and IL-1β activation were determined in mesenteric resistance arteries from normoglicemic and streptozotocin-induced diabetic C57BL/6 and NLRP3 knockout (*Nlrp3*$^{-/-}$) mice. Endothelial cells and mesenteric arteries were stimulated with mDNA from control (cmDNA) and diabetic (dmDNA) mice.

Results: Diabetes reduced endothelium-dependent vasodilation and increased vascular ROS generation and caspase-1 and IL-1β activation in C57BL/6, but not in *Nlrp3*$^{-/-}$ mice. Diabetes increased pancreatic cytosolic mDNA. dmDNA decreased endothelium-dependent vasodilation. In endothelial cells, dmDNA activated NLRP3 via mitochondrial ROS and Ca^{2+} influx. Patients with type 1 diabetes exhibited increased circulating mDNA as well as caspase-1 and IL-1β activation.

Conclusion: dmDNA activates endothelial NLRP3 inflammasome by mechanisms that involve Ca^{2+} influx and mitochondrial ROS generation. NLRP3 deficiency prevents diabetes-associated vascular inflammatory damage and endothelial dysfunction. Our study highlights the importance of NLRP3 inflammasome in diabetes-associated vascular dysfunction, which is key to diabetic complications.

Keywords: type 1 diabetes, endothelial dysfunction, NLRP3 inflammasome, mitochondrial DNA, inflammation, reactive oxygen species

INTRODUCTION

The NLRP3 inflammasome is a multi-protein complex present in cells of the adaptive and innate immune system. NLRP3 regulates inflammatory responses by oligomerization and recruitment of the apoptosis-associated speck-like protein containing a caspase recruit domain (ASC) and pro-caspase-1, causing auto-cleavage and activation of caspase-1, which, in turn, cleaves pro-IL-1β and pro-IL-18 into mature cytokines (Martinon et al., 2002). Mature IL-1β, through the IL-1 receptor (IL-1R), activates various intracellular signaling cascades that trigger transcription of other pro-inflammatory cytokines, adhesion molecules, chemokines and pro-inflammatory enzymes (Palomo et al., 2015). In addition to its role on inflammation, IL-1β is involved in endothelial dysfunction, a hallmark of several cardiovascular and metabolic diseases, including diabetes (Rizzoni et al., 2001; Beckman et al., 2003). IL-1β increases the activity of NADPH oxidase, a key enzyme in oxidative stress-associated conditions, leading to reduced endothelium-dependent vasodilation (Vallejo et al., 2014).

Increased availability of reactive oxygen species (ROS) is a very important mechanism that triggers endothelial dysfunction, being involved in the onset of many diseases. Increased ROS is also a classical mechanism that induces NLRP3 inflammasome activation. Many other stimuli, such as lysosomal damage, potassium (K^+) efflux, calcium (Ca^{2+}) influx, and DAMPs (damage-associated molecular patterns) also induce NLRP3 oligomerization (Brough et al., 2003; Petrilli et al., 2007; Chu et al., 2009; Zhou et al., 2010). Mitochondrial DAMPS, i.e., mitochondrial DNA (mDNA), particularly cytosolic oxidized mDNA, activate the NLRP3 inflammasome and, consequently, increase IL-1β release, as demonstrated in murine macrophages (Shimada et al., 2012).

Increased levels of circulating mDNA were reported in diabetic subjects with microvascular complications, such as retinopathy and nephropathy (Czajka et al., 2015; Malik et al., 2015). In addition, NLRP3 inflammasome activation by mDNA plays a major role in pathogenic cellular immune responses mediated by T lymphocytes during type 1 diabetes development, contributing to damage of insulin-producing β cells, as we recently demonstrated (Carlos et al., 2017).

Although inflammation plays a key role in type 1 diabetes development, few experimental and clinical studies have evaluated the involvement of NLRP3 activation on vascular inflammatory processes and its repercussion on endothelial function. Therefore, this study investigated the functional role of NLRP3 inflammasome, and related signaling pathways, in the development of type 1 diabetes-associated endothelial dysfunction. We tested the hypotheses that mDNA promotes NLRP3 activation in endothelial cells contributing to endothelial dysfunction and that the genetic deficiency of NLRP3 receptor attenuates vascular dysfunction and inflammatory response observed in streptozotocin-induced type 1 diabetes. Considering the high incidence of diabetes, especially its complications, it is important to understand the immunological and pathophysiological mechanisms related to the disease in order to uncover new therapeutic targets for diabetes prevention and treatment.

MATERIALS AND METHODS

Animals

All experimental protocols were performed in accordance with the ARRIVE Guidelines (Animal Research: Reporting of *in vivo* Experiments) and approved by the Ethics Committee on Animal Research of the Ribeirão Preto Medical School – University of São Paulo, Ribeirão Preto, Brazil (protocol no. 26/2015).

Male, 8 to 10 week-old C57BL/6 wild-type (WT) and NLRP3 receptor knockout (*Nlrp3*$^{-/-}$) mice were obtained from the Isogenic Breeding Unit of the Ribeirão Preto Medical School, University of São Paulo, Ribeirão Preto, Brazil. The animals were housed in the animal facility of the Pharmacology Department, Ribeirão Preto Medical School, on 12-h light/dark cycles under controlled temperature (22 ± 1°C) with *ad libitum* access to food and water. After a 1-week acclimatization period, mice were randomly divided into non-diabetic and diabetic groups.

Induction of Diabetes by Multiple Low Doses of Streptozotocin (MLD-STZ)

Mice were given daily intraperitoneal injections of 40 mg/kg of streptozotocin (Sigma-Aldrich®, St. Louis, Missouri, United States) dissolved in 0.1 M sodium citrate (pH 4.5) for five consecutive days. Blood glucose levels, body weight, and diabetes incidence were monitored weekly. Mice were considered diabetic when glucose levels were ≥230 mg/dl after two consecutive determinations under non-fasting conditions. The animals were submitted to experimental protocols 30 days after induction of diabetes. Body weight, blood glucose, and insulin levels are shown in **Supplementary Table S1**.

Mitochondrial DNA Isolation

Pancreata from non-diabetic and diabetic mice were submitted to protocols for mitochondria isolation. The pancreatic tissue was homogenized in 5 ml of medium [(in mM): HEPES 10, sucrose 250 and EGTA 1] at pH 7.2, centrifuged at 600 *g* for 5 min and the supernatant collected and centrifuged at 2,000 *g* for 10 min. The pellet containing the isolated mitochondria was recovered, resuspended and centrifuged at 12,000 *g* for 10 min at 4°C followed by centrifugation at 100,000 *g* at 4°C for 30 min. The supernatant was used for DNA extraction with the phenol–chloroform–isoamyl alcohol mixture (Sigma-Aldrich®, St. Louis, MO, United States). Finally, pancreatic mDNA isolated from control (cmDNA) and diabetic (dmDNA) mice was quantified using an Epoch™ Microplate apparatus (BioTek Instruments®, Winooski, VT, United States).

Vascular Reactivity – Isolated Mesenteric Resistance Arteries

The method described by Mulvany and Halpern (1977) was used. Animals were euthanized in a carbon dioxide (CO_2) chamber. Segments of second-branch mesenteric arteries (2 mm in length)

were mounted in a small vessel myograph (Danish Myo Tech, Model 620M, A/S, Aarhus, Denmark). Arteries were maintained in Krebs Henseleit solution [(in mM) NaCl 130, KCl 4.7, KH_2PO_4 1.18, $MgSO_4$ 1.17, $NaHCO_3$ 14.9, glucose 5.5, EDTA 0.03, $CaCl_2$ 1.6], at 37°C, pH 7.4, and gassed with a mixture of 95% O_2 and 5% CO_2.

Mesenteric arteries preparations were set to reach a tension of 13.3 kPa (kilopascal) and remained at rest for 30 min for stabilization. The arteries were stimulated with Krebs solution containing a high concentration of potassium [K^+ (120 mM)] to evaluate the contractile capacity. After washing and return to the basal tension, arteries were contracted with phenylephrine (10^{-6} M) and stimulated with acetylcholine (10^{-5} M) to determine the presence of a functional endothelium. Arteries exhibiting a vasodilator response to acetylcholine greater than 80% were considered endothelium-intact vessels. The failure of acetylcholine to elicit relaxation of arteries that were subjected to rubbing of the intimal surface was taken as proof of endothelium removal. After washing and another period of stabilization, concentration-response curves to acetylcholine and sodium nitroprusside were performed.

Cumulative Concentration-Response Curves

Mesenteric resistance arteries were pre-contracted with phenylephrine (10^{-6} to 3×10^{-6} M) and concentration-response curves to sodium nitroprusside (10^{-10} to 3×10^{-5} M), acetylcholine (10^{-10} to 3×10^{-5} M) in the presence of vehicle, MCC950 (10^{-6} M), a selective NLRP3 inhibitor, Tiron (10^{-4} M), a superoxide anion scavenger; Peg-catalase (200 U/ml), a catalase mimetic; CCCP (10^{-6} M), an uncoupler of the mitochondrial respiratory chain; and cmDNA and dmDNA (1 μg/ml) were carried out.

Cultured Endothelial Cells – *EA.hy926* (ATCC® CRL-2922™)

EA.hy926 endothelial cells were cultured in Dulbecco's modified Eagle's medium (DMEM) (Sigma-Aldrich®, St. Louis, MO, United States), supplemented with 10% of fetal bovine serum (FBS) (Invitrogen®, Carlsbad, CA, United States), and antibiotics (penicillin and gentamicin), at 37°C and 5% CO_2. Cells (1×10^6/well) were stimulated with cmDNA or dmDNA (1 μg/mL), from 30 min to 1 h. To evaluate caspase-1 and IL-1β activation, cells were primed with lipopolysaccharide (LPS, 1 μg/ml) for 24 h (Sigma-Aldrich®, St. Louis, MO, United States), prior to stimulation with mDNA.

Mitochondrial DNA Quantification

DNA was extracted and purified using the QIAamp DNA Blood Mini kit (Qiagen®, Hilden, Germany). DNA isolated from pancreas of mice or from human serum was amplified and quantified using real time-polymerase chain reaction (RT-PCR). The RT-PCR results are presented as the inverse of cycle threshold (CT) for gene amplification (McCarthy et al., 2015). The murine primers used were cytochrome b [(Cyt B) forward 5′-ACCTCAAAGCAACGAAGCCT-3′ and reverse 5′-GGTTGGCCTCCAATTCAGGT-3′], cytochrome c [(Cyt C) forward 5′-GACTTGCAACCCTACACGGAT-3′ and reverse 5′-CCGGTTAGACCACCAACTGT-3′], and NADH dehydrogenase subunit 6 (forward 5′-ATTCCACCCCCTCACGACTA-3′ and reverse 5′-TGTCGTTTTGGGTGAGAGCA-3′). The human primers used were cytochrome b [(Cyt B) forward 5′-ATGACCCACCAATCACATGC- 3′ and reverse 5′-ATGCCCCA ATACGCAAAAT-3′], cytochrome c [(Cyt C) forward 5′– ATGA CCCACCAATCACATGC-3′ and reverse 5′– ATCACATGGCTA GGCCGGAG-3′], and NADH dehydrogenase subunit 6 (forward 5′ – ATACCCATGGCCAACCTCCT-3′ and reverse 5′ – GGGCCTTTGCGTAGTTGTAT-3′).

Western Blotting

Forty to fifty micrograms of proteins extracted from *EA.hy926* endothelial cells or mesenteric arteries from the different experimental groups were directly loaded into sodium dodecyl sulfate (SDS) sample buffer for 10% SDS- polyacrylamide gel electrophoresis. After protein transfer onto a nitrocellulose membrane (*Trans*-Blot Transfer Medium; Bio-Rad, Hercules, CA, United States), membranes were blocked with 5% bovine serum albumin (BSA) in Tris buffer solution containing 0.1% Tween 20 for 1 h and then incubated with antibodies against NLRP3 (1-500, Abcam, ab4207), Caspase-1 (1-500, Novus Biologicals, 14F468), IL-1β (1-500, Santa Cruz Biotechnology, sc-7884), Nox1 (1-1000, Abcam, ab55831), Nox4 (1-2000, Abcam, ab61248), Catalase (1-2000, Cell Signaling, 8841s), SOD-1 (1-3000, Abcam, ab13498), β-Actin (1-3000, Cell Signaling, #4967) or GAPDH (1-20000, Sigma-Aldrich, G9545) overnight at 4°C. Membranes were then incubated with secondary antibodies, according to species cross-reactivity for each primary antibody, for 1 h at room temperature. After the membranes were rinsed, the immunocomplexes were developed using Luminata™ Forte Western HRP Substrate (Millipore®, Burlington, MA, United States) and the images captured in a ImageQuant 350 Photodocumentation system (GE Healthcare®, Piscata Way, NJ, United States). The images were quantified by the Image J® program and the results were expressed as arbitrary units (AU).

Lucigenin

Superoxide anion generation was determined in mice mesenteric arteries and *EA.hy926* endothelial cells by a chemiluminescence assay. Mesenteric arteries from non-diabetic and diabetic C57BL/6 and *Nlrp3*$^{-/-}$ mice were placed in glass tubes containing 950 μl HANK'S solution [(in mM): NaCl 120, $CaCl_2$ 1.6, KCl 5, $MgCl_2.6\ H_2O$ 1, NaH_2PO_4 0.5, glucose 10, HEPES 10] and 5 μl of lucigenin (5 μM) for basal luminescence reading. Then, 50 μl of NAD(P)H (100 μM) were added to the tube and superoxide anion generation was quantified using the Line TL Tube Luminometer (Titertek-Berthold®, Pforzheim, Germany). Superoxide anion generation was expressed in RLU (relative units of luminescence)/dry weight (g).

mDNA-stimulated endothelial cells were mechanically removed with 100 μl lysis buffer [(mM) KH_2PO_4 20, EGTA 1] containing a protease inhibitor cocktail [aprotinin 1 μg/ml, leupeptin 1 μg/ml, pepstatin 1 μg/ml, phenylmethylsulfonyl fluoride (PMSF 1 mM)], and then transferred to Eppendorf tubes. In a 96-well white plate, 50 μl of sample, 173.75 μl of

phosphate buffer [(in mM): KH_2PO_4 50, EGTA 1, Sucrose 150] and 1.25 μl of lucigenin were pipetted in each well. Basal luminescence reading (3 min) was performed, and 25 μl of NAD(P)H (1 mM) was then added and a new reading (after 15 min) was performed. The Orion II Microplate Luminometer (Titertek-Berthold®, Pforzheim, Germany) was used. Superoxide anion generation was expressed in RLU/μg protein.

Amplex Red

Mesenteric arteries from non-diabetic and diabetic C57BL/6 and *Nlrp3*$^{-/-}$ mice were quickly frozen in liquid nitrogen and subsequently pulverized in ice-cold Krebs solution and centrifuged at 2,000 rpm (1 min). Hydrogen peroxide production was evaluated in aliquots of 50 μl of the supernatant, using an Amplex™ Red Hydrogen Peroxide/Peroxidase Assay Kit (Invitrogen®, Carlsbad, California, EUA). The fluorescence was measured (530–590 μm) using the FlexStation 3 Multi Mode Microplate Reader (Molecular Devices, Sunnyvale, CA, United States) and the software SoftMax® Pro (Molecular Devices, Sunnyvale, CA, United States). A standard curve for hydrogen peroxide was constructed to determine hydrogen peroxide concentration in the samples. The quantification was corrected by the total protein concentration and the results are expressed in μmol/l.

Ca^{2+} Influx

Endothelial cells were seeded in black-walled, clear-bottomed 96-well plates (Corning, NY, United States) at a density of 50,000 cells/well in DMEM with 10% FBS and incubated for 24 h at 37°C in a 5% CO_2. In the following day, cells were incubated with vehicle, cmDNA or dmDNA (1 μg/ml) diluted in DMEM without phenol red for 30 min. The medium was replaced for 100 μL of dye solution (Molecular Devices, Sunnyvale, CA, United States) and plates were incubated for 1 h at room temperature. Transient changes in Ca^{2+} concentration induced by adenosine 5′-triphosphate (ATP) (10^{-5} M) were measured by fluorescence (515–575 nm) using the FlexStation® equipment and SoftMax® Pro software (Molecular Devices, Sunnyvale, CA, United States). ATP-induced responses were determined immediately upon its addition and measured as peak fluorescent intensity minus basal fluorescent intensity and the area under the curve was calculated.

Detection of 8-OHdG Levels

The 8-OHdG levels in serum and pancreatic DNA were evaluated by ELISA using the HT 8-oxo-dG ELISA Kit II (Trevigen®, Gaithersburg, MD, United States). Briefly, 25 μl of serum samples (1:10), DNA extracted from the pancreas (500 μg/ml), and 8-OHdG monoclonal solution were added in a pre-coated 96-well plate and incubated for 1 h at 25°C, and then washed for four times with phosphate buffered saline containing Tween 20 (PBST). Fifty μl of goat anti-mouse IgG-HRP antibody were then added (incubation for 1 h at 25°C). After four washes with PBST, 50 μl of the TACS-Sapphire™ reagent were added in each well. After 15 min at 25°C, 50 μl of hydrochloric acid (0.2 M) were added and 8-OHdG levels were determined (450 μm) using the FlexStation® equipment and SoftMax® Pro software (Molecular Devices, Sunnyvale, California, United States). A standard curve (3.13 to 200 nM) for 8-OHdG was performed following the manufacturer instructions.

Drugs and Salts

Phenylephrine hydrochloride, acetylcholine chloride, LPS, lucigenin (N,N′-Dimethyl-9,9′-biacridinium dinitrate) and peg-catalase (Catalase-polyethylene glycol) were obtained from Sigma-Aldrich (St. Louis, MO, United States), MCC950 from Avistron® (Bude, Cornwall, United Kingdom), Tiron from Santa Cruz Biotechnology® (San Juan, CA, United States) and all reagents used in RT-PCR and murine primers from Invitrogen® (Carlsbad, CA, United States). Human primers from Sigma-Aldrich®, All other salts used were obtained from Merck® (Rio de Janeiro, RJ, Brazil). For cell culture, DMEM was purchased from Sigma®; FBS and antibiotics (Penicillin/Streptomycin) from Gibco Thermo Fisher Scientific® (Waltham, MA, United States).

Patients

Serum samples from 18 patients with type 1 diabetes and 20 age-matched healthy control subjects (non-diabetic) were collected by a specialized professional from the Clinical Laboratory Service of the University of São Paulo Hospital. All procedures were approved by the Research Ethics Committee of the Institute of Psychology of the University of São Paulo (protocol no. 644.869). Clinical and biochemical characteristics are shown in **Supplementary Table S2**.

Statistical Analysis

Results are expressed as mean ±standard error of the mean (E.P.M.). Relaxation responses are expressed as the percentage of relaxation in relation to pre-contraction levels induced by phenylephrine. Concentration-effect curves were submitted to non-linear regression analysis using the GraphPad Prism 6.0 program (GraphPad Software®, La Jolla, CA, United States). Agonist potency and maximal response are expressed as pD_2 [negative log of the molar concentration that produces 50% of maximal response (-log EC_{50})] and Rmax (maximal effect produced by the agonist), respectively.

Statistical analyses were performed by one-way or two-way ANOVA followed by Tukey multiple comparisons post-test for repeated measurements or by Student's *t*-test for unpaired data. The minimum acceptable level of significance was $P < 0.05$.

RESULTS

Type 1 Diabetes Increases Vascular NLRP3 Inflammasome Activation

Vascular expression of NLRP3 [Arbitrary Units (AU), T1D = 3.8 ± 0.1 vs. control = 0.9 ± 0.2; $P < 0.05$] (**Figure 1A**), and caspase-1 [AU, T1D = 3.6 ± 0.5 vs. control = 1.0 ± 0.3;

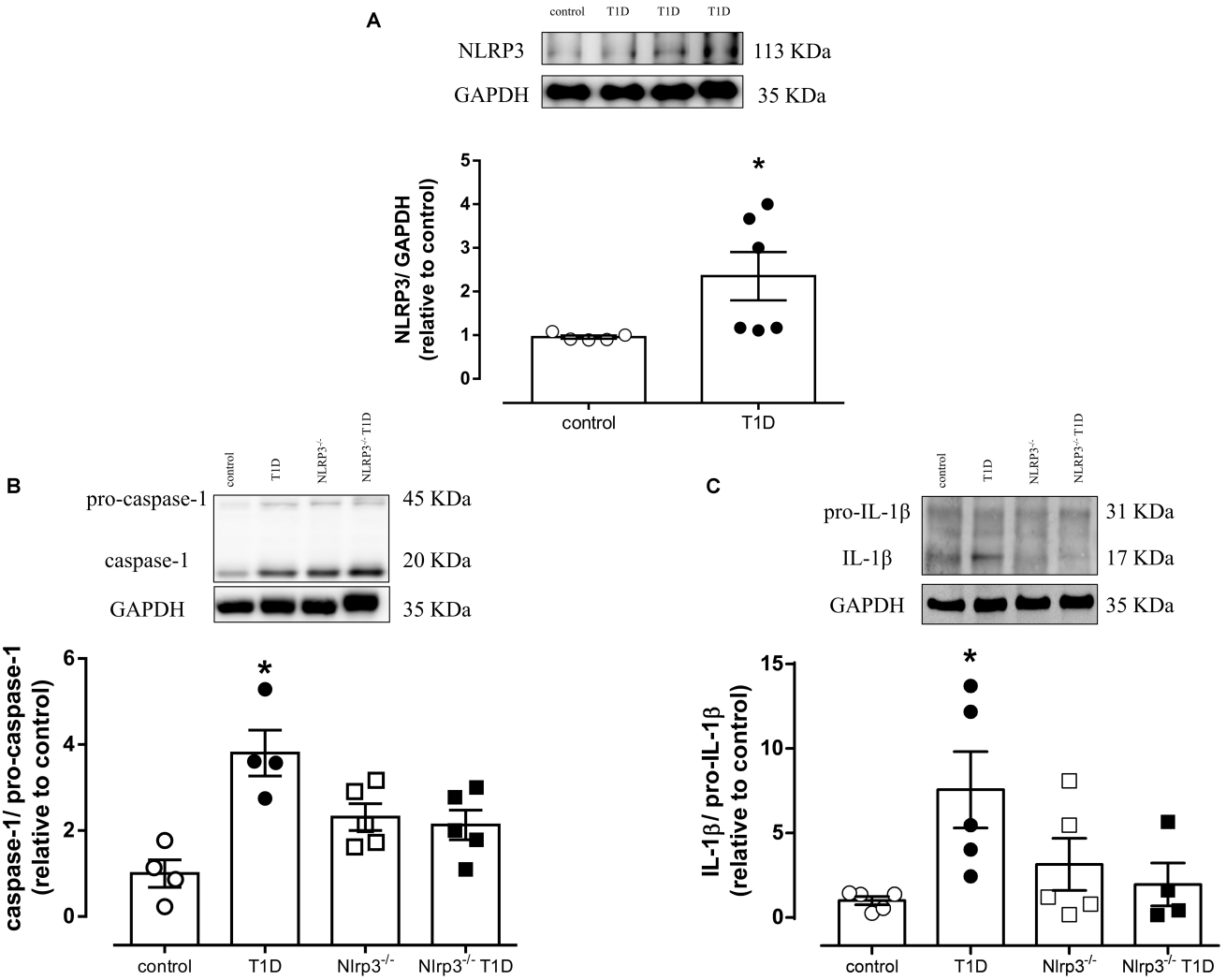

FIGURE 1 | On top, representative images of western blot and, at the bottom, densitometric analysis of protein expression of **(A)** NLRP3, **(B)** caspase-1 and pro-caspase-1 and **(C)** IL-1β and pro-IL-1β in mesenteric arteries from non-diabetic (control, white circles) or diabetic (T1D, black circles) C57BL/6 mice and non-diabetic (*Nlrp3*$^{-/-}$, white squares) or diabetic (*Nlrp3*$^{-/-}$ T1D, black squares) *Nlrp3*$^{-/-}$ mice. Each column represents the mean ±SEM. *$P < 0.05$ vs. control. N = 4–6, Student's t-test **(A)** and two-way ANOVA followed by a Tukey's *post hoc* test **(B,C)**.

$P < 0.05$] (**Figure 1B**) as well as IL-1β activation [AU, T1D = 5.5 ± 2.2 vs. control = 1.4 ± 0.2; $P < 0.05$] (**Figure 1C**) were increased in diabetic WT mice, in comparison to control mice. Diabetic *Nlrp3*$^{-/-}$ mice did not exhibit changes in activation of caspase-1 or IL-1β (**Figures 1B,C**).

NLRP3 Activation Contributes to ROS-Induced Endothelial Dysfunction in Type 1 Diabetes

Endothelium-denuded arteries from control and T1D mice exhibited similar relaxation responses to sodium nitroprusside (**Supplementary Figure S1**). Mesenteric arteries from T1D mice exhibited decreased endothelium-dependent relaxation (pD_2, T1D = 6.2 ± 0.2 vs. control = 6.6 ± 0.1; Rmax, T1D = 47.2 ± 4.9 vs. control = 90.2 ± 0.1; $P < 0.05$) (**Figure 2A**). NLRP3 deficiency prevented diabetes-induced decreased endothelium-dependent relaxation in mesenteric arteries (pD_2, *Nlrp3*$^{-/-}$ T1D = 6.6 ± 0.1 vs. T1D = 6.2 ± 0.2; Rmax, *Nlrp3*$^{-/-}$ T1D = 80.8 ± 3.3 vs. T1D = 47.2 ± 4.9; $P < 0.05$) (**Figure 2A**). Reduced vasodilation in WT diabetic mice was partially reverted by MCC950, a selective NLRP3 inhibitor (pD_2, T1D+MCC950 = 6.9 ± 0.2 vs. T1D = 6.2 ± 0.2; Rmax, T1D+MCC950 = 62.5 ± 3.8 vs. T1D = 46.6 ± 4.1; $P < 0.05$) (**Figure 2B**), and completely reverted by the superoxide anion scavenger Tiron (pD_2, T1D+Tiron = 6.6 ± 0.1 vs. T1D = 6.2 ± 0.2; Rmax, T1D+Tiron = 78.4 ± 3.1 vs. T1D = 46.6 ± 4.1; $P < 0.05$) (**Figure 2C**) and by peg-catalase (pD_2, T1D+Peg-catalase = 6.4 ± 0.1 vs. T1D = 6.2 ± 0.2; Rmax, T1D+Peg-catalase = 86.4 ± 2.8 vs. T1D = 46.6 ± 4.1; $P < 0.05$) (**Figure 2D**). MCC950 treatment did not affect ACh responses in arteries from control mice (pD_2, control+MCC950 = 6.7 ± 0.1

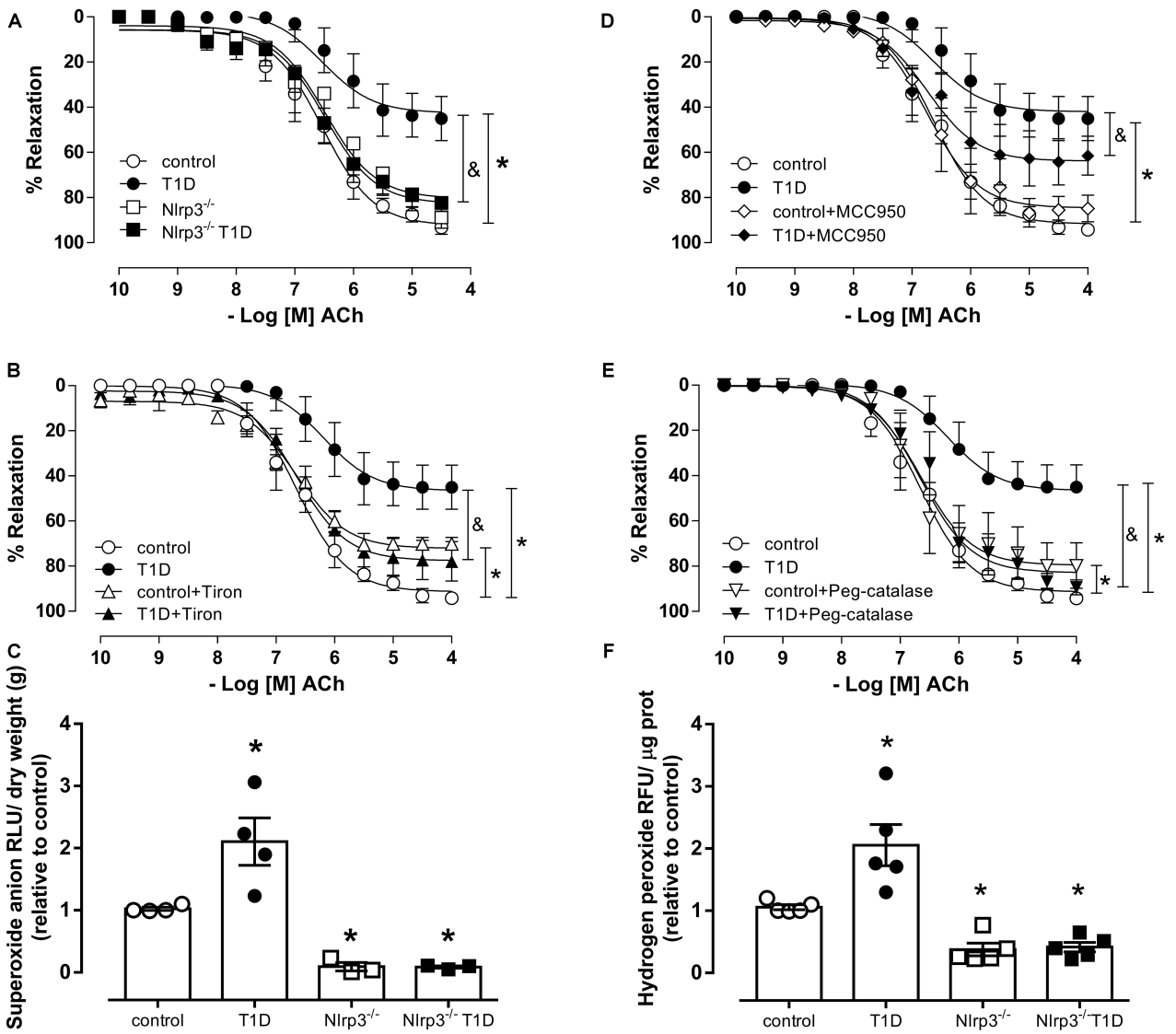

FIGURE 2 | Cumulative concentration-response curves to Acetylcholine (ACh) **(A)**, endothelium-dependent vasodilator, in resistance mesenteric arteries from C57BL/6 non-diabetic (control, white circles) or diabetic (T1D, black circles) and *Nlrp3*$^{-/-}$ non-diabetic (*Nlrp3*$^{-/-}$, white squares) or diabetic (*Nlrp3*$^{-/-}$ T1D, black squares) mice in the presence of **(B)** vehicle (white diamonds) and a NLRP3 inhibitor (MCC950, black diamonds), **(C)** vehicle (white triangles) and superoxide scavenger Tiron (black triangles), and **(D)** vehicle (white triangles down) and catalase mimetic peg-catalase (black triangles down). Generation of **(E)** superoxide anion and **(F)** hydrogen peroxide in mesenteric bed from non-diabetic (control, white circles) or diabetic (T1D, black circles) C57BL/6 mice and non-diabetic (*Nlrp3*$^{-/-}$, white squares) or diabetic (*Nlrp3*$^{-/-}$ T1D, black squares) *Nlrp3*$^{-/-}$ mice. Each point/column represents the mean ±SEM. $^{*}P < 0.05$ vs. control, $^{\&}P < 0.05$ vs. T1D. *N* = 3–7, two-way ANOVA followed by Tukey's *post hoc* test **(A–F)**.

vs. control = 6.6 ± 0.1; Rmax, control+MCC950 = 85.6 ± 6.7 vs. control = 91.3 ± 2.6; $P > 0.05$) (**Figure 2B**), whereas Tiron (pD_2, control+Tiron = 6.8 ± 0.1 vs. control = 6.6 ± 0.1; Rmax, control+Tiron = 70.6 ± 1.5 vs. control = 91.3 ± 2.6; $P > 0.05$) (**Figure 2C**) and Peg-catalase (pD_2, control+Peg-catalase = 6.8 ± 0.2 vs. control = 6.6 ± 0.1; Rmax, control+Peg-catalase = 78.0 ± 4.4 vs. control = 91.3 ± 2.6; $P > 0.05$) (**Figure 2D**) produced small decreases in ACh relaxation.

In addition, diabetes significantly increased superoxide anion generation (AU, T1D = 2.1 ± 0.4 vs. control = 1.0 ± 0.1; $P < 0.05$) (**Figure 2E**) as well as hydrogen peroxide generation (AU, T1D = 2.0 ± 0.4 vs. control = 1.0 ± 0.1; $P < 0.05$) (**Figure 2F**) in mesenteric arteries from C57BL/6 mice, which was not observed in mesenteric arteries from diabetic *Nlrp3*$^{-/-}$ mice.

NLRP3 Deficiency Decreases Nox4 Expression and Prevents Increased SOD-1 Expression

Diabetes did not change expression of Nox1 or catalase (**Figures 3A,B**) in mesenteric arteries. However, diabetes

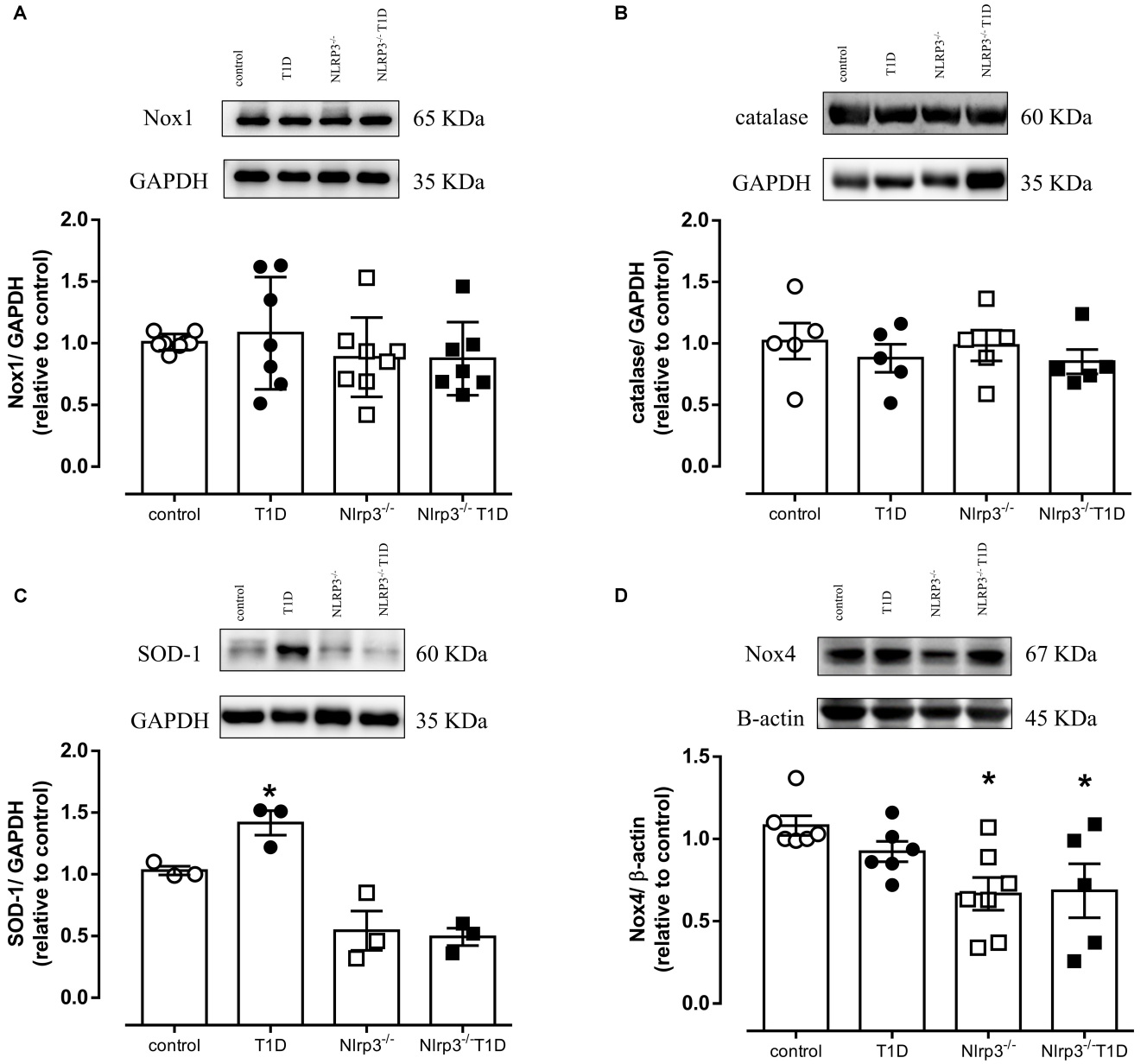

FIGURE 3 | On top, representative images of western blot and, at the bottom, densitometric analysis of the vascular expression of **(A)** Nox1, **(B)** Catalase, **(C)** SOD-1 and **(D)** Nox4 in mesenteric arteries from C57BL/6 non-diabetic (control, white circles) or diabetic (T1D, black circles) and *Nlrp3*$^{-/-}$ non-diabetic (*Nlrp3*$^{-/-}$, white squares) or diabetic (*Nlrp3*$^{-/-}$ T1D, black squares) mice. Each column represents the mean ±SEM. *$P < 0.05$ vs. respective control. $N = 3$–7, two-way ANOVA followed by Tukey's *post hoc* test **(A–D)**.

increased SOD-1 expression in arteries from WT diabetic mice (AU, T1D = 1.4 ± 0.1 vs. control = 1.0 ± 0.1; $P < 0.05$), which was not observed in arteries from *Nlrp3*$^{-/-}$ mice (**Figure 3C**). In addition, *Nlrp3*$^{-/-}$ mice exhibited reduced vascular Nox4 expression when compared to their respective counterpart C57BL/6 mice (AU, *Nlrp3*$^{-/-}$ = 0.7 ± 0.1 vs. control = 1.1 ± 0.1; *Nlrp3*$^{-/-}$ T1D = 0.7 ± 0.2 vs. T1D = 0.9 ± 0.1; $P < 0.05$) (**Figure 3D**).

Type 1 Diabetes Increases Cytosolic mDNA in Pancreatic Cells and dmDNA Promotes Endothelial Dysfunction by Mitochondrial Superoxide Anion Generation

Diabetes increased cytosolic mDNA release (**Figure 4A**), represented by increased Cyt C, Cyt B, and NADH expression. dmDNA, but not cmDNA reduced endothelium-dependent

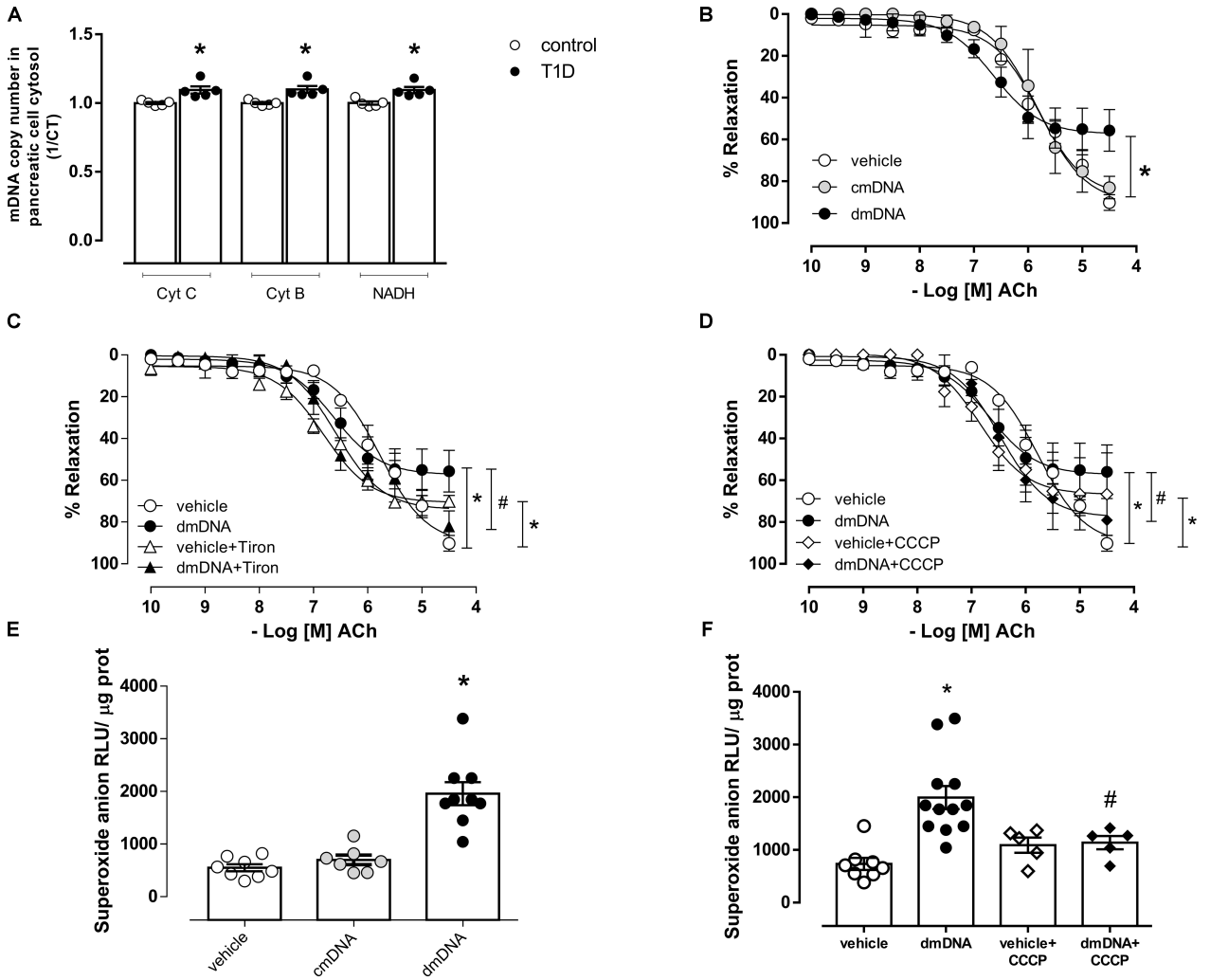

FIGURE 4 | (A) Quantification of mitochondrial DNA genes cytochrome C (Cyt C), cytochrome B (Cyt B) and NADH dehydrogenase (NADH) in the cytosolic fraction of pancreatic cells from non-diabetic (control, white circles) or diabetic (T1D, black circles) C57BL/6 mice. Gene expression was determined by RT-PCR. Each bar represents the mean ±SEM. $^{*}P < 0.05$ vs. control, $N = 3$–5. Cumulative concentration-response curves to Acetylcholine (ACh), endothelium-dependent vasodilator, in resistance mesenteric arteries from C57BL/6 mice incubated with **(B)** vehicle (white circles), mitochondrial DNA from control (cmDNA, gray circles) or diabetic (dmDNA, black circles) mice. Acetylcholine responses in mesenteric arteries incubated with vehicle or dmDNA were also performed in the presence of **(C)** Tiron [vehicle+Tiron (white triangles) or dmDNA+Tiron (black triangles)] and **(D)** CCCP [vehicle+CCCP (white diamonds) or dmDNA+CCCP (black diamonds)]. Superoxide anion generation in endothelial cells incubated with **(E)** vehicle (white circles), cmDNA (gray circles) or dmDNA (black circles) and in the presence of **(F)** CCCP [vehicle+CCCP (white diamonds) or dmDNA+CCCP (black diamonds)]. Each point/column represents the mean ±SEM. $^{*}P < 0.05$ vs. vehicle, $^{\#}P < 0.05$ vs. dmDNA. $N = 5$–12, Student's *t*-test **(A)**, one-way ANOVA **(B–F)**.

relaxation (Rmax, dmDNA = 57.3 ± 3.7 vs. vehicle = 90.5 ± 3.4; $P < 0.05$) (**Figure 4B**) in mesenteric arteries. dmDNA-induced reduced vasodilation was reversed by Tiron (Rmax, dmDNA+Tiron = 74.0 ± 3.4 vs. dmDNA = 57.3 ± 3.7; $P < 0.05$) (**Figure 4C**) and by CCCP (Rmax, dmDNA+CCCP = 77.7 ± 3.3 vs. dmDNA = 57.3 ± 3.7; $P < 0.05$) (**Figure 4D**). dmDNA also increased superoxide anion generation in endothelial cells (RLU/µg prot., dmDNA = 1958 ± 217 vs. vehicle = 550 ± 65; $P < 0.05$) (**Figure 4E**) and CCCP prevented dmDNA-induced increased superoxide anion generation in endothelial cells (RLU/µg prot., dmDNA+CCCP = 1138 ± 126 vs. dmDNA = 1995 ± 219) (**Figure 4F**). Tiron and CCCP reduced the maximum relaxation response in mesenteric arteries incubated with vehicle (vehicle+Tiron = 70.1 ± 1 vs. vehicle = 90.5 ± 3.4 and vehicle+CCCP = 66.8 ± 5.7 vs. vehicle = 90.5 ± 3.4).

NLRP3 Activation Contributes to dmDNA-Induced Endothelial Dysfunction

The incubation of endothelial cells with cmDNA and dmDNA did not activate caspase-1 or IL-1β. However, in cells primed with LPS for 24 h prior to mDNA incubation, dmDNA, but not cmDNA, increased activation

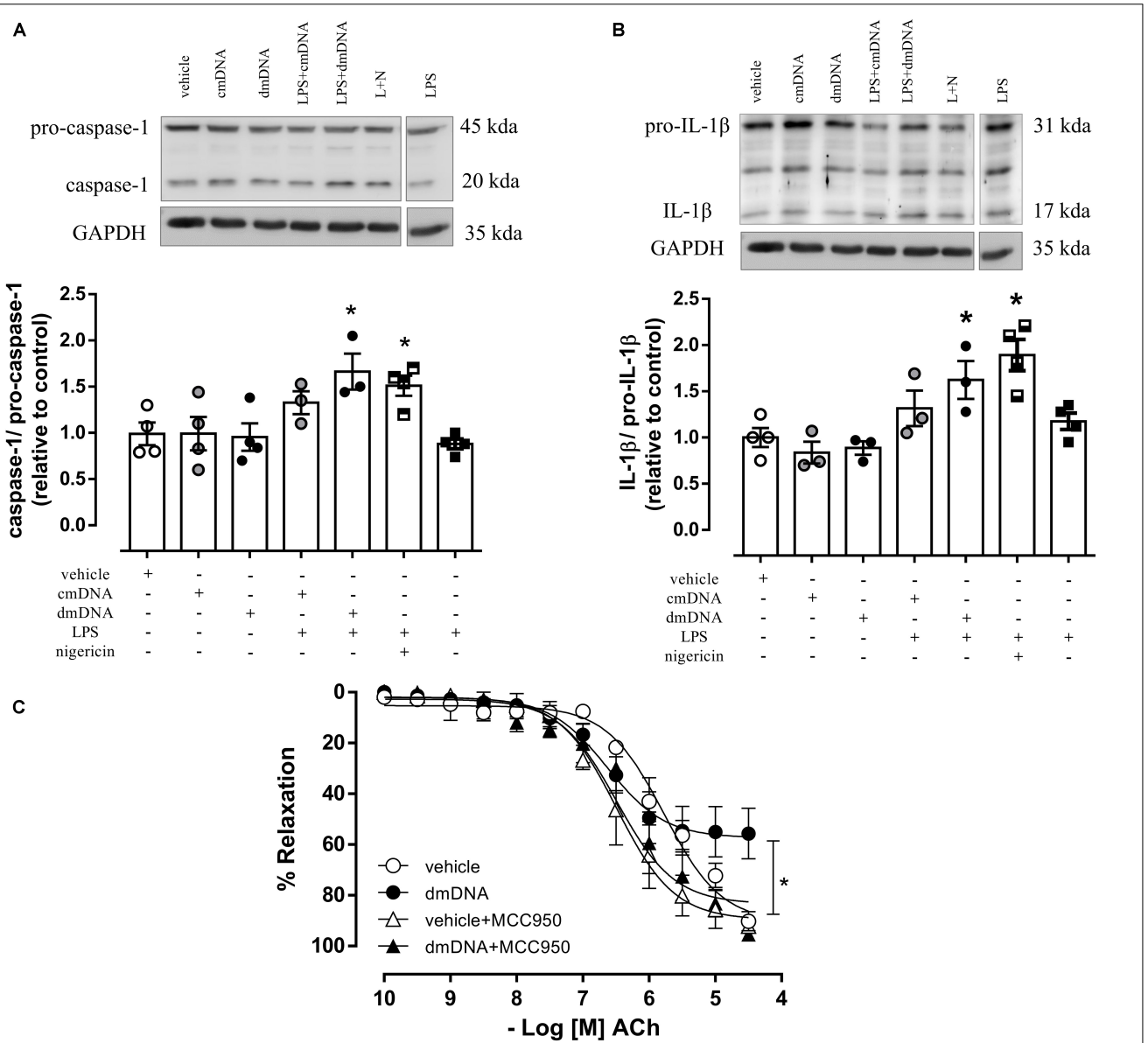

FIGURE 5 | On top, representative images of western blot and, at the bottom, densitometric analysis of the expression of **(A)** caspase-1 and pro-caspase-1 and **(B)** IL-1β and pro-IL-1β in endothelial cells primed with lipopolysaccharide (LPS) and incubated with vehicle (white squares) and mitochondrial DNA from control (cmDNA, white circles) and diabetic (dmDNA, black circles) mice. **(C)** Cumulative concentration-response curves to acetylcholine (ACh), endothelium-dependent vasodilator, in resistance mesenteric arteries from C57BL/6 incubated with vehicle (white circles) or mitochondrial DNA from diabetic mice (dmDNA, black circles) in the presence of vehicle (white triangles) or a NLRP3 inhibitor (MCC950, black triangles). Each point/column represents the mean ±SEM. *$P < 0.05$ vs. vehicle. $N = 3–5$, one-way ANOVA **(A–C)**.

of caspase-1 (AU, LPS+dmDNA = 1.5 ± 0.2 vs. vehicle = 0.8 ± 0.1; $P < 0.05$) (**Figure 5A**) and IL-1β (AU, LPS+dmDNA = 1.6 ± 0.2 vs. vehicle = 1.0 ± 0.1; $P < 0.05$) (**Figure 5B**). MCC950 prevented dmDNA-induced impairment of endothelium-dependent relaxation in mesenteric arteries (Rmax, dmDNA+MCC950 = 91.8 ± 4.9 vs. dmDNA+vehicle = 57.3 ± 3.8; $P < 0.05$) (**Figure 5C**). MCC950 did not alter ACh responses in vehicle-treated arteries (Rmax, vehicle+MCC950 = 89.1 ± 4.1 vs. vehicle = 90.5 ± 3.4; $P > 0.05$).

Ca^{2+} Influx-Induced Mitochondrial ROS Generation by dmDNA Activates Endothelial Cell NLRP3 Inflammasome

Incubation of endothelial cells with dmDNA, but not cmDNA increased ATP-stimulated Ca^{2+} influx (RFU, dmDNA = 315.0 ± 19.0 vs. vehicle = 130.0 ± 8.6; $P < 0.05$) (**Figure 6A**). The presence of a Ca^{2+} chelator, Bapta, prevented the increased dmDNA-induced ROS generation (RFU, dmDNA+Bapta = 980 ± 169 vs. dmDNA = 2380 ± 401;

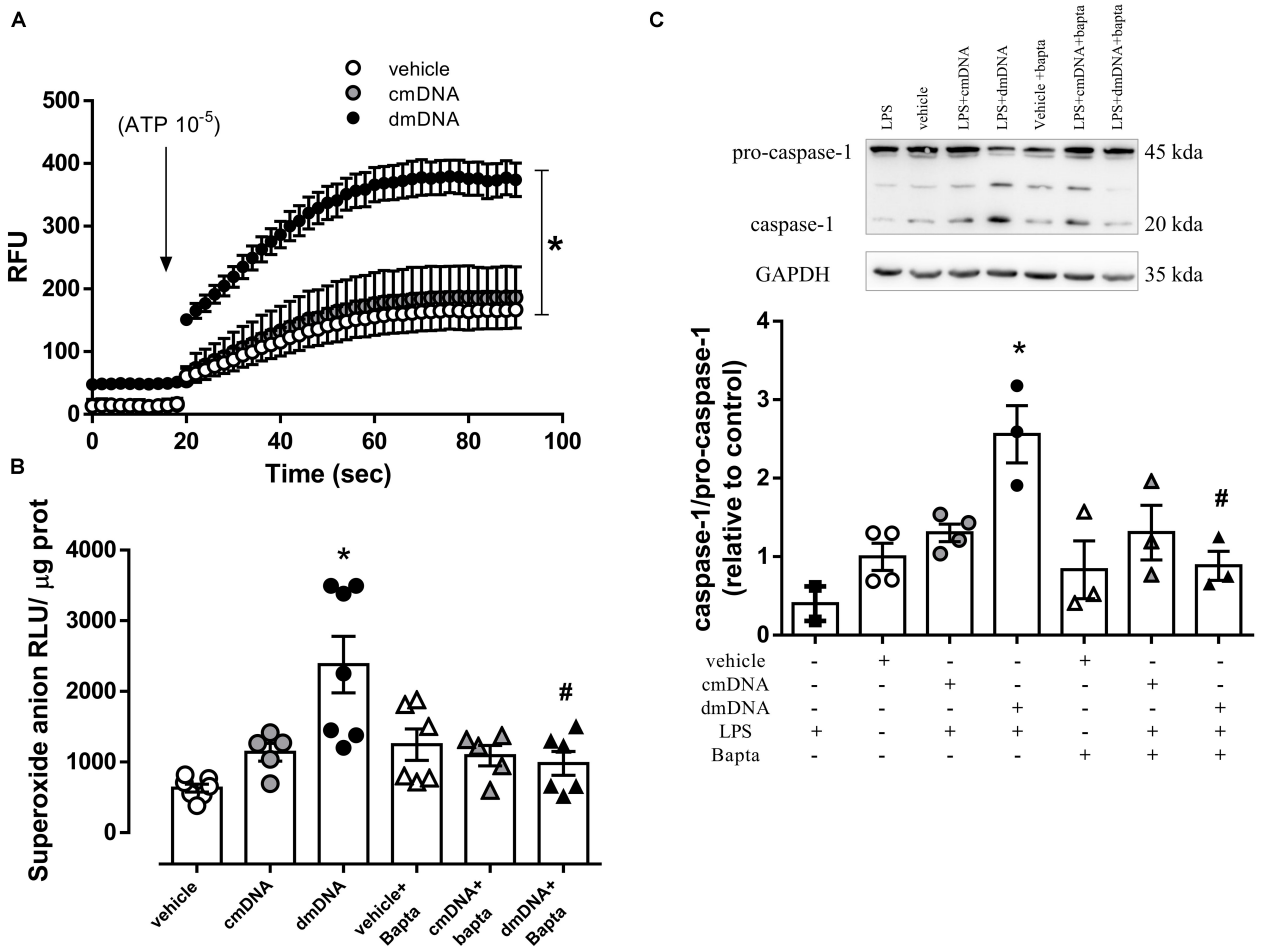

FIGURE 6 | (A) Ca^{2+} influx and **(B)** superoxide anion generation in endothelial cells incubated with vehicle (white circles), mitochondrial DNA from control (cmDNA, gray circles) or diabetic (dmDNA, black circles) mice in the presence of vehicle (white triangles) or a Ca^{2+} chelator (Bapta, gray and black triangles). On top, representative images of western blot and, at the bottom, densitometric analysis of the expression of **(C)** caspase-1 and pro-caspase-1 in endothelial cells primed with lipopolysaccharide (LPS) and incubated with vehicle (white squares), mitochondrial DNA from control (cmDNA, gray circles) or diabetic (dmDNA, black circles) mice in the presence of vehicle (white triangles) or a Ca^{2+} chelator (Bapta, gray and black triangles). Each point/column represents the mean ±SEM. $^{*}P < 0.05$ vs. vehicle, $^{\#}P < 0.05$ vs. dmDNA. N = 5–12, one-way ANOVA **(A–C)**.

$P < 0.05$) (**Figure 6B**) and caspase-1 activation (AU, LPS+dmDNA+Bapta = 0.9 ± 0.2 vs. LPS+dmDNA = 2.6 ± 0.4; $P < 0.05$) in endothelial cells (**Figure 6C**).

Type 1 Diabetes Increases Circulating mDNA and Serum NLRP3 Inflammasome Activation

In humans, type 1 diabetes increased circulating mDNA levels represented by increased CytB and NADH expression (**Figure 7A**). Diabetic patients also exhibited increased NLRP3 expression (AU, Type 1 diabetic = 0.18 ± 0.1 vs. Non-diabetic = 0.13 ± 0.1; $P < 0.05$) (**Figure 7B**), caspase-1 (AU, Type 1 diabetic = 2.0 ± 0.1 vs. Non-diabetic = 1.7 ± 0.1; $P < 0.05$) (**Figure 7C**) and IL-1β activation (AU, Type 1 diabetic = 1.3 ± 0.1 vs. Non-diabetic = 1.0 ± 0.1; $P < 0.05$) (**Figure 7D**). Clinical and biochemical characteristics of control (non-diabetic) subjects and diabetic patients are shown in the (**Supplementary Table S2**).

Type 1 Diabetes Does Not Change 8-OHdG Levels

Diabetes did not change 8-OHdG levels in serum DNA or mouse pancreatic mDNA (**Supplementary Figure S2**).

DISCUSSION

The present study shows that *Nlrp3*$^{-/-}$ mice are protected from diabetes-associated inflammatory vascular damage and endothelial dysfunction. Mitochondrial DNA is key for NLRP3 inflammasome activation in endothelial cells through increased Ca^{2+} influx and mitochondrial ROS generation.

One of the most important findings of this study is the association between NLRP3 and vascular dysfunction in type 1 diabetes. A link between NLRP3 and endothelial (dys)function has been previously suggested in other studies (15–17). In obese

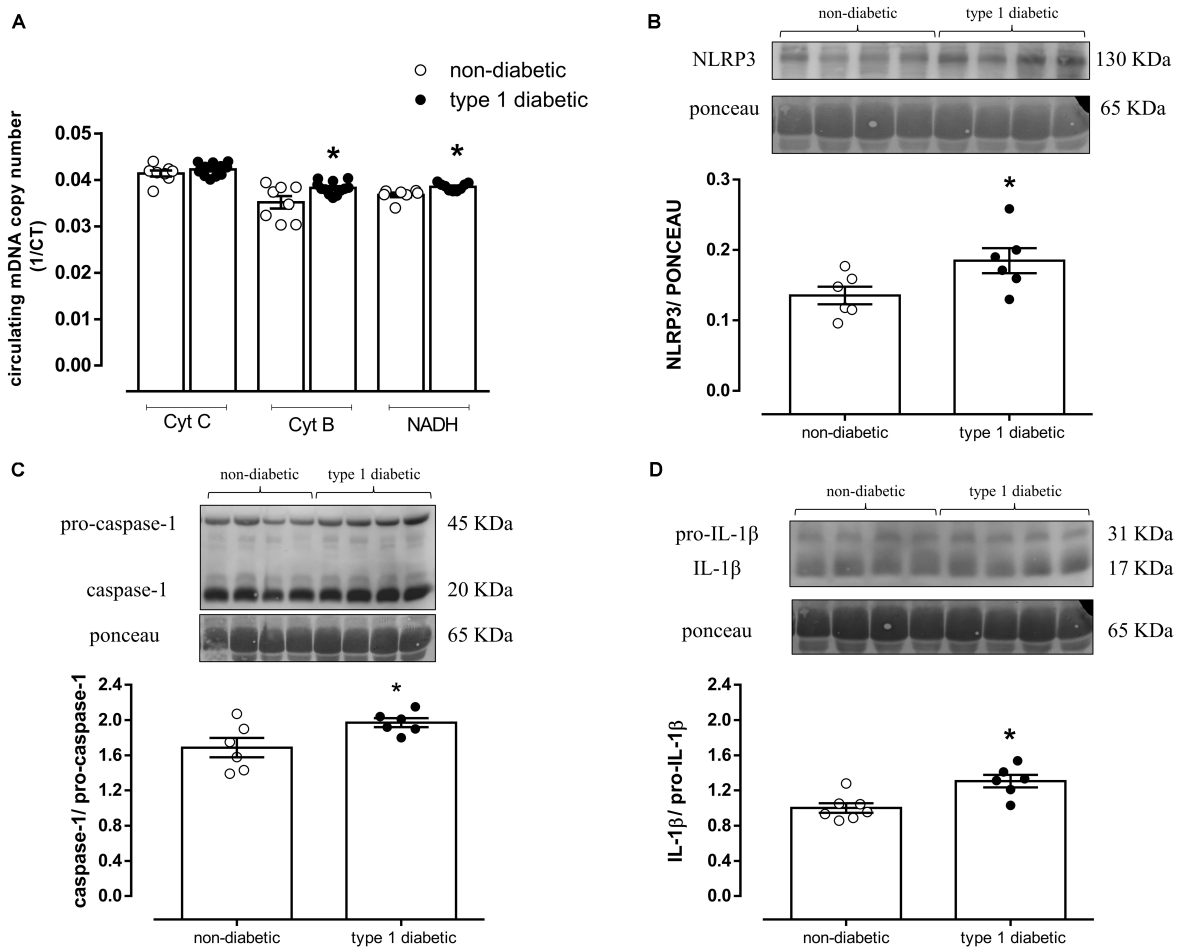

FIGURE 7 | (A) Quantification of mitochondrial DNA genes cytochrome C (Cyt C), cytochrome B (Cyt B) and NADH dehydrogenase (NADH). On top, representative images of western blot and, at the bottom, densitometric analysis of the expression of **(B)** NLRP3, **(C)** caspase-1 and pro-caspase-1, and **(D)** IL-1β and pro-IL-1β in the serum from non-diabetic subjects (white circles) and patients with type 1 diabetes (black circles). Each column represents the mean ±SEM. $^*P < 0.05$ vs. non-diabetic. N = 5–12, Student's t-test **(A–D)**.

rats, vascular dysfunction, represented by impaired endothelium-dependent relaxation, is associated with increased vascular expression of inflammasome markers such as NLRP3, caspase-1 and IL-1β (Liu et al., 2015). Mice with Kawasaki's disease, an inflammatory disease model, present impaired endothelium-dependent vasodilation accompanied by increased caspase-1, IL-1β, and VCAM-1 expression (Chen et al., 2015). In addition, NLRP3 deficiency protects endothelial function in hypercholesterolemic mice by reducing vascular superoxide anion generation and increasing eNOS activity (Zhang et al., 2015). *In vitro* experiments also show a modulatory role of NLRP3 on endothelial function since the silencing of NLRP3 gene prevents caspase-1 and IL-1β activation in endothelial cells stimulated with cell wall fragments of *Lactobacillus casei* (Chen et al., 2015). Furthermore, the expression of NLRP3 inflammasome components is increased in brain areas that control blood pressure in spontaneously hypertensive rats and is linked to increased vascular damage and high blood pressure (Avolio et al., 2018).

Reactive oxygen species modulate endothelial function and IL-1β is an important stimulus for ROS production. IL-1β increases ROS generation in human umbilical vein endothelial cells (HUVECs) (Toniolo et al., 2015) and in vascular smooth muscle cells (VSMC) from human coronary arteries (Kaur et al., 2004) by mechanisms that involve increased NADPH oxidase activation. NADPH oxidase is one of the main sources for ROS generation in different organs, including the vasculature (Hansen et al., 2018). Furthermore, inhibition of IL-1β using anakinra, a recombinant human interleukin-1 receptor antagonist, protects endothelial function and reduces ROS generation in mesenteric arteries of diabetic rats (Vallejo et al., 2014). It is important to mention that not only IL-1β induces ROS generation, but ROS also induce IL-1β production. Cultured astrocytes from BALB/C mice stimulated with high glucose concentrations exhibit increased IL-1β, TNF-α, IL-6, and IL-4 gene expression, which is abrogated by a ROS scavenger (Wang et al., 2012).

In the present study, mesenteric arteries from *Nlrp3*$^{-/-}$ mice with type 1 diabetes displayed decreased expression of Nox4

and reduced ROS levels. Other studies support an interaction between NLRP3 inflammasome and Nox expression and activity. Nox4 inhibition prevents ROS generation and decreases protein expression of NLRP3, caspase-1 and IL-1β in endothelial cells stimulated with high glucose (Wang et al., 2017). Decreased NLRP3 inflammasome activation associated with reduced Nox4 expression and ROS generation was also reported in rat cardioblasts stimulated with TNF-α and submitted to hypoxia (Chen et al., 2018). In addition, Nox4 silencing in rat aortic VSMC prevents IL-1β-induced ROS generation (Ginnan et al., 2013). Treatment of mice exhibiting LPS-induced hyperalgesia with a NLRP3 inhibitor, MCC950, decreases the expression of Nox2 subunits, $gp91^{phox}$ and $p47^{phox}$ in the brain, heart and lungs (Dolunay et al., 2017). These studies corroborate a link between Nox4 and NLRP3 inflammasome.

NLRP3 inflammasome activity is triggered by several stimuli, including mitochondrial DAMPs. The immunostimulatory role of mDNA was first reported by Collins et al. (2004). These authors showed that intra-articular administration of mDNA extracted from human and murine tissues induces inflammatory arthritis in mice, an event associated with increased TNF-α levels (Collins et al., 2004). Moreover, mDNA infusion increases IL-6 and neutrophil migration, causing tissue injury (Zhang et al., 2010). Our findings corroborate an immunostimulatory role of mDNA, since mDNA extracted from the pancreas of diabetic mice stimulates the production of proinflammatory markers in endothelial cells. Potential mechanisms associated with the immunostimulatory effect of mDNA include activation of pattern recognition receptors, such as NOD and Toll receptors, and structural modifications of the DNA. TLR-9 activation is linked to mDNA-induced inflammatory responses. TLR-9 antagonist reduces phosphorylation of MAPKs, such as p38 and p44/42, and IL-8 levels in human neutrophils stimulated with mDNA extracted from various tissues (Zhang et al., 2010). TLR-9 inhibition also decreases IL-8 and TNF-α in mDNA-stimulated cells from humans and mice (Pazmandi et al., 2014). NLRP3 is another receptor associated with mDNA effects. LPS-primed macrophages incubated with mDNA exhibit increased activation of caspase-1 and IL-1β in response to ATP, effects associated with NLRP3 activation (Nakahira et al., 2011). In the present study, cells primed with LPS and incubated with dmDNA exhibited increased activation of caspase-1 and IL-1β, reinforcing a relationship between mDNA and NLRP3.

mDNA oxidation has been associated with structural modifications that increase immunogenesis. Oxidized mDNA potentiates increased pro-inflammatory factors (IL-8 and TNF-α) in plasmocytoid dendritic cells (Pazmandi et al., 2014). One of the most common modifications related to DNA oxidation is represented by increased levels of oxidatively modified guanine bases (8-OHdG) (Kuchino et al., 1987). In diabetes, this modification is reported in the urine, mononuclear cells and skeletal muscle of patients (Dandona et al., 1996; Leinonen et al., 1997; Hinokio et al., 1999). Our results did not show higher circulating or pancreatic 8-OHdG levels in the mDNA. However, other modifications, such as epigenetic alterations may increase mDNA immunogenesis. High glucose concentrations increase mDNA methylation, an epigenetic modification, in retinal endothelial cells, a condition also observed in the retinal microvasculature of human donors with diabetic retinopathy (Mishra and Kowluru, 2015). In diabetes, DNA methylation in several organs is associated with micro and macrovascular complications (Kato and Natarajan, 2014). Mitochondrial DNA methylation is also a potential mechanism for the greater immunogenesis associated with diabetic mitochondrial DNA, which should be investigated in further studies.

Another potential mechanism by which mDNA may activate the NLRP3 inflammasome is mitochondrial ROS generation. Human macrophages incubated with increasing doses of inhibitors of the mitochondrial respiratory chain display increased IL-1β release. This effect is inhibited by NLRP3 and caspase-1 gene deletion in both human and murine macrophages (Zhou et al., 2011). In our study, dmDNA increased mitochondrial ROS, since ROS generation by dmDNA in endothelial cells was attenuated by a mitochondrial antioxidant, CCCP. Similar results were observed in murine macrophages after the incubation with a mitochondrial antioxidant agent, MitoTEMPO (Nakahira et al., 2011), reinforcing the link between mDNA, mitochondrial ROS and NLRP3 inflammasome activation. Thus, mitochondrial ROS generation induced by dmDNA seems to activate NLRP3 inflammasome in endothelial cells.

Ca^{2+} influx is also critical for NLRP3 activation and, consequently, IL-1β release. In LPS-primed and ATP-stimulated macrophages, IL-1β release is prevented by thapsigargin, a Ca^{2+} mobilization agent that inhibits the sarcoplasmic Ca^{2+}-ATPase (Murakami et al., 2012). Furthermore, mDNA increases Ca^{2+} influx and NLRP3 activation. LPS-primed and ATP-stimulated murine macrophages incubated with mDNA display greater Ca^{2+} influx and activation of caspase-1 and IL-1β (Nakahira et al., 2011). Likewise, in the present study, we found increased Ca^{2+} influx in endothelial cells incubated with dmDNA.

Considering the immunogenic role of mDNA, the presence of circulating mDNA, i.e., mDNA released into the blood, has been associated with inflammatory mechanisms under several conditions. Post-myocardial infarction patients have increased circulating mDNA levels, accompanied by higher levels of inflammatory cytokines, such as TNF-α and IL-6, compared to healthy individuals (Qin et al., 2017). Patients with breast cancer (Mahmoud et al., 2015), gastric cancer (Fernandes et al., 2014), diabetes and retinopathy (Malik et al., 2015), coronary artery disease (Liu et al., 2016) also have higher levels of circulating mDNA. These results corroborate data from our study showing that patients with type 1 diabetes present an increase in circulating mDNA and the increased release of mDNA from pancreatic cells observed in our study may be related to the apoptotic and necrotic processes triggered in the endocrine pancreas by diabetes, which enables extracellular genetic content extravasation. Overall, this is the first study that demonstrates a relationship between mDNA, vascular NLRP3 inflammasome activation, Ca^{2+} influx-induced ROS generation and endothelial dysfunction in diabetes.

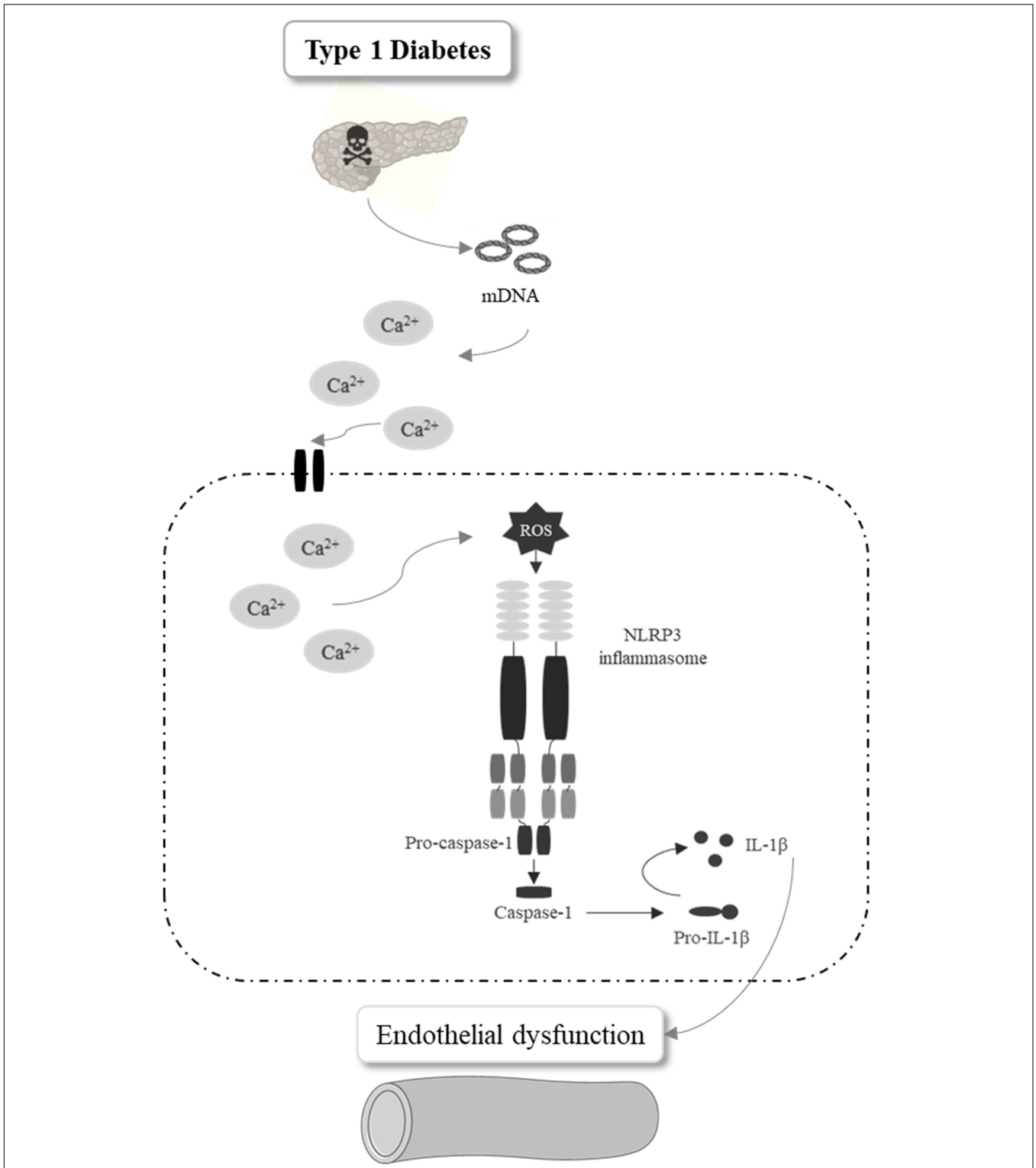

FIGURE 8 | Schematic representation of the conclusion. Pancreatic mitochondrial DNA release in type 1 diabetes increases Ca^{2+} influx and mitochondrial ROS generation in endothelial cells promoting caspase-1 and IL-1 secretion by NLRP3 inflammasome activation, events that contribute to diabetes-associated endothelial dysfunction.

CONCLUSION

In summary, mDNA contributes to endothelial dysfunction in type 1 diabetes, which is linked to increased inflammatory mediators via activation of the NLRP3 inflammasome in endothelial cells (**Figure 8**). Pharmacologic inhibition or genetic deletion of the NLRP3 in mice protects from diabetes-associated inflammatory vascular damage and endothelial dysfunction. Our study highlights the importance of NLRP3 inflammasome in diabetes-associated vascular dysfunction, which is key to diabetes-associated complications.

DATA AVAILABILITY STATEMENT

The raw data supporting the conclusions of this article will be made available by the authors, without undue reservation, to any qualified researcher.

ETHICS STATEMENT

The studies involving human participants were reviewed and approved by the Research Ethics Committee of the Institute of Psychology of the University of São Paulo (protocol no. 644.869). The patients/participants provided their written informed consent to participate in this study. The animal study was reviewed and approved by the Ethics Committee on Animal Research of the Ribeirão Preto Medical School – University of São Paulo, Ribeirão Preto, Brazil (protocol no. 26/2015).

AUTHOR CONTRIBUTIONS

CP, NF, CZ, and JFS performed the wet laboratory experiments. CP, DC, and RT designed the study. VG and DV provided the human samples. DZ and JSS provided the knockout mice used in this study. CP wrote the manuscript. DC, DZ, and RT revised its scientific content.

FUNDING

This work was funded by grants from CAPES (Coordenação de Aperfeiçoamento de Pessoal de Nível Superior), CNPq (Conselho Nacional de Desenvolvimento Científico e Tecnológico), and FAPESP (Fundação de Amparo a Pesquisa do Estado de São Paulo, 2016/17303-4 to CP and 2013/08216-2 to RT at the Center for Research in Inflammatory Diseases – CRID), Brazil.

ACKNOWLEDGMENTS

We thank Dr. Vishva Dixit (Genentech) for providing the *Nlrp3*$^{-/-}$ mice used in this study [CITAR: Mariathasan et al. (2006)].

SUPPLEMENTARY MATERIAL

The Supplementary Material for this article can be found online at: https://www.frontiersin.org/articles/10.3389/fphys.2019.01557/full#supplementary-material

REFERENCES

Avolio, E., Pasqua, T., Di Vito, A., Fazzari, G., Cardillo, G., Alo, R., et al. (2018). Role of brain neuroinflammatory factors on hypertension in the spontaneously hypertensive rat. *Neuroscience* 375, 158–168. doi: 10.1016/j.neuroscience.2018.01.067

Beckman, J. A., Goldfine, A. B., Gordon, M. B., Garrett, L. A., Keaney, J. F. Jr., and Creager, M. A. (2003). Oral antioxidant therapy improves endothelial function in Type 1 but not Type 2 diabetes mellitus. *Am. J. Physiol. Heart Circ. Physiol.* 285, H2392–H2398.

Brough, D., Le Feuvre, R. A., Wheeler, R. D., Solovyova, N., Hilfiker, S., Rothwell, N. J., et al. (2003). Ca2+ stores and Ca2+ entry differentially contribute to the release of IL-1 beta and IL-1 alpha from murine macrophages. *J. Immunol.* 170, 3029–3036. doi: 10.4049/jimmunol.170.6.3029

Carlos, D., Costa, F. R., Pereira, C. A., Rocha, F. A., Yaochite, J. N., Oliveira, G. G., et al. (2017). Mitochondrial DNA activates the NLRP3 inflammasome and predisposes to Type 1 diabetes in murine model. *Front Immunol.* 8:164. doi: 10.3389/fimmu.2017.00164

Chen, A., Chen, Z., Xia, Y., Lu, D., Yang, X., Sun, A., et al. (2018). Liraglutide attenuates NLRP3 inflammasome-dependent pyroptosis via regulating SIRT1/NOX4/ROS pathway in H9c2 cells. *Biochem. Biophys. Res. Commun.* 499, 267–272. doi: 10.1016/j.bbrc.2018.03.142

Chen, Y., Li, X., Boini, K. M., Pitzer, A. L., Gulbins, E., Zhang, Y., et al. (2015). Endothelial Nlrp3 inflammasome activation associated with lysosomal destabilization during coronary arteritis. *Biochim. Biophys. Acta* 1853, 396–408. doi: 10.1016/j.bbamcr.2014.11.012

Chu, J., Thomas, L. M., Watkins, S. C., Franchi, L., Nunez, G., and Salter, R. D. (2009). Cholesterol-dependent cytolysins induce rapid release of mature IL-1beta from murine macrophages in a NLRP3 inflammasome and cathepsin B-dependent manner. *J. Leukoc Bio.* 86, 1227–1238. doi: 10.1189/jlb.0309164

Collins, L. V., Hajizadeh, S., Holme, E., Jonsson, I. M., and Tarkowski, A. (2004). Endogenously oxidized mitochondrial DNA induces in vivo and in vitro inflammatory responses. *J. Leukoc. Biol.* 75, 995–1000. doi: 10.1189/jlb.0703328

Czajka, A., Ajaz, S., Gnudi, L., Parsade, C. K., Jones, P., Reid, F., et al. (2015). Altered mitochondrial function, mitochondrial DNA and reduced metabolic flexibility in patients with diabetic nephropathy. *EBio Med.* 2, 499–512. doi: 10.1016/j.ebiom.2015.04.002

Dandona, P., Thusu, K., Cook, S., Snyder, B., Makowski, J., Armstrong, D., et al. (1996). Oxidative damage to DNA in diabetes mellitus. *Lancet* 347, 444–445. doi: 10.1016/s0140-6736(96)90013-6

Dolunay, A., Senol, S. P., Temiz-Resitoglu, M., Guden, D. S., Sari, A. N., Sahan-Firat, S., et al. (2017). Inhibition of NLRP3 inflammasome prevents LPS-Induced inflammatory hyperalgesia in mice: contribution of NF-kappaB, Caspase-1/11, ASC, NOX, and NOS Isoforms. *Inflammation* 40, 366–386. doi: 10.1007/s10753-016-0483-3

Fernandes, J., Michel, V., Camorlinga-Ponce, M., Gomez, A., Maldonado, C., De Reuse, H., et al. (2014). Circulating mitochondrial DNA level, a noninvasive biomarker for the early detection of gastric cancer. *Cancer Epidemiol. Biomark. Prev.* 23, 2430–2438. doi: 10.1158/1055-9965.EPI-14-0471

Ginnan, R., Jourd'heuil, F. L., Guikema, B., Simons, M., Singer, H. A., and Jourd'heuil, D. (2013). NADPH oxidase 4 is required for interleukin-1beta-mediated activation of protein kinase Cdelta and downstream activation of c-jun N-terminal kinase signaling in smooth muscle. *Free Radic. Biol .Med.* 54, 125–134. doi: 10.1016/j.freeradbiomed.2012.09.026

Hansen, S. S., Aasum, E., and Hafstad, A. D. (2018). The role of NADPH oxidases in diabetic cardiomyopathy. *Biochim. Biophys. Acta* 1864(5 Pt B), 1908–1913. doi: 10.1016/j.bbadis.2017.07.025

Hinokio, Y., Suzuki, S., Hirai, M., Chiba, M., Hirai, A., and Toyota, T. (1999). Oxidative DNA damage in diabetes mellitus: its association with diabetic complications. *Diabetologia* 42, 995–998. doi: 10.1007/s001250051258

Kato, M., and Natarajan, R. (2014). Diabetic nephropathy–emerging epigenetic mechanisms. *Nat. Rev. Nephrol.* 10, 517–530. doi: 10.1038/nrneph.2014.116

Kaur, J., Dhaunsi, G. S., and Turner, R. B. (2004). Interleukin-1 and nitric oxide increase NADPH oxidase activity in human coronary artery smooth muscle cells. *Med. Princ. Pract.* 13, 26–29. doi: 10.1159/000074047

Kuchino, Y., Mori, F., Kasai, H., Inoue, H., Iwai, S., Miura, K., et al. (1987). Misreading of DNA templates containing 8-hydroxydeoxyguanosine at the modified base and at adjacent residues. *Nature* 327, 77–79. doi: 10.1038/327077a0

Leinonen, J., Lehtimaki, T., Toyokuni, S., Okada, K., Tanaka, T., Hiai, H., et al. (1997). New biomarker evidence of oxidative DNA damage in patients with non-insulin-dependent diabetes mellitus. *FEBS Lett.* 417, 150–152. doi: 10.1016/s0014-5793(97)01273-8

Liu, J., Zou, Y., Tang, Y., Xi, M., Xie, L., Zhang, Q., et al. (2016). Circulating cell-free mitochondrial deoxyribonucleic acid is increased in coronary heart disease patients with diabetes mellitus. *J. Diabetes Investig* 7, 109–114. doi: 10.1111/jdi.12366

Liu, P., Xie, Q., Wei, T., Chen, Y., Chen, H., and Shen, W. (2015). Activation of the NLRP3 inflammasome induces vascular dysfunction in obese OLETF rats. *Biochem. Biophys. Res. Commun.* 468, 319–325. doi: 10.1016/j.bbrc.2015.10.105

Mahmoud, E. H., Fawzy, A., Ahmad, O. K., and Ali, A. M. (2015). Plasma circulating cell-free nuclear and mitochondrial DNA as potential biomarkers in the peripheral blood of breast cancer patients. *Asian. Pac. J. Cancer Prev.* 16, 8299–8305. doi: 10.7314/apjcp.2015.16.18.8299

Malik, A. N., Parsade, C. K., Ajaz, S., Crosby-Nwaobi, R., Gnudi, L., Czajka, A., et al. (2015). Altered circulating mitochondrial DNA and increased inflammation in patients with diabetic retinopathy. *Diabetes. Res. Clin. Pract.* 110, 257–265. doi: 10.1016/j.diabres.2015.10.006

Mariathasan, S., Weiss, D. S., Newton, K., McBride, J., O'Rourke, K., Roose-Girma, M., et al. (2006). Cryopyrin activates the inflammasome in response to toxins and ATP. *Nature* 440, 228–232. doi: 10.1038/nature04515

Martinon, F., Burns, K., and Tschopp, J. (2002). The inflammasome: a molecular platform triggering activation of inflammatory caspases and processing of proIL-beta. *Mol. Cell* 10, 417–426.

McCarthy, C. G., Wenceslau, C. F., Goulopoulou, S., Ogbi, S., Baban, B., Sullivan, J. C., et al. (2015). Circulating mitochondrial DNA and Toll-like receptor 9 are associated with vascular dysfunction in spontaneously hypertensive rats. *Cardiovasc. Res.* 107, 119–130. doi: 10.1093/cvr/cvv137

Mishra, M., and Kowluru, R. A. (2015). Epigenetic modification of mitochondrial DNA in the development of diabetic retinopathy. *Invest Ophthalmol. Vis. Sci.* 56, 5133–5142. doi: 10.1167/iovs.15-16937

Mulvany, M. J., and Halpern, W. (1977). Contractile properties of small arterial resistance vessels in spontaneously hypertensive and normotensive rats. *Circ. Res.* 41, 19–26. doi: 10.1161/01.res.41.1.19

Murakami, T., Ockinger, J., Yu, J., Byles, V., McColl, A., Hofer, A. M., et al. (2012). Critical role for calcium mobilization in activation of the NLRP3 inflammasome. *Proc. Natl. Acad. Sci. U.S.A.* 109, 11282–11287. doi: 10.1073/pnas.1117765109

Nakahira, K., Haspel, J. A., Rathinam, V. A., Lee, S. J., Dolinay, T., Lam, H. C., et al. (2011). Autophagy proteins regulate innate immune responses by inhibiting the release of mitochondrial DNA mediated by the NALP3 inflammasome. *Na.t Immunol.* 12, 222–230. doi: 10.1038/ni.1980

Palomo, J., Dietrich, D., Martin, P., Palmer, G., and Gabay, C. (2015). The interleukin (IL)-1 cytokine family–Balance between agonists and antagonists in inflammatory diseases. *Cytokine* 76, 25–37. doi: 10.1016/j.cyto.2015.06.017

Pazmandi, K., Agod, Z., Kumar, B. V., Szabo, A., Fekete, T., Sogor, V., et al. (2014). Oxidative modification enhances the immunostimulatory effects of extracellular mitochondrial DNA on plasmacytoid dendritic cells. *Free Radic. Biol. Med.* 77, 281–290. doi: 10.1016/j.freeradbiomed.2014.09.028

Petrilli, V., Papin, S., Dostert, C., Mayor, A., Martinon, F., and Tschopp, J. (2007). Activation of the NALP3 inflammasome is triggered by low intracellular potassium concentration. *Cell Death Differ.* 14, 1583–1589. doi: 10.1038/sj.cdd.4402195

Qin, C., Gu, J., Liu, R., Xu, F., Qian, H., He, Q., et al. (2017). Release of mitochondrial DNA correlates with peak inflammatory cytokines in patients with acute myocardial infarction. *Anatol. J. Cardiol.* 17, 224–228. doi: 10.14744/AnatolJCardiol.2016.7209

Rizzoni, D., Porteri, E., Guelfi, D., Muiesan, M. L., Valentini, U., Cimino, A., et al. (2001). Structural alterations in subcutaneous small arteries of normotensive and hypertensive patients with non-insulin-dependent diabetes mellitus. *Circulation* 103, 1238–1244. doi: 10.1161/01.cir.103.9.1238

Shimada, K., Crother, T. R., Karlin, J., Dagvadorj, J., Chiba, N., Chen, S., et al. (2012). Oxidized mitochondrial DNA activates the NLRP3 inflammasome during apoptosis. *Immunity* 36, 401–414. doi: 10.1016/j.immuni.2012.01.009

Toniolo, A., Buccellati, C., Trenti, A., Trevisi, L., Carnevali, S., Sala, A., et al. (2015). Antiinflammatory and antioxidant effects of H2O2 generated by natural sources in Il1beta-treated human endothelial cells. *Prostaglandins Other Lipid Mediat.* 121(Pt B), 190–198. doi: 10.1016/j.prostaglandins.2015.09.004

Vallejo, S., Palacios, E., Romacho, T., Villalobos, L., Peiro, C., and Sanchez-Ferrer, C. F. (2014). The interleukin-1 receptor antagonist anakinra improves endothelial dysfunction in streptozotocin-induced diabetic rats. *Cardiovasc. Diabetol.* 13:158. doi: 10.1186/s12933-014-0158-z

Wang, J., Li, G., Wang, Z., Zhang, X., Yao, L., Wang, F., et al. (2012). High glucose-induced expression of inflammatory cytokines and reactive oxygen species in cultured astrocytes. *Neuroscience* 202, 58–68. doi: 10.1016/j.neuroscience.2011.11.062

Wang, W., Wu, Q. H., Sui, Y., Wang, Y., and Qiu, X. (2017). Rutin protects endothelial dysfunction by disturbing Nox4 and ROS-sensitive NLRP3 inflammasome. *Biomed Pharmacother.* 86, 32–40. doi: 10.1016/j.biopha.2016.11.134

Zhang, Q., Raoof, M., Chen, Y., Sumi, Y., Sursal, T., Junger, W., et al. (2010). Circulating mitochondrial DAMPs cause inflammatory responses to injury. *Nature* 464, 104–107. doi: 10.1038/nature08780

Zhang, Y., Li, X., Pitzer, A. L., Chen, Y., Wang, L., and Li, P. L. (2015). Coronary endothelial dysfunction induced by nucleotide oligomerization domain-like receptor protein with pyrin domain containing 3 inflammasome activation during hypercholesterolemia: beyond inflammation. *Antioxid. Redox Signal.* 22, 1084–1096. doi: 10.1089/ars.2014.5978

Zhou, R., Tardivel, A., Thorens, B., Choi, I., and Tschopp, J. (2010). Thioredoxin-interacting protein links oxidative stress to inflammasome activation. *Nat. Immunol.* 11, 136–140. doi: 10.1038/ni.1831

Zhou, R., Yazdi, A. S., Menu, P., and Tschopp, J. (2011). A role for mitochondria in NLRP3 inflammasome activation. *Nature* 469, 221–225. doi: 10.1038/nature09663

Conflict of Interest: The authors declare that the research was conducted in the absence of any commercial or financial relationships that could be construed as a potential conflict of interest.

frontiers in Physiology

ORIGINAL RESEARCH
published: 21 January 2020
doi: 10.3389/fphys.2019.01614

Acute Increase in *O*-GlcNAc Improves Survival in Mice With LPS-Induced Systemic Inflammatory Response Syndrome

*Josiane Fernandes Silva[1†], Vania C. Olivon[2†], Fabiola Leslie A. C. Mestriner[3], Camila Ziliotto Zanotto[1], Raphael Gomes Ferreira[1], Nathanne Santos Ferreira[1], Carlos Alberto Aguiar Silva[4], João Paulo Mesquita Luiz[1], Juliano Vilela Alves[1], Rubens Fazan[4], Fernando Queiróz Cunha[1], Jose Carlos Alves-Filho[1] and Rita C. Tostes[1]**

[1] Department of Pharmacology, Ribeirão Preto Medical School, University of São Paulo, Ribeirão Preto, Brazil, [2] Universidade Anhanguera-UNIDERP, Campo Grande, Brazil, [3] Department of Surgery and Anatomy, Ribeirão Preto Medical School, University of São Paulo, Ribeirão Preto, Brazil, [4] Department of Physiology, Ribeirão Preto Medical School, University of São Paulo, Ribeirão Preto, Brazil

OPEN ACCESS

Edited by:
Shampa Chatterjee,
University of Pennsylvania,
United States

Reviewed by:
Jingyan Han,
Boston University, United States
Suowen Xu,
University of Rochester, United States

***Correspondence:**
Rita C. Tostes
rtostes@usp.br

[†] These authors have equally contributed to this work

Specialty section:
This article was submitted to Vascular Physiology, a section of the journal Frontiers in Physiology

Received: 05 October 2019
Accepted: 23 December 2019
Published: 21 January 2020

Citation:
Silva JF, Olivon VC, Mestriner FLAC, Zanotto CZ, Ferreira RG, Ferreira NS, Silva CAA, Luiz JPM, Alves JV, Fazan R, Cunha FQ, Alves-Filho JC and Tostes RC (2020) Acute Increase in O-GlcNAc Improves Survival in Mice With LPS-Induced Systemic Inflammatory Response Syndrome. Front. Physiol. 10:1614. doi: 10.3389/fphys.2019.01614

Sepsis is a systemic inflammatory response syndrome (SIRS) resulting from a severe infection that is characterized by immune dysregulation, cardiovascular derangements, and end-organ dysfunction. The modification of proteins by *O*-linked N-acetylglucosamine (*O*-GlcNAcylation) influences many of the key processes that are altered during sepsis, including the production of inflammatory mediators and vascular contractility. Here, we investigated whether *O*-GlcNAc affects the inflammatory response and cardiovascular dysfunction associated with sepsis. Mice received an intraperitoneal injection of lipopolysaccharide (LPS, 20 mg/Kg) to induce endotoxic shock and systemic inflammation, resembling sepsis-induced SIRS. The effects of an acute increase in *O*-GlcNAcylation, by treatment of mice with glucosamine (GlcN, 300 mg/Kg, i.v.) or thiamet-G (ThG, 150 μg/Kg, i.v.), on LPS-associated mortality, production and release of cytokines by macrophages and vascular cells, vascular responsiveness to constrictors and blood pressure were then determined. Mice under LPS-induced SIRS exhibited a systemic and local inflammatory response with increased levels of interleukin-1β (IL-1β), interleukin-6 (IL-6) and tumor necrosis factor (TNF-α), as well as severe hypotension and vascular hyporesponsiveness, characterized by reduced vasoconstriction to phenylephrine. In addition, LPS increased neutrophil infiltration in lungs and produced significant lethality. Treatment with GlcN and ThG reduced systemic inflammation and attenuated hypotension and the vascular refractoriness to phenylephrine, improving survival. GlcN and ThG also decreased LPS-induced production of inflammatory cytokines by bone marrow-derived macrophages and nuclear transcription factor-kappa B (NF-κB) activation in RAW 264.7 NF-κB promoter macrophages. Treatment of mice with ThG increased *O*-glycosylation of NF-κB p65 subunit in mesenteric arteries, which was associated with reduced Ser^{536} phosphorylation of NF-κB p65. Finally, GlcN

also increased survival rates in mice submitted to cecal ligation and puncture (CLP), a sepsis model. In conclusion, increased *O*-GlcNAc reduces systemic inflammation and cardiovascular disfunction in experimental sepsis models, pointing this pathway as a potential target for therapeutic intervention.

Keywords: *O*-GlcNAc, sepsis, LPS, inflammation, vascular reactivity, blood pressure

INTRODUCTION

Sepsis is a systemic inflammatory response syndrome (SIRS) resulting from a severe infection that is characterized by immune dysregulation, cardiovascular derangements, and end-organ dysfunction. Despite the significant progress in the understanding of the pathophysiologic processes involved in these diseases, their incidence is remarkable. Estimates point to 31.5 million sepsis cases, and approximately 5.3 million deaths per year in high-income countries (Fleischmann et al., 2016). In a Brazilian observational study, the mortality rate of septic patients reached 55% (Machado et al., 2017). These numbers justify the efforts to clarify the systemic alterations during sepsis progress and to improve its recognition and treatment.

During an infection, the host immune system recognizes invading pathogens by identifying pathogen-associated molecular patterns (PAMPs) through a variety of cell-surface and intracellular pattern recognition receptors (PRRs) on the innate immune cells, such as Toll-like receptors (TLRs), nucleotide-binding oligomerization domain-like receptors (NLRs; which activation leads to inflammasome formation), retinoic acid-inducible gene-like receptors (RLRs) and C-type lectin receptors (CLRs) (Takeuchi and Akira, 2010; van der Poll et al., 2017; Salomão et al., 2019). In most cases, the immune system is able to remove the invading pathogen. However, the predominance of the pathogens and exacerbation of host immune response can lead to an excessive inflammatory response, resulting in cardiovascular collapse and organ dysfunction.

Both in the early and late phases of sepsis, the activation of immune cells initiates a complex signal transduction pathway that culminates in the activation of nuclear transcription factor-kappa B (NF-κB) and mitogen-activated protein kinases (MAPK), with consequent release of large amounts of cytokines, chemokines and activation of the complement system (Munoz et al., 1991; Silasi-Mansat et al., 2010; Takeuchi and Akira, 2010; Wiersinga et al., 2014; Salomão et al., 2019). Indeed, macrophages activated by lipopolysaccharide (LPS), the major component of the outer membrane of Gram-negative bacteria, primarily release inflammatory mediators such as interleukin-1β (IL-1β), interleukin-6 (IL-6) and tumor necrosis factor-alpha (TNF-α), as well as secondary mediators involved in pathogens elimination, such as nitric oxide (NO) and reactive oxygen species (ROS) (Ayala et al., 1996; Lu et al., 2015; Seo et al., 2016). The excessive production of NO and ROS is directly involved in vascular damage, leading to excessive vasodilation, edema formation, leukocytes and platelets adhesion, glycocalyx shedding, and endothelial dysfunction (Huet et al., 2011; Tyml, 2011), critical processes in septic condition.

Cellular metabolism has arisen as a key mechanism that modulate inflammatory responses and may play a crucial role in sepsis. In macrophages, the upregulation of glycolysis, for example, increases the transcription of IL-1β, which is related to succinate accumulation and, subsequently, activation of hypoxia-inducible factor 1α (HIF1α) (Lachmandas et al., 2016). Moreover, LPS stimulation of macrophages increases mitochondrial oxidation and ROS generation and promotes a pro-inflammatory state (Cheng et al., 2016). High-glucose also leads to NF-κB activation in vascular smooth muscle cells (Tannahill et al., 2013) and peripheral blood mononuclear cells as observed in diabetic patients (Mills et al., 2016). In this context, the hexosamine metabolism pathway, through the *O*-glycosylation with N-acetylglucosamine (*O*-GlcNAc) of innumerous proteins, can also contribute to the regulation of the inflammatory response. *O*-GlcNAc, a highly dynamic post-translational modification of nuclear and cytoplasmic proteins (Yang and Qian, 2017; Zachara, 2018), is directly controlled by the activity of two enzymes: *O*-GlcNAc transferase (OGT, uridine diphosphate-N-acetyl glucosamine; β-N-acetylglucosaminyl transferase and UDP-NAc transferase) and β-N-acetylglucosaminidase (O-GlcNAcase or OGA). Whereas OGT catalyzes the addition of N-acetylglucosamine in the hydroxyl group of serine and threonine residues of target proteins, OGA catalyzes the hydrolytic removal of *O*-GlcNAc from proteins (Yang and Qian, 2017). Hence, OGT and OGA expression and activity are important to regulate *O*-GlcNAc and, consequently, proteins function by changing their sub-cellular localization, activity, and interaction with other proteins (Andrali et al., 2007; Guinez et al., 2011; Baudoin and Issad, 2015; Zachara, 2018).

In the cardiovascular system, *O*-GlcNAc modulates cardiac and vascular contractility and remodeling as well as inflammation-related processes (da Costa et al., 2018; Kronlage et al., 2019). Glucosamine, which increases *O*-GlcNAc-modified proteins, reduces the levels of circulating pro-inflammatory cytokines, including TNF-α and IL-6 (Azuma et al., 2015) and attenuates LPS-induced activation of NF-κB in RAW264.7 macrophages (Shin et al., 2013). Glucosamine also reduces vascular expression of pro-inflammatory mediators, inhibiting acute inflammatory responses and neointimal layer formation following balloon catheter injury of the carotid artery in ovariectomized rats (Xing et al., 2008), indicating that *O*-GlcNAc has anti-inflammatory and vasoprotective actions.

Monocytes and macrophages play central roles in acute and chronic inflammatory processes. Disturbed metabolism also shifts the profile production of inflammatory mediators

by macrophages. For instance, high glucose increases IL-1β, TNFα, TLR2, TLR4, and NF-κB signaling (Shanmugam et al., 2003; Dasu et al., 2008; Hua et al., 2012), contributing to diabetes-associated pro-inflammatory state. On the other hand, stimulation of the hexosamine pathway by glucosamine attenuates LPS-induced NO and NF-κB activation in macrophage cells (Hwang et al., 2017) whereas OGT degradation increases endothelial inflammatory responses induced by hypoxia (Liu et al., 2014). Li et al. (2019) observed that mice with OGT deletion exhibit an exacerbated innate immune response and septic inflammation induced by LPS, events dependent on TLR/RIPK3/NF-κB signaling activation. These results demonstrate that reprogramming of cellular metabolic events can be a fine-tuning point to modulate the inflammatory response in septic conditions. However, it is not clear whether activation of the hexosamine pathway has cardiovascular protective effects in sepsis.

Therefore, considering that *O*-GlcNAc modulates the function of the cardiovascular and immune systems, which are key in endotoxemic/sepsis-associated conditions and complications, this study tested the hypothesis that acute increases in *O*-GlcNAc reduce NF-κB activation and expression/release of pro-inflammatory cytokines, improving cardiovascular function in animals with LPS-induced SIRS.

MATERIALS AND METHODS

Animals

Male C57BL6/J mice (8 to 10-week-old, 20–25 g) were used in this study. Mice were kept in the animal facility of the Department of Pharmacology, Ribeirão Preto Medical School, University of São Paulo, under controlled temperature (22–24°C) and humidity, 12-hour (h) light/dark cycles and received standard diet and water *ad libitum*. All experimental procedures were approved by the Ethics Committee on Animal Research of the Ribeirão Preto Medical School, University of São Paulo (protocol n° 196/13) and are in accordance with the Guidelines of the National Council for Animal Experimentation Control (CONCEA).

Experimental Animal Models and Pharmacological Tools to Increase *O*-GlcNAc-Modified Proteins

Severe endotoxemia by LPS was induced with a single dose (20 mg/Kg, i.p.) of LPS (Escherichia coli 0111:B4, Sigma Chemical Co., St. Louis, MO, United States), 30 min after treatment with GlcN (300 mg/Kg/animal, i.v.), or 12 h after treatment with ThG (150 μg/Kg; i.v.). Proper controls were performed with vehicle administration (for LPS, GlcN or ThG) at the same time points. To evaluate the effects of acute increased *O*-GlcNAc in mice with endotoxemia induced by LPS, animals were randomly divided into the following groups: saline (Control); vehicle + 20 mg/Kg LPS (LPS); glucosamine or thiamet-G plus 20 mg/Kg LPS (LPS + GlcN and LPS + ThG, respectively). Six hours after LPS treatment, mice were anesthetized with isoflurane and fluids and tissues were collected. The time for GlcN and ThG administration were determined in preliminary protocols (**Supplementary Material** and **Supplementary Figure S1**).

Some experiments were also performed in mice that received a lower dose of LPS (10 mg/Kg, i.p.), which induces moderate endotoxemia (LPS_{low}). The following groups were tested in specific protocols: saline (Control); vehicle + 10 mg/Kg LPS (LPS_{low}); glucosamine or thiamet-G plus 10 mg/Kg LPS (LPS_{low} + GlcN and LPS_{low} + ThG, respectively). Similarly, GlcN and ThG were administered 30 min and 12 h, respectively, before LPS injection.

Finally, mice with cecal ligation and puncture (CLP)-induced sepsis were used to confirm the effects of GlcN in specific protocols. CLP was induced, as previously described (Alves-Filho et al., 2010). After anesthesia and abdominal wall shaving of the mice, the cecum was exposed through midline laparotomy. The cecum ligation was performed below the ileocecal valve without causing intestinal obstruction and then punctured with a 18G needle. Mice were divided in six groups: (1) Sham, mice submitted to midline laparotomy without cecum ligation and puncture and that received 1 mL of saline i.v.; (2) Sham + hydration + antibiotic therapy, mice submitted to sham operation and that received a single i.v. dose of 1 mL of saline. Antibiotic therapy was performed with sodium Ertapenem (30 mg/Kg, s.c., 1 h) after CLP and every 12 h, for 3 days; (3) Sham + hydration + antibiotic therapy + GlcN treatment, mice submitted to sham operation + hydration + antibiotic therapy + GlcN (300 mg/kg. i.v.); (4) CLP, mice submitted to the CLP procedure; (5) CLP + hydration + antibiotic therapy group (CLP + ATB), CLP mice that received a single dose of 1 mL of saline and were treated with sodium Ertapenem; and (6) CLP + ATB + GlcN, CLP mice submitted to hydration + ATB and that received GlcN.

Survival Rates

Following treatment of mice with GlcN or ThG and LPS-induced SIRS, the survival rates were determined daily, every 12 h, for 7 days. Survival rates were also determined in mice with CLP-induced sepsis for 7 days. The survival rate is expressed as the percentage of live animals, and the Mantel-Cox log-rank test was used to determine differences between the experimental groups (Alves-Filho et al., 2010).

Neutrophil Migration to the Peritoneal Cavity

Neutrophil migration was determined as previously described (Alves-Filho et al., 2010). Peritoneal cavity lavage (PCL) was performed 6 h after LPS-induced SIRS or CLP-induced sepsis using 3 ml of phosphate buffer saline/ethylene diamine tetraacetic acid (PBS/EDTA) 1 mM and peritoneal fluids were collected. A Coulter AcT Diff analyzer (Beckman Coulter) was used to perform total cells counts. Differential cell counts were determined on Cytospin slides stained with Panótico Rápido LB dye (Laborclin, Brazil). The results are expressed as the mean number of neutrophils ± SEM per cavity.

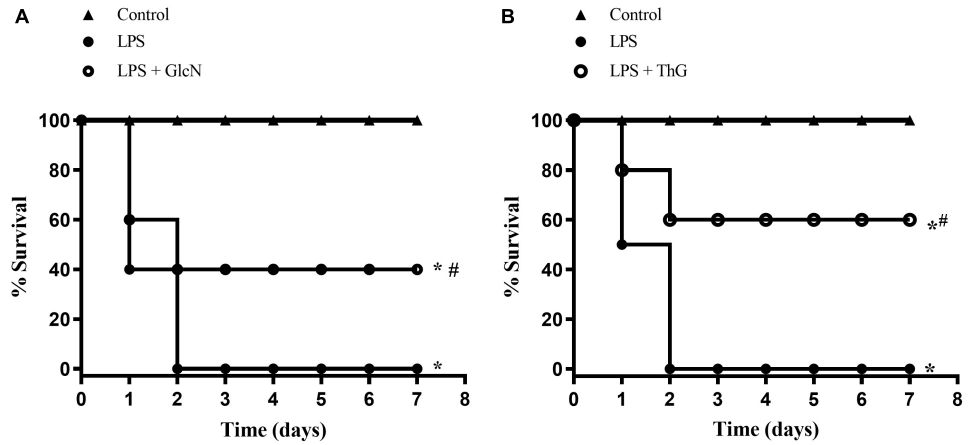

FIGURE 1 | Survival rates in mice submitted to LPS-induced SIRS (20 mg/Kg, i.p.), and pre-treated with vehicle (LPS), **(A)** GlcN (300 mg/Kg, i.v., LPS + GlcN) or **(B)** ThG (150 μg/Kg, i.v., LPS + ThG). Survival rates were determined every 12 h for 7 days and the results are expressed as the percentage of animals alive on each day. $^{*}p < 0.05$ vs. control. $^{\#}p < 0.05$ vs. LPS. $N = 10$ animals per experimental group. Log-rank test.

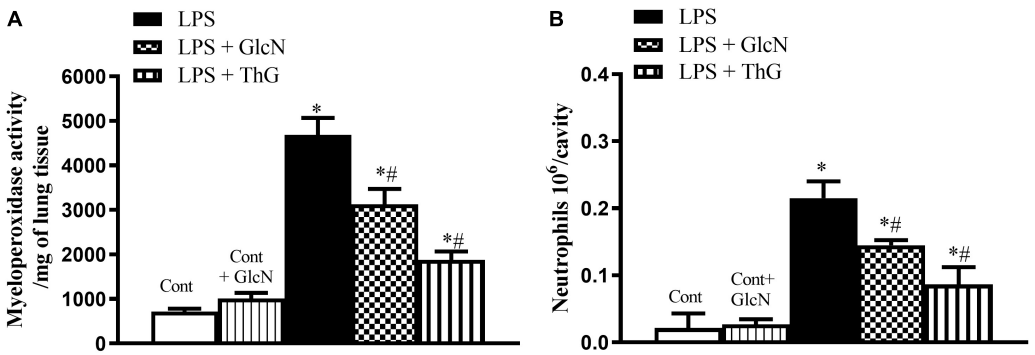

FIGURE 2 | Neutrophil infiltration in the lung and neutrophil migration to the peritoneal cavity. Evaluation of **(A)** neutrophil infiltration in the lungs and **(B)** migration of neutrophils to the peritoneal cavity in mice submitted to LPS-induced SIRS and treated with vehicle (LPS), GlcN (LPS + GlcN) or ThG (LPS + ThG). Lung neutrophil sequestration was estimated by the myeloperoxidase assay (MPO) in the organ homogenate 6 h after LPS-induced SIRS. Neutrophil count into the peritoneal cavity was performed using the Coulter® apparatus. The results are expressed as mean ± SEM and are representative of 4–5 experiments. $^{*}p < 0.05$ vs. control; $^{\#}p < 0.05$ vs. LPS. One-way ANOVA followed by Dunnett's post-test.

Myeloperoxidase Activity Assay

Lipopolysaccharide or CLP-induced leukocyte migration to the lungs was evaluated using a myeloperoxidase kinetic-colorimetric assay. Tissue samples were collected in 50 mM K_2HPO_4 buffer (pH 6.0) containing 13.72 mM hexadecyltrimethylammonium bromide (HTAB) and stored at −80°C until assayed. The samples were homogenized using a Tissue-Tearor (BioSpec), and homogenates were centrifuged (13.000 rpm, 2 min, 4°C). Supernatants were assayed spectrophotometrically for myeloperoxidase activity at 450 nm (Victor3 1420 multilabel counter). Myeloperoxidase activity of samples was compared to a standard curve of neutrophils and is presented as the number of neutrophils per mg of tissue (Alves-Filho et al., 2010).

Determination of Cytokines Levels

TNF-α, IL-1β, and IL-6 concentrations in cell culture supernatant and serum were determined using enzyme-linked immunosorbent assay (ELISA, R&D Systems, United States) according to the manufacturer's instructions. Briefly, each well of flat-bottomed 96-well microliter plates was coated with 100 μL of an antibody specific to one of the above cytokines and incubated overnight at 37°C. Plates were washed, and non-specific binding was blocked with 1% bovine serum for 120 min at 37°C. Samples and standards were loaded onto plates. Recombinant murine (rm) TNF-α, IL-1β, and IL-6 standard curves were used to calculate cytokines concentrations. Plates were thoroughly washed, and the appropriate biotinylated polyclonal or monoclonal anti-cytokine antibody was added. After one h, the plates were washed, avidin-peroxidase was added to each well for 15 min, and plates were thoroughly washed again. After addition of substrate, the reaction was stopped with H_2SO_4 (1 mol/L), and the optical density of the individual samples was measured on an ELISA plate scanner (Spectra Max 250; Molecular Devices, Menlo Park, CA, United States) at 490 nm. The results are expressed as picograms of TNF-α, IL-1β, and

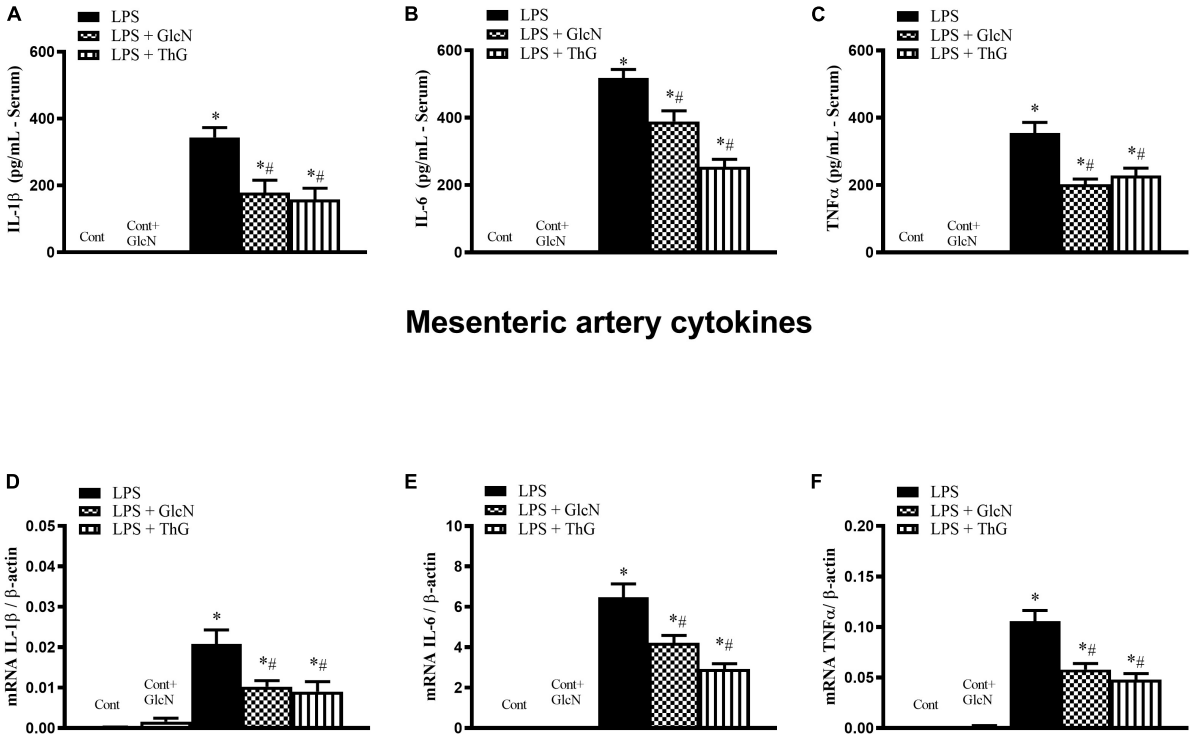

FIGURE 3 | Systemic and vascular production of IL-1β, IL-6, and TNF-α. Evaluation of **(A–C)** serum concentration and **(D–F)** mesenteric artery mRNA of **(A,D)** IL-1β, **(B,E)** IL-6, and **(C,F)** TNF-α in mice submitted to LPS-induced SIRS and treated with vehicle (LPS), GlcN (LPS + GlcN) or ThG (LPS + ThG). The results are expressed as mean ± SEM and are representative of 3–4 experiments. $^{*}p < 0.05$ vs. control; $^{\#}p < 0.05$ vs. LPS. One-way ANOVA followed by Dunnett's post-test.

IL-6 per μL of the cell culture supernatant or serum. Optical density in the samples were derived from standard curves for each specific cytokine.

Real-Time RT-PCR for TNF-α, IL-1β, and IL-6

Gene expression of TNF-α, IL-1β, and IL-6 was determined in mesenteric arteries and macrophages using the RNeasy kit (Qiagen Sciences). One micro gram of total RNA was reverse-transcribed in a final volume of 50 μL using the high-capacity cDNA archive kit (Applied Biosystems). TaqMan probes for TNF-α (Mm00443260_g1), IL-1β (Mm00434228_m1), IL-6 (Mm02620446_s1), and β-actin (Mm00607939_s1) mRNA were obtained from Applied Biosystems. Real-time RT-PCR (quantitative PCR) reactions were performed using the 7500 fast Real-Time PCR system (Applied Biosystems) in a total volume of 20 μL reaction mixture, following the manufacturer's protocol, using the TaqMan fast universal PCR master mix (Applied Biosystems) and 0.1 mmol/L of each primer. Relative gene expression for TNF-α, IL-1β, and IL-6 mRNA were calculated with the $2^{(-\Delta\Delta Ct)}$ method and expressed as n-fold differences in TNF-α, IL-1β, and IL-6 gene expression relative to β-actin.

Quantification of Nitric Oxide Production

The production of NO was indirectly determined by Griess reaction (Green et al., 1982) by measuring the content of nitrite (NO_2^-) in the cell culture supernatant. Fifty microliter of serum were incubated for 10 min (room temperature) in the presence of 50 μL Griess solution [1:1 (v/v) (solutions: sulfanilamide 0.1 mol/L ortho-phosphoric acid 30% and enediamine 7.7 mmol/L and 60% ortho-phosphoric acid]. Nitrite content was determined at 550 nm, and a curve of sodium nitrite ($NaNO_2$) was used as standard.

Blood Pressure Monitoring

To record arterial pressure, randomly selected mice from each experimental group were anesthetized with isoflurane (5% for induction and 2% 100% O_2 for maintenance of anesthesia) for carotid artery catheterization (Intramedic, Becton Dickinson and Company). Three days after the surgical procedure, the catheter was connected to a transducer coupled to an amplifier system and to a computer (Dataquest LabPRO Acquisition System version 3.01, Data Sciences International, St. Paul, MN, United States). After a stabilization period, cardiovascular parameters (blood pressure and heart rate) were monitored for 6 h.

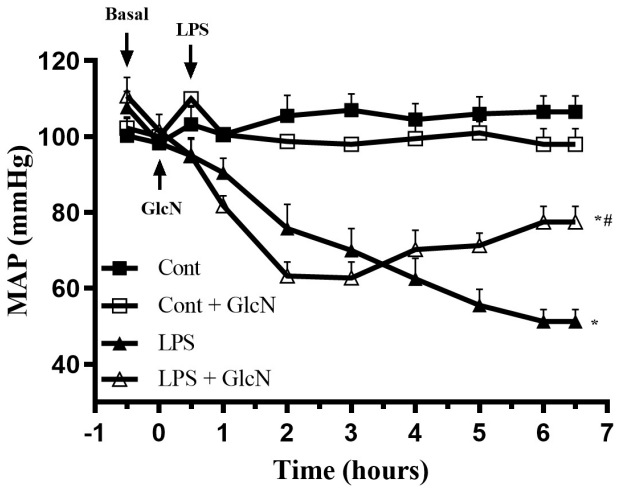

FIGURE 4 | Mean arterial pressure (MAP) in LPS-induced SIRS in mice. Mean arterial pressure (MAP) was recorded, via carotid artery cannulation, for 6 h after LPS administration (20 mg/kg, i.p.). GlcN treatment was performed 30 min before LPS injection. The results are expressed as mean ± SEM and are representative of four experiments. $^{*}p < 0.05$ vs. control; $^{\#}p < 0.05$ vs. LPS. One-way ANOVA followed by Bonferroni's post-test.

Vascular Functional Studies

After euthanasia, the mesenteric beds from mice were rapidly removed and cleaned from fat tissue in an ice-cold (4°C) Krebs–Henseleit modified solution [(in mM): 130 NaCl, 4.7 KCl, 14.9 $NaHCO_3$, 1.18 KH_2PO_4, 1.17 $MgSO_4{\cdot}7H_2O$, 5.5 glucose, 1.56 $CaCl_2{\cdot}2H_2O$, and 0.026 EDTA], gassed with 5% CO_2/95% O_2 to maintain a pH of 7.4. Second-order branches of mesenteric arteries (≈2 mm in length with internal diameter ≈150–200 μm) were carefully dissected and mounted as rings in an isometric Mulvany–Halpern myograph (model 610 M; Danish Myo Technology – DMT, Copenhagen, Denmark) (Halpern et al., 1978). Changes in force were recorded by a PowerLab 8/SP data acquisition system (ADInstruments). Second-order mesenteric arteries were adjusted to maintain a passive force of 13,3 kPa and allowed to equilibrate for about 30 min in Krebs–Henseleit solution. After the stabilization period, arterial integrity was assessed first by stimulation of vessels with 120 mM of KCl. After washing and a new stabilization period, endothelial function was assessed by testing the relaxant effect of acetylcholine (ACh, 10 μM) on vessels contracted with phenylephrine (PE, 2 μM). Mesenteric arteries exhibiting a relaxant response to ACh greater than 90% were considered endothelium-intact vessels. All experiments were performed in endothelium-intact vessels. Concentration-response curves to phenylephrine (PE; 1 nM to 100 μM) were performed. Endothelium-dependent relaxation was assessed by measuring the relaxation response to ACh (1 nM to 100 μM) in PE-contracted vessels (1 μM).

Bone Marrow-Derived Macrophages

Bone marrow cells were harvested from femurs of control mice and differentiated in the presence of L929-conditioned medium (30%) in complete RPMI 1640 medium containing 10 mM glucose, 2 mM L-glutamine, 100 U/ml of penicillin/streptomycin and 20% fetal bovine serum (FBS). The culture medium was replaced on day 4. After 7 days, bone marrow-derived macrophages (BMDM) were counted and 2×10^6 cells were incubated with glucosamine (GlcN, 5 mM, 30 min) or thiamet-G (ThG, 1 μM, 12 h) prior to 6 h stimulation with ultrapure LPS, 1 μM. Gene expression of cytokines was determined by Real-Time PCR.

NF-κB Activity

To analyze whether *O*-GlcNAc modulates NF-κB activity, NF-κB luciferase stable RAW264.7 cells were used (Cooper et al., 2010). The murine leukaemic monocyte macrophage 264.7 cell line bearing the luciferase vector inserted in the NF-κB promoter (pNF-κB-Luc) was cultured in RPMI1640 medium supplemented with 10% FBS and antibiotics at 37°C in a humidified atmosphere of 5% CO_2. For luciferase assay, 3×10^5 cells were grown in 24 well-plates for 2 h. The cells were incubated with glucosamine (GlcN, 5 mM, 30 min), thiamet-G (ThG, 1 μM, 12 h) or vehicle, before stimulation with LPS (1 μM for 6 h). After LPS stimulation, cells were harvested and disrupted in lysis buffer (Tris–HCl 0.02 M, NaCl 0.08 M, TritonX-100 1%). The luciferase activity in the cell lysates was measured with the Luciferase Assay System (Promega, WI, United States), according to the manufacturer's instructions using FlexStation® 3 (Molecular Devices, United States).

Western Blot Analysis

Aorta and mesenteric arteries were frozen in liquid nitrogen and homogenized in a lysis buffer [50 mM Tris/HCl, 150 mM NaCl, 1% Nonidet P40, 1 mM EDTA, 1 μg/ml leupeptin, 1 μg/ml pepstatin, 1 μg/ml aprotinin, 1 mM sodium orthovanadate, 1 mM phenylmethylsulfonyl fluoride (PMSF), and 1 mM sodium fluoride]. Proteins were extracted and separated (60 μg) by electrophoresis. Non-specific binding sites were blocked with 5% bovine serum albumin (BSA) in Tris-buffered saline (TBS) containing 0.1% Tween 20 (for 1 h at 24°C). Membranes were incubated with antibodies (at the indicated dilutions) at 4°C overnight. Antibodies were as follows: anti–*O*-GlcNAc antibody, CTD 110.6 (1:500; Sigma-Aldrich, O7764), phosphor-Ser^{536}-p65 (cell signaling, #3033); NF-κB subunit p65 (cell signaling, #8242) and β-actin (1:2000; Sigma-Aldrich, A3854). After incubation with secondary antibodies, signals were obtained by chemiluminescence, and optical densitometry units were measured using Image Quant software (GE healthcare life sciences). Data are shown as the ratio of interest protein by β-actin band densitometry.

Immunoprecipitation Assay

To verify whether NF-κB p65 subunit was modified by *O*-GlcNAc, NF-κB p65 subunit was immunoprecipitated, using magnetic beads (Millipore, LSKMAGG02) and anti-p65 subunit antibody (Cell Signaling #8242), from mesenteric arteries of control and LPS-induced SIRS mice treated with Thiamet-G or vehicle. *O*-GlcNAc levels were determined by western blot analysis using a monoclonal anti-β-*O*-Linked N-acetylglucosamine antibody (Sigma-Aldrich, O7764), as

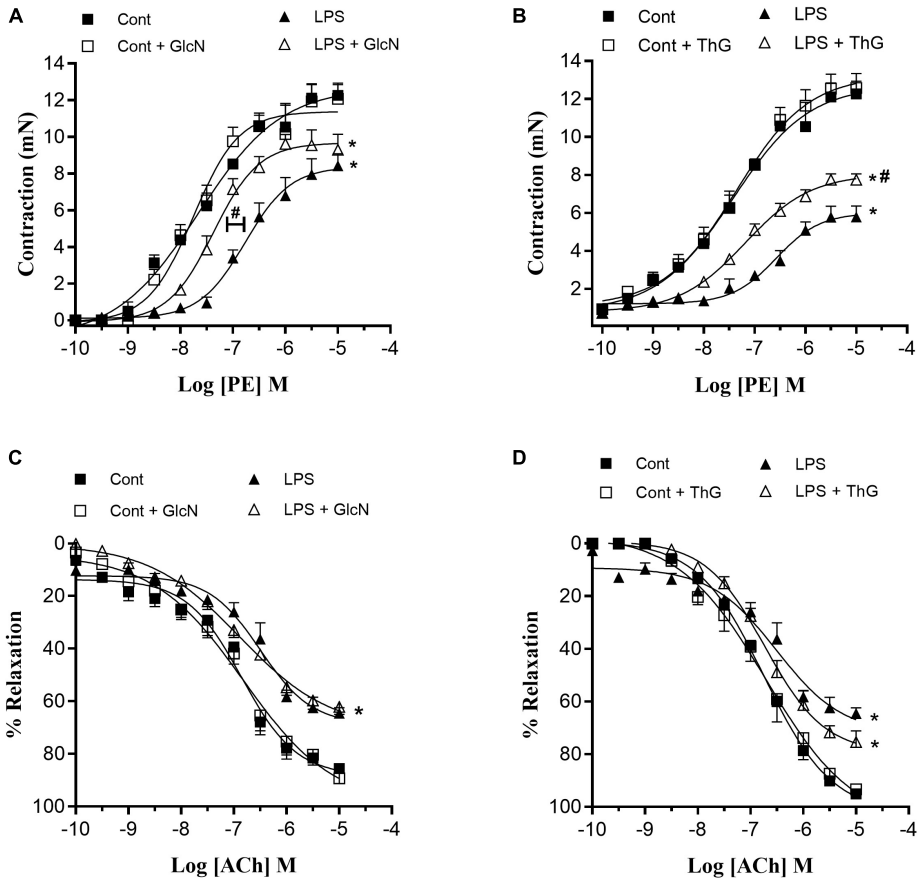

FIGURE 5 | Mesenteric artery reactivity. **(A,B)** Contractile responses to phenylephrine (PE) and **(C,D)** relaxation responses to acetylcholine (ACh) in mesenteric arteries from control and LPS-induced SIRS (LPS) mice treated with **(A,C)** vehicle or glucosamine (GlcN) and **(B,D)** vehicle or thiamet-G (ThG). Data are expressed as mean ± SEM of contraction and relaxation values and are representative of 4–5 experiments. Cont, vehicle-treated control mice; LPS, LPS (20 mg/Kg i.P.)-treated mice; Cont + GlcN and LPS + GlcN, mice treated with glucosamine (GlcN); Cont + ThG and LPS + ThG, mice treated with thiamet-G (ThG). $^{*}p < 0.05$ vs. respective control; $^{\#}p < 0.05$ vs. LPS. ANOVA followed by Bonferroni's post-test.

described above. Data are shown as the densitometric ratio of *O*-GlcNAc by NF-κB p65 subunit.

Statistical Analysis

Prism software, version 5.0 (GraphPad Software Inc., San Diego, CA, United States) was used to analyze the parameters. Data are presented as mean ± SEM. Groups were compared using one-way ANOVA. ANOVA was followed by the Bonferroni's or Dunnett's post-test. Survival curves were analyzed with the log-rank test. *N* represents the number of animals used and *p* values less than 0.05 were considered significant.

RESULTS

Effects of Increased *O*-GlcNAc on LPS-Induced Mice Mortality

To determine whether acute increases in *O*-GlcNAc levels affects survival rates in mice with LPS-induced SIRS, animals were followed for 7 days, and checked every 12 h. Mice undergoing LPS-induced SIRS (20 mg/Kg, i.p., LPS) died within 48 h. Treatment of LPS mice with GlcN, which increases the synthesis of UDP-GlcNAc in the hexosamine pathway, increased survival to 40%, when compared to mice that received only LPS (**Figure 1A**). Additionally, inhibition of the OGA enzyme with ThG improved survival of LPS-treated mice by up to 60% (**Figure 1B**).

Effects of Increased *O*-GlcNAc on Inflammatory Response

Leukocyte Infiltration in Lungs and Leukocyte Migration to the Peritoneal Cavity

Sequestration of neutrophils from the circulation is an event that can compromise an appropriate response to infection (Sumi et al., 2014). To evaluate the effect of increased *O*-GlcNAc on neutrophil infiltration in the lungs, myeloperoxidase (MPO) activity was determined. **Figure 2A** demonstrates that treatment with both GlcN and ThG significantly reduced neutrophil sequestration in the lung of LPS mice as compared to vehicle-treated mice. In addition to reducing pulmonary neutrophil

sequestration, increased *O*-GlcNAc also decreased neutrophil migration to the peritoneal cavity (**Figure 2B**).

Systemic Levels and Vascular Expression of Inflammatory Cytokines

The production of inflammatory cytokines coordinates the response to infectious agents through the activation and recruitment of immune cells (Dinarello, 1997; Alves-Filho et al., 2010; Li et al., 2019). To determine the production of inflammatory mediators, serum concentrations of IL-1β, IL-6, and TNFα were quantified. mRNA expression of these cytokines was determined in mesenteric arteries. LPS increased both serum levels and vascular expression of IL-1β, IL-6 and TNFα (**Figure 3**). Treatment of LPS-mice with GlcN and ThG attenuated systemic levels (**Figures 3A,C**) and vascular expression (**Figures 3D,F**) levels of cytokines. These results suggest that increased *O*-GlcNAc reduces LPS-associated pro-inflammatory cytokines production.

To confirm that acute increases in *O*-GlcNAc protein levels has anti-inflammatory effects, we also used a lower dose of LPS (LPS_{low}) to induce SIRS. Accordingly, experiments were performed in mice injected via the intraperitoneal route with 10 mg/Kg LPS.

Supplementary Figure S2 shows that treatment of LPS_{low} mice with GlcN and ThG decreased systemic levels of IL-1β, IL-6 and TNFα, indicating that acute increase in *O*-GlcNAc reduces pro-inflammatory events in mice subjected to both low and high doses of LPS.

Effect of Increased *O*-GlcNAc Levels in the Cardiovascular System

LPS-Induced Hypotension

Hypotension contributes to organ failure in SIRS-associated conditions (De Backer et al., 2014; Coeckelenbergh et al., 2019). LPS induces a progressive decrease in mean arterial blood pressure (MAP) in mice. Although GlcN did not prevent LPS-induced hypotension, the fall of MAP was attenuated 5 h after LPS injection (**Figure 4**).

Mice that received a moderate dose of LPS (10 mg/Kg i.p.) also exhibited hypotension, as shown in **Supplementary Figure S3**. Similarly, GlcN treatment did not prevent hypotension in mice with LPS_{low} (LPS_{low} + GlcN), but MAP was significantly higher 5 h after LPS-induced endotoxemia (**Supplementary Figure S3**).

Vascular Reactivity

In sepsis, hyporesponsiveness to vasopressor agents contributes to the reduction of MAP and organ perfusion (De Backer et al., 2014; Ozer et al., 2017). Therefore, vascular function was determined by evaluating mesenteric artery responses to phenylephrine (PE) and acetylcholine (ACh). LPS-induced SIRS reduced mesenteric artery reactivity to phenylephrine and reduced vasodilator responses to ACh (**Figures 5A,C**). Moreover, the concentration-response curves to phenylephrine in mesenteric arteries from LPS mice treated with GlcN and ThG showed a shift to the left, indicating improvement of contractile vascular responses (**Figures 5A,B** and **Tables 1**, **2**). Treatment with GlcN and ThG did not restore maximal contractile responses (Emax) to phenylephrine (**Figures 5A,B**) or the reduced vasodilation to ACh induced by LPS (**Figures 5C,D** and **Table 1**).

TABLE 1 | Effect of GlcN treatment on Emax and pD_2 values for phenylephrine and acetylcholine in mesenteric arteries from mice submitted to LPS-induced SIRS and treated with vehicle or GlcN.

	PE		ACh	
	Emax	**pD_2**	**Emax**	**pD_2**
Cont	12.69 ± 0.73	7.65 ± 0.14	87.18 ± 2.89	7.65 ± 0.08
Cont + GlcN	11.75 ± 0.54	7.76 ± 0.12	95.04 ± 4.51	7.39 ± 0.11
LPS	8.40 ± 0.49*	6.76 ± 0.10*	66.70 ± 1.40*	7.03 ± 0.08*
LPS + GlcN	9.53 ± 0.30*	7.37 ± 0.07*,#	66.56 ± 2.89*	7.48 ± 0.10*

*Emax and pD_2 values for phenylephrine (PE) and acetylcholine (ACh) in mesenteric arteries from mice of the following groups: control (Cont), control + GlcN treatment (cont + GlcN), LPS (LPS), and LPS + GlcN treatment (LPS + GlcN). Data are expressed as mean ± SEM of contraction and relaxation values and are representative of 4–5 experiments. *$p < 0.05$ vs. control group; #$p < 0.05$ vs. LPS group. ANOVA followed by Bonferroni's post-test.*

TABLE 2 | Effect of ThG treatment on Emax and pD_2 values for phenylephrine (PE) and acetylcholine (ACh) in mesenteric arteries from mice submitted to LPS-induced SIRS and treated with thiamet-G.

	PE		ACh	
	Emax	**pD_2**	**Emax**	**pD_2**
Cont	12.72 ± 0.73	7.43 ± 0.14	95.05 ± 0.71	6.73 ± 0.05
Cont + ThG	13.24 ± 0.68	7.36 ± 0.12	93.30 ± 1.14	6.70 ± 0.18
LPS	6.30 ± 0.57*	6.54 ± 0.18*	64.54 ± 2.07*	6.50 ± 0.16*
LPS + ThG	8.05 ± 0.28*	7.19 ± 0.08*,#	75.36 ± 4.18*	6.72 ± 0.80*

*Emax and pD_2 values for PE contraction and ACh relaxation in mesenteric arteries from mice of the following groups: control (Cont), control treated with ThG (cont + ThG), treated with LPS (LPS), and LPS + ThG treatment (LPS + ThG). Data are expressed as mean ± SEM of contraction and relaxation values and are representative of 4–5 experiments. *$p < 0.05$ vs. control; #$p < 0.05$ vs. LPS. ANOVA followed by Bonferroni's post-test.*

Similarly, OGA inhibition by treatment with ThG improved mesenteric artery contractile responses to phenylephrine (**Figure 5B** and **Table 2**), but it did not change the decreased relaxation responses to ACh in LPS mice (**Figure 5D** and **Table 2**).

Similar responses were observed in mesenteric arteries from mice treated with the lower dose of LPS (10 mg/kg i.p.), i.e., responses to phenylephrine were decreased in LPS_{low} mice. Arteries from LPS_{low} mice treated with ThG showed increased responses to phenylephrine, indicating improvement of contractile vascular responses (**Supplementary Figure S4**).

Nitrite Quantification and Inducible Nitric Oxide Synthase Expression

Vascular hyporesponsiveness in LPS-induced SIRS has been attributed to an excessive production of vasodilator mediators, such as nitric oxide (NO) (Kandasamy et al., 2011). To determine NO production, its secondary metabolite (nitrite) was measured. LPS mice showed a significant increase in nitrite serum levels, which was prevented by

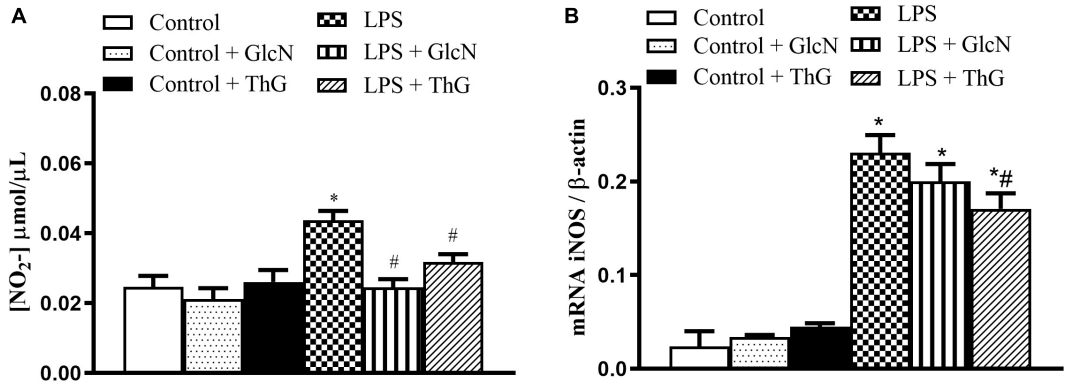

FIGURE 6 | Nitrite levels and vascular iNOS mRNA expression. **(A)** Glucosamine (GlcN) and Thiamet G (ThG) treatment prevented the increase in systemic nitrite levels in LPS mice. Serum was collected 6 h after induction of SIRS (LPS). Nitrite production was determined by the Griess method. **(B)** ThG treatment attenuated inducible nitric oxide synthase (iNOS) gene expression in mesenteric arteries from mice with SIRS ($2^{-\Delta\Delta CT}$). Results are expressed as mean ± SEM and are representative of 3–4 experiments. $^{*}p < 0.05$ vs. control; $^{\#}p < 0.05$ vs. LPS. ANOVA followed by Dunnett's multiple comparisons test.

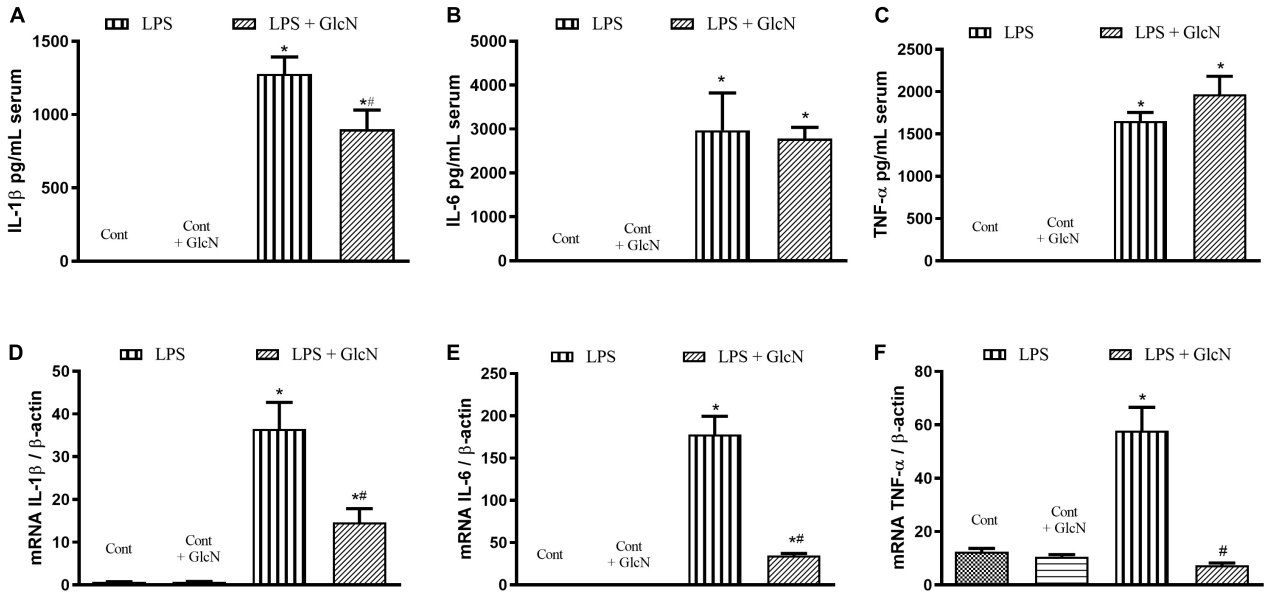

FIGURE 7 | LPS-induced pro inflammatory profile of bone marrow-derived macrophages (BMDM) treated with vehicle or glucosamine. BMDM were isolated from control mice. BMDM were treated with glucosamine (GlcN, 1 μM, 30 min) and then with LPS (1 μM for 6 h). The supernatant was collected to measure IL-1β **(A)**, IL-6 **(B)**, and TNFα **(C)** cytokines by ELISA. Macrophages mRNA levels of IL-1β **(D)**, IL-6 **(E)**, and TNFα **(F)** were determined by qPCR. Data are represented by mean ± SEM and are representative of 3–5 experiments. $^{*}p < 0.05$ vs. control; $^{\#}p < 0.05$ vs. LPS. ANOVA followed by Dunnett's multiple comparisons test.

GlcN and ThG treatments (**Figure 6A**). In addition, OGA inhibition with ThG, but not GlcN treatment, attenuated the increased iNOS mRNA vascular expression induced by LPS (**Figure 6B**).

Cytokine Production by Macrophages

Acute increases in *O*-GlcNAc proteins reduced LPS-associated inflammatory processes in mice, as shown in **Figure 3**. Considering that macrophages are important cells in the response to infectious agents, LPS-induced pro-inflammatory response was determined in bone marrow-derived macrophages (BMDM). BMDM were isolated from control naïve mice and treated *in vitro* with LPS (1 μM, 6 h). LPS-treated BMDM showed increased secretion of pro-inflammatory cytokines (**Figures 7A–C**) as well as increased mRNA expression of IL-1β (**Figure 7D**), IL-6 (**Figure 7E**), and TNFα (**Figure 7F**). GlcN treatment reduced LPS-induced IL-1β secretion in BMDM (**Figure 7A**). Also, GlcN treatment decreased mRNA levels of IL-1β (**Figure 7D**), IL-6 (**Figure 7E**), and TNFα (**Figure 7F**) in BMDM stimulated with LPS.

Moreover, OGA inhibition with ThG also decreased LPS-induced pro-inflammatory responses in BMDM, reducing cytokines secretion and mRNA expression of IL-1β (**Figures 8A,D**), IL-6 (**Figures 8B,E**), and TNFα (**Figures 8C,F**).

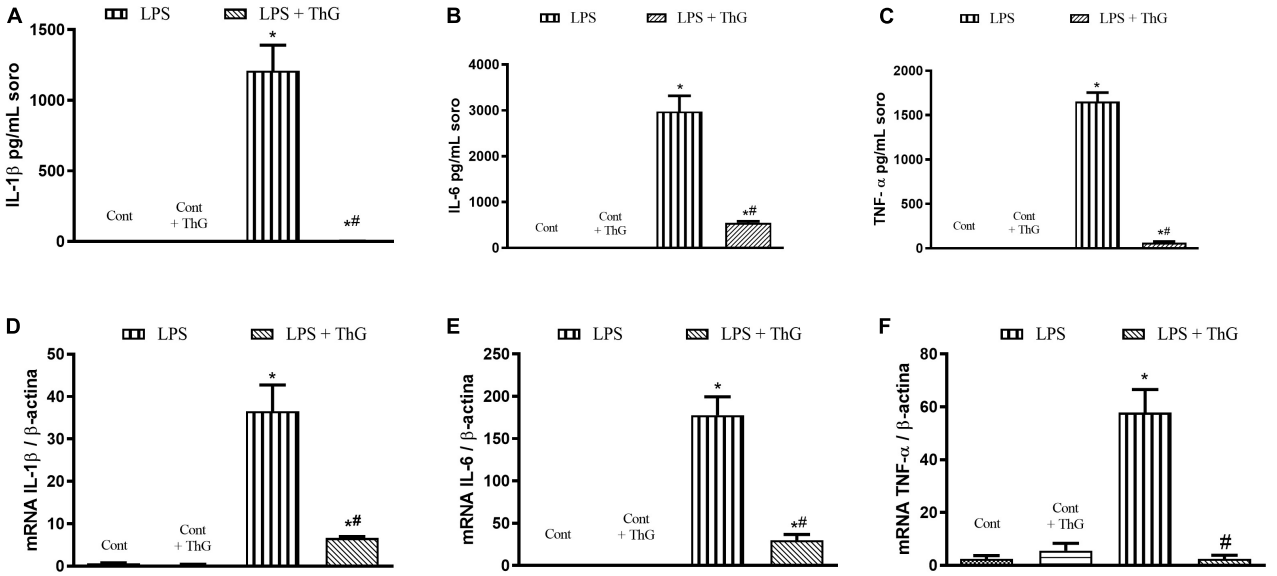

FIGURE 8 | Pro inflammatory profile of bone marrow-derived macrophages (BMDM) from control mice stimulated with LPS in the presence of vehicle or thiamet G. BMDM were isolated from control mice. BMDM were treated with thiamet G (ThG, 1 μM, 12 h) and then, with LPS (1 μM, 6 h). The supernatant was collected to measure cytokines IL-1β **(A)**, IL-6 **(B)**, and TNFα **(C)** by ELISA. The cells were lysed to evaluate mRNA levels of IL-1β **(D)**, IL-6 **(E)**, and TNFα **(F)** by qPCR. Data are represented by mean ± SEM and are representative of 3–5 experiments. $^{*}p < 0.05$ vs. control; $^{\#}p < 0.05$ vs. LPS. ANOVA followed by Dunnett's multiple comparisons test.

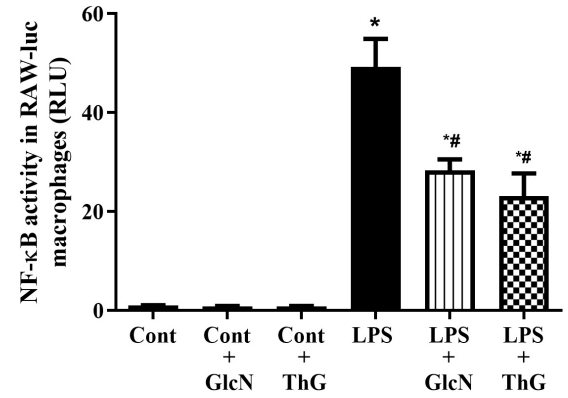

FIGURE 9 | NF-κB activation in macrophages. Glucosamine (GlcN, 5 mM, 30 min) and thiamet G (ThG, 1 μM 12 h) attenuated LPS-induced NF-κB activation in RAW 264.7 macrophages. NF-κB activity was measured after incubation with LPS (1 μM for 6 h). Data are represented as mean ± SEM of RLU (relative luminescence unit) and are representative of 4–8 experiments. $^{*}p < 0.05$ vs. control; $^{\#}p < 0.05$ vs. LPS. ANOVA followed by Dunnett's multiple comparisons test.

NF-κB Activity

Considering that acute increases in *O*-GlcNAc proteins reduced cytokines production and that NF-κB is a key transcription factor that induces IL-1β and TNF-α mRNA expression, we determined whether acute increase in *O*-GlcNAc proteins reduces NF-κB signaling. As shown in **Figure 9**, treatment of RAW 264.7 NF-κB promoter macrophages with GlcN or ThG reduced LPS-induced NF-κB activation.

O-GlcNAc Modification of NF-κB p65 Subunit in Mesenteric Arteries

Expression of Total, Phosphorylated and *O*-GlcNAc-Modified NF-κB p65 Subunit

Since activation of the hexosamine pathway decreased inflammatory responses and improved vascular function in mice with LPS-induced SIRS, *O*-GlcNAc protein levels in mesenteric arteries were quantified by western blot analysis. ThG increased *O*-GlcNAc levels in mesenteric arteries from control ($p = 0.06$) and LPS-treated mice ($p < 0.05$) (**Figures 10A,B**). LPS-treated mice showed a decrease in *O*-GlcNAc-modified NF-κB p65 subunit, which was not observed in mice treated with ThG (**Figure 10C**). Mesenteric arteries from mice with LPS-induced SIRS showed increased expression of the total (**Figure 11A**) and phosphorylated (**Figure 11B**) forms of NF-κB p65 subunit, which was not observed in mice treated with ThG (**Figure 11C**).

Cecal Ligation and Puncture (CLP) Sepsis Model in Mice

Effect of GlcN on CLP-Induced Mortality

To evaluate the effects of increased *O*-GlcNAc proteins in a second experimental model, GlcN was administrated to mice with sepsis induced by CLP. CLP-induced sepsis was lethal in 24 h. Treatment of mice with hydration plus antibiotic (Ertapenem, 30 mg/Kg) every 12 h for three consecutive days reduced mortality by approximately 50%. Moreover, GlcN improved the hydration + antibiotic effect, resulting in survival rates of 80% (**Figure 12**).

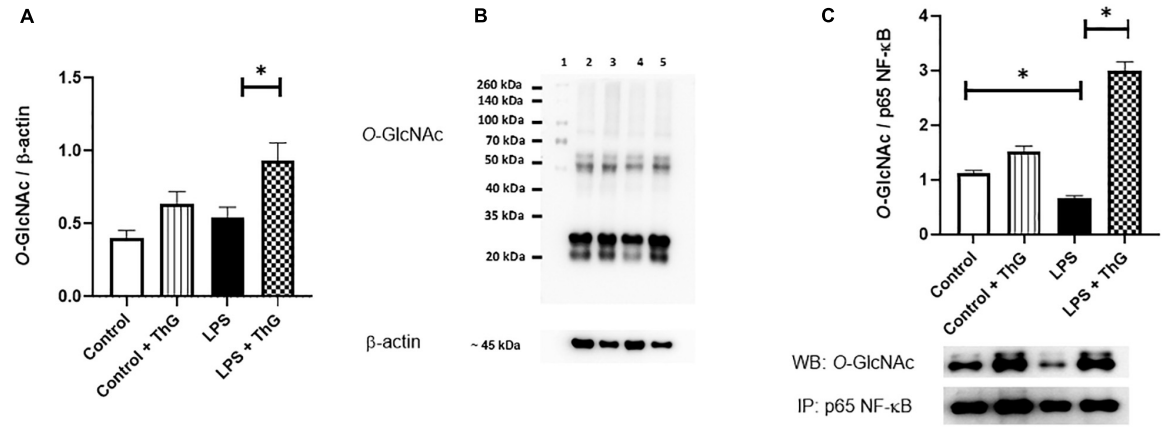

FIGURE 10 | *O*-GlcNAc protein levels in mesenteric arteries from Control and LPS mice treated with vehicle or Thiamet-G. **(A)** Global quantification and **(B)** representative images of *O*-GlcNAc protein levels in mesenteric arteries from the experimental groups. Lanes: (1) molecular standard protein weight; (2) control group with saline; (3) control group treated with Thiamet-G (ThG, 1 μM 12 h); (4) LPS-induced SIRS group treated with saline; (5) LPS-induced SIRS group treated with ThG. **(C)** *O*-GlcNAcylated NF-κB p65 subunit, determined by immunoprecipitation, in mesenteric arteries from control and LPS mice. Data are represented as mean ± SEM $^*p < 0.05$, N = 3–5 different experiments. One-way ANOVA followed by Tukey's multiple comparisons test.

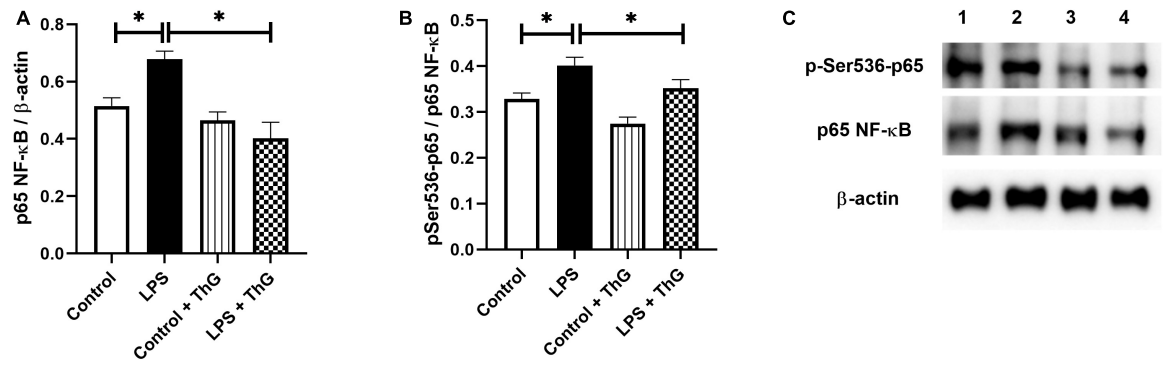

FIGURE 11 | Expression of total and phosphorylated NF-κB p65 subunit. Graphs show expression of **(A)** total and **(B)** phosphorylated (at the residue serine^{536}) forms of the p65 subunit. **(C)** Representative image of 4 different experiments. Lanes in C: (1) control group with saline, (2) LPS-induced SIRS group treated with saline, (3) control group treated with Thiamet-G (1 μM, 12 h) and (4) LPS-induced SIRS group treated with Thiamet-G (1 μM, 12 h). Data are represented as mean ± SEM. $^*p < 0.05$. One-way ANOVA followed by Tukey's multiple comparisons test.

Leukocyte Infiltration in Lungs and Leukocyte Migration to the Peritoneal Cavity in CLP Treated Mice

Treatment with GlcN significantly reduced neutrophil sequestration in the lung in mice with CLP-induced sepsis as compared to Sham mice (**Figure 13A**). GlcN treatment increased neutrophil migration to the peritoneal cavity (**Figure 13B**).

DISCUSSION

Early events in an inflammatory process involve the activation of immune cells such as polymorphonuclear leukocytes (neutrophils), monocytes/macrophages and lymphocytes. Activation of immune cells leads to production and secretion of proinflammatory mediators, which are responsible for most of the pathophysiological changes in endotoxemia/sepsis (Dinarello, 1997; De Backer et al., 2014; Li et al., 2019). Here, we show that acute increase in *O*-glycosylation with N-acetylglucosamine (*O*-GlcNAc) reduces inflammatory processes and improves cardiovascular function in mice with moderated and severe endotoxemia. More specifically, increased *O*-GlcNAc attenuates hypotension, improves contractile vascular responses and reduces systemic and local proinflammatory cytokine production by mechanisms that involve reduced NF-κB activity.

In conditions of systemic inflammatory responses, such as sepsis, exacerbated inflammation contributes to multiple organ dysfunction, that is strictly related to loss of vasomotor tone, decreased peripheral vascular resistance, decreased blood pressure and cardiac output, hypoperfusion, and hypoxygenation of tissues and organs leading to a significant mortality in intensive care units (De Backer et al., 2014; Hotchkiss et al., 2016; Machado et al., 2017; Salomão et al., 2019). This study shows that acute protein glycosylation, either by increasing flux in the hexosamine pathway, with glucosamine, or by OGA inhibition, with thiamet-G, improves survival of mice with severe

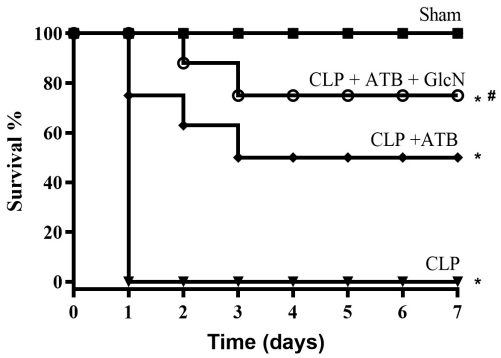

FIGURE 12 | Survival rate in mice of the control group (Sham) and mice submitted to cecal ligation and puncture-induced sepsis (CLP); CLP + ATB (treatment with sodium ertapenem 30 mg/kg s.c.), and CLP + ATB + GlcN (300 mg/Kg, i.v.). Survival rates were determined every 12 h for 7 days and the results are expressed as the percentage of animals alive on each day. $^{*}p < 0.05$ vs. control. $^{\#}p < 0.05$ vs. CLP + ATB. $N = 10$ animals per experimental group. Log-rank test.

endotoxemia in 40 and 60% (**Figure 1**), respectively, suggesting that acute increase in *O*-GlcNAc reduces mortality associated to septic condition. Furthermore, in the CLP-induced sepsis model, that is an important model of sepsis (Alves-Filho et al., 2010), GlcN treatment potentialized the antibiotic effect in improving septic animal survival (**Figure 12**).

The disarrangement in the immune response in the septic patient is an important risk factor that leads to tissue injury and organ dysfunction. This process involves the activation of components of the innate immune response, including humoral and cellular components. An efficient immune response is critical for local control and inhibition of the inflammatory process in LPS-induced SIRS (Cohen, 2002) and neutrophil migration is key in the pathogenesis of endotoxemia (Alves-Filho et al., 2010). Accordingly, increased pulmonary neutrophil sequestration, increased neutrophil numbers in abdominal cavity and high levels of systemic IL-1β, IL-6, and TNFα (**Figures 2**, **3**, **13** and **Supplementary Figures S2, S5**) were observed in LPS-treated and CLP-induced septic mice, depicting a disruption and uncontrolled activation of the immune system in septic mice. Moreover, GlcN and ThG attenuated lung neutrophil sequestration and the number of neutrophils in the abdominal cavity (**Figures 2**, **13**). The reduction in lung neutrophil accumulation can related a lower lung injury and contribute to improvement in animal survival. In CLP model, GlcN also reduce the lung neutrophils sequestration (**Figure 13A**). Moreover, in this septic model, increase in O-GlcNAc protein levels result in higher neutrophils migration to peritoneal cavity (**Figure 13B**). This result could suggest that GlcN improve the neutrophils response to migrate to the focus of the infection. Although the mechanisms involved in neutrophil migration are not fully understood, it is known that high levels of circulating cytokines/chemokines (including TNF-α and IL-1β) modulate the failure of neutrophil migration during SIRS, by releasing nitric oxide (NO), mainly produced by NO inducible synthase (iNOS) (Farias Benjamim et al., 2002; Mestriner et al., 2007).

It is important to highlight that the treatment of LPS mice with GlcN and ThG prevented LPS-induced increase in nitrite serum concentration and ThG also reduced iNOS mRNA in mice (**Figure 6**). Additionally, GlcN- and ThG-treated animals also showed lower serum concentration of IL-1β, TNFα, and IL-6 (**Figure 3** and **Supplementary Figure S5**). These *O*-GlcNAc-induced modifications potentially explain the reduction of lung neutrophil sequestration in this study.

GlcN has anti-inflammatory properties in various animal models and cell types (Shikhman et al., 2001; Gouze et al., 2002; Largo et al., 2003; Chen et al., 2006; Zou et al., 2009; Shin et al., 2013). GlcN treatment reduces the expression of inflammatory mediators, such as IL-6 and cyclooxygenase 2 (COX2) in human chondrocytes (Shikhman et al., 2001; Largo et al., 2003), inhibits IL-1β activity in rat chondrocytes

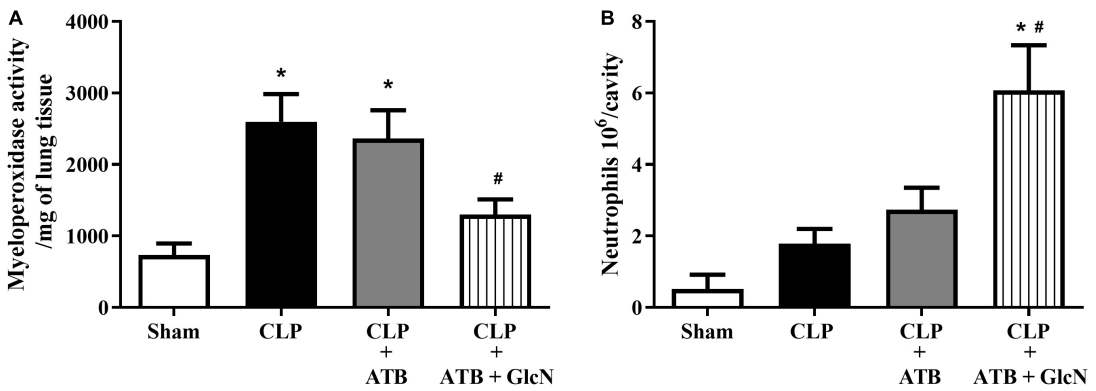

FIGURE 13 | Neutrophil infiltration in the lung and neutrophil migration to the peritoneal cavity in CLP mice. Evaluation of **(A)** neutrophil infiltration in the lungs and **(B)** migration of neutrophils to the peritoneal cavity in control mice (Sham) and mice submitted to CLP-induced sepsis; CLP mice treated with sodium ertapenem (30 mg/kg s.c., CLP + ATB), or CLP + ATB + GlcN (300 mg/Kg, i.v., CLP + ATB + GlcN). Lung neutrophil sequestration was estimated by the myeloperoxidase assay (MPO) in the organ homogenate 6 h after CLP-induced sepsis. Neutrophil count into the peritoneal cavity was performed using the Coulter® apparatus. The results are expressed as mean ± SEM and are representative of 4–5 experiments. $^{*}p < 0.05$ vs. sham; $^{\#}p < 0.05$ vs. CLP + ATB. One-way ANOVA followed by Dunnett's post-test.

(Gouze et al., 2002), decreases TNF-α-induced ICAM expression in human conjunctival epithelial cells (Chen et al., 2006) as well as LPS-induced NO production in macrophage cell lines (Shin et al., 2013). These studies corroborate the hypothesis that increased *O*-GlcNAc-modified proteins reduce levels of circulating pro-inflammatory cytokines with potential protective effects in septic conditions, as observed in our study.

In septic conditions, decreased arterial blood pressure, arterial hyporesponsiveness to contractile agents and vasoplegia are the main symptoms that lead to diminished circulatory blood volume and poor septic patient prognosis (Kandasamy et al., 2011; De Backer et al., 2014; Sumi et al., 2014; Ozer et al., 2017; Coeckelenbergh et al., 2019). For this reason, restoration of vascular function is key in sepsis therapy. In this study, we observed that GlcN treatment attenuated arterial hypotension induced by LPS (**Figure 4**) and increased mesenteric artery sensitivity to phenylephrine (**Figure 5**). OGA inhibition also improved mesenteric artery contractile response to phenylephrine in moderated and severe LPS-induced SIRS (**Figure 5** and **Supplementary Figure S4**). Taken together, these results suggest that increased *O*-GlcNAc protein levels have positive effects in septic condition, improving MAP, vascular function and, consequently, animal survival.

Excessive inflammatory response promotes vascular damage, intravascular systemic vasodilation, hyporesponsiveness to vasopressors, multiple organ failure, and mortality. In our study, SIRS significantly increased cytokines circulating levels, which can contribute to vascular dysfunction in septic animals. Previous studies have shown that pro-inflammatory cytokines, such as IL-1β and TNFα, activate vascular cells to produce more proinflammatory cytokines, which exacerbates the inflammatory response and stimulates generation of vasoactive molecules, such as NO. For instance, Xing et al. (2011) showed that TNF-α induces iNOS expression through the NF-κB signaling pathway in aortic smooth muscle cells and Dalvi et al. (2017) observed that activated monocyte exosomes stimulate IL-1β and IL-6 production by endothelial cells. Corroborating these studies, we observed an increase in mesenteric artery mRNA levels of IL-1β, TNFα, and IL-6 (**Figure 3**), which was paralleled by increased expression of the total and phosphorylated forms of the NF-κB p65 subunit (**Figure 11**), suggesting a local proinflammatory vascular response in septic animals by activation of NF-κB signaling. Activation of the hexosamine pathway by GlcN and OGA inhibition by ThG prevented the systemic and local production of pro-inflammatory cytokines. Furthermore, treatment of mice with ThG increased *O*-glycosylation of the NF-κB p65 subunit in mesenteric arteries, which was associated with reduced Ser^{536} phosphorylation of the p65 subunit (**Figures 10**, **11**, respectively). NF-κB p65 subunit phosphorylation is key to NF-κB-dependent TNFα production (Ahmed et al., 2014) and decreased phosphorylation of NF-κB p65 may explain the anti-inflammatory effect of ThG treatment. All these effects may synergistically contribute to ThG-mediated improved vascular function in LPS-treated animals.

Macrophages have a crucial role in septic inflammatory response. During infection, activated macrophages increase the production of inflammatory mediators to fight the infectious agent and to recruit other immune cells. However, a massive synthesis of proinflammatory mediators contributes to all sepsis-related deleterious effects, as discussed above (Cohen, 2002; van der Poll et al., 2017; Salomão et al., 2019). In our study, BMDM isolated from animals produced the highest levels of cytokines when they were challenged with LPS (**Figures 7**, **8**). Furthermore, *in vitro* experiments, GlcN and ThG treatments attenuated the production and secretion of IL-1β, TNFα, and IL-6 by BMDM (**Figures 7**, **8**). These results suggest that the positive effects induced by GlcN and ThG treatment in septic animals may result from reduced macrophages response.

A recent study showed that LPS-activated macrophages show lower levels of *O*-GlcNAc proteins and activation of OGT-mediated *O*-GlcNAcylation reduces pro-inflammatory macrophages response by inhibition of receptor-interacting serine/threonine-protein kinase 3 (RIPK3), which regulates diverse intracellular signaling, including NF-κB (Li et al., 2019). However, the cardiovascular impact of increased *O*-GlcNAc protein levels in the septic mice were not investigated. The inhibition of RIPK3 may help to explain how GlcN and ThG treatments improve cardiovascular function in septic mice. Additionally, we also observed that acute increase in *O*-GlcNAc proteins attenuates LPS-induced NF-κB activation in macrophages (**Figure 9**), indicating that modulation of NF-κB signaling in macrophages is important for the positive effect induced by *O*-GlcNAcylation in septic mice.

CONCLUSION

In conclusion, our result provides strong evidence that acute increase of *O*-GlcNAc protein levels increases survival by reducing systemic inflammation and vascular dysfunction, suggesting that reprogramming of cellular metabolism, by stimulating the hexosamine pathway, may represent a therapeutic approach in septic conditions.

DATA AVAILABILITY STATEMENT

The datasets generated for this study are available on request to the corresponding author.

ETHICS STATEMENT

The animal study was reviewed and approved by Ethics Committee on Animal Research of the Ribeirão Preto Medical School, University of São Paulo (protocol no 196/13) and are in accordance with the Guidelines of the National Council for Animal Experimentation Control (CONCEA).

AUTHOR CONTRIBUTIONS

VO, JA-F, and RT participated in the design of the study. JS, VO, CZ, RGF, NF, CS, JA, JL, and FM conducted the experiments. FC, JA-F, RF, and RT contributed with reagents or analytical tools. JS, VO, CZ, and RT performed the data analysis. JS,

VO, and RT wrote the manuscript. All authors discussed and reviewed the manuscript.

FUNDING

This work was supported by grants from Fundação de Amparo à Pesquisa do Estado de São Paulo (FAPESP-CRID 2013/08216-2 to RT, FC, and JA-F; 2016/16207-1 to JS), and grants from Coordenação de Aperfeiçoamento de Pessoal de Nível Superior (CAPES) and Conselho Nacional de Desenvolvimento Científico e Tecnológico (CNPq), Brazil, to RT.

SUPPLEMENTARY MATERIAL

The Supplementary Material for this article can be found online at: https://www.frontiersin.org/articles/10.3389/fphys.2019.01614/full#supplementary-material

REFERENCES

Ahmed, A. U., Sarvestani, S. T., Gantier, M. P., Williams, B. R., and Hannigan, G. E. (2014). Integrin-linked kinase modulates lipopolysaccharide- and *Helicobacter pylori*-induced nuclear factor κB-activated tumor necrosis factor-α production via regulation of p65 serine 536 phosphorylation. *J. Biol. Chem.* 289, 27776–27793. doi: 10.1074/jbc.M114.574541

Alves-Filho, J. C. I., Sônego, F., Souto, F. O., Freitas, A., Verri, W. A. Jr., Auxiliadora-Martins, M., et al. (2010). Interleukin-33 attenuates sepsis by enhancing neutrophil influx to the site of infection. *Nat. Med.* 16, 708–712. doi: 10.1038/nm.2156

Andrali, S. S., Qian, Q., and Ozcan, S. (2007). Glucose mediates the translocation of NeuroD1 by O-linked glycosylation. *J. Biol. Chem.* 282, 15589–15596. doi: 10.1074/jbc.M701762200

Ayala, A., Urbanich, M. A., Herdon, C. D., and Chaudry, I. H. (1996). Is sepsis-induced apoptosis associated with macrophage dysfunction? *J. Trauma.* 40, 568–573. doi: 10.1097/00005373-199604000-00008

Azuma, K., Osaki, T., Kurozumi, S., Kiyose, M., Tsuka, T., Murahata, Y., et al. (2015). Anti-inflammatory effects of orally administered glucosamine oligomer in an experimental model of inflammatory bowel disease. *Carbohydr. Polym.* 22, 448–456. doi: 10.1016/j.carbpol.2014.09.012

Baudoin, L., and Issad, T. (2015). O-GlcNAcylation and inflammation: a vast territory to explore. *Front. Endocrinol.* 5:235. doi: 10.3389/fendo.2014.00235

Chen, J. T., Chen, C. H., Horng, C. T., Chien, M. W., Lu, D. W., Liang, J. B., et al. (2006). Glucosamine sulfate inhibits proinflammatory cytokine-induced icam-1 production in human conjunctival cells in vitro. *J. Ocul. Pharmacol. Ther.* 22, 402–416. doi: 10.1089/jop.2006.22.402

Cheng, S. C., Scicluna, B. P., Arts, R. J., Gresnigt, M. S., Lachmandas, E., Giamarellos-Bourboulis, E. J., et al. (2016). Broad defects in the energy metabolism of leukocytes underlie immunoparalysis in sepsis. *Nat. Immunol.* 17, 406–413. doi: 10.1038/ni.3398

Coeckelenbergh, S., Van Nuffelen, M., and Mélot, C. (2019). Sepsis is frequent in initially non-critical hypotensive emergency department patients and is associated with increased mortality. *Am. J. Emerg. Med.* 23:158360. doi: 10.1016/j.ajem.2019.158360

Cohen, J. (2002). The immunopathogenesis of sepsis. *Nature* 420, 885–891. doi: 10.1038/nature01326

Cooper, Z. A. I., Ghosh, A., Gupta, A., Maity, T., Benjamin, I. J., and Vogel, S. N. (2010). Febrile-range temperature modifies cytokine gene expression in LPS-stimulated macrophages by differentially modifying NF-{kappa}B recruitment to cytokine gene promoters. *Am. J. Physiol. Cell. Physiol.* 298, C171–C181. doi: 10.1152/ajpcell.00346.2009

da Costa, R. M., da Silva, J. F., Alves, J. V., Dias, T. B., Rassi, D. M., Garcia, L. V., et al. (2018). Increased O-GlcNAcylation of endothelial nitric oxide synthase compromises the anti-contractile properties of perivascular adipose tissue in metabolic syndrome. *Front. Physiol.* 9:341. doi: 10.3389/fphys.2018.00341

Dalvi, P., Sun, B., Tang, N., and Pulliam, L. (2017). Immune activated monocyte exosomes alter microRNAs in brain endothelial cells and initiate an inflammatory response through the TLR4/MyD88 pathway. *Sci. Rep.* 7:9954. doi: 10.1038/s41598-017-10449-0

Dasu, M. R., Devaraj, S., Zhao, L., Hwang, D. H., and Jialal, I. (2008). High glucose induces toll-like receptor expression in human monocytes: mechanism of activation. *Diabetes* 57, 3090–3098. doi: 10.2337/db08-0564

De Backer, D., Orbegozo Cortes, D., Donadello, K., and Vincent, J. L. (2014). Pathophysiology of microcirculatory dysfunction and the pathogenesis of septic shock. *Virulence* 5, 73–79. doi: 10.4161/viru.26482

Dinarello, C. A. (1997). Proinflammatory and anti-inflammatory cytokines as mediators in the pathogenesis of septic shock. *Chest* 112, 321S–329S. doi: 10.1378/chest.112.6_supplement.321s

Farias Benjamim, C., Santana Silva, J., Bruno Fortes, Z., Aparecida Oliveira, M., Henrique Ferreira, S., and Queiroz Cunha, F. (2002). Inhibition of leukocyte rolling by nitric oxide during sepsis leads to reduced migration of active microbicidal neutrophils. *Infect. Immun.* 70, 3602–3610. doi: 10.1128/iai.70.7.3602-3610.2002

Fleischmann, C., Scherag, A., Adhikari, N. K., Hartog, C. S., Tsaganos, T., Schlattmann, P., et al. (2016). Assessment of global incidence and mortality of hospital-treated sepsis. Current estimates and limitations. *Am. J. Respir. Crit. Care Med.* 193, 259–272. doi: 10.1164/rccm.201504-0781OC

Gouze, J. N., Bianchi, A., Bécuwe, P., Dauça, M., Netter, P., Magdalou, J., et al. (2002). Glucosamine modulates IL-1-induced activation of rat chondrocytes at a receptor level, and by inhibiting the NF-kappa B pathway. *FEBS Lett.* 510, 166–170. doi: 10.1016/s0014-5793(01)03255-0

Green, L. C., Wagner, D. A., Glogowski, J., Skipper, P. L., Wishnok, J. S., and Tannenbaum, S. R. (1982). Analysis of nitrate, nitrite, and [15N]nitrate in biological fluids. *Anal. Biochem.* 126, 131–138. doi: 10.1016/0003-2697(82)90118-x

Guinez, C., Filhoulaud, G., Rayah-Benhamed, F., Marmier, S., Dubuquoy, C., Dentin, R., et al. (2011). O-GlcNAcylation increases ChREBP protein content and transcriptional activity in the liver. *Diabetes* 60, 1399–1413. doi: 10.2337/db10-0452

Halpern, W., Mulvany, M. J., and Warshaw, D. M. (1978). Mechanical properties of smooth muscle cells in the walls of arterial resistance vessels. *J. Physiol.* 275, 85–101. doi: 10.1113/jphysiol.1978.sp012179

Hotchkiss, R. S., Moldawer, L. L., Opal, S. M., Reinhart, K., Turnbull, I. R., and Vincent, J. L. (2016). Sepsis and septic shock. *Nat. Rev. Dis. Primers.* 2:16045. doi: 10.1038/nrdp.2016.45

Hua, K. F., Wang, S. H., Dong, W. C., Lin, C. Y., Ho, C. L., and Wu, T. H. (2012). High glucose increases nitric oxide generation in lipopolysaccharide-activated macrophages by enhancing activity of protein kinase C-α/δ and NF-κB. *InflammRes* 61, 1107–1116. doi: 10.1007/s00011-012-0503-1

Huet, O., Dupic, L., Harrois, A., and Duranteau, J. (2011). Oxidative stress and endothelial dysfunction during sepsis. *Front. Biosci.* 16:1986–1995.

Hwang, J. S., Kwon, M. Y., Kim, K. H., Lee, Y., Lyoo, I. K., Kim, J. E., et al. (2017). Lipopolysaccharide (LPS)-stimulated iNOS induction is increased by glucosamine under normal glucose conditions but is inhibited by glucosamine under high glucose conditions in macrophage cells. *J. Biol. Chem.* 292, 1724–1736. doi: 10.1074/jbc.M116.737940

Kandasamy, K., Prawez, S., Choudhury, S., More, A. S., Ahanger, A. A., Singh, T. U., et al. (2011). Atorvastatin prevents vascular hyporeactivity to norepinephrine in sepsis: role of nitric oxide and α1-adrenoceptor mRNA expression. *Shock* 36, 76–82. doi: 10.1097/SHK.0b013e31821a4002

Kronlage, M., Dewenter, M., Grosso, J., Fleming, T., Oehl, U., Lehmann, L. H., et al. (2019). O-GlcNAcylation of histone deacetylase 4 protects the diabetic Heart From Failure. *Circulation* 140, 580–594. doi: 10.1161/CIRCULATIONAHA.117.031942

Lachmandas, E., Boutens, L., Ratter, J. M., Hijmans, A., Hooiveld, G. J., Joosten, L. A., et al. (2016). Microbial stimulation of different Toll-like receptor signaling

pathways induces diverse metabolic programmes in human monocytes. *Nat. Microbiol.* 2:16246. doi: 10.1038/nmicrobiol.2016.246

Largo, R., Alvarez-Soria, M. A., Díez-Ortego, I., Calvo, E., Sánchez-Pernaute, O., Egido, J., et al. (2003). Glucosamine inhibits IL-1beta-induced NFkappaB activation in human osteoarthritic chondrocytes. *Osteoarthritis Cartilage* 11, 290–298. doi: 10.1016/0003-2697(82)90118-X

Li, X., Gong, W., Wang, H., Li, T., Attri, K. S., Lewis, R. E., et al. (2019). O-GlcNAc transferase suppresses inflammation and necroptosis by targeting receptor-interacting serine/Threonine-protein kinase 3. *Immunity* 50:576-590.e6. doi: 10.1016/j.immuni.2019.01.007

Liu, H., Wang, Z., Yu, S., and Xu, J. (2014). Proteasomal degradation of O-GlcNAc transferase elevates hypoxia-induced vascular endothelial inflammatory response. *Cardiovasc. Res.* 103, 131–139. doi: 10.1093/cvr/cvu116

Lu, G., Zhang, R., Geng, S., Peng, L., Jayaraman, P., Chen, C., et al. (2015). Myeloid cell-derived inducible nitric oxide synthase suppresses M1 macrophage polarization. *Nat. Commun.* 27:6676. doi: 10.1038/ncomms7676

Machado, F. R., Cavalcanti, A. B., Bozza, F. A., Ferreira, E. M., Angotti Carrara, F. S., Sousa, J. L., et al. (2017). The epidemiology of sepsis in Brazilian intensive care units (the Sepsis Prevalence Assessment Database, SPREAD): an observational study. *Lancet Infect. Dis* 17, 1180–1189. doi: 10.1016/S1473-3099(17)30322-5

Mestriner, F. L., Spiller, F., Laure, H. J., Souto, F. O., Tavares-Murta, B. M., Rosa, J. C., et al. (2007). Acute-phase protein alpha-1-acid glycoprotein mediates neutrophil migration failure in sepsis by a nitric oxide-dependent mechanism. *Proc. Natl. Acad. Sci.U.S.A.* 104, 19595–19600. doi: 10.1073/pnas.0709681104

Mills, E. L., Kelly, B., Logan, A., Costa, A. S. H., Varma, M., Bryant, C. E., et al. (2016). Succinate dehydrogenase supports metabolic repurposing of mitochondria to drive inflammatory macrophages. *Cell* 167:457-470.e13. doi: 10.1016/j.cell.2016.08.064

Munoz, C., Carlet, J., Fitting, C., Misset, B., Blériot, J. P., and Cavaillon, J. M. (1991). Dysregulation of in vitro cytokine production by monocytes during sepsis. *J. Clin. Invest.* 88, 1747–1754. doi: 10.1172/JCI115493

Ozer, E. K., Goktas, M. T., Toker, A., Bariskaner, H., Ugurluoglu, C., and Iskit, A. B. (2017). Effects of carvacrol on survival, mesenteric blood flow, aortic function and multiple organ injury in a murine model of polymicrobial sepsis. *Inflammation* 40, 1654–1663. doi: 10.1007/s10753-017-0605-6

Salomão, R., Ferreira, B. L., Salomão, M. C., Santos, S. S., Azevedo, L. C. P., and Brunialti, M. K. C. (2019). Sepsis: evolving concepts and challenges. *Braz. J. Med. Biol. Res.* 52:e8595. doi: 10.1590/1414-431X20198595

Seo, Y. J., Jeong, M., Lee, K. T., Jang, D. S., and Choi, J. H. (2016). Isocyperol, isolated from the rhizomes of Cyperus rotundus, inhibits LPS-induced inflammatory responses via suppression of the NF-κB and STAT3 pathways and ROS stress in LPS-stimulated RAW 264.7 cells. *Int. Immunopharmacol.* 38, 61–69. doi: 10.1016/j.intimp.2016.05.017

Shanmugam, N., Reddy, M. A., Guha, M., and Natarajan, R. (2003). High glucose-induced expression of proinflammatory cytokine and chemokine genes in monocytic cells. *Diabetes* 52, 1256–1264. doi: 10.2337/diabetes.52.5.1256/

Shikhman, A. R., Kuhn, K., Alaaeddine, N., and Lotz, M. (2001). N-acetylglucosamine prevents IL-1 beta-mediated activation of human chondrocytes. *J. Immunol.* 166, 5155–5160. doi: 10.4049/jimmunol.166.8.5155

Shin, J. A., Hwang, J. S., Kim, S. Y., Oh, S. K., Nam, G., and Han, I. O. (2013). A novel glucosamine derivative exerts anti-inflammatory actions via inhibition of nuclear factor-kappaB. *Neurosci. Lett.* 29, 162–167. doi: 10.1016/j.neulet.2013.06.053

Silasi-Mansat, R., Zhu, H., Popescu, N. I., Peer, G., Sfyroera, G., Magotti, P., et al. (2010). Complement inhibition decreases the procoagulant response and confers organ protection in a baboon model of *Escherichia coli* sepsis. *Blood* 116, 1002–1010. doi: 10.1182/blood-2010-02-269746

Sumi, Y., Woehrle, T., Chen, Y., Bao, Y., Li, X., Yao, Y., et al. (2014). Plasma ATP is required for neutrophil activation in a mouse sepsis model. *Shock* 42, 142–147. doi: 10.1097/SHK.0000000000000180

Takeuchi, O., and Akira, S. (2010). Pattern recognition receptors and inflammation. *Cell* 140, 805–820. doi: 10.1016/j.cell.2010.01.022

Tannahill, G. M., Curtis, A. M., Adamik, J., Palsson-McDermott, E. M., McGettrick, A. F., Goel, G., et al. (2013). Succinate is an inflammatory signal that induces IL 1β through HIF 1α. *Nature* 496, 238–242. doi: 10.1038/nature11986

Tyml, K. (2011). Critical role for oxidative stress, platelets, and coagulation in capillary blood flow impairment in sepsis. *Microcirculation* 18, 152–162. doi: 10.1111/j.1549-8719.2010.00080.x

van der Poll, T., van de Veerdonk, F. L., Scicluna, B. P., and Netea, M. G. (2017). The immunopathology of sepsis and potential therapeutic targets. *Nat. Rev. Immunol.* 17, 407–420. doi: 10.1038/nri.2017.36

Wiersinga, W. J., Leopold, S. J., Cranendonk, D. R., and van der Poll, T. (2014). Host innate immune responses to sepsis. *Virulence* 5, 36–44. doi: 10.4161/viru.25436

Xing, D., Feng, W., Nöt, L. G., Miller, A. P., Zhang, Y., Chen, Y. F., et al. (2008). Increased protein O-GlcNAc modification inhibits inflammatory and neointimal responses to acute endoluminal arterial injury. *Am. J. Physiol. Heart Circ. Physiol.* 295, H335–H342. doi: 10.1152/ajpheart.01259.2007

Xing, D., Gong, K., Feng, W., Nozell, S. E., Chen, Y. F., Chatham, J. C., et al. (2011). O-GlcNAc modification of NF-kB p65 inhibits TNF-α-induced inflammatory mediator expression in rat aortic smooth muscle cells. *PLoS One* 6:e24021. doi: 10.1371/journal.pone.0024021

Yang, X., and Qian, K. (2017). Protein O-GlcNAcylation: emerging mechanisms and functions. *Nat. Rev. Mol. Cell Biol.* 18, 452–465. doi: 10.1038/nrm.2017.22

Zachara, N. E. (2018). Critical observations that shaped our understanding of the function(s) of intracellular glycosylation (O-GlcNAc). *FEBS Lett.* 592, 3950–3975. doi: 10.1002/1873-3468.13286

Zou, L., Yang, S., Champattanachai, V., Hu, S., Chaudry, I. H., Marchase, R. B., et al. (2009). Glucosamine improves cardiac function following trauma-hemorrhage by increased protein O-GlcNAcylation and attenuation of NF-{kappa}B signaling. *Am. J. Physiol.* 296, H515–H523. doi: 10.1152/ajpheart.01025.2008

Conflict of Interest: The authors declare that the research was conducted in the absence of any commercial or financial relationships that could be construed as a potential conflict of interest.

frontiers in Physiology

REVIEW
published: 22 January 2020
doi: 10.3389/fphys.2019.01583

Vascular Integrity and Signaling Determining Brain Development, Network Excitability, and Epileptogenesis

Jugajyoti Baruah[1,2], Anju Vasudevan[1,2] and Rüdiger Köhling[3]**

[1]*Department of Psychiatry, Harvard Medical School, Boston, MA, United States,* [2]*Angiogenesis and Brain Development Laboratory, Division of Basic Neuroscience, McLean Hospital, Belmont, MA, United States,* [3]*Oscar-Langendorff-Institute of Physiology, Rostock University Medical Center, Rostock, Germany*

Our understanding of the etiological mechanisms leading up to epilepsy has undergone radical changes over time due to more insights into the complexity of the disease. The traditional hypothesis emphasized network hyperexcitability and an imbalance of inhibition and excitation, eventually leading to seizures. In this context, the contribution of the vascular system, and particularly the interactions between blood vessels and neuronal tissue, came into focus only recently. Thus, one highly exciting causative or contributing factor of epileptogenesis is the disruption of the blood-brain barrier (BBB) in the context of not only posttraumatic epilepsy, but also other etiologies. This hypothesis is now recognized as a synergistic mechanism that can give rise to epilepsy, and BBB repair for restoration of cerebrovascular integrity is considered a therapeutic alternative. Endothelial cells lining the inner surface of blood vessels are an integral component of the BBB system. Sealed by tight junctions, they are crucial in maintaining homeostatic activities of the brain, as well as acting as an interface in the neurovascular unit. Additional potential vascular mechanisms such as inflammation, altered neurovascular coupling, or changes in blood flow that can modulate neuronal circuit activity have been implicated in epilepsy. Our own work has shown how intrinsic defects within endothelial cells from the earliest developmental time points, which preclude neuronal changes, can lead to vascular abnormalities and autonomously support the development of hyperexcitability and epileptiform activity. In this article, we review the importance of vascular integrity and signaling for network excitability and epilepsy by highlighting complementary basic and clinical research studies and by outlining possible novel therapeutic strategies.

Keywords: vascular endothelia, development, blood-brain barrier, inflammation, hyperexcitability, epileptogenesis

OPEN ACCESS

Edited by:
Shampa Chatterjee, University of Pennsylvania, United States

Reviewed by:
Jingjing Zhang, Affiliated Hospital of Guangdong Medical University, China
Xin Wu, Texas A&M University, United States

****Correspondence:***
Anju Vasudevan
avasudevan@mclean.harvard.edu
Rüdiger Köhling
ruediger.koehling@uni-rostock.de

Specialty section:
This article was submitted to Vascular Physiology, a section of the journal Frontiers in Physiology

Received: *13 September 2019*
Accepted: *17 December 2019*
Published: *22 January 2020*

Citation:
Baruah J, Vasudevan A and Köhling R (2020) Vascular Integrity and Signaling Determining Brain Development, Network Excitability, and Epileptogenesis. Front. Physiol. 10:1583. doi: 10.3389/fphys.2019.01583

INTRODUCTION

Epileptogenesis is the process of developing epilepsy, that is, a chronic neurological disorder characterized by seizures. During this process, a normally functioning brain gradually develops the chronic susceptibility to generate intermittent or recurrent seizures. Epilepsy is a neurological disorder that not only impairs quality of life but also can lead to increased mortality (Devinsky et al., 2018; Beghi et al., 2019). Epileptogenesis can be precipitated by multifactorial events that

can be either genetic or environmental. Nevertheless, the macro- or micro-molecular events that lead to epileptogenesis are poorly elucidated, and the disease mechanisms that lead to epilepsy are still unknown in 50% of the global cases (Neligan et al., 2012). Although extensive research using animal models of epilepsy has highlighted the wide array of molecular and cellular events that predict epileptogenesis (Avoli et al., 2005), the "missing link" between the primal events leading up to epileptogenesis in a human brain still persists. In an interesting editorial, a vivid interpretation of historical texts from the works of novelist and painter August Strindberg (1849–1912) was made. In his writings, he describes a person who, after several episodes with loss of tone and consciousness, shows a syndrome of complete hemiparesis due to stroke. This has been interpreted as *vascular precursor epilepsy* (Trinka et al., 2015), and therefore, it is safe to comprehend that the vascular component of epilepsy has been a topic of subtle discussion in history as well. However, it was not until the nineteenth century that an alternate hypothesis, which today is known as the "blood-brain barrier (BBB) hypothesis," was proposed to explain some of the phenotypic consequences of epilepsy (Cornford and Oldendorf, 1986; Cornford, 1999). Studies from several other groups later added insights that directly implicated dysfunction in blood vessels to seizure disorders (Seiffert et al., 2004; van Vliet et al., 2006; Ivens et al., 2007; Marchi et al., 2007; Weissberg et al., 2011). In this context, our own work has depicted that selective deletion of vascular endothelial growth factor (VEGF), gamma aminobutyric acid (GABA) A receptor subunit beta 3 (GABRB3), or the vesicular GABA transporter (VGAT) from endothelial cells during early development affects forebrain vascular networks, leads to brain morphological defects, and makes lasting changes to cortical circuits (Li et al., 2013, 2018). Importantly, vascular health is of significance not only for epilepsy but also for several neuropsychiatric disorders (Baruah and Vasudevan, 2019). In **Figure 1**, we present a pictorial representation of "the vascular landscape in epilepsy," highlighting different vascular or neurovascular abnormalities that are implicated in epilepsy through basic and clinical research. Many seminal reviews have addressed the role of BBB dysfunction in the etiology of epilepsy (van Vliet et al., 2006; Marchi et al., 2007, 2011; Kim et al., 2017), and therefore, the current review focuses on some of the studies in the last two decades and how information gained from these studies can be applied for novel therapeutic interventions.

VASCULAR-NEURONAL INTERACTIONS DURING BRAIN DEVELOPMENT

The similarities between vascular and neuronal development in the brain are striking initially at a phenomenological level. In

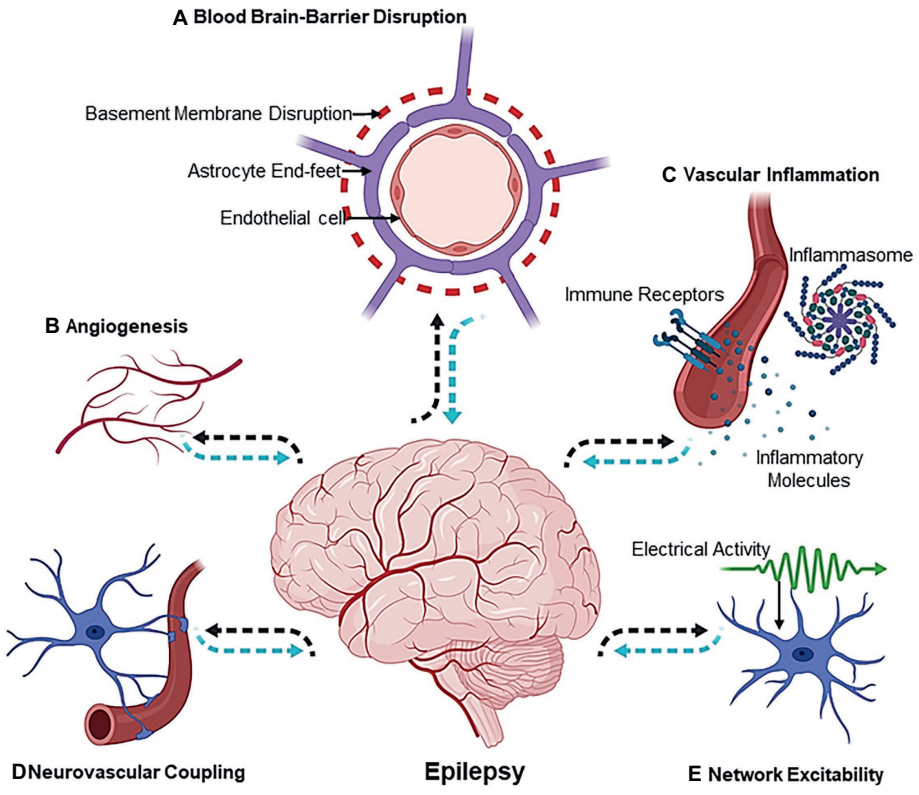

FIGURE 1 | The Vascular Landscape in Epilepsy. The mechanisms involved in the etiology of epileptogenesis are multiphasic [**(A)** blood-brain-barrier disruption, **(B)** angiogenesis, **(C)** vascular inflammation, **(D)** neurovascular coupling and, lastly, **(E)** network excitability] and exist at the crossroads of the neurovascular network. Dotted black arrows indicate the sequence of events leading up to epileptogenesis, whereas dotted blue arrows show the sequence of events that affect the neuron or vascular interface in an epileptic brain. Illustration was created using Biorender.com.

both the vascular and nervous systems, generation of the different types of cells begins with the proliferation of stem cells. Common mechanisms operate at the level of the cell cycle to regulate proliferation of angioblasts and neuronal precursors. In both, cell generation epochs result in an initial overproduction of cellular elements, and later, the excess elements are eliminated by apoptosis or pruning. Both vascular and neuronal elements undergo significant activity-dependent remodeling during development. In the case of the vasculature, the activity is generated by shearing force of blood flow, and in the case of the nervous system, the activity is generated by electrical impulses in the neuronal networks. Just as neuronal networks show plasticity in response to changing electrical activity, vascular endothelial cells also show remarkable plasticity in response to changing tissue oxygenation level or blood flow. Process outgrowth and guidance in the nervous system involve axon growth cone guidance, pathfinding, axon branching, and arborization. The corresponding events in the vascular system are filopodial extensions of tip cells (specialized endothelial cells at the growing tips of navigating vessels), migration of endothelial cells, vessel elongation, and sprouting. Thus, common mechanisms regulate the genesis of endothelial cells and neurons. A review of the literature indicates that not only an overlapping repertoire of signaling molecules but also intrinsic regulation by compartment-specific transcription factors controls angiogenesis, neurogenesis, and neuronal migration in the embryonic brain (Carmeliet, 2003; Haigh et al., 2003; Carmeliet and Tessier-Lavigne, 2005; Eichmann et al., 2005; Vasudevan et al., 2008; Li et al., 2013, 2018; Paredes et al., 2018; Karakatsani et al., 2019). Importantly, molecules produced in one system influence the other to promote proliferation, differentiation, migration, or process outgrowth in both the systems. This developmental phase is very crucial because improper neuro-vascular interactions can precipitate into a spectrum of neurological disorders including epilepsy (Carmeliet, 2005; Vasudevan and Bhide, 2008; Obermeier et al., 2013; Ruhrberg and Bautch, 2013; Stern, 2018). A common pathology seen in epileptic brains is the presence of widespread structural alterations in brain regions, such as the hippocampus, thalamus, or neocortex (Barkovich et al., 2015). Taken together, epilepsy can be characterized by shared disturbance in the cortico-subcortical brain network (Stafstrom and Carmant, 2015), and often times, it is concomitant with vascular malformation in young patients (Hauser and Mohr, 2011). Given that the blood vessels or the vasculature plays an important role in defining brain architecture and circuitry, any aberrant vascular-neuronal interactions during development stages when the brain is "wiring up" can be expected to make the brain more prone to develop epilepsy at postnatal stages or during adulthood.

ABNORMAL ANGIOGENESIS AND EPILEPTOGENESIS

Angiogenesis is the spatio-temporal event where blood vessels are formed from preexisting vessels to perfuse tissues, establish circulation, and provide instructional cues both during development as well as in postnatal life as part of therapeutic angiogenesis. One of the earliest studies conducted by Rigau et al. showed an increase in angiogenic processes in the hippocampi that were surgically removed from patients with chronic intractable temporal lobe epilepsy (TLE; Rigau et al., 2007). An important set of molecules that regulates both developmental and pathological angiogenesis and is upregulated in patients with medically intractable epilepsy is the family of vascular endothelial growth factor (VEGF; Croll et al., 2004; Vezzani, 2005; Li et al., 2013; Sun et al., 2016). Interestingly, the subtypes A and B, and the VEGF receptors 1 and 2, were highly expressed in the dysplastic neurons. Since VEGF is expressed by both neuronal and endothelial cell populations, the authors concluded that VEGF-mediated signaling can act *via* autocrine or paracrine mechanisms that can lead to astroglial activation and precipitate events associated with epilepsy (Nicoletti et al., 2008, 2010; Li et al., 2013). The VEGF signaling pathway is also active in hippocampi, exhibiting epileptiform activity (Morin-Brureau et al., 2011). In a rat model of pilocarpine-induced epilepsy, there was an increased angiogenesis in the CA3 region of the hippocampus, which was also accompanied by an increase in cerebral blood flow. The increased angiogenic sprouting was accompanied by neurodegeneration, ectopic neurogenesis, mossy fiber sprouting in the hippocampus, and most importantly BBB leakage (Ndode-Ekane et al., 2010). In another rat model of mesial temporal lobe epilepsy, inhibition of angiogenesis *via* a chemical inhibitor, sunitinib, resulted in the absence of seizures when compared to sham-treated mice (Benini et al., 2016). Similar studies suggested that morphological changes observed in the epileptic foci were consistent with an increase in angiogenic processes. Most recently, patients who have mammalian target of rapamycin (mTOR)-dependent malformations of cortical development (MCDs) displayed hyperperfusion and an increased vessel density of the dysmorphic cortical tissue (Zhang et al., 2019). Ephrin receptor A4 that mediates neurogenesis and angiogenesis in the dentate gyrus was also found to increase angiogenesis in the CA1 and CA2 regions of the hippocampus in a mouse model of TLE (Feng et al., 2017). In another interesting study, astrocytes were shown to regulate angiogenesis *via* the activities of Jagged/Notch1 signaling pathway in a kainic acid-induced mouse model of epilepsy (Zhai et al., 2016). All of these studies have implicated abnormal angiogenesis in epilepsy.

DEVELOPMENTAL ANGIOGENESIS AND ORIGIN OF EPILEPSY

A new perspective is that abnormalities in developmental angiogenesis can now be directly linked with the etiopathophysiology of epilepsy. Our studies have shown that during development, preformed vascular networks serve as a cellular substrate for long distance migration of GABAergic interneurons (Vasudevan et al., 2008; Won et al., 2013). Projection neuron precursors also interact closely with blood vessels during cerebral cortex development (Stubbs et al., 2009). Cortical abnormalities by virtue of defective migration and neuronal positioning are a commonly observed phenomenon in epileptic brains (Blinder et al., 2013; Whelan et al., 2018). Interestingly,

the laminar position of cortical neuronal subsets has very little effect on the overall vascular pattern in the cortex in the shaking rat Kawasaki (SRK) and reeler mutants, despite inversion of cortical layers, suggesting the autonomous roles for vascular components in neurogenesis and neuronal migration (Vasudevan et al., 2008; Stubbs et al., 2009). Moreover, periventricular endothelial cells of the embryonic forebrain have a unique gene expression signature compared to pial endothelial cells or endothelial cells from the midbrain or hindbrain. Of significance, gene expression profiling depicted the disease category "epilepsy" to be significantly enriched in genes expressed in periventricular endothelial cells, whereas genes in pial endothelial cells showed enrichment in inflammation and pathological process categories. These observations implicate a new cell type, "periventricular endothelial cells," as being contributory to epilepsy (Won et al., 2013).

Defects in $GABA_A$ receptor regulation or mutations in $GABA_A$ receptor subunits and polymorphisms have also been associated with genetic epilepsies that cause seizures as one of the primary symptoms (Kang and Macdonald, 2009). In this respect, our work has unraveled a novel $GABA_A$ receptor-GABA signaling pathway in periventricular endothelial cells of the embryonic

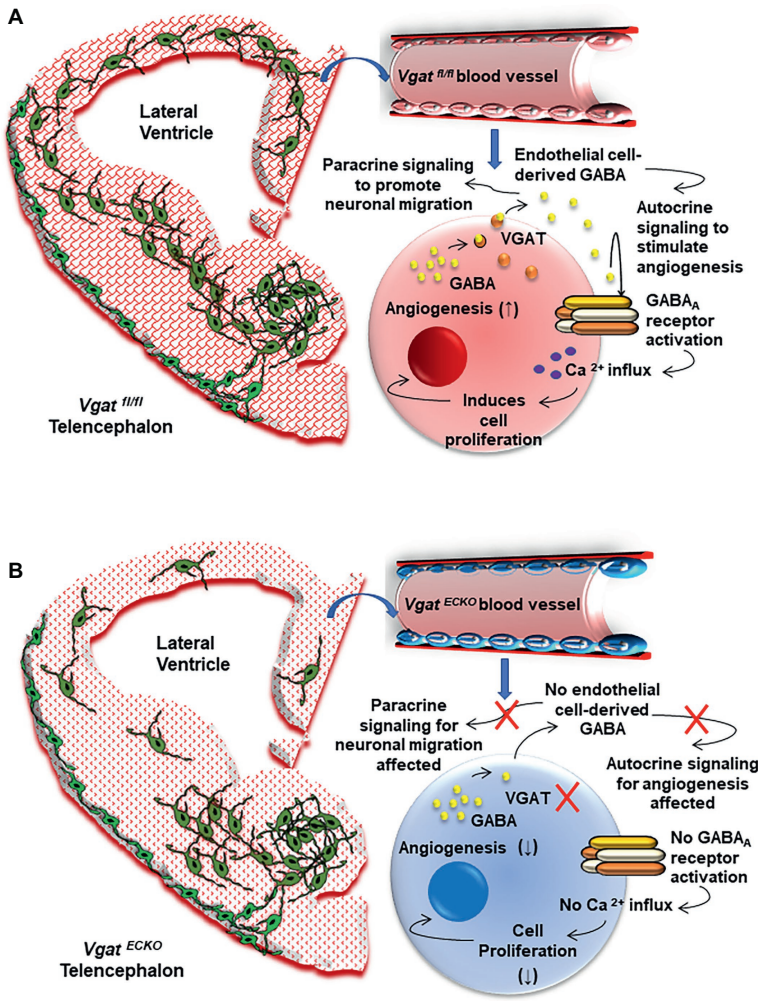

FIGURE 2 | The Vascular Origin of Epilepsy. **(A)** Schema depicting the *Vgat* $^{fl/fl}$ or control embryonic telencephalon at day 15 that has normal periventricular vascular network (red lattice pattern) and a normal endothelial GABA signaling pathway that promotes long distance tangential migration of GABAergic interneurons (green) from the ventral telencephalon. A single vessel has been magnified to illustrate the positive feedback GABA signaling pathway that exists in normal telencephalic endothelial cells (red). Endothelial GABA activates $GABA_A$ receptors, thereby triggering Ca^{2+} influx and endothelial cell proliferation. Vesicular GABA transporter (VGAT) is the primary mechanism for GABA release from telencephalic endothelial cells at embryonic day 15 (Li et al., 2018). Endothelial GABA release thus has autocrine roles in stimulating angiogenesis (↑) and paracrine roles in promoting long distance GABAergic neuronal migration in the embryonic telencephalon. **(B)** Schema depicting altered vascular profiles in *Vgat* ^{ECKO} telencephalon (red dotted pattern) in which there is complete loss of endothelial GABA secretion that causes GABAergic interneurons to stall in the ventral telencephalon. This has significant consequences for GABAergic neuronal tangential migration, resulting in neuronal reductions and abnormal cortical distribution in *Vgat* ^{ECKO} telencephalon. Magnification of a single vessel to depict abnormal *Vgat* ^{ECKO} endothelial cells (blue) and how lack of GABA release from these endothelial cells affects the positive feedback of GABA-$GABA_A$ receptor signaling, which in turn significantly affects angiogenesis-related gene expression (↓). Lack of endothelial GABA release also affects paracrine signaling and impairs long-distance migration of GABAergic interneurons.

brain that is distinct from the neuronal GABA signaling pathway. Selective deletion of the $GABA_A$ receptor β3 subunit from endothelial cells resulted in seizure-like symptoms in 15% of the mice. On the other hand, deletion of the vesicular GABA transporter (*Vgat*) from endothelial cells resulted in a mouse model of epilepsy. We have shown that *Vgat* is the primary mechanism for GABA release from endothelial cells at early embryonic stages. Therefore, when *Vgat* was deleted specifically from endothelial cells, endothelial GABA secretion was turned off during embryonic brain development. In the absence of endothelial GABA release, all of the key cellular events during forebrain development – angiogenesis, neurogenesis, radial migration of projection neurons, and tangential migration of GABA interneurons – were affected to some degree, indicative of the autocrine and paracrine roles of EC-derived GABA signaling. Strikingly, gene expression profiling of *Vgat* endothelial cell conditional knockout ($Vgat^{ECKO}$) embryonic telencephalon at embryonic stages was able to predict the postnatal phenotype of the mouse model. Significant enrichment was seen in disease categories "epilepsy" and "seizures," and several of the epilepsy-related genes were isolated and grouped (Li et al., 2018; Choi and Vasudevan, 2019). The $Vgat^{ECKO}$ mice were smaller in size at birth when compared to littermate controls and developed severe seizures during the postnatal period P7–P14. Reduction in vascular densities was associated with a layer-specific loss of GABAergic interneurons along with abnormal GABAergic and glutamatergic neuronal distribution in $Vgat^{ECKO}$ cerebral cortex indicative of a highly asynchronous cortical circuitry. $Vgat^{ECKO}$ mice showed periods of quiescence, interrupted by tremors and reductions in movement, and did not survive beyond 2 months of age. Field potential recordings depicted a high degree of hyperexcitability in the hippocampus. Collectively, our work has provided mechanistic understanding of how intrinsic defects within blood vessels from the earliest developmental time points can directly contribute to epilepsy (**Figure 2**).

BASEMENT MEMBRANE DYSFUNCTION AND EPILEPSY

The basement membrane is a specialized form of extracellular matrix that encases the endothelial cells. Pericytes are also embedded in the basement membrane, situated between endothelial cells and astroglial endfeet. The composition and structure of the basement membrane affect the permeability of the vessel. Basement membrane constituents include collagens, laminins, fibronectin, fibrillin, vitronectin, perlecan, and nidogen, as well as growth factors and cytokines, enzymes responsible for matrix degradation, and proteins that adhere to the extracellular matrix, for instance, the semaphorins and lectins. Apart from providing a structural base for cells to adhere to, individual basement membrane components serve as regulators of many biological activities, such as cell growth, repair, differentiation, migration, proliferation, and morphogenesis. The effects of various basement membrane components on cell functions are mediated *via* cell surface receptors, such as integrins and dystroglycan. Mechanosensitive signals conveyed by the extracellular matrix have also been shown to converge with microenvironmental cues, such as growth factors (VEGF) to control transcription factors essential for angiogenesis (Mammoto et al., 2009). However, there is significant variability in the composition of basement membranes between small and large blood vessels throughout the brain. Targeted deletion of basement membrane components causes extensive cortical ectopias and dysplasia (Georges-Labouesse et al., 1998; Anton et al., 1999; Halfter et al., 2002). Although several neurological disturbances have been described as a result of basement membrane disruption, the knockout of nidogen-1 was the first report of a basement membrane gene that resulted in epilepsy. Interestingly, interference with nidogen altered neuronal excitability and synaptic plasticity without obvious underlying structural damage. Our work has shown that nidogen ablation leads to epileptic activity *in vivo* and the appearance of spontaneous epileptiform activity *in vitro* and opened the possibility of modulatory mechanisms of synaptic plasticity and excitability reaching beyond classical processes confined to cellular interactions (Köhling et al., 2006; Vasudevan et al., 2010).

Additionally, 8–20% of patients with laminin α2 deficiency suffer from seizures that arise in early childhood. Seizures were also observed in 8% patients with *LAMA2* mutations, suggesting that seizures may be present in a significant proportion of patients with primary laminin α2 mutations (Jones et al., 2001). Alterations in vasoregulation that included degeneration of pericytes, accompanied by abnormal basement membrane thickening in cerebral microvessels, have been reported in patients with intractable complex partial seizures (Liwnicz et al., 1990). Together, these studies establish contributions of basement membrane dysfunction in epilepsy.

BLOOD-BRAIN BARRIER FAILURE IN EPILEPTOGENESIS

The BBB is a highly complex and dynamic structure that separates the circulating blood from the brain and is mainly composed of endothelial cells, pericytes, astrocytes, and the basement membrane. While an activated vascular system leads to altered angiogenesis, the common phenotype associated with this is an increase in barrier permeability or alteration of adherens junction protein that ultimately leads to disruption of the BBB system (David et al., 2009; Friedman, 2011; Abbott and Friedman, 2012; Bar-Klein et al., 2017; Stern, 2018). The disruption of the BBB can induce a multifaceted pathological process including but not limited to changes in the brain environment, altered neuroglial interactions, maladaptive angiogenesis, and hemodynamic changes in different brain regions. At the cellular level, the BBB is a micro-anatomic structure that mediates exchange of nutrients, xenobiotics, blood components, and cells, which is necessary for brain homeostatic functions (Obermeier et al., 2013). Given the proximity of the BBB microvessels to neurons, it is now increasingly accepted as a cause-effect factor in epilepsy, meaning that BBB failure may result in abnormal excitability of neurons or the neuronal network. Regarding the pathogenesis of epilepsy, after initial speculations on BBB failure leading to epilepsy in the 1960s (Quadbeck, 1968) and experimental studies in the

1970s confirming edema formation in focal experimental epilepsy (Nagy and Fischer, 1978), several seminal papers by the Friedman lab (Seiffert et al., 2004; Ivens et al., 2007; Bar-Klein et al., 2017; Lippmann et al., 2017) established a causality between BBB breakdown and epilepsy, mediated *via* albumin release into the brain parenchyma and subsequent TGF-β-dependent albumin glial uptake. The link between BBB disruption and epileptogenesis was consecutively confirmed in different models. Thus, recent evidence indicates that the dysfunctional BBB can (1) promote seizures, (2) contribute to epileptogenesis, and (3) favor seizure recurrence in patients with epilepsy (Daneman and Prat, 2015; Zhao et al., 2015; Rüber et al., 2018). One of the many proposed mechanisms by which BBB damage can lead to epileptogenesis is *via* a systemic intravascular inflammation (Vezzani and Friedman, 2011; Kim et al., 2017). In light of these findings, one can assume that BBB disruption is the pivotal event, which subsequently can lead to secondary events, such as altered neurovascular coupling (NVC), changes in the morphology of neurovascular network, and altered cerebral blood flow to different brain areas and systemic vascular inflammation (**Figure 1**).

The BBB is far from mature at birth. By embryonic day 15 (E15) in mice, the primitive BBB system is established *via* recruitment of pericytes to blood vessels, interaction of endothelial cells with the astrocytic endfeet, and further modifying the cell-cell junctions (Zhao et al., 2015). The BBB continues to mature after birth, although it is a species-specific temporal event (Daneman and Prat, 2015; Zhao et al., 2015). As the BBB continues to mature, improper establishment can lead to long-term implications in the brain and contribute to epileptogenesis. While a compromised BBB can have severe implications for the availability of glucose or drugs (Cornford and Oldendorf, 1986; Cornford, 1999), the experimental evidence cited above demonstrated direct seizure-promoting effects of a disrupted BBB. From a developmental standpoint, due to the fact that seizure activity is recorded in the postnatal stages, much of the current evidence is based on either animal or human systems analyzed at postnatal stages or during adulthood. One commonality observed in these cases was the presence of a leaky BBB system. A curious question is whether malformed BBB during development predicts epileptogenesis in a brain or whether ectopic events that result in a leaky BBB transform an otherwise healthy brain into an epileptic one? This remains an open-ended question, which Freidman famously stated as the "chicken and the egg puzzle" (Friedman, 2011). The above statement stems from experiments where either acute or chronic disruption of the endothelial tight junctions was induced that resulted in a hypersynchronous epileptiform activity (Seiffert et al., 2004; Marchi et al., 2007). Interestingly in our *Vgat* ^{ECKO} model of epilepsy, we observed a reduction in tight junction proteins (claudin-5 and ZO1), IgG leakage, and increased vascular permeability at embryonic day 17 (Li et al., 2018). Endothelial GABA thus seems to have novel roles in strengthening tight junctions and is important for BBB development (Li et al., 2018).

The mechanisms by which a disrupted BBB in the affected brain can lead to epileptogenesis are multifold. One current hypothesis is that a leaky BBB can cause seizure-promoting components, such as albumin extravasation, excitatory glutamate neurotransmitter, and K^+ ions to act on neuronal cells, which then increase network excitability (Ivens et al., 2007; Köhling and Wolfart, 2016). Pivotally, Ivens et al. found that a leaky BBB releases albumin that binds to TGF-β1 receptors on astrocytes and leads to astrocytic impairment of K^+ spatial buffering and hence increased excitability. In a similar way, after BBB breakdown, glutamate uptake into astrocytes is compromised, thus possibly leading to a loss of excitability regulation as warranted by glutamate buffering (Heinemann et al., 2012). Apart from depolarizing neurons, higher levels of glutamate could also affect endothelial cells. Endothelial cells, including the neuronal cells, express the N-methyl-D-aspartate receptor (NMDAR), which is responsive to glutamate. A study conducted by Vazana et al. (2016) showed that glutamate can act on endothelial NMDAR, thereby inducing a leaky BBB; however, a separate commentary by Xhima et al. (2016) mentioned that since NMDARs are pantropic receptors expressed in the brain, the exclusive role of endothelial cells may not be central to the barrier disruption. In fact, the events might have resulted from an interplay of both vascular and neuronal NMDAR activities (Vazana et al., 2016; Xhima et al., 2016). In addition to endothelial cells, pericytes are also an integral component of the BBB system, and deficiency of pericytes is implicated in barrier disruption (Winkler et al., 2011). Pericytes along with vascular smooth muscle cells have been reported to play a central role in seizure-induced neurovascular remodeling, and these cells are added and removed from veins, arterioles, and capillaries after seizure induction with severe consequences for vessel physiology (Arango-Lievano et al., 2018). Another interesting aspect that is implicated in epilepsy and BBB breakdown, both in TLE patients and in animal experimental models of epilepsy, is the altered expression of aquaporins, the water channels responsible for maintaining fluid homeostasis (Binder et al., 2012; Heinemann et al., 2012). Lastly, also a reduction in GABAergic inhibition could be a factor of BBB breakdown, as demonstrated experimentally in peri-infarct hippocampal tissue (Lippmann et al., 2017).

NEUROVASCULAR COUPLING

The aspect of NVC is an emerging area in the etiology of epilepsy. NVC mechanism broadly entails the relationship between neuronal activity, tissue level oxygenation, and the flow of blood in the affected area (Schwartz, 2007). Cellular contributors to NVC in the neocortex include different types of neurons, endothelial cells, pericytes, vascular smooth muscle cells, and astrocytes. In an epileptic brain, this mechanism is compromised or uncoupled to meet the metabolic demands around epileptic focus and in deep cortical layers (Zhao et al., 2011). Prager et al. reported that seizure-induced injury to the microvasculature is associated with impaired NVC, which ultimately led to BBB dysfunction (Prager et al., 2019). Using a rat ictal model, Ma and colleagues demonstrated, in real time, the dynamics of NVC and uncoupling, during the initiation and events leading up to the termination of an ictal propagation (Ma et al., 2013). The use of voltage-sensitive dyes (VSDs) in their study helped image

the cerebral blood flow (CBF) as well as changes in the membrane potential, indicative of ongoing coupling and uncoupling events in real time. Similarly, through the use of simultaneous three-dimensional (3-D) photoacoustic tomography and EEG, NVC events were validated in an animal model of epilepsy (Wang et al., 2014). Interestingly, in a case study of a patient with acute subarachnoid hemorrhage, events such as impaired NVC to ictal epileptic activity and spreading depolarization were seen. The authors posit that this might be a potential link to the BBB dysfunction (Winkler et al., 2012).

During epileptogenesis, in parallel to the vascular responses, neuronal responses also mediate blood vessel function, such as modulating blood flow or inducing angiogenic activities in the responding niche (Attwell et al., 2010). The two major signaling events involved in this process are the neuronal and the astrocytic signaling. Nitric oxide synthase containing neurons have been reported to participate in coupling between local cortical blood flow and synaptic signaling, a form of NVC that does not depend on metabolic needs (Estrada and DeFelipe, 1998). With respect to the neuronal signaling, NMDA or glutamate activates NMDA receptors on cortical neurons that trigger calcium influx, membrane depolarization, activation of intracellular nitric oxide synthase (neuronal; nNOS), and subsequent release of nitric oxide (Busija et al., 2007). This nitric oxide diffuses to cerebral arteries and arterioles and causes vasodilation, modulating the blood flow. The mechanism causes relaxation of the vascular smooth muscles without the involvement of astrocytes or endothelial cells. In astrocyte signaling, it is theorized that blood vessel dilation may occur through a K^+-based mechanism *via* modulatory effects of oxygen (O_2; Attwell et al., 2010).

GABAergic interneurons are also known to provide an exceptionally rich innervation to local microvessels and can transmute afferent neuronal signals to appropriate vascular responses, thus acting as local integrators of NVC (Vaucher et al., 2000; Cauli et al., 2004). Changes in blood flow have also been implicated in providing spatial and temporal information by modulating the neural activity and regulating the excitability of cortical circuits (Moore and Cao, 2008). Thus, a deeper understanding of hemodynamics and neural activity can be applied for elucidating vascular dysfunctions in epilepsy.

INFLAMMATION AND NETWORK EXCITABILITY

The mature vasculature and the mature nervous system can respond to infection or injury by activating defense mechanisms including inflammation. Another aspect in the development

TABLE 1 | Studies of interest in vascular-based human studies of epilepsy.

Method	Type of sample	Findings	References
Immunohistochemistry	Post mortem hippocampal sections	Altered microvascular network	Kastanauskaite et al. (2009) and Alonso-Nanclares and DeFelipe (2014)
ESI/MSI and BOLD	Patient population	Blood oxygenation level-dependent (BOLD) signal changes at the time of interictal epileptic discharges (IEDs) to identify their associated vascular/hemodynamic responses	Heers et al. (2014)
Sandwich enzyme-linked immunosorbent assay to determine Adhesion Molecules in CSF and sera	Patient group	Detection of soluble vascular cell adhesion molecule-1 (sVCAM-1) and soluble intercellular adhesion molecule-1 (sICAM-1) in sera, and CSF	Luo et al. (2014)
7T imaging	Patient group	Vascular dysgenesis implicated in the pathogenesis of polymicrogyria and epilepsy	De Ciantis et al. (2015)
Protein expression *via* Western Blotting	Patient group	Increased protein expression of VEGF-A, VEGF-B, VEGF-C, and their receptors in the temporal neocortex of pharmacoresistant temporal lobe epilepsy patients.	Castañeda-Cabral et al. (2019)
		Elevated expression of VEGF-C and its receptors, VEGFR-2 and VEGFR-3, in patients with mesial temporal lobe epilepsy	Sun et al. (2016)
Neuropsychological assessment, clinical examination, and fasting blood evaluation for quantification of vascular status	Patient group	Aging persons with chronic epilepsy exhibit multiple abnormalities in metabolic, inflammatory, and vascular health that are associated with poorer cognitive function	Hermann et al. (2017)
Molecular and biochemical methods	Patient group	cDNA microarray showed the presence of CYP enzymes in isolated human primary brain endothelial cells	Ghosh et al. (2010)
Molecular and Biochemical methods	Post mortem and patient group	Endothelial cells of blood vessels are the major source of IL-17	He et al. (2016)
Immunohistochemistry	Patient group	Reduced ratio of afferent to total vascular density in mesial temporal sclerosis. Significant reduction in the density of afferent vessels	Mott et al. (2009)

ESI/MSI, electric source imaging/magnetic source imaging; BOLD, blood-oxygen-level-dependent; VEGF, vascular endothelial growth factor receptor; CYP, cytochrome P-450.

of epileptogenesis is inflammation in the brain that serves as an essential feature in hyperexcitable brain regions or tissues. Interestingly, endothelial cells are at the forefront of an inflammatory cascade. In this context, given the heterogeneity of the cerebral vasculature, pathological deviations from normal functions can directly impact neuronal firing events (Librizzi et al., 2018). Therefore, it is not surprising that an event that triggers seizure or epileptic activity in the brain will directly or indirectly affect the vasculature (Vezzani et al., 2010, 2013). Studies reveal that the inflammatory receptor TGF-β-mediated signaling cascade is one of the central processes that mediate key events associated with epileptogenesis (Cacheaux et al., 2009). *In vivo* studies utilizing a murine model of CD8 T-cell-mediated central nervous system inflammation demonstrated that neuronal VEGF is significantly upregulated, which is typical of neuroinflammation-induced BBB disruption (Suidan et al., 2010). While the group did not measure epileptic events in these mice, this study demonstrates the cellular interplay that can precipitate into epileptic events. Similarly, CCR5, a chemokine that regulates inflammatory processes was shown to control vascular inflammation and leukocyte recruitment during acute excitotoxic seizure induction and neural damage (Louboutin et al., 2011). Endothelial inflammasome molecules, such as NLRP1 and NLRP3, NOD1 and NOD2, and NLRC4 and NLRC5, have been implicated in brain injury processes, and these molecules can further our understanding of functional congruence at the vascular-neuron interface (Lénárt et al., 2016). Indeed, various neurological insults result in alterations of inflammatory mechanisms (Kim et al., 2017). The reports included in this review are not exhaustive. A similar correlation can be inferred from additional scientific evidences supported by either non-rodent or primate models of epilepsy. We have summarized some of the key studies in the epileptic patient population that were vascular centric in **Table 1**.

VASCULAR THERAPY FOR EPILEPSY

Today, most of the pharmacological compounds available for epilepsy treatment are partially effective. One major reason is that the majority of people exhibit drug-resistant epilepsy (Walker and Köhling, 2013). An emerging consensus for this ineffectiveness of clinically available drugs is because majority of the drugs are designed in a way to target molecules and receptors specific to the neuronal cells. This is where we reiterate the need for pharmacologic compounds or biologics that can also target the non-neuronal cell population, such as the endothelial cells. Additionally, it is important to have a better understanding of cell type-specific contributions in epilepsy disease origin and a realization that it is not primarily a neuronal dysfunction. Remediating the BBB could be one option to prevent or shunt epileptogenesis (Shlosberg et al., 2010). Thus, BBB-affecting drugs such glucocorticosteroids have been used in children with difficult-to-treat epilepsies and were effective in reducing drug-resistant seizures and for restoration of BBB function (Marchi et al., 2012). Additionally, BBB-affecting drugs like natalizumab and IL-1RA act on proinflammatory mediators and have been tested in cases of refractory epilepsy, initially leading to suppression of seizures (Sotgiu et al., 2010), however, harboring the risk of severe side effects in the long run (Abkur et al., 2018). Thus, a search for less strongly interfering drugs is clearly necessary.

One possible intervention may be a modulation of mammalian target of rapamycin (mTOR). In neuron-specific (NS)-PTEN-depleted mice, progression into epileptogenesis was blocked by inhibiting mTOR signaling (Sunnen et al., 2011). Because aberrant mTOR signaling is concomitant with an increase in vessel density in epileptic patients, it will be interesting to see if targeting endothelial mTOR might alleviate or lead to a remission of epilepsy symptoms. In addition, an adjunct area that can be explored is the hormone therapy in epileptic patients. To this end, convincing data indicate that endothelial cells express estrogen or progesterone receptors, and both of these hormones have been shown to protect from vascular injury/BBB dysfunction in rodent models (Si et al., 2014; Shin et al., 2016; Yu et al., 2017). Therefore, targeting the vascular hormone receptors may serve as another approach to restore BBB defects, as well as for improving the angiogenic outcome in epileptogenesis. The vasoactive effects of soluble matrix proteins and integrin ligands may be tapped into in order to regulate calcium influx and modulate blood flow in arteries (Wu et al., 1998). For instance, identification of alterations in extracellular matrix-integrin signaling and treatment of epileptic mice with integrin blockers resulted in a significant reduction in kindling epileptogenesis (Wu et al., 2017). Another study has reported that loss of mural cells (that includes pericytes and vascular smooth muscle cells) is proportional to seizure severity and vascular pathology. Interestingly, intravenous treatment with platelet-derived growth factor subunits BB (PDGF-BB) activated PDGFRβ in mural cells, ameliorating vessel coverage with mural cells, vessel functions, and reducing spontaneous EEG epileptiform activity (Arango-Lievano et al., 2018). An added perspective in managing intractable epilepsy is introducing the ketogenic diet (KD). At least experimentally, KD may also positively affect astrocytic monocarboxylate transporters, and this change in turn in a recent study was associated with seizure reduction (Forero-Quintero et al., 2017). Since the molecular mechanisms of KD are far from understood, it would be interesting to understand the implication of KD on blood vessels, which can further our knowledge in designing effective diet-based interventions for epileptogenesis. While the list is not extensive, collectively, these studies bring to light the importance of vascular therapy in epilepsy.

In continuation, another experimental treatment for epilepsy is stem cell-based therapy. Human pluripotent stem cell (hPSC)-derived GABAergic interneurons can serve as a potential cell therapy for epilepsy because the therapeutic strategies are multiple: general secretion of GABA by the grafted cells to increase the seizure threshold, direct replacement of malfunctioning or lost GABAergic interneurons, or modulation of the excitatory hyperactive system (Cunningham et al., 2014; Zhu et al., 2018). However, one issue that needs improvement is the migration efficiency of transplanted cells.

Transplanted human interneurons displayed minimal migration and distribution at 2 weeks posttransplantation. It was only at 4–7 months posttransplantation that migration and integration into the host brain were observed (Cunningham et al., 2014; Kim et al., 2014; Zhu et al., 2018; Upadhya et al., 2019). Therefore, the beneficial effects of interneuron graft-in-disease models were delayed to several months after transplantation. Another drawback is a reduction in GABA levels after transplantation that has been reported by some groups (Nolte et al., 2008; Alvarez Dolado and Broccoli, 2011). These are some current issues with moving this promising therapeutic treatment to the clinic. Vascular therapy could serve to improve this treatment strategy. Since the periventricular vascular network is the natural substrate for GABAergic neuronal migration in the embryonic forebrain, it can serve to improve hPSC-derived GABAergic neuronal migration. We have generated human periventricular-like endothelial cells in our laboratory using the hPSC technology that significantly improved the rate of human GABAergic neuronal migration after transplantation, with high GABA release levels (Datta et al., 2018). This endothelial-neuronal cotransplantation strategy may have significant benefits for brain repair in epilepsy.

CONCLUSION AND PERSPECTIVES

In this review, we attempt to shed light on how vascular health is crucial, if not one of the primary factors leading up to epileptogenesis. Greater challenges in the field are some of these lingering questions: (1) How to effectively target and prevent the brain from becoming hyperexcitable and seizure-prone after the first episode of seizure? (2) Which parameters in the blood vessel can help identify a brain that can become epileptic after ictal events? (3) Can we tap into the gene expression in embryonic forebrain blood vessels for better understanding of epilepsy? (4) Can we effectively use knowledge gained from developmental and vasculature-related studies to design interventions that will be effective in the clinic? These unmet questions warrant a deeper understanding and more research, necessitating new work highlighting vascular health. Molecular and mechanism-based studies can provide deeper understanding of pathways or genetic components involved in epileptogenesis. Translational studies or patient-based studies should be carefully evaluated to design targeted therapies in better management of this disease. Perhaps, fine tuning the vascular contribution or role in epileptogenesis can help find a "missing link" in epileptogenesis and will potentially serve as diagnostic or prognostic marker in years to come.

AUTHOR CONTRIBUTIONS

All authors listed have made a substantial, direct and intellectual contribution to the work, and approved it for publication.

FUNDING

This work was supported by awards from the National Institute of Mental Health (R01MH110438) and National Institute of Neurological Disorders and Stroke (R01NS100808) to AV and the DFG (KO 1779 14-1, as well as TPC03 of CRC 1270 ELAINE) to RK.

REFERENCES

Abbott, N. J., and Friedman, A. (2012). Overview and introduction: the blood-brain barrier in health and disease. *Epilepsia* 53(Suppl. 6), 1–6. doi: 10.1111/j.1528-1167.2012.03696.x

Abkur, T. M., Kearney, H., and Hennessy, M. J. (2018). Refractory epilepsy following natalizumab associated PML. *Mult. Scler. Relat. Disord.* 20, 1–2. doi: 10.1016/j.msard.2017.12.004

Alonso-Nanclares, L., and DeFelipe, J. (2014). Alterations of the microvascular network in the sclerotic hippocampus of patients with temporal lobe epilepsy. *Epilepsy Behav.* 38, 48–52. doi: 10.1016/j.yebeh.2013.12.009

Alvarez Dolado, M., and Broccoli, V. (2011). GABAergic neuronal precursor grafting: implications in brain regeneration and plasticity. *Neural Plast.* 2011:384216. doi: 10.1155/2011/384216

Anton, E. S., Kreidberg, J. A., and Rakic, P. (1999). Distinct functions of α3 and αV integrin receptors in neuronal migration and laminar organization of the cerebral cortex. *Neuron* 22, 277–289. doi: 10.1016/S0896-6273(00)81089-2

Arango-Lievano, M., Boussadia, B., De Terdonck, L. D. T., Gault, C., Fontanaud, P., Lafont, C., et al. (2018). Topographic reorganization of cerebrovascular mural cells under seizure conditions. *Cell Rep.* 23, 1045–1059. doi: 10.1016/j.celrep.2018.03.110

Attwell, D., Buchan, A. M., Charpak, S., Lauritzen, M., Macvicar, B. A., and Newman, E. A. (2010). Glial and neuronal control of brain blood flow. *Nature* 468, 232–243. doi: 10.1038/nature09613

Avoli, M., Louvel, J., Pumain, R., and Köhling, R. (2005). Cellular and molecular mechanisms of epilepsy in the human brain. *Prog. Neurobiol.* 77, 166–200. doi: 10.1016/j.pneurobio.2005.09.006

Bar-Klein, G., Lublinsky, S., Kamintsky, L., Noyman, I., Veksler, R., Dalipaj, H., et al. (2017). Imaging blood–brain barrier dysfunction as a biomarker for epileptogenesis. *Brain* 140, 1692–1705. doi: 10.1093/brain/awx073

Barkovich, A. J., Dobyns, W. B., and Guerrini, R. (2015). Malformations of cortical development and epilepsy. *Cold Spring Harb. Perspect. Med.* 5:a022392. doi: 10.1101/cshperspect.a022392

Baruah, J., and Vasudevan, A. (2019). The vessels shaping mental health or illness. *Open Neurol. J.* 13, 1–9. doi: 10.2174/1874205X01913010001

Beghi, E., Giussani, G., Nichols, E., Abd-Allah, F., Abdela, J., Abdelalim, A., et al. (2019). Global, regional, and national burden of epilepsy, 1990–2016: a systematic analysis for the global burden of disease study 2016. *Lancet Neurol.* 18, 357–375. doi: 10.1016/S1474-4422(18)30454-X

Benini, R., Roth, R., Khoja, Z., Avoli, M., and Wintermark, P. (2016). Does angiogenesis play a role in the establishment of mesial temporal lobe epilepsy? *Int. J. Dev. Neurosci.* 49, 31–36. doi: 10.1016/j.ijdevneu.2016.01.001

Binder, D. K., Nagelhus, E. A., and Ottersen, O. P. (2012). Aquaporin-4 and epilepsy. *Glia* 60, 1203–1214. doi: 10.1002/glia.22317

Blinder, P., Tsai, P. S., Kaufhold, J. P., Knutsen, P. M., Suhl, H., and Kleinfeld, D. (2013). The cortical angiome: an interconnected vascular network with noncolumnar patterns of blood flow. *Nat. Neurosci.* 16, 889–897. doi: 10.1038/nn.3426

Busija, D. W., Bari, F., Domoki, F., and Louis, T. (2007). Mechanisms involved in the cerebrovascular dilator effects of N-methyl-d-aspartate in cerebral cortex. *Brain Res. Rev.* 56, 89–100. doi: 10.1016/j.brainresrev.2007.05.011

Cacheaux, L. P., Ivens, S., David, Y., Lakhter, A. J., Bar-Klein, G., Shapira, M., et al. (2009). Transcriptome profiling reveals TGF-β signaling involvement in epileptogenesis. *J. Neurosci.* 29, 8927–8935. doi: 10.1523/JNEUROSCI.0430-09.2009

Carmeliet, P. (2003). Angiogenesis in health and disease. *Nat. Med.* 9, 653–660. doi: 10.1038/nm0603-653

Carmeliet, P. (2005). Angiogenesis in life, disease and medicine. *Nature* 438, 932–936. doi: 10.1038/nature04478

Carmeliet, P., and Tessier-Lavigne, M. (2005). Common mechanisms of nerve and blood vessel wiring. *Nature* 436, 193–200. doi: 10.1038/nature03875

Castañeda-Cabral, J. L., Beas-Zárate, C., Rocha-Arrieta, L. L., Orozco-Suárez, S. A., Alonso-Vanegas, M., Guevara-Guzmán, R., et al. (2019). Increased protein expression of VEGF-A, VEGF-B, VEGF-C and their receptors in the temporal neocortex of pharmacoresistant temporal lobe epilepsy patients. *J. Neuroimmunol.* 328, 68–72. doi: 10.1016/j.jneuroim.2018.12.007

Cauli, B., Tong, X.-K., Rancillac, A., Serluca, N., Lambolez, B., Rossier, J., et al. (2004). Cortical GABA interneurons in neurovascular coupling: relays for subcortical vasoactive pathways. *J. Neurosci.* 24, 8940–8949. doi: 10.1523/JNEUROSCI.3065-04.2004

Choi, Y. K., and Vasudevan, A. (2019). Mechanistic insights into autocrine and paracrine roles of endothelial GABA signaling in the embryonic forebrain. *Sci. Rep.* 9, 16256.

Cornford, E. M. (1999). Epilepsy and the blood brain barrier: endothelial cell responses to seizures. *Adv. Neurol.* 79, 845–862.

Cornford, E. M., and Oldendorf, W. H. (1986). Epilepsy and the blood-brain barrier. *Adv. Neurol.* 44, 787–812.

Croll, S. D., Goodman, J. H., and Scharfman, H. E. (2004). Vascular endothelial growth factor (VEGF) in seizures: a double-edged sword. *Adv. Exp. Med. Biol.* 548, 57–68. doi: 10.1007/978-1-4757-6376-8_4

Cunningham, M., Cho, J.-H., Leung, A., Savvidis, G., Ahn, S., Moon, M., et al. (2014). hPSC-derived maturing GABAergic interneurons ameliorate seizures and abnormal behavior in epileptic mice. *Cell Stem Cell* 15, 559–573. doi: 10.1016/j.stem.2014.10.006

Daneman, R., and Prat, A. (2015). The blood–brain barrier. *Cold Spring Harb. Perspect. Biol.* 7:a020412. doi: 10.1101/cshperspect.a020412

David, Y., Cacheaux, L. P., Ivens, S., Lapilover, E., Heinemann, U., Kaufer, D., et al. (2009). Astrocytic dysfunction in epileptogenesis: consequence of altered potassium and glutamate homeostasis? *J. Neurosci.* 29, 10588–10599. doi: 10.1523/JNEUROSCI.2323-09.2009

Datta, D., Subburaju, S., Kaye, S., and Vasudevan, A. (2018). "Human forebrain endothelial cells for cell-based therapy of neuropsychiatric disorders" in *Proceedings of 22nd Biennial Meeting of the International Society for Developmental Neuroscience*. Nara, Japan.

De Ciantis, A., Barkovich, A. J., Cosottini, M., Barba, C., Montanaro, D., Costagli, M., et al. (2015). Ultra-high-field MR imaging in polymicrogyria and epilepsy. *AJNR Am. J. Neuroradiol.* 36, 309–316. doi: 10.3174/ajnr.A4116

Devinsky, O., Vezzani, A., O'Brien, T. J., Jette, N., Scheffer, I. E., de Curtis, M., et al. (2018). Epilepsy. *Nat. Rev. Dis. Primers.* 4:18024. doi: 10.1038/nrdp.2018.24

Eichmann, A., Noble, F. L., Autiero, M., and Carmeliet, P. (2005). Guidance of vascular and neural network formation. *Curr. Opin. Neurobiol.* 15, 108–115. doi: 10.1016/j.conb.2005.01.008

Estrada, C., and DeFelipe, J. (1998). Nitric oxide-producing neurons in the neocortex: morphological and functional relationship with intraparenchymal microvasculature. *Cereb. Cortex* 8, 193–203. doi: 10.1093/cercor/8.3.193

Feng, L., Shu, Y., Wu, Q., Liu, T., Long, H., Yang, H., et al. (2017). EphA4 may contribute to microvessel remodeling in the hippocampal CA1 and CA3 areas in a mouse model of temporal lobe epilepsy. *Mol. Med. Rep.* 15, 37–46. doi: 10.3892/mmr.2016.6017

Forero-Quintero, L. S., Deitmer, J. W., and Becker, H. M. (2017). Reduction of epileptiform activity in ketogenic mice: the role of monocarboxylate transporters. *Sci. Rep.* 7:4900. doi: 10.1038/s41598-017-05054-0

Friedman, A. (2011). Blood-brain barrier dysfunction, status epilepticus, seizures, and epilepsy: a puzzle of a chicken and egg? *Epilepsia* 52(Suppl. 8), 19–20. doi: 10.1111/j.1528-1167.2011.03227.x

Georges-Labouesse, E., Mark, M., Messaddeq, N., and Gansmüller, A. (1998). Essential role of α6 integrins in cortical and retinal lamination. *Curr. Biol.* 8, 983–986. doi: 10.1016/S0960-9822(98)70402-6

Ghosh, C., Gonzalez-Martinez, J., Hossain, M., Cucullo, L., Fazio, V., Janigro, D., et al. (2010). Pattern of P450 expression at the human blood-brain barrier: roles of epileptic condition and laminar flow. *Epilepsia* 51, 1408–1417. doi: 10.1111/j.1528-1167.2009.02428.x

Haigh, J. J., Morelli, P. I., Gerhardt, H., Haigh, K., Tsien, J., Damert, A., et al. (2003). Cortical and retinal defects caused by dosage-dependent reductions in VEGF-A paracrine signaling. *Dev. Biol.* 262, 225–241. doi: 10.1016/S0012-1606(03)00356-7

Halfter, W., Dong, S., Yip, Y.-P., Willem, M., and Mayer, U. (2002). A critical function of the pial basement membrane in cortical histogenesis. *J. Neurosci.* 22, 6029–6040. doi: 10.1523/JNEUROSCI.22-14-06029.2002

Hauser, W. A., and Mohr, J. P. (2011). Seizures, epilepsy, and vascular malformations. *Neurology* 76, 1540–1541. doi: 10.1212/WNL.0b013e318219fb97

He, J.-J., Sun, F.-J., Wang, Y., Luo, X.-Q., Lei, P., Zhou, J., et al. (2016). Increased expression of interleukin 17 in the cortex and hippocampus from patients with mesial temporal lobe epilepsy. *J. Neuroimmunol.* 298, 153–159. doi: 10.1016/j.jneuroim.2016.07.017

Heers, M., Hedrich, T., An, D., Dubeau, F., Gotman, J., Grova, C., et al. (2014). Spatial correlation of hemodynamic changes related to interictal epileptic discharges with electric and magnetic source imaging. *Hum. Brain Mapp.* 35, 4396–4414. doi: 10.1002/hbm.22482

Heinemann, U., Kaufer, D., and Friedman, A. (2012). Blood-brain barrier dysfunction, TGFβ signaling, and astrocyte dysfunction in epilepsy. *Glia* 60, 1251–1257. doi: 10.1002/glia.22311

Hermann, B. P., Sager, M. A., Koscik, R. L., Young, K., and Nakamura, K. (2017). Vascular, inflammatory, and metabolic factors associated with cognition in aging persons with chronic epilepsy. *Epilepsia* 58, e152–e156. doi: 10.1111/epi.13891

Ivens, S., Kaufer, D., Flores, L. P., Bechmann, I., Zumsteg, D., Tomkins, O., et al. (2007). TGF-β receptor-mediated albumin uptake into astrocytes is involved in neocortical epileptogenesis. *Brain* 130, 535–547. doi: 10.1093/brain/awl317

Jones, K. J., Morgan, G., Johnston, H., Tobias, V., Ouvrier, R. A., Wilkinson, I., et al. (2001). The expanding phenotype of laminin alpha2 chain (merosin) abnormalities: case series and review. *J. Med. Genet.* 38, 649–657. doi: 10.1136/jmg.38.10.649

Kang, J.-Q., and Macdonald, R. L. (2009). Making sense of nonsense GABA(A) receptor mutations associated with genetic epilepsies. *Trends Mol. Med.* 15, 430–438. doi: 10.1016/j.molmed.2009.07.003

Karakatsani, A., Shah, B., and Ruiz de Almodovar, C. (2019). Blood vessels as regulators of neural stem cell properties. *Front. Mol. Neurosci.* 12:85. doi: 10.3389/fnmol.2019.00085

Kastanauskaite, A., Alonso-Nanclares, L., Blazquez-Llorca, L., Pastor, J., Sola, R. G., and DeFelipe, J. (2009). Alterations of the microvascular network in sclerotic hippocampi from patients with epilepsy. *J. Neuropathol. Exp. Neurol.* 68, 939–950. doi: 10.1097/NEN.0b013e3181b08622

Kim, S. Y., Senatorov, V. V. Jr., Morrissey, C. S., Lippmann, K., Vazquez, O., Milikovsky, D. Z., et al. (2017). TGFβ signaling is associated with changes in inflammatory gene expression and perineuronal net degradation around inhibitory neurons following various neurological insults. *Sci. Rep.* 7:7711. doi: 10.1038/s41598-017-07394-3

Kim, T.-G., Yao, R., Monnell, T., Cho, J.-H., Vasudevan, A., Koh, A., et al. (2014). Efficient specification of interneurons from human pluripotent stem cells by dorsoventral and rostrocaudal modulation. *Stem Cells* 32, 1789–1804. doi: 10.1002/stem.1704

Köhling, R., Nischt, R., Vasudevan, A., Ho, M., Weiergräber, M., Schneider, T., et al. (2006). Nidogen and nidogen-associated basement membrane proteins and neuronal plasticity. *Neurodegener Dis.* 3, 56–61. doi: 10.1159/000092094

Köhling, R., and Wolfart, J. (2016). Potassium channels in epilepsy. *Cold Spring Harb. Perspect. Med.* 6:a022871. doi: 10.1101/cshperspect.a022871

Lénárt, N., Brough, D., and Dénes, Á. (2016). Inflammasomes link vascular disease with neuroinflammation and brain disorders. *J. Cereb. Blood Flow Metab.* 36, 1668–1685. doi: 10.1177/0271678X16662043

Li, S., Haigh, K., Haigh, J. J., and Vasudevan, A. (2013). Endothelial VEGF sculpts cortical cytoarchitecture. *J. Neurosci.* 33:14809. doi: 10.1523/JNEUROSCI.1368-13.2013

Li, S., Kumar, T. P., Joshee, S., Kirschstein, T., Subburaju, S., Khalili, J. S., et al. (2018). Endothelial cell-derived GABA signaling modulates neuronal migration and postnatal behavior. *Cell Res.* 28, 221–248. doi: 10.1038/cr.2017.135

Librizzi, L., de Cutis, M., Janigro, D., Runtz, L., de Bock, F., Barbier, E. L., et al. (2018). Cerebrovascular heterogeneity and neuronal excitability. *Neurosci. Lett.* 667, 75–83. doi: 10.1016/j.neulet.2017.01.013

Lippmann, K., Kamintsky, L., Kim, S. Y., Lublinsky, S., Prager, O., Nichtweiss, J. F., et al. (2017). Epileptiform activity and spreading depolarization in the

blood-brain barrier-disrupted peri-infarct hippocampus are associated with impaired GABAergic inhibition and synaptic plasticity. *J. Cereb. Blood Flow Metab.* 37, 1803–1819. doi: 10.1177/0271678X16652631

Liwnicz, B. H., Leach, J. L., Yeh, H.-S., and Privitera, M. (1990). Pericyte degeneration and thickening of basement membranes of cerebral microvessels in complex partial seizures: electron microscopic study of surgically removed tissue. *Neurosurgery* 26, 409–420. doi: 10.1227/00006123-199003000-00006

Louboutin, J.-P., Chekmasova, A., Marusich, E., Agrawal, L., and Strayer, D. S. (2011). Role of CCR5 and its ligands in the control of vascular inflammation and leukocyte recruitment required for acute excitotoxic seizure induction and neural damage. *FASEB J.* 25, 737–753. doi: 10.1096/fj.10-161851

Luo, J., Wang, W., Xi, Z., Dan, C., Wang, L., Xiao, Z., et al. (2014). Concentration of soluble adhesion molecules in cerebrospinal fluid and serum of epilepsy patients. *J. Mol. Neurosci.* 54, 767–773. doi: 10.1007/s12031-014-0366-8

Ma, H., Zhao, M., and Schwartz, T. H. (2013). Dynamic neurovascular coupling and uncoupling during ictal onset, propagation, and termination revealed by simultaneous in vivo optical imaging of neural activity and local blood volume. *Cereb. Cortex* 23, 885–899. doi: 10.1093/cercor/bhs079

Mammoto, A., Connor, K. M., Mammoto, T., Yung, C. W., Huh, D., Aderman, C. M., et al. (2009). A mechanosensitive transcriptional mechanism that controls angiogenesis. *Nature* 457, 1103–1108. doi: 10.1038/nature07765

Marchi, N., Angelov, L., Masaryk, T., Fazio, V., Granata, T., Hernandez, N., et al. (2007). Seizure-promoting effect of blood–brain barrier disruption. *Epilepsia* 48, 732–742. doi: 10.1111/j.1528-1167.2007.00988.x

Marchi, N., Granata, T., Ghosh, C., and Janigro, D. (2012). Blood-brain barrier dysfunction and epilepsy: pathophysiologic role and therapeutic approaches. *Epilepsia* 53, 1877–1886. doi: 10.1111/j.1528-1167.2012.03637.x

Marchi, N., Tierney, W., Alexopoulos, A. V., Puvenna, V., Granata, T., and Janigro, D. (2011). The etiological role of blood-brain barrier dysfunction in seizure disorders. *Cardiovasc. Psychiatry Neurol.* 2011:482415. doi: 10.1155/2011/482415

Moore, C. I., and Cao, R. (2008). The hemo-neural hypothesis: on the role of blood flow in information processing. *J. Neurophysiol.* 99, 2035–2047. doi: 10.1152/jn.01366.2006

Morin-Brureau, M., Lebrun, A., Rousset, M.-C., Fagni, L., Bockaert, J., de Bock, F., et al. (2011). Epileptiform activity induces vascular remodeling and zonula occludens 1 downregulation in organotypic hippocampal cultures: role of VEGF signaling pathways. *J. Neurosci.* 31, 10677–10688. doi: 10.1523/JNEUROSCI.5692-10.2011

Mott, R. T., Thore, C. R., Moody, D. M., Glazier, S. S., Ellis, T. L., and Brown, W. R. (2009). Reduced ratio of afferent to total vascular density in mesial temporal sclerosis. *J. Neuropathol. Exp. Neurol.* 68, 1147–1154. doi: 10.1097/NEN.0b013e3181b9d75f

Nagy, Z., and Fischer, J. (1978). Development of periforcal edema in experimental epilepsy induced by cobalt-gelatin. *Acta Neuropathol.* 41, 191–195. doi: 10.1007/BF00690434

Ndode-Ekane, X. E., Hayward, N., Gröhn, O., and Pitkänen, A. (2010). Vascular changes in epilepsy: functional consequences and association with network plasticity in pilocarpine-induced experimental epilepsy. *Neuroscience* 166, 312–332. doi: 10.1016/j.neuroscience.2009.12.002

Neligan, A., Hauser, W. A., and Sander, J. W. (2012). "Chapter 6—The epidemiology of the epilepsies" in *Handbook of clinical neurology*. eds. H. Stefan and W. H. Theodore (Amsterdam, Netherlands: Elsevier), 113–133.

Nicoletti, J. N., Lenzer, J., Salerni, E. A., Shah, S. K., Elkady, A., Khalid, S., et al. (2010). Vascular endothelial growth factor attenuates status epilepticus-induced behavioral impairments in rats. *Epilepsy Behav.* 19, 272–277. doi: 10.1016/j.yebeh.2010.07.011

Nicoletti, J. N., Shah, S. K., McCloskey, D. P., Goodman, J. H., Elkady, A., Atassi, H., et al. (2008). Vascular endothelial growth factor is up-regulated after status epilepticus and protects against seizure-induced neuronal loss in hippocampus. *Neuroscience* 151, 232–241. doi: 10.1016/j.neuroscience.2007.09.083

Nolte, M. W., Löscher, W., Herden, C., Freed, W. J., and Gernert, M. (2008). Benefits and risks of intranigral transplantation of GABA-producing cells subsequent to the establishment of kindling-induced seizures. *Neurobiol. Dis.* 31, 342–354. doi: 10.1016/j.nbd.2008.05.010

Obermeier, B., Daneman, R., and Ransohoff, R. M. (2013). Development, maintenance and disruption of the blood-brain barrier. *Nat. Med.* 19, 1584–1596. doi: 10.1038/nm.3407

Paredes, I., Himmels, P., and Ruiz de Almodóvar, C. (2018). Neurovascular communication during CNS development. *Dev. Cell* 45, 10–32. doi: 10.1016/j.devcel.2018.01.023

Prager, O., Kamintsky, L., Hasam-Henderson, L. A., Schoknecht, K., Wuntke, V., Papageorgiou, I., et al. (2019). Seizure-induced microvascular injury is associated with impaired neurovascular coupling and blood–brain barrier dysfunction. *Epilepsia* 60, 322–336. doi: 10.1111/epi.14631

Quadbeck, G. (1968). "Clinical importance of alterations in barrier" in *Progress in brain research*. eds. A. Lajtha and D. H. Ford (Amsterdam, Netherlands: Elsevier), 343–348.

Rigau, V., Morin, M., Rousset, M.-C., de Bock, F., Lebrun, A., Coubes, P., et al. (2007). Angiogenesis is associated with blood–brain barrier permeability in temporal lobe epilepsy. *Brain* 130, 1942–1956. doi: 10.1093/brain/awm118

Rüber, T., David, B., Lüchters, G., Nass, R. D., Friedman, A., Surges, R., et al. (2018). Evidence for peri-ictal blood–brain barrier dysfunction in patients with epilepsy. *Brain* 141, 2952–2965. doi: 10.1093/brain/awy242

Ruhrberg, C., and Bautch, V. L. (2013). Neurovascular development and links to disease. *Cell. Mol. Life Sci.* 70, 1675–1684. doi: 10.1007/s00018-013-1277-5

Schwartz, T. H. (2007). Neurovascular coupling and epilepsy: hemodynamic markers for localizing and predicting seizure onset. *Epilepsy Curr.* 7, 91–94. doi: 10.1111/j.1535-7511.2007.00183.x

Seiffert, E., Dreier, J. P., Ivens, S., Bechmann, I., Tomkins, O., Heinemann, U., et al. (2004). Lasting blood-brain barrier disruption induces epileptic focus in the rat somatosensory cortex. *J. Neurosci.* 24, 7829–7836. doi: 10.1523/JNEUROSCI.1751-04.2004

Shin, J. A., Yoon, J. C., Kim, M., and Park, E.-M. (2016). Activation of classical estrogen receptor subtypes reduces tight junction disruption of brain endothelial cells under ischemia/reperfusion injury. *Free Radic. Biol. Med.* 92, 78–89. doi: 10.1016/j.freeradbiomed.2016.01.010

Shlosberg, D., Benifla, M., Kaufer, D., and Friedman, A. (2010). Blood-brain barrier breakdown as a therapeutic target in traumatic brain injury. *Nat. Rev. Neurol.* 6, 393–403. doi: 10.1038/nrneurol.2010.74

Si, D., Li, J., Liu, J., Wang, X., Wei, Z., Tian, Q., et al. (2014). Progesterone protects blood-brain barrier function and improves neurological outcome following traumatic brain injury in rats. *Exp. Ther. Med.* 8, 1010–1014. doi: 10.3892/etm.2014.1840

Sotgiu, S., Murrighile, M. R., and Constantin, G. (2010). Treatment of refractory epilepsy with natalizumab in a patient with multiple sclerosis. Case report. *BMC Neurol.* 10:84. doi: 10.1186/1471-2377-10-84

Stafstrom, C. E., and Carmant, L. (2015). Seizures and epilepsy: an overview for neuroscientists. *Cold Spring Harb. Perspect. Med.* 5:a022426. doi: 10.1101/cshperspect.a022426

Stern, P. (2018). Developing the blood-brain barrier. *Science* 361, 763–765. doi: 10.1126/science.361.6404.763-k

Stubbs, D., DeProto, J., Nie, K., Englund, C., Mahmud, I., Hevner, R., et al. (2009). Neurovascular congruence during cerebral cortical development. *Cereb. Cortex* 19(Suppl. 1), i32–i41. doi: 10.1093/cercor/bhp040

Suidan, G. L., Dickerson, J. W., Chen, Y., McDole, J. R., Tripathi, P., Pirko, I., et al. (2010). CD8 T cell-initiated vascular endothelial growth factor expression promotes central nervous system vascular permeability under neuroinflammatory conditions. *J. Immunol.* 184, 1031–1040. doi: 10.4049/jimmunol.0902773

Sun, F.-J., Wei, Y.-J., Li, S., Guo, W., Chen, X., Liu, S.-Y., et al. (2016). Elevated expression of VEGF-C and its receptors, VEGFR-2 and VEGFR-3, in patients with mesial temporal lobe epilepsy. *J. Mol. Neurosci.* 59, 241–250. doi: 10.1007/s12031-016-0714-y

Sunnen, C. N., Brewster, A. L., Lugo, J. N., Vanegas, F., Turcios, E., Mukhi, S., et al. (2011). Inhibition of the mammalian target of rapamycin blocks epilepsy progression in NS-Pten conditional knockout mice. *Epilepsia* 52, 2065–2075. doi: 10.1111/j.1528-1167.2011.03280.x

Trinka, E., Krämer, G., and Werhahn, K. (2015). Vascular precursor epilepsy — old wine in new skins? *Epilepsy Behav.* 48, 103–104. doi: 10.1016/j.yebeh.2015.03.026

Upadhya, D., Hattiangady, B., Castro, O. W., Shuai, B., Kodali, M., Attaluri, S., et al. (2019). Human induced pluripotent stem cell-derived MGE cell grafting after status epilepticus attenuates chronic epilepsy and comorbidities via synaptic integration. *Proc. Natl. Acad. Sci. USA* 116, 287–296. doi: 10.1073/pnas.1814185115

van Vliet, E. A., da Costa Araújo, S., Redeker, S., van Schaik, R., Aronica, E., and Gorter, J. A. (2006). Blood–brain barrier leakage may lead to progression of temporal lobe epilepsy. *Brain* 130, 521–534. doi: 10.1093/brain/awl318

Vasudevan, A., and Bhide, P. G. (2008). Angiogenesis in the embryonic CNS. *Cell Adhes. Migr.* 2, 167–169. doi: 10.4161/cam.2.3.6485

Vasudevan, A., Ho, M. S. P., Weiergräber, M., Nischt, R., Schneider, T., Lie, A., et al. (2010). Basement membrane protein nidogen-1 shapes hippocampal synaptic plasticity and excitability. *Hippocampus* 20, 608–620. doi: 10.1002/hipo.20660

Vasudevan, A., Long, J. E., Crandall, J. E., Rubenstein, J. L. R., and Bhide, P. G. (2008). Compartment-specific transcription factors orchestrate angiogenesis gradients in the embryonic brain. *Nat. Neurosci.* 11, 429–439. doi: 10.1038/nn2074

Vaucher, E., Tong, X.-K., Cholet, N., Lantin, S., and Hamel, E. (2000). GABA neurons provide a rich input to microvessels but not nitric oxide neurons in the rat cerebral cortex: a means for direct regulation of local cerebral blood flow. *J. Comp. Neurol.* 421, 161–171. doi: 10.1002/(SICI)1096-9861(20000529)421:2<161::AID-CNE3>3.0.CO;2-F

Vazana, U., Veksler, R., Pell, G. S., Prager, O., Fassler, M., Chassidim, Y., et al. (2016). Glutamate-mediated blood–brain barrier opening: implications for neuroprotection and drug delivery. *J. Neurosci.* 36, 7727–7739. doi: 10.1523/JNEUROSCI.0587-16.2016

Vezzani, A. (2005). VEGF and seizures: cross-talk between endothelial and neuronal environments. *Epilepsy Curr.* 5, 72–74. doi: 10.1111/j.1535-7597.2005.05209.x

Vezzani, A., French, J., Bartfai, T., and Baram, T. Z. (2010). The role of inflammation in epilepsy. *Nat. Rev. Neurol.* 7, 31–40. doi: 10.1038/nrneurol.2010.178

Vezzani, A., and Friedman, A. (2011). Brain inflammation as a biomarker in epilepsy. *Biomark. Med* 5, 607–614. doi: 10.2217/bmm.11.61

Vezzani, A., Friedman, A., and Dingledine, R. J. (2013). The role of inflammation in epileptogenesis. *Neuropharmacology* 69, 16–24. doi: 10.1016/j.neuropharm.2012.04.004

Walker, M. C., and Köhling, R. (2013). The problems facing epilepsy therapy. *Neuropharmacology* 69, 1–2. doi: 10.1016/j.neuropharm.2013.02.007

Wang, B., Xiao, J., and Jiang, H. (2014). Simultaneous real-time 3D photoacoustic tomography and EEG for neurovascular coupling study in an animal model of epilepsy. *J. Neural Eng.* 11:046013. doi: 10.1088/1741-2560/11/4/046013

Weissberg, I., Reichert, A., Heinemann, U., and Friedman, A. (2011). Blood-brain barrier dysfunction in epileptogenesis of the temporal lobe. *Epilepsy Res. Treat.* 2011:143908. doi: 10.1155/2011/143908

Whelan, C. D., Altmann, A., Botía, J. A., Jahanshad, N., Hibar, D. P., Absil, J., et al. (2018). Structural brain abnormalities in the common epilepsies assessed in a worldwide ENIGMA study. *Brain* 141, 391–408. doi: 10.1093/brain/awx341

Winkler, E. A., Bell, R. D., and Zlokovic, B. V. (2011). Central nervous system pericytes in health and disease. *Nat. Neurosci.* 14, 1398–1405. doi: 10.1038/nn.2946

Winkler, M. K. L., Chassidim, Y., Lublinsky, S., Revankar, G. S., Major, S., Kang, E.-J., et al. (2012). Impaired neurovascular coupling to ictal epileptic activity and spreading depolarization in a patient with subarachnoid hemorrhage: possible link to blood–brain barrier dysfunction. *Epilepsia* 53, 22–30. doi: 10.1111/j.1528-1167.2012.03699.x

Won, C., Lin, Z., Kumar, T. P., Li, S., Ding, L., Elkhal, A., et al. (2013). Autonomous vascular networks synchronize GABA neuron migration in the embryonic forebrain. *Nat. Commun.* 4:2149. doi: 10.1038/ncomms3149

Wu, X., Mogford, J. E., Platts, S. H., Davis, G. E., Meininger, G. A., and Davis, M. J. (1998). Modulation of calcium current in arteriolar smooth muscle by αvβ3 and α5β1 integrin ligands. *J. Cell Biol.* 143, 241–252. doi: 10.1083/jcb.143.1.241

Wu, X., Muthuchamy, M., and Reddy, D. S. (2017). Atomic force microscopy investigations of fibronectin and α5β1-integrin signaling in neuroplasticity and seizure susceptibility in experimental epilepsy. *Epilepsy Res.* 138, 71–80. doi: 10.1016/j.eplepsyres.2017.10.013

Xhima, K., Weber-Adrian, D., and Silburt, J. (2016). Glutamate induces blood–brain barrier permeability through activation of N-methyl-D-aspartate receptors. *J. Neurosci.* 36, 12296–12298. doi: 10.1523/JNEUROSCI.2962-16.2016

Yu, P., Li, S., Zhang, Z., Wen, X., Quan, W., Tian, Q., et al. (2017). Progesterone-mediated angiogenic activity of endothelial progenitor cell and angiogenesis in traumatic brain injury rats were antagonized by progesterone receptor antagonist. *Cell Prolif.* 50:e12362. doi: 10.1111/cpr.12362

Zhai, X., Liang, P., Li, Y., Li, L., Zhou, Y., Wu, X., et al. (2016). Astrocytes regulate angiogenesis through the Jagged1-mediated Notch1 pathway after status epilepticus. *Mol. Neurobiol.* 53, 5893–5901. doi: 10.1007/s12035-015-9492-8

Zhang, L., Huang, T., Teaw, S., and Bordey, A. (2019). Hypervascularization in mTOR-dependent focal and global cortical malformations displays differential rapamycin sensitivity. *Epilepsia* 60, 1255–1265. doi: 10.1111/epi.15969

Zhao, Z., Nelson, A. R., Betsholtz, C., and Zlokovic, B. V. (2015). Establishment and dysfunction of the blood-brain barrier. *Cell* 163, 1064–1078. doi: 10.1016/j.cell.2015.10.067

Zhao, M., Nguyen, J., Ma, H., Nishimura, N., Schaffer, C. B., and Schwartz, T. H. (2011). Preictal and ictal neurovascular and metabolic coupling surrounding a seizure focus. *J. Neurosci.* 31, 13292–13300. doi: 10.1523/JNEUROSCI.2597-11.2011

Zhu, Q., Naegele, J. R., and Chung, S. (2018). Cortical GABAergic interneuron/progenitor transplantation as a novel therapy for intractable epilepsy. *Front. Cell. Neurosci.* 12:167. doi: 10.3389/fncel.2018.00167

Conflict of Interest: The authors declare that the research was conducted in the absence of any commercial or financial relationships that could be construed as a potential conflict of interest.

frontiers in Physiology

REVIEW
published: 11 February 2020
doi: 10.3389/fphys.2020.00098

Immune and Apoptosis Mechanisms Regulating Placental Development and Vascularization in Preeclampsia

*Nozha Raguema, Sarah Moustadraf and Mariane Bertagnolli**

Laboratory of Maternal-Child Health, Centre de Recherche de l'Hôpital du Sacré-Coeur de Montréal, Centre Intégré Universitaire de Santé et de Services Sociaux du Nord-de-l'Île-de-Montréal, Montreal, QC, Canada

Preeclampsia is the most severe type of hypertensive disorder of pregnancy, affecting one in 10 pregnancies worldwide and increasing significantly maternal and neonatal morbidity and mortality. Women developing preeclampsia display an array of symptoms encompassing uncontrolled hypertension and proteinuria, with neurological symptoms including seizures at the end of pregnancy. The main causes of preeclampsia are still unknown. However, abnormal placentation and placenta vascularization seem to be common features in preeclampsia, also leading to fetal growth restriction mainly due to reduced placental blood flow and chronic hypoxia. An over activation of maternal immunity cells against the trophoblasts, the main cells forming the placenta, has been recently shown as an important mechanism triggering trophoblast apoptosis and death. This response will further disrupt the remodeling of maternal uterine arteries, in a first stage, and the formation of new placental vessels in a later stage. A consequent chronic hypoxia stress will further contribute to increase placental stress and exacerbate systemic circulatory changes in the mother. The molecular mechanisms driving these processes of apoptosis and anti-angiogenesis are also not well-understood. In this review, we group main evidences suggesting potential targets and molecules that should be better investigated in preeclampsia. This knowledge will contribute to improve therapies targeting a better placenta formation, having a positive impact on maternal disease prevention and on fetal development.

Keywords: apoptosis, preeclampsia, placental development, vascular remodeling, hypoxia

OPEN ACCESS

Edited by:
Silvia Lacchini,
University of São Paulo, Brazil

Reviewed by:
Loren P. Thompson,
University of Maryland, Baltimore, United States
Keshari Thakali,
University of Arkansas for Medical Sciences, United States

***Correspondence:**
Mariane Bertagnolli
mariane.bertagnolli@umontreal.ca

Specialty section:
This article was submitted to Vascular Physiology, a section of the journal Frontiers in Physiology

Received: *18 September 2019*
Accepted: *27 January 2020*
Published: *11 February 2020*

Citation:
Raguema N, Moustadraf S and Bertagnolli M (2020) Immune and Apoptosis Mechanisms Regulating Placental Development and Vascularization in Preeclampsia. Front. Physiol. 11:98. doi: 10.3389/fphys.2020.00098

INTRODUCTION

Pregnancy is a major physiologic event in a woman's life, leading to significant body and metabolic changes. During the implantation of the embryo, a new transient organ is formed connecting mother and fetus, the placenta (Burton and Fowden, 2015). The structure of the placenta will, during pregnancy, provide a range of functions such as fetal nutrition and oxygenation, as well as the secretion of endocrine factors, also building a maternal-fetal immune tolerance (Heerema-McKenney, 2018).

During the first three gestational weeks, the blastocyst implants in the decidual endometrium, developing the placenta. The implantation is mediated by the invasion of trophoblasts, the main cells forming the placenta (Knofler et al., 2019). Trophoblasts are primitive cells giving origin to different cell lineages such as the cytotrophoblasts and the syncytiotrophoblasts. More specifically, during invasion, the cytotrophoblasts form a cell layer under the syncytiotrophoblasts, so these can infiltrate in between uterine epithelial cells in order to ensure the implantation of the embryo (Knofler et al., 2019).

During the implantation process, endometrial cells, and uterine vessels, in addition to uterine immune cells, are modified to form the decidua. Trophoblasts will, in addition, invade the spiral arteries of the uterus. In order to reach this goal, trophoblasts differentiate into villous trophoblasts, ensuring the feto-maternal exchanges and the endocrine functions of the placenta, and in invasive extravillous trophoblasts, essential for the implantation and remodeling of the uterine vessels. The extravillous trophoblast proliferates and becomes invasive, migrating into the decidua and myometrium.

The migration of the extravillous trophoblasts into the maternal spiral arteries also represents another key step of human placentation (Baker et al., 2009). There, extravillous trophoblasts will replace maternal arteries endothelium and smooth muscle cells by stimulating their apoptosis and ultimately promote vessel remodeling (Whitley and Cartwright, 2009). The invasion of extravillous trophoblasts further reduces vasomotor tonus and responses of spiral arteries to vasoactive factors (Baker et al., 2009), causing a permanent arterial dilation and ensuring an increased blood flow to the placenta and growing fetus (Salamonsen et al., 2003). This remodeling process is completed around 20 gestational weeks in healthy pregnancies (Osol and Mandala, 2009).

However, some pregnancies are associated with complications. Indeed, several studies have demonstrated defects in the vascular remodeling process in more severe complications such as preeclampsia (da Cunha Castro and Popek, 2018). In abnormal placentation with poor vascularization of the placenta, the transition of increased oxygenation does not occur, resulting in tissue hypoxia. In addition, the failure of vascular remodeling can reduce significantly the blood supply to the placenta, stimulating a placental metabolic stress and the release of vasoactive factors. As a result, maternal blood pressure can increase significantly either directly due to the chronic rise in uterine vascular resistance, or in response to placental vasoactive factors, causing hypertension in the mother (Karthikeyan and Lip, 2011; American College of Obstetricians and Gynecologists, and Task Force on Hypertension in Pregnancy, 2013; Chaiworapongsa et al., 2014; Dymara-Konopka et al., 2018). Indeed, hypertension occurs in 10% of all pregnancies in the world. If it is not treated or is not well-monitored during pregnancy, it can predispose to more severe outcomes such as preterm delivery, low birth weight and preeclampsia.

In this review, we will describe one of the most severe hypertensive disorders of pregnancy, preeclampsia. We will discuss how the molecular mechanisms linked to abnormal placentation involving maternal inflammation by activation of immune cells and apoptosis can alter placental vascularization and contribute to the unfavorable progression of preeclampsia.

PATHOGENESIS OF PREECLAMPSIA

Preeclampsia is a disorder emerging around 20 gestational weeks; however, it is diagnosed through high blood pressure values ($\geq$140/90 mmHg) and proteinuria of $\geq$ 0.3 g per day later during gestation. Other symptoms can be also associated such as edema, severe headaches and visual disturbance (Ben Ali Gannoun et al., 2016). Considered a major cause of maternal and fetal mortality and morbidity, preeclampsia affects 2 to 10% of all pregnancies worldwide with nearly 70,000 maternal deaths annually (Duhig et al., 2018). It can lead to multi-systemic and serious complications in the mother such as cerebral hemorrhage, renal failure, HELLP syndrome, which is characterized by associated hemolysis and liver injury, and even eclampsia with severe seizures in more severe cases.

In addition, the fetus can also be affected by preeclampsia since it is one of the leading cause of premature birth and intrauterine growth restriction, mainly due to insufficient nutrient supply and chronic hypoxia exposure (Redman and Sargent, 2005). In addition, the only known treatment of preeclampsia to date is premature delivery. Nevertheless, there are risk factors already identified and they include previous history of preeclampsia or family history, multiple pregnancies, as well as cardiometabolic factors such as obesity, diabetes and chronic hypertension (Dong et al., 2017).

The pathogenesis of preeclampsia is still not well-understood and seems to associate differential complex alterations in the placenta and maternal circulation, turning this disorder a major subject of a large amount of studies. Some, however, agree that the preeclampsia origin is an abnormal placentation, which can be defined by two distinct developmental stages: the pre-clinical and the clinical stages (Mayrink et al., 2018). While the pre-clinical stage is determined by critical changes in placental structure and development, the clinical stage is characterized by circulatory systemic changes and symptoms in the mother.

The pre-clinical stage corresponds to inefficient trophoblast invasion in the maternal decidua (Tsatsaris et al., 2008). If the cell invasion occurs only superficially at this stage, trophoblasts will fail to reach the maternal spiral arteries and to promote the vascular remodeling, resulting in increased arterial resistance and reduced blood flow (Roberts and Hubel, 2009). A disrupted remodeling of maternal spiral arteries is, therefore, a major consequence of the pre-clinical stage. It further contributes to promote placental ischemia and to stimulate the secretion of pro-inflammatory factors by the placenta, leading to the second stage of abnormal placentation (Mayrink et al., 2018). Following the pre-clinical stage, the clinical stage corresponds to the manifestation of symptoms in the mother such as severe, and sometimes uncontrolled, high blood pressure, and proteinuria followed by the dysfunction of multiple organs (Chaiworapongsa et al., 2014).

Therefore, it is now well-understood that a healthy placentation depends on the essential steps of placental

development and the ability to respond or adapt to different types of stress. The dysfunction of one of these processes can have harmful repercussions on maternal circulation and fetal development.

In the pre-clinical and clinical stages, the maternal immune cells are also active. Lymphocyte T cells can significantly increase the production of inflammatory cytokines such as tumor necrosis factor alpha (TNFα) and interleukin-6 (IL6), as shown in preeclampsia. Pro-inflammatory responses are also associated with a reduction in anti-inflammatory cytokines (de Oliveira et al., 2010; Hutabarat et al., 2017). In maternal vessels, an increase in pro-inflammatory TNFα and IL6 contributes to causing endothelial dysfunction, which is a hallmark of preeclampsia mainly characterized by reduced production of vasodilation factors and an increase in the permeability of endothelial cells (de Oliveira et al., 2010). TNFα is also shown to decrease nitric oxide synthase (NOS) gene transcription while increasing the production of the potent vasoconstrictor endothelin-1 (Cornelius, 2018). Further, placental ischemia can trigger an oxidative stress state, characterized by the bursting of large quantities of reactive oxygen species (ROS) in the cell membrane, the endoplasmic reticulum and the compartments of the mitochondria, causing protein and DNA damage (Schoots et al., 2018). Hence, all these mechanisms contribute to stimulate a state of chronic inflammation during abnormal placentation.

Inflammation can further activate and promote the programed death of trophoblasts, a process called apoptosis. In normal healthy pregnancies, the mechanisms of apoptosis can be of crucial importance to protect the trophoblasts from the attack of maternal immune cells and to promote the death of uterine arteries endothelial cells and their replacement by extravillous trophoblasts (Abrahams et al., 2004; Ashton et al., 2005). However, under inflammation, activation of apoptosis can backfire on the trophoblasts, significantly disrupting trophoblast migration and placental vascularization, also exacerbating immune responses (Sharp et al., 2010).

In addition, it has been described that abnormal placentation can be associated with an imbalance in the production of pro-angiogenic and antiangiogenic factors by the placenta. Increased secretion of antiangiogenic factors soluble fms-like tyrosine kinase 1 (sFlt1) and soluble endoglin (sEng), as well as reduced production of pro-angiogenic factors vascular endothelial growth factor (VEGF) and placental growth factor (PlGF) during exposure to ischemia, likely contributes to the pathogenesis of preeclampsia (Karthikeyan et al., 2011; Helmo et al., 2018). An increasing number of studies have identified enhanced sFlt1 expression in placentas of pregnancies with preeclampsia (Helmo et al., 2018). sFlt1 is the soluble form of VEGF receptor 1 (VEGFR1) and antagonizes the pro-angiogenic effects of VEGF. In addition, sEng, another key antiangiogenic protein, is also shown to be up-regulated in preeclampsia (Dymara-Konopka et al., 2018). On the other hand, the synthesis of pro-angiogenic PlGF was associated with an exacerbated production of anti-angiogenic factors during preeclampsia (Karthikeyan et al., 2011). These results indicate that abnormal placentation does not only cause changes in uterine vessels but also a systemic damage to the maternal endothelium and the angiogenesis capacity, which can lead to endothelial dysfunction (Eddy et al., 2018).

In the next sessions, we describe how these two interconnected mechanisms involving the maternal immune system and cell death act during placentation and placental vascularization in healthy pregnancies and in the pathology of preeclampsia.

IMMUNE SYSTEM IN PREECLAMPSIA

Several hypotheses have been proposed to explain an abnormal trophoblast invasion and the over activation of placental inflammation in early pregnancies with preeclampsia. Some support an impaired maternal immune response or a defective maternal immune-tolerance to the semi-allogeneic fetus (Racicot et al., 2014). A successful invasion in normal pregnancies relies on an adequate interaction between trophoblast cells and maternal epithelial, immune and endothelial cells and tissues (Liu et al., 2017). In this regard, the maternal immune system plays a key role in facilitating the interaction of two immunologically different beings, the mother and the fetus (Baker et al., 2009).

In normal pregnancies, the processes of trophoblast invasion and spiral artery remodeling are highly dependent on the maternal immune system to allow significant tissue changes (Faas and de Vos, 2017a). During trophoblast invasion, the decidua contains a high number of immune cells necessary for the migration of trophoblasts (Racicot et al., 2014). They include macrophages, natural killer cells (NK), dendritic cells (DCs), T lymphocyte and T regulatory cells (Tregs) (Liu et al., 2017). These cells infiltrate the decidua and gather around the trophoblasts allowing them to reach the endometrium and spiral arteries (Figueiredo and Schumacher, 2016). On the other hand, Tregs and regulatory cytokines ensure the proper control and function of pro-inflammatory cells and their actions during invasion (Baker et al., 2009). In mouse models, it is well-documented that Treg cells are important for maternal-fetal immune tolerance (Faas and de Vos, 2017a). In addition, it is believed that the DCs present in the decidua can promote a dominant presence of T helper type 2 cells (Th2) in the uterus and placenta in order to induce immune tolerance of mother to fetus (Figueiredo and Schumacher, 2016; Cornelius, 2018).

However, an over activated immune system can play a significant negative role in placental development and the progression of preeclampsia. Epidemiological evidence supports this role, indicating an association between adverse changes in maternal immune responses and preeclampsia (Kestlerova et al., 2012). In particular, the fact that preeclampsia can surge more frequently in the first pregnancy, and also that long-term exposure to partner's sperm has been described as reducing the risk of preeclampsia, or that risks may increase during artificial reproduction, for example, support the hypothesis that the immune system can have a direct impact and perhaps even induce preeclampsia (Matthiesen et al., 2005). In addition, the mechanisms allowing the semi-allogenic trophoblast cell to invade maternal tissues by outwitting maternal processes of non-self recognition can also fail during preeclampsia (Cornelius, 2018).

One hypothesis is that over activation of immune cells stimulates trophoblast apoptosis in preeclampsia (Jafri and Ormiston, 2017). Indeed, during healthy pregnancies, the non-recognition of trophoblasts by maternal immune cells reduces the activation of inflammation, and this will consequently decrease the lysis of the trophoblasts present in the decidua (Cornelius, 2018). In addition, a recent study showed a very low presence of macrophages during trophoblast invasion in normal pregnancies (Taylor and Sasser, 2017). However, in preeclampsia, their numbers can be dramatically increased, notably in the uterine artery wall of patients, where very few extravillous trophoblasts were also present.

T lymphocytes along with NKs and DCs have also been found to respond differently in preeclampsia compared to normal pregnancies, tending to develop a pro-inflammatory state (Faas and de Vos, 2017b). These cells produce and respond to a broad spectrum of cytokines and are involved in paracrine mechanisms regulating trophoblast invasion (Moffett-King, 2002). *In vitro*, maternal macrophages could further induce apoptosis of periarterial extravillous trophoblasts (Miko et al., 2009; Faas and de Vos, 2017b; Taylor and Sasser, 2017). In addition, excessive activation of neutrophils and monocytes in clinical and experimental preeclampsia have also been described (Faas and de Vos, 2017a; Cornelius, 2018). Monocytes have been found to spontaneously synthesize larger quantities of pro-inflammatory cytokines such as IL1b, IL6, and IL8 (Faas and de Vos, 2017a).

Another defective system appears to be involved in the dysfunctional invasion of trophoblasts in the spiral arteries. Human leukocyte antigens (HLAs) are major histocompatibility complex (MHC) molecules expressed on different cells of the placenta. Invasive extravillous trophoblasts express Class I HLA-C and the atypical class Ib antigens HLA-G, which promote immune-regulation between extravillous trophoblasts and maternal decidual NK cells. HLA-G is a ligand for the inhibitory receptor KIR2DL4 of NK cells (Chen et al., 2010). Consequently, the expression of HLA-G by the extravillous trophoblast can defend it against cell death mediated by NKs. This is an essential mechanism of extravillous trophoblast protection to allow cell invasion during healthy pregnancies mainly by inhibiting NK cytotoxicity and cytokine production (Chen et al., 2010; Liu et al., 2013). HLA-G can also directly modify the biological function of trophoblast cells stimulating invasiveness by different cell signaling pathways (Liu et al., 2013). However, a lower HLA-G expression in the placenta, more specifically in extravillous trophoblasts, has been described in preeclampsia (Yie et al., 2004; Robillard et al., 2011).

Lower expression of other HLA genes can inversely protect the placenta. For example, syncytiotrophoblasts do not express HLA-A and HLA-B genes, which leads to not expressing MHC-I, a major binding site for lymphocyte T cells (Thellin and Heinen, 2003; Racicot et al., 2014; Cornelius, 2018). Therefore, by being in close contact with the activated maternal immune system, the lack of HLA-A and -B protects the syncytiotrophoblasts from maternal T cells, hence preventing tissue rejection (Hutabarat et al., 2017).

APOPTOSIS IN PREECLAMPSIA

An important mechanisms involved in maternal-fetal immune tolerance is apoptosis, which is defined as a programed cell death that can be induced by two different pathways: the extrinsic and the intrinsic (Elmore, 2007). The mechanisms of activation of these two pathways are illustrated in **Figure 1**. The extrinsic pathway is initiated when a cell expressing a FAS receptor on the surface binds to its FAS ligand (FASL), activating a cascade of pro-apoptotic elements and leading to cell death. The binding of FASL to the transmembrane receptor FAS recruits procaspase 8, further activated to caspase 8. This then cleaves another type of procaspase generating the active form of caspase 3. Active caspase 3 will also recruit other downstream effectors, promoting the final steps of cell death (Elmore, 2007).

The intrinsic pathway is usually activated during intracellular stress such as ischemia and DNA damage, or when cells receive signals from certain pro-apoptotic factors. During intracellular stress, P53 is also activated, a protein which main role is to stimulate cascades of pro-apoptotic factors mainly targeting the mitochondria (Harris and Levine, 2005). One of these factors, a pro-apoptotic member of the BCL2 family called Bax, releases cytochrome C from the inner mitochondrial membrane during stress (Sharp et al., 2014). Subsequently, cytochrome C can form an apoptosome in the cytosol, a complex comprising active caspase 9 and Apaf-1, in order to cleave procaspase 3 to its active form and, therefore, cause cell death (Sharp et al., 2010).

Figure 1 also illustrates the critical changes in apoptosis pathways during normal healthy and complicated pregnancies. During healthy and abnormal placentation, the mechanisms of apoptosis, as noted above, occur in the vast majority of placental cells and likewise in placental villous trophoblasts. They regulate the number and type of trophoblast population in the placenta and decidua, greatly influencing maternal-fetal immune tolerance (Sharp et al., 2010). Apoptosis is particularly important in the initial and final stages of placental development and function. Apoptotic cells have been found in the maternal and embryonic parts of the placenta during normal pregnancy. The presence of these cells is associated with stages of placental development, including the invasion of trophoblast, remodeling of the spiral arteries, differentiation of trophoblasts and childbirth (Abrahams et al., 2004). However, stimulation of placental apoptosis is also regulated by maternal immune cells, although the main mechanisms activated by these cells in normal and complicated pregnancies are not yet fully understood.

Evidence supports that in normal pregnancies, trophoblasts secrete FASL rather than expressing the FAS receptor (Kauma et al., 1999), as shown in **Figure 1A**. The predominance of FASL secretion reduces their susceptibility to activate themselves and enter apoptosis (Bamberger et al., 1997). Therefore, the higher FASL secretion combined with lower FAS receptor expression may protect trophoblasts against cytolytic activation of maternal immune cells. Instead, they can stimulate the extrinsic apoptosis pathway in maternal immune cells such as T lymphocytes and macrophages, naturally expressing higher amounts of FAS receptor (Kauma et al., 1999;

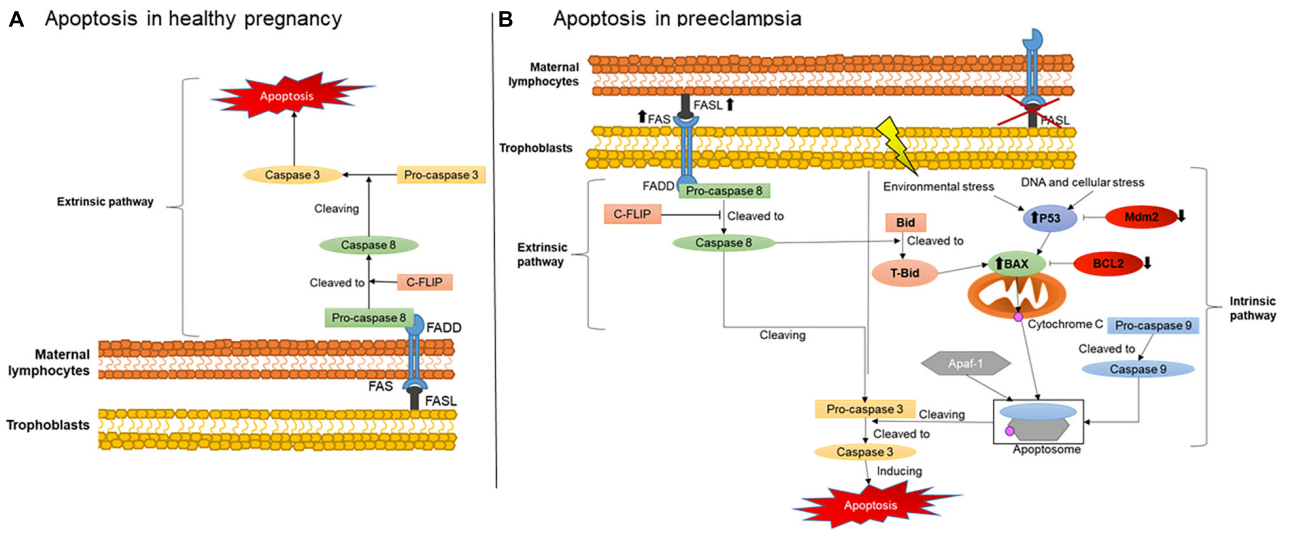

FIGURE 1 | Placental apoptosis mechanisms. **(A)** Extrinsic apoptosis pathway activation in maternal immune cells stimulated by trophoblasts producing FASL. **(B)** Extrinsic apoptosis activation in trophoblasts stimulated by FASL produced by the maternal immune system and intrinsic pathway activated by environmental stress such as hypoxia and DNA damage. FAS, FAS receptor; FASL, FAS ligand; FADD, Fas-associated protein with death domain; C-FLIP, cellular FLICE (FADD-like IL-1β-converting enzyme)-inhibitory protein; P53, apoptosis inductor; BCL-2, B-cell lymphoma 2; BAX, BCL2-associated X apoptosis regulator; Mdm2, Human mouse double minute 2; Bid, BH3 interacting-domain death agonist; tBid, truncated p15 BID; Apaf-1, apoptotic protease activating factor 1.

Roh et al., 2002). In addition, the higher secretion of FASL by trophoblasts is an important mechanism activating apoptosis of endothelial cells in the maternal spiral arteries (Pongcharoen et al., 2004). This process is therefore critical for their replacement by extravillous trophoblasts during normal placentation (Pongcharoen et al., 2004).

On the other hand, changes in this process and on main players have a significant negative impact on placental development, contributing to the establishment of placental abnormalities. In hypertensive pregnancies, for example, increased trophoblast apoptosis and reduced cell invasion were described (Whitley et al., 2007). More specifically, during preeclampsia, apoptosis was described in extravillous trophoblasts in the vicinity of the wall of the spiral arteries, rather than in maternal endothelial cells (Whitley et al., 2007). It has also been shown that these extravillous trophoblasts, instead of mainly expressing FASL, express FAS receptor and the TNF-α receptor 1, another pro-apoptotic factor. They also had lower expression of anti-apoptotic factors BCL2 and Mcl-1.

Consistent with these findings, we and others have also shown that the expression of FAS and FASL in serum and in maternal lymphocytes also occurs in preeclampsia (Miko et al., 2009; Raguema et al., 2018). We also described the polymorphisms of FAS-670A/G and FASL IVS2nt124A/G genes in the lymphocytes of pregnant women with preeclampsia. These polymorphisms were characterized by a higher production of FASL by the maternal immune cells, supporting the postulate of an over activation of pro-apoptosis responses in the trophoblasts, as illustrated in **Figure 1B**, which could contribute to alter the placentation during preeclampsia (Abrahams et al., 2004). In line with our findings, another study also described increased expression of the FAS receptor and reduced expression of FASL in the placentas of pregnancies with hypertensive disorders (Roh et al., 2002).

In addition, over activation of the intrinsic pathway may also occur due to reduced anti-apoptotic factors, being another potential origin of exacerbated apoptosis in preeclampsia (**Figure 1B**) (Hung et al., 2002; Sharp et al., 2010). Indeed, several studies have shown that, during the development of the trophoblastic villi, an early stage of apoptosis is activated, specifically targeting cytotrophoblasts, whereas later stages of apoptosis are more likely to affect syncytiotrophoblasts (Hutabarat et al., 2017). Syncytiotrophoblasts are multinucleated cells with number of nuclei increasing up to nine times from the beginning of gestation to term. These nuclei can form aggregates called syncytial knots. In normal pregnancies, knots are rarely seen before 20 weeks of gestation and their frequency increases in mature placentas (Loukeris et al., 2010). They are also very frequent in the placentas of complicated pregnancies, being present on almost all terminal villi in preeclamptic placentas (Tomas et al., 2011). Currently, the presence of a large number of syncytial knots can indicate premature aging of the placentas (Loukeris et al., 2010).

Syncytiotrophoblast apoptosis in preeclampsia has also been associated with larger numbers of syncytial knots and higher oxidative stress (Tomas et al., 2011; Fogarty et al., 2013). Rajakumar et al. have also described the presence of syncytial knots in the bloodstream of preeclamptic mothers (Rajakumar et al., 2012). In their study, they described the presence of large structures of 50–150 μm consistent with detached syncytial knots after gently rinsing the placentas of preeclamptic pregnancies. The syncytial origin was determined by the fact that these structures were always membrane-bound and multinucleated. Interestingly, in normal term placentas, very few multi-nucleated

structures were observed in the effluent. Their data indicated that the abundant syncytial knots in the preeclamptic placentas can easily detach from the syncytial layer to become free aggregates of syncytial origin. Furthermore, these syncytial aggregates have been described as containing a large expression of sFlt1, potentially contributing to impair placental angiogenesis in preeclampsia (Rajakumar et al., 2012).

The increase of syncytial knots in trophoblasts has been observed and associated with down regulation of anti-apoptotic factors of the intrinsic pathway such as BCL2 and Mdm2 and with premature aging of the placenta in preeclampsia (Coleman et al., 2013). In addition, they can also increase significantly when exposed to hyperoxia, hypoxia or greater amounts of ROS in the placental villi (Heazell et al., 2007). These findings indicate that the presence of knots in syncytiotrophoblasts may reflect placental responses to environmental stress and the activation of intrinsic apoptosis pathways in abnormal placentation and preeclampsia.

SUMMARY

Despite the increasing number of studies reporting the involvement of the maternal immune system and apoptosis in the development of the placenta and preeclampsia, the main mechanisms promoting cell death and ineffective vascular remodeling in abnormal placentation are still unclear. It is well-known that close interaction between the maternal immune system and trophoblasts is essential during placentation. However, in the presence of an over activation of inflammation and apoptosis of the trophoblasts, it leads to abnormal placentation with impaired invasion, vascular remodeling and microcirculation in the placenta. Activation of different pathways of apoptosis also depends on pathological processes in the placenta. More specifically, activation of the FAS/FASL extrinsic pathway and of the intrinsic pathway mediated by P53, Bax, and BCL2 have been systematically reported in normal and complicated pregnancies such as preeclampsia although their mechanisms are not yet fully understood.

Future studies are therefore necessary to better understand the mechanisms of activation of the extrinsic and intrinsic apoptosis pathways in hypertensive disorders of pregnancy and whether their activation may also depend on different pathological stimuli associated with preeclampsia. Current data support that activation of the extrinsic pathway is largely associated with systemic and local immune and inflammatory responses in the placenta. The intrinsic pathway is primarily described as a consequence of trophoblasts disruption under severe and chronic hypoxia, DNA damage and environmental stress conditions. Importantly, the close interaction of these two pathways can help promote abnormal placentation and vascularization, aggravating placental stress during preeclampsia. More studies evaluating these mechanisms are therefore needed to elucidate these interactions and to investigate new therapies capable of reducing the activation of apoptosis at different stages of the development of preeclampsia.

AUTHOR CONTRIBUTIONS

NR wrote the manuscript and supervised figures edition. SM designed the figures and collaborated in writing. MB reviewed and edited the text and figures.

FUNDING

NR has a postdoctoral fellowship from the Société Québécoise d'Hypertension Artérielle/Servier. MB laboratory is funded with grants from the CIUSSS Nord-de-l'Île-de-Montréal, SickKids Foundation and Canadian Institutes of Health Research. This work was funded by the SickKids Foundation and Canadian Institutes of Health Research (NI20-1037).

REFERENCES

Abrahams, V. M., Straszewski-Chavez, S. L., Guller, S., and Mor, G. (2004). First trimester trophoblast cells secrete Fas ligand which induces immune cell apoptosis. *Mol. Hum. Reprod.* 10, 55–63. doi: 10.1093/molehr/gah006

American College of Obstetricians and Gynecologists, and Task Force on Hypertension in Pregnancy, (2013). Hypertension in pregnancy. Report of the american college of obstetricians and gynecologists' task force on hypertension in pregnancy. *Obstet Gynecol.* 122, 1122–1131.

Ashton, S. V., Whitley, G. S., Dash, P. R., Wareing, M., Crocker, I. P., Baker, P. N., et al. (2005). Uterine spiral artery remodeling involves endothelial apoptosis induced by extravillous trophoblasts through Fas/FasL interactions. *Arterioscler. Thromb. Vasc. Biol.* 25, 102–108. doi: 10.1161/01.atv.0000148547.70187.89

Baker, C. D., Ryan, S. L., Ingram, D. A., Seedorf, G. J., Abman, S. H., and Balasubramaniam, V. (2009). Endothelial colony-forming cells from preterm infants are increased and more susceptible to hyperoxia. *Am. J. Respir. Crit. Care Med.* 180, 454–461. doi: 10.1164/rccm.200901-0115OC

Bamberger, A. M., Schulte, H. M., Thuneke, I., Erdmann, I., Bamberger, C. M., and Asa, S. L. (1997). Expression of the apoptosis-inducing Fas ligand (FasL) in human first and third trimester placenta and choriocarcinoma cells. *J. Clin. Endocrinol. Metab.* 82, 3173–3175. doi: 10.1210/jcem.82.9.4360

Ben Ali Gannoun, M., Bourrelly, S., Raguema, N., Zitouni, H., Nouvellon, E., and Maleh, W. (2016). Placental growth factor and vascular endothelial growth factor serum levels in tunisian arab women with suspected preeclampsia. *Cytokine* 79, 1–6. doi: 10.1016/j.cyto.2015.12.005

Burton, G. J., and Fowden, A. L. (2015). The placenta: a multifaceted, transient organ. *Philos. Trans. R. Soc. Lond. B Biol. Sci.* 370:20140066. doi: 10.1098/rstb.2014.0066

Chaiworapongsa, T., Chaemsaithong, P., Yeo, L., and Romero, R. (2014). Pre-eclampsia part 1: current understanding of its pathophysiology. *Nat. Rev. Nephrol.* 10, 466–480. doi: 10.1038/nrneph.2014.102

Chen, L. J., Han, Z. Q., Zhou, H., Zou, L., and Zou, P. (2010). Inhibition of HLA-G expression via RNAi abolishes resistance of extravillous trophoblast cell line TEV-1 to NK lysis. *Placenta* 31, 519–527. doi: 10.1016/j.placenta.2010.03.008

Coleman, S. J., Gerza, L., Jones, C. J., Sibley, C. P., Aplin, J. D., and Heazell, A. E. (2013). Syncytial nuclear aggregates in normal placenta show increased nuclear condensation, but apoptosis and cytoskeletal redistribution are uncommon. *Placenta* 34, 449–455. doi: 10.1016/j.placenta.2013.02.007

Cornelius, D. C. (2018). Preeclampsia: from inflammation to immunoregulation. *Clin. Med. Insights Blood Disord.* 11:1179545x17752325. doi: 10.1177/1179545X17752325

da Cunha Castro, E. C., and Popek, E. (2018). Abnormalities of placenta implantation. *APMIS* 126, 613–620. doi: 10.1111/apm.12831

de Oliveira, L. G., Karumanchi, A., and Sass, N. (2010). Preeclampsia: oxidative stress, inflammation and endothelial dysfunction. *Revist. Bras. Ginecol. Obstetr.* 32, 609–616.

Dong, X., Gou, W., Li, C., Wu, M., Han, Z., Li, X., et al. (2017). Proteinuria in preeclampsia: not essential to diagnosis but related to disease severity and fetal outcomes. *Pregnancy Hypertens.* 8, 60–64. doi: 10.1016/j.preghy.2017.03.005

Duhig, K., Vandermolen, B., and Shennan, A. (2018). Recent advances in the diagnosis and management of pre-eclampsia. *F1000Research* 7:242. doi: 10.12688/f1000research.12249.1

Dymara-Konopka, W., Laskowska, M., and Blazewicz, A. (2018). Angiogenic imbalance as a contributor of preeclampsia. *Curr. Pharm. Biotechnol.* 19, 797–815. doi: 10.2174/1389201019666180925115559

Eddy, A. C., Bidwell, G. L. III, and George, E. M. (2018). Pro-angiogenic therapeutics for preeclampsia. *Biol. Sex Differ.* 9:36. doi: 10.1186/s13293-018-0195-5

Elmore, S. (2007). Apoptosis: a review of programmed cell death. *Toxicol. Pathol.* 35, 495–516.

Faas, M. M., and de Vos, P. (2017a). Maternal monocytes in pregnancy and preeclampsia in humans and in rats. *J. Reprod. Immunol.* 119, 91–97. doi: 10.1016/j.jri.2016.06.009

Faas, M. M., and de Vos, P. (2017b). Uterine NK cells and macrophages in pregnancy. *Placenta* 56, 44–52. doi: 10.1016/j.placenta.2017.03.001

Figueiredo, A. S., and Schumacher, A. (2016). The T helper type 17/regulatory T cell paradigm in pregnancy. *Immunology* 148, 13–21. doi: 10.1111/imm.12595

Fogarty, N. M., Ferguson-Smith, A. C., and Burton, G. J. (2013). Syncytial knots (Tenney-Parker changes) in the human placenta: evidence of loss of transcriptional activity and oxidative damage. *Am. J. Pathol.* 183, 144–152. doi: 10.1016/j.ajpath.2013.03.016

Harris, S. L., and Levine, A. J. (2005). The p53 pathway: positive and negative feedback loops. *Oncogene* 24, 2899–2908. doi: 10.1038/sj.onc.1208615

Heazell, A. E., Moll, S. J., Jones, C. J., Baker, P. N., and Crocker, I. P. (2007). Formation of syncytial knots is increased by hyperoxia, hypoxia and reactive oxygen species. *Placenta* 28(Suppl. A), S33–S40.

Heerema-McKenney, A. (2018). Defense and infection of the human placenta. *APMIS* 126, 570–588. doi: 10.1111/apm.12847

Helmo, F. R., Lopes, A. M. M., Carneiro, A., Campos, C. G., Silva, P. B., and Dos Reis Monteiro, M. L. G. (2018). Angiogenic and antiangiogenic factors in preeclampsia. *Pathol. Res. Pract.* 214, 7–14. doi: 10.1016/j.prp.2017.10.021

Hung, T. H., Skepper, J. N., Charnock-Jones, D. S., and Burton, G. J. (2002). Hypoxia-reoxygenation: a potent inducer of apoptotic changes in the human placenta and possible etiological factor in preeclampsia. *Circ. Res.* 90, 1274–1281. doi: 10.1161/01.res.0000024411.22110.aa

Hutabarat, M., Wibowo, N., and Huppertz, B. (2017). The trophoblast survival capacity in preeclampsia. *PLoS One* 12:e0186909. doi: 10.1371/journal.pone.0186909

Jafri, S., and Ormiston, M. L. (2017). Immune regulation of systemic hypertension, pulmonary arterial hypertension, and preeclampsia: shared disease mechanisms and translational opportunities. *Am. J. Physiol. Regul. Integr. Comp. Physiol.* 313, R693–R705. doi: 10.1152/ajpregu.00259.2017

Karthikeyan, V. J., and Lip, G. Y. (2011). Endothelial damage/dysfunction and hypertension in pregnancy. *Front. Biosci.* 3, 1100–1108. doi: 10.2741/e314

Karthikeyan, V. J., Lip, G. Y., Lane, D. A., and Blann, A. D. (2011). Angiogenin and apoptosis in hypertension in pregnancy. *Pregnancy Hypertens.* 1, 191–196. doi: 10.1016/j.preghy.2011.07.002

Kauma, S. W., Huff, T. F., Hayes, N., and Nilkaeo, A. (1999). Placental Fas ligand expression is a mechanism for maternal immune tolerance to the fetus. *J. Clin. Endocrinol. Metab.* 84, 2188–2194. doi: 10.1210/jc.84.6.2188

Kestlerova, A., Feyereisl, J., Frisova, V., Mechurova, A., Sula, K., Zima, T., et al. (2012). Immunological and biochemical markers in preeclampsia. *J. Reprod. Immunol.* 96, 90–94. doi: 10.1016/j.jri.2012.10.002

Knofler, M., Haider, S., Saleh, L., Pollheimer, J., Gamage, T., and James, J. (2019). Human placenta and trophoblast development: key molecular mechanisms and model systems. *Cell. Mol. Life Sci.* 76, 3479–3496. doi: 10.1007/s00018-019-03104-6

Liu, H., Liu, X., Jin, H., Yang, F., Gu, W., and Li, X. (2013). Proteomic analysis of knock-down HLA-G in invasion of human trophoblast cell line JEG-3. *Int. J. Clin. Exp. Pathol.* 6, 2451–2459.

Liu, S., Diao, L., Huang, C., Li, Y., Zeng, Y., and Kwak-Kim, J. Y. H. (2017). The role of decidual immune cells on human pregnancy. *J. Reprod. Immunol.* 124, 44–53. doi: 10.1016/j.jri.2017.10.045

Loukeris, K., Sela, R., and Baergen, R. N. (2010). Syncytial knots as a reflection of placental maturity: reference values for 20 to 40 weeks' gestational age. *Pediatr. Dev. Pathol.* 13, 305–309. doi: 10.2350/09-08-0692-OA.1

Matthiesen, L., Berg, G., Ernerudh, J., Ekerfelt, C., Jonsson, Y., and Sharma, S. (2005). Immunology of preeclampsia. *Chem. Immunol. Allergy* 89, 49–61. doi: 10.1159/000087912

Mayrink, J., Costa, M. L., and Cecatti, J. G. (2018). Preeclampsia in 2018: revisiting concepts, physiopathology, and prediction. *Sci. World J.* 2018:6268276. doi: 10.1155/2018/6268276

Miko, E., Szereday, L., Barakonyi, A., Jarkovich, A., Varga, P., and Szekeres-Bartho, J. (2009). Immunoactivation in preeclampsia: Vdelta2+ and regulatory T cells during the inflammatory stage of disease. *J. Reprod. Immunol.* 80, 100–108. doi: 10.1016/j.jri.2009.01.003

Moffett-King, A. (2002). Natural killer cells and pregnancy. *Nat. Rev. Immunol.* 2, 656–663.

Osol, G., and Mandala, M. (2009). Maternal uterine vascular remodeling during pregnancy. *Physiology* 24, 58–71. doi: 10.1152/physiol.00033.2008

Pongcharoen, S., Searle, R. F., and Bulmer, J. N. (2004). Placental Fas and Fas ligand expression in normal early, term and molar pregnancy. *Placenta* 25, 321–330. doi: 10.1016/j.placenta.2003.08.020

Racicot, K., Kwon, J. Y., Aldo, P., Silasi, M., and Mor, G. (2014). Understanding the complexity of the immune system during pregnancy. *Am. J. Reprod. Immunol.* 72, 107–116. doi: 10.1111/aji.12289

Raguema, N., Zitouni, H., Ben Ali Gannoun, M., Benletaifa, D., Almawi, W. Y., Mahjoub, T., et al. (2018). FAS A-670G and Fas ligand IVS2nt A 124G polymorphisms are significantly increased in women with pre-eclampsia and may contribute to HELLP syndrome: a case-controlled study. *BJOG* 125, 1758–1764. doi: 10.1111/1471-0528.15412

Rajakumar, A., Cerdeira, A. S., Rana, S., Zsengeller, Z., Edmunds, L., and Jeyabalan, A. (2012). Transcriptionally active syncytial aggregates in the maternal circulation may contribute to circulating soluble fms-like tyrosine kinase 1 in preeclampsia. *Hypertension* 59, 256–264. doi: 10.1161/HYPERTENSIONAHA.111.182170

Redman, C. W., and Sargent, I. L. (2005). Latest advances in understanding preeclampsia. *Science* 308, 1592–1594. doi: 10.1126/science.1111726

Roberts, J. M., and Hubel, C. A. (2009). The two stage model of preeclampsia: variations on the theme. *Placenta* 30(Suppl. A), S32–S37. doi: 10.1016/j.placenta.2008.11.009

Robillard, P. Y., Dekker, G., Chaouat, G., Hulsey, T. C., and Saftlas, A. (2011). Epidemiological studies on primipaternity and immunology in preeclampsia–a statement after twelve years of workshops. *J. Reprod. Immunol.* 89, 104–117. doi: 10.1016/j.jri.2011.02.003

Roh, C. R., Lee, J. W., Kang, B. H., Yang, S. H., Kim, B. G., Bae, D. S., et al. (2002). Differential expressions of Fas and Fas ligand in human placenta. *J. Korean Med. Sci.* 17, 213–216.

Salamonsen, L. A., Dimitriadis, E., Jones, R. L., and Nie, G. (2003). Complex regulation of decidualization: a role for cytokines and proteases–a review. *Placenta* 24(Suppl. A), S76–S85.

Schoots, M. H., Gordijn, S. J., Scherjon, S. A., van Goor, H., and Hillebrands, J. L. (2018). Oxidative stress in placental pathology. *Placenta* 69, 153–161. doi: 10.1016/j.placenta.2018.03.003

Sharp, A. N., Heazell, A. E., Baczyk, D., Dunk, C. E., Lacey, H. A., and Jones, C. J. (2014). Preeclampsia is associated with alterations in the p53-pathway in villous trophoblast. *PLoS One* 9:e87621. doi: 10.1371/journal.pone.0087621

Sharp, A. N., Heazell, A. E., Crocker, I. P., and Mor, G. (2010). Placental apoptosis in health and disease. *Am. J. Reprod. Immunol.* 64, 159–169. doi: 10.1111/j.1600-0897.2010.00837.x

Taylor, E. B., and Sasser, J. M. (2017). Natural killer cells and T lymphocytes in pregnancy and pre-eclampsia. *Clin. Sci.* 131, 2911–2917. doi: 10.1042/CS20171070

Thellin, O., and Heinen, E. (2003). Pregnancy and the immune system: between tolerance and rejection. *Toxicology* 185, 179–184. doi: 10.1016/s0300-483x(02)00607-8

Tomas, S. Z., Prusac, I. K., Roje, D., and Tadin, I. (2011). Trophoblast apoptosis in placentas from pregnancies complicated by preeclampsia. *Gynecol. Obstet. Invest.* 71, 250–255. doi: 10.1159/000320289

Tsatsaris, V., Fournier, T., and Winer, N. (2008). Pathophysiology of preeclampsia. *J. Gynecol. Obstet. Biol. Reprod.* 37, 16–23.

Whitley, G. S., and Cartwright, J. E. (2009). Trophoblast-mediated spiral artery remodelling: a role for apoptosis. *J. Anat.* 215, 21–26. doi: 10.1111/j.1469-7580.2008.01039.x

Whitley, G. S., Dash, P. R., Ayling, L. J., Prefumo, F., Thilaganathan, B., and Cartwright, J. E. (2007). Increased apoptosis in first trimester extravillous trophoblasts from pregnancies at higher risk of developing preeclampsia. *Am. J. Pathol.* 170, 1903–1909. doi: 10.2353/ajpath.2007.070006

Yie, S. M., Li, L. H., Li, Y. M., and Librach, C. (2004). HLA-G protein concentrations in maternal serum and placental tissue are decreased in preeclampsia. *Am. J. Obstet. Gynecol.* 191, 525–529. doi: 10.1016/j.ajog.2004.01.033

Conflict of Interest: The authors declare that the research was conducted in the absence of any commercial or financial relationships that could be construed as a potential conflict of interest.

frontiers in Physiology

MINI REVIEW
published: 28 February 2020
doi: 10.3389/fphys.2020.00120

Quantitative and Dynamic MRI Measures of Peripheral Vascular Function

Erin K. Englund[1] and Michael C. Langham[2]*

[1] Department of Orthopaedic Surgery, University of California, San Diego, La Jolla, CA, United States, [2] Department of Radiology, University of Pennsylvania, Philadelphia, PA, United States

The endothelium regulates and mediates vascular homeostasis, allowing for dynamic changes of blood flow in response to mechanical and chemical stimuli. Endothelial dysfunction underlies many diseases and is purported to be the earliest pathologic change in the progression of atherosclerotic disease. Peripheral vascular function can be interrogated by measuring the response kinetics following induced ischemia or exercise. In the presence of endothelial dysfunction, there is a blunting and delay of the hyperemic response, which can be measured non-invasively using a variety of quantitative magnetic resonance imaging (MRI) methods. In this review, we summarize recent developments in non-contrast, proton MRI for dynamic quantification of blood flow and oxygenation. Methodologic description is provided for: blood oxygenation-level dependent (BOLD) signal that reflect combined effect of blood flow and capillary bed oxygen content; arterial spin labeling (ASL) for quantification of regional perfusion; phase contrast (PC) to quantify arterial flow waveforms and macrovascular blood flow velocity and rate; high-resolution MRI for luminal flow-mediated dilation; and dynamic MR oximetry to quantify oxygen saturation. Overall, results suggest that these dynamic and quantitative MRI methods can detect endothelial dysfunction both in the presence of overt cardiovascular disease (such as in patients with peripheral artery disease), as well as in sub-clinical settings (i.e., in chronic smokers, non-smokers exposed to e-cigarette aerosol, and as a function of age). Thus far, these tools have been relegated to the realm of research, used as biomarkers of disease progression and therapeutic response. With proper validation, MRI-measures of vascular function may ultimately be used to complement the standard clinical workup, providing additional insight into the optimal treatment strategy and evaluation of treatment efficacy.

Keywords: MRI, reactive hyperemia, blood flow, endothelial (dys)function, flow mediated dilatation, perfusion

OPEN ACCESS

Edited by:
Shampa Chatterjee, University of Pennsylvania, United States

Reviewed by:
Markus Hecker, Heidelberg University, Germany
Erik Josef Behringer, Loma Linda University, United States

****Correspondence:***
Erin K. Englund
eenglund@ucsd.edu

Specialty section:
This article was submitted to Vascular Physiology, a section of the journal Frontiers in Physiology

Received: *21 September 2019*
Accepted: *03 February 2020*
Published: *28 February 2020*

Citation:
Englund EK and Langham MC (2020) Quantitative and Dynamic MRI Measures of Peripheral Vascular Function. Front. Physiol. 11:120. doi: 10.3389/fphys.2020.00120

INTRODUCTION

Blood flow is necessary to sustain life through the delivery of substrates for cellular metabolism including oxygen and nutrients, and the removal of waste products. Regulation of blood flow to tissue is a complex and dynamically controlled process mediated in large part by the vascular endothelium (Furchgott and Zawadzki, 1980). Endothelial dysfunction, the phenotypic presentation of a vasoconstricted, pro-inflammatory, thrombogenic state, underlies many diseases

including atherosclerosis (Harrison et al., 1987) and diabetes (Yamauchi et al., 1990), and is present in patients with significant risk factors for cardiovascular disease including smoking (Messner and Bernhard, 2014), aging (Lakatta and Levy, 2003) and hypertension (Zeiher et al., 1993). A reduced bioavailability or activity of nitric oxide is thought to be the predominant mechanism underlying endothelial dysfunction, resulting in reduced vasodilation and delayed vascular reactivity (Davignon, 2004). Other articles in this special issue will focus on the physiologic importance of mediators that maintain vascular homeostasis in the microvasculature and endothelium, but here, we briefly overview some emerging non-invasive magnetic resonance imaging (MRI) methods to evaluate peripheral vascular function in the context of injury and inflammation.

In general, assessment of endothelial function can be accomplished by measuring the magnitude and temporal dynamics of blood flow and oxygenation in response to a vasoactive stimulus such as exercise, induced ischemia, or chemical stimulation (e.g., Acetylcholine). To evaluate peripheral vascular function, a reactive hyperemia protocol is commonly used, in which the response following a period of induced ischemia is interrogated (**Figure 1**). During the period of arterial occlusion, blood flow in the arteries, capillaries, and veins is suspended. The stagnant blood in the capillary bed is subjected to continued oxygen extraction (in short, the desaturated blood serves as an endogenous tracer), though the oxygen diffusion gradient between blood and tissue decreases as a function of ischemic duration (Lebon et al., 1998). Meanwhile, there is local accumulation of vasodilators, activation of inwardly rectifying potassium channels and Na + /K + -ATPase (Crecelius et al., 2013), and a reduction in arteriolar pressure, causing an overall decrease in vascular resistance (Carlsson et al., 1987). Following cuff release, reactive hyperemia ensues with a transient surge of macrovascular flow rate as much as five-fold increase owing to the decrease in microvascular resistance downstream at the level of the arterioles. This increase of blood flow also amplify shear stress at the vessel wall, ultimately triggering additional arteriolar vasodilation (Tagawa et al., 1994; Widlansky et al., 2003). The return of blood flow causes an increase in perfusion, delivering oxygenated blood to the ischemic tissue and driving out the accumulated vasodilators and deoxygenated capillary blood. In the presence of endothelial dysfunction, the reactive hyperemia response in dampened and/or delayed (Fronek et al., 1973; Lieberman et al., 1996; Ledermann et al., 2006; Isbell et al., 2007). Changes in vascular reactivity may therefore provide insight into early, sub-clinical disease states (Flammer et al., 2012).

Conventional physiologic measurements used to assess surrogate markers of endothelial function include ultrasound to quantify blood flow and arterial diameter, strain gauge plethysmography to measure tissue perfusion, and invasive catheterization for blood gas analysis to determine oxygen saturation in the arteries and veins. Though commonly used clinically for evaluation of anatomy, MRI technology is far richer and has the greater potential to quantify a spectrum of physiologic parameters of interest, non-invasively across multiple vascular beds in a single session. Other imaging modalities including contrast-enhanced MRI (Isbell et al., 2007; Zhang et al., 2019), positron emission tomography (PET) (Heinonen et al., 2010), near infrared spectroscopy (NIRS) (Nioka et al., 2006; Baker et al., 2017), and ultrasound (Celermajer et al., 1992) have also been used to evaluate peripheral vascular function. However, non-contrast MRI has the advantage of

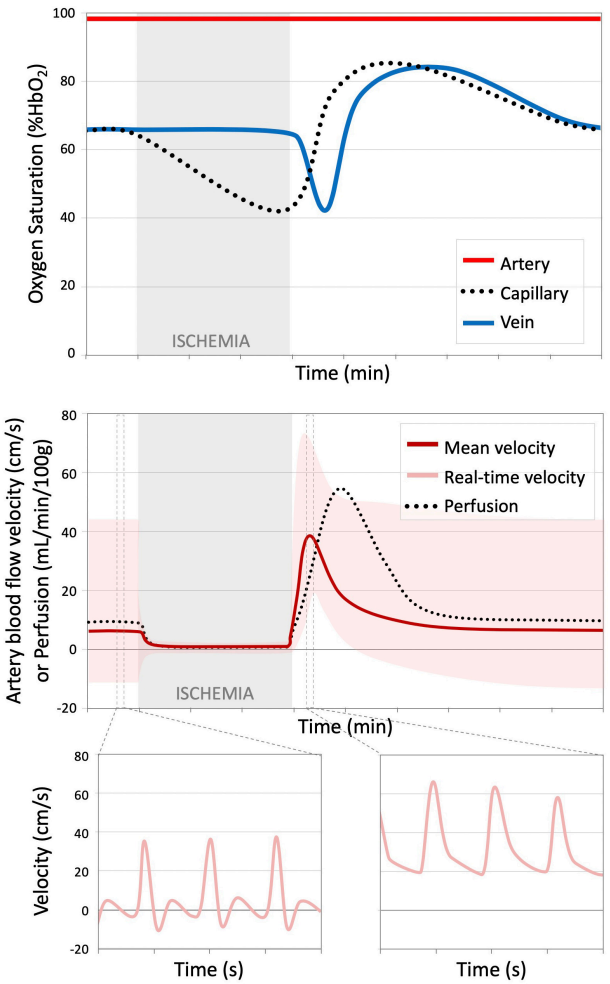

FIGURE 1 | Time course oxygen saturation and blood flow over a reactive hyperemia protocol. (Top) Illustration of hemoglobin oxygen saturation (%HbO_2) measured in the artery, proximal to the cuff (red), capillary (black dotted line), and venous (blue) circulations. During the period of ischemia, arterial and venous %HbO_2 remain constant, but progressively decreases in the stagnant blood in the capillaries. Upon cuff release, the deoxygenated blood from the capillaries serves as an endogenous tracer and can be tracked as it flows into the large draining veins. The capillary bed and venous oxygen saturations surpass the baseline condition during hyperemia. (Bottom) Blood flow velocity and tissue perfusion decrease from the relative low baseline value to approximately zero during induced ischemia. Following cuff release, there is a transient surge in arterial flow velocity, which translates to increased perfusion, albeit at a slight lag. This figure shows the mean arterial velocity averaged over a cardiac cycle (dark red) and the real-time flow waveform (light red). The arterial flow waveform, initially triphasic at rest in healthy subjects, becomes entirely antegrade during the period of hyperemia. Dynamic, temporally resolved MRI methods can quantify various aspects of the illustrated processes. Figure adapted from Englund et al. (2013) and Englund et al. (2016) with permission.

being spatially resolved (unlike plethysmography) with a fixed frame of reference (compared to NIRS or ultrasound) and is entirely non-invasive (compared to contrast-enhanced MRI or catheterization) and does not expose the subjects to ionizing radiation (in contrast to PET). Specific tailoring of the MRI pulse sequence allows for quantification of various parameters which can be expressed in physiologic units, including for instance, blood flow velocity (cm/s) or flow rate (mL/min), tissue perfusion (mL/min/100g), and oxygen saturation (% hemoglobin oxygen saturation, $\%HbO_2$).

Here, we review recent developments and results from quantitative, dynamic, non-contrast MRI studies for evaluation of vascular function and reactivity including blood oxygen level-dependent (BOLD) imaging, arterial spin labeling (ASL), phase contrast (PC), including MR-measured pulse wave velocity (PWV), luminal flow mediated dilation (FMD), and dynamic MR oximetry, summarized in **Table 1**. The goal of this manuscript is to introduce the reader to these MRI methods and to review studies that have employed these methods as biomarkers of disease presence, severity, and in the evaluation of treatment response.

BOLD MRI TO ASSESS CAPILLARY OXYGEN CONTENT

The most widely used MRI method to evaluate changes in blood flow and oxygenation is the measurement of the BOLD response (Raichle, 1998; Kim and Ogawa, 2012). BOLD MRI is perhaps best known as the basis for functional neuroimaging experiments, providing insight into patterns of neural activity in response to a specified task (Glover, 2011). Similar principles may be applied to the peripheral circulation, allowing BOLD MRI of skeletal muscle to inform on vasoactive changes in response to exercise or induced ischemia.

The BOLD signal arises due to changes in the local content of paramagnetic deoxyhemoglobin. In the context of a reactive hyperemia paradigm, during the period of induced ischemia constant oxidative metabolism in nearby cells will cause blood in the capillary bed to desaturate, increasing the local concentration of deoxyhemoglobin. This accumulation of paramagnetic deoxyhemoglobin will cause the local magnetic field to become more inhomogeneous, ultimately leading to faster decay of the MR signal (e.g., decreased effective transverse relaxation time, T_2^*). Following release of the cuff, the surge of oxygenated blood decreases the concentration of deoxyhemoglobin in the capillaries (increasing T_2^*), while at the same time, expanding the blood volume, which tends to decrease T_2^*. Thus, the BOLD signal serves as a surrogate marker of capillary bed oxygen content, mediated by both changes in blood flow/volume and oxygen extraction. Complicating the physiologic interpretation even more, BOLD signal is also sensitive to changes in cellular pH, vessel diameter, and vessel orientation (Lebon et al., 1998; Damon et al., 2007; Sanchez et al., 2010; Partovi et al., 2012a), and is significantly impacted by static magnetic field inhomogeneities.

Despite the complicated origin of the BOLD signal, its implementation is quite straightforward. Gradient-recalled echo MR images are acquired with echo time approximately equal to the expected T_2^* (yielding T_2^*- or BOLD-weighted images), or with multiple echoes to quantify T_2^* from the rate of signal decay. The dynamic data, generally measured at a temporal resolution of 1 s (Huegli et al., 2008; Schulte et al., 2008; Kos et al., 2009; Towse et al., 2016; Tonson et al., 2017; Larsen et al., 2019), are normalized by the baseline signal intensity and the relative changes in response to the vasoactive stimulus (e.g., exercise or induced ischemia) are then evaluated. The relative magnitude of the response (e.g., maximum signal change following cuff release/exercise, or minimum during induced ischemia) and the temporal response kinetics (e.g., time to half maximum/minimum, time to peak response) provide insight into the combined blood flow and oxygenation responses that are occurring locally at the level of the capillary bed.

Early manifestations of endothelial dysfunction, even in the absence of overt cardiovascular disease, have been observed with BOLD MRI. In general, those with risk factors for cardiovascular disease such as older subjects versus younger individuals (Schulte et al., 2008; Kos et al., 2009) and smokers compared to non-smokers (Nishii et al., 2015), demonstrated a blunting and delay of the BOLD response following induced ischemia (i.e., reactive hyperemia). In addition, impaired vascular function has been observed from BOLD imaging in clinically overt diseases including peripheral artery disease (PAD) (Ledermann et al., 2006; Englund et al., 2015; Li et al., 2016; Bakermans et al., 2019), critical limb ischemia (CLI) (Huegli et al., 2008), and systemic sclerosis (Partovi et al., 2012b, 2013). Assessment of treatment response following percutaneous transluminal angioplasty in patients with CLI (Huegli et al., 2008; Bajwa et al., 2016), showed that patients had improvements in the reactive hyperemia response as assessed by BOLD imaging. Another recent study used BOLD MRI to investigate the therapeutic effect of antioxidants on the response to exercise and induced ischemia following eccentric exercise, but contrary to their hypothesis found no significant effect (Larsen et al., 2019).

These results are, in general, promising for the use of BOLD imaging during reactive hyperemia as a biomarker for disease

TABLE 1 | Summary of MRI methods to dynamically evaluate vascular function.

MR method	Measurement	Units	Site	Typical temporal resolution
BOLD	Relative capillary bed oxygen content	% change from baseline	Microvasculature	1–2 s
ASL	Tissue perfusion	mL/min/100g	Microvasculature	2–16 s
PC	Blood flow velocity, flow rate, PWV	cm/s or mL/min	Large arteries, veins	5–60 ms
FMD	Vessel diameter or area	% change from baseline	Large arteries	12 s
Oximetry	Hemoglobin oxygen saturation	$\%HbO_2$	Microvasculature or large draining veins	2–228 s

BOLD, blood oxygen level-dependent; ASL, arterial spin labeling; PC, phase contrast; PWV, pulse wave velocity; FMD, flow-mediated dilation.

progression and therapeutic response, particularly due to the ease of implementation. However, the BOLD response is inherently measured relative to some initial condition, is not quantified in physiologic units, and it is difficult to separate the contributions of flow and oxygenation changes to the measured signal.

ASL MRI FOR PERFUSION QUANTIFICATION

To quantify tissue perfusion in physiologically relevant units, another type of non-contrast MRI acquisition, ASL, can be used (Detre et al., 1992; Williams et al., 1992; Kim, 1995; Kim et al., 1997; Wong et al., 1997). In ASL, a magnetic label (i.e., inversion pulse) is applied to water protons in arterial blood, allowing the blood, serving as an endogenous tracer, to be tracked as it flows from the large arteries into the capillary bed and perfuses the tissue. The perfusion signal is isolated by pairwise subtraction between two images, the second acquired without application of the arterial tagging pulse. The difference between these two images removes the contribution from static background tissue, leaving behind only signal related to perfusion of the labeled blood. This signal can be converted into perfusion in physiologic units of mL/min/100g through application of various models that describe the exchange of the labeled protons between arterial blood and tissue (Buxton et al., 1998; Raynaud et al., 2001; Alsop et al., 2014).

In reactive hyperemia experiments, the time course of perfusion, measured at temporal resolution up to 2 s (e.g., Englund et al., 2016) is analyzed to determine the speed (e.g., time to peak), and magnitude (e.g., peak hyperemic flow) of the post-ischemic perfusion response. Unlike BOLD, the magnitude of the response quantifies the amount of tissue perfusion, and the timing is unimpacted by the concurrent changes in capillary bed oxygen saturation. Prior studies have uncovered an association between these ASL-based measures and PAD disease presence and severity (Wu et al., 2009; Englund et al., 2015). Compared to healthy controls, patients with PAD had a decrease in peak perfusion, and with worsening disease severity, there was a prolongation of the time to peak perfusion.

In addition to the muscles of the leg, perfusion of the foot has also been interrogated (Zheng et al., 2014), finding that patients with diabetes had impaired perfusion following toe extension exercise compared to healthy controls. Finally, investigation of the impact of percutaneous transluminal angioplasty with reactive hyperemia ASL measurements showed that patients with CLI had improvements in perfusion in some but not all muscles following intervention (Grözinger et al., 2013), which may be reflective of the heterogeneity seen between muscles prior to intervention (Wu et al., 2008, 2009).

While ASL measures microvascular perfusion, the blood flow response in the capillary bed following induced ischemia is mediated by both the macro- and microvascular reactivity. This means that it's not possible to separate the effects from macrovascular stenoses from potential primary microvascular dysfunction. In PAD, the macrovascular lesions are generally unmodified by conservative therapies such as exercise (Sanne and Sivertsson, 1968), thus there is significant interest in isolating the microvascular response. Efforts to disentangle these two effects has come in the form of physiologic models of the reactive hyperemia perfusion response (Chen and Wright, 2017), or through simultaneous measurement of microvascular and macrovascular blood flow responses (Englund et al., 2017). Additional work to clearly define and isolate the microvascular contribution is necessary.

PHASE CONTRAST MRI FOR QUANTIFICATION OF MACROVASCULAR FLOW

In addition to quantifying perfusion in the microcirculation, MRI can also be used to measure blood flow in the large arteries and veins via PC. In PC-MRI, magnetic field gradients are used to encode the motion of the water protons into the signal phase (Moran, 1982; Bryant et al., 1984; Moran et al., 1985). A thorough technical explanation of PC-MRI can be found in Nayak et al. (2015), but briefly, application of bi-polar magnetic field gradients will impart a residual phase offset in moving protons relative to static tissue as a function of velocity and gradient parameters (e.g., duration, temporal separation, and strength). Since the timing and gradient strength are chosen pulse sequence parameters, the measured phase can be converted to velocity (in cm/s).

By gating the phase contrast acquisition to the electrocardiogram, time-resolved images of blood flow throughout the cardiac cycle can be reconstructed (Nayler et al., 1986). Acquisition generally takes several seconds to minutes depending on the desired apparent temporal resolution, as data are sampled over several heartbeats and synthesized together to create images over the cardiac cycle. In young healthy subjects, the baseline flow waveform of arteries in the high-resistance peripheral circulation (e.g., superficial femoral artery) is triphasic, with high velocity antegrade flow during the systolic phase of the cardiac cycle, followed by retrograde flow during early and late diastole, respectively. In contrast, patients with flow-limiting stenoses in the peripheral arteries generally have a monophasic flow waveform, attributed to decreased vascular resistance distal to the stenosis (Akbari, 2012). In these patients, the flow profile loses the retrograde flow during diastole, remaining antegrade throughout the cardiac cycle (Bernstein et al., 1970; Mohajer et al., 2006; Langham et al., 2013a; Versluis et al., 2014).

Furthering this technique, velocity vector components can be resolved by encoding motion in each of the three directions in succession, and if 3-dimensional spatial encoding is implemented at the same time, 4D flow images can be reconstructed (i.e., velocity vector is time-resolved (Buonocore, 1998; Frydrychowicz et al., 2007). 4D flow MRI data allow assessment of complex flow dynamics and can provide striking visualization of the impact of macrovascular lesions, showing flow jets, vortices, and areas of turbulence, which may be useful for understanding the patterns of atherosclerotic plaque development (Markl et al., 2012). Additionally, simultaneous quantification of the temporally

resolved blood flow waveform at two distinct locations along the artery of interest can be used to compute PWV, a measure of arterial stiffness (Wentland et al., 2014). In contrast to the traditional arterial applanation tonometry, MR-measured PWV is not limited to superficial arteries, can provide accurate path length measurements, and can probe shorter segments of the artery, providing regional PWV of the aortic arch or femoral artery (Langham et al., 2011).

In addition to this baseline characterization of the arterial flow waveform, the dynamics of the arterial blood flow response during reactive hyperemia (Mohiaddin et al., 2002; Langham et al., 2010b, 2013a, 2015) or following exercise (Englund et al., 2017) provide insight into endothelial function, vascular reactivity, and flow reserve (Versluis et al., 2012). By quantifying macrovascular blood flow dynamically in the feeding artery, the time to peak flow and the duration of forward flow can be measured. These parameters are increased in the presence of PAD (Langham et al., 2013a) and are sensitive to early changes in endothelial function that occur with smoking, aging (Langham et al., 2015), and have recently been shown to be acutely impaired following nicotine-free e-cigarette aerosol inhalation (Caporale et al., 2019).

FLOW-MEDIATED DILATION FOR EVALUATION OF ENDOTHELIAL FUNCTION

Perhaps the most widely studied surrogate marker of endothelial function is ultrasound measurements of FMD in the brachial artery following cuff-induced ischemia (Celermajer et al., 1992). While often regarded as an effective surrogate marker for endothelial function (or dysfunction), the method's poor intra-subject reproducibility (Hardie et al., 1997) plague brachial artery FMD. The reported coefficients of variation of FMD measurements vary widely from as little as 1.5% to approximately 50% in others (Sorensen et al., 1995; Andrews et al., 1997; Hardie et al., 1997; de Roos et al., 2001). This limitation is magnified since the average magnitude of FMD is approximately 5% (Boushel and Piantadosi, 2000) and ultrasound settings such as dynamic range, gain and probe distance are known to significantly affect diameter measurements (Potter et al., 2008). For these reasons, the value of ultrasound-based FMD measurement in routine clinical practice has been put into question (Bhagat et al., 1997; Pyke and Tschakovsky, 2005; Sejda et al., 2005) since its introduction over 25 years ago.

Magnetic resonance imaging (MRI) can also be used to quantify vessel cross-sectional area through a variety of measures including phase contrast angiography (Silber et al., 2001), high-resolution cine bright-blood imaging (Wiesmann et al., 2004), and dynamic vessel wall imaging methods (Langham et al., 2013b). In addition to the measurement of vessel diameter needed for FMD quantification, these MRI methods, depending on the sequence used, can be used to evaluate the vessel wall or flow dynamics. Brachial artery FMD measured by MRI was found to be lower in smokers compared to non-smokers (Wiesmann et al., 2004), and in long-term users of birth control (contraceptive depot medroxyprogesterone acetate) during menstruation compared to control women with no intake of progestogens (Sorensen et al., 2002).

A new approach to rapidly acquire high-resolution vessel-wall images to assess plaque burden in PAD have been modified to quantify superficial femoral artery FMD at 60, 90, and 120 s after cuff release (Langham et al., 2013b, 2016). Of note is that the luminal FMD (denoted FMD_L), consisting of a measurement of the change in cross-sectional area ($FMD_L \equiv \delta A/A_o \approx 2\delta r/r_o$), where δr and r_0 are the changes in radius, and radius at rest, respectively, yields greater detection sensitivity compared to ultrasound-based-measurement of the change in arterial diameter, i.e., $FMD \equiv \delta d/d_0 = \delta r/r_o$. Recent work indicates that the superficial femoral artery FMD_L is sensitive enough to detect acute effects of nicotine-free electronic cigarette aerosol inhalation (Caporale et al., 2019).

DYNAMIC OXIMETRY FOR QUANTIFICATION OF VASCULAR REACTIVITY

While the previous methods generally focused on the dynamic quantification of blood flow, measurement of blood oxygen saturation (e.g., $\%HbO_2$) may also be useful for understanding the underlying tissue metabolism. Differences in the magnetic susceptibility of oxygenated and deoxygenated hemoglobin (Pauling and Coryell, 1936) can be exploited to quantify $\%HbO_2$ in the microvasculature based on the irreversible transverse relaxation time, T_2' (He and Yablonskiy, 2006), or $\%HbO_2$ in large vessels via T_2- (Lu and Ge, 2008) or MR susceptometry- (Haacke et al., 1997; Fernández-Seara et al., 2006) based oximetry. Furthermore, when these measures of oxygen extraction are combined with the previously described measures of blood flow, the muscle oxidative metabolism can be computed via Fick's principle (Zheng et al., 2013; Mathewson et al., 2014; Englund et al., 2017).

In addition, temporally resolved measurement of intravascular venous oxygen saturation (SvO_2) throughout an ischemia-reperfusion paradigm allows for the intravascular blood to act as an endogenous tracer as it transits from the capillary bed to the large draining vein. During the period of induced ischemia, oxygen extraction continues in the stationary blood of the capillary bed and upon cuff release, the hyperemic arterial inflow drives deoxygenated blood from the capillary bed into the collecting veins, causing the measured SvO_2 to drop sharply (Langham et al., 2010a, 2013a, 2015; Langham and Wehrli, 2011). Thus blood flow, tissue metabolism, and endothelium-mediated dilation underlie the measured SvO_2 dynamics measured in the large draining vein.

Washout time (time to minimum SvO_2), upslope – representing the rate of resaturation (maximum slope during recovery), and overshoot (peak SvO_2 minus baseline SvO_2) can be extracted from the SvO_2 time course data. These metrics reflect the reactivity of the microvessels to NO-mediated vasodilation. Langham et al. revealed an association between alterations in the SvO_2 time course-derived metrics in the

femoral (Langham et al., 2010a; Langham and Wehrli, 2011) or posterior tibial (Englund et al., 2015) veins and the presence of PAD. Compared to age-matched healthy controls and young healthy subjects, patients with PAD had a longer washout time, diminished upslope, and lower overshoot, suggesting endothelial dysfunction. Furthermore, these dynamic measurement of SvO_2 are altered in pre-clinical disease states including aging and smoking (Langham et al., 2015), and most recently have been shown to be sensitive to acute effects of nicotine-free e-cig aerosol inhalation (Caporale et al., 2019).

DISCUSSION

The methods and results described herein illustrate the vast capability of MRI for dynamic evaluation of endothelial function. While there are many other approaches to quantify blood flow, arterial diameter, or oxygen saturation, MR imaging is the only modality capable of providing all parameters, non-invasively, without being limited by depth or radiation exposure. However, many of the described methods are not standard acquisition schemes available on clinical MRI scanners. Thus, there is a need for open-access to the acquisition and image analysis software packages, which would help to expand the availability of these advanced methods to researchers without dedicated MR physicists and image analysis experts.

In general, the findings reviewed herein revealed that the reactive hyperemia response was blunted and delayed in various diseases and conditions with underlying endothelial dysfunction, regardless of the measurement method, corroborating prior non-MR-based research (e.g., Fronek et al., 1973). While these methods have been described in the context of investigation of peripheral vascular function, similar strategies could be used to measure cerebrovascular reactivity albeit in response to different vasoactive stimuli (Fisher et al., 2018).

Use of MRI and selection of imaging contrast may ultimately help to unveil the mechanism of action for disease progression or therapeutic response. For example, it is known that exercise improves pain-limited walking distance in patients with PAD (Murphy et al., 2012), but the mechanism is not entirely understood. Using MRI, changes in tissue perfusion could be used to assess the contribution of microvascular angiogenesis, while measurement of venous oxygen saturation may provide insight into changes in the mitochondrial efficiency and metabolic processes, and the combined effect of these factors may be unveiled by BOLD imaging. Finally, MR-measured perfusion, FMD, and oximetry could replace plethysmography, ultrasound, or invasive catheter-based measures for studies investigating the specific signaling pathways involved in vasodilation (e.g., Crecelius et al., 2013), or the effect of dietary supplements on blood flow during exercise (e.g., Richards et al., 2018).

The methods described herein have thus far been largely relegated to the realm of research. Use as a clinical tool and biomarker for disease progression and therapeutic response mandates that the accuracy, precision, and repeatability of the measurements be well documented, and that the methods be accessible on clinical scanners. Future studies combining such MRI methods with clinical measures and outcomes will help to define the additive benefit of these imaging metrics in cohorts of subjects as well as individual patients.

AUTHOR CONTRIBUTIONS

EE and ML drafted, edited, and approved the final version of the manuscript.

FUNDING

This work was supported by NIH grants U01 HD087180 and R01 HL139358.

REFERENCES

Akbari, C. M. (2012). "Clinical features and diagnosis of peripheral arterial disease," in *The Diabetic Foot*, eds A. Piaggesi, and J. Apelqvist (Totowa, NJ: Humana Press), 75–85. doi: 10.1007/978-1-61779-791-0_5

Alsop, D. C., Detre, J. A., Golay, X., Günther, M., Hendrikse, J., Hernandez-Garcia, L., et al. (2014). Recommended implementation of arterial spin-labeled perfusion MRI for clinical applications: a consensus of the ISMRM perfusion study group and the European consortium for ASL in dementia. *Magn. Reson. Med.* 73, 102–116. doi: 10.1002/mrm.25197

Andrews, T. C., Whitney, E. J., Green, G., Kalenian, R., and Personius, B. E. (1997). Effect of gemfibrozil +/- niacin +/- cholestyramine on endothelial function in patients with serum low-density lipoprotein cholesterol levels <160 mg/dl and high-density lipoprotein cholesterol levels <40 mg/dl. *Am. J. Cardiol.* 80, 831–835. doi: 10.1016/s0002-9149(97)00531-6

Bajwa, A., Wesolowski, R., Patel, A., Saha, P., Ludwinski, F., Ikram, M., et al. (2016). Blood Oxygenation level-dependent CMR-derived measures in critical limb ischemia and changes with revascularization. *JACC* 67, 420–431. doi: 10.1016/j.jacc.2015.10.085

Baker, W. B., Li, Z., Schenkel, S. S., Chandra, M., Busch, D. R., Englund, E. K., et al. (2017). Effects of exercise training on calf muscle oxygen extraction and blood flow in patients with peripheral artery disease. *J. Appl. Physiol.* 123, 1599–1609. doi: 10.1152/japplphysiol.00585.2017

Bakermans, A. J., Wessel, C. H., Zheng, K. H., Groot, P. F. C., Stroes, E. S. G., and Nederveen, A. J. (2019). Dynamic magnetic resonance measurements of calf muscle oxygenation and energy metabolism in peripheral artery disease. *J. Magn. Reson. Imaging* 51, 98–107. doi: 10.1002/jmri.26841

Bernstein, E. F., Murphy, A. E., Shea, M. A., and Housman, L. B. (1970). Experimental and clinical experience with transcutaneous doppler ultrasonic flowmeters. *AMA Arch. Surg.* 101, 21–25.

Bhagat, K., Hingorani, A., and Vallance, P. (1997). Flow associated or flow mediated dilatation? More than just semantics. *Heart* 78, 7–8. doi: 10.1136/hrt.78.1.7

Boushel, R., and Piantadosi, C. A. (2000). Near-infrared spectroscopy for monitoring muscle oxygenation. *Acta Physiol. Scand.* 168, 615–622. doi: 10.1046/j.1365-201x.2000.00713.x

Bryant, D. J., Payne, J. A., Firmin, D. N., and Longmore, D. B. (1984). Measurement of flow with NMR imaging using a gradient pulse and phase difference technique. *J. Comput. Assist. Tomogr.* 8, 588–593. doi: 10.1097/00004728-198408000-00002

Buonocore, M. H. (1998). Visualizing blood flow patterns using streamlines, arrows, and particle paths. *Magn. Reson. Med.* 40, 210–226. doi: 10.1002/mrm.1910400207

Buxton, R. B., Frank, L. R., Wong, E. C., Siewert, B., Warach, S., and Edelman, R. R. (1998). A general kinetic model for quantitative perfusion imaging with arterial spin labeling. *Magn. Reson. Med.* 40, 383–396. doi: 10.1002/mrm.1910400308

Caporale, A., Langham, M. C., Guo, W., Johncola, A., Chatterjee, S., and Wehrli, F. W. (2019). Acute effects of electronic cigarette aerosol inhalation on vascular function detected at quantitative MRI. *Radiology* 293, 97–106. doi: 10.1148/radiol.2019190562

Carlsson, I., Sollevi, A., and Wennmalm, A. (1987). The role of myogenic relaxation, adenosine and prostaglandins in human forearm reactive hyperaemia. *J. Physiol.* 389, 147–161. doi: 10.1113/jphysiol.1987.sp016651

Celermajer, D. S., Sorensen, K. E., Gooch, V. M., Spiegelhalter, D. J., Miller, O. I., Sullivan, I. D., et al. (1992). Non-invasive detection of endothelial dysfunction in children and adults at risk of atherosclerosis. *Lancet* 340, 1111–1115. doi: 10.1016/0140-6736(92)93147-f

Chen, H.-J., and Wright, G. A. (2017). A physiological model for interpretation of arterial spin labeling reactive hyperemia of calf muscles. *PLoS One* 12:e0183259. doi: 10.1371/journal.pone.0183259

Crecelius, A. R., Richards, J. C., Luckasen, G. J., Larson, D. G., and Dinenno, F. A. (2013). Reactive hyperemia occurs via activation of inwardly rectifying potassium channels and Na +/K +-ATPase in Humans. *Circ. Res.* 113, 1023–1032. doi: 10.1161/CIRCRESAHA.113.301675

Damon, B. M., Hornberger, J. L., Wadington, M. C., Lansdown, D. A., and Kent-Braun, J. A. (2007). Dual gradient-echo MRI of post-contraction changes in skeletal muscle blood volume and oxygenation. *Magn. Reson. Med.* 57, 670–679. doi: 10.1002/mrm.21191

Davignon, J. (2004). Role of Endothelial Dysfunction In Atherosclerosis. *Circulation* 109, III–27–III–32. doi: 10.1161/01.CIR.0000131515.03336.f8

de Roos, N. M., Bots, M. L., and Katan, M. B. (2001). Replacement of dietary saturated fatty acids by trans fatty acids lowers serum HDL cholesterol and impairs endothelial function in healthy men and women. *Atheroscler. Thromb. Vasc Biol.* 21, 1233–1237. doi: 10.1161/hq0701.092161

Detre, J. A., Leigh, J. S., Williams, D. S., and Koretsky, A. P. (1992). Perfusion imaging. *Magn. Reson. Med.* 23, 37–45. doi: 10.1002/mrm.1910230106

Englund, E. K., Langham, M. C., Li, C., Rodgers, Z. B., Floyd, T. F., Mohler, E. R., et al. (2013). Combined measurement of perfusion, venous oxygen saturation, and skeletal muscle T_2^* during reactive hyperemia in the leg. *J. Cardiovasc. Magn. Reson.* 15:70. doi: 10.1186/1532-429X-15-70

Englund, E. K., Langham, M. C., Ratcliffe, S. J., Fanning, M. J., Wehrli, F. W., Mohler, E. R., et al. (2015). Multiparametric assessment of vascular function in peripheral artery disease: dynamic measurement of skeletal muscle perfusion, blood-oxygen-level dependent signal, and venous oxygen saturation. *Circ.Cardiovasc. Imaging* 8:e002673. doi: 10.1161/CIRCIMAGING.114.002673

Englund, E. K., Rodgers, Z. B., Langham, M. C., Mohler, E. R. III, Floyd, T. F., and Wehrli, F. W. (2016). Measurement of skeletal muscle perfusion dynamics with pseudo-continuous arterial spin labeling (pCASL): assessment of relative labeling efficiency at rest and during hyperemia, and comparison to pulsed arterial spin labeling (PASL). *J. Magn. Reson. Imaging* 44, 929–939. doi: 10.1002/jmri.25247

Englund, E. K., Rodgers, Z. B., Langham, M. C., Mohler, E. R. III, Floyd, T. F., and Wehrli, F. W. (2017). Simultaneous measurement of macro- and microvascular blood flow and oxygen saturation for quantification of muscle oxygen consumption. *Magn. Reson. Med.* 79, 846–855. doi: 10.1002/mrm.26744

Fernández-Seara, M. A., Techawiboonwong, A., Detre, J. A., and Wehrli, F. W. (2006). MR susceptometry for measuring global brain oxygen extraction. *Magn. Reson. Med.* 55, 967–973. doi: 10.1002/mrm.20892

Fisher, J. A., Venkatraghavan, L., and Mikulis, D. J. (2018). Magnetic resonance imaging-based cerebrovascular reactivity and hemodynamic reserve. *Stroke* 49, 2011–2018. doi: 10.1161/STROKEAHA.118.021012

Flammer, A. J., Anderson, T., Celermajer, D. S., Creager, M. A., Deanfield, J., Ganz, P., et al. (2012). The assessment of endothelial function: from research into clinical practice. *Circulation* 126, 753–767. doi: 10.1161/CIRCULATIONAHA.112.093245

Fronek, A., Johansen, K., Dilley, R. B., and Bernstein, E. F. (1973). Ultrasonographically monitored postocclusive reactive hyperemia in diagnosis of peripheral arterial occlusive disease. *Circulation* 48, 149–152. doi: 10.1161/01.cir.48.1.149

Frydrychowicz, A., Winterer, J. T., Zaitsev, M., Jung, B., Hennig, J., Langer, M., et al. (2007). Visualization of iliac and proximal femoral artery hemodynamics using time-resolved 3D phase contrast MRI at 3T. *J. Magn. Reson. Imaging* 25, 1085–1092. doi: 10.1002/jmri.20900

Furchgott, R. F., and Zawadzki, J. V. (1980). The obligatory role of endothelial-cells in the relaxation of arterial smooth-muscle by acetylcholine. *Nature* 288, 373–376. doi: 10.1038/288373a0

Glover, G. H. (2011). Overview of functional magnetic resonance imaging. *Neurosurg. Clin. N. Am.* 22, 133–139. doi: 10.1016/j.nec.2010.11.001

Grözinger, G., Pohmann, R., Schick, F., Grosse, U., Syha, R., Brechtel, K., et al. (2013). Perfusion measurements of the calf in patients with peripheral arterial occlusive disease before and after percutaneous transluminal angioplasty using Mr arterial spin labeling. *J. Magn. Reson. Imaging* 40, 980–987. doi: 10.1002/jmri.24463

Haacke, E. M., Lai, S., Reichenbach, J. R., Kuppusamy, K., Hoogenraad, F., Takeichi, H., et al. (1997). In vivo measurement of blood oxygen saturation using magnetic resonance imaging: a direct validation of the blood oxygen level-dependent concept in functional brain imaging. *Hum Brain Mapp* 5, 341–346. doi: 10.1002/(SICI)1097-019319975:5

Hardie, K. L., Kinlay, S., Hardy, D. B., Wlodarczyk, J., Silberberg, J. S., and Fletcher, P. J. (1997). Reproducibility of brachial ultrasonography and flow-mediated dilatation (FMD) for assessing endothelial function. *Aust. N. Z. J. Med.* 27, 649–652. doi: 10.1111/j.1445-5994.1997.tb00992.x

Harrison, D. G., Freiman, P. C., Armstrong, M. L., Marcus, M. L., and Heistad, D. D. (1987). Alterations of vascular reactivity in atherosclerosis. *Circ. Res.* 61, II74–II80.

He, X., and Yablonskiy, D. A. (2006). Quantitative BOLD: mapping of human cerebral deoxygenated blood volume and oxygen extraction fraction: default state. *Magn. Reson. Med.* 57, 115–126. doi: 10.1002/mrm.21108

Heinonen, I., Kemppainen, J., Kaskinoro, K., Peltonen, J. E., Borra, R., Lindroos, M. M., et al. (2010). Comparison of exogenous adenosine and voluntary exercise on human skeletal muscle perfusion and perfusion heterogeneity. *J. Appl. Physiol.* 108, 378–386. doi: 10.1152/japplphysiol.00745.2009

Huegli, R. W., Schulte, A.-C., Aschwanden, M., Thalhammer, C., Kos, S., Jacob, A. L., et al. (2008). Effects of percutaneous transluminal angioplasty on muscle BOLD-MRI in patients with peripheral arterial occlusive disease: preliminary results. *Eur. Radiol.* 19, 509–515. doi: 10.1007/s00330-008-1168-6

Isbell, D. C., Epstein, F. H., Zhong, X., DiMaria, J. M., Berr, S. S., Meyer, C. H., et al. (2007). Calf muscle perfusion at peak exercise in peripheral arterial disease: measurement by first-pass contrast-enhanced magnetic resonance imaging. *J. Magn. Reson. Imaging* 25, 1013–1020. doi: 10.1002/jmri.20899

Kim, S. G. (1995). Quantification of relative cerebral blood flow change by flow-sensitive alternating inversion recovery (FAIR) technique: application to functional mapping. *Magn. Reson. Med.* 34, 293–301. doi: 10.1002/mrm.1910340303

Kim, S.-G., and Ogawa, S. (2012). Biophysical and physiological origins of blood oxygenation level-dependent fMRI signals. *JCBFM* 32, 1188–1206. doi: 10.1038/jcbfm.2012.23

Kim, S. G., Tsekos, N. V., and Berr, S. S. (1997). Perfusion imaging by a flow-sensitive alternating inversion recovery (FAIR) technique: application to functional brain imaging. *Magn. Reson. Med.* 37, 425–435. doi: 10.1002/mrm.1910370321

Kos, S., Klarhöfer, M., and Aschwanden, M. (2009). Simultaneous dynamic blood oxygen level-dependent magnetic resonance imaging of foot and calf muscles: aging effects at ischemia and postocclusive hyperemia in .... *Invest. Radiol.* 44, 741–747. doi: 10.1097/rli.0b013e3181b248f9

Lakatta, E. G., and Levy, D. (2003). Arterial and cardiac aging: major shareholders in cardiovascular disease enterprises. *Circulation* 107, 139–146. doi: 10.1161/01.CIR.0000048892.83521.58

Langham, M. C., Desjardins, B., Englund, E. K., Mohler, E. R. III, Floyd, T. F., and Wehrli, F. W. (2016). Rapid high-resolution, self-registered, dual lumen-contrast MRI method for vessel-wall assessment in peripheral artery disease. *Acad. Radiol.* 23, 457–467. doi: 10.1016/j.acra.2015.12.015

Langham, M. C., Englund, E. K., Mohler, E. R. III, Li, C., Rodgers, Z. B., Floyd, T. F., et al. (2013a). Quantitative CMR markers of impaired vascular reactivity associated with age and peripheral artery disease. *J. Cardiovasc. Magn. Reson.* 15, 1–10. doi: 10.1186/1532-429X-15-17

Langham, M. C., Floyd, T. F., Mohler, E. R., Magland, J. F., and Wehrli, F. W. (2010a). Evaluation of cuff-induced ischemia in the lower extremity by

magnetic resonance oximetry. *JACC* 55, 598–606. doi: 10.1016/j.jacc.2009.08.068

Langham, M. C., Jain, V., Magland, J. F., and Wehrli, F. W. (2010b). Time-resolved absolute velocity quantification with projections. *Magn. Reson. Med.* 64, 1599–1606. doi: 10.1002/mrm.22559

Langham, M. C., Li, C., Englund, E. K., Chirico, E. N., Mohler, E. R., Floyd, T. F., et al. (2013b). Vessel-wall imaging and quantification of flow-mediated dilation using water-selective 3D SSFP-echo. *J. Cardiovasc. Magn. Reson.* 15, 1–9. doi: 10.1186/1532-429X-15-100

Langham, M. C., Li, C., and Wehrli, F. W. (2011). Non-triggered quantification of central and peripheral pulse-wave velocity. *J. Cardiovasc. Magn. Reson.* 13:81. doi: 10.1186/1532-429X-13-81

Langham, M. C., and Wehrli, F. W. (2011). Simultaneous mapping of temporally-resolved blood flow velocity and oxygenation in femoral artery and vein during reactive hyperemia. *J. Cardiovasc. Magn. Reson.* 13, 66–68. doi: 10.1186/1532-429X-13-66

Langham, M. C., Zhou, Y., Chirico, E. N., Magland, J. F., Sehgal, C. M., Englund, E. K., et al. (2015). Effects of age and smoking on endothelial function assessed by quantitative cardiovascular magnetic resonance in the peripheral and central vasculature. *J. Cardiovasc. Magn. Reson.* 17:19. doi: 10.1186/s12968-015-0110-8

Larsen, R. G., Thomsen, J. M., Hirata, R. P., Steffensen, R., Poulsen, E. R., Frøkjær, J. B., et al. (2019). Impaired microvascular reactivity after eccentric muscle contractions is not restored by acute ingestion of antioxidants or dietary nitrate. *Physiol. Rep.* 7, 1102–1115. doi: 10.14814/phy2.14162

Lebon, V., Brillault-Salvat, C., Bloch, G., Leroy-Willig, A., and Carlier, P. G. (1998). Evidence of muscle BOLD effect revealed by simultaneous interleaved gradient-echo NMRI and myoglobin NMRS during leg ischemia. *Magn. Reson. Med.* 40, 551–558. doi: 10.1002/mrm.1910400408

Ledermann, H. P., Schulte, A. C., Heidecker, H. G., Aschwanden, M., Jager, K. A., Scheffler, K., et al. (2006). Blood oxygenation level-dependent magnetic resonance imaging of the skeletal muscle in patients with peripheral arterial occlusive disease. *Circulation* 113, 2929–2935. doi: 10.1161/CIRCULATIONAHA.105.605717

Li, Z., Muller, M. D., Wang, J., Sica, C. T., Karunanayaka, P., Sinoway, L. I., et al. (2016). Dynamic characteristics of T2*-weighted signal in calf muscles of peripheral artery disease during low-intensity exercise. *J. Magn. Reson. Imaging* 46, 40–48. doi: 10.1002/jmri.25532

Lieberman, E. H., Gerhard, M. D., Uehata, A., Selwyn, A. P., Ganz, P., Yeung, A. C., et al. (1996). Flow-induced vasodilation of the human brachial artery is impaired in patients <40 years of age with coronary artery disease. *Am. J. Cardiol.* 78, 1210–1214. doi: 10.1016/s0002-9149(96)00597-8

Lu, H., and Ge, Y. (2008). Quantitative evaluation of oxygenation in venous vessels using T2-Relaxation-Under-Spin-Tagging MRI. *Magn. Reson. Med.* 60, 357–363. doi: 10.1002/mrm.21627

Markl, M., Frydrychowicz, A., Kozerke, S., Hope, M., and Wieben, O. (2012). 4D flow MRI. *J. Magn. Reson. Imaging* 36, 1015–1036. doi: 10.1002/jmri.23632

Mathewson, K. W., Haykowsky, M. J., and Thompson, R. B. (2014). Feasibility and reproducibility of measurement of whole muscle blood flow, oxygen extraction, and VO 2with dynamic exercise using MRI. *Magn. Reson. Med.* 74, 1640–1651. doi: 10.1002/mrm.25564

Messner, B., and Bernhard, D. (2014). Smoking and cardiovascular disease. *Atheroscler. Thromb. Vasc Biol.* 34, 509–515. doi: 10.1161/ATVBAHA.113.300156

Mohajer, K., Zhang, H., Gurell, D., Ersoy, H., Ho, B., Kent, K. C., et al. (2006). Superficial femoral artery occlusive disease severity correlates with MR cine phase-contrast flow measurements. *J. Magn. Reson. Imaging* 23, 355–360. doi: 10.1002/jmri.20514

Mohiaddin, R. H., Gatehouse, E. D., Moon, J. C. C., Youssuffidin, M., Yang, G. Z., Firmin, D. N., et al. (2002). Assessment of reactive hyperaemia using real time zonal echo-planar flow imaging. *J. Cardiovasc. Magn. Reson.* 4, 283–287. doi: 10.1081/jcmr-120003954

Moran, P. R. (1982). A flow velocity zeugmatographic interlace for NMR imaging in humans. *Magn. Reson. Imaging* 1, 197–203. doi: 10.1016/0730-725x(82)90170-9

Moran, P. R., Moran, R. A., and Karstaedt, N. (1985). Verification and evaluation of internal flow and motion. True magnetic resonance imaging by the phase gradient modulation method. *Radiology* 154, 433–441. doi: 10.1148/radiology.154.2.3966130

Murphy, T. P., Cutlip, D. E., Regensteiner, J. G., Mohler, E. R., Cohen, D. J., Reynolds, M. R., et al. (2012). Supervised exercise versus primary stenting for claudication resulting from aortoiliac peripheral artery disease. *Circulation* 125, 130–139. doi: 10.1161/CIRCULATIONAHA.111.075770

Nayak, K. S., Nielsen, J.-F., Bernstein, M. A., Markl, M., Gatehouse, P., Botnar, R., et al. (2015). Cardiovascular magnetic resonance phase contrast imaging. *J. Cardiovasc. Magn. Reson.* 17:71. doi: 10.1186/s12968-015-0172-7

Nayler, G. L., Firmin, D. N., and Longmore, D. B. (1986). Blood flow imaging by cine magnetic resonance. *J. Comput. Assist. Tomogr.* 10, 715–722.

Nioka, S., Kime, R., Sunar, U., Im, J., Izzetoglu, M., Zhang, J., et al. (2006). A novel method to measure regional muscle blood flow continuously using NIRS kinetics information. *Dyn. Med.* 5:5. doi: 10.1186/1476-5918-5-5

Nishii, T., Kono, A. K., Nishio, M., Kyotani, K., Nishiyama, K., and Sugimura, K. (2015). Dynamic blood oxygen level-dependent MR imaging of muscle: comparison of postocclusive reactive hyperemia in young smokers and nonsmokers. *MRMS* 14, 275–283. doi: 10.2463/mrms.2014-0105

Partovi, S., Aschwanden, M., Jacobi, B., Schulte, A.-C., Walker, U. A., Staub, D., et al. (2013). Correlation of muscle BOLD MRI with transcutaneous oxygen pressure for assessing microcirculation in patients with systemic sclerosis. *J. Magn. Reson. Imaging* 38, 845–851. doi: 10.1002/jmri.24046

Partovi, S., Karimi, S., Jacobi, B., Schulte, A.-C., Aschwanden, M., Zipp, L., et al. (2012a). Clinical implications of skeletal muscle blood-oxygenation-level-dependent (BOLD) MRI. *Magn. Reson. Mater. Phy.* 25, 251–261. doi: 10.1007/s10334-012-0306-y

Partovi, S., Schulte, A.-C., Aschwanden, M., Staub, D., Benz, D., Imfeld, S., et al. (2012b). Impaired skeletal muscle microcirculation in systemic sclerosis. *Arthritis Res. Ther.* 14:R209. doi: 10.1186/ar4047

Pauling, L., and Coryell, C. D. (1936). The magnetic properties and structure of hemoglobin, oxyhemoglobin and carbonmonoxyhemoglobin. *PNAS* 22, 210–216. doi: 10.1073/pnas.22.4.210

Potter, K., Reed, C. J., Green, D. J., Hankey, G. J., and Arnolda, L. F. (2008). Ultrasound settings significantly alter arterial lumen and wall thickness measurements. *Cardiovasc Ultrasound* 6, doi: 10.1186/1476-7120-6-6

Pyke, K. E., and Tschakovsky, M. E. (2005). The relationship between shear stress and flow-mediated dilatation: implications for the assessment of endothelial function. *J. Physiol.* 568, 357–369. doi: 10.1113/jphysiol.2005.089755

Raichle, M. E. (1998). Behind the scenes of functional brain imaging: a historical and physiological perspective. *PNAS* 95, 765–772. doi: 10.1073/pnas.95.3.765

Raynaud, J. S., Duteil, S., Vaughan, J. T., Hennel, F., Wary, C., Leroy-Willig, A., et al. (2001). Determination of skeletal muscle perfusion using arterial spin labeling NMRI: validation by comparison with venous occlusion plethysmography. *Magn. Reson. Med.* 46, 1–7. doi: 10.1002/mrm.1192

Richards, J. C., Racine, M. L., Hearon, C. M. Jr., Kunkel, M., Luckasen, G. J., Larson, D. G., et al. (2018). Acute ingestion of dietary nitrate increases muscle blood flow via local vasodilation during handgrip exercise in young adults. *Physiol. Rep.* 6:e13572 doi: 10.14814/phy2.13572

Sanchez, O. A., Copenhaver, E. A., Elder, C. P., and Damon, B. M. (2010). Absence of a significant extravascular contribution to the skeletal muscle BOLD effect at 3 T. *Magn. Reson. Med.* 64, 527–535. doi: 10.1002/mrm.22449

Sanne, H., and Sivertsson, R. (1968). The effect of exercise on the development of collateral circulation after experimental occlusion of the femoral artery in the cat. *Acta Physiol. Scand.* 73, 257–263. doi: 10.1111/j.1748-1716.1968.tb04104.x

Schulte, A.-C., Aschwanden, M., and Bilecen, D. (2008). Calf muscles at blood oxygen level–dependent MR imaging: aging effects at postocclusive reactive hyperemia. *Radiology* 247, 482–489. doi: 10.1148/radiol.2472070828

Sejda, T., Pit'ha, J., Svandova, E., and Poledne, R. (2005). Limitations of non-invasive endothelial function assessment by brachial artery flow-mediated dilatation. *Clin. Physiol. Funct. Imaging* 25, 58–61. doi: 10.1111/j.1475-097X.2004.00590.x

Silber, H. A., Bluemke, D. A., Ouyang, P., Du, Y. P., Post, W. S., and Lima, J. A. C. (2001). The relationship between vascular wall shear stress and flow-mediated dilation: endothelial function assessed by phase-contrast magnetic resonance angiography. *JACC* 38, 1859–1865. doi: 10.1016/S0735-1097(01)01649-7

Sorensen, K. E., Celermajer, D. S., Spiegelhalter, D. J., Georgakopoulos, D., Robinson, J., Thomas, O., et al. (1995). Non-invasive measurement of human endothelium dependent arterial responses: accuracy and reproducibility. *Br. Heart J.* 74, 247–253. doi: 10.1136/hrt.74.3.247

Sorensen, M. B., Collins, P., Ong, P. J. L., Webb, C. M., Hayward, C. S., Asbury, E. A., et al. (2002). Long-term use of contraceptive depot medroxyprogesterone acetate in young women impairs arterial endothelial function assessed by cardiovascular magnetic resonance. *Circulation* 106, 1646–1651. doi: 10.1161/01.CIR.0000030940.73167.4E

Tagawa, T., Imaizumi, T., Endo, T., Shiramoto, M., Harasawa, Y., and Takeshita, A. (1994). Role of nitric oxide in reactive hyperemia in human forearm vessels. *Circulation* 90, 2285–2290. doi: 10.1161/01.cir.90.5.2285

Tonson, A., Noble, K. E., Meyer, R. A., Rozman, M. R., Foley, K. T., and Slade, J. M. (2017). Age reduces microvascular function in the leg independent of physical activity. *Med. Sci. Sports Exerc.* 49, 1623–1630. doi: 10.1249/MSS.0000000000001281

Towse, T. F., Elder, C. P., Bush, E. C., Klockenkemper, S. W., Bullock, J. T., Dortch, R. D., et al. (2016). Post-contractile BOLD contrast in skeletal muscle at 7 T reveals inter-individual heterogeneity in the physiological responses to muscle contraction. *NMR Biomed.* 29, 1720–1728. doi: 10.1002/nbm.3593

Versluis, B., Dremmen, M. H. G., Nelemans, P. J., Wildberger, J. E., Schurink, G.-W., Leiner, T., et al. (2012). MRI of arterial flow reserve in patients with intermittent claudication: feasibility and initial experience. *PLoS One* 7:e31514. doi: 10.1371/journal.pone.0031514

Versluis, B., Nelemans, P. J., Wildberger, J. E., Schurink, G. W., Leiner, T., and Backes, W. H. (2014). Magnetic resonance imaging-derived arterial peak flow in peripheral arterial disease: towards a standardized measurement. *Eur. J. Vasc Endovasc. Surg.* 48, 185–192. doi: 10.1016/j.ejvs.2014.04.022

Wentland, A. L., Grist, T. M., and Wieben, O. (2014). Review of MRI-based measurements of pulse wave velocity: a biomarker of arterial stiffness. *Cardiovasc. Diagn. Ther.* 4, 193–206. doi: 10.3978/j.issn.2223-3652.2014.03.04

Widlansky, M. E., Gokce, N., Keaney, J. F. Jr., and Vita, J. A. (2003). The clinical implications of endothelial dysfunction. *JACC* 42, 1149–1160. doi: 10.1016/S0735-1097(03)00994-X

Wiesmann, F., Petersen, S. E., Leeson, P. M., Francis, J. M., Robson, M. D., Wang, Q., et al. (2004). Global impairment of brachial, carotid, and aortic vascular function in young smokers. *JACC* 44, 2056–2064. doi: 10.1016/j.jacc.2004.08.033

Williams, D. S., Detre, J. A., Leigh, J. S., and Koretsky, A. P. (1992). Magnetic resonance imaging of perfusion using spin inversion of arterial water. *PNAS* 89, 212–216.

Wong, E. C., Buxton, R. B., and Frank, L. R. (1997). Implementation of quantitative perfusion imaging techniques for functional brain mapping using pulsed arterial spin labeling. *NMR Biomed.* 10, 237–249. doi: 10.1002/(sici)1099-1492(199706/08)10:4/5<237::aid-nbm475>3.0.co;2-x

Wu, W.-C., Mohler, E., Ratcliffe, S. J., Wehrli, F. W., Detre, J. A., and Floyd, T. F. (2009). Skeletal muscle microvascular flow in progressive peripheral artery disease: assessment with continuous arterial spin-labeling perfusion magnetic resonance imaging. *JACC* 53, 2372–2377. doi: 10.1016/j.jacc.2009.03.033

Wu, W. C., Wang, J., Detre, J. A., Wehrli, F. W., Mohler, E., Ratcliffe, S. J., et al. (2008). Hyperemic flow heterogeneity within the calf, foot, and forearm measured with continuous arterial spin labeling MRI. *AJP Heart Circ. Physiol.* 294, H2129–H2136. doi: 10.1152/ajpheart.01399.2007

Yamauchi, T., Ohnaka, K., Takayanagi, R., Umeda, F., and Nawata, H. (1990). Enhanced secretion of endothelin-1 by elevated glucose levels from cultured bovine aortic endothelial cells. *FEBS Lett.* 267, 16–18. doi: 10.1016/0014-5793(90)80276-o

Zeiher, A. M., Drexler, H., Saurbier, B., and Just, H. (1993). Endothelium-mediated coronary blood flow modulation in humans. Effects of age, atherosclerosis, hypercholesterolemia, and hypertension. *J. Clin. Invest.* 92, 652–662. doi: 10.1172/JCI116634

Zhang, J. L., Layec, G., Hanrahan, C., Conlin, C. C., Hart, C., Hu, N., et al. (2019). Exercise-induced calf muscle hyperemia: quantitative mapping with low-dose dynamic contrast enhanced magnetic resonance imaging. *AJP Heart Circ. Physiol.* 316, H201–H211. doi: 10.1152/ajpheart.00537.2018

Zheng, J., An, H., Coggan, A. R., Zhang, X., Bashir, A., Muccigrosso, D., et al. (2013). Noncontrast skeletal muscle oximetry. *Magn. Reson. Med.* 71, 318–325. doi: 10.1002/mrm.24669

Zheng, J., Hastings, M. K., Muccigross, D., Fan, Z., Gao, F., Curci, J., et al. (2014). Non-contrast MRI perfusion angiosome in diabetic feet. *Eur. Radiol.* 25, 99–105. doi: 10.1007/s00330-014-3337-0

Conflict of Interest: The authors declare that the research was conducted in the absence of any commercial or financial relationships that could be construed as a potential conflict of interest.

The handling Editor declared a shared affiliation and past co-authorship with one of the authors ML.

frontiers in Physiology

REVIEW
published: 08 May 2020
doi: 10.3389/fphys.2020.00443

Vascular Signaling in Allogenic Solid Organ Transplantation – The Role of Endothelial Cells

*Laura Kummer[1], Marcin Zaradzki[2], Vijith Vijayan[3], Rawa Arif[2], Markus A. Weigand[1], Stephan Immenschuh[3], Andreas H. Wagner[4] and Jan Larmann[1]**

[1] Department of Anesthesiology, University Hospital Heidelberg, Heidelberg, Germany, [2] Institute of Cardiac Surgery, University Hospital Heidelberg, Heidelberg, Germany, [3] Institute for Transfusion Medicine, Hannover Medical School, Hanover, Germany, [4] Institute of Physiology and Pathophysiology, Heidelberg University, Heidelberg, Germany

Graft rejection remains the major obstacle after vascularized solid organ transplantation. Endothelial cells, which form the interface between the transplanted graft and the host's immunity, are the first target for host immune cells. During acute cellular rejection endothelial cells are directly attacked by HLA I and II-recognizing NK cells, macrophages, and T cells, and activation of the complement system leads to endothelial cell lysis. The established forms of immunosuppressive therapy provide effective treatment options, but the treatment of chronic rejection of solid organs remains challenging. Chronic rejection is mainly based on production of donor-specific antibodies that induce endothelial cell activation—a condition which phenotypically resembles chronic inflammation. Activated endothelial cells produce chemokines, and expression of adhesion molecules increases. Due to this pro-inflammatory microenvironment, leukocytes are recruited and transmigrate from the bloodstream across the endothelial monolayer into the vessel wall. This mononuclear infiltrate is a hallmark of transplant vasculopathy. Furthermore, expression profiles of different cytokines serve as clinical markers for the patient's outcome. Besides their effects on immune cells, activated endothelial cells support the migration and proliferation of vascular smooth muscle cells. In turn, muscle cell recruitment leads to neointima formation followed by reduction in organ perfusion and eventually results in tissue injury. Activation of endothelial cells involves antibody ligation to the surface of endothelial cells. Subsequently, intracellular signaling pathways are initiated. These signaling cascades may serve as targets to prevent or treat adverse effects in antibody-activated endothelial cells. Preventive or therapeutic strategies for chronic rejection can be investigated in sophisticated mouse models of transplant vasculopathy, mimicking interactions between immune cells and endothelium.

Keywords: endothelial activation, donor-specific antibodies, transplant vasculopathy, vascular signaling, HLA I and II

OPEN ACCESS

Edited by:
Shampa Chatterjee, University of Pennsylvania, United States

Reviewed by:
Michael Autieri, Temple University, United States
Federico Sertic, University of Pennsylvania, United States

****Correspondence:***
Jan Larmann
Jan.Larmann@med.uni-heidelberg.de

Specialty section:
This article was submitted to Vascular Physiology, a section of the journal Frontiers in Physiology

Received: *19 December 2019*
Accepted: *09 April 2020*
Published: *08 May 2020*

Citation:
Kummer L, Zaradzki M, Vijayan V, Arif R, Weigand MA, Immenschuh S, Wagner AH and Larmann J (2020) Vascular Signaling in Allogenic Solid Organ Transplantation – The Role of Endothelial Cells. Front. Physiol. 11:443. doi: 10.3389/fphys.2020.00443

INTRODUCTION

Endothelial cells (ECs) are semiprofessional antigen-presenting cells; furthermore they express all major sets of antigens that can be recognized by immune cells. Therefore, they constitute a preferential target in vascularized grafts for the host immune system to discriminate between self and non-self (Piotti et al., 2014). Various transplantation-dependent factors lead to EC activation,

and upon reperfusion ECs themselves trigger T cell co-stimulation and specific immune cell activation. It has been shown *in vitro* that the co-stimulation properties of ECs are influenced by their vascular origin, the presented antigen, and the maturity of the T cell (Rothermel et al., 2004). So far, rejection after allogeneic solid organ transplantation remains the major limiting factor for graft survival. Allograft rejection can be categorized as hyperacute, acute, or chronic, depending on the time of onset after the transplant procedure. In addition, it can be classified on the basis of the principal mechanism, such as cell-mediated or antibody-mediated rejection.

Preformed Antibodies Against ECs Elicit Hyperacute Rejection

In vascularized grafts, hyperacute rejection is seen within minutes after organ reperfusion. The underlying mechanism is the presence of preformed anti-donor specific antibodies in the recipient prior to transplantation (Moreau et al., 2013). Common reasons for these preformed antibodies are previous blood transfusions, transplantations, and in women, a history of one or more pregnancies. The preformed anti-donor specific antibodies are directed against ECs and other vascular cells. Deposition of antibodies on the EC surface is sufficient to activate the complement system, both distinct mechanisms result in formation of an interstitial neutrophilic infiltrate, intravascular platelet adhesion, and aggregation. One observation, specific for hyperacute rejection after lung transplantation, is diffuse alveolar damage promoted by donor-specific IgG antibodies that induce T cell-mediated lymphocytotoxicity (Frost et al., 1996). In addition to its effects on immune cells and platelets, the activated complement system initiates an enzymatic cascade that forms the membrane attack complex (MAC), resulting in pores in the plasma membrane of ECs and subsequent cell lysis (Wehner et al., 2007). Nowadays hyperacute organ rejection has become rare because the detection of anti-donor specific antibodies is a routine procedure performed before any organ transplantation (Moreau et al., 2013).

T Cell- and B Cell-Dependent Pathways Contribute to Acute Rejection

Whereas hyperacute rejection occurs within the first few minutes after organ reperfusion, acute rejection refers to graft rejection days or months after transplantation (Mengel et al., 2012). While features of adaptive immunity are used to describe and characterize acute rejection, the innate immune system also plays a crucial role in acute transplant rejection. Importantly, its effects are in part independent of adaptive immunity. For example, in mice lacking an adaptive immune system but developing normal NK and myeloid cell compartments, pro-inflammatory cytokines, such as interleukin-1β (IL-1β) and interleukin-6 (IL-6), are significantly upregulated after heterotopic heart transplantation (He et al., 2003). Besides several immunological factors there are various non-immunological factors, e.g., ischemia–reperfusion (I/R) injury or infections during transplantation, that are harmful to graft ECs (Chong and Alegre, 2012; Krezdorn et al., 2017). Similar to hyperacute rejection, acute rejection can arise in a T cell-mediated fashion, the so-called acute cellular rejection or in a B cell-dependent mechanism termed antibody-mediated rejection. The two mechanisms can occur independently of each other, but the immunological pathways of acute cellular rejection and antibody-mediated rejection overlap (Moreau et al., 2013). In acute cellular rejection, there are two known antigen-dependent T cell-activating pathways. In the direct pathway, T cells of the host immune system recognize intact foreign HLA: antigen complexes presented on the surface of donor-derived antigen presenting cells (APCs) in the host lymphoid organs. In contrast, in the indirect pathway, recipient T cells recognize fragments of donor HLA peptides bound to HLA molecules on recipient APCs (Ochando et al., 2006). Both pathways contribute to B cell activation which plays a crucial role in developing antibody-mediated rejection. Antibody-mediated rejection is driven by generation of antibodies directed against HLA I and HLA II molecules or other immunogenic targets on the surface of graft ECs. In early antibody-mediated rejection, *de novo* synthesized donor-specific antibodies against HLA I and HLA II molecules are equally common. During late antibody-mediated rejection, however, donor-specific antibodies are mainly directed against HLA II molecules. This finding is interpreted as an indicator for two distinct pathways in the development of antibody-mediated rejection (Walsh et al., 2011). Persistent occurrence of antibodies against the graft endothelium results in chronic antibody-mediated rejection.

The past few years have seen improvements in immunosuppressive therapies and concepts to tackle acute rejection. As a result, acute rejection is now seen in less than 15% of patients that lack preformed anti-donor specific antibodies. With fewer episodes of acute rejection and improved short-term graft survival, chronic rejection has become increasingly relevant (Najarian et al., 1985; Gonzalez-Molina et al., 2014).

Chronic Rejection Arises From Persistent Inflammation of the Endothelium

Chronic allograft rejection develops over a period of months to years and is described as transplant vasculopathy (TV), characterized by neointima formation. With further progression, the luminal diameter decreases and the internal elastic lamina is destroyed. Intima thickening, as a hallmark of TV, is manifested by proliferation of myofibroblasts and accumulation of extracellular matrix, both seen on histopathological examination. TV is found as bronchiolitis obliterans syndrome (BOS) in lung transplantation, as cardiac allograft vasculopathy after cardiac transplantation, and as renal transplant arteriosclerosis following kidney transplantation (Pedagogos et al., 1997; Pilmore et al., 2000). One risk factor for the development of chronic rejection is the occurrence of donor-specific antibodies. In a prospective, single-center cohort study, 47% of the patients were serum positive for antibodies against graft ECs after lung

transplantation (Tikkanen et al., 2016).This agreed with an earlier study's finding of a negative correlation between the appearance of anti-donor specific antibodies and graft survival (Mao et al., 2007). Antibodies against the major histocompatibility complex (MHC) I can elicit chronic allograft rejection in mice lacking functional T and B cells (Uehara et al., 2007). Even in the absence of an intact complement system, one of the generally accepted criteria for antibody-mediated rejection, a mononuclear infiltrate is formed by NK cells and macrophages (Hirohashi et al., 2010).

Figure 1 provides an overview of the interplay of different cellular compartments of the innate and adaptive immune system as well as soluble factors such as antibodies and complement factors. All of the pathways, starting with allorecognition of the graft and leading to rejection, interfere with others. The time of occurrence and concentration of each factor determine the phenotype of rejection.

In acute inflammation, ECs undergo transcriptional and translational changes and are converted into an activated state. Activated ECs are phenotypically characterized by increased permeability and cytokine release, enhanced adhesiveness for leukocytes, and pro-thrombic features (Pober and Cotran, 1990). These reactions serve to effectively eliminate invading pathogens and destroy potentially harmful agents. However, when the immune system fails to resolve inflammation a chronic inflammatory state will persist, involving subsequent destruction of primarily unaffected tissue (Ryan and Majno, 1977). Altogether, ECs in a transplanted solid organ can be activated during the surgical procedure of transplantation, either by presenting antigens bound to their HLA molecules or by antigens expressed by themselves.

The major questions we address in this review include the following:

- What are the main target structures on the vascular endothelium of the transplanted organ that can be recognized by immunological and non-immunological factors?
- How will the endothelial phenotype be affected during activation?
- What role plays the immune system during activation of ECs and in organ rejection?
- How is the vascular structure altered due to organ rejection?
- What kind of research models do we have to address further questions, and what are the advantages and limitations of the different models?

IMMUNOLOGICAL ENDOTHELIAL ACTIVATION FACTORS

A major goal after solid organ transplantation remains prevention of an ongoing inflammatory process in the vessel wall, which is the pathological correlate of chronic rejection. Therefore, a reduced donor-specific immune response in a mature immune system is desirable. Graft-infiltrating, innate immune cells comprise a major pro-inflammatory stimulus driving TV and putting graft function at risk.

Endothelial Interactions of Anti-HLA Antibodies

It is established that antibodies against molecules of the major histocompatibility complex (MHC), which is termed human leukocyte antigen (HLA) in humans, play a critical role in transplant rejection after solid organ transplantation via fixation and activation of complement, which in turn causes cytotoxicity in the graft endothelium (Patel and Terasaki, 1969). In addition to these so-called complement-dependent effects, more recent evidence suggests that ligation of anti-HLA antibodies can also cause complement-independent effects in the graft endothelium via induction of intracellular signaling cascades (Thomas et al., 2015). In particular, binding of anti-HLA class I (HLA I) antibodies has been shown to cause phenotypical alterations of the endothelium, including pro-inflammatory activation via up-regulation of inducible pro-inflammatory adhesion molecules and cytokines such as intercellular cell adhesion molecule-1 (ICAM-1), vascular adhesion molecule-1 (VCAM-1), and monocyte chemoattractant protein-1 (MCP-1) (Naemi et al., 2013; Zilian et al., 2015), as well as increased adhesion of inflammatory leukocytes via Fcγ receptor (FcγR)-dependent mechanisms (Hirohashi et al., 2012; Valenzuela et al., 2013b). Moreover, binding of anti-HLA I antibodies has been associated with proliferation of ECs (Jindra et al., 2008; Thomas et al., 2015). The complement-independent effects of anti-HLA antibodies in ECs are mediated via activation of a variety of signaling cascades including, but not limited to, mitogen-activated protein (MAP) kinase pathway, the extracellular-regulated kinase (ERK) pathway, and the nuclear factor (NF)-kappa B and fibroblast growth factor (FGF) pathway (Thomas et al., 2015). Another important intracellular signal transducer in ECs is mechanistic target of rapamycin (mTOR). HLA I crosslinking on ECs triggers mTOR/Rictor/Sin1 association, which results in formation of mTORC2 complex (Jin et al., 2014). Rearrangement of the cytoskeleton and cell migration is mediated through activation of mTORC2 and the downstream-located Rho GTPases. Furthermore, anti-HLA I antibodies mediate mTORC1 formation by inducing the mTOR-Raptor complex, resulting in increased EC proliferation (Sarbassov et al., 2004). Binding of anti-HLA I antibodies induces phosphorylation of Akt at Ser473 and ERK at Thr202/Tyr204, inducing expression of the anti-apoptotic genes Bcl-2 and Bcl-xL (Jin et al., 2004). Another way for anti-HLA I antibodies to induce EC proliferation is via the generation of inositol phosphate, which serves as a messenger of Akt signaling (Bian et al., 1997). *In vitro* treatment of ECs with the mTOR inhibitors sirolimus and everolimus reduces monocyte adhesion by repressing mTORC1- and mTORC2-dependent pathways. Accordingly, administering mTOR inhibitors in a mouse model of fully mismatched cardiac transplantation results in reduced mononuclear infiltration (Salehi et al., 2018). Furthermore, anti-HLA I antibodies induce tyrosine phosphorylation of members of the Src family, regulating complex signal transduction pathways (Jin et al., 2002). Activated

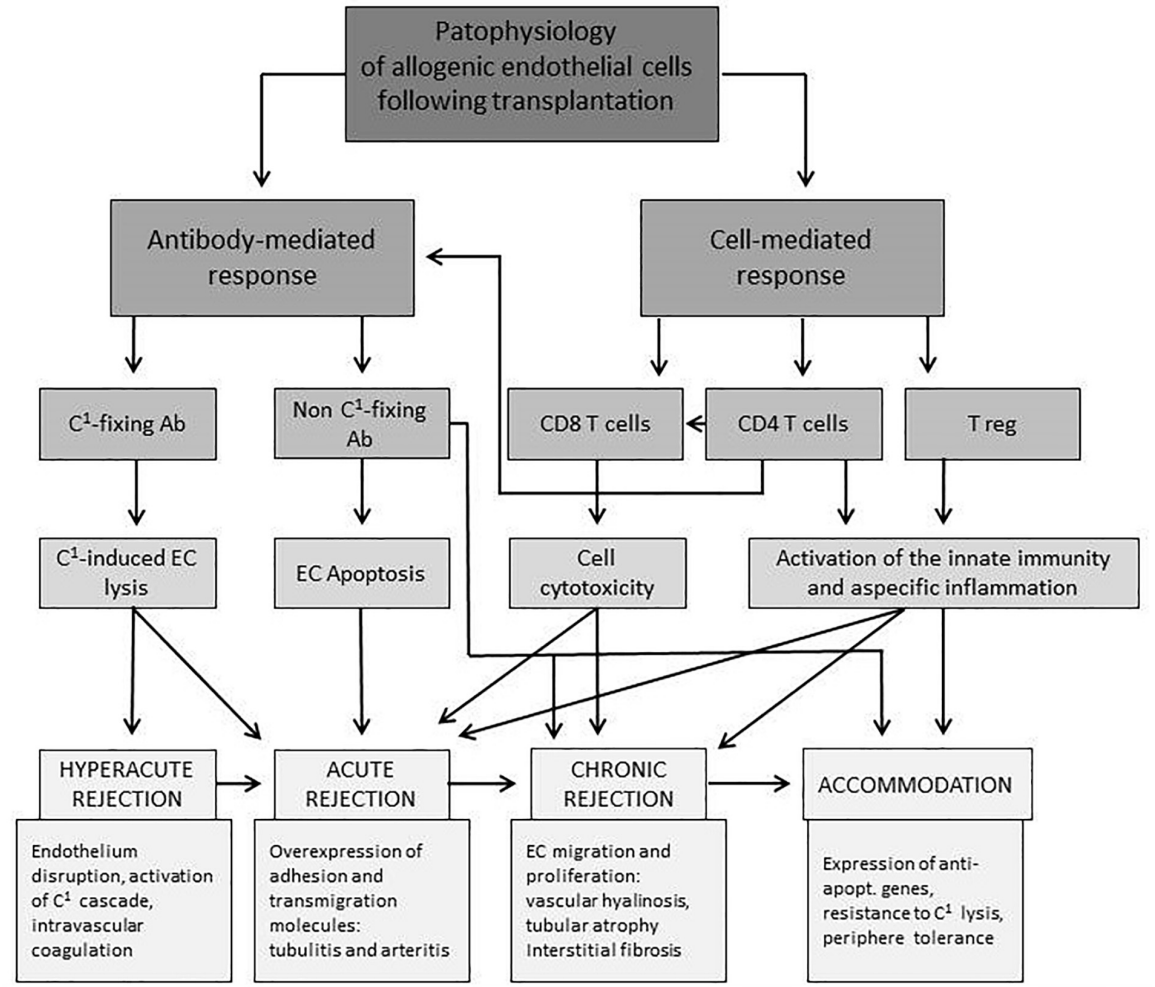

FIGURE 1 | Overview of interactions of endothelial and immune cells leading to different forms of rejection after solid organ transplantation. EC, endothelial cell; C^1, complement factor; Ab, antibody; expr., expression; apopt., apoptotic (Piotti et al., 2014).

Src is required for phosphorylation of cortactin, an actin-binding molecule, which is part of the adhesion molecule ICAM-1 cluster. Phosphorylated cortactin stabilizes ICAM-1 clusters and induces cytoskeletal remodeling with improved leukocyte transmigration capacity (Yang et al., 2006). In contrast with the regulatory events mediated by anti-HLA I antibodies in the endothelium, the effects of anti-HLA II antibodies are less well established. Le Bas-Bernadet and colleagues demonstrated that the monoclonal HLA-DR antibody L243 caused differential effects in human vascular ECs and B cells, such as activation of the protein kinase C and protein kinase B/Akt signaling cascades (Le Bas-Bernardet et al., 2004). A more recent report demonstrated that HLA II antibody-dependent interaction with human ECs induced a complex TH17 cell-dependent immunological mechanism that might mediate humoral kidney transplant rejection. Specifically, endothelial ligation of a monoclonal anti-HLA II antibody and native allospecific anti-HLA II antibodies from patient sera activated this pathway via up-regulation of interleukin (IL)-6 in a co-culture model of a human EC line and primary peripheral blood monocytes (Lion et al., 2016). Independently, Zhang and colleagues have demonstrated that endothelial HLA II ligation caused proliferation and migration of ECs via the induction of a complex network of signaling cascades including Src, focal adhesion kinase, phosphatidyl-inositol-3 kinase (PI3K), and ERK (Jin et al., 2018). Finally, the monoclonal anti-HLA II antibody L243 and native anti-HLA II antibodies from allosera have recently been shown to cause complement-independent non-apoptotic cytotoxicity in human ECs via a lysosomal membrane-mediated cell death pathway (Aljabri et al., 2019).

Endothelial Interactions of Non-HLA Antibodies

Numerous experimental and clinical studies have demonstrated that antibodies directed against endothelial non-HLA antigens are also critically involved in acute and chronic AMR after transplantation of various solid organs (Opelz, 2005). However, compared with anti-HLA antibodies, much less is known on the

generation and functional significance of non-HLA antibodies in transplant rejection.

Two major groups of non-HLA antibodies are known. The first group is directed against polymorphic alloantigens, whereas the second group interacts with a variety of autoantigens of the endothelium (Zhang and Reed, 2016). A prototypical alloantigen targeted by antibodies of the first group is the endothelial MHC I chain-related gene A (MICA) (Zou and Stastny, 2009). The clinical importance of antibodies against MICA has been demonstrated in a study on kidney transplant patients (Zou et al., 2007). Non-HLA antibodies of the second group are directed against numerous endothelial autoantigens, including several cell surface or intracellular proteins (Dragun et al., 2016). Importantly, non-HLA antibodies directed against autoantigens appear to be of major clinical significance, because their presence in the circulation is associated with adverse clinical outcome, as recently reported by independent groups for renal transplantation (Cardinal et al., 2017; Delville et al., 2019; Lefaucheur et al., 2019). For example, an autoantigen targeted by non-HLA antibodies is the G protein-coupled receptor anti-angiotensin type I receptor (AT1R), which is critical for mediating the effects of angiotensin II in blood vessels (Dragun et al., 2016). The clinical significance of AT1R antibodies for rejection has been demonstrated in kidney transplantation patients (Dragun et al., 2005). Other examples of autoantigens targeted by non-HLA antibodies include the endothelial receptor endothelin type A receptor (ET1AR), perlecan, and endoglin (Dragun et al., 2016). Interestingly, a large number of other non-HLA candidate proteins that may serve as endothelial autoantigens associated with transplant rejection have been identified by array approaches (Li et al., 2009; Sigdel et al., 2012). The mechanisms by which non-HLA antibodies mediate transplant rejection are currently under intense investigation. Similar to what has been explained for complement-independent signaling of HLA antibodies in the endothelium, non-HLA antibodies may mediate their detrimental effects in transplantation via the induction of endothelial signal transduction (Zhang and Reed, 2009). An important issue for future studies will be to improve our understanding of the interrelationship of HLA alloantibodies and non-HLA autoantibodies in the pathogenesis of humoral rejection.

Figure 2 shows different effects of antibodies towards ECs. Due to complement activation, antibodies may induce acute rejection of the graft by directly damaging the endothelium or, if the antibody titer reaches a sub-lytic level, EC expression profile is altered, leading to a more chronic rejection phenotype.

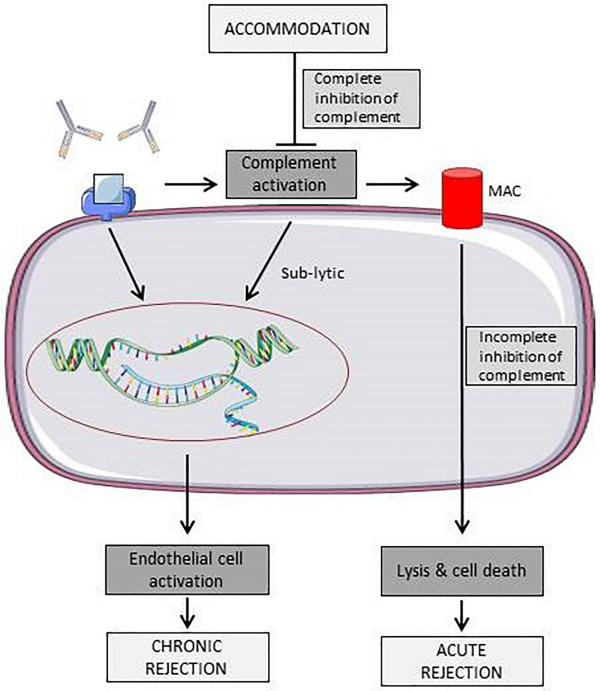

FIGURE 2 | Schematic representation of known effects of antibodies towards surface antigens on endothelial cells. Binding of antibodies can either leads to acute rejection due to immune cell or complement mediated lysis or to a state of chronic rejection due to endothelial cell activation (Colvin and Smith, 2005). Elements of **Figures 2**, **3** and **4** were taken and adjusted from Servier Medical Art at http://smart.servier.com, licensed under a Creative Commons Attribution 3.0 Unported License.

NON-IMMUNOLOGICAL ENDOTHELIAL ACTIVATION FACTORS

Non-immunological factors activating the endothelium of vascular allografts are still not fully understood but have been best investigated in cardiac, lung and renal transplantation. Activation of ECs is a multifactorial process that is regularly initiated long before the donor's brain death. Factors associated with critical illness, pain, infections, and treatment contribute to EC activation. When brain death is diagnosed, the therapeutic goals are revised with the aim of protecting organs from further adverse events. Still, factors such as I/R injury and systemic inflammatory reaction caused by the artificial surface of the cardiopulmonary bypass (during heart transplantation) contribute to ongoing endothelial injury.

Brain Death of Organ Donors Is the First Inducer of Endothelial Dysfunction During the Process of Transplantation

Organ donors are predominantly diagnosed with brain death due to cerebral damage following intracranial bleeding or trauma (McKeown et al., 2012). During this process, before organ retrieval is initiated, the donor organism undergoes profound systemic changes. Consequently, approximately 25% of potential organ donors are excluded from explantation due to hemodynamic instability (Szabo, 2004; Girlanda, 2016). Furthermore, the process of organ retrieval—as a multi-visceral operation—also causes systemic inflammation, altering vascular structures, which requires intensive hemodynamic management to minimize the risk of organ hypoperfusion, arrhythmia or cardiac arrest.

Acute cerebral damage is immediately followed by a rapid increase of intracranial pressure and is compensated by a catecholamine storm, resulting in arterial hypertension and

bradycardia (Smith, 2004). The acute catecholamine-mediated compensatory mechanisms are followed by a loss of sympathetic activity and consecutive peripheral vasodilatation with the risk of hypoperfusion of possible allografts. Changes of plasma catecholamines during the late phase after brain death result in endothelial dysfunction (Szabo et al., 2002). Szabo et al. established a canine model of induced brain death (inflation of a subdural balloon) to assess coronary blood flow and the influence of the endothelium on vasodilatation. Besides changes in blood flow, the authors observed severe endothelial dysfunction by impaired vasodilation caused by application of endothelium-dependent acetylcholine (Szabo et al., 2002). The same group demonstrated in a large animal model, that coronary blood flow increases approximately threefold but drops significantly below baseline levels as soon as the acute phase is over. They hypothesized that nitric oxide supply improves endothelial function, because after infusion of L-arginine, the substrate for nitric oxide supply, the decrease in coronary blood flow was less pronounced. They concluded that enhancement of endogenous nitric oxide synthesis due to L-arginine treatment is beneficial for endothelial function and thus for myocardial performance after brain death (Szabo et al., 2006).

Takada et al. (1998) showed in a rat model, that experimentally induced explosive brain death is followed by an up-regulation of immunoregulatory and cell adhesion molecules (CAMs) compared to animals with non-explosive brain death). They postulated a preconditioning effect on allografts leading to adverse donor–host reactions after transplantation. Segel et al. found an abundance of CAMs and increased cytokine expression in animal models of brain death and searched for an association with endothelial dysfunction. Relative expression of ICAM-1, VCAM-1, IL-1, and IL-6 mRNAs was significantly elevated in brain-dead animals, while the hemodynamics remained uncompromised (Segel et al., 2002). The authors concluded that an increase in IL-1 might mediate the overexpression of the adhesion molecules and IL-6 mRNAs. Similar effects have been proven for humans by Mehra et al., who divided recipients into groups that received cardiac allografts from donors with either explosive or non-explosive brain death (EBD vs. non-EBD). EBD was defined as acutely increased intracranial pressure (Mehra et al., 2004). No significant differences were found in posttransplant survival and distribution of immunological and non-immunological variables between recipients of organs from EBD donors and recipients of organs from non-EBD donors. Interestingly, allografts from EBD donors demonstrated advanced intimal thickening and a higher cardiac event rate, by contrast with grafts from non-EBD donors. Consequently, hearts from donors with EBD had lower organ survival than those from non-EBD donors. These findings were attributed to a release of cytokines following leukocyte activation in vascular beds of all peripheral organs including the heart (Mehra et al., 2004).

Koo et al. (1999) found lower E-selectin, DR locus of HLA (HLA-DR), ICAM-1, and VCAM-1 expression in biopsies from human living-related kidney donors than from cadaveric donors, which may be associated with beneficial graft survival). Similar findings were also observed in cadaveric and living-donor livers before transplantation (Jassem et al., 2003). These results are further supported by Anyanwu et al. (2002) investigating domino hearts (living-related heart transplantation from recipients who require heart-lung transplantation). Domino hearts also tend to develop less allograft vasculopathy than cadaveric grafts.

Ex vivo lung perfusion models have widely been used to assess endothelial activation during transplantation in lungs. Park et al. showed in a xenotransplant model, that nitric oxide donor treatment reduced platelet adhesion and vascular resistance of the lung (Park et al., 2015). Von Willebrand factor (vWF) secretion from ECs was reduced; complement activation and thrombin generation were inhibited. Another treatment strategy to prevent EC activation was investigated by Kim et al., who showed that aurintricarboxylic acid (ATA), a platelet inhibitor, significantly inhibited tumor necrosis factor alpha (TNF-α)- or lipopolysaccharide-induced endothelial E-selectin expression. As a result of inhibited E-selectin expression, adhesiveness of monocyte to ECs was impeded (Kim et al., 2008). Thrombin-induced vWF secretion and complement activation were reduced, although *in vitro* findings revealed that ATA induced endothelial tissue factor expression and platelet activation (Kim et al., 2008).

Altogether, ECs of transplanted organs are already affected during brain death and before the process of transplantation is initiated. This leads to EC activation and facilitates increased leukocyte–endothelial interactions. Thus, treatment of organ donors prior to explantation focuses on prevention of vascular allograft injury and needs to be developed further.

I/R Injury Contributes to Further Endothelial Activation After Transplantation

Another non-immunological factor that causes endothelial dysfunction is I/R injury. Reperfusion injury develops hours or days after the initial phase of blood flow suppression or disruption during organ explantation and occurs either as cold or warm ischemia. Despite restoration of flow, further tissue and microcirculation injury occurs during reperfusion. The associated damage even exceeds the injury during the initial ischemic phase. Within the damaged tissue, apoptosis, autophagy, and necrosis are induced concurrently to start repair and regeneration processes. Predomination of regeneration processes leads to organ survival, while prevailing damaging processes result in organ failure (Nordling et al., 2018).

A common feature of graft I/R injury is increased vascular permeability caused by endothelial dysfunction and microvascular damage. The most important factor is the adhesion of neutrophils to the activated endothelium. Neutrophil adhesion to ECs is mediated by interactions between CAMs on the surface of neutrophils and ECs, e.g., P-selectin, E-selectin, and ICAM-1. The abundance of these factors depends strongly on the local tissue conditions after explantation, e.g., time of ischemia (Tsukimori et al., 2008). P-selectin expression occurs acutely following I/R injury due to its storage in preformed intracellular Weibel–Palade bodies, whereas expression of other CAMs is delayed depending on their translation process.

Neutrophil–EC adherence not only provides physical interactions but also results in altered intracellular signaling

in both cell populations (Saragih et al., 2014). For instance, adhesion of neutrophils to ECs induces intracellular Ca^{2+} increases, F-actin stress fiber formation, myosin light chain kinase activation, and isometric tension generation in ECs (Wang and Doerschuk, 2000). In addition to these structural changes in the endothelium, neutrophil adherence to activated ECs induces reactive oxygen species (ROS) production only in ECs, not in neutrophils. Due to increased ROS production, neutrophil–EC interactions lead to typical necrosis (Francis and Baynosa, 2017). This appears to mediate cytoskeletal remodeling, which may stimulate subsequent inflammatory responses.

Ischemic injury and the subsequent interaction between immune cells and ECs cannot fully explain the damage observed during I/R injury. Several non-immunological conditions play a pivotal role. This includes pro-coagulatory and pro-thrombotic changes on the surface of the endothelium, resulting in vascular occlusion (Nordling et al., 2015).

Recent studies have shown that a healthy EC layer is the most important factor in maintaining proper control over inflammation and hemostasis, as described above. Alphonsus and Rodseth showed that the endothelial glycocalyx (eGC) modulates vascular homeostasis through its physical barrier properties (Alphonsus and Rodseth, 2014). Mounting evidence suggests that I/R injury causes the degradation of eGC, associated with postischemic oxidative stress and increased leukocyte and platelet adhesion. ROS may account for damage to the eGC as well (Kolarova et al., 2014). In patients suffering from sepsis, an ablated layer of eGC is negatively correlated with leukocyte–endothelial interactions, thrombogenicity, and vascular permeability. These effects could be reversed when the eGC was restored. Degradation of eGC reinforces plasminogen activator inhibitor-1 release and ICAM-1 expression, with the consequence of intensified attachment of monocytes to ECs. Furthermore, reduced eGC is associated with increased endothelial nitric oxide synthase (eNOS) activity, which is associated with impaired vascular homeostasis. These findings illustrate that physical factors also make an important contribution to regulation of the vascular inflammatory responses and blood clotting function (Cao et al., 2019).

Other work has highlighted that stressed ECs release high quantities of adenosine triphosphate (ATP) and adenosine diphosphate (ADP) into the extracellular environment. These mediators act as early stimulators of inflammatory responses, which, in turn, catalyze additional platelet aggregation, resulting in microthrombus formation and further microvascular damage. ATP and ADP can also directly stimulate macrophages and neutrophils to release pro-inflammatory mediators and express leukocyte adhesion molecules (Sugimoto et al., 2009). In several rodent transplantation models, a direct linear correlation was found between cold ischemic time, I/R injury, and early allograft dysfunction. Prolonged ischemic time was associated with increased ROS production, cytokine expression, cardiomyocyte apoptosis, and caspase activity (Yun et al., 2000; Krishnadasan et al., 2004; Tanaka et al., 2005; Lemke et al., 2015).

To date, the treatment of I/R injury relies heavily on immune-modulating drugs with undesirable side effects, but recent studies suggest new therapeutic targets (Tarjus et al., 2019). After renal transplantation, many patients develop hypertension under treatment with the immunosuppressive drug tacrolimus to suppress rejection. This is a risk factor for allograft vasculopathy and lower overall patient survival, but the underlying mechanisms have not yet been completely elucidated. A decrease in production of the vasodilator nitric oxide (NO) by eNOS has been suggested to be responsible for the endothelial dysfunction and hypertension elicited by tacrolimus (Cook et al., 2009). Therefore, immunosuppressive drugs are suspected to amplify the damage to an already critically stressed and dysfunctional endothelium. One potential new therapeutic target could be the epithelial sodium channel (ENaC). Active ENaC decreases eNOS activity and therefore reduces NO release, which in turn leads to stiffer ECs. This could explain the observed prevention of renal tubular injury and renal dysfunction after kidney I/R injury in mice with endothelial αENaC deficiency. Moreover, in human ECs, pharmacological ENaC inhibition promoted eNOS coupling and activation, resulting in NO release and vasodilatation. Altogether, the authors conclude that endothelial αENaC influences vasoconstriction and vasodilatation and plays an important role in recovery from ischemic injury (Tarjus et al., 2019).

SOLUBLE FACTORS ORCHESTRATE INTERPLAY BETWEEN ECs AND IMMUNE CELLS

Chemokines

Besides their prominent effects on promoting signal transduction between different cell populations, chemokines are also able to induce angiogenesis and vascular remodeling (Belperio et al., 2005). Chemokines, as well as their corresponding receptors, can be expressed in a constitutive or inducible manner on leukocytes, neurons, astrocytes, epithelial cells, or ECs and on vascular smooth muscle cells (VSMCs).

In heart transplantation models of acute allograft rejection, the chemokines CCL3 and CCL5 were upregulated and the subsequent mononuclear infiltrate could be diminished by blocking the CCL3 and CCL5 receptor CCR1 (Gao et al., 2000; Horuk et al., 2001). Another chemokine that serves as immune cell recruiter into the vessel wall during rejection is ITAC. In a prospective study with patients suffering transplant coronary artery disease, elevated peripheral blood levels of ITAC were measured and could serve as a clinical marker for patients at elevated risk of developing chronic rejection (Kao et al., 2003). ITAC binds to CXCR3 receptors on immune cells, and immunohistochemical analysis showed mononuclear infiltrates of $CXCR3^{+}$ cells within the vasculature (Kao et al., 2003). In addition to chronic rejection after cardiac transplantation, elevated levels of CXCR3 ligands were found in patients at high risk of developing chronic lung allograft dysfunction. In this setting, CXCR3 ligands serve as chemoattractants for activated T and NK cells (Shino et al., 2017). CXCR3 and its ligands are involved in a broad spectrum of inflammatory and/or vasculature-affecting diseases (e.g., atherosclerosis, hepatitis, and

systemic sclerosis). Therefore, preventing CXCR3 activation might be a promising therapeutic approach to delay graft failure (Van Raemdonck et al., 2015). On the other hand, modulation of CXCR3 expression might be a therapeutic tool to orchestrate recruitment of anti-inflammatory cells with the aim of resolving the chronic inflammation state during organ rejection. Intensive research efforts are being devoted to a next-generation DNA methyltransferase inhibitor (DMTi) in breast cancer. DMTi upregulates CXCR3 ligands and recruits $CD8^+$ cells into the tumor, thereby enhancing their anti-tumor immune capacity (Luo et al., 2018).

If ECs are stimulated synergistically with IL-17 and TNF-α, *in vitro* expression of the neutrophil-specific chemokines KC, MIP2α, and LIX increases and overexpression of co-stimulatory molecules such as LFA-3 or OX-40L occurs (Griffin et al., 2012). This leads to the recruitment of leukocytes with enhanced activity, reinforcing a pro-inflammatory environment. In addition, co-culturing of allogeneic $CD4^+$ T cells and ECs enhances release of IL-1α by ECs. IL-1α stimulates allogeneic memory $CD4^+$ T cells to produce IFN-γ and IL-17. IL-17, in turn, stimulates predominantly smooth muscle cells (SMCs) to release cytokines and to selectively recruit $CCR6^+$ T cells into allograft arteries, leading to an amplification of the immune response. These cell–cell interactions lead to memory $CD4^+$ T-cell proliferation and Th1/Th17 expansion and have been verified in a humanized mouse model (Rao et al., 2008).

Damage-Associated Molecular Patterns

Damage associated molecular patterns (DAMPs) can be released by all cell types and serve as homeostatic danger signals, indicating pathological stress during transplantation or chronic rejection (Bianchi, 2007; Gallo and Gallucci, 2013).They can be recognized either by innate lymphocytes or by pattern recognition receptors (PRR) such as toll-like receptors (TLRs) (Land, 2012a). It has been shown that the high-mobility group box protein-1 (HMGB1) is upregulated in a kidney I/R injury mouse model. HMGB1 can be released from apoptotic cells or actively secreted, maintaining nucleosomal structure and regulating gene transcription (Herzog et al., 2014). It induces up-regulation of adhesion molecules on ECs, which in turn intensifies leukocyte–EC interaction and finally leads to graft damage. This effect could be abolished by blocking HMGB1, and it was not seen in $TLR4^{-/-}$ mice lacking its receptor, which suggests involvement of the TLR4 pathway in HMGB1 signal transduction (Wu et al., 2010; Chen et al., 2011). Downstream of TLR4, both mitogen-activated protein kinase 8 (MAPK8) and apoptosis signal-regulating kinase 1 (ASK1) are activated following HMGB1–TLR4 interactions, and could thus serve as new therapeutic targets to prevent apoptosis during I/R injury (Mkaddem et al., 2009). It has been demonstrated that HMGB1 can be released from necrotic ECs and cardiomyocytes in the setting of heart transplantation and activates pro-inflammatory pathways (Park et al., 2004; Rovere-Querini et al., 2004; Bell et al., 2006). Yao et al. have shown that overexpression of microRNA26a, which plays an important role in apoptosis (Zhang et al., 2010) and induces VSMC growth (Leeper et al., 2011), inhibits HMGB1 expression and decreases cardiac I/R injury (Yao et al., 2016). Further studies are needed to investigate the mechanistic pathway of microRNA26a and to make it available as a therapy.

TRANSMIGRATION OF LEUKOCYTES ACROSS THE ENDOTHELIUM

During inflammation, leukocytes are actively recruited into the vessel wall to resolve the inflammatory state, so cell–cell contact between ECs and leukocytes must be established. Alongside other triggers, donor-derived vascular cells, e.g., ECs and VSMCs, produce and release ROS as well as cytokines into the extracellular environment, recruiting neutrophils and macrophages to the site of injury. In turn, recruited and activated cells themselves start to produce, inter alia, ROS, which acts as an amplification loop for immune cell stimulation (Land, 2012b).

Activation of ECs Induces Expression of Adhesion Molecules and Growth Factors

Activation of ECs leads to rapid release of vWF. Also, adhesion molecules, such as E-selectin, P-selectin, ICAM-1, and VCAM-1, are upregulated on the surface of ECs (Salom et al., 1998; Valenzuela et al., 2013a; Fenton et al., 2016). Interestingly, Fenton et al. found a decrease of E- and P-selectin expression on the endothelium in their patient cohort of heart-transplanted children compared to age- and sex-matched controls from healthy siblings. All patients had been treated with immunosuppressant and 90% with statins after heart transplantation (Fenton et al., 2016). A direct contact of dendritic cells (DCs) and ECs, provided by adhesion molecules, leads to the transfer of intact MHC:peptide complexes from activated ECs to DCs. This offers recipient DCs to present foreign MHC molecules to T cells and serves as a link between direct and indirect allorecognition (Herrera et al., 2004).

Activation of ECs is not only characterized by intensified expression of adhesion receptors but also by enhanced synthesis of numerous growth factors (PDGF, EGF, FGF, VEGF, TGF-β, etc.) and synthesis of endothelin I (ET-1) as well as expression of the corresponding receptors (Bian and Reed, 2001; Chen et al., 2001; Rossini et al., 2005).

The presence of higher numbers of FGF receptors (FGFR) on the surface of ECs facilitates increased binding capacity of FGF, which activates the MAPK/ERK pathway and results in enhanced EC proliferation (Jin et al., 2007). ET-1 is one of the most potent vasoconstrictors in humans, and its antagonists are used to treat pulmonary arterial hypertension, but it also exerts pro-inflammatory effects (Davenport et al., 2016). In a retrospective study of heart transplantations, elevated ET-1 has been established as an independent predictor of accelerated cardiac allograft rejection (Parikh et al., 2019).

Sunitinib, a tyrosine kinase inhibitor, is already used for gastrointestinal stromal tumor and metastatic renal cell carcinoma, blocking PDGF and VEGF receptors (Chow and Eckhardt, 2007). In a rat kidney rejection model, orally administered Sunitinib was successfully used to prevent

neointima hyperplasia, one hallmark of renal transplant arteriosclerosis (Rintala et al., 2016).

Transmigration of Leukocytes Is a Multistep Progress

For immune cells, up-regulation of transmigration molecules on the surface of ECs is essential for migration from the circulation across the endothelial monolayer into the vessel wall. Before transmigration, leukocytes tether and roll along the EC monolayer, which is mediated by selectins and integrins (Muller, 2003). Subsequent leukocyte transmigration is mediated by specialized molecules (Muller et al., 1993). PECAM, CD99, or JAM-A are partially stored in lateral border recycling compartments (LBRCs) within ECs beneath the plasma membrane near endothelial junctions. To achieve sufficient transmigration, leukocytes are surrounded by LBRC membrane to provide unligated receptors for the immune cells (Mamdouh et al., 2003, 2009). Recent studies suggest relevance of IQ-domain GTPase-activating protein 1 (IQGAP1), bearing an actin-binding as well as a calmodulin-binding domain, for leukocyte transmigration. It has been shown that IQGAP1 interacts with LBRC, and knockdown of the protein prevents LBRC movement and leukocyte transmigration (Dalal et al., 2018, 2019). For the transient receptor potential canonical 6 (TRPC6), a ubiquitously expressed Ca^{2+} channel, co-localization with PECAM at endothelial junctions during transmigration has been proven. Chelation of Ca^{2+} as well as disruption of TRPC6 function stops leukocytes on the apical surface of ECs, suggesting a pivotal role for Ca^{2+} influx during transmigration. A TRPC6 function is likely located downstream of PECAM, because transmigration occurs after selective activation of TRPC6 and simultaneous PECAM blockade (Weber et al., 2015). Taking these findings together, interfering with Ca2+ currents might be a therapeutic approach for TV.

Leukocytes can either transmigrate paracellularly across ECs–ECs junctions or migrate transcellularly through single ECs (Vestweber, 2015). Paracellular transmigration requires loosening of endothelial junctions, with VE-cadherin as an important regulator of these junctional connections (Gotsch et al., 1997). To leave the bloodstream and invade the vessel wall, leukocytes must penetrate the basement membrane, which is composed of laminins and connects the endothelial monolayer with the underlying SMCs. Laminin 411 is ubiquitously expressed, whereas laminin 511 is expressed in distinct spots, and these spots are not preferred sites of leukocyte transmigration (Sixt et al., 2001). Laminin 511 induces VE-cadherin localization at endothelial junctions, which results in a RhoA-dependent stabilization of these cell junctions and reduced leukocyte transmigration (Song et al., 2017). Yeh and colleagues have shown that leukocytes are capable of generating 3D traction stresses to mechanically widen gaps between ECs and initiate transmigration (Yeh et al., 2018). Immunohistochemical analysis of the vessel wall of explanted organs with TV revealed that the majority of infiltrating cells are T cells. Macrophages account for 8–15% of infiltrating cells, whereas B cells and NK cells are encountered infrequently (van Loosdregt et al., 2006; Hidalgo et al., 2010).

Figure 3 is a schematic summary of transcellular and paracellular transmigration. The most prominent receptors involved in these two distinct pathways of leukocyte migration across the endothelial monolayer are depicted.

Prevention of leukocyte recruitment is a putative therapeutic intervention to prevent TV. It has been shown, that adding the heparin-based macromolecule Corline Heparin Conjugate (CHC) to the preservation solution forms a protective coating on the renal endothelium during cold storage after kidney explantation. Kidneys were analyzed 24 hours after transplantation, and the number of infiltrated leukocytes and the thrombotic area was significantly greater in control kidneys. CHC treatment is a promising strategy for prevention of I/R injury-induced leukocyte transmigration (Nordling et al., 2018).

A further means of delaying graft failure is to actively recruit suppressive, i.e., beneficial leukocytes into the graft. Application of depletional antibodies or the use of specific knockout and transgenic mouse strains enabled demonstration of the impact of different immune cell subtypes on ongoing graft failure. In various animal experiments, tolerogenic characteristics have been revealed for regulatory T cells (Tregs), T cells, B cells, NK cells, and NKT cells (Sakaguchi et al., 1995; Niimi et al., 1998; Seino et al., 2001; Yu et al., 2006; Haudebourg et al., 2007).

CHANGES IN VASCULAR STRUCTURE

Transplant vasculopathy is characterized by accumulation of extracellular matrix (ECM) (Lin et al., 1996), endothelial dysfunction, and VSMC proliferation, which result in diffuse, concentric intimal thickening (Rahmani et al., 2006). TV differs in appearance depending on the vessel structure: large coronary segments are affected by artery shrinkage, resulting in a loss of luminal diameter, whereas new intimal growth and subsequent loss of luminal diameter occurs in both large and small segments (Wong et al., 2001; Suzuki et al., 2010). In addition to the lumen narrowing, production of vasoconstrictors such as ET-1 and thromboxane is impaired and vascular resistance increases, which may result in ischemia (Rahmani et al., 2006). After activation, ECs elicit the differentiation and proliferation of quiescent medial VSMCs. VSMCs transdifferentiate from a contractile phenotype to dedifferentiated synthetic cells. Dedifferentiated VSMCs migrate from the media into the neointima and interstitial space, where they proceed to proliferate. VSMC proliferation and ECM production aggravate lumen narrowing. Furthermore, VSMCs produce cytokines which act in an autocrine fashion and strengthen proliferation (Michael, 2003; Dewald et al., 2005; Kennard et al., 2008; Wynn, 2008). Most neointimal muscle cells that evolved from VSMCs are similar in appearance to their medial progenitors; nevertheless, on the basis of some important functional differences, neointimal muscle cells are generally labeled smooth muscle-like cells (SMLCs) (Wong et al., 2001; Suzuki et al., 2010).

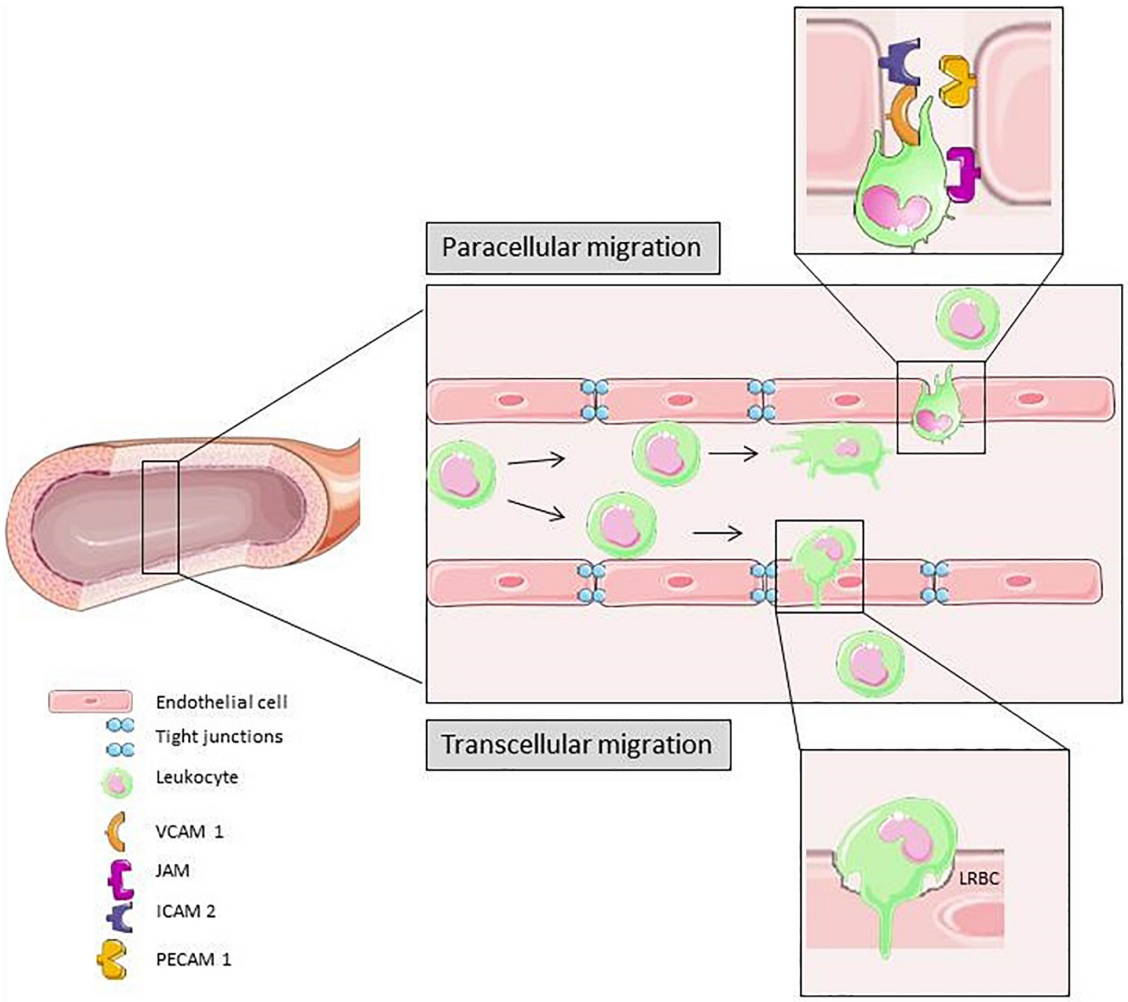

FIGURE 3 | In response to different pro-inflammatory signals the leukocyte adhesion and transmigration cascade is activated. Slow down, rolling, firm adhesion and transmigration is mediated by different cytokines and molecules on the surface of leukocytes and ECs. Para-cellular transmigration through EC junctions is the primary route for extravasation (Vestweber, 2015). Elements of **Figures 2**, **3** and **4** were taken and adjusted from Servier Medical Art at http://smart.servier.com, licensed under a Creative Commons Attribution 3.0 Unported License.

Not only ECs but also VSMCs can be directly affected by donor-specific anti-HLA I antibodies. *In vitro* stimulation with anti-HLA I antibodies induces VSMC proliferation in a dose-dependent manner. Also, migration is promoted, even in the presence of the proliferation inhibitor mitomycin C. As underlying mechanism for the observed effect, increased phosphorylation of FAK Tyr576, Akt Ser473, and ERK1/2 Thr202/Tyr204 is postulated (Li et al., 2011). In a humanized mouse model, human arteries were grafted into SCID/beige mice lacking functional T and B cell compartments. In this mouse model, passively transferred anti-HLA I antibodies were able to evoke neointima thickening and VSMC proliferation (Galvani et al., 2009). Recent studies demonstrated a pivotal role for sphingosine-1-phosphate (S1P) in anti-HLA I-induced intimal hyperplasia because treatment with anti-S1P antibodies and siRNA knockdown of sphingosine kinase-1 (SK1) inhibitor prevents intimal hyperplasia in mice (Trayssac et al., 2015). S1P is a mediator within signaling pathways for cell survival, proliferation, and migration (Herzog et al., 2010) and provides another potential therapeutic target for preventing TV (Spiegel and Milstien, 2003).

Figure 4 illustrates the vascular changes during alloresponse after solid organ transplantation. EC activation due to I/R injury predominantly leads to neutrophil recruitment into the vessel wall. At a later stage, lymphocytes and macrophages transmigrate into the vasculature and drive rejection. In the end, due to SMLC proliferation, TV with hallmark lumen narrowing is established.

EFFECTS OF THE COMPLEMENT SYSTEM ON ECs

The complement system is part of the innate immune system and provides a link to adaptive immunity. It can be activated

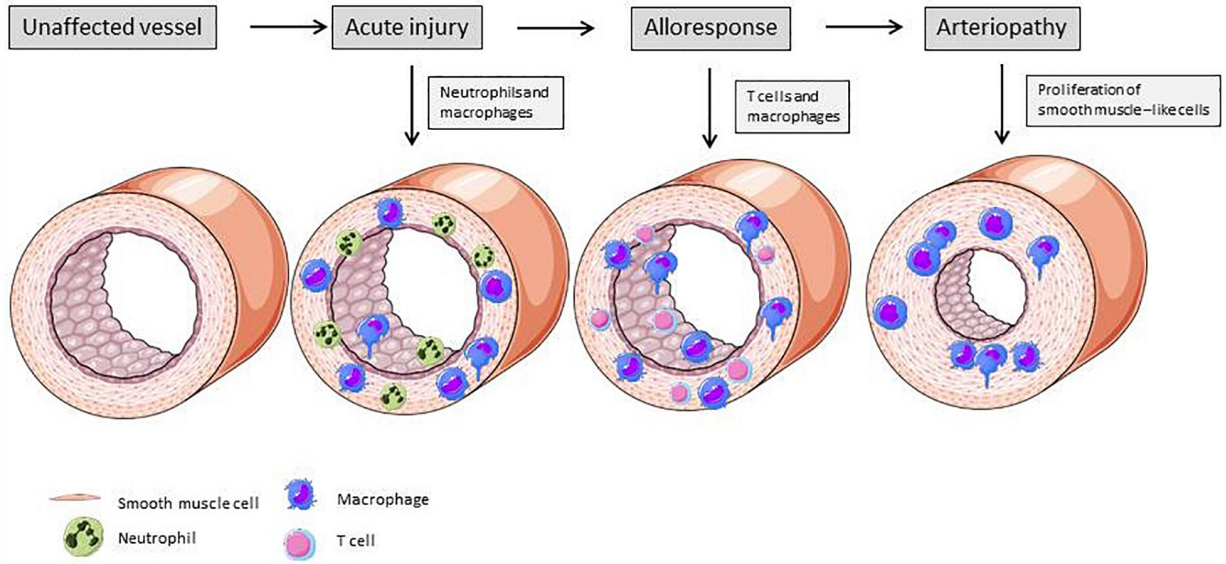

FIGURE 4 | Changes of vascular structure due alloresponse following solid organ transplantation. Acute injury is mainly mediated by neutrophiles ans macrophages. These immune cells produce cytokines and induce expression of adhesion molecules on ECs, leading to further recruitment of immune cells. Activated ECs exert a pro-inflammatory phenotype and activate smooth muscle-like cells, resulting in their proliferation and lumen narrowing (Mitchell, 2009). Elements of **Figures 2**, **3** and **4** were taken and adjusted from Servier Medical Art at http://smart.servier.com, licensed under a Creative Commons Attribution 3.0 Unported License.

in three different ways: complement proteins bind to (1) antibodies bound to ECs, (2) proteins on cell membranes, or (3) carbohydrate residues on the surface. Independent of the mode of activation, all three pathways have in common protein C3 cleavage and subsequent membrane attack complex (MAC) formation. The MAC consists of complement proteins C5b-C9, and its activity results in cell lysis. Deposition of the complement fragment C4d on ECs was established as an independent marker for acute allograft rejection and as a predictor for long-term graft loss (Collins et al., 1999; Herzenberg et al., 2002; Racusen et al., 2003).

Nevertheless, there are some mechanisms that protect against EC damage due to an activated complement system. Expressed on human ECs, CD59 binds tightly into the forming MAC, thus preventing further MAC assembly (Davies and Lachmann, 1993). Another complement regulatory protein is CD55, which is also expressed on ECs. Incubation of ECs with CD55- and CD59-blocking antibodies induces complement fixation, which results in vWF release and platelet adhesion. Interestingly, complement fixation was increased in ECs from patients with type 3 von Willebrand disease lacking functional vWF. vWF seems to act as a complement regulator on the surface of ECs (Noone et al., 2016). Renal transplantation models in rats showed a decrease in mRNA expression of the complement regulators CD59 and Crry in allografts, and administration of anti-Crry and anti-CD59 antibodies results in reduced graft survival. A subsequent clinical study showed significantly increased graft survival in patients with high expression of complement regulatory proteins (Yamanaka et al., 2016).

It has been shown that assembly of MAC at sublytic levels has various effects in different cell types. *In vitro* stimulation of human ECs with C5b-C9 induces proliferation and migration. Furthermore, C5b-C9 promotes the release of pro-inflammatory cytokines, such as IL-6, MCP-1, and epidermal growth factor (Fosbrink et al., 2006), which contribute to recruitment of immune cells and ongoing inflammation.

In a mouse model of vascularized composite allografts, it was documented that the neutrophil and macrophage infiltrate was impaired in C3-deficient mice. Treatment with the C3 inhibitor CR2-Crry was associated with significantly prolonged graft survival (Zhu et al., 2017). Accordingly, the results of a clinical study in patients after kidney transplantation demonstrated that a local upregulation of C3 expression in glomeruli and tubuli was associated with ongoing acute cellular rejection (Serinsoz et al., 2005). Neutrophil recruitment to sites of inflammation can also be reduced by interfering with C5a and its receptor (Mueller et al., 2013).

WHAT KIND OF RESEARCH MODELS DO WE HAVE?

Humanized Mouse Models

As there are several examples of successful therapy approaches in mice that failed to provide similar efficacy in humans, the transferability of preclinical animal studies to humans might seem doubtful (Mestas and Hughes, 2004). Species-specific differences between the murine and human immune systems should be taken into account. To overcome this limitation in the field of solid organ transplantation, the use of humanized mice to study human allografts and xenograft rejection may

provide insights into the immune mechanisms responsible for graft rejection [recently reviewed by Kenney et al. (2016)].

Humanized mice have become an important preclinical tool in translational biomedical research (Walsh et al., 2017) and serve as a preclinical bridge in several fields [reviewed in Allen et al. (2019)]. Generally, these mice are reconstituted with human $CD34^+$ stem cells derived from human cord blood, bone marrow, and peripheral blood (Lee et al., 2019). This is made possible by a targeted mutation in the interleukin 2 (IL-2) receptor common gamma chain [IL2rg(null)] in mice that are already deficient in T and B cells (Brehm et al., 2013). The most widely used immunodeficient strains engrafted with human hematopoietic cells are listed in **Table 1** [modified after (Kenney et al., 2016); a more detailed list with immunodeficient mice that have been engrafted with human immune systems has been published elsewhere (Shultz et al., 2012; Hogenes et al., 2014)]. Among other immune defects, these animals do not develop functional NK cells. This allows efficient engraftment with human hematopoietic cells, generating a functional human immune system (Brehm et al., 2013).

BLT(**b**one marrow, **l**iver, **t**hymus) humanized mice are generated by implantation of human fetal thymus and liver tissue into immunodeficient mice followed by systemic reconstitution with human innate (monocytes/macrophages, DCs, NK cells) and adaptive immune cells (B cells and T cells) (Wahl et al., 2019). The presence of a human thymic tissue allows human T cell education depending on HLA and the induction of HLA-restricted T cell responses in these mice is comparable with the human system (Wahl et al., 2019). Even though mice have a significantly shorter life span than humans, age-associated DNA methylation changes in the transplanted hematopoietic stem cells were not found to be increased (Frobel et al., 2018).

Recently, a humanized lung mouse model has been generated by subcutaneously implanting human lung tissue into the back of immunodeficient mice (Wahl et al., 2019). The human lung tissue vascularizes, expands and persists as a human lung implant. The engraftment of human non-hematopoietic cells, which are able to present antigens to autologous human immune cells in the full context of HLA (Wahl et al., 2019), will broaden the use of humanized mice for research in the field of transplantation.

Heterotopic Versus Orthotopic Transplantation of Different Organs

Solid organ transplantation is an established treatment option for patients with end-organ dysfunction (Black et al., 2018). Progress in surgical techniques has minimized complications and reduced ischemic injury events. The more common orthotopic transplantation includes removal of the recipient's organ and the insertion of the donor organ in the normal anatomic position, while in the case of heterotopic or "piggy-back" transplantation the diseased organ is retained.

Heterotopic heart transplantation (HHT) is extensively used in murine animal models in the non-working mode (Flecher et al., 2013). HHT in human patients, first performed by Barnard and Losman in 1974 (Barnard and Losman, 1975) is used rarely in comparison with orthotopic heart transplantation (OHT). The reason for this is major progress in immunosuppression therapy with the expansion of immunosuppressive protocols to dampen the host immune response and improve short- and long-term graft survival (Black et al., 2018). However, HHT may experience a renaissance, especially for children with advanced cardiomyopathy, where cardiac transplantation is limited by pediatric donor availability, by increasing the size of the donor pool. Beyond that, HHT also enables transplantations in adults previously not eligible for transplantation. It may be used especially in recipients with significant pulmonary hypertension (Flecher et al., 2013). Another advantage is that during temporary graft dysfunction due to early graft rejection the recipient heart could serve as an auxiliary pump (Holinski et al., 2016).

TABLE 1 | Immunodeficient mouse strains engrafted with human hematopoietic cells (modified after Kenney et al., 2016)

Strain	Abbreviation	*Il2rg* mutation	Characteristics	Immunological Characteristics	Availability [Refences]
NOD.Cg-*Prkdc*^{scid} *Il2rg*^{tm1Wjl}/*SzJ*	NSG	Do not express the DNA repair complex protein Prkdc nor the X-linked Il2rg gene, the IL2rg^{null} mutation prevents cytokine signaling through multiple receptors	NOD strain. Immunodeficient and relatively radiosensitive due to a defect in DNA repair	Deficient in mature lymphocytes, serum Ig is not detectable and natural killer cell cytotoxic activity is extremely low	The Jackson Laboratory Stock: 005557 (Shultz et al., 2005)
NOD.*cg-Prkdc*^{scid} *Il2rg*^{tm1Sug}/*JicTac*	NOG	Lacks the intracytoplasmic domain and will bind cytokines but will not signal	NOD strain. Immunodeficient and relatively radiosensitive due to a defect in DNA repair	Lacks T, B and NK cells, additional defects in innate immune cells	Taconic Bioscience Stock: CIEA NOG mouse (Ito et al., 2002)
NOD.Cg-*Rag1*^{tm1Mom} *IL2rg*^{tm1Wjl}/*SzJ*	NRG	Rag1null mutation renders the mice B and T cell deficient and the IL2rg^{null} mutation prevents cytokine signaling through multiple receptors,	NOD strain. Extremely immunodeficient and relatively radioresistant	Lacks T, B and NK cells, additional defects in innate immune cells	The Jackson Laboratory Stock: 007799 (Pearson et al., 2008)
C.Cg-*Rag2*^{tm1Fwa} *Il2rg*^{tm1Sug}*JicTac*	BRG	Lacks the intracytoplasmic domain and will bind cytokines but will not signal	Mixed background, predominately BALB/c strain: Immunodeficient and relatively radioresistant	Lacks T, B and NK cells, remaining innate immune cells are functional	Taconic Bioscience Stock: 11503 (Traggiai et al., 2004)

The prognosis for long-term graft survival and retention depends mainly on revascularization. Injury to the donor-derived microvasculature during organ explantation and subsequent ischemia may account for the documented clinical variability (Soares et al., 2015). Thereby, replacement of the donor graft vasculature by recipient-derived endothelial and endothelial progenitor cells may be a strategy for all non-vascularized free grafts or vascularization of tissue constructs engineered *in vitro* (Capla et al., 2006). Exogenous liposomal delivery of the angiogenic inducer VEGF gene prior to bone marrow–derived endothelial precursor cell transplantation has been shown to improve orthotopic liver transplantation-induced hepatic I/R injury (Cao et al., 2017). In this study, the transfer of the VEGF gene significantly increased hepatotrophic mitogen expression, in common with, for example, hepatocyte growth factor, angiogenesis, and NOS activity (Cao et al., 2017). In another study, the phosphodiesterase-5 inhibitor sildenafil citrate protected the graft microvasculature of warm ischemic kidney transplants (Lledo-Garcia et al., 2009) and autologous fat grafts (Soares et al., 2015). Sildenafil also decreased edema in lung I/R injury and ROS formation in a lung I/R injury model (Guerra-Mora et al., 2017).

The endothelial hypoxia-inducible factor HIF-2α has been shown to be essential for airway microvascular health and to play an important role in maintaining lung homeostasis (Jiang et al., 2019). In an orthotopic tracheal transplantation model, the genetic deletion of HIF-2α but not HIF-1α caused tracheal endothelial cell apoptosis. HIF-1α overexpression induced the expression of proangiogenic factors such as stromal cell-derived factor 1 (Sdf1) and VEGF, and promoted the recruitment of vasoreparative $Tie2^{+}$ endothelial progenitor cells to the allograft (Jiang et al., 2019). These results are in line with the findings of a previous study using immortalized human microvascular endothelial cells (HMEC-1), demonstrating that reduction of both HIFs reduced cell survival, gene expression of glycolytic enzymes and pro-angiogenic factors compared with the corresponding control (Hahne et al., 2018).

ACCOMMODATION: THE ROLE OF PROTECTIVE GENE EXPRESSION IN ECs

Accommodation in solid organ transplantation has been defined as stable allograft function without evidence of pathological alterations in the presence of alloantibodies and graft deposition of the complement component C4d (Smith and Colvin, 2012). The term accommodation was proposed at the beginning of the 1990s and was initially been demonstrated in the setting of xenotransplantation (Bach et al., 1991). It was later shown in a hamster-to-rat xenotransplantation model that increased expression of protective genes, i.e., anti-apoptotic and anti-oxidant genes, in ECs of the grafted organ was critical for mediating transplant survival (Bach et al., 1997). Moreover, it was found that regulation of endothelial gene expression patterns was accompanied by a host T_H2 cell response. A follow-up study in a mouse-to-rat cardiac xenograft model demonstrated that the inducible anti-oxidant heme-degrading enzyme heme oxygenase-1 (HO-1) plays a key role in mediating anti-inflammatory protective effects. These protective effects were important for mediating transplant survival, possibly via the generation of the gaseous molecule carbon monoxide and biliverdin/bilirubin (Soares et al., 1998) [for a review see Soares et al. (1999)]. In accordance with these findings, Salama and colleagues showed, in studies on sensitized kidney transplantation patients with anti-HLA antibodies, that accommodation appears to be dependent on the expression of the anti-apoptotic gene Bcl-xL in the endothelium (Salama et al., 2001). Interestingly, this study demonstrates that low titers of anti-HLA antibodies can cause accommodation.

In a more recent HLA-mismatched, humanized murine HHT model, it was demonstrated that up-regulation of protective genes, including Bcl-2, Bcl-xL, and HO-1, was associated with protection against transplant rejection. Furthermore, expression of inducible inflammatory genes, e.g., ICAM-1 and VCAM-1, and pro-inflammatory cytokines such as IL-1β, TNF-α, and IL-6 was decreased in accommodated grafts (Fukami et al., 2012). In accordance with these findings, targeted up-regulation of HO-1 protected against anti-HLA class I antibody-mediated pro-inflammatory activation of ECs (Zilian et al., 2015).

Interestingly, a recent report compared the regulatory effects of interactions of the endothelium with antibodies against either AB0 or HLA antigens in a cell culture model of EA.hy926 ECs. It was demonstrated that ligation of ECs with anti-AB0 antibodies but not with anti-HLA antibodies caused accommodation (Iwasaki et al., 2012). The principal findings of these *in vitro* studies appear to be in accordance with a report on AB0-incompatible living kidney donor transplantation (Brocker et al., 2013).

Furthermore, ligation of anti-AB0 antibodies to EA.hy926 ECs induced upregulation of the complement regulatory proteins CD55 and CD59 on the RNA as well as on the protein level (Iwasaki et al., 2012). The first *in vivo* studies showed that overexpression of human CD55 and CD59 (hCD55, hCD59) protects mice from impaired kidney function in an experimental renal I/R injury model (Bongoni et al., 2017). A recent retrospective study of 150 patients after kidney transplantation, confirmed that lower intragraft expression of CD55 is a risk factor for rapid progression of chronic renal rejection (Cernoch et al., 2018). A more detailed study of kidney transplantations demonstrated a correlation between promotor polymorphisms in complement-regulatory proteins and graft survival (Michielsen et al., 2018).

CONCLUSION

Graft rejection after transplantation of vascularized solid organs remains the main obstacle for graft survival. This complex disease pattern is caused by the interplay of different immune cell subsets and soluble factors from the recipient's and the donor's immune system. Graft rejection has heterogeneous characteristics, depending on the affected organ and whether it arises from cellular- or humoral-dependent pathways, but in any

case, it leads to organ failure. While medication to treat acute rejection episodes is available, the therapeutic options for chronic rejection are limited.

The first target structure to be attacked after transplantation is the endothelium of the graft vessel wall. ECs are recognized by the recipient's immune system due to the expression of surface molecules such as HLA and others, and activation of ECs is induced. Beside immunological components, brain death and I/R injury promote activation of donor-derived ECs. Activated ECs upregulate expression of various pro-inflammatory cytokines, and immune cells will be recruited. Various cytokines have been established as clinical markers to facilitate early diagnosis of graft failure and allow for treatment optimization. Furthermore, ECs present an amended expression pattern of adhesion and transmigration receptors on the surface to promote transmigration of leukocytes from the bloodstream across the EC monolayer into the vessel wall. Due to cytokines released from ECs as well as leukocytes, a pro-inflammatory microenvironment is built up and cannot be resolved.

The mononuclear infiltrate and growth factors further induce migration and proliferation of VSMCs and the resulting concentric intimal hyperplasia is a hallmark of long-term graft rejection. Crosslinking of antibodies on the surface induces phosphorylation and formation of intermediate signal transducers within the mTOR pathway, which regulates cytoskeletal changes, proliferation, and expression activity.

Further research is needed to gain deeper insight into how innate and adaptive immune responses contribute to graft rejection and how activation of ECs might be prevented. One therapeutic approach could be blocking ECs from presenting antigens, to prevent direct cellular cytotoxicity and to avoid synthesis of *de novo* donor-specific antibodies. Another option could be inhibiting recruitment of immune cells into the vessel wall, a concept of interest for other vascular diseases such as atherosclerosis. Humanized mouse models are important preclinical tools to study the underlying mechanisms of graft rejection. Despite many differences between the species, these mice represent a model system to evaluate new drugs and other treatment options without putting patients at risk.

AUTHOR CONTRIBUTIONS

LK and JL contributed conception and design of the Review. LK, MZ, VV, RA, SI, MW, and AW wrote separate sections of the manuscript. All authors conducted extensive literature research, read and approved the submitted version.

FUNDING

The work was supported by grants from the Deutsche Forschungsgemeinschaft (LA 2343/7-1 and IM 20/4-1) to JL and SI.

REFERENCES

Aljabri, A., Vijayan, V., Stankov, M., Nikolin, C., Figueiredo, C., Blasczyk, R., et al. (2019). HLA class II antibodies induce necrotic cell death in human endothelial cells via a lysosomal membrane permeabilization-mediated pathway. *Cell Death Dis.* 10:235. doi: 10.1038/s41419-019-1319-5

Allen, T. M., Brehm, M. A., Bridges, S., Ferguson, S., Kumar, P., Mirochnitchenko, O., et al. (2019). Humanized immune system mouse models: progress, challenges and opportunities. *Nat. Immunol.* 20, 770–774. doi: 10.1038/s41590-019-0416-z

Alphonsus, C. S., and Rodseth, R. N. (2014). The endothelial glycocalyx: a review of the vascular barrier. *Anaesthesia* 69, 777–784. doi: 10.1111/anae.12661

Anyanwu, A. C., Banner, N. R., Radley-Smith, R., Khaghani, A., and Yacoub, M. H. (2002). Long-term results of cardiac transplantation from live donors: the domino heart transplant. *J. Heart Lung Transplant.* 21, 971–975. doi: 10.1016/s1053-2498(02)00406-0

Bach, F. H., Ferran, C., Hechenleitner, P., Mark, W., Koyamada, N., Miyatake, T., et al. (1997). Accommodation of vascularized xenografts: expression of "protective genes" by donor endothelial cells in a host Th2 cytokine environment. *Nat. Med.* 3, 196–204. doi: 10.1038/nm0297-196

Bach, F. H., Turman, M. A., Vercellotti, G. M., Platt, J. L., and Dalmasso, A. P. (1991). Accommodation: a working paradigm for progressing toward clinical discordant xenografting. *Transplant. Proc.* 23(Pt 1), 205–207.

Barnard, C. N., and Losman, J. G. (1975). Left ventricular bypass. *S. Afr. Med. J.* 49, 303–312.

Bell, C. W., Jiang, W., Charles, F., Reich, I., and Pisetsky, D. S. (2006). The extracellular release of HMGB1 during apoptotic cell death. *Am. J. Physiol. Cell Physiol.* 291, C1318–C1325. doi: 10.1152/ajpcell.00616.2005

Belperio, J. A., Keane, M. P., Burdick, M. D., Gomperts, B., Xue, Y. Y., Hong, K., et al. (2005). Role of CXCR2/CXCR2 ligands in vascular remodeling during bronchiolitis obliterans syndrome. *J. Clin. Invest.* 115, 1150–1162. doi: 10.1172/JCI24233

Bian, H., Harris, P. E., Mulder, A., and Reed, E. F. (1997). Anti-HLA antibody ligation to HLA class I molecules expressed by endothelial cells stimulates tyrosine phosphorylation, inositol phosphate generation, and proliferation. *Hum. Immunol.* 53, 90–97. doi: 10.1016/S0198-8859(96)00272-8

Bian, H., and Reed, E. F. (2001). Anti-HLA class I antibodies transduce signals in endothelial cells resulting in FGF receptor translocation, down-regulation of ICAM-1 and cell proliferation. *Transplant. Proc.* 33:311. doi: 10.1016/s0041-1345(00)02022-4

Bianchi, M. E. (2007). DAMPs, PAMPs and alarmins: all we need to know about danger. *J. Leukoc. Biol.* 81, 1–5. doi: 10.1189/jlb.0306164

Black, C. K., Termanini, K. M., Aguirre, O., Hawksworth, J. S., and Sosin, M. (2018). Solid organ transplantation in the 21(st) century. *Ann. Transl. Med.* 6:409. doi: 10.21037/atm.2018.09.68

Bongoni, A. K., Lu, B., Salvaris, E. J., Roberts, V., Fang, D., McRae, J. L., et al. (2017). Overexpression of human CD55 and CD59 or treatment with human CD55 protects against renal ischemia-reperfusion injury in mice. *J. Immunol.* 198, 4837–4845. doi: 10.4049/jimmunol.1601943

Brehm, M. A., Shultz, L. D., Luban, J., and Greiner, D. L. (2013). Overcoming current limitations in humanized mouse research. *J. Infect. Dis.* 208(Suppl. 2), S125–S130. doi: 10.1093/infdis/jit319

Brocker, V., Pfaffenbach, A., Habicht, A., Chatzikyrkou, C., Kreipe, H. H., Haller, H., et al. (2013). Beyond C4d: the ultrastructural appearances of endothelium in ABO-incompatible renal allografts. *Nephrol. Dial. Transplant.* 28, 3101–3109. doi: 10.1093/ndt/gft373

Cao, D., Wang, M., Gong, J., Wei, S., and Li, J. (2017). Exogenous vascular endothelial growth factor delivery prior to endothelial precursor cell transplantation in orthotopic liver transplantation-induced hepatic ischemia/reperfusion injury. *Liver Transpl.* 23, 804–812. doi: 10.1002/lt.24745

Cao, R. N., Tang, L., Xia, Z. Y., and Xia, R. (2019). Endothelial glycocalyx as a potential theriapeutic target in organ injuries. *Chin. Med. J. (Engl.)* 132, 963–975. doi: 10.1097/cm9.0000000000000177

Capla, J. M., Ceradini, D. J., Tepper, O. M., Callaghan, M. J., Bhatt, K. A., Galiano, R. D., et al. (2006). Skin graft vascularization involves precisely regulated regression and replacement of endothelial cells through both angiogenesis and vasculogenesis. *Plast. Reconstr. Surg.* 117, 836–844. doi: 10.1097/01.prs.0000201459.91559.7f

Cardinal, H., Dieude, M., and Hebert, M. J. (2017). The emerging importance of non-HLA autoantibodies in kidney transplant complications. *J. Am. Soc. Nephrol.* 28, 400–406. doi: 10.1681/ASN.2016070756

Cernoch, M., Hruba, P., Kollar, M., Mrazova, P., Stranavova, L., Lodererova, A., et al. (2018). Intrarenal complement system transcripts in chronic antibody-mediated rejection and recurrent IgA nephropathy in kidney transplantation. *Front. Immunol.* 9:2310. doi: 10.3389/fimmu.2018.02310

Chen, J., Fabry, B., Schiffrin, E. L., and Wang, N. (2001). Twisting integrin receptors increases endothelin-1 gene expression in endothelial cells. *Am. J. Physiol. Cell Physiol.* 280, C1475–C1484. doi: 10.1152/ajpcell.2001.280.6.C1475

Chen, J. L., John, R., Richardson, J. A., Shelton, J. M., Zhou, X. J., Wang, Y. X., et al. (2011). Toll-like receptor 4 regulates early endothelial activation during ischemic acute kidney injury. *Kidney Int.* 79, 288–299. doi: 10.1038/ki.2010.381

Chong, A. S., and Alegre, M. L. (2012). The impact of infection and tissue damage in solid-organ transplantation. *Nat. Rev. Immunol.* 12, 459–471. doi: 10.1038/nri3215

Chow, L. Q. M., and Eckhardt, S. G. (2007). Sunitinib: from rational design to clinical efficacy. *J. Clin. Oncol.* 25, 884–896. doi: 10.1200/jco.2006.06.3602

Collins, A. B., Schneeberger, E. E., Pascual, M. A., Saidman, S. L., Williams, W. W., Tolkoff-Rubin, N., et al. (1999). Complement activation in acute humoral renal allograft rejection: diagnostic significance of C4d deposits in peritubular capillaries. *J. Am. Soc. Nephrol.* 10, 2208–2214.

Colvin, R. B., and Smith, R. N. (2005). Antibody-mediated organ-allograft rejection. *Nat. Rev. Immunol.* 5, 807–817. doi: 10.1038/nri1702

Cook, L. G., Chiasson, V. L., Long, C., Wu, G.-Y., and Mitchell, B. M. (2009). Tacrolimus reduces nitric oxide synthase function by binding to FKBP rather than by its calcineurin effect. *Kidney Int.* 75, 719–726. doi: 10.1038/ki.2008.697

Dalal, P. J., Sullivan, D. P., and Muller, W. A. (2018). Exploring the role of calmodulin and calcium signaling in leukocyte transmigration. *FASEB J.* 32(Suppl. 1):280.7. doi: 10.1096/fasebj.2018.32.1_supplement.280.7

Dalal, P. J., Sullivan, D. P., and Muller, W. A. (2019). Endothelial calmodulin and CaMKII play a role in leukocyte transmigration. *FASEB J.* 33(Suppl. 1):375.5. doi: 10.1096/fasebj.2019.33.1_supplement.375.5

Davenport, A. P., Hyndman, K. A., Dhaun, N., Southan, C., Kohan, D. E., Pollock, J. S., et al. (2016). Endothelin. *Pharmacol. Rev.* 68, 357–418. doi: 10.1124/pr.115.011833

Davies, A., and Lachmann, P. J. (1993). Membrane defence against complement lysis: the structure and biological properties of CD59. *Immunol. Res.* 12, 258–275. doi: 10.1007/bf02918257

Delville, M., Lamarthee, B., Pagie, S., See, S. B., Rabant, M., Burger, C., et al. (2019). Early acute microvascular kidney transplant rejection in the absence of anti-HLA antibodies is associated with preformed IgG antibodies against diverse glomerular endothelial cell antigens. *J. Am. Soc. Nephrol.* 30, 692–709. doi: 10.1681/ASN.2018080868

Dewald, O., Zymek, P., Winkelmann, K., Koerting, A., Ren, G., Abou-Khamis, T., et al. (2005). CCL2/monocyte chemoattractant protein-1 regulates inflammatory responses critical to healing myocardial infarcts. *Circ. Res.* 96, 881–889. doi: 10.1161/01.RES.0000163017.13772.3a

Dragun, D., Catar, R., and Philippe, A. (2016). Non-HLA antibodies against endothelial targets bridging allo- and autoimmunity. *Kidney Int.* 90, 280–288. doi: 10.1016/j.kint.2016.03.019

Dragun, D., Muller, D. N., Brasen, J. H., Fritsche, L., Nieminen-Kelha, M., Dechend, R., et al. (2005). Angiotensin II type 1-receptor activating antibodies in renal-allograft rejection. *N. Engl. J. Med.* 352, 558–569.

Fenton, M., Simmonds, J., Shah, V., Brogan, P., Klein, N., Deanfield, J., et al. (2016). Inflammatory cytokines, endothelial function, and chronic allograft vasculopathy in children: an investigation of the donor and recipient vasculature after heart transplantation. *Am. J. Transplant.* 16, 1559–1568. doi: 10.1111/ajt.13643

Flecher, E., Fouquet, O., Ruggieri, V. G., Chabanne, C., Lelong, B., and Leguerrier, A. (2013). Heterotopic heart transplantation: where do we stand? *Eur. J. Cardiothorac. Surg.* 44, 201–206. doi: 10.1093/ejcts/ezt136

Fosbrink, M., Niculescu, F., Rus, V., Shin, M. L., and Rus, H. (2006). C5b-9-induced endothelial cell proliferation and migration are dependent on Akt inactivation of forkhead transcription factor FOXO1. *J. Biol. Chem.* 281, 19009–19018. doi: 10.1074/jbc.M602055200

Francis, A., and Baynosa, R. (2017). Ischaemia-reperfusion injury and hyperbaric oxygen pathways: a review of cellular mechanisms. *Diving Hyperb. Med.* 47, 110–117. doi: 10.28920/dhm47.2.110-117

Frobel, J., Rahmig, S., Franzen, J., Waskow, C., and Wagner, W. (2018). Epigenetic aging of human hematopoietic cells is not accelerated upon transplantation into mice. *Clin. Epigenet.* 10:67. doi: 10.1186/s13148-018-0499-7

Frost, A. E., Jammal, C. T., and Cagle, P. T. (1996). Hyperacute rejection following lung transplantation. *Chest* 110, 559–562. doi: 10.1378/chest.110.2.559

Fukami, N., Ramachandran, S., Narayanan, K., Liu, W., Nath, D. S., Jendrisak, M., et al. (2012). Mechanism of accommodation in a sensitized human leukocyte antigen transgenic murine cardiac transplant model. *Transplantation* 93, 364–372. doi: 10.1097/TP.0b013e3182406a6b

Gallo, P. M., and Gallucci, S. (2013). The dendritic cell response to classic, emerging, and homeostatic danger signals. Implications for autoimmunity. *Front. Immunol.* 4:138. doi: 10.3389/fimmu.2013.00138

Galvani, S., Auge, N., Calise, D., Thiers, J. C., Canivet, C., Kamar, N., et al. (2009). HLA class I antibodies provoke graft arteriosclerosis in human arteries transplanted into SCID/beige mice. *Am. J. Transplant.* 9, 2607–2614. doi: 10.1111/j.1600-6143.2009.02804.x

Gao, W., Topham, P. S., King, J. A., Smiley, S. T., Csizmadia, V., Lu, B., et al. (2000). Targeting of the chemokine receptor CCR1 suppresses development of acute and chronic cardiac allograft rejection. *J. Clin. Invest.* 105, 35–44. doi: 10.1172/JCI8126

Girlanda, R. (2016). Deceased organ donation for transplantation: challenges and opportunities. *World J. Transplant.* 6, 451–459. doi: 10.5500/wjt.v6.i3.451

Gonzalez-Molina, M., Burgos, D., Cabello, M., Ruiz-Esteban, P., Rodriguez, M. A., Gutierrez, C., et al. (2014). Impact of immunosuppression treatment on the improvement in graft survival after deceased donor renal transplantation: a long-term cohort study. *Nefrologia* 34, 570–578. doi: 10.3265/Nefrologia.pre2014.Jun.12327

Gotsch, U., Borges, E., Bosse, R., Boggemeyer, E., Simon, M., Mossmann, H., et al. (1997). VE-cadherin antibody accelerates neutrophil recruitment in vivo. *J. Cell. Sci.* 110(Pt 5), 583–588.

Griffin, G. K., Newton, G., Tarrio, M. L., Bu, D. X., Maganto-Garcia, E., Azcutia, V., et al. (2012). IL-17 and TNF-alpha sustain neutrophil recruitment during inflammation through synergistic effects on endothelial activation. *J. Immunol.* 188, 6287–6299. doi: 10.4049/jimmunol.1200385

Guerra-Mora, J. R., Perales-Caldera, E., Aguilar-Leon, D., Nava-Sanchez, C., Diaz-Cruz, A., Diaz-Martinez, N. E., et al. (2017). Effects of sildenafil and tadalafil on edema and reactive oxygen species production in an experimental model of lung ischemia-reperfusion injury. *Transplant. Proc.* 49, 1461–1466. doi: 10.1016/j.transproceed.2017.03.089

Hahne, M., Schumann, P., Mursell, M., Strehl, C., Hoff, P., Buttgereit, F., et al. (2018). Unraveling the role of hypoxia-inducible factor (HIF)-1alpha and HIF-2alpha in the adaption process of human microvascular endothelial cells (HMEC-1) to hypoxia: redundant HIF-dependent regulation of macrophage migration inhibitory factor. *Microvasc. Res.* 116, 34–44. doi: 10.1016/j.mvr.2017.09.004

Haudebourg, T., Dugast, A. S., Coulon, F., Usal, C., Triebel, F., and Vanhove, B. (2007). Depletion of LAG-3 positive cells in cardiac allograft reveals their role in rejection and tolerance. *Transplantation* 84, 1500–1506. doi: 10.1097/01.tp.0000282865.84743.9c

He, H., Stone, J. R., and Perkins, D. L. (2003). Analysis of differential immune responses induced by innate and adaptive immunity following transplantation. *Immunology* 109, 185–196. doi: 10.1046/j.1365-2567.2003.01641.x

Herrera, O. B., Golshayan, D., Tibbott, R., Salcido Ochoa, F., James, M. J., Marelli-Berg, F. M., et al. (2004). A novel pathway of alloantigen presentation by dendritic cells. *J. Immunol.* 173, 4828–4837. doi: 10.4049/jimmunol.173.8.4828

Herzenberg, A. M., Gill, J. S., Djurdjev, O., and Magil, A. B. (2002). C4d deposition in acute rejection: an independent long-term prognostic factor. *J. Am. Soc. Nephrol.* 13, 234–241.

Herzog, C., Lorenz, A., Gillmann, H. J., Chowdhury, A., Larmann, J., Harendza, T., et al. (2014). Thrombomodulin's lectin-like domain reduces myocardial damage

by interfering with HMGB1-mediated TLR2 signalling. *Cardiovasc. Res.* 101, 400–410. doi: 10.1093/cvr/cvt275

Herzog, C., Schmitz, M., Levkau, B., Herrgott, I., Mersmann, J., Larmann, J., et al. (2010). Intravenous sphingosylphosphorylcholine protects ischemic and postischemic myocardial tissue in a mouse model of myocardial ischemia/reperfusion injury. *Mediat. Inflamm.* 2010:425191. doi: 10.1155/2010/425191

Hidalgo, L. G., Sis, B., Sellares, J., Campbell, P. M., Mengel, M., Einecke, G., et al. (2010). NK cell transcripts and NK cells in kidney biopsies from patients with donor-specific antibodies: evidence for NK cell involvement in antibody-mediated rejection. *Am. J. Transplant.* 10, 1812–1822. doi: 10.1111/j.1600-6143.2010.03201.x

Hirohashi, T., Chase, C. M., Della Pelle, P., Sebastian, D., Alessandrini, A., Madsen, J. C., et al. (2012). A novel pathway of chronic allograft rejection mediated by NK cells and alloantibody. *Am. J. Transplant.* 12, 313–321. doi: 10.1111/j.1600-6143.2011.03836.x

Hirohashi, T., Uehara, S., Chase, C. M., DellaPelle, P., Madsen, J. C., Russell, P. S., et al. (2010). Complement independent antibody-mediated endarteritis and transplant arteriopathy in mice. *Am. J. Transplant.* 10, 510–517. doi: 10.1111/j.1600-6143.2009.02958.x

Hogenes, M., Huibers, M., Kroone, C., and de Weger, R. (2014). Humanized mouse models in transplantation research. *Transplant. Rev. (Orlando)* 28, 103–110. doi: 10.1016/j.trre.2014.02.002

Holinski, S., Hausdorf, G., and Konertz, W. (2016). From baby to man with a piggyback heart: long-term success of heterotopic heart transplantation. *Eur. J. Cardiothorac. Surg.* 49, 348–349. doi: 10.1093/ejcts/ezv055

Horuk, R., Clayberger, C., Krensky, A. M., Wang, Z., Grone, H. J., Weber, C., et al. (2001). A non-peptide functional antagonist of the CCR1 chemokine receptor is effective in rat heart transplant rejection. *J. Biol. Chem.* 276, 4199–4204. doi: 10.1074/jbc.M007457200

Ito, M., Hiramatsu, H., Kobayashi, K., Suzue, K., Kawahata, M., Hioki, K., et al. (2002). NOD/SCID/gamma(c)(null) mouse: an excellent recipient mouse model for engraftment of human cells. *Blood* 100, 3175–3182. doi: 10.1182/blood-2001-12-0207

Iwasaki, K., Miwa, Y., Ogawa, H., Yazaki, S., Iwamoto, M., Furusawa, T., et al. (2012). Comparative study on signal transduction in endothelial cells after anti-a/b and human leukocyte antigen antibody reaction: implication of accommodation. *Transplantation* 93, 390–397. doi: 10.1097/TP.0b013e3182424df3

Jassem, W., Koo, D. D., Cerundolo, L., Rela, M., Heaton, N. D., and Fuggle, S. V. (2003). Leukocyte infiltration and inflammatory antigen expression in cadaveric and living-donor livers before transplant. *Transplantation* 75, 2001–2007. doi: 10.1097/01.TP.0000061605.30685.03

Jiang, X., Tian, W., Tu, A. B., Pasupneti, S., Shuffle, E., Dahms, P., et al. (2019). Endothelial hypoxia-inducible factor-2alpha is required for the maintenance of airway microvasculature. *Circulation* 139, 502–517. doi: 10.1161/circulationaha.118.036157

Jin, Y.-P., Korin, Y., Zhang, X., Jindra, P. T., Rozengurt, E., and Reed, E. F. (2007). RNA interference elucidates the role of focal adhesion kinase in HLA class I-mediated focal adhesion complex formation and proliferation in human endothelial cells. *J. Immunol.* 178, 7911–7922. doi: 10.4049/jimmunol.178.12.7911

Jin, Y. P., Fishbein, M. C., Said, J. W., Jindra, P. T., Rajalingam, R., Rozengurt, E., et al. (2004). Anti-HLA class I antibody-mediated activation of the PI3K/Akt signaling pathway and induction of Bcl-2 and Bcl-xL expression in endothelial cells. *Hum. Immunol.* 65, 291–302. doi: 10.1016/j.humimm.2004.01.002

Jin, Y. P., Singh, R. P., Du, Z. Y., Rajasekaran, A. K., Rozengurt, E., and Reed, E. F. (2002). Ligation of HLA class I molecules on endothelial cells induces phosphorylation of Src, paxillin, and focal adhesion kinase in an actin-dependent manner. *J. Immunol.* 168, 5415–5423. doi: 10.4049/jimmunol.168.11.5415

Jin, Y. P., Valenzuela, N. M., Zhang, X., Rozengurt, E., and Reed, E. F. (2018). HLA class II-triggered signaling cascades cause endothelial cell proliferation and migration: relevance to antibody-mediated transplant rejection. *J. Immunol.* 200, 2372–2390. doi: 10.4049/jimmunol.1701259

Jin, Y. P., Valenzuela, N. M., Ziegler, M. E., Rozengurt, E., and Reed, E. F. (2014). Everolimus inhibits anti-HLA I antibody-mediated endothelial cell signaling, migration and proliferation more potently than sirolimus. *Am. J. Transplant.* 14, 806–819. doi: 10.1111/ajt.12669

Jindra, P. T., Hsueh, A., Hong, L., Gjertson, D., Shen, X. D., Gao, F., et al. (2008). Anti-MHC class I antibody activation of proliferation and survival signaling in murine cardiac allografts. *J. Immunol.* 180, 2214–2224. doi: 10.4049/jimmunol.180.4.2214

Kao, J., Kobashigawa, J., Fishbein, M. C., MacLellan, W. R., Burdick, M. D., Belperio, J. A., et al. (2003). Elevated serum levels of the CXCR3 chemokine ITAC are associated with the development of transplant coronary artery disease. *Circulation* 107, 1958–1961. doi: 10.1161/01.CIR.0000069270.16498.75

Kennard, S., Liu, H., and Lilly, B. (2008). Transforming growth factor-beta (TGF-1) down-regulates Notch3 in fibroblasts to promote smooth muscle gene expression. *J. Biol. Chem.* 283, 1324–1333. doi: 10.1074/jbc.M706651200

Kenney, L. L., Shultz, L. D., Greiner, D. L., and Brehm, M. A. (2016). Humanized mouse models for transplant immunology. *Am. J. Transplant.* 16, 389–397. doi: 10.1111/ajt.13520

Kim, H. K., Kim, J. E., Wi, H. C., Lee, S. W., Kim, J. Y., Kang, H. J., et al. (2008). Aurintricarboxylic acid inhibits endothelial activation, complement activation, and von Willebrand factor secretion in vitro and attenuates hyperacute rejection in an ex vivo model of pig-to-human pulmonary xenotransplantation. *Xenotransplantation* 15, 246–256. doi: 10.1111/j.1399-3089.2008.00481.x

Kolarova, H., Ambruzova, B., Svihalkova Sindlerova, L., Klinke, A., and Kubala, L. (2014). Modulation of endothelial glycocalyx structure under inflammatory conditions. *Mediat. Inflamm.* 2014:694312. doi: 10.1155/2014/694312

Koo, D. D., Welsh, K. I., McLaren, A. J., Roake, J. A., Morris, P. J., and Fuggle, S. V. (1999). Cadaver versus living donor kidneys: impact of donor factors on antigen induction before transplantation. *Kidney Int.* 56, 1551–1559. doi: 10.1046/j.1523-1755.1999.00657.x

Krezdorn, N., Tasigiorgos, S., Wo, L., Turk, M., Lopdrup, R., Kiwanuka, H., et al. (2017). Tissue conservation for transplantation. *Innov. Surg. Sci.* 2, 171–187. doi: 10.1515/iss-2017-0010

Krishnadasan, B., Farivar, A. S., Naidu, B. V., Woolley, S. M., Byrne, K., Fraga, C. H., et al. (2004). Beta-chemokine function in experimental lung ischemia-reperfusion injury. *Ann. Thorac. Surg.* 77, 1056–1062. doi: 10.1016/S0003-4975(03)01600-X

Land, W. G. (2012a). Emerging role of innate immunity in organ transplantation part II: potential of damage-associated molecular patterns to generate immunostimulatory dendritic cells. *Transplant. Rev. (Orlando)* 26, 73–87. doi: 10.1016/j.trre.2011.02.003

Land, W. G. (2012b). Emerging role of innate immunity in organ transplantation: part I: evolution of innate immunity and oxidative allograft injury. *Transplant. Rev. (Orlando)* 26, 60–72. doi: 10.1016/j.trre.2011.05.001

Le Bas-Bernardet, S., Coupel, S., Chauveau, A., Soulillou, J. P., and Charreau, B. (2004). Vascular endothelial cells evade apoptosis triggered by human leukocyte antigen-DR ligation mediated by allospecific antibodies. *Transplantation* 78, 1729–1739. doi: 10.1097/01.tp.0000147339.31581.99

Lee, J. Y., Han, A. R., and Lee, D. R. (2019). T lymphocyte development and activation in humanized mouse model. *Dev. Reprod.* 23, 79–92. doi: 10.12717/dr.2019.23.2.079

Leeper, N. J., Raiesdana, A., Kojima, Y., Chun, H. J., Azuma, J., Maegdefessel, L., et al. (2011). MicroRNA-26a is a novel regulator of vascular smooth muscle cell function. *J. Cell. Physiol.* 226, 1035–1043. doi: 10.1002/jcp.22422

Lefaucheur, C., Viglietti, D., Bouatou, Y., Philippe, A., Pievani, D., Aubert, O., et al. (2019). Non-HLA agonistic anti-angiotensin II type 1 receptor antibodies induce a distinctive phenotype of antibody-mediated rejection in kidney transplant recipients. *Kidney Int.* 96, 189–201. doi: 10.1016/j.kint.2019.01.030

Lemke, A., Noriega, M., Roske, A. M., Kemper, M. J., Nashan, B., Falk, C. S., et al. (2015). Rat renal transplant model for mixed acute humoral and cellular rejection: weak correlation of serum cytokines/chemokines with intragraft changes. *Transpl. Immunol.* 33, 95–102. doi: 10.1016/j.trim.2015.08.003

Li, F., Zhang, X., Jin, Y. P., Mulder, A., and Reed, E. F. (2011). Antibody ligation of human leukocyte antigen class I molecules stimulates migration and proliferation of smooth muscle cells in a focal adhesion kinase-dependent manner. *Hum. Immunol.* 72, 1150–1159. doi: 10.1016/j.humimm.2011.09.004

Li, L., Wadia, P., Chen, R., Kambham, N., Naesens, M., Sigdel, T. K., et al. (2009). Identifying compartment-specific non-HLA targets after renal transplantation by integrating transcriptome and "antibodyome" measures. *Proc. Natl. Acad. Sci. U.S.A.* 106, 4148–4153. doi: 10.1073/pnas.0900563106

Lin, H., Wilson, J. E., Roberts, C. R., Horley, K. J., Winters, G. L., Costanzo, M. R., et al. (1996). Biglycan, decorin, and versican protein expression patterns in coronary arteriopathy of human cardiac allograft: distinctness as compared to native atherosclerosis. *J. Heart Lung Transplant.* 15, 1233–1247.

Lion, J., Taflin, C., Cross, A. R., Robledo-Sarmiento, M., Mariotto, E., Savenay, A., et al. (2016). HLA class II antibody activation of endothelial cells promotes Th17 and disrupts regulatory T lymphocyte expansion. *Am. J. Transplant.* 16, 1408–1420. doi: 10.1111/ajt.13644

Lledo-Garcia, E., Subira-Rios, D., Rodriguez-Martinez, D., Dulin, E., Alvarez-Fernandez, E., Hernandez-Fernandez, C., et al. (2009). Sildenafil as a protecting drug for warm ischemic kidney transplants: experimental results. *J. Urol.* 182, 1222–1225. doi: 10.1016/j.juro.2009.05.006

Luo, N., Nixon, M. J., Gonzalez-Ericsson, P. I., Sanchez, V., Opalenik, S. R., Li, H., et al. (2018). DNA methyltransferase inhibition upregulates MHC-I to potentiate cytotoxic T lymphocyte responses in breast cancer. *Nat. Commun.* 9:248. doi: 10.1038/s41467-017-02630-w

Mamdouh, Z., Chen, X., Pierini, L. M., Maxfield, F. R., and Muller, W. A. (2003). Targeted recycling of PECAM from endothelial surface-connected compartments during diapedesis. *Nature* 421, 748–753. doi: 10.1038/nature01300

Mamdouh, Z., Mikhailov, A., and Muller, W. A. (2009). Transcellular migration of leukocytes is mediated by the endothelial lateral border recycling compartment. *J. Exp. Med.* 206, 2795–2808. doi: 10.1084/jem.20082745

Mao, Q., Terasaki, P. I., Cai, J., Briley, K., Catrou, P., Haisch, C., et al. (2007). Extremely high association between appearance of HLA antibodies and failure of kidney grafts in a five-year longitudinal study. *Am. J. Transplant.* 7, 864–871. doi: 10.1111/j.1600-6143.2006.01711.x

McKeown, D. W., Bonser, R. S., and Kellum, J. A. (2012). Management of the heartbeating brain-dead organ donor. *Br. J. Anaesth.* 108(Suppl 1), i96–i107. doi: 10.1093/bja/aer351

Mehra, M. R., Uber, P. A., Ventura, H. O., Scott, R. L., and Park, M. H. (2004). The impact of mode of donor brain death on cardiac allograft vasculopathy: an intravascular ultrasound study. *J. Am. Coll. Cardiol.* 43, 806–810. doi: 10.1016/j.jacc.2003.08.059

Mengel, M., Sis, B., Haas, M., Colvin, R. B., Halloran, P. F., Racusen, L. C., et al. (2012). Banff 2011 meeting report: new concepts in antibody-mediated rejection. *Am. J. Transplant.* 12, 563–570. doi: 10.1111/j.1600-6143.2011.03926.x

Mestas, J., and Hughes, C. C. (2004). Of mice and not men: differences between mouse and human immunology. *J. Immunol.* 172, 2731–2738. doi: 10.4049/jimmunol.172.5.2731

Michael, V. A. (2003). Allograft-induced proliferation of vascular smooth muscle cells: potential targets for treating transplant vasculopathy. *Curr. Vasc. Pharmacol.* 1, 1–9. doi: 10.2174/1570161033386772

Michielsen, L. A., van Zuilen, A. D., Kardol-Hoefnagel, T., Verhaar, M. C., and Otten, H. G. (2018). Association between promoter polymorphisms in CD46 and CD59 in kidney donors and transplant outcome. *Front. Immunol.* 9:972. doi: 10.3389/fimmu.2018.00972

Mitchell, R. N. (2009). Graft vascular disease: immune response meets the vessel wall. *Annu. Rev. Pathol.* 4, 19–47. doi: 10.1146/annurev.pathol.3.121806.151449

Mkaddem, S. B., Werts, C., Goujon, J.-M., Bens, M., Pedruzzi, E., Ogier-Denis, E., et al. (2009). Heat shock protein gp96 interacts with protein phosphatase 5 and controls toll-like receptor 2 (TLR2)-mediated activation of extracellular signal-regulated kinase (ERK) 1/2 in post-hypoxic kidney cells. *J. Biol. Chem.* 284, 12541–12549. doi: 10.1074/jbc.M808376200

Moreau, A., Varey, E., Anegon, I., and Cuturi, M. C. (2013). Effector mechanisms of rejection. *Cold Spring Harb. Perspect. Med.* 3:a015461. doi: 10.1101/cshperspect.a015461

Mueller, M., Herzog, C., Larmann, J., Schmitz, M., Hilfiker-Kleiner, D., Gessner, J. E., et al. (2013). The receptor for activated complement factor 5 (C5aR) conveys myocardial ischemic damage by mediating neutrophil transmigration. *Immunobiology* 218, 1131–1138. doi: 10.1016/j.imbio.2013.03.006

Muller, W. A. (2003). Leukocyte-endothelial-cell interactions in leukocyte transmigration and the inflammatory response. *Trends Immunol.* 24, 327–334. doi: 10.1016/s1471-4906(03)00117-0

Muller, W. A., Weigl, S. A., Deng, X., and Phillips, D. M. (1993). PECAM-1 is required for transendothelial migration of leukocytes. *J. Exp. Med.* 178, 449–460. doi: 10.1084/jem.178.2.449

Naemi, F. M., Carter, V., Kirby, J. A., and Ali, S. (2013). Anti-donor HLA class I antibodies: pathways to endothelial cell activation and cell-mediated allograft rejection. *Transplantation* 96, 258–266. doi: 10.1097/TP.0b013e3182985504

Najarian, J. S., Fryd, D. S., Strand, M., Canafax, D. M., Ascher, N. L., Payne, W. D., et al. (1985). A single institution, randomized, prospective trial of cyclosporin versus azathioprine-antilymphocyte globulin for immunosuppression in renal allograft recipients. *Ann. Surg.* 201, 142–157. doi: 10.1097/00000658-198502000-00003

Niimi, M., Hara, M., Witzke, O., Morris, P. J., and Wood, K. J. (1998). Donor resting B cells induce indefinite prolongation of fully allogeneic cardiac grafts when delivered with anti-immunoglobulin-D monoclonal antibody: evidence for tolerogenicity of donor resting B cells in vivo. *Transplantation* 66, 1786–1792. doi: 10.1097/00007890-199812270-00037

Noone, D. G., Riedl, M., Pluthero, F. G., Bowman, M. L., Liszewski, M. K., Lu, L., et al. (2016). Von Willebrand factor regulates complement on endothelial cells. *Kidney Int.* 90, 123–134. doi: 10.1016/j.kint.2016.03.023

Nordling, S., Brannstrom, J., Carlsson, F., Lu, B., Salvaris, E., Wanders, A., et al. (2018). Enhanced protection of the renal vascular endothelium improves early outcome in kidney transplantation: preclinical investigations in pig and mouse. *Sci. Rep.* 8:5220. doi: 10.1038/s41598-018-21463-1

Nordling, S., Hong, J., Fromell, K., Edin, F., Brannstrom, J., Larsson, R., et al. (2015). Vascular repair utilising immobilised heparin conjugate for protection against early activation of inflammation and coagulation. *Thromb. Haemost.* 113, 1312–1322. doi: 10.1160/th14-09-0724

Ochando, J. C., Krieger, N. R., and Bromberg, J. S. (2006). Direct versus indirect allorecognition: visualization of dendritic cell distribution and interactions during rejection and tolerization. *Am. J. Transplant.* 6, 2488–2496. doi: 10.1111/j.1600-6143.2006.01494.x

Opelz, G. (2005). Non-HLA transplantation immunity revealed by lymphocytotoxic antibodies. *Lancet* 365, 1570–1576. doi: 10.1016/S0140-6736(05)66458-6

Parikh, R. V., Khush, K., Pargaonkar, V. S., Luikart, H., Grimm, D., Yu, M., et al. (2019). Association of endothelin-1 with accelerated cardiac allograft vasculopathy and late mortality following heart transplantation. *J. Cardiac. Failure* 25, 97–104. doi: 10.1016/j.cardfail.2018.12.001

Park, H. S., Kim, J. E., You, H. J., Gu, J., Yoo, B., Lee, S., et al. (2015). Beneficial effect of a nitric oxide donor in an ex vivo model of pig-to-human pulmonary xenotransplantation. *Xenotransplantation* 22, 391–398. doi: 10.1111/xen.12195

Park, J. S., Svetkauskaite, D., He, Q. B., Kim, J. Y., Strassheim, D., Ishizaka, A., et al. (2004). Involvement of toll-like receptors 2 and 4 in cellular activation by high mobility group box 1 protein. *J. Biol. Chem.* 279, 7370–7377. doi: 10.1074/jbc.M306793200

Patel, R., and Terasaki, P. I. (1969). Significance of the positive crossmatch test in kidney transplantation. *N. Engl. J. Med.* 280, 735–739. doi: 10.1097/00007890-199308000-00007

Pearson, T., Shultz, L. D., Miller, D., King, M., Laning, J., Fodor, W., et al. (2008). Non-obese diabetic-recombination activating gene-1 (NOD-Rag1 null) interleukin (IL)-2 receptor common gamma chain (IL2r gamma null) null mice: a radioresistant model for human lymphohaematopoietic engraftment. *Clin. Exp. Immunol.* 154, 270–284. doi: 10.1111/j.1365-2249.2008.03753.x

Pedagogos, E., Hewitson, T. D., Walker, R. G., Nicholis, K. M., and Becker, G. J. (1997). Myofibroblast involvement in chronic transplant rejection. *Transplantation* 64, 1192–1197. doi: 10.1097/00007890-199710270-00019

Pilmore, H. L., Painter, D. M., Bishop, G. A., McCaughan, G. W., and Eris, J. M. (2000). Early up-regulation of macrophages and myofibroblasts: a new marker for development of chronic renal allograft rejection. *Transplantation* 69, 2658–2662. doi: 10.1097/00007890-200006270-00028

Piotti, G., Palmisano, A., Maggiore, U., and Buzio, C. (2014). Vascular endothelium as a target of immune response in renal transplant rejection. *Front. Immunol.* 5:505. doi: 10.3389/fimmu.2014.00505

Pober, J. S., and Cotran, R. S. (1990). The role of endothelial cells in inflammation. *Transplantation* 50, 537–544. doi: 10.1097/00007890-199010000-00001

Racusen, L. C., Colvin, R. B., Solez, K., Mihatsch, M. J., Halloran, P. F., Campbell, P. M., et al. (2003). Antibody-mediated rejection criteria - an addition to the Banff 97 classification of renal allograft rejection. *Am. J. Transplant.* 3, 708–714. doi: 10.1034/j.1600-6143.2003.00072.x

Rahmani, M., Cruz Rani, P., Granville David, J., and McManus Bruce, M. (2006). Allograft vasculopathy versus atherosclerosis. *Circ. Res.* 99, 801–815. doi: 10.1161/01.RES.0000246086.93555.f3

Rao, D. A., Eid, R. E., Qin, L., Yi, T., Kirkiles-Smith, N. C., Tellides, G., et al. (2008). Interleukin (IL)-1 promotes allogeneic T cell intimal infiltration and IL-17 production in a model of human artery rejection. *J. Exp. Med.* 205, 3145–3158. doi: 10.1084/jem.20081661

Rintala, J. M., Savikko, J., Palin, N., Rintala, S. E., Koskinen, P. K., and von Willebrand, E. (2016). Oral platelet-derived growth factor and vascular endothelial growth factor inhibitor sunitinib prevents chronic allograft injury in experimental kidney transplantation model. *Transplantation* 100, 103–110. doi: 10.1097/tp.0000000000000837

Rossini, M., Cheunsuchon, B., Donnert, E., Ma, L. J., Thomas, J. W., Neilson, E. G., et al. (2005). Immunolocalization of fibroblast growth factor-1 (FGF-1), its receptor (FGFR-1), and fibroblast-specific protein-1 (FSP-1) in inflammatory renal disease. *Kidney Int.* 68, 2621–2628. doi: 10.1111/j.1523-1755.2005.00734.x

Rothermel, A. L., Wang, Y., Schechner, J., Mook-Kanamori, B., Aird, W. C., Pober, J. S., et al. (2004). Endothelial cells present antigens in vivo. *BMC Immunol.* 5:5. doi: 10.1186/1471-2172-5-5

Rovere-Querini, P., Capobianco, A., Scaffidi, P., Valentinis, B., Catalanotti, F., Giazzon, M., et al. (2004). HMGB1 is an endogenous immune adjuvant released by necrotic cells. *EMBO Rep.* 5, 825–830. doi: 10.1038/sj.embor.7400205

Ryan, G. B., and Majno, G. (1977). Acute-inflammation – Review. *Am. J. Pathol.* 86, 183–276.

Sakaguchi, S., Sakaguchi, N., Asano, M., Itoh, M., and Toda, M. (1995). Immunologic self-tolerance maintained by activated T cells expressing IL-2 receptor alpha-chains (CD25). Breakdown of a single mechanism of self-tolerance causes various autoimmune diseases. *J. Immunol.* 155, 1151–1164.

Salama, A. D., Delikouras, A., Pusey, C. D., Cook, H. T., Bhangal, G., Lechler, R. I., et al. (2001). Transplant accommodation in highly sensitized patients: a potential role for Bcl-xL and alloantibody. *Am. J. Transplant.* 1, 260–269. doi: 10.1034/j.1600-6143.2001.001003260.x

Salehi, S., Sosa, R. A., Jin, Y.-P., Kageyama, S., Fishbein, M. C., Rozengurt, E., et al. (2018). Outside-in HLA class I signaling regulates ICAM-1 clustering and endothelial cell-monocyte interactions via mTOR in transplant antibody-mediated rejection. *Am. J. Transplant.* 18, 1096–1109. doi: 10.1111/ajt.14544

Salom, R. N., Maguire, J. A., and Hancock, W. W. (1998). Endothelial activation and cytokine expression in human acute cardiac allograft rejection. *Pathology* 30, 24–29. doi: 10.1080/00313029800169625

Saragih, H., Zilian, E., Jaimes, Y., Paine, A., Figueiredo, C., Eiz-Vesper, B., et al. (2014). PECAM-1-dependent heme oxygenase-1 regulation via an Nrf2-mediated pathway in endothelial cells. *Thromb. Haemost.* 111, 1077–1088. doi: 10.1160/TH13-11-0923

Sarbassov, D. D., Ali, S. M., Kim, D. H., Guertin, D. A., Latek, R. R., Erdjument-Bromage, H., et al. (2004). Rictor, a novel binding partner of mTOR, defines a rapamycin-insensitive and raptor-independent pathway that regulates the cytoskeleton. *Curr. Biol.* 14, 1296–1302. doi: 10.1016/j.cub.2004.06.054

Segel, L. D., vonHaag, D. W., Zhang, J., and Follette, D. M. (2002). Selective overexpression of inflammatory molecules in hearts from brain-dead rats. *J. Heart Lung Transplant.* 21, 804–811. doi: 10.1016/s1053-2498(02)00382-0

Seino, K. I., Fukao, K., Muramoto, K., Yanagisawa, K., Takada, Y., Kakuta, S., et al. (2001). Requirement for natural killer T (NKT) cells in the induction of allograft tolerance. *Proc. Natl. Acad. Sci. U.S.A.* 98, 2577–2581. doi: 10.1073/pnas.041608298

Serinsoz, E., Bock, O., Gwinner, W., Schwarz, A., Haller, H., Kreipe, H., et al. (2005). Local complement C3 expression is upregulated in humoral and cellular rejection of renal allografts. *Am. J. Transplant.* 5, 1490–1494. doi: 10.1111/j.1600-6143.2005.00873.x

Shino, M. Y., Weigt, S. S., Li, N., Palchevskiy, V., Derhovanessian, A., Saggar, R., et al. (2017). The prognostic importance of CXCR3 chemokine during organizing pneumonia on the risk of chronic lung allograft dysfunction after lung transplantation. *PLoS ONE* 12:e0180281. doi: 10.1371/journal.pone.0180281

Shultz, L. D., Brehm, M. A., Garcia-Martinez, J. V., and Greiner, D. L. (2012). Humanized mice for immune system investigation: progress, promise and challenges. *Nat. Rev. Immunol.* 12, 786–798. doi: 10.1038/nri3311

Shultz, L. D., Lyons, B. L., Burzenski, L. M., Gott, B., Chen, X., Chaleff, S., et al. (2005). Human lymphoid and myeloid cell development in NOD/LtSz-scid IL2R gamma null mice engrafted with mobilized human hemopoietic stem cells. *J. Immunol.* 174, 6477–6489. doi: 10.4049/jimmunol.174.10.6477

Sigdel, T. K., Li, L., Tran, T. Q., Khatri, P., Naesens, M., Sansanwal, P., et al. (2012). Non-HLA antibodies to immunogenic epitopes predict the evolution of chronic renal allograft injury. *J. Am. Soc. Nephrol.* 23, 750–763. doi: 10.1681/ASN.2011060596

Sixt, M., Engelhardt, B., Pausch, F., Hallmann, R., Wendler, O., and Sorokin, L. M. (2001). Endothelial cell laminin isoforms, laminins 8 and 10, play decisive roles in T cell recruitment across the blood-brain barrier in experimental autoimmune encephalomyelitis. *J. Cell Biol.* 153, 933–946. doi: 10.1083/jcb.153.5.933

Smith, M. (2004). Physiologic changes during brain stem death–lessons for management of the organ donor. *J. Heart Lung Transplant.* 23(Suppl. 9), S217–S222. doi: 10.1016/j.healun.2004.06.017

Smith, R. N., and Colvin, R. B. (2012). Chronic alloantibody mediated rejection. *Semin. Immunol.* 24, 115–121. doi: 10.1016/j.smim.2011.09.002

Soares, M. A., Ezeamuzie, O. C., Ham, M. J., Duckworth, A. M., Rabbani, P. S., Saadeh, P. B., et al. (2015). Targeted protection of donor graft vasculature using a phosphodiesterase inhibitor increases survival and predictability of autologous fat grafts. *Plast. Reconstr. Surg.* 135, 488–499. doi: 10.1097/prs.0000000000000909

Soares, M. P., Lin, Y., Anrather, J., Csizmadia, E., Takigami, K., Sato, K., et al. (1998). Expression of heme oxygenase-1 can determine cardiac xenograft survival. *Nat. Med.* 4, 1073–1077. doi: 10.1038/2063

Soares, M. P., Lin, Y., Sato, K., Stuhlmeier, K. M., and Bach, F. H. (1999). Accommodation. *Immunol. Today* 20, 434–437.

Song, J., Zhang, X., Buscher, K., Wang, Y., Wang, H., Di Russo, J., et al. (2017). Endothelial basement membrane laminin 511 contributes to endothelial junctional tightness and thereby inhibits leukocyte transmigration. *Cell Rep.* 18, 1256–1269. doi: 10.1016/j.celrep.2016.12.092

Spiegel, S., and Milstien, S. (2003). Sphingosine-1-phosphate: an enigmatic signalling lipid. *Nat. Rev. Mol. Cell Biol.* 4, 397–407. doi: 10.1038/nrm1103

Sugimoto, S., Lin, X., Lai, J., Okazaki, M., Das, N. A., Li, W., et al. (2009). Apyrase treatment prevents ischemia-reperfusion injury in rat lung isografts. *J. Thorac. Cardiovasc. Surg.* 138, 752–759. doi: 10.1016/j.jtcvs.2009.04.049

Suzuki, J., Isobe, M., Morishita, R., and Nagai, R. (2010). Characteristics of chronic rejection in heart transplantation: important elements of pathogenesis and future treatments. *Circ. J.* 74, 233–239. doi: 10.1253/circj.cj-09-0809

Szabo, G. (2004). Physiologic changes after brain death. *J. Heart Lung Transplant.* 23(Suppl. 9), S223–S226. doi: 10.1016/j.healun.2004.04.005

Szabo, G., Buhmann, V., Bahrle, S., Vahl, C. F., and Hagl, S. (2002). Brain death impairs coronary endothelial function. *Transplantation* 73, 1846–1848. doi: 10.1097/00007890-200206150-00027

Szabo, G., Soos, P., Heger, U., Mandera, S., Buhmann, V., Bahrle, S., et al. (2006). L-arginine improves endothelial and myocardial function after brain death. *Transplantation* 82, 108–112. doi: 10.1097/01.tp.0000225778.49388.f5

Takada, M., Nadeau, K. C., Hancock, W. W., Mackenzie, H. S., Shaw, G. D., Waaga, A. M., et al. (1998). Effects of explosive brain death on cytokine activation of peripheral organs in the rat. *Transplantation* 65, 1533–1542. doi: 10.1097/00007890-199806270-00001

Tanaka, M., Mokhtari, G. K., Terry, R. D., Gunawan, F., Balsam, L. B., Hoyt, G., et al. (2005). Prolonged cold ischemia in rat cardiac allografts promotes ischemia-reperfusion injury and the development of graft coronary artery disease in a linear fashion. *J. Heart Lung Transplant.* 24, 1906–1914. doi: 10.1016/j.healun.2004.06.007

Tarjus, A., González-Rivas, C., Amador-Martínez, I., Bonnard, B., López-Marure, R., Jaisser, F., et al. (2019). The absence of endothelial sodium channel α (αENaC) reduces renal ischemia/reperfusion injury. *Int. J. Mol. Sci.* 20:3132. doi: 10.3390/ijms20133132

Thomas, K. A., Valenzuela, N. M., and Reed, E. F. (2015). The perfect storm: HLA antibodies, complement, FcgammaRs, and endothelium in transplant rejection. *Trends Mol. Med.* 21, 319–329. doi: 10.1016/j.molmed.2015.02.004

Tikkanen, J. M., Singer, L. G., Kim, S. J., Li, Y., Binnie, M., Chaparro, C., et al. (2016). De Novo DQ donor-specific antibodies are associated with chronic lung allograft dysfunction after lung transplantation. *Am. J. Respir. Crit. Care Med.* 194, 596–606. doi: 10.1164/rccm.201509-1857OC

Traggiai, E., Chicha, L., Mazzucchelli, L., Bronz, L., Piffaretti, J. C., Lanzavecchia, A., et al. (2004). Development of a human adaptive immune system in cord blood cell-transplanted mice. *Science* 304, 104–107. doi: 10.1126/science.1093933

Trayssac, M., Galvani, S., Auge, N., Sabbadini, R., Calise, D., Mucher, E., et al. (2015). Role of sphingosine-1-phosphate in transplant vasculopathy evoked by anti-HLA antibody. *Am. J. Transplant.* 15, 2050–2061. doi: 10.1111/ajt.13264

Tsukimori, K., Tsushima, A., Fukushima, K., Nakano, H., and Wake, N. (2008). Neutrophil-derived reactive oxygen species can modulate neutrophil adhesion to endothelial cells in preeclampsia. *Am. J. Hypertens.* 21, 587–591. doi: 10.1038/ajh.2007.87

Uehara, S., Chase, C. M., Cornell, L. D., Madsen, J. C., Russell, P. S., and Colvin, R. B. (2007). Chronic cardiac transplant arteriopathy in mice: relationship of alloantibody. C4d deposition and neointimal fibrosis. *Am. J. Transplant.* 7, 57–65. doi: 10.1111/j.1600-6143.2006.01599.x

Valenzuela, N. M., Hong, L., Shen, X. D., Gao, F., Young, S. H., Rozengurt, E., et al. (2013a). Blockade of p-selectin is sufficient to reduce MHC I antibody-elicited monocyte recruitment in vitro and in vivo. *Am. J. Transplant.* 13, 299–311. doi: 10.1111/ajt.12016

Valenzuela, N. M., Mulder, A., and Reed, E. F. (2013b). HLA class I antibodies trigger increased adherence of monocytes to endothelial cells by eliciting an increase in endothelial P-selectin and, depending on subclass, by engaging FcgammaRs. *J. Immunol.* 190, 6635–6650. doi: 10.4049/jimmunol.1201434

van Loosdregt, J., van Oosterhout, M. F., Bruggink, A. H., van Wichen, D. F., van Kuik, J., de Koning, E., et al. (2006). The chemokine and chemokine receptor profile of infiltrating cells in the wall of arteries with cardiac allograft vasculopathy is indicative of a memory T-helper 1 response. *Circulation* 114, 1599–1607. doi: 10.1161/CIRCULATIONAHA.105.597526

Van Raemdonck, K., van den Steen, P. E., Liekens, S., Van Damme, J., and Struyf, S. (2015). CXCR3 ligands in disease and therapy. *Cytokine Growth Fact. Rev.* 26, 311–327. doi: 10.1016/j.cytogfr.2014.11.009

Vestweber, D. (2015). How leukocytes cross the vascular endothelium. *Nat. Rev. Immunol.* 15, 692–704. doi: 10.1038/nri3908

Wahl, A., De, C., Abad Fernandez, M., Lenarcic, E. M., Xu, Y., Cockrell, A. S., et al. (2019). Precision mouse models with expanded tropism for human pathogens. *Nat. Biotechnol.* 37, 1163–1173. doi: 10.1038/s41587-019-0225-9

Walsh, N. C., Kenney, L. L., Jangalwe, S., Aryee, K. E., Greiner, D. L., Brehm, M. A., et al. (2017). Humanized mouse models of clinical disease. *Annu. Rev. Pathol.* 12, 187–215. doi: 10.1146/annurev-pathol-052016-100332

Walsh, R. C., Brailey, P., Girnita, A., Alloway, R. R., Shields, A. R., Wall, G. E., et al. (2011). Early and late acute antibody-mediated rejection differ immunologically and in response to proteasome inhibition. *Transplantation* 91, 1218–1226. doi: 10.1097/TP.0b013e318218e901

Wang, Q., and Doerschuk, C. M. (2000). Neutrophil-induced changes in the biomechanical properties of endothelial cells: roles of ICAM-1 and reactive oxygen species. *J. Immunol.* 164, 6487–6494. doi: 10.4049/jimmunol.164.12.6487

Weber, E. W., Han, F., Tauseef, M., Birnbaumer, L., Mehta, D., and Muller, W. A. (2015). TRPC6 is the endothelial calcium channel that regulates leukocyte transendothelial migration during the inflammatory response. *J. Exp. Med.* 212, 1883–1899. doi: 10.1084/jem.20150353

Wehner, J., Morrell, C. N., Reynolds, T., Rodriguez, E. R., and Baldwin, W. M. III (2007). Antibody and complement in transplant vasculopathy. *Circ. Res.* 100, 191–203. doi: 10.1161/01.RES.0000255032.33661.88

Wong, C., Ganz, P., Miller, L., Kobashigawa, J., Schwarzkopf, A., Valantine, et al. (2001). Role of vascular remodeling in the pathogenesis of early transplant coronary artery disease: a multicenter prospective intravascular ultrasound study. *J. Heart Lung Transplant.* 20, 385–392. doi: 10.1016/s1053-2498(00)00230-8

Wu, H., Ma, J., Wang, P., Corpuz, T. M., Panchapakesan, U., Wyburn, K. R., et al. (2010). HMGB1 contributes to kidney ischemia reperfusion injury. *J. Am. Soc. Nephrol.* 21, 1878–1890. doi: 10.1681/asn.2009101048

Wynn, T. A. (2008). Cellular and molecular mechanisms of fibrosis. *J. Pathol.* 214, 199–210. doi: 10.1002/path.2277

Yamanaka, K., Kakuta, Y., Miyagawa, S., Nakazawa, S., Kato, T., Abe, T., et al. (2016). Depression of complement regulatory factors in rat and human renal grafts is associated with the progress of acute T-cell mediated rejection. *PLoS ONE* 11:e0148881. doi: 10.1371/journal.pone.0148881

Yang, L., Kowalski, J. R., Zhan, X., Thomas, S. M., and Luscinskas, F. W. (2006). Endothelial cell cortactin phosphorylation by Src contributes to polymorphonuclear leukocyte transmigration in vitro. *Circ. Res.* 98, 394–402. doi: 10.1161/01.RES.0000201958.59020.1a

Yao, L., Lv, X., and Wang, X. (2016). MicroRNA 26a inhibits HMGB1 expression and attenuates cardiac ischemia-reperfusion injury. *J. Pharmacol. Sci.* 131, 6–12. doi: 10.1016/j.jphs.2015.07.023

Yeh, Y. T., Serrano, R., Francois, J., Chiu, J. J., Li, Y. J., Del Alamo, J. C., et al. (2018). Three-dimensional forces exerted by leukocytes and vascular endothelial cells dynamically facilitate diapedesis. *Proc. Natl. Acad. Sci. U.S.A.* 115, 133–138. doi: 10.1073/pnas.1717489115

Yu, G., Xu, X., Vu, M. D., Kilpatrick, E. D., and Li, X. C. (2006). NK cells promote transplant tolerance by killing donor antigen-presenting cells. *J. Exp. Med.* 203, 1851–1858. doi: 10.1084/jem.20060603

Yun, J. J., Fischbein, M. P., Laks, H., Fishbein, M. C., Espejo, M. L., Ebrahimi, K., et al. (2000). Early and late chemokine production correlates with cellular recruitment in cardiac allograft vasculopathy. *Transplantation* 69, 2515–2524. doi: 10.1097/00007890-200006270-00009

Zhang, B., Liu, X.-X., He, J.-R., Zhou, C.-X., Guo, M., He, M., et al. (2010). Pathologically decreased miR-26a antagonizes apoptosis and facilitates carcinogenesis by targeting MTDH and EZH2 in breast cancer. *Carcinogenesis* 32, 2–9. doi: 10.1093/carcin/bgq209

Zhang, Q., and Reed, E. F. (2016). The importance of non-HLA antibodies in transplantation. *Nat. Rev. Nephrol.* 12, 484–495. doi: 10.1038/nrneph.2016.88

Zhang, X., and Reed, E. F. (2009). Effect of antibodies on endothelium. *Am. J. Transplant.* 9, 2459–2465. doi: 10.1111/j.1600-6143.2009.02819.x

Zhu, P., Bailey, S. R., Lei, B., Paulos, C. M., Atkinson, C., and Tomlinson, S. (2017). Targeted complement inhibition protects vascularized composite allografts from acute graft injury and prolongs graft survival when combined with subtherapeutic cyclosporine A therapy. *Transplantation* 101, e75–e85. doi: 10.1097/TP.0000000000001625

Zilian, E., Saragih, H., Vijayan, V., Hiller, O., Figueiredo, C., Aljabri, A., et al. (2015). Heme oxygenase-1 inhibits HLA class I antibody-dependent endothelial cell activation. *PLoS ONE* 10:e0145306. doi: 10.1371/journal.pone.0145306

Zou, Y., and Stastny, P. (2009). The role of major histocompatibility complex class I chain-related gene A antibodies in organ transplantation. *Curr. Opin. Organ Transplant.* 14, 414–418. doi: 10.1097/mot.0b013e32832d835e

Zou, Y., Stastny, P., Susal, C., Dohler, B., and Opelz, G. (2007). Antibodies against MICA antigens and kidney-transplant rejection. *N. Engl. J. Med.* 357, 1293–1300. doi: 10.1056/NEJMoa067160

Conflict of Interest: The authors declare that the research was conducted in the absence of any commercial or financial relationships that could be construed as a potential conflict of interest.

frontiers in Physiology

REVIEW
published: 21 May 2020
doi: 10.3389/fphys.2020.00492

New Insights From MRI and Cell Biology Into the Acute Vascular-Metabolic Implications of Electronic Cigarette Vaping

Felix W. Wehrli[1], Alessandra Caporale[1], Michael C. Langham[1] and Shampa Chatterjee[2]*

[1] Laboratory for Structural Physiologic and Functional Imaging, Department of Radiology, University of Pennsylvania, Philadelphia, PA, United States, [2] Department of Physiology and Institute for Environmental Medicine, University of Pennsylvania, Philadelphia, PA, United States

The popularity of electronic cigarettes (e-cigs) has grown at a startling rate since their introduction to the United States market in 2007, with sales expected to outpace tobacco products within a decade. Spurring this trend has been the notion that e-cigs are a safer alternative to tobacco-based cigarettes. However, the long-term health impacts of e-cigs are not yet known. Quantitative magnetic resonance imaging (MRI) approaches, developed in the authors' laboratory, provide conclusive evidence of acute deleterious effects of e-cig aerosol inhalation in the absence of nicotine in tobacco-naïve subjects. Among the pathophysiologic effects observed are transient impairment of endothelial function, vascular reactivity, and oxygen metabolism. The culprits of this response are currently not fully understood but are likely due to an immune reaction caused by the aerosol containing thermal breakdown products of the e-liquid, including radicals and organic aldehydes, with particle concentrations similar to those emitted by conventional cigarettes. The acute effects observed following a single vaping episode persist for 1–3 h before subsiding to baseline and are paralleled by build-up of biological markers. Sparse data exist on long-term effects of vaping, and it is likely that repeated regular exposure to e-cig aerosol during vaping will lead to chronic conditions since there would be no return to baseline conditions as in the case of an isolated vaping episode. This brief review aims to highlight the potential of pairing MRI, with its extraordinary sensitivity to structure, physiology and metabolism at the holistic level, with biologic investigations targeting serum and cellular markers of inflammation and oxidative stress. Such a multi-modal framework should allow interpretation of the impact of e-cigarette vaping on vascular health at the organ level in the context of the underlying biological alterations. Applications of this approach to the study of other lifestyle-initiated pathologies including hypertension, hypercholesterolemia, and metabolic syndrome are indicated.

Keywords: E-cigarette, endothelium, MRI, vaping, vascular

OPEN ACCESS

Edited by:
Eduardo Nava, University of Castilla La Mancha, Spain

Reviewed by:
Giuseppe Biondi-Zoccai, Sapienza University of Rome, Italy
Fabiano E. Xavier, Federal University of Pernambuco, Brazil

****Correspondence:***
Felix W. Wehrli
felix.wehrli@pennmedicine.upenn.edu

Specialty section:
This article was submitted to Vascular Physiology, a section of the journal Frontiers in Physiology

Received: *14 January 2020*
Accepted: *22 April 2020*
Published: *21 May 2020*

Citation:
Wehrli FW, Caporale A, Langham MC and Chatterjee S (2020) New Insights From MRI and Cell Biology Into the Acute Vascular-Metabolic Implications of Electronic Cigarette Vaping. Front. Physiol. 11:492. doi: 10.3389/fphys.2020.00492

INTRODUCTION

The popularity of electronic cigarettes (e-cigs) has grown at a startling rate since their introduction to the United States market in 2007, with sales expected to outpace tobacco products within a decade. Spurring this trend has been the notion that e-cigs are a safer alternative to tobacco-based cigarettes. However, the long-term health impact of e-cigs are not yet known, and the existing

research does not support such a conclusion (Kligerman et al., 2020). The most urgent concern is the huge rise in the use of e-cigs by adolescents, showing an increase of over 87% in 12th graders from 2017 to 2019 with a 2019 prevalence of 35.1% (16.1% in 8th graders) (Miech et al., 2019).

Even though it has been conjectured that e-cig use may be less deleterious to human health than tobacco smoking, or perhaps not harmful at all, this notion has been challenged by a number of reports that appeared during the past several years, in the form of studies *in vitro* (Schweitzer et al., 2015), in animal models (Lerner et al., 2015) and, importantly, involving human subjects (Vlachopoulos et al., 2016; Biondi-Zoccai et al., 2019).

Besides nicotine, which has long been known to cause endothelial dysfunction (EDF) (Neunteufl et al., 2002), e-cig users are exposed to a host of toxic compounds generated by thermal degradation of solvents (Bekki et al., 2014; Jensen et al., 2017), and possibly flavorings (Omaiye et al., 2019), along with metal contaminants and ultrafine metal particles ejected by the heating element (Williams et al., 2013, 2017; Olmedo et al., 2018). Recent findings from the authors' laboratories indicate that a single vaping episode involving non-nicotinized e-liquid provoked an inflammatory immune response and oxidative stress along with reduced nitric oxide (NO) bioavailability (Chatterjee et al., 2019b). The latter also manifested in impaired peripheral vascular reactivity and endothelial function as determined by a battery of quantitative magnetic resonance imaging (MRI) metrics (Caporale et al., 2019). Almost coincidentally with the release of our findings, a surge in vaping-related lung illnesses and deaths had been reported, variably attributed to additives such as vitamin-E acetate in cannabis-based vaping liquids (Lewis et al., 2019).

The purpose of this brief review is to highlight some of the recent findings from imaging studies, with particular focus on magnetic resonance, and to elaborate on the potential of these methods to gain insight into the vascular-metabolic consequences of e-cig vaping, notably EDF. We further show that the transient imaging findings are paralleled by rapid formation of signaling molecules, both in serum and in pulmonary endothelial cells, in response to e-cig aerosol exposure. The vascular-metabolic effects of other risk-alleviating tobacco products, e.g., heat-not-burn cigarettes, are not discussed here but we refer the reader to the key paper by Biondi-Zoccai et al. (2019).

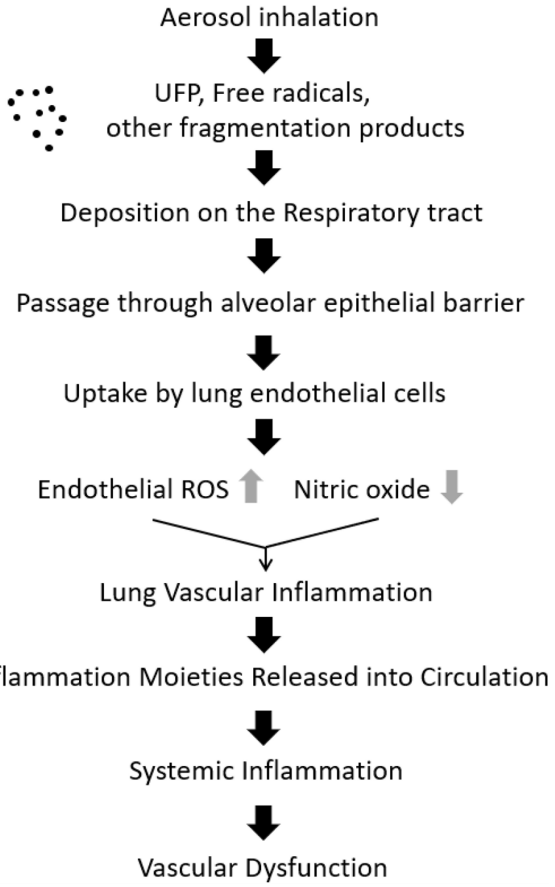

FIGURE 1 | Cascade of events following e-cigarette inhalation, initiating vascular inflammation and dysfunction. Ultra-fine particles (UFP) and free radicals, deposited on the respiratory tract are taken up by endothelial cells. This process drives endothelial activation that triggers inflammation signaling, eventually leading to vascular dysfunction (original figure).

ENDOTHELIAL DYSFUNCTION AND ITS MANIFESTATIONS AT MICRO AND MACRO-CELLULAR LEVEL

The vascular circulatory system is a network that integrates all organ systems via the transport of blood, nutrients, and pathogenic stimuli. Chemical or physical alterations (Herrmann and Lerman, 2001) within the vascular system play a major role in vasodilatation and vasoconstriction of blood vessels. The endothelial layer that lines these vessels functions as a mechanical barrier, regulating fluid movement through blood vessels, but also participates in regulation of vessel tone. This process is mediated via endothelial derived relaxing factor (Furchgott and Zawadzki, 1980) later recognized to be NO, a product of endothelial cells. The endothelium is by virtue of its location, the converging site of inflammation toward which immune cells are recruited and into which these cells later adhere and extravasate. Indeed, as natural barrier to inflammatory moieties and microorganisms (from invading tissues) in the blood, the endothelium is also integral to innate immune activation in response to microbial attack. These events are facilitated by endothelial signaling that leads to production of adhesion molecules, cytokines and chemokines that drive immune cell adherence, inflammation, and endothelial oxidative stress. A major participant in endothelial signaling is reactive oxygen species (ROS). Endothelial cells produce ROS in response to stimuli ranging from physical (shear stress) to chemical (inflammatory agents, microbes, and smoke, etc.). ROS in turn activate signaling cascades that induce inflammation and oxidative stress leading to EDF, which entails compromised vasodilatory capacity. Vasorelaxation is expected, for example, in response to increased shear stress or pharmacologic stimuli (e.g., acetylcholine), but can be impaired as a result of reduced synthesis or depressed bioavailability

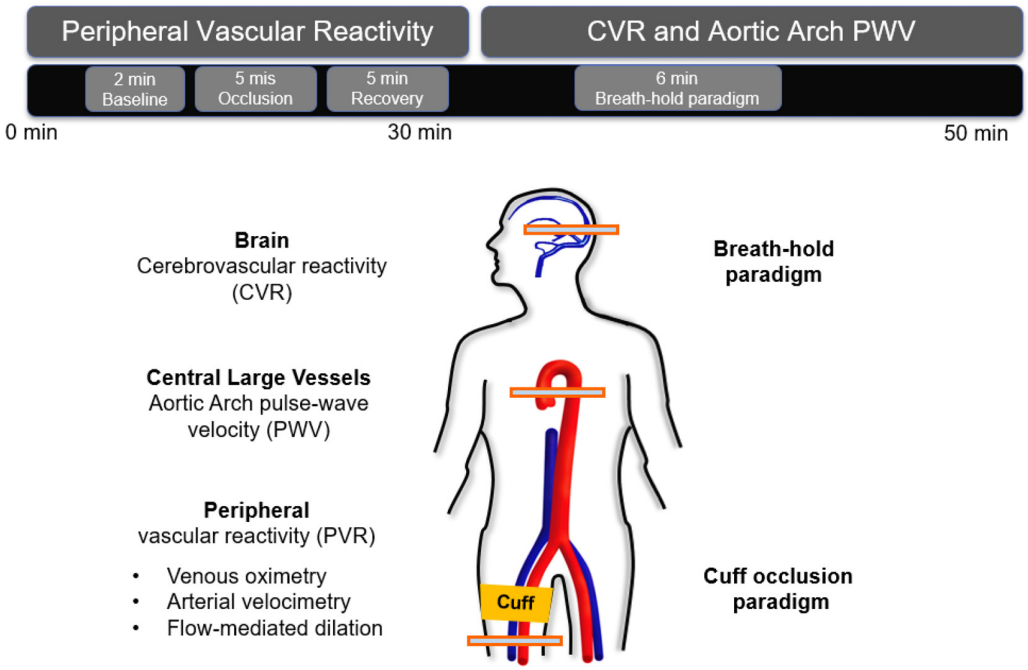

FIGURE 2 | Multi-vascular MRI protocol. The 50-min MRI protocol included a measure of peripheral vascular reactivity (PVR) to cuff-induced ischemia, followed by cerebrovascular reactivity (CVR) and aortic pulse wave velocity (PWV) quantification. PVR was assessed in the femoral vessels via multiple techniques. To stimulate reactive hyperemia the cuff was placed around the upper thigh and inflated for 5 min. CVR to hypercapnia in the form of volitional apnea was measured in the superior sagittal sinus (artwork modified from Caporale et al., 2019; Supplementary Figure B1, with permission from RSNA publisher).

of NO, the most potent endogenous vasodilator promoting activation of proinflammatory and prothrombic pathways, which in turn cause reduced blood fluidity (Bleakley et al., 2015). EDF is often found with pre-clinical inflammatory or autoimmune diseases [e.g., rheumatoid arthritis (Kerekes et al., 2008), diabetes mellitus (Tabit et al., 2010)], and promoted by hypertension (Bleakley et al., 2015) and unhealthy lifestyle (e.g., tobacco abuse, lack of physical activity, and improper diet) leading to hypercholesterolemia (Defago et al., 2014), as well as environmental factors such as air pollution (Bourdrel et al., 2017).

Of all the organs in the body, the lung is possibly the most vascularized. The pulmonary system is also in direct contact with the environment and for gas exchange to occur at the air-water interface, inhaled gases or particles must pass through alveolar surfactant, alveolar epithelium, and basement membrane into the capillary endothelium. In the case of inhaled smoke or particulate matter such as fine or ultra-fine particles associated with tobacco or e-cigs, the pulmonary endothelium responds to this exposure by activation of the endothelial enzyme NADPH oxidase to produce ROS (Chatterjee et al., 2019a). Pulmonary endothelial ROS produce intercellular adhesion molecule (ICAM) which is key to recruitment and adherence of immune cells from the circulation. ROS also react with NO, to form the highly reactive peroxynitrite that curtails NO bioavailability. As the production of peroxynitrite is accompanied by reduction in NO, it is also linked to EDF (Cannon, 1998). The cascade of events following e-cig aerosol inhalation is illustrated in **Figure 1**.

In addition to these changes occurring at the cellular level of the endothelium, inflammatory moieties that increase in the bloodstream in response to smoking or exposure to particulate matter, entail increased circulatory burden. In the long term, such insults can amplify inflammation along the endothelial layer by enhanced expression of cell surface adhesion molecules, enabling docking of circulating polymorphonuclear neutrophils to endothelial cells and their transmigration in the interstitium and airspace. It can also lead to changes between interconnected endothelial cells via increasing gap junctions (Doerschuk et al., 1999) making it more permissive to the spread of inflammation over large areas of the lung and compromising vascular properties such as vasodilation or vasoconstriction.

Thus, evaluation of changes at the microcellular level are crucial in gaining insights into events as they occur sequentially post inhalation: from the initial signals at the endothelial cellular level, to its macro-manifestations on the vascular network changes.

ROLE OF MRI AS AN INVESTIGATIONAL TOOL OF E-CIGARETTE INDUCED VASCULAR AND METABOLIC EFFECTS IN HUMANS

The literature on image-based assessment of the effects of e-cigarettes on the cardiovascular system is sparse. Recent work

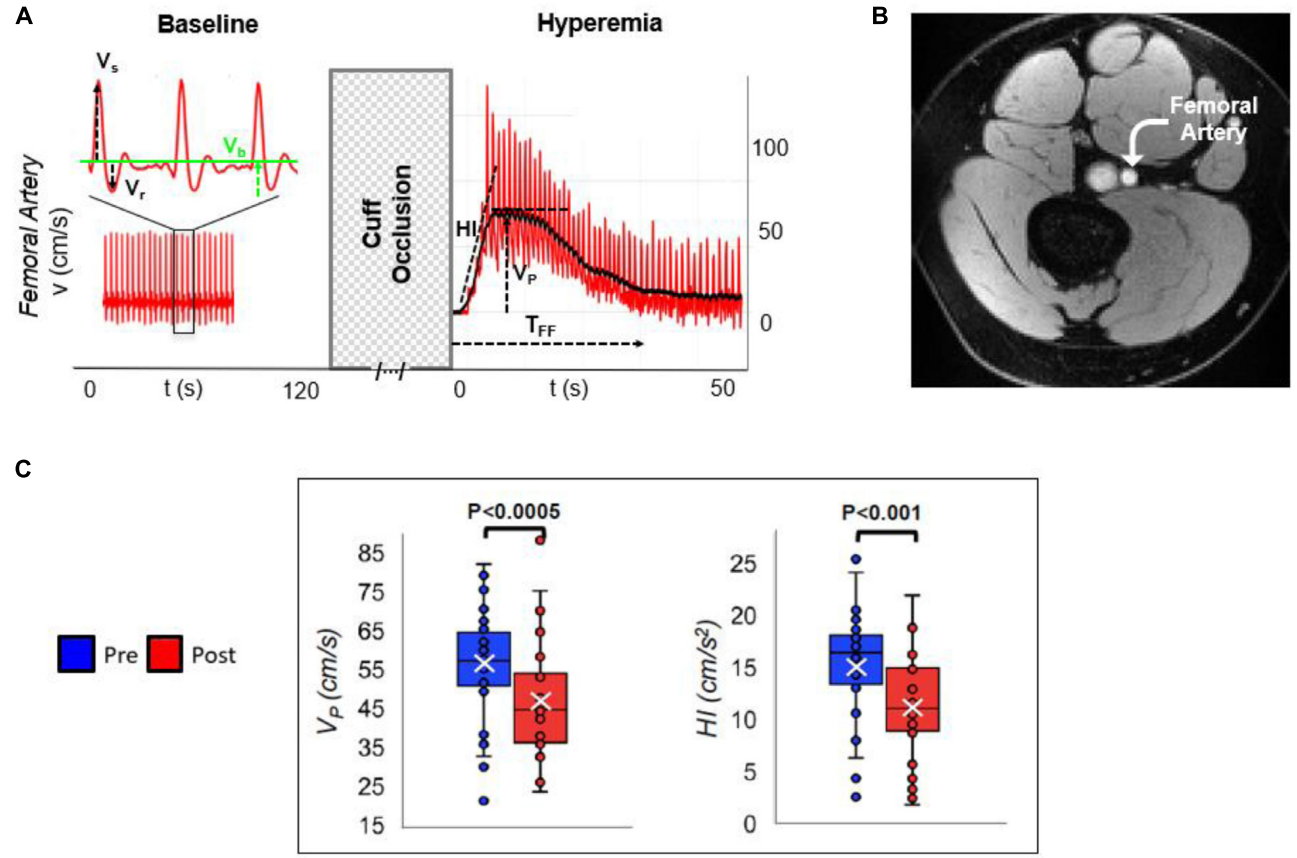

FIGURE 3 | Arterial velocimetry at baseline and hyperemia. **(A)** Blood flow velocity in the superficial femoral artery, during baseline and post-cuff occlusion (reactive hyperemia). Systolic, retrograde, and baseline velocities are indicated (V_s, V_r, and V_b, respectively). Post-ischemia, hyperemia is evaluated in terms of hyperemic index (HI) as the slope of the initial part of the velocity-time curve, peak average velocity (V_P), and duration of hyperemia, referred to as time of forward flow (T_{FF}). **(B)** Axial MR image of the thigh perpendicular to the femoral artery. **(C)** Pre- vs. post-electronic cigarette (e-cig) vaping differences for two parameters, in non-smokers, after a single episode of non-nicotinized e-cig vaping. The same MRI protocol was executed before and after e-cig use (modified from Caporale et al., 2019; Figures 2, 5, with permission from RSNA publisher).

using B-mode ultrasound has provided some insight into the acute effects of e-cigarette exposure in smokers in the form of flow-mediated dilation (*FMD*). A group of Italian investigators found brachial artery *FMD* in e-cigarette users to be impaired following a single vaping episode (Carnevale et al., 2016; Biondi-Zoccai et al., 2019).

Flow-mediated dilation is induced by transient increase in conduit blood flow velocity due to reduced microvascular resistance as the organism's mechanism to re-oxygenate hypoxic tissue. The resulting increase in shear stress to the endothelium leads to vasodilation of the conduit artery via NO release (Widlansky et al., 2003). While often regarded as an effective surrogate marker for endothelial function (or dysfunction), the method's poor intra-and inter-session reproducibility plague brachial artery *FMD* (Hardie et al., 1997; Ghiadoni et al., 2012).

Carotid-femoral pulse-wave velocity (*PWV*) has also been explored as a tool to study the acute impact of e-cigarette vaping (Vlachopoulos et al., 2016; Franzen et al., 2018). Both studies provided evidence of transient arterial wall stiffening following vaping and tobacco smoking. *PWV* is typically obtained by measuring the time delay of the systolic pressure wave at some downstream location, using pressure transducers placed at two locations (typically carotid and common femoral arteries) (Asmar et al., 1995; Wilkinson et al., 1998) or Doppler ultrasound (Sutton-Tyrrell et al., 2001).

Magnetic resonance imaging (MRI) is unmatched in its ability to provide structural information at high resolution and contrast, as well as quantitative physiologic and functional information non-invasively. It has provided pivotal insight into the vascular system in the form of quantitative perfusion data in the brain (Detre et al., 2009) and musculoskeletal system (Wu et al., 2009), blood flow velocity and flow rate of major arteries and veins (Markl et al., 2003) and, more recently, the metabolic rate of oxygen consumption, MRO_2 (Xu et al., 2009; Jain et al., 2010), or parameters assessing vascular compliance (Mohiaddin et al., 1989) and *PWV* (Grotenhuis et al., 2009; Langham et al., 2011). MRI quantification of each of these physiologic quantities is able to yield results expressed in absolute physiologic units. MRI thus provides us with a sensitive

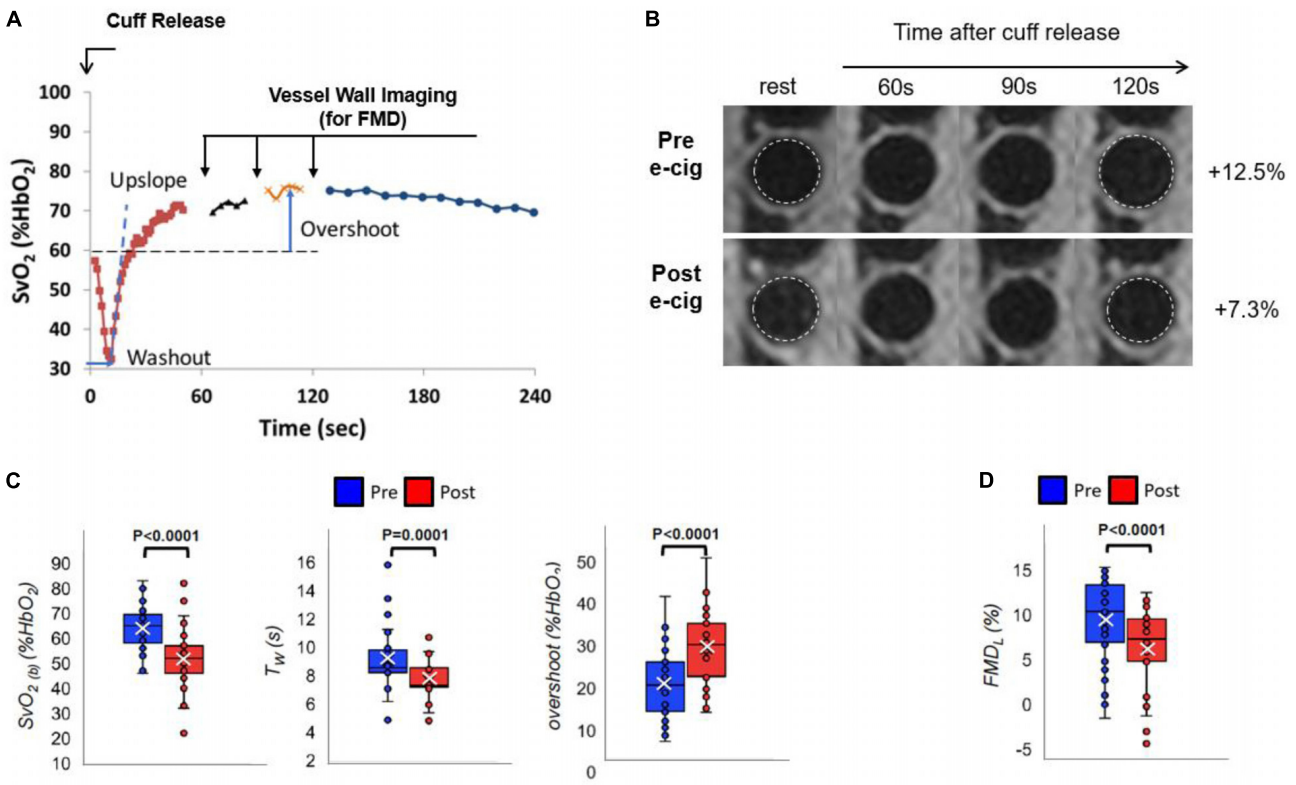

FIGURE 4 | Venous oximetry and flow-mediated dilation. **(A)** Post-cuff release venous oxygen saturation (SvO_2) interleaved with vessel wall imaging to derive femoral artery flow-mediated dilation (FMD) measurement at 60, 90, and 120 s following cuff deflation, with respect to the lumen at rest **(B)**. **(B–D)** Pre vs. post-e-cig vaping differences for the extracted metrics: **(B,D)** luminal FMD (FMD_L), **(C)** pre-cuff occlusion baseline SvO_2 [$SvO_{2(b)}$], washout time (T_W), and overshoot (**A**,**B** are original, produced from data already published in Caporale et al., 2019; **(C,D)** are modified from Caporale et al., 2019; Figure 5, with permission from RSNA publisher).

toolbox to study vascular-metabolic disturbances such as acute and chronic effects of smoking and vaping, the topic of this review. Thus, unlike competing techniques, which evaluate a single physiologic property, MRI is able to measure a host of parameters covering multiple vascular territories in a single session, as first demonstrated in a study of the acute effects of tobacco smoking (Langham et al., 2015). In comparison to non-smokers, smokers had reduced endothelial function and vascular reactivity independent of subjects' age. In that work, both measures of post-occlusion hyperemia and femoral *FMD* were assessed with an upper leg cuff-occlusion protocol disrupting both arterial inflow and venous return, along with parameters describing the time-course of femoral vein oxygen saturation (SvO_2). The latter also yielded significant group differences, interpreted in terms of compromised microvascular reactivity (Langham et al., 2015).

The above multi-vascular MRI procedure, which has since been refined, permits concurrent measurement of arterial and venous post-ischemia reactivity and endothelial function (Caporale et al., 2019), central aortic PWV (Langham et al., 2011) as well as cerebrovascular reactivity (Wu et al., 2019), to study acute effects of e-cigarette vaping (**Figure 2**; Caporale et al., 2019). The enhanced efficiency allows running the entire protocol in back-to-back sessions separated by a vaping episode. The objective of the latter study was to evaluate the acute transient effects of inhalation of nicotine-free e-cig aerosol in smoking-naïve young subjects (Caporale et al., 2019). The work was motivated by prior data indicating aerosol and its breakdown products to contain toxic compounds that can enter the vascular system through upper respiratory pathways (Bakand et al., 2012; Nakane, 2012). Excerpts of the protocol, along with pre/post comparison data are shown in **Figures 3**, **4**. The principle, along with sample data, for quantification of metrics of hyperemia of the femoral artery is illustrated in **Figure 3**, together with a comparison of two of the extracted parameters before and after vaping (**Figures 3A,C**, respectively). **Figure 4A** displays the femoral vein oxygen saturation curve following cuff release, interleaving this measurement with high-resolution femoral artery vessel wall images (**Figure 4B**) to derive FMD at three time-points. Pre/post plots of the oximetric parameter derived from the SvO_2 recovery curve are presented in **Figure 4C**, the change in FMD in **Figure 4D**. All data are highly significant and consistent with the notion that the aerosol (supplemented with tobacco flavor), or the breakdown products (Wang et al., 2017), possibly micro-particles emanating from the heating elements (Williams et al., 2013, 2017), cause an immune response [as shown by the authors' data in Chatterjee et al. (2019b)], leading to acute EDF.

RELATIONSHIP OF IMAGING FINDINGS TO BIOLOGICAL MARKERS

Endothelial dysfunction, a process occurring at the microvascular level, is highly predictive of future macrovascular events (Bleakley et al., 2015). Microvascular dysfunction manifests in alterations of endothelial receptors, and reduction in NO availability due to reduced biosynthesis and increased scavenging by oxygen radicals linked to oxidative stress. One consequence is impaired anti-inflammatory protection, leading to increased systemic inflammation, represented, for instance, by C-reactive protein (CRP) (Bleakley et al., 2015). Associations between subclinical vascular disease established by means of MRI and other quantitative imaging modalities, and vascular inflammation is well established [see, for instance (McEvoy et al., 2015) as well as some of the current authors' prior work (Langham et al., 2015)]. Arterial FMD, as pointed out earlier, is mediated by NO release in the endothelium (Kooijman et al., 2008). The substantial reduction in femoral artery FMD measured with MRI in non-smokers approximately 20–30 min after inhalation of nicotine-free-cig aerosol (Caporale et al., 2019) is paralleled by a decrease in NO and increase in CRP in the circulating serum, recovering to baseline values within 2–3 h (Chatterjee et al., 2019b). Similarly, a decrease on the order of 20–30% in NO bioavailability was found in non-smokers, whose brachial artery FMD was reduced by almost 40% after exposure to nicotinized e-cigarette in two crossover studies comparing the effects of e-cig vaping to tobacco smoking (Carnevale et al., 2016; Biondi-Zoccai et al., 2019), where tobacco smoking was found to cause a larger decrement in both quantities). The above two studies further provided evidence of increased oxidative stress expressed by augmented NADPH oxidase activation, and increased 8-iso prostaglandin F2α, and reduced levels of vitamin E, an anti-oxidant, following exposure to both, e-cig aerosol and tobacco smoke (Carnevale et al., 2016; Biondi-Zoccai et al., 2019).

DISCUSSION AND CONCLUSION

The data reviewed above compellingly show that quantitative MRI is extraordinarily sensitive to detect single events, in this case a vaping episode of nicotine-free aerosol. These results, though limited, demonstrate adverse effects consistent with transient impairment of endothelial function, along with reduced micro- and macrovascular reactivity. The time window for the observed effects is in the order of 1–3 h, which begs the question whether repeated vaping on this time scale causes a chronic response without the vascular system allowed to return to baseline conditions. Another question is which, among the myriad possible sources of toxins, would be the key culprit eliciting the observed responses. The studies reviewed in section "Role of MRI as an Investigational Tool of E-Cigarette Induced Vascular and Metabolic Effects in Humans" involved healthy, smoking naïve, young subjects rather than smokers/vapers. The latter would require study of both, acute and chronic exposure, which is currently in progress in the authors' laboratory. The other unknown is the added effect of nicotine that, alone, can promote EDF.

AUTHOR CONTRIBUTIONS

FW, AC, and SC conceived and drafted the manuscript. FW, SC, AC, and ML read, edited, and approved the final manuscript.

FUNDING

Our research of which we report results published elsewhere (see specific references) was supported by the National Institutes of Health, National Heart, Lung, and Blood Institute (R01HL139358).

REFERENCES

Asmar, R., Benetos, A., Topouchian, J., Laurent, P., Pannier, B., and Brisac, A. M. (1995). Assessment of arterial distensibility by automatic pulse wave velocity measurement. Validation and clinical application studies. *Hypertension* 26, 485–490. doi: 10.1161/01.hyp.26.3.485

Bakand, S., Hayes, A., and Dechsakulthorn, F. (2012). Nanoparticles: a review of particle toxicology following inhalation exposure. *Inhal. Toxicol.* 24, 125–135. doi: 10.3109/08958378.2010.642021

Bekki, K., Uchiyama, S., Ohta, K., Inaba, Y., Nakagome, H., and Kunugita, N. (2014). Carbonyl compounds generated from electronic cigarettes. *Intern. J. Environ. Res. Public Health* 11, 11192–11200. doi: 10.3390/ijerph111111192

Biondi-Zoccai, G., Sciarretta, S., Bullen, C., Nocella, C., Violi, F., and Loffredo, L. (2019). Acute Effects of heat-not-burn, electronic vaping, and traditional tobacco combustion cigarettes: the sapienza university of rome-vascular assessment of proatherosclerotic effects of smoking (SUR - VAPES) 2 randomized trial. *J. Am. Heart Assoc.* 8:e010455. doi: 10.1161/JAHA.118.010455

Bleakley, C., Hamilton, P. K., Pumb, R., Harbinson, M., and Mcveigh, G. E. (2015). Endothelial function in hypertension: victim or culprit? *J. Clin. Hypertens.* 17, 651–654. doi: 10.1111/jch.12546

Bourdrel, T., Bind, M. A., Bejot, Y., Morel, O., and Argacha, J. F. (2017). Cardiovascular effects of air pollution. *Arch. Cardiovasc. Dis.* 110, 634–642.

Cannon, R. O. III (1998). Role of nitric oxide in cardiovascular disease: focus on the endothelium. *Clin. Chem.* 44, 1809–1819.

Caporale, A., Langham, M. C., Guo, W., Johncola, A., Chatterjee, S., and Wehrli, F. W. (2019). Acute effects of e-cigarette aerosol inhalation on vascular function detected by quantitative MRI. *Radiology* 293, 97–106. doi: 10.1148/radiol.2019190562

Carnevale, R., Sciarretta, S., Violi, F., Nocella, C., Loffredo, L., and Perri, L. (2016). Acute impact of tobacco vs electronic cigarette smoking on oxidative stress and vascular function. *Chest* 150, 606–612. doi: 10.1016/j.chest.2016.04.012

Chatterjee, S., Pietrofesa, R. A., Park, K., Tao, J. Q., Carabe-Fernandez, A., Berman, A. T., et al. (2019a). LGM2605 reduces space radiation-induced NLRP3 inflammasome activation and damage in vitro lung vascular networks. *Intern. J. Mol. Sci.* 20:176. doi: 10.3390/ijms20010176

Chatterjee, S., Tao, J. Q., Johncola, A., Guo, W., Caporale, A., Langham, M. C., et al. (2019b). Acute exposure to e-cigarettes causes inflammation and pulmonary endothelial oxidative stress in nonsmoking, healthy young subjects. *Am. J. Physiol. Lung. Cell Mol. Physiol.* 317, L155–L166. doi: 10.1152/ajplung.00110.2019

Defago, M. D., Elorriaga, N., Irazola, V. E., and Rubinstein, A. L. (2014). Influence of food patterns on endothelial biomarkers: a systematic review. *J. Clin. Hypertens.* 16, 907–913. doi: 10.1111/jch.12431

Detre, J. A., Wang, J., Wang, Z., and Rao, H. (2009). Arterial spin-labeled perfusion MRI in basic and clinical neuroscience. *Curr. Opin. Neurol.* 22, 348–355. doi: 10.1097/WCO.0b013e32832d9505

Doerschuk, C. M., Mizgerd, J. P., Kubo, H., Qin, L., and Kumasaka, T. (1999). Adhesion molecules and cellular biomechanical changes in acute lung injury: giles F. *Filley Lecture Chest.* 116, 37S–43S. doi: 10.1378/chest.116.suppl_1.37s-a

Franzen, K. F., Willig, J., Cayo Talavera, S., Meusel, M., Sayk, F., Reppel, M., et al. (2018). E-cigarettes and cigarettes worsen peripheral and central hemodynamics as well as arterial stiffness: a randomized, double-blinded pilot study. *Vasc. Med.* 23, 419–425. doi: 10.1177/1358863X18779694

Furchgott, R., and Zawadzki, J. (1980). The obligatory role of endothelial cells in the relaxation of arterial smooth muscle by acetylcholine. *Nature* 288, 373–376. doi: 10.1038/288373a0

Ghiadoni, L., Faita, F., Salvetti, M., Cordiano, C., Biggi, A., Puato, M., et al. (2012). Assessment of flow-mediated dilation reproducibility: a nationwide multicenter study. *J. Hypertens.* 30, 1399–1405. doi: 10.1097/HJH.0b013e328353f222

Grotenhuis, H. B., Westenberg, J. J., Steendijk, P., Van Der Geest, R. J., Ottenkamp, J., Bax, J. J., et al. (2009). Validation and reproducibility of aortic pulse wave velocity as assessed with velocity-encoded MRI. *J. Magn. Reson. Imaging* 30, 521–526. doi: 10.1002/jmri.21886

Hardie, K. L., Kinlay, S., Hardy, D. B., Wlodarczyk, J., Silberberg, J. S., and Fletcher, P. J. (1997). Reproducibility of brachial ultrasonography and flow-mediated dilatation (FMD) for assessing endothelial function. *Aust. N. Z. J. Med.* 27, 649–652. doi: 10.1111/j.1445-5994.1997.tb00992.x

Herrmann, J., and Lerman, A. (2001). The endothelium: dysfunction and beyond. *J. Nucl. Cardiol.* 8, 197–206.

Jain, V., Langham, M. C., and Wehrli, F. W. (2010). MRI estimation of global brain oxygen consumption rate. *J. Cereb. Blood Flow Metab.* 30, 1598–1607. doi: 10.1038/jcbfm.2010.49

Jensen, R. P., Strongin, R. M., and Peyton, D. H. (2017). Solvent chemistry in the electronic cigarette reaction vessel. *Sci. Rep.* 7:42549. doi: 10.1038/srep42549

Kerekes, G., Szekanecz, Z., Der, H., Sandor, Z., Lakos, G., Muszbek, L., et al. (2008). Endothelial dysfunction and atherosclerosis in rheumatoid arthritis: a multiparametric analysis using imaging techniques and laboratory markers of inflammation and autoimmunity. *J. Rheumatol.* 35, 398–406.

Kligerman, S., Raptis, C., Larsen, B. T., Henry, T. S., Caporale, A., Tazelaar, H. D., et al. (2020). Radiologic, pathologic, clinical, and physiologic findings of evali: evolving knowledge and remaining questions. *Radiology* 294, 491–505. doi: 10.1148/radiol.2020192585

Kooijman, M., Thijssen, D. H., De Groot, P. C., Bleeker, M. W., Van Kuppevelt, H. J., and Green, D. J. (2008). Flow-mediated dilatation in the superficial femoral artery is nitric oxide mediated in humans. *J. Physiol.* 586, 1137–1145. doi: 10.1113/jphysiol.2007.145722

Langham, M. C., Li, C., Magland, J. F., and Wehrli, F. W. (2011). Nontriggered MRI quantification of aortic pulse-wave velocity. *Magn. Reson. Med.* 65, 750–755. doi: 10.1002/mrm.22651

Langham, M. C., Zhou, Y., Chirico, E. N., Magland, J. F., Sehgal, C. M., and Englund, E. K. (2015). Effects of age and smoking on endothelial function assessed by quantitative cardiovascular magnetic resonance in the peripheral and central vasculature. *J. Cardiovasc. Magn. Reson.* 17:19. doi: 10.1186/s12968-015-0110-8

Lerner, C. A., Sundar, I. K., Yao, H., Gerloff, J., Ossip, D. J., Mcintosh, S., et al. (2015). Vapors produced by electronic cigarettes and e-juices with flavorings induce toxicity, oxidative stress, and inflammatory response in lung epithelial cells and in mouse lung. *PLoS One* 10:e0116732. doi: 10.1371/journal.pone.0116732

Lewis, N., Mccaffrey, K., Sage, K., Cheng, C.-J., Green, J., Goldstein, L., et al. (2019). E-cigarette use, or vaping, practices and characteristics among persons with associated lung injury - utah, April-October 2019. *Morbid. Mortal. Weekly Rep.* 68, 953–956. doi: 10.15585/mmwr.mm6842e1

Markl, M., Chan, F. P., Alley, M. T., Wedding, K. L., Draney, M. T., Elkins, C. J., et al. (2003). Time-resolved three-dimensional phase-contrast MRI. *J. Magnet. Reson. Imaging* 17, 499–506.

McEvoy, J. W., Nasir, K., Defilippis, A. P., Lima, J. A., Bluemke, D. A., Hundley, W. G., et al. (2015). Relationship of cigarette smoking with inflammation and subclinical vascular disease: the multi-ethnic study of atherosclerosis. *Arterioscler. Thromb. Vasc. Biol.* 35, 1002–1010. doi: 10.1161/ATVBAHA.114.304960

Miech, R., Johnston, L., O'malley, P. M., Bachman, J. G., and Patrick, M. E. (2019). Trends in adolescent vaping, 2017–2019. *N. Engl. J. Med.* 381, 1490–1491. doi: 10.1056/NEJMc1910739

Mohiaddin, R. H., Underwood, S. R., Bogren, H. G., Firmin, D. N., Klipstein, R. H., Rees, R. S., et al. (1989). Regional aortic compliance studied by magnetic resonance imaging: the effects of age, training, and coronary artery disease. *Br. Heart J.* 62, 90–96. doi: 10.1136/hrt.62.2.90

Nakane, H. (2012). Translocation of particles deposited in the respiratory system: a systematic review and statistical analysis. *Environ. Health Prevent. Med.* 17:263. doi: 10.1007/s12199-011-0252-8

Neunteufl, T., Heher, S., Kostner, K., Mitulovic, G., Lehr, S., Khoschsorur, G., et al. (2002). Contribution of nicotine to acute endothelial dysfunction in long-term smokers. *J. Am. Coll. Cardiol.* 39, 251–256. doi: 10.1016/s0735-1097(01)01732-6

Olmedo, P., Goessler, W., Tanda, S., Grau-Perez, M., Jarmul, S., Aherrera, A., et al. (2018). Metal concentrations in e-cigarette liquid and aerosol samples: the contribution of metallic coils. *Environ. Health Perspect.* 126:027010. doi: 10.1289/EHP2175

Omaiye, E. E., Mcwhirter, K. J., Luo, W., Pankow, J. F., and Talbot, P. (2019). High-nicotine electronic cigarette products: toxicity of JUUL fluids and aerosols correlates strongly with nicotine and some flavor chemical concentrations. *Chem. Res. Toxicol.* 32, 1058–1069. doi: 10.1021/acs.chemrestox.8b00381

Schweitzer, K. S., Chen, S. X., Law, S., Van Demark, M., Poirier, C., Justice, M. J., et al. (2015). Endothelial disruptive proinflammatory effects of nicotine and e-cigarette vapor exposures. *Am. J. Physiol. Lung. Cell Mol. Physiol.* 309, L175–L187. doi: 10.1152/ajplung.00411.2014

Sutton-Tyrrell, K., Mackey, R. H., Holubkov, R., Vaitkevicius, P. V., Spurgeon, H. A., and Lakatta, E. G. (2001). Measurement variation of aortic pulse wave velocity in the elderly. *Am. J. Hypertens.* 14, 463–468. doi: 10.1016/s0895-7061(00)01289-9

Tabit, C. E., Chung, W. B., Hamburg, N. M., and Vita, J. A. (2010). Endothelial dysfunction in diabetes mellitus: molecular mechanisms and clinical implications. *Rev. Endocr. Metab. Disord.* 11, 61–74. doi: 10.1007/s11154-010-9134-4

Vlachopoulos, C., Ioakeimidis, N., Abdelrasoul, M., Terentes-Printzios, D., Georgakopoulos, C., Pietri, P., et al. (2016). Electronic cigarette smoking increases aortic stiffness and blood pressure in young smokers. *J. Am. Coll. Cardiol.* 67, 2802–2803. doi: 10.1016/j.jacc.2016.03.569

Wang, P., Chen, W., Liao, J., Matsuo, T., Ito, K., Fowles, J., et al. (2017). A device-independent evaluation of carbonyl emissions from heated electronic cigarette solvents. *PLoS One* 12:e0169811. doi: 10.1371/journal.pone.0169811

Widlansky, M. E., Gokce, N., Keaney, J. F. Jr., and Vita, J. A. (2003). The clinical implications of endothelial dysfunction. *J. Am. Coll. Cardiol.* 42, 1149–1160.

Wilkinson, I. B., Fuchs, S. A., Jansen, I. M., Spratt, J. C., Murray, G. D., Cockcroft, J. R., et al. (1998). Reproducibility of pulse wave velocity and augmentation index measured by pulse wave analysis. *J. Hypertens.* 16, 2079–2084. doi: 10.1097/00004872-199816121-00033

Williams, M., Bozhilov, K., Ghai, S., and Talbot, P. (2017). Elements including metals in the atomizer and aerosol of disposable electronic cigarettes and electronic hookahs. *PLoS One* 12:e0175430. doi: 10.1371/journal.pone.0175430

Williams, M., Villarreal, A., Bozhilov, K., Lin, S., and Talbot, P. (2013). Metal and silicate particles including nanoparticles are present in electronic cigarette cartomizer fluid and aerosol. *PLoS One* 8:e57987. doi: 10.1371/journal.pone.057987

Wu, P. H., Rodriguez-Soto, A. E., Rodgers, Z. B., Englund, E. K., Wiemken, A., Langham, M. C., et al. (2019). MRI evaluation of cerebrovascular reactivity

in obstructive sleep apnea. *J. Cereb. Blood Flow Metab.* 15:0271678X19862182. doi: 10.1177/0271678X19862182

Wu, W.-C., Mohler, E. III, Ratcliffe, S. J., Wehrli, F. W., Detre, J. A., and Floyd, T. F. (2009). Skeletal muscle microvascular flow in progressive peripheral artery disease: assessment with continuous arterial spin-labeling perfusion magnetic resonance imaging. *J. Am. Coll. Cardiol.* 53, 2372–2377. doi: 10.1016/j.jacc.2009.03.033

Xu, F., Ge, Y., and Lu, H. (2009). Noninvasive quantification of whole-brain cerebral metabolic rate of oxygen (CMRO2) by MRI. *Magn. Reson. Med.* 62, 141–148. doi: 10.1002/mrm.21994

Conflict of Interest: The authors declare that the research was conducted in the absence of any commercial or financial relationships that could be construed as a potential conflict of interest.

frontiers in Physiology

ORIGINAL RESEARCH
published: 29 July 2020
doi: 10.3389/fphys.2020.00879

Cystic Fibrosis Transmembrane Conductance Regulator (CFTR) in Human Lung Microvascular Endothelial Cells Controls Oxidative Stress, Reactive Oxygen-Mediated Cell Signaling and Inflammatory Responses

*Maha Khalaf[1], Toby Scott-Ward[1], Adam Causer[2], Zoe Saynor[2], Anthony Shepherd[2], Dariusz Górecki[1], Anthony Lewis[1], David Laight[1] and Janis Shute[1]**

[1] School of Pharmacy and Biomedical Sciences, Institute of Biological and Biomedical Sciences, University of Portsmouth, Portsmouth, United Kingdom, [2] Department of Sport and Exercise Science, University of Portsmouth, Portsmouth, United Kingdom

OPEN ACCESS

Edited by:
Shampa Chatterjee, University of Pennsylvania, United States

Reviewed by:
Sirajudheen Anwar, University of Hail, Saudi Arabia
Azizah Ugusman, National University of Malaysia, Malaysia

***Correspondence:**
Janis Shute
jan.shute@port.ac.uk

Specialty section:
This article was submitted to Vascular Physiology, a section of the journal Frontiers in Physiology

Received: *30 July 2019*
Accepted: *29 June 2020*
Published: *29 July 2020*

Citation:
Khalaf M, Scott-Ward T, Causer A, Saynor Z, Shepherd A, Górecki D, Lewis A, Laight D and Shute J (2020) Cystic Fibrosis Transmembrane Conductance Regulator (CFTR) in Human Lung Microvascular Endothelial Cells Controls Oxidative Stress, Reactive Oxygen-Mediated Cell Signaling and Inflammatory Responses. Front. Physiol. 11:879. doi: 10.3389/fphys.2020.00879

Background: Perturbation of endothelial function in people with cystic fibrosis (CF) has been reported, which may be associated with endothelial cell expression of the cystic fibrosis transmembrane conductance regulator (CFTR). Previous reports indicate that CFTR activity upregulates endothelial barrier function, endothelial nitric oxide synthase (eNOS) expression and NO release, while limiting interleukin-8 (IL-8) release, in human umbilical vein endothelial cells (HUVECs) in cell culture. In view of reported microvascular dysfunction in people with CF we investigated the role of CFTR expression and activity in the regulation of oxidative stress, cell signaling and inflammation in human lung microvascular endothelial cells (HLMVECs) in cell culture.

Methods: HLMVECs were cultured in the absence and presence of the CFTR inhibitor GlyH-101 and CFTR siRNA. CFTR expression was analyzed using qRT-PCR, immunocytochemistry (IHC) and western blot, and function by membrane potential assay. IL-8 expression was analyzed using qRT-PCR and ELISA. Nrf2 expression, and NF-κB and AP-1 activation were determined using IHC and western blot. The role of the epidermal growth factor receptor (EGFR) in CFTR signaling was investigated using the EGFR tyrosine kinase inhibitor AG1478. Oxidative stress was measured as intracellular ROS and hydrogen peroxide (H_2O_2) concentration. VEGF and SOD-2 were measured in culture supernatants by ELISA.

Results: HLMVECs express low levels of CFTR that increase following inhibition of CFTR activity. Inhibition of CFTR, significantly increased intracellular ROS and H_2O_2 levels over 30 min and significantly decreased Nrf2 expression by 70% while increasing SOD-2 expression over 24 h. CFTR siRNA significantly increased constitutive expression of IL-8 by HLMVECs. CFTR inhibition activated the AP-1 pathway and increased IL-8

expression, without effect on NF-κB activity. Conversely, TNF-α activated the NF-κB pathway and increased IL-8 expression. The effects of TNF-α and GlyH-101 on IL-8 expression were additive and inhibited by AG1478. Inhibition of both CFTR and EGFR in HLMVECs significantly increased VEGF expression. The antioxidant N-acetyl cysteine significantly reduced ROS production and the increase in IL-8 and VEGF expression following CFTR inhibition.

Conclusion: Functional endothelial CFTR limits oxidative stress and contributes to the normal anti-inflammatory state of HLMVECs. Therapeutic strategies to restore endothelial CFTR function in CF are warranted.

Keywords: endothelium, CFTR, cystic fibrosis, inflammation, oxidative stress, cell signaling

INTRODUCTION

Cystic fibrosis (CF) lung disease is associated with neutrophilic airway inflammation, bronchiectasis, respiratory failure, and early mortality (Nichols and Chmiel, 2015). Defective or deficient expression of the cystic fibrosis transmembrane conductance regulator (CFTR) protein, an anion channel conducting mainly chloride and bicarbonate ions in airway epithelial cells (Saint-Criq and Gray, 2017), leads to dehydration of airway secretions with failure of mucociliary clearance and mucus plugging. In the early stages of CF lung disease this may lead to sterile inflammation (Zhou-Suckow et al., 2017), but inevitably the airways become chronically infected leading to further interleukin-8 (IL-8) driven neutrophilic inflammation (Nichols and Chmiel, 2015). In more severe disease, increased expression of vascular endothelial growth factor (VEGF) and associated peribronchial vascularity contributes to the immune and inflammatory responses in the CF airway, as well as the risk of hemoptysis (Martin et al., 2013).

A number of studies have indicated macro- and microvascular endothelial perturbation in people with CF (Romano et al., 2001; Solic et al., 2005; Poore et al., 2013; Rodriguez-Miguelez et al., 2016; Vizzardi et al., 2019) that may be associated with defective endothelial CFTR function (Noe et al., 2009; Brown et al., 2014; Peters et al., 2015; Totani et al., 2017). Increased circulating levels of von Willebrand factor (vWF) and tissue plasminogen activator (tPA), indicative of endothelial damage and altered hemostasis (Romano et al., 2001), and reduced flow-mediated dilation of the brachial artery, which was associated with more severe airway disease and symptomatic of reduced NO availability (Poore et al., 2013), were reported in CF. Hydrogen peroxide (H_2O_2)-induced oxidative stress and apoptosis required functional CFTR in human lung microvascular cells (HLMVEC), effects that were reversed by the CFTR inhibitor CFTRinh-172 (Noe et al., 2009). Reduced endothelial apoptosis in the vasculature of the CF lung has previously been reported which may be associated with reduced endothelial ceramide concentration (Noe et al., 2009). Endothelial CFTR plays an important role in maintaining hydration of the endothelial glycocalyx (Peters et al., 2015), the endothelial barrier function (Brown et al., 2014; Totani et al., 2017) and the availability of NO, while limiting IL-8 release (Totani et al., 2017).

Thus, together with reports of endothelial expression of CFTR in human umbilical vein endothelial cells (HUVEC) (Tousson et al., 1998; Totani et al., 2017), HLMVEC (Tousson et al., 1998), and human pulmonary artery endothelial cells (HPAEC) (Plebani et al., 2017; Totani et al., 2017), there is a growing body of evidence for expression and function of CFTR in the endothelium.

Previous studies have shown that functional CFTR at the epithelial cell surface is critical for limiting NF-κB mediated cell signaling leading to IL-8 expression both at baseline and following activation with pro-inflammatory cytokines IL-1 and TNF-α (Perez et al., 2007; Vij et al., 2009), for inhibiting epidermal growth factor receptor (EGFR)-mediated IL-8 (Kim et al., 2013) and VEGF synthesis (Martin et al., 2013) and for Nrf-2-mediated adaptive responses to oxidative stress (Chen et al., 2008).

The present study focuses on the pulmonary microvasculature and investigates the expression and function of CFTR as a regulator of oxidative stress, expression of the key transcriptional regulator of antioxidant defenses nuclear factor erythroid 2 [NF-E2]-related factor 2 (Nrf2), expression of pro-angiogenic VEGF and of the neutrophil chemoattractant IL-8, and reactive oxygen species (ROS)-mediated inflammatory cell signaling in HLMVECs grown on the basement membrane component, collagen IV.

The overall aim is to identify a role for dysfunctional endothelial CFTR in systemic inflammation and oxidative stress and, importantly, new therapeutic targets to reduce systemic inflammation and oxidative stress in people with CF.

MATERIALS AND METHODS

Materials

All reagents were from Merck unless indicated otherwise.

Cell Culture

Human lung microvascular endothelial cells (HLMVECs) from non-smoking donors (Lonza Biologics) were maintained in complete EGM-2MV medium (EBM-2MV basal medium supplemented with 5% FBS, 0.04% hydrocortisone, 0.4% hFGF, 0.1% VEGF, 0.1% IGF-1, 0.1% ascorbic acid, 0.1% hEGF and 0.1%

GA-100 (Lonza Biologics) and used at passage 5–8. The growth medium was changed 1 day after seeding and then every other day to 90% confluence. Cells were passaged using trypsin-EDTA to detach them, neutralized with warmed FBS and pelleted by centrifugation. The cell pellet was re-suspended in full growth medium (FGM) and seeded in multi-well plates (25×10^4/6-well plate, 5×10^4/24-well plate) coated with human collagen IV (0.1 mg/ml) and allowed to adhere overnight before treatment at the indicated times with the CFTR inhibitor GlyH-101 [5, 10, 20 μM (Friard et al., 2017)], dimethyl sulfoxide (DMSO, 0.1%) as vehicle control or TNF-α [10 ng/ml (Chen et al., 2008), Peprotech] for up to 24 h, which was established by cell viability testing in the presence of GlyH-101, as described below.

The specificity of GlyH-101 as a CFTR inhibitor was confirmed using inhibitors of other chloride ion channels. DCPIB (4-(2-butyl-6,7-dichlor-2-cyclopentyl-indan-1-on-5-yl) oxybutyric acid) (Tocris), a potent (IC_{50} 4.8 μM) and specific Volume-Regulated Anion Channel (VRAC) inhibitor was used at 20 μM (Friard et al., 2017), and Ani9 (2-(4-chloro-2-methylphenoxy)-N-[(2-methoxyphenyl)methylideneamino]-acetamide), a potent (IC_{50} 77 nM) and specific inhibitor of the calcium-activated chloride ion channel Transmembrane Member 16A (TMEM16A), also known as Anoctamin-1 (Ano-1), that lacks inhibitory activity against CFTR and VRAC (Seo et al., 2016), was used at 10 μM in HLMVEC cultures. HLMVECs were cultured in 5% CO_2 at 37°C and used until passage 8.

In separate experiments, HLMVECs were treated with N-acetyl cysteine [NAC, 5 or 10 mM (Chen et al., 2008), as indicated] and the EGFR inhibitor AG-1478 [10 μM (Kim et al., 2013)] for 3 h, followed by incubation with GlyH-101 (20 μM) alone, and with TNF-α (10 ng/ml) for 16 and 24 h in FGM.

Human embryonic kidney cells (HEK-293) which do not express CFTR (Friard et al., 2017) and human bronchial epithelial cells (the human bronchial epithelial cell line 16HBE14o-) which do express CFTR (Cozens et al., 1994) were used as negative and positive controls, respectively. HEK-293 and 16HBE cells were cultured as described above in DMEM or MEM media, respectively, supplemented with 10% FBS, 1% penicillin-streptomycin, 1% L-glutamine. Cells were maintained until passage 30.

MTT Assay for Cell Viability

Human lung microvascular endothelial cells were seeded at a density of 1×10^4 cells/well/100 μl of FGM in collagen-coated 96 well plates and left to adhere overnight at 37°C and 5% CO2. Next day the cells were treated with GlyH-101 and DMSO (0.1%) as vehicle control in FGM for 16, 24, and 48 h. In order to eliminate the effect of ascorbic acid in FGM on MTT color changes, the medium were replaced with 100 μl phenol red free medium (MEM) containing 0.3% of FBS per well. MTT 3-(4,5-dimethylthiazol-2-yl)-2,5-diphenyltetrazolium bromide (to a final concentration of 0.5 mg/ml) added to cells for 4 h at 37°C and 5% CO2 was reduced by cellular metabolic activity to insoluble formazan, which was solubilized with 100 μl 10% SDS in 0.01 M HCl overnight, and the absorbance read at 570 nm using a Spectramax i3x plate reader (Molecular Devices).

CFTR Activity Assay

Cystic fibrosis transmembrane conductance regulator activity was measured in HLMVECs, 16HBE and HEK-293 cells using the FLIPR Blue membrane potential assay (Molecular Devices), according to the manufacturer's instructions, and as described by Maitra et al. (2013). Cells were seeded at 8×10^3 cells per well and cultured overnight in collagen IV-coated optical-bottom black 96-well plates in 100 μl FGM. FLIPR Blue (100 μl) was directly added to the wells for 45 min at 37°C in FGM. Agonists, forskolin (100 μM)/IBMX (1000 μM), concentrations that significantly increase endothelial intracellular cAMP (Hopkins and Gorman, 1981; Sayner et al., 2004), were applied for 2 min and fluorescence measured with excitation 530 nm and emission 565 nm, using the Spectramax® i3x fluorescent plate reader (Molecular Devices). GlyH-101 (20 μM) or DMSO (0.1%) control were applied 15 min before the agonists. Changes in membrane polarization are reported as changes in relative fluorescence units (ΔRFU). CFTR activity was detected as membrane depolarization at baseline, and in response to IBMX plus forskolin leading to increased uptake and fluorescence of intracellular FLIPR Blue, that could be inhibited by GlyH-101 (Maitra et al., 2013). Experimental conditions were tested in quadruplicate in each of three independent experiments.

Preparation of Cell Lysates for CFTR and Nrf2 Protein Assessment by Western Blot

Cells were lysed directly with 35 μl/well for 24-well (Nrf2) and 75 μl/well for 6-well (CFTR) plates of 1X sample buffer [7.5% (v/v) glycerol, 50 mM Tris-Base, 2% (w/v) sodium dodecyl sulfate (SDS), 100 mM DL-dithiothreitol (DTT), 0.01% (w/v) bromophenol blue, 2 mM MgCl2, 0.05% (v/v) benzonase nuclease, 2x protease inhibitor cocktail I], on ice for 10 min. Finally 1 μl of 0.25 M EDTA was added to each lysate and samples heated in a water bath at 50°C for 20 min.

Preparation of Cell Lysates for Phospho-c-Jun Protein Assessment by Western Blot

Human lung microvascular endothelial cells in 6-well plates were treated with DMSO (0.1%), GlyH-101 (20 μM) or TNF-α (10 ng/ml) for 30 min and the cells lysed in 100 μl/well lysis buffer [125 mM NaCl, 1 mM MgCl2, 20 mM Tris–HCl, 1% Triton X-100, Complete protease inhibitor cocktail (Roche) and phosphatase inhibitor (PhosSTOP, Roche)] at 4°C for 30 min. The cell lysates were centrifuged at 24000 RCF, at 4°C for 30 min and stored at −80°C. Cell lysates (30 μl) were mixed with 10 μl 4X sample loading buffer (30% v/v glycerol, 200 mM Tris–HCl pH 6.8, 8% w/v SDS, 400 mM DTT, 0.04% w/v bromophenol blue), and placed in a water bath (95°C) for 4 min.

Gel Electrophoresis and Western Blotting

Samples (35 μl) were loaded onto 7.5% (CFTR) or 10% (Nrf2, p-c-Jun) SDS-PAGE gels, with 5 μl of a molecular weight ladder with pre-stained proteins in the molecular size range 8–220 kDa (Sigma) or 10–250 kDa (Bio-Rad) loaded on each gel, and resolved proteins transferred using a *Trans*-Blot semi-dry transfer cell (Bio-Rad, United Kingdom) to

0.45 μm nitrocellulose membrane (Bio-Rad, United Kingdom). Membranes were blocked with 3% (w/v) skimmed milk powder in PBS (without Ca/Mg) with 0.1% Tween-20 (PBS-T), overnight at 4°C.

For CFTR, blots were incubated with 2 μg/ml "Mr. Pink" rabbit polyclonal antibody (kindly provided by Prof. Ineke Braakman, Utrecht University through the CFTR Folding Consortium, United States) diluted 1:500 in PBS-T. Blots were incubated with antibody for 1 h at room temperature (RT), washed and incubated with 0.05 μg/ml goat anti-rabbit-HRP (Dako) for 1 h at RT.

For Nrf-2, membranes were stained with 1 μg/ml rabbit polyclonal anti-Nrf2 (Santa Cruz) in blocking buffer for 1 h at RT, washed in PBS-T, and incubated with 0.125 μg/ml goat anti-rabbit-HRP (Dako) for 1 h at RT.

For p-c-Jun, membranes were stained with 0.2 μg/ml rabbit polyclonal anti-p-c-Jun [(Ser 63/73) Santa Cruz] overnight at 4°C in blocking buffer, and then 0.125 μg/ml goat anti-rabbit-HRP (DAKO) for 2 h at RT.

After washing in PBS, blots were incubated for 5 min in the dark with chemiluminescence substrate (Promega), followed by detection of the bands with ChemiDoc^{TM} MP System (Bio-Rad). The bands were normalized to β-actin in the samples, which was detected after stripping with Restore Western Blot Stripping Buffer (Thermo Fisher, United Kingdom) for 15 min and re-probing membranes with rabbit polyclonal anti-β-actin for 1 h at RT followed by 1 h incubation at RT with 0.05 μg/ml goat anti-rabbit HRP (DAKO). Bands were quantified using scanning densitometry and Quantiscan software.

Preparation of Supernatants and Cell Lysates for Quantification of IL-8, VEGF, SOD-2 and Catalase by ELISA

Supernatants from HLMVECs grown in 24-well plates were cleared by centrifugation (1500 RCF for 10 min at 4°C). Cells were lysed for 10 min on ice in hypotonic buffer (20 mM NaCl, 1% Triton X-100, and 20 mM Tris-base, pH 7.4), containing Complete protease inhibitors (Roche), and protease inhibitor cocktail I (Calbiochem). Lysates were centrifuged at 5000 RCF for 10 min at 4°C and samples stored at −80°C prior to analysis. IL-8 and VEGF were measured using Duo-Set ELISA kits (R&D Systems) according to the manufacturer's instruction. Mitochondrial Mn-dependent superoxide dismutase (SOD-2) and catalase were quantified in neat cell lysates using ELISA kits (AbCam) according to manufacturer's instructions, with standard curves prepared in the range 7.8–500 ng/ml.

Measurement of Intracellular ROS and H_2O_2

Human lung microvascular endothelial cells were seeded in 35 mm dishes for live cell imaging (25×10^4 cells/dish), and HLMVECs and 16HBEs were seeded (8×10^3/well/100 μl) for quantification of ROS in 96-well plates coated with collagen IV and incubated overnight. In some experiments, NAC (10 mM) was added for 3 h in FGM before adding the ROS detector, carboxy-H2DFFDA (5-(and-6)-carboxy-2′,7′-difluorodihydrofluorescein diacetate, (Invitrogen) in serum-free HBSS (+Ca/Mg) at 10 μM for 30 min. Cells were washed and incubated for 30 min in FGM, before being challenged with GlyH-101 and TNF-α for 5, 10, and 30 min in FGM. Changes in relative fluorescent units (ΔRFU) were compared with cells treated with 0.1% DMSO or media alone, as controls for GlyH-101 and TNF-α, respectively, and designated 100% at each time point. In some experiments, the mitochondrial targeting antioxidant MitoQ was added at 1 μM for 30 min in FGM prior to challenge of the cells with GlyH-101 for 5 min. Plates were read at 37°C in 5% CO2, Polar Star Optima plate reader, (BMG Labtech), with excitation at 485 nm and emission at 520 nm. For live cell imaging, dishes were examined on a LSM 710 confocal microscope (ZEISS) with immersion objectives and stage with temperature control, but without atmospheric control.

Hydrogen peroxide (H_2O_2) was measured in HLMVECs seeded at 5×10^4 cells/well/300 μl FGM in wells of 24-well plates, incubated in the absence and presence of 10 μM diphenyleneiodonium chloride (DPI) in FGM for 1 h, before challenge with CFTR inhibitor GlyH-101 (20 μM) and control DMSO (0.1%) for 5, 10, 30 min. Cells were lysed in 125 μl of hypotonic lysis buffer [20 mM NaCl, 1% Triton X-100, 20 mM Tris-base, and pH to 7.4, with protease inhibitors (Calbiochem), and sodium azide (0.1% w/v), to inhibit catalase and peroxidase activity] and H_2O_2 quantified against an H_2O_2 standard in the range 3.125–200 μM using the Amplex Red assay (Chen et al., 2008).

Immunocytochemistry for CFTR, Nrf2, NF-κB and Phospho-c-Jun

HLMVECs, 16HBE or HEK293 cells in collagen-coated eight-well chamber slides were fixed in paraformaldehyde (4%) and permeabilized with Triton X-100 (0.1%). No primary antibody controls were included for each analysis.

For CFTR staining, non-specific antibody-binding sites were blocked with BSA (2%, for 16 h at 4°C) and HLMVECs, 16HBE or HEK293 cells incubated with rabbit anti-CFTR antibody "Mr. Pink" (1/500), followed by goat anti-rabbit antibody conjugated to Alexa Fluor-555 (2 μg/ml; Molecular Probes).

For NF-κB localization, non-specific antibody-binding sites were blocked with rabbit serum (5%, for 1 h) and HLMVECs incubated with mouse anti-p65 (4 μg/ml; Santa Cruz), for 16 h at 4°C, followed by rabbit anti-mouse antibody conjugated to Alexa Fluor-488 (2 μg/ml; Molecular Probes) for 1 h at RT.

For Nrf2 staining, HLMVECs were blocked with 5% goat serum overnight at 4°C, then rabbit polyclonal anti-Nrf2 (Santa Cruz) at 4 μg/ml was added for 1 h at 4°C, followed by Alexa Fluor-555 goat anti-rabbit IgG (2 μg/ml; Molecular Probes) for 1 h at RT.

For phospho-c-Jun staining HLMVECs were blocked with 5% goat serum overnight at 4°C, then rabbit anti-p-c-Jun [(Ser 63/73), Santa Cruz] at 0.8 μg/ml was added for 1 h at 4°C, followed by goat anti-rabbit Alexa Fluor-555 (Molecular Probes) at 2 μg/ml for 1 h at RT.

Nuclei were stained with 5 μg/ml Hoechst 33342 (Molecular Probes) for 10 min, and slides mounted in Fluor-Preserve Reagent for imaging with a LSM 710 confocal microscope (Zeiss).

RNA Extraction and Reverse Transcription

Total RNA was extracted using ReliaPrep RNA Cell Miniprep System (Promega) according to manufacturers' instructions. The concentration and purity (absorbance ratios at 260/230 and 260/280 of ≥2.0) of RNA in samples was determined using a Nanodrop spectrophotometer. RNA was then reverse transcribed into cDNA using the first step of the GoTaq 2-Step RT-qPCR System (Promega) and either stored at −20°C or immediately used in quantitative PCR.

Quantitative Real-Time Polymerase Chain Reaction (qRT-PCR)

Cystic fibrosis transmembrane conductance regulator, IL-8 and β-actin transcripts were amplified from cDNA (1 μg), using the following primers: CFTR (105 bp) sense 5′- ATG CCC TTC GGC GAT GTT TT -3′and antisense 5′- TGA TTC TTC CCA GTA AGA GAG GC -3′;

IL-8 (194 bp) sense 5′- TTT TGC CAA GGA GTG CTA AAG A -3′ and antisense 5′- AAC CCT CTG CAC CCA GTT TTC -3′: and β-actin (93 bp) sense 5′- CGC GAG AAG ATG ACC CAG AT -3′ and antisense 5′- GCC AGA GGC GTA CAG GGA TA -3. The cycles for the qRT-PCR were: 2 min at 95°C, then 35 cycles for quantitation of IL-8 expression and 40 cycles for detection of CFTR mRNA of 10 s at 95°C, 20 s at 62°C, and 60 s at 72°C. Data were collected using a LightCycler 96 (Roche Diagnostics International Ltd.).

For nested or two-step, quantitative PCR, a 526 bp region of CFTR was first amplified using primers: sense 5′- ACA GCG CCT GGA ATT GTC AGA C -3′and antisense 5′- AGC GAT CCA CAC GAA ATG TGC C -3′, followed by a second round of amplification using the CFTR-specific primers and conditions used in the single-step quantitative PCR.

To exclude the possibility of amplification from contaminating genomic DNA during the qRT-PCR reaction, we utilized a DNAse step in the ReliaPrep protocol during mRNA extraction, and primers were designed to span at least one or more large (>20,000 bp) introns, precluding amplification from genomic DNA directly. Negative control reactions, not including template cDNA (no template control) or reverse transcriptase ("-RT," or no amplification control), were also performed and accepted when the threshold value (Ct) was at least five cycles greater than the experimental amplifications. Measurements were performed in duplicate and accepted if the difference between the Ct values of the duplicates was less than 1. The generation of a single product of appropriate size was routinely checked by the presence of a single melt peak and by agarose gel electrophoresis. Data were analyzed using Roche LightCycler software. A relative expression method was implemented, normalizing the data by the internal control β-actin and expressing the final result relative to the control group.

Electroporation and CFTR Silencing

Electroporation were used to introduce small interfering RNA to target the CFTR gene in HLMVECs. HLMVECs (0.75 × 106) were suspended in 100 μl of OptiMEM medium and transferred to a sterile cuvette for the NEPA21 electroporator (NepaGene) and 2 μl of siRNA for CFTR or validated non-targeting siRNA pool (50 μM) was added to a final concentration of 1 μM. For CFTR siRNA (ON-TARGET plus Human CFTR (1080) siRNA-SMART pool (Dharmacon) was used, which consists of a mixture of four siRNA with target sequence as the following:

1-GAACACAUACCUUCGAUAU
2-GUACAAACAUGGUAUGACU
3-GUGAAAGACUUGUGAUUAC
4-GCAGGUGGGAUUCUUAAUA

The cells were electroporated according to the pulse settings in **Table 1**.

After electroporation cells were transferred to the wells of a collagen-coated 6 well plate at a final concentration of 1.5 × 106 cell/well/2 ml of FGM. The medium then was changed every 24 h, for a total of 72 h, then the supernatants for the last 24 h were harvested and processed and used to analyze IL-8 concentrations by ELISA.

Statistical Analysis

Statistical analysis was carried out using GraphPad Prism version 8. Data is presented graphically as mean ± SEM, and analyzed by one-way or two-way ANOVA with two-tailed *post hoc* tests for multiple comparisons as appropriate and as indicated in the Figure legends. A directional one-tailed *t*-test was applied in the case of the hypothesized increase in CFTR expression following inhibition of CFTR activity (**Figure 1F**). Multiplicity adjusted *p* values are given in the text to four decimal places.

The relative effect size, Cohen's d, was determined by calculating the mean difference between two groups and dividing the result by the pooled standard deviation. Cohen's $d = (M_2 - M_1)/SD_{pooled}$, where:

$SD_{pooled} = \sqrt{((SD_1{}^2 + SD_2{}^2)/2)}$, and Cohen's $d > 0.8$ is considered a large effect size.

RESULTS

CFTR Expression

Western blotting and RT-PCR were used to confirm CFTR expression in HLMVEC under the cell culture conditions used

TABLE 1 | Electroporation pulse settings.

Poring pulse						Transfer pulse					
V	Length ms	Interval ms	No.	D. Rate (%)	Polarity	V	Length ms	Interval ms	No.	D. Rate (%)	Polarity
170	2.5	50	2	10	+	20	50	50	5	40	±

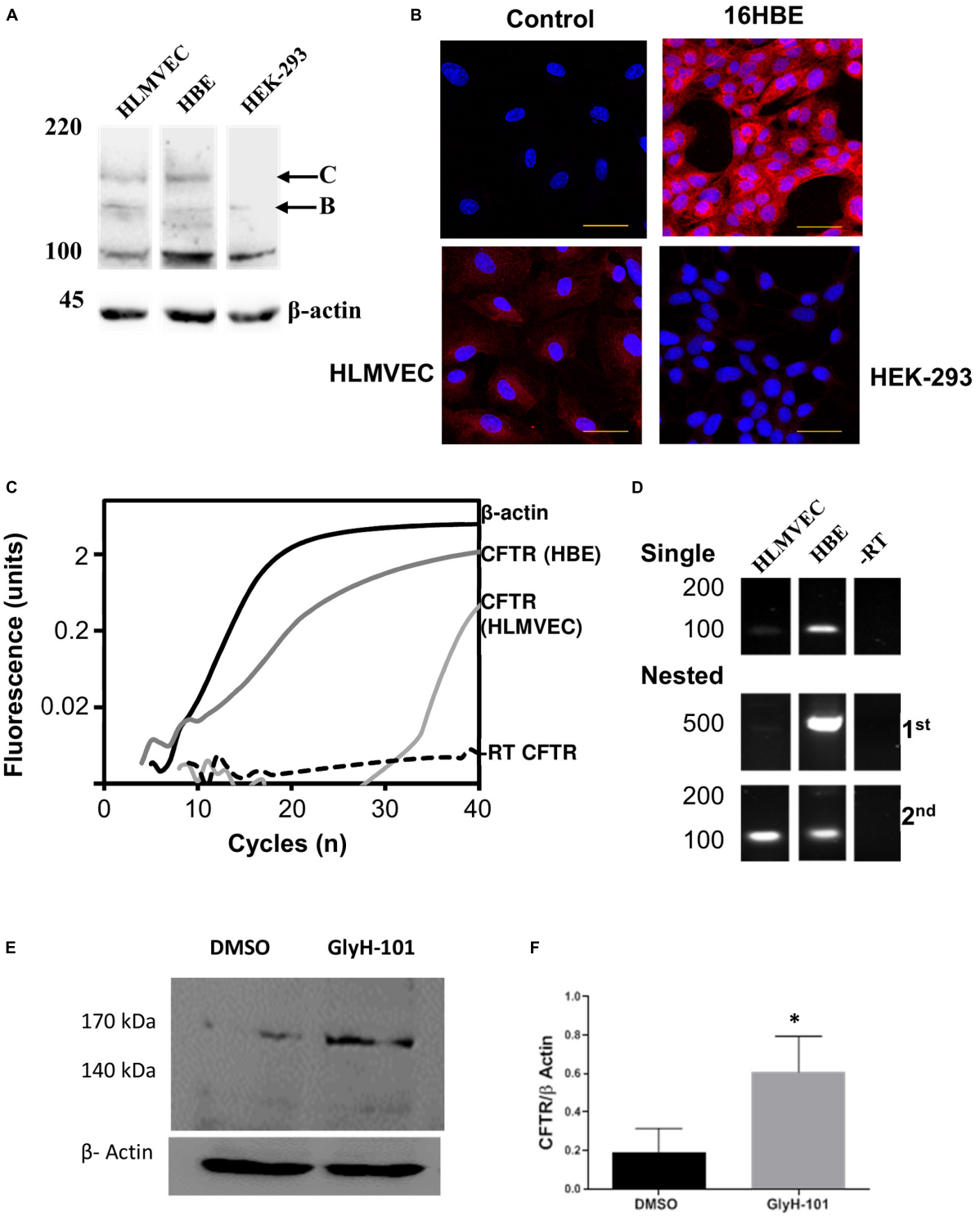

FIGURE 1 | CFTR expression in HLMVECs. **(A)** Immunoblot of CFTR in whole cell extracts of HLMVEC, 16HBE and HEK-293 cells. All data are representative of that obtained in at least three independent experiments. **(B)** Immunolocalization of CFTR in HLMVEC, 16HBE and HEK-293 cells (the control refers to the no-primary antibody negative control). All images were acquired and displayed under identical conditions. **(C)** RT-PCR amplification of CFTR (light gray), β-actin (solid) and reverse-transcription negative control (-RT CFTR, dotted line) in HLMVECs, and CFTR in 16HBE cells (positive control, dark gray). **(D)** Gel analysis of CFTR cDNA amplified from HLMVEC, 16HBE mRNA and -RT control following single and nested RT-PCR. **(E,F)** CFTR expression in HLMVECs cell lysate by western blot after 16 h incubation with GlyH-101 (20 μM) and DMSO (0.1%) vehicle control. Data were normalized to β-actin, numbers expressed as average of three independent experiments. Each experiment was conducted on HLMVECs obtained from three different donors (*$p < 0.05$ for the difference between GlyH-101 and control). The scale bar represents 50 μm.

in these experiments, including growth on collagen IV coated cultureware. CFTR could be detected on western blot as two high molecular weight bands in HLMVEC lysates, the partially glycosylated band B (140 kDa) and fully mature band C (170 kDa) (**Figure 1A**). However, the level of expression was highly variable between preparations. In separate experiments, the same CFTR protein bands were detected in 16HBE, but not in HEK293 cells. Levels of CFTR detected by IHC appeared to be lower in HLMVECs than in the 16HBE bronchial epithelial cell line and, in addition to the plasma membrane, CFTR was detected in association with intracellular organelles possibly the endoplasmic reticulum around the nucleus (**Figure 1B**). Additionally, expression of CFTR mRNA was detected in HLMVECs (ΔCT = 25.35 $\pm$ 0.55, n = 3), although at much lower levels that in 16HBEs (ΔCT = 3.78 $\pm$ 0.53, n = 3; $p < 0.0001$), when normalized to housekeeping β-actin expression at threshold of 0.02 ΔRFU (**Figure 1C**). The expression of CFTR mRNA In HLMVECs was confirmed by nested PCR (**Figure 1D**) which increased the intensity of the expected 100 bp CFTR product observed in single round PCR while the expected 500 bp product was faintly detected.

In view of previous reports of the negative regulation of CFTR expression by CFTR activity (Wang et al., 2016), we tested the hypothesis that CFTR inhibition would increase CFTR expression. Indeed, the abundance of CFTR in cells treated for 16 h with GlyH-101 (20 μM) was significantly higher (p = 0.035, one-tailed t-test) with a large effect size (Cohen's d = 1.55) compared to control cells treated with DMSO (0.1%) (**Figures 1E,F**).

GlyH-101 and HLMVEC Viability

In order to investigate the effect of the CFTR inhibitor and the vehicle control on metabolic activity as a measure of cell cytotoxicity, cells were grown in medium (FGM) alone, or incubated with GlyH-101 (5, 10, 20 μM) or DMSO (0.1%), as the vehicle control, for the times indicated (**Figure 2**) and metabolic activity measured using the MTT assay. Data was normalized to the metabolic activity of cells grown in medium alone. Incubation of cells with GlyH-101 at concentrations of 5–20 μM for up to 24 h had no significant effect on HLMVEC metabolic activity (MTT reduction) compared to the vehicle control (**Figure 2**). After 48 h incubation with the highest (20 μM) GlyH-101 concentration, the significant (p = 0.002) decrease in MTT reduction (74.2 $\pm$ 15.4%) compared with the DMSO control (123.6 $\pm$ 22.0%) was associated with a reduction in the number of cells adherent to the plate. Experiments using GlyH-101 to inhibit CFTR were therefore conducted over periods of up to 24 h.

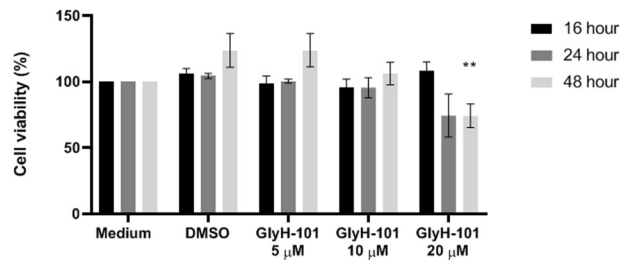

FIGURE 2 | Effect of GlyH-101 on HLMVEC viability. HLMVECs were grown in FGM medium alone (medium), or treated for 16, 24, and 48 h with CFTR inhibitor GlyH-101 at 5, 10, and 20 μM or 1% DMSO as vehicle control. Results were normalized for the cells grown in medium alone, and data for the effect of GlyH-101 compared with DMSO (0.1%) vehicle control data. Data were expressed as mean ± SEM (**p value < 0.01 comparing GlyH-101 (20 μM) to DMSO (0.1%) at 48 h, n = 3 independent experiments). Data were analyzed with two-way ANOVA and Tukey's multiple comparison test.

CFTR Activity

Cystic fibrosis transmembrane conductance regulator activity was detected as membrane depolarization at baseline, and in response to IBMX plus forskolin leading to increased uptake and fluorescence of intracellular FLIPR Blue, that could be inhibited by GlyH-101 (Maitra et al., 2013). The significant (p = 0.0002) inhibitory effect (Cohen's d = 1.32) of GlyH-101 on control cells indicates constitutive activity of CFTR in HLMVECs (**Figure 3A**). This was not seen in HEK293 cells used as a negative control or 16HBE cells used as a positive control. The cAMP-elevating agent forskolin (an adenylate cyclase activator) together with IBMX (a cAMP-phosphodiesterase inhibitor) strongly ($p < 0.0001$) stimulated HLMVEC membrane depolarization in all cells (**Figure 3B**, black bars) compared to baseline (**Figure 3A**, black bars). CFTR activity was measured as the increase in membrane depolarization (increase in Δ RFU) that was significantly inhibited by GlyH-101 (20 μM) (**Figure 3B**, gray bars). In HLMVEC, GlyH-101 significantly (p = 0.0495) inhibited membrane depolarization by 34% (Cohen's d = 1.17). The depolarization response of 16HBE cells was significantly (p = 0.0095) greater than that of HLMVECs and was significantly (p = 0.0068) inhibited 26.4% (Cohen's d = 1.08) by GlyH-101. This decrease in fluorescence was attributed to inhibition of CFTR activity. HEK293 cells that do not express CFTR (Friard et al., 2017) showed a greater depolarization in response to forskolin/IBMX than HLMVECs, but there was no significant inhibitory effect of GlyH-101 (**Figure 3B**) and no effect on unstimulated control cells (**Figure 3A**).

CFTR and Oxidative Stress

In view of previous reports of the effect of dysfunctional epithelial CFTR on increased intracellular H_2O_2 (Chen et al., 2008), we investigated the effect of CFTR inhibition on the generation of intracellular ROS and, specifically, H_2O_2 levels. Using live-cell imaging, low levels of intracellular ROS were observed at time zero, which increased over 30 min after treating the cells with GlyH-101 (**Figure 4A**). However, using a quantitative approach to measuring ROS generation, a faster response was detected in stimulated cells compared to unstimulated control cells (**Figure 4B**). The slower response during live cell imaging may reflect the absence of atmospheric control during the experiment.

Both TNF-α, included as a positive control, and GlyH-101 induced a significant (p = 0.0012 and p = 0.0004, respectively) increase in ROS of 165.2 $\pm$ 35.1% and 170 $\pm$ 11.5% compared to unstimulated control cells at 5 min. The response to GlyH-101 was sustained over 30 min and was significantly higher than the response to TNF-α at 10 and 30 min (p = 0.003 and p = 0.0173,

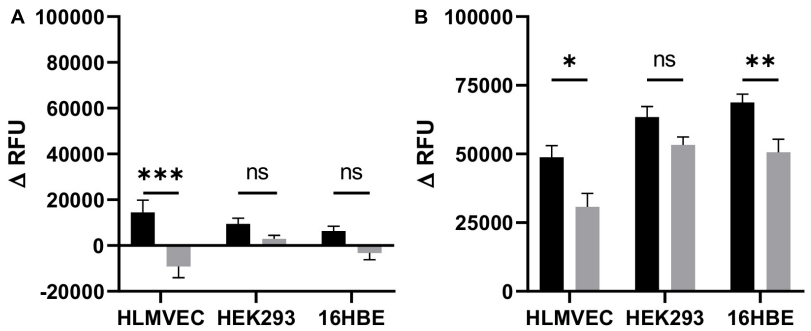

FIGURE 3 | CFTR activity in HLMVECs at baseline and following cAMP-dependent activation. CFTR activity was measured at baseline **(A)** and following cAMP-dependent activation **(B)** of HLMVECs, non-CFTR expressing HEK-293 cells and CFTR expressing 16HBE cells for comparison. CFTR activity at baseline was measured as a decrease in relative fluorescence units (ΔRFU) following treatment of cells with the CFTR inhibitor GlyH-101 (20 μM, gray bars), reflecting membrane hyperpolarization and decreased uptake of FLIPR compared to cells treated with 0.1% DMSO vehicle control (black bars). Activation of CFTR **(B)** was measured as an increase in fluorescence (ΔRFU) following membrane depolarization of HLMVECs, HEK-293, and 16HBE cells activated with forskolin (100 μM) plus IBMX (1000 μM) (F/I) for 2 min in the absence (black bars) and presence (gray bars) of GlyH-101 (n = 3 independent experiments, each carried out in quadruplicate). Data were analyzed by two-way ANOVA and Holm-Sidak multiple comparisons test (*$p < 0.05$, **$p < 0.01$, ***$p < 0.001$ for the comparisons indicated).

respectively), while the response to TNF-α was back to control levels at 10 min (**Figure 4B**).

N-acetyl cysteine (10 mM), added 3 h before GlyH-101, had no effect on ROS production at 5 and 10 min following stimulation with GlyH-101. After 10 min, ROS production in response to GlyH-101 was 164.5 ± 9.9% of the control value, and in the presence of NAC was still 156.9 ± 50% of the control value ($n = 6$). However, NAC (10 mM) not only reversed the effect of GlyH-101 on ROS levels at 30 min, but also significantly ($p = 0.005$) reduced the level of ROS to 42.8 ± 28.1% fluorescence intensity, below that observed in control cells (**Figure 4B**).

H2DFFDA detects intracellular oxidative stress rather than a specific reactive species (Eruslanov and Kusmartsev, 2010). We therefore measured H_2O_2, one of the major ROS in cells. H_2O_2 was not detected in supernatants, but intracellular H_2O_2 was significantly ($p = 0.0022$) increased (Cohen's $d = 4.39$) following 30 min treatment with GlyH-101 (36.1 ± 2.7 μM) compared to control (13.2 ± 2.5 μM), with no significant changes at earlier time points (**Figure 4C**). Incubation of cells with 10 μM DPI for 1 h prior to and during GlyH-101 challenge had no effect on H_2O_2 concentrations.

Intracellular SOD-2 protein levels were significantly increased at 16 h ($p = 0.05$, Cohen's $d = 1.58$) and at 24 h ($p = 0.0054$, Cohen's $d = 2.63$) following CFTR inhibition (**Figure 4D**). No significant changes in catalase protein levels were observed over 24 h (data not shown).

The staining pattern observed during live cell imaging of ROS was punctuate (**Figure 4A**), which suggested a mitochondrial source of ROS. However, the mitochondrial-targeting antioxidant MitoQ had no effect in HLMVEC or 16HBE cells on ROS production, measured as a change in ΔRFU of carboxy-H2DFFDA over 5 min following challenge with GlyH-101 (**Figures 4E,F**). GlyH-101 induced a significant increase in ROS in HLMVECs in the absence ($p = 0.0043$, Cohen's $d = 1.65$) and presence ($p = 0.0042$) of MitoQ, and in the 16HBE bronchial epithelial cell line in the absence ($p = 0.0275$, Cohen's $d = 1.3$) and presence ($p = 0.0474$) of MitoQ, which had no significant effect.

CFTR and Nrf-2 Expression

Chen et al. (2008) reported significantly reduced Nrf2 expression in CF epithelia and in normal epithelial cells treated with the CFTR inhibitor $CFTR_{inh}$-172 (Chen et al., 2008). Therefore, Nrf2 expression in HLMVECs was investigated following CFTR inhibition with GlyH-101 (20 μM) for up to 24 h. IHC demonstrated that Nrf2 was mostly absent from the cytoplasm after 24 h incubation with GlyH-101, compared to control cells (**Figure 5A**). The overall abundance of Nrf2 was significantly ($p = 0.0425$) decreased at 6 h and had decreased further still at 16 h ($p = 0.0032$) and by 70.8 ± 11.6% at 24 h, ($p = 0.0034$, Cohen's $d = 4.82$), compared to control cells (**Figures 5B,C**).

CFTR and VEGF Expression

Since ROS induce the expression of endothelial VEGF (Kim and Byzova, 2014), we investigated the effect of GlyH-101 on VEGF levels in HLMVEC culture supernatants. Initial experiments established that GlyH-101 (5, 10, 20 μM) increased endothelial VEGF expression over 16 h, with a significant effect at 20 μM GlyH-101 (**Figure 6**), but not at lower concentrations (data not shown). GlyH-101 (20 μM) significantly ($p = 0.0375$, Cohen's $d = 2.95$) increased VEGF concentration in the supernatants (202.1 ± 22.1 pg/ml) compared to control (74.24 ± 11.8 pg/ml) over 16 h (**Figure 6A**). TNF-α, alone, did not have a significant effect on VEGF levels, but further significantly ($p = 0.0019$, Cohen's $d = 2.01$) increased the VEGF response to GlyH-101 to 394.5 ± 50.4 pg/ml. Treatment of cells with NAC (5 mM) significantly ($p = 0.0056$) reduced VEGF levels in the presence of GlyH-101 plus TNF-α to 105.6 ± 21.8 pg/ml, which was thus found not significantly higher than control levels (data not presented graphically).

In cultured airway epithelial cells, treatment with CFTR inhibitors triggered EGFR phosphorylation and activation that was required for VEGF synthesis (Martin et al., 2013). We therefore investigated the effect of EGFR inhibition on VEGF synthesis in HLMVECs. Pre-treatment with the EGFR tyrosine

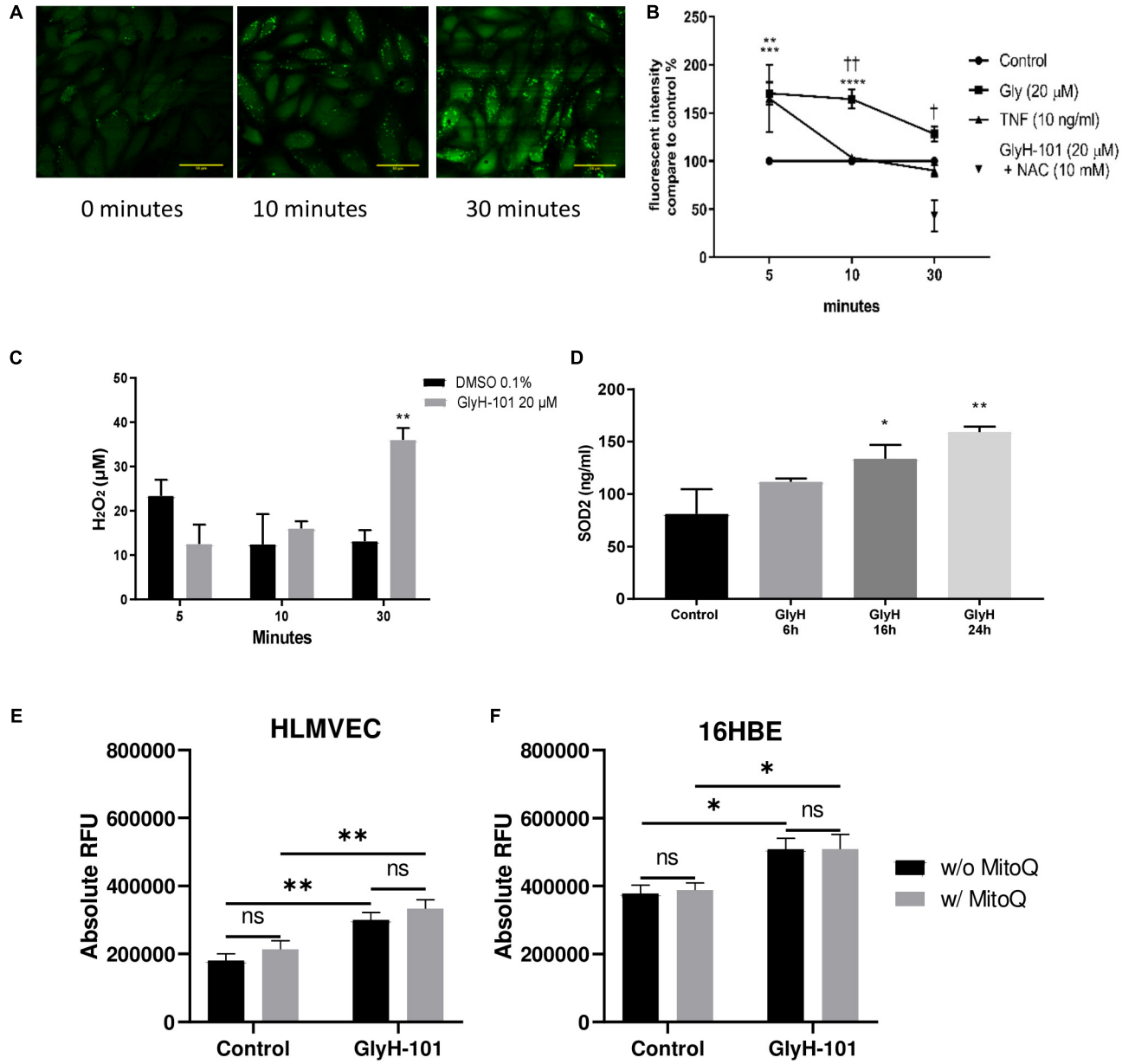

FIGURE 4 | Oxidative stress in HLMVECs following CFTR inhibition with GlyH-101. **(A)** Intracellular ROS in HLMVECs using live cell imaging. Intracellular ROS in HLMVECs detected using carboxy H2-DFFDA. GlyH-101 (20 μM) was added and the fluorescence detected at 0, 10, and 30 min. Scale bar 50 μm. Images representative of duplicate wells in a single experiment. **(B)** Quantification of intracellular ROS in HLMVECs using carboxy-H2DFFDA. HLMVECs were incubated for 5–30 min in the absence and presence of GlyH-101 (20 μM) and TNF-α (10 ng/ml) and ROS detected by intracellular DFFDA. The experiments were conducted in triplicate, $n = 6$ independent experiments for GlyH-101 in the absence and presence of 10 mM NAC, and $n = 3$ for TNF-α. Control values at each time point were designated 100% (filled circles). Data points represent the mean ± SEM. Results were analyzed with two-way ANOVA and Tukey's multiple comparisons test. (**** p value < 0.0001, *** p value < 0.001) comparing GlyH-101 to control and (** p value < 0.01) comparing TNF-α to control, (††, p value < 0.01, † p value < 0.05 comparing GlyH-101 and TNF-α). **(C)** Quantification of intracellular H_2O_2 using Amplex Red. HLMVECs were treated with GlyH-101 for 5–30 min, and H_2O_2 measured in cell lysates using Amplex Red reagent. ** p value < 0.01 in comparison to DMSO after 30 min, ($n = 4$). Data were expressed as average ± SEM and analyzed with two way ANOVA and Tukey's *post hoc* test. **(D)** Intracellular SOD2. SOD2 was measured by ELISA in HLMVECs cell lysates following CFTR inhibition with GlyH-101 (20 μM). Data were analyzed with one way ANOVA and Dunnett's test, $n = 3$ (* $p < 0.05$, ** p value < 0.01 compared to DMSO control at 24 h). **(E)** Quantification of intracellular ROS in HLMVECs using carboxy-H2DFFDA. HLMVECs were incubated for 30 min with/without MitoQ (1 μM) followed by 5 min incubation with GlyH-101 (20 μM) and ROS detected by intracellular DFFDA. The experiments were conducted in quadruplicate, $n = 3$ independent experiments. (** p value < 0.01 for the comparisons indicated). Data were analyzed by two-way ANOVA with Tukey's multiple comparison *post hoc* test. RFU, relative fluorescence units. **(F)** Quantification of intracellular ROS in 16HBEs using carboxy-H2DFFDA. 16HBEs were incubated for 30 min with/without MitoQ (1 μM) followed by 5 min incubation with GlyH-101 (20 μM) and ROS detected by intracellular DFFDA. The experiments were conducted in quadruplicate, $n = 3$ independent experiments. (* $p < 0.05$ for the comparisons indicated). Data were analyzed by two-way ANOVA with Tukey's multiple comparison *post hoc* test. RFU, relative fluorescence units.

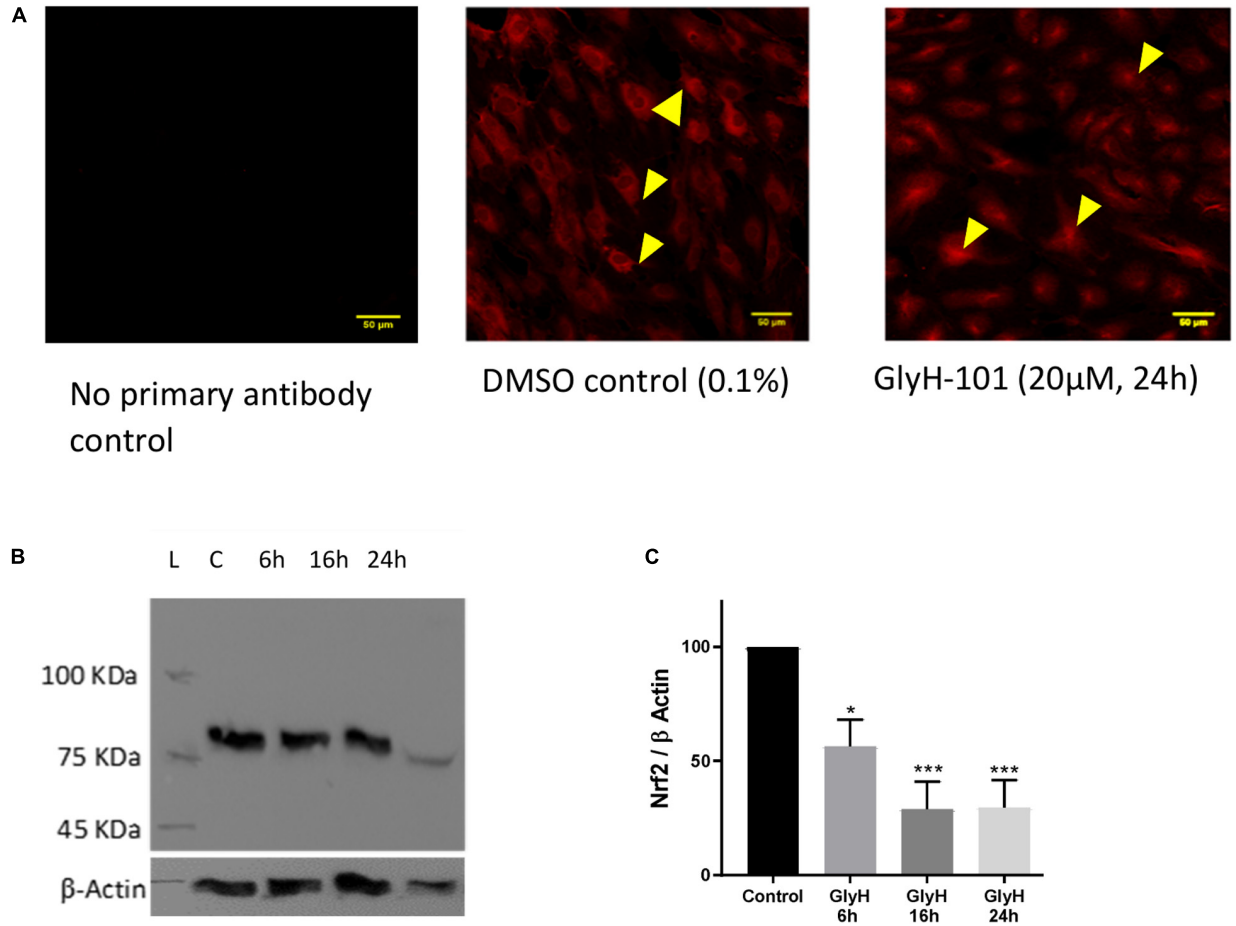

FIGURE 5 | The effect of CFTR inhibition on Nrf-2 expression. The effect of CFTR inhibition on Nrf2 expression in HLMVECs over 24 h was investigated by immunocytochemistry **(A)** and by western blot **(B,C)**. **(A)** CFTR inhibition by GlyH-101 (20 μM) results in loss of cytosolic Nrf2 (arrows in control) with residual Nrf2 in nuclei. Scale bar 50 μm. Images are representative of two independent experiments. **(B,C)** Nrf2 was detected on western blot as an 85 kDa band in control cells (lane C) at 24 h **(B)**, this value was significantly reduced by 70% with GlyH-101 over 24 h **(C)**. Bars indicate mean ± SEM (* $p < 0.05$, *** p value < 0.001) for comparison with 24 h control, $n = 3$ independent experiments. Data were analyzed by one-way ANOVA with Dunnett's *post hoc* test.

kinase inhibitor AG1478 (10 μM) caused a non-significant increase in VEGF levels at 16 h (results not shown). However, a significant ($p < 0.0001$) increase in VEGF (481.6 ± 59.2 pg/ml) was seen following EGFR inhibition with AG1478, alone, compared to control (13.48 ± 2.9 pg/ml) over 24 h (**Figure 6B**). Although GlyH-101 alone had no significant effect on VEGF synthesis over 24 h, AG1478 increased VEGF synthesis in the presence of GlyH-101 ($p < 0.0001$), and in the presence of both the CFTR inhibitor and EGFR inhibitor VEGF levels were 598.8 ± 63.7 pg/ml. Addition of TNF-α to GlyH-101 at this time point induced a small significant ($p = 0.046$) increase in VEGF levels, and addition of AG1478 further significantly ($p < 0.0001$) increased VEGF levels in the presence of GlyH-101 plus TNF-α.

CFTR and IL-8 Expression

Functional CFTR was reported to limit bronchial epithelial expression of IL-8 (Perez et al., 2007). We therefore investigated the effect of CFTR inhibition on IL-8 expression by HLMVECs. Control, unstimulated, HLMVECs expressed IL-8 that was predominantly in soluble form and released into supernatants (**Figure 7A**). The CFTR inhibitor GlyH-101 (20 μM) significantly increased IL-8 protein levels in both supernatants ($p = 0.0359$) and HLMVEC cell lysates ($p = 0.0234$) (**Figure 7A**). This effect was not seen with GlyH-101 added at 5 μM and 10 μM. IL-8 concentrations were significantly ($p < 0.0001$) higher in supernatants than lysates under all conditions. TNF-α (10 ng/ml) further significantly ($p < 0.0001$) increased IL-8 levels in the presence of GlyH-101 (20 μM) in both fractions over 16 h. In the presence of TNF-α, GlyH-101 (20 μM) significantly increased IL-8 levels in cell lysates ($p = 0.0193$) and supernatants ($p = 0.0047$) compared to TNF-α alone.

Over a 24-h time course, TNF-α (10 ng/ml) and the combination of TNF-α (10 ng/ml) plus GlyH-101 (20 μM) significantly ($p < 0.0001$) increased supernatant IL-8 levels at both 16 h and 24 h (**Figure 7B**). The response to TNF-α alone plateaued at 16 h (**Figure 7B**), but the combination of GlyH-101 plus TNF-α significantly increased IL-8 levels at 16 h ($p = 0.0043$) and at 24 h ($p < 0.0001$) compared to the effect of TNF-α alone.

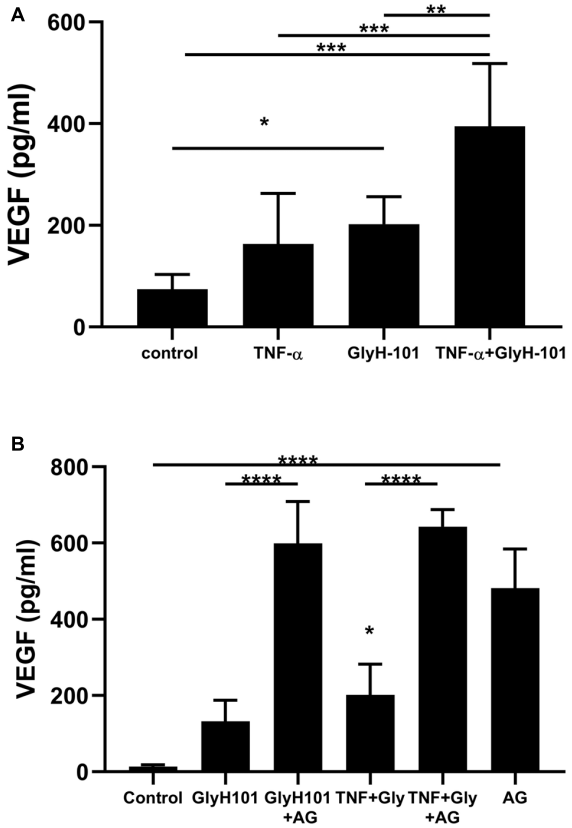

FIGURE 6 | The effect of CFTR inhibition on VEGF concentrations in HLMVEC culture supernatants. **(A)** VEGF concentration after 16 h CFTR inhibition with GlyH-101 (20 μM), in the absence and presence of TNF-α (10 ng/ml). VEGF was measured by ELISA, and concentrations expressed as average ± SEM (* p value < 0.05, ** p value < 0.01, *** p value < 0.001 for the comparisons indicated). Data were analyzed with one-way ANOVA test and Tukey's multiple comparison test, n = 6 independent experiments, each carried out in triplicate. **(B)** The effect of AG1478 on VEGF concentration alone, and after 24 h CFTR inhibition with GlyH-101 (20 μM) in the absence and presence of TNF-α. VEGF was measured by ELISA, and concentrations expressed as average ± SEM (**** p value < 0.0001 for the comparisons indicated, * p value < 0.05 for TNF + Gly compared to the control value). Data were analyzed with one-way ANOVA test and Tukey's multiple comparison test, n = 3 independent experiments, each carried out in triplicate.

AG1478 (10 μM) and NAC (5 mM) significantly (p = 0.0028 and p = 0.0444, respectively) inhibited the response to the combination of TNF-α plus GlyH-101 at 24 h.

The increase in protein concentration mirrored the increase in IL-8 mRNA expression following 16 h incubation with GlyH-101 (20 μM) and TNF-α (10 ng/ml), alone and in combination (**Figure 7C**). The normalized relative expression of IL-8 mRNA was significantly (p = 0.0258, Cohen's d = 17.82) increased in the presence of GlyH-101 alone. GlyH-101 also further significantly (p = 0.0004, Cohen's d = 3.72) enhanced the response to TNF-α.

Specificity of GlyH-101

Melis et al. (2014) reported non-specific inhibitory effects of GlyH-101 on volume-sensitive outwardly rectifying chloride conductance (VSORC), also termed volume-regulated anion channel current (VRAC), and calcium-activated chloride conductance (CaCC) in murine cell lines expressing CFTR (Melis et al., 2014). More recently, Friard et al. (2017) also reported inhibitory effects of GlyH-101 on VRAC conductance in the immortalized human embryonic kidney cell line, HEK-293 cells, with an IC_{50} of 9.5 μM and 80% inhibition at 20 μM (Friard et al., 2017).

HEK-293 cells, unlike endothelial cells, do not express CFTR or the calcium-activated chloride ion channels anoctamin-1 and anoctamin-2 (ANO1/2, also termed TMEM16A and TMEM16B, respectively) (Friard et al., 2017). Therefore to investigate whether the pro-inflammatory effects of GlyH-101 effects on HLMVEC were due to inhibitory effects on VRAC activity, HEK-293 cells were incubated with 20 μM GlyH-101 for 24 h and IL-8 levels measured in cell culture supernatants. Because HEK-293 cells express moderate levels of endogenous TNFα receptors (Greco et al., 2015), TNFα (10 ng/ml) was used as a positive control. TNFα (10 ng/ml) significantly (p < 0.0001, Cohen's d = 42.1) increased IL-8 concentrations in HEK-293 cell culture supernatant compared to control levels (**Figure 8A**), whereas GlyH-101 had no effect, indicating that effects of GlyH-101 on IL-8 expression are not mediated by VRAC.

This was confirmed using the potent (IC_{50} 4.8 μM) and specific VRAC inhibitor DCPIB (4-(2-butyl-6,7-dichlor-2-cyclopentyl-indan-1-on-5-yl) oxybutyric acid (Friard et al., 2017), in cultures of HLMVECs with GlyH-101 (20 μM) and TNFα (10 ng/ml) as positive controls. Both TNFα (p < 0.0001, Cohen's d = 16.73) and GlyH-101 (p = 0.017, Cohen's d = 4.7) significantly increased IL-8 in culture supernatants, but DCPIB at 20 μM had no effect (**Figure 8B**).

Additionally, the potent (IC_{50} 77 nM) TMEM16A-specific inhibitor Ani9 (2-(4-chloro-2-methylphenoxy)-N-[(2-methoxyphenyl)methylideneamino]-acetamide), that lacks inhibitory activity against CFTR and VRAC (Seo et al., 2016) did not induce significant IL-8 expression by HLMVECs at the relatively high concentration of 10 μM (**Figure 8B**).

Effect of CFTR Gene Silencing

The anti-inflammatory function of endothelial CFTR was confirmed using a siRNA approach to CFTR gene silencing. A significantly (p = 0.041, Cohen's d = 1.84) higher concentration of IL-8 was measured in the supernatants of HLMVECs transfected with CFTR siRNA compared with cells transfected with non-targeting siRNA. The non-targeted cells yielded 160.01 ± 17.2 pg/ml IL-8 in HLMVEC supernatants, while silencing of CFTR (siCFTR) in HLMVECs gave 265.4 ± 36.7 pg/ml IL-8 in the supernatant (**Figure 9**) confirming constitutive CFTR activity in HLMVECs.

CFTR and Inflammatory Cell Signaling

Functional CFTR was reported to be a negative regulator of NF-κB and inflammatory cell signaling (Vij et al., 2009). We therefore investigated the effect of CFTR inhibition on activation of NF-kB and AP-1, two key ROS-dependent signaling pathways leading to IL-8 expression (Hoffmann et al., 2002), with TNF-α (10 ng/ml) as a positive control stimulus. While TNF-α

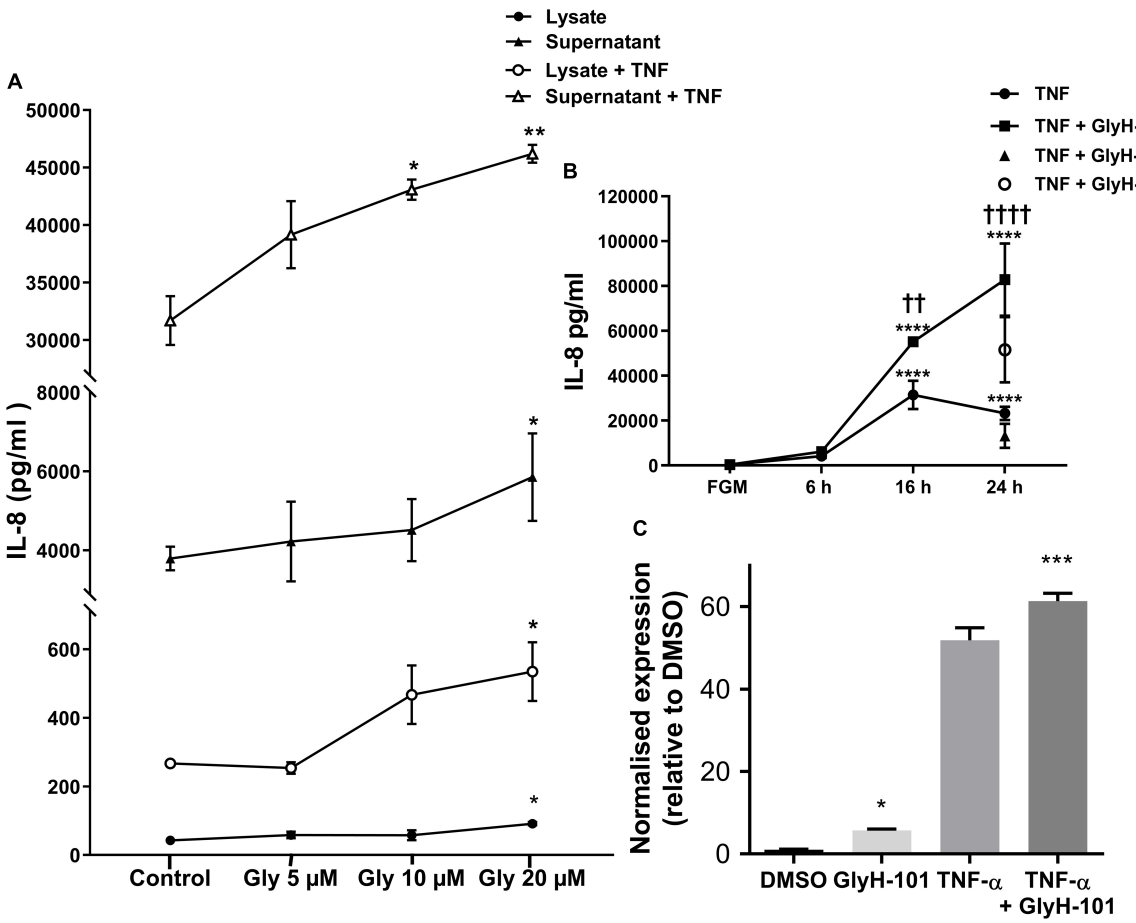

FIGURE 7 | IL-8 in HLMVEC cells and supernatants. **(A)** Concentration response curve for CFTR inhibitor GlyH-101 in the absence and presence of TNF-α (10 ng/ml) for 16 h. GlyH-101 at 20 μM significantly increased IL-8 in supernatant, cell lysate, with and without TNF-α (* $p < 0.05$, ** $p < 0.01$) comparing GlyH-101 with control for each condition using one-way ANOVA ($n = 3$). **(B)** Time course for the effect of TNF-α (10 ng/ml) alone and in the presence of GlyH-101 (20 μM) on IL-8 levels in HLMVEC supernatants. (**** $p < 0.0001$ compared to 24 h control, FGM), (†† value < 0.01, † † †† value < 0.0001 compared to TNF-α alone), ($n = 3$). AG1478 (10 μM, filled triangle) and NAC (5 mM, open circle) significantly ($p < 0.01$ and $p < 0.05$, respectively) inhibited the response to the combination of TNF-α plus GlyH-101 at 24 h. Numbers were expressed as mean ± SEM. The data were analyzed with two-way ANOVA and Tukey's multiple comparison test, or one-way ANOVA for the effects of AG1478 and NAC on the response to the combination of TNF-α plus GlyH-101. **(C)** Relative changes in IL-8 mRNA levels normalized to β-actin (2-delta delta Ct values), following 16 h incubation with GlyH-101 (20 μM) and TNF-α (10 ng/ml), alone and together, compared to DMSO (0.1%) control, $n = 3$. (* $p < 0.05$ comparing GlyH-101 with DMSO control, and *** $p < 0.001$ comparing TNF-α + GlyH-101 with TNF-α alone).

clearly stimulated nuclear translocation of the NF-kB p65 subunit (**Figure 10A**, panel 2), CFTR inhibition with GlyH-101 (20 μM) had no effect (**Figure 10A**, panel 3). However, both GlyH-101 and TNF-α significantly ($p = 0.0326$ with Cohen's $d = 1.86$ and $p = 0.035$ with Cohen's $d = 2.37$, respectively) increased phosphorylation of the AP-1 c-Jun subunit (**Figures 10C1,C2**) and significantly ($p = 0.0476$ with Cohen's $d = 1.96$, and $p = 0.0094$ with Cohen's $d = 1.99$, respectively) increased its nuclear translocation (**Figures 10B,D**).

DISCUSSION

Summary of Key Findings

We have shown that lung microvascular endothelial cells respond to CFTR inhibition with significantly increased levels of ROS, increased IL-8, VEGF and SOD-2 expression, and a significant 70% decrease in Nrf2 protein levels. GlyH-101, a CFTR-specific inhibitor, increased IL-8 expression via ROS-dependent activation of AP-1 signaling with increased nuclear phospho-c-Jun in HLMVECs, but no evidence of NF-κB activation. Further, CFTR inhibition enhanced TNFα-stimulated IL-8 expression, which occurs via both AP-1 and NF-κB signaling pathways. We show that dysfunctional CFTR enhanced EGFR-dependent expression of IL-8, which was inhibited using the EGFR tyrosine kinase specific inhibitor AG1478. Conversely, the increased expression of VEGF following CFTR inhibition was significantly enhanced in the presence of AG1478, and in this respect these endothelial cells differ from airway epithelial cells. Overall, the data indicate that suppression of endothelial CFTR activity activates production of intracellular ROS, and ROS-dependent signaling cascades leading

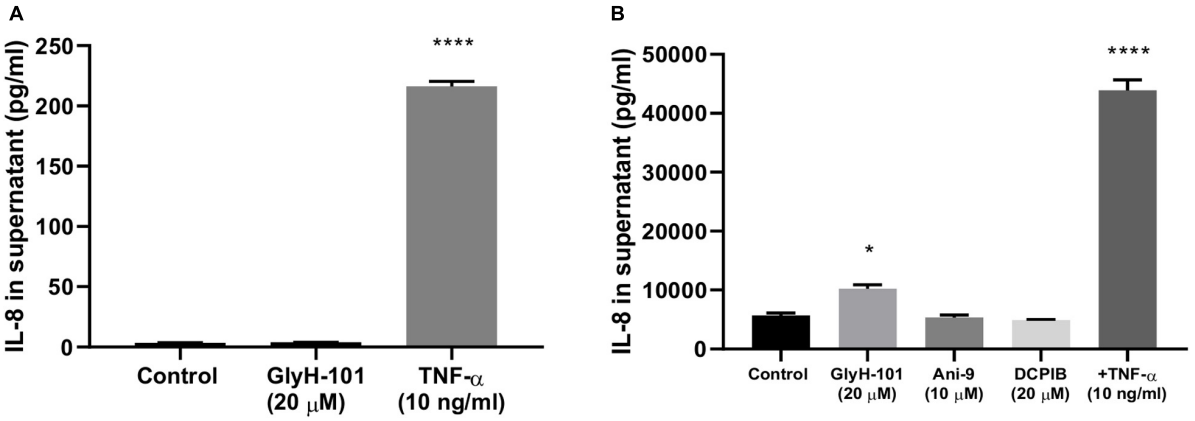

FIGURE 8 | CFTR-specific inhibition mediates pro-inflammatory effects in HLMVECs. **(A)** non-CFTR expressing HEK-293 cells were incubated with GlyH-101 (20 μM) and TNF-α (10 ng/ml) as a positive control, and IL-8 was measured in culture supernatants by ELISA ($n = 3$) (**** $p < 0.0001$ compared to control). **(B)** HLMVECs were cultured for 24 h in the absence and presence of the CFTR inhibitor GlyH-101 (20 μM), the calcium-activated chloride ion channel Transmembrane Member 16A (TMEM16A)-specific inhibitor Ani-9 (10 μM), the Volume-Regulated Anion Channel (VRAC)-specific inhibitor DCPIB (20 μM) and TNF-α (10 ng/ml) as a positive control, and IL-8 was measured in culture supernatants by ELISA ($n = 3$). Data were analyzed by one-way ANOVA with Dunnett's multiple comparisons *post hoc* test. (* $p < 0.05$ comparing GlyH-101 with control, and **** $p < 0.0001$ comparing TNF-α with control).

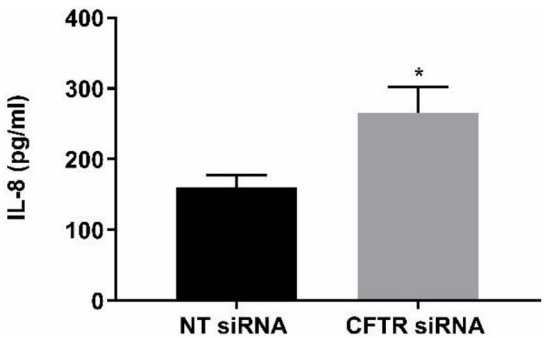

FIGURE 9 | CFTR gene silencing. CFTR gene silencing using siRNA in HLMVECs induced a significant increase in IL-8 in supernatants. After targeting CFTR mRNA for 72 h, the results were compared with non-targeting siRNA as negative control. (*$p < 0.05$, $n = 4$ independent experiments, with each experiment carried out in duplicate). Data were expressed as mean ± SEM and analyzed by *t*-test.

to activation of nuclear transcription factors involved in IL-8 and VEGF synthesis.

CFTR Expression

Endothelial CFTR expression was confirmed in the present study, but appeared to be lower in our model than previously reported in HLMVECs (Tousson et al., 1998), possibly reflecting growth on collagen IV, which is an exclusive component of basement membranes that regulates endothelial cell function (Wang and Su, 2011). Levels of expression varied greatly between HLMVEC preparations, as reported for other tissues (Riordan et al., 1989), and appeared to be largely associated with intracellular organelles with punctate staining indicating localization in the endoplasmic reticulum surrounding the nucleus, as previously reported in endothelial cells (Tousson et al., 1998).

Since we found that the CFTR inhibitor GlyH-101 does not activate endothelial NF-κB (**Figure 10**), the increased expression of CFTR following CFTR inhibition is unlikely to be via activation of the TNF-R adaptor molecule, TRADD, and NF-κB activation, as has been previously described in bronchial epithelial cells (Wang et al., 2016). However, Nrf2 has an inhibitory effect on CFTR expression (Rene et al., 2010) and repression of CFTR expression occurs under conditions of prolonged oxidative stress in bronchial epithelial cells (Zhang et al., 2015). Thus, the significantly reduced levels of endothelial Nrf2 we detected in HLMVECs following CFTR inhibition (**Figure 5**) may contribute to the observed increase in endothelial CFTR expression following treatment with GlyH-101.

However, the low levels of mature CFTR in the plasma membrane were activated by the cAMP-elevating agents, forskolin plus IBMX, to cause cell depolarization. This response was inhibited by GlyH-101, a water-soluble glycine hydrazide reported to bind to CFTR externally in the channel pore where, at 10 μM, it rapidly and completely inhibited CFTR chloride channel activity in human airway epithelial cells (Muanprasat et al., 2004). The cAMP-elevating agents stimulated membrane depolarization in both HLMVECs and 16HBEs and the non-CFTR expressing HEK293 cells. Significant inhibition of the response by GlyH-101 in HLMVECs and 16HBEs indicated that depolarization was partly due to CFTR. However, other cAMP-activated channels, such as cAMP-gated non-selective cation channels (Nilius and Droogmans, 2001), which are not inhibited by GlyH-101, may also contribute to membrane depolarization in these cells.

CFTR and Oxidative Stress

Oxidative stress is a key contributor to vascular endothelial dysfunction in people with CF (Tucker et al., 2019). In the present

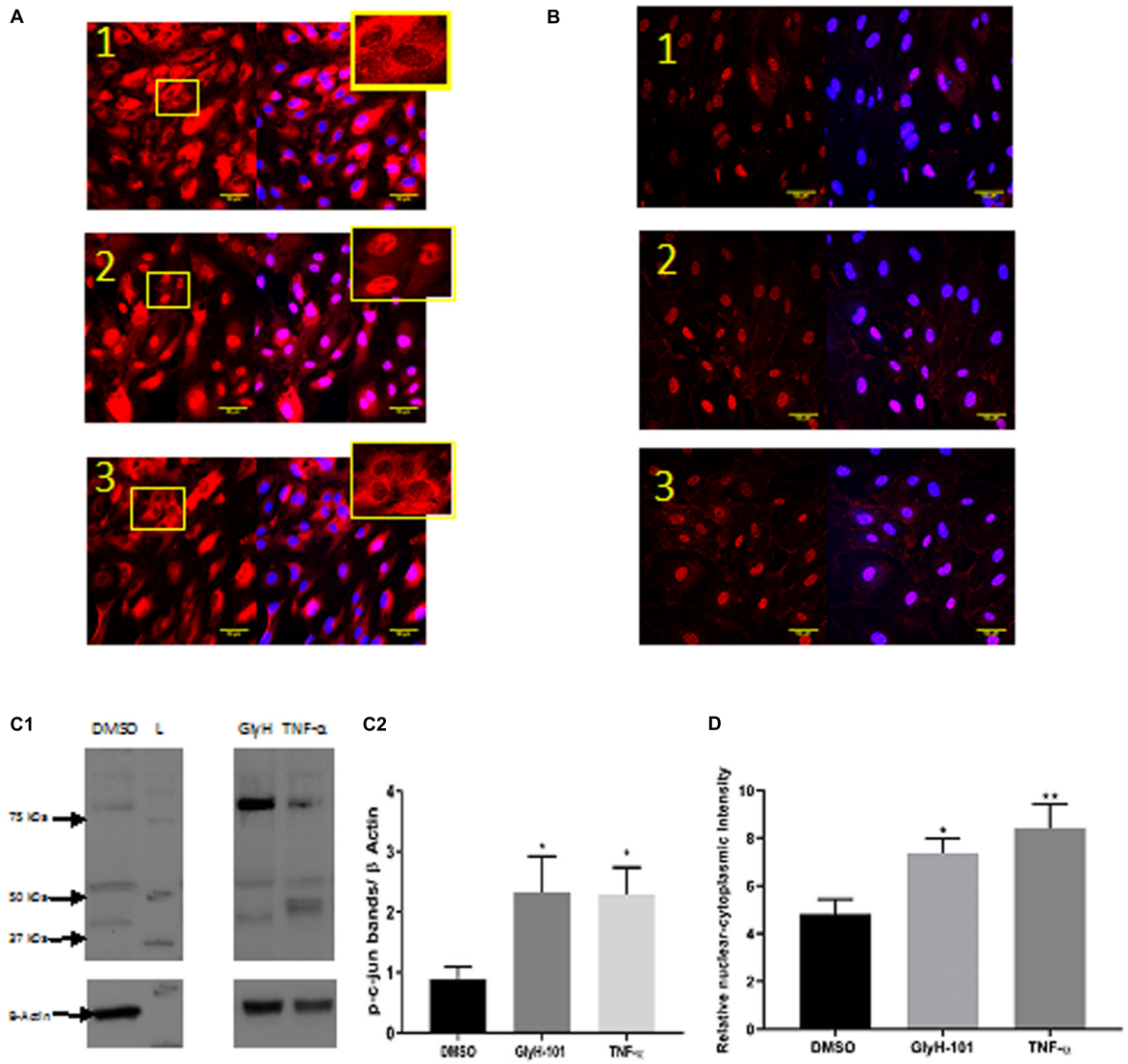

FIGURE 10 | The effect of GlyH-101 on cell signaling. **(A)** NF-κB immunocytochemistry of HLMVECS after 1 h of 1; DMSO (0.1%), 2; TNF-α (10 ng/ml), 3; GlyH-101 (20 μM). No primary antibody controls showed no positive staining. **(B)** p-c-jun immunocytochemistry of HLMVECs after 30 min of 1; DMSO (0.1%), 2; TNF-α (10 ng/ml), 3; GlyH-101 (20 μM). No primary antibody controls showed no positive staining. **(C)** p-c-jun western blotting. **(C1)** image of whole cell lysate after treating HLMVECs with DMSO (0.1%), TNF-α (10 ng/ml), GlyH-101 (20 μM) for 30 min. L; molecular weight ladder. **(C2)** quantification p-c-jun on western blots from three independent experiments. Data were analyzed with one-way ANOVA and Fisher *post hoc* test. (* $p < 0.05$ compared with DMSO control, $n = 3$). **(D)** Immunocytochemistry quantification of relative nuclear to cytoplasmic p-c-jun intensity, data represent three independent experiments, in which 20 cells were quantified from each condition. Data were analyzed with one-way ANOVA, and Fisher test (* $p < 0.05$, ** $p < 0.01$,compared with DMSO control, $n = 3$).

study, increased intracellular oxidative stress in HLMVECs and 16HBEs was demonstrated in response to CFTR inhibition. Chen et al. (2008) previously reported an increase in intracellular H_2O_2 following 72 h of CFTR inhibition in human bronchial epithelial cells. The difference lies in the rapid response in HLMVECs, in which intracellular ROS were significantly induced over 5–30 min following CFTR inhibition with GlyH-101 and was reflected in a significant increase in intracellular H_2O_2 concentrations at 30 min compared to baseline levels. H_2O_2 is a highly diffusible cell signaling molecule with multiple redox-sensitive molecular targets. These include oxidative inactivation of protein phosphatases and direct or indirect activation of kinases, converging in the regulation of transcription factor activity and effects on endothelial cell function via increased expression of growth factors including VEGF and transactivation of growth factor receptors including EGFR (Bretón-Romero and Lamas, 2014; Kim and Byzova, 2014; Marinho et al., 2014).

The ROS signal following CFTR inhibition was completely ablated in the presence of NAC, despite the fact that NAC has only weak direct antioxidant properties toward superoxide anions and H_2O_2 (Aldini et al., 2018). However, as a precursor

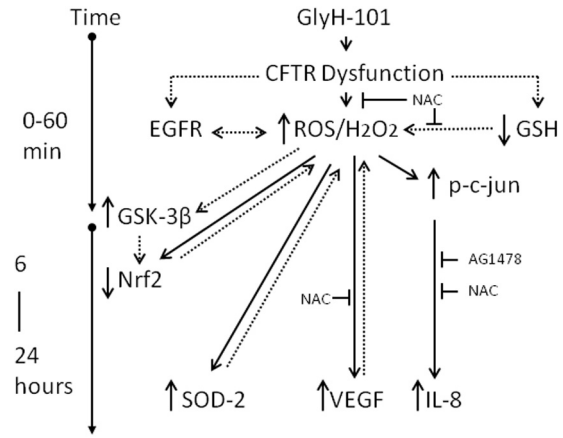

FIGURE 11 | Schematic of the impact of CFTR dysfunction in HLMVEC on oxidative stress, inflammation and angiogenesis. Specific pharmacological inhibition of endothelial CFTR activity is associated with an increase in intracellular ROS (5 min) and hydrogen peroxide (30 min), an increase in phosphorylation of c-jun and activation of AP-1 (30 min) leading to transcription of IL-8 (16–24 h). These responses are inhibited by the antioxidant NAC and the EGFR inhibitor AG1478, indicating a role for EGFR-mediated ROS/H_2O_2 generation in the induction of IL-8 synthesis. The increase in ROS/H_2O_2 is associated with increased VEGF and SOD2 expression which serve to sustain high levels of intracellular hydrogen peroxide, via effects on VEGFR and superoxide dismutation, respectively. Under these conditions Nrf2, the master regulator of oxidative stress, is significantly depleted, which is proposed to occur via prolonged exposure to high levels of H_2O_2, activation of GSK-3β and labeling of Nrf2 for β-TrCP recognition, ubiquitination and degradation. The suppression of Nrf2 levels to below normal will further sensitize endothelial cells to oxidative stress by reducing expression of antioxidant genes. Dotted lines indicate proposed pathways. T indicates inhibition of a pathway.

of cysteine and thus of glutathione (GSH) synthesis, NAC is effectively an indirect antioxidant, GSH being a direct antioxidant and a substrate of several antioxidant enzymes (Aldini et al., 2018). CFTR may be a major transporter of GSH in both epithelial and endothelial cells (Roum et al., 1993; Gao et al., 1999). Impaired CFTR activity diminishes both intracellular and extracellular GSH levels in bronchial epithelial cells (de Bari et al., 2018), and impaired endothelial CFTR activity may contribute to the systemic deficiency in GSH in CF (Roum et al., 1993). A rapid, within 10 min, significant 50% decrease in GSH in airway epithelial cells following CFTR inhibition with the CFTR inhibitor CFTRinh-172 was recently reported (de Bari et al., 2018). Thus, if CFTR inhibition similarly lowers intracellular GSH concentrations in HLMVECs, this may contribute to the observed rapid increase in ROS/H_2O_2 following treatment with GlyH-101. On the other hand, the significant decrease in ROS observed in the presence of 10 mM NAC may reflect an increase in intracellular GSH, as previously reported for human pulmonary vascular endothelial cells treated with 10 mM NAC (Hashimoto et al., 2001).

Major sources of ROS production in vascular endothelial cells include the mitochondria, endoplasmic reticulum, plasma membrane and cytosolic enzymes (Bretón-Romero and Lamas, 2014). Mitochondrial defects and increased production of ROS, although controversial (Schwarzer et al., 2007), have been reported in CF lung (Valdivieso and Santa-Coloma, 2013; Atlante et al., 2016), and gut (Kleme et al., 2018) epithelial cells. However, the mitochondrially targeting antioxidant MitoQ did not attenuate ROS production in HLMVEC or 16HBEs, and since the NOX/Duox inhibitor, diphenyleneiodonium (DPI) at 10 μM, failed to inhibit H_2O_2 formation, another source of endothelial ROS is indicated (Cai, 2005), which warrants further investigation.

Cystic fibrosis transmembrane conductance regulator dysfunction in airway epithelial cells was previously reported to significantly increase SOD-2, while reducing catalase, expression (Chen et al., 2008). Similarly, inhibition of endothelial CFTR induced a significant increase in SOD-2, albeit in the absence of a significant decrease in catalase expression.

SOD-2 is localized in the mitochondrial matrix and catalyzes the dismutation of $O2^{\cdot-}$ to H_2O_2. The observed increase in SOD-2 expression 16–24 h following CFTR inhibition, in the absence of any increase in catalase expression, would serve to maintain relatively high intracellular H_2O_2 levels in our endothelial cell cultures, as previously reported in airway epithelial cells over 72 h (Chen et al., 2008). SOD-2 expression is not reported to be regulated by Nrf2 (Türei et al., 2013) and, considering the loss of Nrf2 function over 16–24 h (**Figure 5**), we propose that SOD-2 expression is upregulated in response to H_2O_2 - mediated activation of other redox sensitive transcription factors (Yoshioka et al., 1994).

CFTR and Nrf2 Expression

Previous work has demonstrated, in intestinal epithelial cells, that CFTR knockout significantly increased mitochondrial levels of H_2O_2 and decreased mitochondrial levels of Nrf2 (Kleme et al., 2018). As in bronchial epithelial cells (Chen et al., 2008), CFTR inhibition in HLMVECs led to a 70% decrease in endothelial Nrf2 expression in the present study, although further work is needed to demonstrate the subcellular organelle distribution of Nrf2 in HLMVECs.

Since Nrf2 is a transcription factor and a master regulator of the adaptive cellular response to oxidative stress in endothelial cells, one would expect that oxidative stress would induce an adaptive response (reviewed in 53). Adaptive responses are characterized by increased Nrf2 expression and activity, upregulated antioxidant response element (ARE)-regulated gene expression with co-ordinated induction of endogenous cytoprotective enzymes. In view of our evidence of oxidative stress in endothelial cells following CFTR inhibition (increased ROS/H_2O_2), the observed decrease in Nrf2 is a paradox, but one which was also previously reported in airway epithelial cells (Chen et al., 2008). H_2O_2 is further metabolized by catalase in the peroxisomes or by the glutathione peroxidase, peroxiredoxin/thioredoxin system, isoforms of which are found in the mitochondria and the cytosol, and whose expression is normally regulated by Nrf2. However, expression of these cytoprotective proteins is decreased in CF epithelial cells, and CF nasal and lung tissue, and this was linked to the decreased expression of Nrf2 (Chen et al., 2008).

Nuclear related factor 2 is normally maintained at low levels intracellularly by its association with Kelch-like ECH-associated protein 1 (Keap-1), a substrate adapter in an E3 ubiquitin ligase complex, leading to Nrf2 ubiquitination and proteosomal degradation (Rada et al., 2011; Marinho et al., 2014). H_2O_2 oxidizes critical cysteine residues in Keap-1, inducing conformational changes affecting the interaction between Keap-1 and Nrf2, thereby inhibiting Nrf2 ubiquitination and degradation. In this way, stabilization of Nrf2 by H_2O_2 leads to translocation and accumulation of Nrf2 in the nucleus, upregulation of ARE-driven gene expression and coordinated induction of endogenous cytoprotective proteins. However, Nrf2 can also be tagged for degradation by phosphorylation mediated by glycogen synthase kinase-3β (GSK-3β). Phosphorylated Nrf2 is recognized and bound by the β-transducin repeat containing protein (β-TrCP), a substrate adapter forming an E3 ligase complex, followed by ubiquitination and proteosomal degradation of Nrf2. Since GSK-3β is *inhibited* by PKB/Akt-mediated phosphorylation, and H_2O_2 is an activator of the PI3K/Akt pathway, then H_2O_2 can also activate Nrf2 in a Keap-1 independent manner (Rada et al., 2011; Marinho et al., 2014).

However, while short-term exposure to H_2O_2 inhibits GSK-3β and activates Nrf2, prolonged exposure to high H_2O_2 concentrations *activates* GSK-3β, which could terminate the Nrf2 signal by degradation of Nrf2 through the β-TrCP pathway leading to lower than normal levels of Nrf2 (Rada et al., 2011; Marinho et al., 2014). These pathways are outlined in **Figure 11**. Thus it would be of future interest to investigate if antioxidants, such as NAC, could prevent the loss of Nrf2 following CFTR inhibition in endothelial cell cultures.

Nrf2 as a Therapeutic Target

Since, Nrf2 expression is central to limiting oxidative stress and inflammation, the reduced expression of Nrf2 in CF airway epithelium (Chen et al., 2008), and now also demonstrated in pulmonary endothelial cells with dysfunctional CFTR, strongly indicate Nrf2 may be a therapeutic target to limit oxidative stress and airway inflammation by increasing its expression and activation in CF. Such an approach has been demonstrated using the synthetic triterpenoid CDDO (2-cyano-3,12-dioxooleana-1,9 (Peters et al., 2015)-dien-28-oic acid) in airway epithelial cell and animal models of CF (Nichols et al., 2009). Further, since CDDO activates PI3K-PKB/Akt signaling (reviewed in 53), the increase in Nrf2 activity in CF airway epithelial cells following treatment with CDDO (Nichols et al., 2009), suggests the reduced Nrf2 activity in preclinical models of CF lung disease is associated with GSK-3β activity. It would therefore be of future interest to investigate the effect of specific pharmacological activators of PI3K-PKB/Akt and inhibitors of GSK-3β activity on Nrf2 activity in pulmonary endothelial cells. Other Nrf2 activators include natural products such as curcumin (Balogun et al., 2003) and sulforaphane, an isothiocyanate enriched in broccoli sprouts, which has been proposed as a dietary supplement to activate Nrf2 (Galli et al., 2012).

In addition to regulation by proteosomal degradation, cytosolic Nrf2 levels are regulated at the stage of Nrf2 gene transcription. Amongst factors that increase Nrf2 transcripts is Nrf2 itself (Suzuki et al., 2013), possibly contributing to the overall significant decrease in Nrf2 levels following CFTR inhibition. Of interest, is the recent observation that clinically approved CFTR modulators rescue Nrf2 dysfunction in CF airway epithelial cells (Borcherding et al., 2019). The effect of CFTR modulators on endothelial Nrf-2 expression and activity remains to be investigated.

CFTR and VEGF Expression

Increased VEGF expression and peribronchial angiogenesis is a feature of the CF airway. VEGF promotes angiogenesis and increased vascular permeability, enhancing inflammatory cell recruitment and plasma exudation in the airway. Inhibition of airway epithelial CFTR increased VEGF expression, an effect that was dependent on EGFR activity and inhibited by the receptor tyrosine kinase inhibitor AG1478 (Martin et al., 2013). Further, CF airway epithelial cells have increased EGFR activity and phosphorylation compared to normal cells (Stolarczyk et al., 2018). Thus it was suggested that EGFR tyrosine kinase inhibitors, such as AG1478, might be useful in the treatment of CF. However, the findings in the present study clearly indicate that such an approach further enhances the increased VEGF expression observed following CFTR inhibition in HLMVECs, and in this respect these endothelial cells differ from epithelial cells.

Conversely, EGFR inhibition reduced IL-8 expression in CFTR-inhibited epithelial cells (Kim et al., 2013) and, as demonstrated in the present study, also in HLMVECs. Since anti-inflammatory therapies targeting inhibition of EGFR are likely to increase VEGF expression in endothelial cells, other approaches such as those that target oxidative stress (Kim and Byzova, 2014) are needed. This notion is supported by our evidence that the antioxidant NAC significantly reduced ROS, and both IL-8 and VEGF expression in HLMVECs. In addition, others have recently demonstrated that ingestion of an antioxidant cocktail can improve vascular endothelial cell function and oxidative stress in patients with CF (Tucker et al., 2019).

CFTR and IL-8 Expression

Dysfunctional CFTR significantly increased endothelial IL-8 expression both in the absence and presence of TNFα, a pro-inflammatory cytokine that enhances neutrophil responses in CF airways (Nichols and Chmiel, 2015). Increased expression of IL-8 in pulmonary epithelial cells with dysfunctional CFTR was previously associated with increased activation of the transcription factor NF−κB (Vij et al., 2009), which works with other transcription factors, including AP−1, as a central transcriptional regulator of airway inflammation in CF (Nichols and Chmiel, 2015). Diminished Nrf2 levels are proposed to exacerbate activation of redox sensitive pathways including activation of AP-1 and NF-κB signaling leading to increased IL-8 expression (Hoffmann et al., 2002) and activation of EGFR signaling pathways (Burgel and Nadel, 2008). GlyH-101 induced a rapid (within 30 min) significant increase in the cellular abundance of phospho-c-Jun, including an increase in the concentration of nuclear phospho-c-Jun. These changes are

indicative of increased c-Jun expression and activation of AP-1 signaling, which contribute to a self-amplifying cycle of increased c-Jun abundance (Marinho et al., 2014). However, no nuclear translocation of p65, an indicator of NF-κB activation, was seen following treatment of HLMVECs with GlyH-101 alone for up to 1 h, ruling out a role for NF-κB activation via the canonical pathway in the IL-8 response to inhibition of CFTR activity. Similarly, the CFTR inhibitor CFTRinh172 also did not induce NF-κB activation and nuclear translocation in airway epithelial cells (Perez et al., 2007).

Unlike GlyH-101, TNFα induced activation of both NF-κB and AP-1 signaling, leading to significantly increased IL-8 expression in HLMVECs, beyond the response to GlyH-101 alone. Of particular interest in this respect is the recent report that JNK is activated in CF epithelial cells and further activated in response to TNFα (Saadane et al., 2011).

The complete inhibitory effect of AG1478 on the GlyH101-induced increase in IL8 synthesis indicates that this response occurred via a signaling cascade leading to ligand-dependent EGFR signaling, as previously described for human airway epithelial cells exposed to the CFTRinh172 (Kim et al., 2013). EGFR activation leads to rapid (within 5 min) generation of H_2O_2 (Bae et al., 1997) by mechanisms which are not yet described (Weng et al., 2018), with immediate response gene expression, including JUN and FOS, occurring over the first 45 min (Avraham and Yarden, 2011). Our data therefore indicate the early, 30 min, increase in phospho-c-Jun observed in response to GlyH-101 is mediated via H_2O_2-activated EGFR signaling (Weng et al., 2018) and involved in AP-1-mediated IL-8 expression.

The inhibitory effect of NAC on IL-8 production in response to GlyH-101 in the presence of TNFα further indicates that ROS are involved in signaling pathways leading to IL-8 synthesis in endothelial cells. Following CFTR inhibition, GlyH-101 appears to act solely through the EGFR cascade and AP-1 activation, while TNF-α activates both NF-κB and AP-1 signaling pathways. ROS contribute to EGFR activation, and activation of NF-κB and AP-1 signaling pathways, as described above. Whether endothelial oxidative stress further contributes to increased IL-8 gene expression through remodeling of chromatin structure and increased histone H4 acetylation at the IL-8 promoter, as seen in CF airway epithelial cell models (Bartling and Drumm, 2009), is not known.

GlyH-101 Is a Specific Inhibitor of Endothelial CFTR

Some degree of non-specificity for GlyH-101 has been reported in murine epithelial cell lines (Melis et al., 2014), although these effects appear to be species specific (Stahl et al., 2012). In murine cells, GlyH-101 inhibited the volume-sensitive outwardly rectifying Cl^- conductance (VSORC) and the calcium dependent Cl^- conductance (CaCC), which in endothelial cells is predominantly TMEM16A. However, although TMEM16A activity was reported to negatively regulate pro-inflammatory cytokine, including IL-8, synthesis in human CF bronchial epithelia (Veit et al., 2012), TMEM16A is a positive regulator of endothelial ROS (Ma et al., 2017), and its inhibition would lead to decreased ROS in endothelial cells, and not the increase reported in the current study, supporting the involvement of CFTR in the observed responses to GlyH-101. In our control experiments, specific inhibition of other chloride ion channels, VRAC and TMEM16A had no effect on IL-8 expression, and GlyH-101 had no effect on IL-8 expression in HEK-293 cells that do not express CFTR. Together these experiments indicate that the observed effects of GlyH-101 in HLMVECs reflect inhibition of CFTR activity without off-target effects.

Others reported non-specific effects of GlyH-101 on mitochondrial respiration and a rapid increase in ROS levels that were independent of CFTR channel inhibition, although these were largely abrogated in the presence of 10% serum, and under these conditions GlyH-101 had no effect on basal oxygen consumption (Kelly et al., 2010). Serum (5%) was present in our HLMVEC cultures to provide a reducing extracellular environment (Chan et al., 2001) and as a source of albumin to increase intracellular glutathione that protects pulmonary cells from oxidant-mediated cytotoxicity (Cantin et al., 2000). Under these conditions, but not in the absence of serum, NAC acts as an anti-oxidant (Chan et al., 2001), as we observed. Further, we saw no effect of MitoQ on the GlyH-101 stimulated ROS production in HLMVECs or 16HBEs, ruling out a direct effect of GlyH-101 on mitochondrial ROS.

Therapeutic Relevance

Systemic inflammation and oxidative stress are characteristics of people with CF and it is proposed that dysfunctional endothelial cells contribute to these changes in the circulation in people with CF (Declercq et al., 2019; Causer et al., 2020). Further, systemic inflammation, oxidative stress and endothelial dysfunction were proposed to be major risk factors for cardiovascular disease in the aging CF population (Reverri et al., 2014). Our data now point to a role for dysfunctional endothelial CFTR in systemic oxidative stress and inflammation in CF.

However, to date, there are limited options for anti-inflammatory therapy for CF (Cantin et al., 2015). Targeting endothelial CFTR for correction and/or potentiation would seem to be a logical therapeutic approach, as small molecule correctors and potentiators are already in development to restore epithelial CFTR function. It was surprising that 6 months treatment with ivacaftor in CF patients with the G551D mutation improved lung function, and reduced sweat chloride, indicating an effect on CFTR function, without an effect on pulmonary inflammation (Rowe et al., 2014). Systemic inflammation was not measured in the study, so it is not possible to appreciate the effect of the oral drug, ivacaftor, on endothelial function. The combination of lumacaftor with ivacaftor (Orkambi) for delF508 patients was approved in 2015, but to our knowledge no studies have reported effects on systemic inflammation.

Correction of CFTR expression in the bronchial epithelium by gene transfer in 10–25% of cells in a population was sufficient to restore normal chloride conductance and epithelial function (Johnson et al., 1992; Zhang et al., 2009). However, it is currently unclear whether low-level expression in many cells (e.g., 10% of

residual CFTR expression) or a low number of cells expressing high levels of CFTR are required to restore normal function and achieve clinical benefit after gene therapy (Griesenbach et al., 2015). Recent revised estimates of the number of endothelial cells in the human body indicate a total of 6×10^{11} cells (Sender et al., 2016), and low level of expression of CFTR in all of them may be sufficient to maintain normal barrier, anti-inflammatory and anti-oxidant endothelial function.

In addition to inherited defects in CFTR in people with CF, inhibition of CFTR on endothelial cells increased the loss of barrier function induced by exposure of endothelial cells to cigarette smoke (Brown et al., 2014). Raju et al. (2013) showed that smoking causes systemic CFTR dysfunction and that acrolein present in cigarette smoke mediates CFTR defects in extrapulmonary tissues in smokers. Endothelial dysfunction is associated with loss of lung function, severity of disease and reduced exercise capacity in COPD (Green and Turner, 2017). Together, these findings indicate that acquired loss of endothelial CFTR function in response to cigarette smoking may be relevant to the development of vascular disease and other co-morbidities in COPD, and a further target for therapy.

Limitations

While our data identify CFTR expressed in human lung microvascular endothelium as a controller of oxidative stress, ROS-mediated cell signaling and inflammatory responses, it was based on a limited number ($n = 3$–6) of independent experiments. In addition, this study was performed in a model in which normal endothelial CFTR function was inhibited pharmacologically. To better understand the role of dysfunctional endothelial CFTR in people with CF, studies could be conducted using primary endothelial cells or cell lines from people with CF in cell culture models under shear flow, for example, and eventually in the *in vivo* situation, given the importance of various cellular interactions in inflammatory responses.

CONCLUSION

In conclusion, our study points to restoring endothelial CFTR and Nrf2 activity as therapeutic targets in people with CF, and supports the use of systemic antioxidants to reduce vascular inflammation and angiogenesis in CF.

DATA AVAILABILITY STATEMENT

All datasets generated for this study are included in the article/supplementary material.

AUTHOR CONTRIBUTIONS

MK, TS-W, AC, and JS acquired and statistically analyzed the data. ZS, AS, DG, AL, DL, and JS contributed to conception and design of the study. JS wrote the first draft of the manuscript. All authors contributed to manuscript revision and approval of the submitted version.

FUNDING

This research was supported by The Dunhill Medical Trust, grant number SA25/0712 and a University of Portsmouth Ph.D. studentship for AC.

REFERENCES

Aldini, G., Altomare, A., Baron, G., Vistoli, G., Carini, M., Borsani, L., et al. (2018). N-Acetylcysteine as an antioxidant and disulphide breaking agent: the reasons why. *Free Radic. Res.* 52, 751–762. doi: 10.1080/10715762.2018.1468564

Atlante, A., Favia, M., Bobba, A., Guerra, L., Casavola, V., and Reshkin, S. J. (2016). Characterization of mitochondrial function in cells with impaired cystic fibrosis transmembrane conductance regulator (CFTR) function. *J. Bioenerg. Biomemb.* 48, 197–210. doi: 10.1007/s10863-016-9663-y

Avraham, R., and Yarden, Y. (2011). Feedback regulation of EGFR signalling: decision making by early and delayed loops. *Nat. Rev. Mol. Cell Biol.* 12, 104–117. doi: 10.1038/nrm3048

Bae, Y. S., Kang, S. W., Seo, M. S., Baines, I. C., Tekle, E., Chock, P. B., et al. (1997). Epidermal growth factor (EGF)-induced generation of hydrogen peroxide. Role in EGF receptor-mediated tyrosine phosphorylation. *J. Biol. Chem.* 272, 217–221. doi: 10.1074/jbc.272.1.217

Balogun, E., Hoque, M., Gong, P., Killeen, E., Green, C. J., Foresti, R., et al. (2003). Curcumin activates the haem oxygenase-1 gene via regulation of Nrf2 and the antioxidant-responsive element. *Biochem. J.* 371(Pt 3), 887–895. doi: 10.1042/bj20021619

Bartling, T. R., and Drumm, M. L. (2009). Oxidative stress causes IL8 promoter hyperacetylation in cystic fibrosis airway cell models. *Am. J. Respir. Cell Mol. Biol.* 40, 58–65. doi: 10.1165/rcmb.2007-0464oc

Borcherding, D. C., Siefert, M. E., Lin, S., Brewington, J., Sadek, H., Clancy, J. P., et al. (2019). Clinically-approved CFTR modulators rescue Nrf2 dysfunction in cystic fibrosis airway epithelia. *J. Clin. Invest.* 129, 3448–3463. doi: 10.1172/jci96273

Bretón-Romero, R., and Lamas, S. (2014). Hydrogen peroxide signaling in vascular endothelial cells. *Redox Biol.* 2, 529–534. doi: 10.1016/j.redox.2014.02.005

Brown, M. B., Hunt, W. R., Noe, J. E., Rush, N. I., Schweitzer, K. S., Leece, T. C., et al. (2014). Loss of cystic fibrosis transmembrane conductance regulator impairs lung endothelial cell barrier function and increases susceptibility to microvascular damage from cigarette smoke. *Pulm. Circ.* 4, 260–268. doi: 10.1086/675989

Burgel, P. R., and Nadel, J. A. (2008). Epidermal growth factor receptor-mediated innate immune responses and their roles in airway diseases. *Eur. Respir. J.* 32, 1068–1081. doi: 10.1183/09031936.00172007

Cai, H. (2005). Hydrogen peroxide regulation of endothelial function: origins, mechanisms, and consequences. *Cardiovasc. Res.* 68, 26–36. doi: 10.1016/j.cardiores.2005.06.021

Cantin, A. M., Hartl, D., Konstan, M. W., and Chmiel, J. F. (2015). Inflammation in cystic fibrosis lung disease: pathogenesis and therapy. *J. Cyst. Fibros.* 14, 419–430. doi: 10.1016/j.jcf.2015.03.003

Cantin, A. M., Paquette, B., Richter, M., and Larivee, P. (2000). Albumin-mediated regulation of cellular glutathione and nuclear factor kappa B activation. *Am. J. Respir. Crit. Care Med.* 162(4 Pt 1), 1539–1546. doi: 10.1164/ajrccm.162.4.9910106

Causer, A. J., Shute, J. K., Cummings, M. H., Shepherd, A. I., Gruet, M., Costello, J. T., et al. (2020). Circulating biomarkers of antioxidant status and oxidative stress in people with cystic fibrosis: a systematic review and meta-analysis. *Redox Biol.* 23:101436. doi: 10.1016/j.redox.2020.101436

Chan, E. D., Riches, D. W., and White, C. W. (2001). Redox paradox: effect of N-acetylcysteine and serum on oxidation reduction-sensitive mitogen-activated

protein kinase signaling pathways. *Am. J. Respir. Cell Mol. Biol.* 24, 627–632. doi: 10.1165/ajrcmb.24.5.4280

Chen, J., Kinter, M., Shank, S., Cotton, C., Kelley, T. J., and Ziady, A. G. (2008). Dysfunction of Nrf-2 in CF epithelia leads to excess intracellular H_2O_2 and inflammatory cytokine production. *PLoS One* 3:e3367. doi: 10.1371/journal.pone.0003367

Cozens, A. L., Yezzi, M. J., Kunzelmann, K., Ohrui, T., Chin, L., Eng, K., et al. (1994). CFTR expression and chloride secretion in polarized immortal human bronchial epithelial cells. *Am. J. Respir. Cell Mol. Biol.* 10, 38–47. doi: 10.1165/ajrcmb.10.1.7507342

de Bari, L., Favia, M., Bobba, A., Lassandro, R., Guerra, L., and Atlante, A. (2018). Aberrant GSH reductase and NOX activities concur with defective CFTR to pro-oxidative imbalance in cystic fibrosis airways. *J. Bioenerg. Biomembr.* 50, 117–129. doi: 10.1007/s10863-018-9748-x

Declercq, M., Treps, L., Carmeliet, P., and Witters, P. (2019). The role of endothelial cells in cystic fibrosis. *J. Cyst. Fibros.* 18, 752–761. doi: 10.1016/j.jcf.2019.07.005

Eruslanov, E., and Kusmartsev, S. (2010). Identification of ROS using oxidized DCFDA and flow-cytometry. *Methods Mol. Biol.* 594, 57–72. doi: 10.1007/978-1-60761-411-1_4

Friard, J., Tauc, M., Cougnon, M., Compan, V., Duranton, C., and Rubera, I. (2017). Comparative effects of chloride channel inhibitors on LRRC8/VRAC-mediated chloride conductance. *Front. Pharmacol.* 8:328. doi: 10.3389/fphar.2017.00328

Galli, F., Battistoni, A., Gambari, R., Pompella, A., Bragonzi, A., Pilolli, F., et al. (2012). Oxidative stress and antioxidant therapy in cystic fibrosis. *Biochim. Biophys. Acta* 1822, 690–713.

Gao, L., Kim, K. J., Yankaskas, J. R., and Forman, H. J. (1999). Abnormal glutathione transport in cystic fibrosis airway epithelia. *Am. J. Physiol.* 277, L113–L118.

Greco, E., Aita, A., Galozzi, P., Gava, A., Sfriso, P., Negm, O. H., et al. (2015). The novel S59P mutation in the TNFRSF1A gene identified in an adult onset TNF receptor associated periodic syndrome (TRAPS) constitutively activates NF-kappaB pathway. *Arthritis Res. Ther.* 17:93.

Green, C. E., and Turner, A. M. (2017). The role of the endothelium in asthma and chronic obstructive pulmonary disease (COPD). *Respir. Res.* 18:20.

Griesenbach, U., Pytel, K. M., and Alton, E. W. (2015). Cystic fibrosis gene therapy in the UK and elsewhere. *Hum. Gene Ther.* 26, 266–275. doi: 10.1089/hum.2015.027

Hashimoto, S., Gon, Y., Matsumoto, K., Takeshita, I., and Horie, T. (2001). N-acetylcysteine attenuates TNF-alpha-induced p38 MAP kinase activation and p38 MAP kinase-mediated IL-8 production by human pulmonary vascular endothelial cells. *Br. J. Pharmacol.* 132, 270–276. doi: 10.1038/sj.bjp.0703787

Hayes, J. D., and Dinkova-Kostova, A. T. (2014). The Nrf2 regulatory network provides an interface between redox and intermediary metabolism. *Trends Biochem. Sci.* 39, 199–218. doi: 10.1016/j.tibs.2014.02.002

Hoffmann, E., Dittrich-Breiholz, O., Holtmann, H., and Kracht, M. (2002). Multiple control of interleukin-8 gene expression. *J. Leukocyte Biol.* 72, 847–855.

Hopkins, N. K., and Gorman, R. R. (1981). Regulation of endothelial cell cyclic nucleotide metabolism by prostacyclin. *J. Clin. Invest.* 67, 540–546. doi: 10.1172/jci110064

Johnson, L. G., Olsen, J. C., Sarkadi, B., Moore, K. L., Swanstrom, R., and Boucher, R. C. (1992). Efficiency of gene transfer for restoration of normal airway epithelial function in cystic fibrosis. *Nat. Genet.* 2, 21–25. doi: 10.1038/ng0992-21

Kelly, M., Trudel, S., Brouillard, F., Bouillaud, F., Colas, J., Nguyen-Khoa, T., et al. (2010). Cystic fibrosis transmembrane regulator inhibitors CFTR(inh)-172 and GlyH-101 target mitochondrial functions, independently of chloride channel inhibition. *J. Pharmacol. Exp. Ther.* 333, 60–69. doi: 10.1124/jpet.109.162032

Kim, S., Beyer, B. A., Lewis, C., and Nadel, J. A. (2013). Normal CFTR inhibits epidermal growth factor receptor-dependent pro-inflammatory chemokine production in human airway epithelial cells. *PLoS One* 8:e72981. doi: 10.1371/journal.pone.0072981

Kim, Y. W., and Byzova, T. V. (2014). Oxidative stress in angiogenesis and vascular disease. *Blood* 123, 625–631. doi: 10.1182/blood-2013-09-512749

Kleme, M. L., Sane, A., Garofalo, C., Seidman, E., Brochiero, E., Berthiaume, Y., et al. (2018). CFTR deletion confers mitochondrial dysfunction and disrupts lipid homeostasis in intestinal epithelial cells. *Nutrients* 10:836. doi: 10.3390/nu10070836

Ma, M. M., Gao, M., Guo, K. M., Wang, M., Li, X. Y., Zeng, X. L., et al. (2017). TMEM16A contributes to endothelial dysfunction by facilitating Nox2 NADPH oxidase-derived reactive oxygen species generation in hypertension. *Hypertension* 69, 892–901. doi: 10.1161/hypertensionaha.116.08874

Maitra, R., Sivashanmugam, P., and Warner, K. (2013). A rapid membrane potential assay to monitor CFTR function and inhibition. *J. Biomol. Screen.* 18, 1132–1137. doi: 10.1177/1087057113488420

Marinho, H. S., Real, C., Cyrne, L., Soares, H., and Antunes, F. (2014). Hydrogen peroxide sensing, signaling and regulation of transcription factors. *Redox Biol.* 2, 535–562. doi: 10.1016/j.redox.2014.02.006

Martin, C., Coolen, N., Wu, Y., Thevenot, G., Touqui, L., Pruliere-Escabasse, V., et al. (2013). CFTR dysfunction induces vascular endothelial growth factor synthesis in airway epithelium. *Eur. Respir. J.* 42, 1553–1562. doi: 10.1183/09031936.00164212

Melis, N., Tauc, M., Cougnon, M., Bendahhou, S., Giuliano, S., Rubera, I., et al. (2014). Revisiting CFTR inhibition: a comparative study of CFTRinh -172 and GlyH-101 inhibitors. *Br. J. Pharmacol.* 171, 3716–3727. doi: 10.1111/bph.12726

Muanprasat, C., Sonawane, N. D., Salinas, D., Taddei, A., Galietta, L. J., and Verkman, A. S. (2004). Discovery of glycine hydrazide pore-occluding CFTR inhibitors: mechanism, structure-activity analysis, and in vivo efficacy. *J. Gen. Physiol.* 124, 125–137. doi: 10.1085/jgp.200409059

Nichols, D. P., and Chmiel, J. F. (2015). Inflammation and its genesis in cystic fibrosis. *Pediatric Pulmonol.* 50(Suppl. 40), S39–S56.

Nichols, D. P., Ziady, A. G., Shank, S. L., Eastman, J. F., and Davis, P. B. (2009). The triterpenoid CDDO limits inflammation in preclinical models of cystic fibrosis lung disease. *Am. J. Physiol. Lung Cell Mol. Physiol.* 297, L828–L836.

Nilius, B., and Droogmans, G. (2001). Ion channels and their functional role in vascular endothelium. *Physiol. Rev.* 81, 1415–1459. doi: 10.1152/physrev.2001.81.4.1415

Noe, J., Petrusca, D., Rush, N., Deng, P., VanDemark, M., Berdyshev, E., et al. (2009). CFTR regulation of intracellular pH and ceramides is required for lung endothelial cell apoptosis. *Am. J. Respir. Cell Mol. Biol.* 41, 314–323. doi: 10.1165/rcmb.2008-0264oc

Perez, A., Issler, A. C., Cotton, C. U., Kelley, T. J., Verkman, A. S., and Davis, P. B. (2007). CFTR inhibition mimics the cystic fibrosis inflammatory profile. *Am. J. Physiol. Lung Cell Mol. Physiol.* 292, L383–L395.

Peters, W., Kusche-Vihrog, K., Oberleithner, H., and Schillers, H. (2015). Cystic fibrosis transmembrane conductance regulator is involved in polyphenol-induced swelling of the endothelial glycocalyx. *Nanomed. Nanotechnol. Biol. Med.* 11, 1521–1530. doi: 10.1016/j.nano.2015.03.013

Plebani, R., Tripaldi, R., Lanuti, P., Recchiuti, A., Patruno, S., Di Silvestre, S., et al. (2017). Establishment and long-term culture of human cystic fibrosis endothelial cells. *Lab. Invest.* 97, 1375–1384. doi: 10.1038/labinvest.2017.74

Poore, S., Berry, B., Eidson, D., McKie, K. T., and Harris, R. A. (2013). Evidence of vascular endothelial dysfunction in young patients with cystic fibrosis. *Chest* 143, 939–945. doi: 10.1378/chest.12-1934

Rada, P., Rojo, A. I., Chowdhry, S., McMahon, M., Hayes, J. D., and Cuadrado, A. S. C. F. (2011). /{beta}-TrCP promotes glycogen synthase kinase 3-dependent degradation of the Nrf2 transcription factor in a Keap1-independent manner. *Mol. Cell Biol.* 31, 1121–1133. doi: 10.1128/mcb.01204-10

Raju, S. V., Jackson, P. L., Courville, C. A., McNicholas, C. M., Sloane, P. A., Sabbatini, G., et al. (2013). Cigarette smoke induces systemic defects in cystic fibrosis transmembrane conductance regulator function. *Am. J. Respir. Crit. Care Med.* 188, 1321–1330.

Rene, C., Lopez, E., Claustres, M., Taulan, M., and Romey-Chatelain, M. C. N. F. - (2010). E2-related factor 2, a key inducer of antioxidant defenses, negatively regulates the CFTR transcription. *Cell Mol. Life Sci.* 67, 2297–2309. doi: 10.1007/s00018-010-0336-4

Reverri, E. J., Morrissey, B. M., Cross, C. E., and Steinberg, F. M. (2014). Inflammation, oxidative stress, and cardiovascular disease risk factors in adults with cystic fibrosis. *Free Radic. Biol. Med.* 76, 261–277. doi: 10.1016/j.freeradbiomed.2014.08.005

Riordan, J. R., Rommens, J. M., Kerem, B., Alon, N., Rozmahel, R., Grzelczak, Z., et al. (1989). Identification of the cystic fibrosis gene: cloning and characterization of complementary DNA. *Science* 245, 1066–1073. doi: 10.1126/science.2475911

Rodriguez-Miguelez, P., Thomas, J., Seigler, N., Crandall, R., McKie, K. T., Forseen, C., et al. (2016). Evidence of microvascular dysfunction in patients with cystic fibrosis. *Am. J. Physiol. Heart Circ. Physiol.* 310, H1479–H1485.

Romano, M., Collura, M., Lapichino, L., Pardo, F., Falco, A., Chiesa, P. L., et al. (2001). Endothelial perturbation in cystic fibrosis. *Thromb. Haemost.* 86, 1363–1367. doi: 10.1055/s-0037-1616736

Roum, J. H., Buhl, R., McElvaney, N. G., Borok, Z., and Crystal, R. G. (1993). Systemic deficiency of glutathione in cystic fibrosis. *J. Appl. Physiol.* 75, 2419–2424. doi: 10.1152/jappl.1993.75.6.2419

Rowe, S. M., Heltshe, S. L., Gonska, T., Donaldson, S. H., Borowitz, D., Gelfond, D., et al. (2014). Clinical mechanism of the cystic fibrosis transmembrane conductance regulator potentiator ivacaftor in G551D-mediated cystic fibrosis. *Am. J. Respir. Crit. Care Med.* 190, 175–184. doi: 10.1164/rccm.201404-0703oc

Saadane, A., Eastman, J., Berger, M., and Bonfield, T. L. (2011). Parthenolide inhibits ERK and AP-1 which are dysregulated and contribute to excessive IL-8 expression and secretion in cystic fibrosis cells. *J. Inflamm.* 8:26. doi: 10.1186/1476-9255-8-26

Saint-Criq, V., and Gray, M. A. (2017). Role of CFTR in epithelial physiology. *Cell. Mol. Life Sci.* 74, 93–115. doi: 10.1007/s00018-016-2391-y

Sayner, S. L., Frank, D. W., King, J., Chen, H., VandeWaa, J., and Stevens, T. (2004). Paradoxical cAMP-induced lung endothelial hyperpermeability revealed by *Pseudomonas aeruginosa* ExoY. *Circ. Res.* 95, 196–203. doi: 10.1161/01.res.0000134922.25721.d9

Schwarzer, C., Illek, B., Suh, J. H., Remington, S. J., Fischer, H., and Machen, T. E. (2007). Organelle redox of CF and CFTR-corrected airway epithelia. *Free Radic. Biol. Med.* 43, 300–316. doi: 10.1016/j.freeradbiomed.2007.04.015

Sender, R., Fuchs, S., and Milo, R. (2016). Revised estimates for the number of human and bacteria cells in the body. *PLoS Biol.* 14:e1002533. doi: 10.1371/journal.pbio.1002533

Seo, Y., Lee, H. K., Park, J., Jeon, D. K., Jo, S., Jo, M., et al. (2016). Ani9, a novel potent small-molecule ANO1 inhibitor with negligible effect on ANO2. *PLoS One* 11:e0155771. doi: 10.1371/journal.pone.0155771

Solic, N., Wilson, J., Wilson, S. J., and Shute, J. K. (2005). Endothelial activation and increased heparan sulfate expression in cystic fibrosis. *Am. J. Respir. Crit. Care Med.* 172, 892–898. doi: 10.1164/rccm.200409-1207oc

Stahl, M., Stahl, K., Brubacher, M. B., and Forrest, J. N. Jr. (2012). Divergent CFTR orthologs respond differently to the channel inhibitors CFTRinh-172, glibenclamide, and GlyH-101. *Am. J. Physiol. Cell Physiol.* 302:C76.

Stolarczyk, M., Veit, G., Schnur, A., Veltman, M., Lukacs, G. L., and Scholte, B. J. (2018). Extracellular oxidation in cystic fibrosis airway epithelium causes enhanced EGFR/ADAM17 activity. *Am. J. Physiol. Lung Cell Mol. Physiol.* 314, L555–L568.

Suzuki, T., Shibata, T., Takaya, K., Shiraishi, K., Kohno, T., Kunitoh, H., et al. (2013). Regulatory nexus of synthesis and degradation deciphers cellular Nrf2 expression levels. *Mol. Cell Biol.* 33, 2402–2412. doi: 10.1128/mcb.00065-13

Totani, L., Plebani, R., Piccoli, A., Di Silvestre, S., Lanuti, P., Recchiuti, A., et al. (2017). Mechanisms of endothelial cell dysfunction in cystic fibrosis. *Biochim. Biophys. Acta* 1863, 3243–3253.

Tousson, A., Van Tine, B. A., Naren, A. P., Shaw, G. M., and Schwiebert, L. M. (1998). Characterization of CFTR expression and chloride channel activity in human endothelia. *Am. J. Physiol.* 275, C1555–C1564.

Tucker, M. A., Fox, B. M., Seigler, N., Rodriguez-Miguelez, P., Looney, J., Thomas, J., et al. (2019). Endothelial dysfunction in cystic fibrosis: role of oxidative stress. *Oxidat. Med. Cell. Longev.* 2019:8.

Türei, D., Papp, D., Fazekas, D., Földvári-Nagy, L., Módos, D., Lenti, K., et al. (2013). NRF2-ome: an integrated web resource to discover protein interaction and regulatory networks of NRF2. *Oxid. Med. Cell Longev.* 2013:737591.

Valdivieso, A. G., and Santa-Coloma, T. A. (2013). CFTR activity and mitochondrial function. *Redox Biol.* 1, 190–202. doi: 10.1016/j.redox.2012.11.007

Veit, G., Bossard, F., Goepp, J., Verkman, A. S., Galietta, L. J., Hanrahan, J. W., et al. (2012). Proinflammatory cytokine secretion is suppressed by TMEM16A or CFTR channel activity in human cystic fibrosis bronchial epithelia. *Mol. Biol. Cell* 23, 4188–4202. doi: 10.1091/mbc.e12-06-0424

Vij, N., Mazur, S., and Zeitlin, P. L. (2009). CFTR is a negative regulator of NFkappaB mediated innate immune response. *PLoS One* 4:e4664. doi: 10.1371/journal.pone.0004664

Vizzardi, E., Sciatti, E., Bonadei, I., Cani, D. S., Menotti, E., Prati, F., et al. (2019). Macro- and microvascular functions in cystic fibrosis adults without cardiovascular risk factors: a case-control study. *Monaldi Arch. Chest Dis.* 89.

Wang, H., Cebotaru, L., Lee, H. W., Yang, Q., Pollard, B. S., Pollard, H. B., et al. (2016). CFTR controls the activity of NF-kappaB by enhancing the degradation of TRADD. *Cell Physiol. Biochem.* 40, 1063–1078. doi: 10.1159/000453162

Wang, H., and Su, Y. (2011). Collagen IV contributes to nitric oxide-induced angiogenesis of lung endothelial cells. *Am. J. Physiol. Cell Physiol.* 300, C979–C988.

Weng, M. S., Chang, J. H., Hung, W. Y., Yang, Y. C., and Chien, M. H. (2018). The interplay of reactive oxygen species and the epidermal growth factor receptor in tumor progression and drug resistance. *J. Exp. Clin. Cancer Res.* 37:61.

Yoshioka, T., Homma, T., Meyrick, B., Takeda, M., Moore-Jarrett, T., Kon, V., et al. (1994). Oxidants induce transcriptional activation of manganese superoxide dismutase in glomerular cells. *Kidney Int.* 46, 405–413. doi: 10.1038/ki.1994.288

Zhang, L., Button, B., Gabriel, S. E., Burkett, S., Yan, Y., Skiadopoulos, M. H., et al. (2009). CFTR delivery to 25% of surface epithelial cells restores normal rates of mucus transport to human cystic fibrosis airway epithelium. *PLoS Biol.* 7:e1000155. doi: 10.1371/journal.pbio.1000155

Zhang, Z., Leir, S. H., and Harris, A. (2015). Oxidative stress regulates CFTR gene expression in human airway epithelial cells through a distal antioxidant response element. *Am. J. Respir. Cell Mol. Biol.* 52, 387–396. doi: 10.1165/rcmb.2014-0263oc

Zhou-Suckow, Z., Duerr, J., Hagner, M., Agrawal, R., and Mall, M. A. (2017). Airway mucus, inflammation and remodeling: emerging links in the pathogenesis of chronic lung diseases. *Cell Tissue Res.* 367, 537–550. doi: 10.1007/s00441-016-2562-z

Conflict of Interest: The authors declare that the research was conducted in the absence of any commercial or financial relationships that could be construed as a potential conflict of interest.

frontiers in Physiology

ORIGINAL RESEARCH
published: 27 August 2020
doi: 10.3389/fphys.2020.00898

Additional Improvement of Respiratory Technique on Vascular Function in Hypertensive Postmenopausal Women Following Yoga or Stretching Video Classes: The YOGINI Study

*Cláudia Fetter[1], Juliana Romeu Marques[1], Liliane Appratto de Souza[1], Daniela Ravizzoni Dartora[1,2], Bruna Eibel[1], Liliana Fortini Cavalheiro Boll[1], Sílvia Noll Goldmeier[1], Danielle Dias[3,4], Katia De Angelis[3,4] and Maria Cláudia Irigoyen[1,5]**

[1] Clinical Investigation Laboratory (LIC), Cardiology Institute of Rio Grande do Sul/Cardiology University Foundation (IC-FUC), Porto Alegre, Brazil, [2] Sainte Justine Hospital and Research Center, Montreal, QC, Canada, [3] Department of Physiology, Federal University of São Paulo (UNIFESP), São Paulo, Brazil, [4] Laboratory of Translational Physiology, Universidade Nove de Julho (UNINOVE), São Paulo, Brazil, [5] Experimental Laboratory of Hypertension, Heart Institute (InCor), University of São Paulo (USP), São Paulo, Brazil

OPEN ACCESS

Edited by:
Felix W. Wehrli,
University of Pennsylvania,
United States

Reviewed by:
Barbara Ruszkowska-Ciastek,
Nicolaus Copernicus University in Torun, Poland
María S. Fernández-Alfonso,
Complutense University of Madrid, Spain

***Correspondence:**
Maria Cláudia Irigoyen
hipirigoyen@incor.usp.br

Specialty section:
This article was submitted to Vascular Physiology, a section of the journal Frontiers in Physiology

Received: 09 December 2019
Accepted: 06 July 2020
Published: 27 August 2020

Citation:
Fetter C, Marques JR, de Souza LA, Dartora DR, Eibel B, Boll LFC, Goldmeier SN, Dias D, De Angelis K and Irigoyen MC (2020) Additional Improvement of Respiratory Technique on Vascular Function in Hypertensive Postmenopausal Women Following Yoga or Stretching Video Classes: The YOGINI Study. Front. Physiol. 11:898. doi: 10.3389/fphys.2020.00898

Background: Hypertension remains highly prevalent in postmenopausal women, along with vascular dysfunction and increased oxidative stress. In such context, regular exercises, yoga practice, and slow breathing have been recommended to treat hypertension. However, the effects of the multiple components of yoga, including the respiratory techniques involved in the practice, on hypertension and on vascular and endothelial function have never been evaluated.

Objective: This study aimed to investigate the additional effects of respiratory technique on vascular function and oxidative stress profile in hypertensive postmenopausal women (HPMWs) following yoga or stretching video classes.

Study Design: Hypertensive postmenopausal women were recruited and randomized for 12 weeks, twice a week, of supervised yoga or stretching video classes of 75 min for 12 weeks associated or not with respiratory technique. Baseline and post-intervention measurements included pulse wave velocity (PWV), flow-mediated dilation (FMD), and oxidative stress parameters. Hypertensive postmenopausal women (59 ± 0.7 years) who ended the protocol were distributed into three groups: (1) control group (yoga or stretching, C, $n = 14$); (2) yoga + respiratory technique (Y+, $n = 10$); (3) stretching + respiratory technique (S+, $n = 9$).

Results: Diastolic blood pressure and FMD [baseline: C: 6.94 ± 1.97%, Y+: 7.05 ± 1.65%, and S+: 3.54 ± 2.01% vs. post: C: 16.59 ± 3.46% ($p = 0.006$), Y+: 13.72 ± 2.81% ($p = 0.005$), and S+: 11.79 ± 0.99% ($p = 0.0001$)] have significantly increased in all groups when baseline and post-practice values were compared. However, resting heart rate and PWV [baseline: Y+: 10.44 ± 3.69 and S+: 9.50 ± 0.53 m/s vs. post:

Y+: 9.45 ± 0.39 (p = 0.003) and S+: 8.02 ± 0.47 m/s (p = 0.003)] decreased significantly only in the Y+ and S+ groups (baseline vs. post). Systemic antioxidant enzyme activities (superoxide dismutase and catalase) increased in all groups, and hydrogen peroxide and lipoperoxidation reduced in Y+ and S+ (baseline vs. post).

Conclusions: Twelve weeks of yoga or stretching video classes promoted positive changes in several outcomes generally regarded as cardiovascular risk factors in HPMWs, and these changes were even more pronounced by the association with respiratory technique.

Keywords: hypertension, arterial stiffness, endothelial function, yoga, breathing, oxidative stress

INTRODUCTION

There is a remarkable increased prevalence of hypertension in postmenopausal women (Yanes and Reckelhoff, 2011; Modena, 2014). Hypoestrogenism caused by menopause exerts deleterious effects on several tissues and organs, including vessels (Somani et al., 2019). This may lead to endothelial dysfunction (Sanchez-Barajas et al., 2018) arterial stiffness (Muka et al., 2016; Costa-Hong et al., 2018), and unfavorable oxidative stress profile (Dinh et al., 2014).

The mechanisms by which menopause leads to changes in vascular bed and impairment in endothelial function are complex and diverse, including decreasing vasodilation capacity and impairing the ability of signaling of blood flow, endothelium, and smooth muscle cells of the media layer (Somani et al., 2019). This process improperly generates reactive oxygen species (ROS), causing losses for vascular homeostasis (Hsieh et al., 2014). Along with this, increasing vascular resistance may represent a burden for hypertension and an overload for central arteries (Thijssen et al., 2016). Damage caused by mechanic stress of blood flow on walls of central arteries leads to lower compliance and arterial stiffness (Mitchell, 2009; Laurent, 2012). Arterial stiffness, in turn, increases with age, but the deleterious effects of menopause should not be seen as part of the natural aging process (Costa-Hong et al., 2018).

Taken together, these conditions demand appropriate clinical management, which should include non-pharmacological strategies in order to prevent their progression to cardiovascular diseases (Yanes and Reckelhoff, 2011). Among others, regular physical exercises and slow breathing are highly recommended to treat the effects of hypertension (Cornelissen and Smart, 2013), and in recent years, yoga also has been found to be an effective intervention (Hagins et al., 2013). Despite controversial results of yoga on arterial stiffness (Patil et al., 2015, 2017), an association between poor trunk flexibility and arterial stiffness has already been demonstrated (Yamamoto et al., 2009). Regarding endothelial function, several studies have demonstrated the effectiveness of yoga (Hunter et al., 2017, 2018). However, the impact of slow breathing on endothelial and vascular function has not yet been demonstrated (Limberg et al., 2013; DeLucia et al., 2018). Multiple components of yoga such as physical poses (*asanas*), respiratory exercises (*pranayamas*), meditation, and devotional and lifestyle aspects have never been analyzed separately in order to assess specific benefits (Hartley et al., 2014).

Pranayamas present different forms and speeds of inhalation, exhalation, and retentions (Jerath et al., 2006). *Ujjayi* is a slow-breathing *pranayama,* which narrows the glottis and extends respiratory phases. It decreases respiratory rate, and it is usually performed along with physical poses (Satin et al., 2014). Physical poses take limbs and spine to great range of motion, demanding mostly agonists' isometric contractions and antagonists' muscle group stretching (Jorge et al., 2016). In recent years, stretching has been regarded as an exercise able to promote changes on vascular function (Kato et al., 2017). Positive effects of single bouts of stretching have been reported, although mechanisms involved in such responses are not fully elucidated, and no studies have been carried out on chronic effects of this kind of exercise (Kruse et al., 2016; Kruse and Scheuermann, 2017).

As an innovative investigation, we may well hypothesize that in hypertensive postmenopausal women (HPMWs) additional improvements resulting from yoga poses and respiratory technique may be expected for blood pressure, vascular, and endothelial function, and oxidative stress profile after 12 weeks of video classes twice a week. Therefore, the aim of this study was to investigate the additional effect of respiratory techniques on vascular function and oxidative stress profile in HPMWs, following 12 weeks of yoga or stretching video classes.

METHODS

Ethical Considerations

The Ethical Committee of Instituto de Cardiologia do Rio Grande do Sul/Fundação Universitária de Cardiologia approved this study, which is in accordance with CONSORT statement. All participants signed an informed written consent form. Data have been collected between July 2018 and December 2019. The study was registered in the Clinical Trials Registry (NCT03137849). All data have been fed into the REDCap Platform (www.redcap.cardiology.org.br).

Participants

Patients have been recruited from the institution patient data, along with a social media network (i.e., Facebook). Inclusion criteria were as follows: age 45 to 68 years old, minimum of 12 months of amenorrhea, follicle-stimulating hormone >35

mUI/mL, blood pressure >140/90, or in continuous use of medication [diuretics, Ca^{+} channel inhibitors, angiotensin-converting enzyme (ACE) inhibitors, ARA2], not undergoing hormone replacement therapy, leading a sedentary lifestyle, and no previous yoga practice. Exclusion criteria were as follows: use of β-blockers and/or psychiatric medication, recent cardiovascular events or surgery, renal alterations, respiratory, and/or neuromotor pathologies, smoking, and body mass index >34.9 kg/m^2.

Randomization and Outcome Measures

After signing the informed consent form, participants were randomized and underwent baseline assessments at Clinical Investigation Laboratory and Ergometry Room of Institute of Cardiology of Rio Grande do Sul/Cardiology University Foundation by trained personnel blinded to the randomization. They were randomized into yoga, stretching, yoga + respiratory technique, and stretching + respiratory technique interventions. Given the dropout of subjects, and the lack of differences between yoga and stretching in baseline and post-interventions in the assessed parameters, participants were assigned into three groups: (1) control (yoga or stretching interventions alone, C, $n = 14$); (2) yoga + respiratory technique (Y+, $n = 10$), and (3) stretching + respiratory technique (S+, $n = 9$).

The participants were previously advised to fast overnight (12 h) and to refrain from alcohol, caffeine, and intensive exercise practice and were told to have proper night of sleep 24 h prior the examination day.

On the day of the evaluation, anthropometric measures, and body composition by bioimpedance were taken (BIODYNAMICS 310^{TM}). Systolic (SBP), diastolic blood pressure (DBP), and heart rate were assessed according to the American Health Association guideline recommendations. Blood sample were collected for biochemical analysis and systemic oxidative stress evaluations.

Arterial stiffness and endothelial function were assessed as described in the following section. Exercise electrocardiogram was performed to rule out any cardiac disease and to estimate maximal oxygen uptake (VO_{2max}). Flexibility was evaluated with "Sit and Reach" test (Ayala et al., 2012).

After baseline assessments, participants attended 12 weeks (24 classes) of intervention and underwent final evaluations in the same baseline order. All participants have been told they were attending a yoga protocol. Blind investigators have taken all outcomes assessments to the interventions.

All evaluations have been repeated in the same order after completion of protocol, as follows:

Biochemical Analyses

Fasting blood samples were collected to analyze fasting glucose (automated enzymatic method). Total cholesterol, high-density lipoprotein cholesterol, and triglycerides were assessed by the enzymatic colorimetric method. Follicle-stimulating hormone was assessed by the electrochemiluminescence method.

Arterial Stiffness

Arterial stiffness was assessed by pulse wave velocity (PWV), which refers to the time a systolic wave travels in an arterial segment (Costa-Hong et al., 2018). Augmentation Index (Aix) refers to the sum of both anterograde systolic wave and the previously reflected systolic wave, and it is considered a reliable measure for vascular resistance along the arterial tree (Mitchell, 2009). Arterial stiffness was assessed by Complior Analyzer^{TM} (ALAM Medical, France). Sensors were positioned upon the right carotid and femoral arteries. Distance between carotid and femoral pulse was provided by the investigator. Measures of blood pressure, height, and weight were fed into the software. Three consecutive measures were obtained from the equipment at a quality signal >90%. The mean of these three measures was considered for analysis of PWV, Aix, and central SBP and DBP (cSBP and cDBP, respectively) (Townsend et al., 2015).

Endothelial Function (Flow-Mediated Dilation)

A high-resolution ultrasonography equipment (Esaote My Lab 70X Vision) was used for the evaluation of endothelial function through a high-frequency transducer to obtain longitudinal images of the brachial artery. The transducer was positioned upon the brachial artery in the 1/3 arm size of superior antecubital fossa. Baseline images were recorded for 1 min, and this was immediately followed by a cuffing inflated up to 200 mmHg and kept for 5 min in order to characterize reactive hyperemia. Thirty seconds before the cuffing was released, new images started to be recorded for 3 min, considered endothelium-dependent dilation, and were analyzed by the Cardiovascular Suite^{TM} software (Quipu, Italy). The software demands to specify the interest area of the arterial segment and flow using visual selection. Baseline and post-hyperemia diameter and flow were computed to obtain the percentage of dilation, volume, and shear stress (Thijssen et al., 2019).

Oxidative Stress Evaluations

Blood Sample Collection and Preparation

Whole blood was sampled from the participants in EDTA tubes and then centrifuged at 2,000 rotations per minute (rpm) during 10 min at 4°C. Plasma was removed and kept aside for further analysis. Mononuclear cell fraction was removed, and the red blood cells were washed with phosphate-buffered saline and centrifuged three times, for 5 min each, at 2,000 rpm. Further, in 100 μL of washed red blood cells, 1 mL of acetic acid (1 mM) and $MgSO_4$ (4 mM) was centrifuged at 3,000 rpm for 30 min at 4°C. The supernatant was stored at −80°C for subsequent assessments. Proteins were quantified by the method described by Lowry et al. (1951).

Antioxidant Enzymes: Catalase and Superoxide Dismutase

Catalase (CAT) activity was evaluated by spectrophotometry (240 nm), through the consumption of hydrogen peroxide (H_2O_2; Sigma–Aldrich Corporation, H3410) by measuring decreasing absorbance, whose rate of decomposition is straightly proportional to its activity. Superoxide dismutase (SOD) activity

was determined through measures of oxidative pirogalol (Sigma–Aldrich Corporation, P0381). A colorful by-product based on oxidation of pirogalol was detected by spectrophotometry (420 nm, SP22, Bioespectro) (Fridovich, 1986).

Nicotinamide Adenine Dinucleotide Phosphate Oxidase

Nicotinamide adenine dinucleotide phosphate oxidase (NADPH) oxidase was determined by the rate of NADPH consumption assessed by measuring the decline in absorbance (340 nm) every 10 min, using a plate reader spectrophotometer (Espectra Max 2, Molecular Devices) (Wei et al., 2006). For the assay, we used a 50 mM phosphate buffer containing EDTA (2 mM, Nuclear, 311737), sucrose (150 mM, Sigma–Aldrich Corporation, S7903), NADPH (1.3 mM, Sigma–Aldrich Corporation, N1630) and 10 μL of sample.

Hydrogen Peroxide (H_2O_2)

H_2O_2 was analyzed through measuring of oxidation of phenol red (Sigma–Aldrich Corporation, H3410) mediated by radish peroxidase (Sigma–Aldrich Corporation, P8250), using a plate reader spectrophotometer (610 nm, Espectra Max 2, Molecular Devices) (Pick and Keisari, 1980).

Lipoperoxidation

Plasma lipid peroxide levels were determined by measuring thiobarbituric acid reactive substances (TBARSs), a common method for measuring the concentration of malondialdehyde, the main breakdown product of oxidized lipids. For the TBARS assay, using 250 μL of sample, trichloroacetic acid (10%, wt/vol, Dinamica, 1072-1) was added to the homogenate to precipitate proteins and to acidify the samples. This mixture was then centrifuged (4,000 rpm, 10 min), the protein free sample was extracted, and thiobarbituric acid (0.67%, wt/vol, Sigma–Aldrich Corporation, T-550-0) was added to the reaction medium. The tubes were placed in a water bath (100°C) for 30 min. The absorbences were measured at 535 nm using a spectrophotometer (SP22, Bioespectro) (Buege and Aust, 1978).

Protein Oxidation

Carbonyls represent a marker of the oxidative damage to proteins and were assessed by the reaction of oxidative proteins in plasma with 2,4-dinitrophenylhydrazine (DNPH, Sigma–Aldrich Corporation, D199303) in acid mean. This was followed by successive washings with acid and organic solvents in the final incubation with guanidine hydrochloride solution (6M, Sigma–Aldrich Corporation, G4505). Absorbance of carbonyls was measured by spectrophotometry (360 nm, SP22, Bioespectro) (Reznick and Packer, 1994).

Intervention

The 12 week supervised video classes occurred twice a week between 2:00 and 6:00 P.M and have taken place in a room equipped with a 32-inch-screen television and yoga mats.

Four video classes have been created as intervention: yoga, stretching, yoga + respiratory technique, and stretching + respiratory technique. The respiratory technique employed as intervention was *ujjayi pranayama* (victorious breath), a nasal respiration that narrows the glottis in order to extend both inspiratory and expiratory phases, and was performed along with yoga or stretching poses. Yoga and stretching, as control intervention, took only "inhale/exhale" commands. After the 60 min of yoga or stretching, all groups underwent the same yoga-based relaxation technique in supine position (15 min). The protocols were developed by same experienced yoga and stretching licensed instructor.

Yoga included three full sequences of sun salutations, followed by traditional standing poses, balance poses, stabilizations (core positions) and retroversion poses, sit poses, and final poses in supine position.

Stretching was based on dynamic (warm-up) and static exercises excluding those similar to yoga poses, attaining great range of motion of the main body joints and muscle groups, and did not include any body weight bearing, thus avoiding isometric contractions.

Full video classes of yoga and stretching were compiled as yoga (**Videos 1–6**) and stretching (**Videos 7–12**) for electronic version (in Portuguese audio, associated with respiratory technique).

A comparative plot of interventions is displayed in **Supplemental Table 1**.

Data Analysis

The study was not analyzed as "intention to treat." A secondary analysis of those participants who ended the protocol was provided. Because of losses in the follow-up, yoga and stretching not associated with respiratory technique were considered as one active control group, so statistical analyses were performed for three intervention groups: (1) control group (yoga or stretching), (2) yoga + respiratory technique (Y+), (3) stretching + respiratory technique (S+). Power of study was calculated *a posteriori* considering PWV variance among groups for post-intervention values, which was determined as $\beta = 0.83$. Medication classes used by participants were divided into five categories: (1) none, (2), diuretics, (3) angiotensin-converting enzyme inhibitor, (4) angiotensin II receptor blockers (ARBs), (5) combination of any class. This classification was taken to determine any differences among groups concerning the use of drug classes.

Collected data were processed by SPSS Statistics for Windows, version 25.0. Differences between post-intervention and baseline measures and among groups were calculated to determine changes in the outcome measures by GEE (generalized estimating equation), in order to obtain population-averaged effects. Bonferroni *post-hoc* test was performed. Two factors have been considered for analysis: intervention group, named "group," and moment of evaluation (baseline and post-intervention), named "moment," as well as interaction between them, called "interaction." Data are shown as mean (M) ± standard error (SE). Correlations of Pearson for parametric data and Spearman (non-parametric) have been taken. Significance considered a $p \leq 0.05$.

RESULTS

Study Population

The eligible study population consisted of 50 women, of which 33 completed the 12 week protocol (**Figure 1**). Participants'

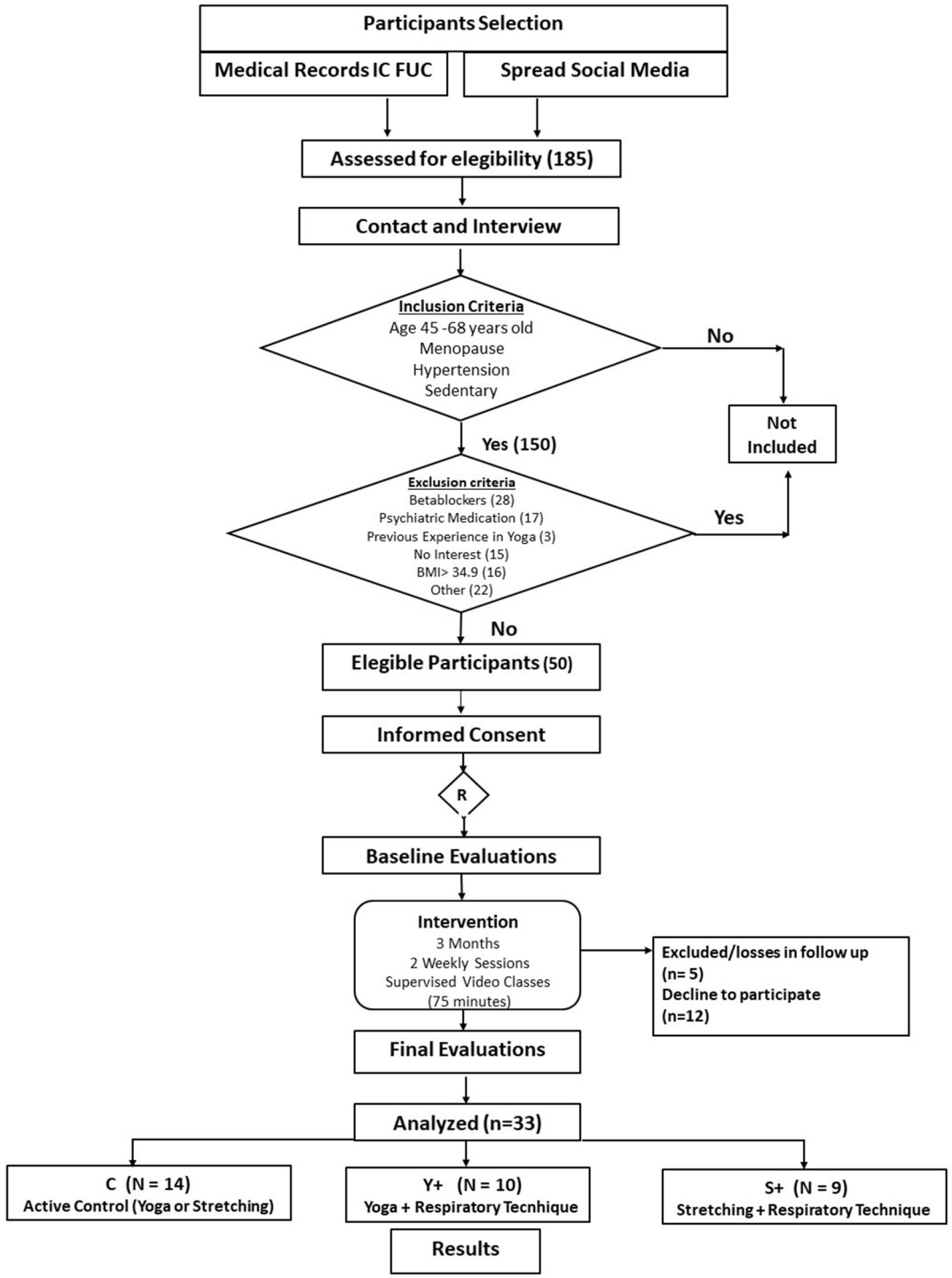

FIGURE 1 | Flowchart of recruitment.

age and time of menopause were similar among groups (**Table 1**).

Five participants were not taking any medication, three participants used only diuretics, 4 participants used ACE inhibitors, nine participants used ARBs, and 12 used a combination of drugs, including three who used of calcium-channel blockers. There were no differences between treated and untreated participants and the type of drugs used in all groups.

Body mass index was not changed significantly in any group from baseline to post-intervention moments. However,

TABLE 1 | Characterization of participants after randomization, at baseline, and post-intervention for 12 weeks of video classes two times a week.

	C ($n = 14$)		Y + ($n = 10$)		S + ($n = 9$)		GEE		
	Baseline	**Post**	**Baseline**	**Post**	**Baseline**	**Post**	***P* group**	***P* moment**	***p* interaction**
Age (years)	59 ± 1,1	_	58.00 ± 1.2	_	60.44 ± 1.1	_			
Time of menopause (years)	9.5 ± 1.6	_	9.40 ± 1.54	_	10.22 ± 1.65	_			
Anthropometric measures									
BMI (kg/cm^2)	27.68 ± 0.7	27.36 ± 0.7	25.93 ± 1.33	26.09 ± 1.33	29.43 ± 0.47	29.08 ± 0.50*	0.019	0.105	0.047
Fat Percentage (%)	35.66 ± 1.1	35.79 ± 1.16	34.34 ± 1.30	34.80 ± 1.44	38.94 ± 0.72	39.32 ± 0.63	0.001	0.233	0.984
Abdom circunference (cm)	85.25 ± 2.08	82.57 ± 2.38*	84.06 ± 3.15	82.39 ± 2.95	92.67 ± 1.55	88.83 ± 2.29*	0.019	0.001	0.601
Biochemychal analyses									
Glucose (mg/dL)	107.9 ± 5.3	103.6 ± 4.9	92.9 ± 2.6	96.4 ± 3.9	100.9 ± 6.8	100.7 ± 3.8	0.145	0.835	0.100
Total cholesterol (mg/dL)	217.3 ± 7.5	199.8 ± 7.9*	237.3 ± 11.0	227.6 ± 11.1*	192.8 ± 13.0	189.5 ± 12.1	0.037	<0.001	0.132
Cholesterol HDL (mg/dL)	53.6 ± 2.0	55.1 ± 3.0	63.5 ± 6.5	62.2 ± 5.9	64.1 ± 6.8	65.4 ± 6.5	0.176	0.658	0.655
Cholesterol LDL (mg/dL)	130.2 ± 7.5	114.6 ± 7.9*	148.1 ± 12.9	134.1 ± 11.5*	105.1 ± 14.3	97.8 ± 11.9	0.077	<0.001	0.552
Triglycerides (mg/dL)	167.5 ± 20.1	145.5 ± 15.5	124.2 ± 11.8	117.2 ± 12.9	117.8 ± 12.3	120.8 ± 16.6	0.110	0.302	0.474
FSH (mUI/mL)	71.5 ± 5.4	67.7 ± 5.9	82.5 ± 11.3	85.1 ± 9.9	66.3 ± 9.2	64.6 ± 9.0	0.374	0.585	0.429
Functional measures									
VO_2max (ml/kg/min)	30.1 ± 1.7	31.4 ± 1.6	31.85 ± 2.2	33.89 ± 2.3	27.6 ± 1.4	29.5 ± 1.9	0.167	0.110	0.927
Flexibility test (cm)	23.9 ± 2.0	29.1 ± 2.5*	21.6 ± 3.2	30.6 ± 3.1*	19.6 ± 3.0	24.9 ± 2.4*	0.388	<0.001	0.410
Hemodynamic measures									
SBP (mmHg)	142.9 ± 5.8	134.5 ± 4.1*	137.4 ± 3.8	136.9 ± 4.0	141.2 ± 4.7	125.6 ± 5.0*	0.70	<0.001	<0.001
DBP (mmHg)	82.66 ± 2.7	78.66 ± 2.5*	86.23 ± 2.18	83.10 ± 2.35*	87.15 ± 2.98	76.37 ± 3.01*	0.418	<0.001	0.015
Heart rate (bpm)	67.7 ± 1.9	66.9 ± 2.1	68.7 ± 2.6	63.7 ± 2.7*	66.4 ± 2.2	63.4 ± 2.0*	0.683	0.005	0.269
Respiratory rate (cpm)	15.5 ± 0.9	14.7 ± 0.9	14.2 ± 0.9	13.9 ± 0.9	16.5 ± 1.8	15.9 ± 0.9	0.145	0.090	0.807

*Data shown as mean (M) ± standard error (SE). C, control group (yoga poses or stretching); Y+, yoga poses plus respiratory technique group; S+, stretching plus respiratory technique group; BMI, body mass index; HDL, high-density lipoprotein; LDL, low-density lipoprotein; FSH, follicle-stimulating hormone; VO_2max, maximal oxygen uptake; SBP, systolic blood pressure; DPB, diastolic blood pressure. *Intragroup analyses, $p \leq 0.05$ baseline vs. post by GEE.*

abdominal circumference was significantly decreased when baseline and post-intervention were compared. This is displayed in **Table 1**, which shows a significant decrease in the C ($p = 0.031$) and in S+ groups ($p = 0.009$), but not in the Y+ group ($p = 0.294$).

Biochemical Analysis

Total cholesterol levels and low-density lipoprotein (LDL) cholesterol decreased significantly in the C and Y+ groups when baseline and post-intervention were compared ($p = 0.009$, and $p = 0.039$). S+ did not present significant changes in these parameters. Other biochemical assessments were similar among groups and time of evaluation (**Table 1**).

Functional Measures

Estimated maximal oxygen consumption was not changed in any group after intervention. Significantly increased flexibility was noticed in all groups through flexibility test (C: $p = 0.034$, Y+: $p = 0.0001$, and S+: $p = 0.001$; **Table 1**).

Hemodynamic Measures

This study has demonstrated a significant improvement from baseline to post-intervention values concerning hemodynamic measures, as demonstrated in **Table 1** (moment baseline vs. post by GEE). Systolic blood pressure was decreased significantly in both the C and S+ groups (**Figure 2A**), whereas DBP decreased significantly in all groups (**Figure 2B**). Heart rates at rest decreased significantly in the Y+ and S+ groups, whereas the C group has not changed significantly when baseline and post-intervention were compared (**Figure 2C**). Respiratory rate was not changed significantly in any group (**Figure 2D**).

Arterial Stiffness

Pulse wave velocity and years of menopause showed a moderate significant correlation at baseline ($r = 0.613$, $p < 0.001$), which was non-significant in the post-intervention assessment ($r = 0.243$, $p = 0.187$; **Figure 3**). Most outcomes of arterial stiffness demonstrated a significant improvement when baseline and post-intervention measurements were compared, as demonstrated in **Table 2** (moment baseline vs. post by GEE). Augmentation Index was significantly decreased in the C group, and central DBP

decreased in all groups when baseline and post-intervention were compared. The PWV decreased significantly only in both groups with respiratory technique post-intervention, but not in the control group (**Figure 4**).

Endothelial Function

Rest value diameters were no changed significantly, but flow-mediated dilation (FMD) (%) had a significant increase in all groups after interventions (**Figure 5**). Time to peak (TP), mean flow of FMD, and mean shear stress of FMD did not present any significant change. However, rest mean flow and mean shear stress were increased significantly only in the Y+ group. The data are shown in **Table 2**.

Oxidative Stress

All systemic oxidative stress parameters demonstrated significant improvement when baseline and post-intervention measurements were compared (moment baseline vs. post by GEE), as demonstrated in **Table 3**. Regarding antioxidants, SOD, and CAT activities showed significant increases in all intervention groups when baseline and post-intervention values were compared. Although NADPH oxidase was not different, H_2O_2 concentration and lipoperoxidation (TBARS) decreased significantly in the Y+ and S+ groups after interventions. Protein oxidation (carbonyls) showed significant decrease in C and Y+ groups.

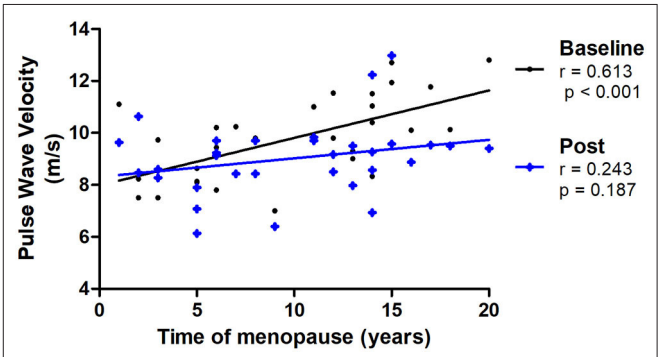

FIGURE 3 | Correlations of PWV (pulse wave velocity) and time of menopause at baseline and post-intervention ($N = 31$).

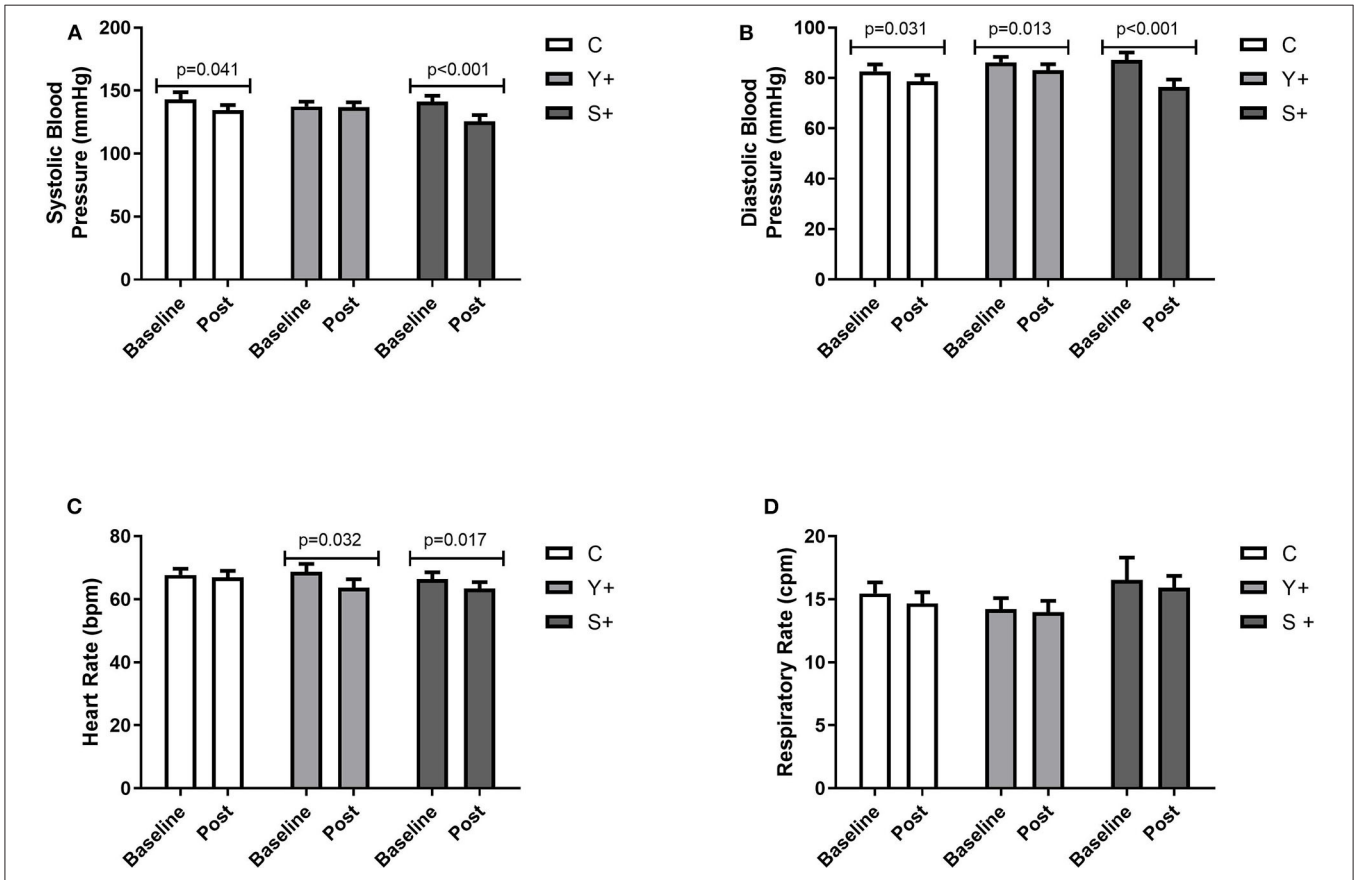

FIGURE 2 | Hemodynamic and respiratory measures. **(A)** Systolic blood pressure expressed in mmHg. **(B)** Diastolic blood pressure expressed in mmHg. **(C)** Heart rate at rest expressed in beats per minute (bpm). **(D)** Respiratory rate expressed in cycles per minute (cpm). Baseline and post-intervention variations by generalized estimation equation (GEE) determined as Mean ± standard error. C, control group (yoga poses or stretching); Y+, yoga poses plus stretching technique group; S+, stretching plus control technique group.

TABLE 2 | Vascular function-arterial stiffness and endothelial function [flow-mediated dilation (FMD)].

	C ($n = 14$)		Y + ($n = 9$)		S + ($n = 8$)		GEE		
	Baseline	**Post**	**Baseline**	**Post**	**Baseline**	**Post**	***P* group**	***P* moment**	***p* interaction**
Arterial stiffness									
Pulse wave velocity (m/s)	9.5 ± 0.4	9.3 ± 0.4	10.4 ± 0.4	9.5 ± 0.4*	9.5 ± 0.5	8.1 ± 0.5*	0.132	<0.001	0.076
Augmentation Index (%)	32.9 ± 4.2	22.7 ± 4.3*	29.2 ± 4.8	29.6 ± 3.4	39.9 ± 7.7	28.7 ± 2.9	0.525	0.032	0.221
cSBP (mmHg)	124.0 ± 4.3	119.8 ± 5.2	125.3 ± 3.9	123.0 ± 3.2	125.5 ± 5.9	119.2 ± 5.7	0.893	0.058	0.681
cDBP (mmHg)	79.8 ± 2.7	76.5 ± 2.7*	87.9 ± 2.8	83.2 ± 2.1*	87.3 ± 2.8	79.5 ± 3.2*	0.085	<0.001	0.293
Endothelial function									
Rest diameter (mm)	4.05 ± 0.17	3.89 ± 0.16	3.95 ± 0.26	3.87 ± 0.20	4.00 ± 0.24	3.83 ± 0.23	0.963	0.331	0.973
FMD diameter (mm)	4.30 ± 0.15	4.50 ± 017	4..22 ± 0.28	4.42 ± 0.30	4.13 ± 0.24	4.29 ± 0.28	0.767	0.291	0.988
FMD (%)	6.94 ± 1.97	16.59 ± 3.46*	7.05 ± 1.65	13.72 ± 2.81*	3.54 ± 2.01	11.79 ± 0.99*	0.187	<0.001	0.764
TP (s)	64 ± 14	63 ± 12	42 ± 11	83.0 ± 16.	83 ± 21	75 ± 15	0.388	0.450	0.250
Rest mean flow (ml)	129 ± 23	103 ± 17	83 ± 15	133 ± 16*	64 ± 22	104 ± 18	0.332	0.106	0.022
Mean flow FMD (ml)	316 ± 32	304 ± 45	393 ± 47	455 ± 61	250 ± 53	341 ± 75	0.036	0.268	0.501
Rest mean shear stress (dynes/cm^2)	170 ± 34	164 ± 29	126 ± 26	216 ± 38*	137 ± 61	206 ± 57	0.994	0.022	0.116
Mean shear stress FMD (dynes/cm^2)	381 ± 44	324 ± 36	555 ± 79	571 ± 63	436 ± 119	498 ± 64	0.001	0.907	0.641

Arterial stiffness assessed by Complior™ and flow-mediated dilation (FMD) at baseline and post-intervention for 12 weeks of video classes two times a week. Data shown as mean (M) ± standard error (SE). C, control group (yoga poses or stretching); Y+, yoga poses plus respiratory technique group; S+, stretching plus respiratory technique group. Pulse wave velocity (m/s), Augmentation Index (%), cSBP, central systolic blood pressure (mmHg); cDBP, central diastolic blood pressure (mmHg); FMD, flow-mediated dilation; TP, time to peak.

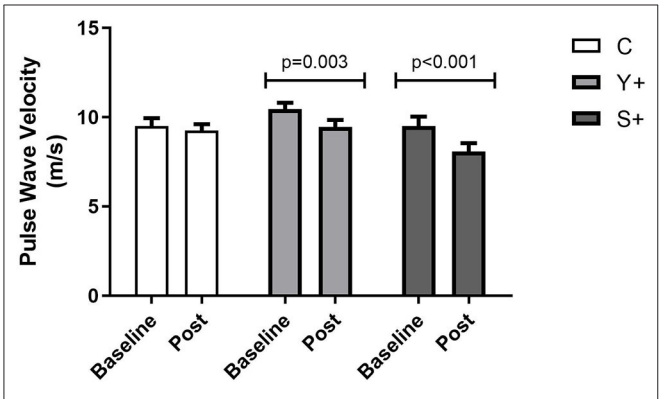

FIGURE 4 | Arterial Stiffness assessed by pulse wave velocity (PWV) by Complior. Baseline and post-intervention variations determined by generalized estimation equation (GEE) determined as mean ± standard error. C, control group (yoga poses or stretching); Y+, yoga poses plus respiratory technique group; S+, stretching plus respiratory technique group.

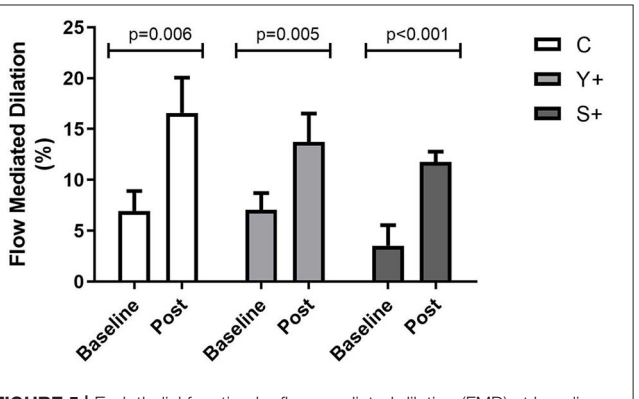

FIGURE 5 | Endothelial function by flow-mediated dilation (FMD) at baseline and post-intervention variations determined by generalized estimation equation (GEE) determined as mean ± standard error. C, control group (Yoga poses or stretching); Y+, yoga poses plus respiratory technique group; S+, stretching plus respiratory technique group.

DISCUSSION

This innovative investigative study was able to demonstrate multiple significant improvements in HPMWs after 12 weeks of yoga or stretching video classes, with additional effects of respiratory technique. General decreases in blood pressure concur to beneficial effects of these practices and are in accordance with previous findings for yoga (Hagins et al., 2014) and respiratory techniques (Pinheiro et al., 2007).

Along with decreased heart rate at rest, both groups with respiratory technique were able to significantly decrease PWV. Previous findings for yoga have demonstrated decreased PWV (Patil et al., 2015), but to our knowledge, this is the first study to demonstrate that protocols including respiratory technique may influence PWV in HPMWs.

TABLE 3 | Oxidative stress.

	C ($n = 12$)		Y+ ($n = 9$)		S + ($n = 8$)		GEE		
	Baseline	**Post**	**Baseline**	**Post**	**Baseline**	**Post**	***P* group**	***P* moment**	***p* interaction**
SOD (USOD/mg protein)	5.15 ± 0.097	6.15 ± 0.13*	5.36 ± 0.12	6.11 ± 0.16*	5.01 ± 0.19	6.11 ± 0.18*	0.566	<0.001	0.533
CAT (nmol/mg protein)	2.17 ± 0.07	2.34 ± 0.06*	2.28 ± 0.11	2.59 ± 0.12*	2.00 ± 0.11	2.47 ± 0.13*	0.290	<0.001	0.229
NADPH (nmol/mg protein)	0.031 ± 0.003	0.026 ± 0.002	0.029 ± 0.003	0.026 ± 0.002	0.030 ± 0.004	0.027 ± 0.002	0.575	0.056	0.082
H_2O_2 (μM H_2O_2)	23.6 ± 2.38	21.7 ± 2.94	26.5 ± 3.41	18.6 ± 3.54*	32.9 ± 3.42	22.3 ± 3.83*	0.272	0.005	0.078
TBARS (μmol/mg protein)	0.41 ± 0.03	0.36 ± 0.03	0.38 ± 0.04	0.26 ± 0.03*	0.39 ± 0.04	0.27 ± 0.03*	0.281	0.001	0.885
Carbonyls (nmol/mg protein)	1.85 ± 0.13	1.43 ± 0.09*	1.86 ± 0.16	1.49 ± 0.12*	1.69 ± 0.05	1.51 ± 0.09	0.685	0.003	0.476

*Oxidative stress variables at baseline and post-intervention for 12 weeks of video classes two times a week. Data shown as mean (M) ± standard error (SE). C, control group (yoga poses or stretching); Y+, yoga poses plus respiratory technique group; S+, stretching plus respiratory technique group; SOD, superoxide dismutase; CAT, catalase; H_2O_2, hydrogen peroxide; NADPH, nicotinamide adenine dinucleotide phosphate oxidase; TBARS, thiobarbituric acid reactive substances. *Intragroup analyses, $p \leq 0.05$ baseline vs. post by GEE.*

Respiration and heart rhythms respond to their interrelated changes (Dick et al., 2014) and heart rate may modulate vascular endothelium, acting on mechanical pulsatile stress (Laosiripisan et al., 2017). Changes in intrathoracic and transmural pressure during inspiration influences cardiac filling and stroke volume, generating stroke volume variability (Shibata et al., 2006). Thus, changes in pattern of respiration such as expansibility of rib cage may influence hemodynamics. Responses of venous return and atrial filling to respiration may be associated to the pattern of respiration, instead of rate (Byeon et al., 2012). Increasing venous return due to diaphragmatic breathing has been demonstrated in healthy individuals (Miller et al., 2005; Balzan et al., 2014). We may speculate that the decreased PWV and rest heart rate in both groups with respiratory technique in the present study are, at least in part, mediated by these mechanisms.

A moderate significant correlation between PWV and years of menopause at baseline was noticed, as expected (Thijssen et al., 2016). At the end of interventions, this correlation disappeared, showing an attenuation of the effects of menopause on PWV, possibly caused by these non-pharmacological interventions.

Moreover, the prevention of losses in nitric oxide bioavailability should be a goal in HPMWs because estrogen deprivation reduces it and increases ROS (Green et al., 2014) thus increasing risk for atherosclerosis (Witkowski and Serviente, 2018). The increase in FMD in all intervention groups found in this study corroborates previous findings of increased FMD after Bikram yoga (hot yoga) (Hunter et al., 2018) and strengthens the potential role of this practice to prevent deleterious effects of menopause. Increased FMD has also been found after some types of exercise training (Early et al., 2017) including isometric exercises (Badrov et al., 2016) which are present in many yoga poses of this study protocol.

Accordingly, increased systemic antioxidant defenses were noticed in this study, once SOD and CAT, as a frontline expression of it, were increased in all groups. As a unique complex producing only ROS, the tendency to decrease ($p = 0.056$, moment baseline vs. post by GEE) in NADPH oxidase (an important source of superoxide anion) and the reduction in systemic hydrogen peroxide (H_2O_2) concentration in the Y+ and S+ groups indicate an overall decrease of pro oxidants. Regarding oxidative stress damage, lipoperoxidation (TBARS) was reduced when baseline and post-intervention values were compared in the Y+ and S+ groups. Moreover, carbonyls, as markers of oxidative damage to proteins were significantly decreased in groups undergoing yoga intervention (C and Y+, baseline vs. post). Taken together, our findings demonstrate markedly improvements in antioxidant, pro-oxidants, and biomolecule damage after interventions, suggesting additional effects in yoga groups and in the groups undergoing respiratory technique. In fact, beneficial effects of yoga on oxidative stress in elderly hypertensive subjects have been previously demonstrated (Patil et al., 2014) along with the beneficial effects of stretching on oxidative stress profile of heart failure patients (Sankaralingam et al., 2011; Kato et al., 2017).

Perhaps increasing fascicle length and local shear stress by ischemia during stretching, present in both yoga poses and stretching, may provide an overall reduction in peripheral resistance through reducing smooth muscle cells tone, besides other adaptations that may induce changes in endothelial function and oxidative stress profile (Wong and Figueroa, 2014; Kruse and Scheuermann, 2017).

Increased flexibility might be considered a functional achievement, once losses in flexibility are expected in postmenopausal women. Although there were no significant increases in estimated VO_{2max}, decreases in total cholesterol and LDL in C and S+ point to a possible metabolic improvement.

The main limitation of this study lies in the relatively high number of dropouts−17 out of 50 recruited HPMWs—higher than other yoga studies (most carried out in developed countries), which reduced the number of subjects in each group. However, despite that, the power of study calculated *a posteriori*—considering PWV variance among groups for post-intervention—was $\beta = 0.83$.

In summary, our findings demonstrated that yoga poses and stretching supervised video classes for 12 weeks improved blood pressure, arterial stiffness, endothelial function, and

oxidative stress profile in HPMWs. Effects of respiratory technique along with yoga poses or stretching point to possible improvement in arterial stiffness. Therefore, yoga or stretching, even when administered through video classes seems to have a positive impact on several outcomes regarded as cardiovascular risk factors, and these benefits are extended by the association of respiratory technique. Nevertheless, more research based on more robust yoga and stretching interventions and a larger sample are needed to lend further support to our findings.

DATA AVAILABILITY STATEMENT

All data supporting the conclusions of this study will be fully provided on request by authors.

ETHICS STATEMENT

The studies involving human participants were reviewed and approved by Comitê de Ética do Instituto de Cardiologia - 5273/16 - 03/11/2016. The patients/participants provided their written informed consent to participate in this study.

AUTHOR CONTRIBUTIONS

All authors listed have made a substantial, direct and intellectual contribution to the work, and approved it for publication.

FUNDING

This work was supported by CNPQ (Conselho Nacional de Desenvolvimento Científico e Tecnológico) and CAPES (Comissão de Aperfeiçoamento de Pessoal do Nível Superior). KD and MI are recipients of CNPQ-BPQ.

ACKNOWLEDGMENTS

The authors express deep gratitude to all participants of the research, as well as the valuable help of the institutional coworkers that made it possible.

SUPPLEMENTARY MATERIAL

The Supplementary Material for this article can be found online at: https://www.frontiersin.org/articles/10.3389/fphys.2020.00898/full#supplementary-material

REFERENCES

Ayala, F., Sainz de Baranda, P., De Ste Croix, M., and Santonja, F. (2012). Reproducibility and criterion-related validity of the sit and reach test and toe touch test for estimating hamstring flexibility in recreationally active young adults. *Phys. Ther. Sport* 13, 219–226. doi: 10.1016/j.ptsp.2011.11.001

Badrov, M. B., Freeman, S. R., Zokvic, M. A., Millar, P. J., and McGowan, C. L. (2016). Isometric exercise training lowers resting blood pressure and improves local brachial artery flow-mediated dilation equally in men and women. *Eur. J. Appl. Physiol.* 116, 1289–1296. doi: 10.1007/s00421-016-3366-2

Balzan, F. M., da Silva, R. C., da Silva, D. P., Sanches, P. R., Tavares, A. M., Ribeiro, J. P., et al. (2014). Effects of diaphragmatic contraction on lower limb venous return and central hemodynamic parameters contrasting healthy subjects versus heart failure patients at rest and during exercise. *Physiol. Rep.* 2:e12216. doi: 10.14814/phy2.12216

Buege, J., and Aust, S. (1978). Microsomal lipid peroxidation. *Meth. Enzymol* 52, 302–310. doi: 10.1016/S0076-6879(78)52032-6

Byeon, K., Choi, J. O., Yang, J. H., Sung, J., Park, S. W., Oh, J. K., et al. (2012). The response of the vena cava to abdominal breathing. *J. Altern. Complement Med.* 18, 153–157. doi: 10.1089/acm.2010.0656

Cornelissen, V. A., and Smart, N. A. (2013). Exercise training for blood pressure: a systematic review and meta-analysis. *J. Am. Heart Assoc.* 2:e004473. doi: 10.1161/JAHA.112.004473

Costa-Hong, V. A., Muela, H. C. S., Macedo, T. A., Sales, A. R. K., and Bortolotto, L. A. (2018). Gender differences of aortic wave reflection and influence of menopause on central blood pressure in patients with arterial hypertension. *BMC Cardiovasc. Disord.* 18:123. doi: 10.1186/s12872-018-0855-8

DeLucia, C. M., De Asis, R. M., and Bailey, E. F. (2018). Daily inspiratory muscle training lowers blood pressure and vascular resistance in healthy men and women. *Exp. Physiol.* 103, 201–211. doi: 10.1113/EP086641

Dick, T. E., Hsieh, Y. H., Dhingra, R. R., Baekey, D. M., Galan, R. F., Wehrwein, E., et al. (2014). Cardiorespiratory coupling: common rhythms in cardiac, sympathetic, and respiratory activities. *Prog. Brain Res.* 209, 191–205. doi: 10.1016/B978-0-444-63274-6.00010-2

Dinh, Q. N., Drummond, G. R., Sobey, C. G., and Chrissobolis, S. (2014). Roles of inflammation, oxidative stress, and vascular dysfunction in hypertension. *Biomed. Res. Int.* 2014:406960. doi: 10.1155/2014/406960

Early, K. S., Stewart, A., Johannsen, N., Lavie, C. J., Thomas, J. R., and Welsch, M. (2017). The effects of exercise training on brachial artery flow-mediated dilation: a meta-analysis. *J. Cardiopulm. Rehabil. Prev.* 37, 77–89. doi: 10.1097/HCR.0000000000000206

Fridovich, I. (1986). Superoxide dismutases. *Adv. Enzymol Relat. Areas Mol. Biol.* 58, 61–97. doi: 10.1002/9780470123041.ch2

Green, D. J., Dawson, E. A., Groenewoud, H. M., Jones, H., and Thijssen, D. H. (2014). Is flow-mediated dilation nitric oxide mediated?: a meta-analysis. *Hypertension* 63, 376–382. doi: 10.1161/HYPERTENSIONAHA.113.02044

Hagins, M., Rundle, A., Consedine, N. S., and Khalsa, S. B. S. (2014). A randomized controlled trial comparing the effects of yoga with an active control on ambulatory blood pressure in individuals with prehypertension and stage 1 hypertension. *J. Clin. Hypertens.* 16, 54–62. doi: 10.1111/jch.12244

Hagins, M., States, R., Selfe, T., and Innes, K. (2013). Effectiveness of yoga for hypertension: systematic review and meta-analysis. *Evid. Based Complement Alternat. Med.* 2013:649836. doi: 10.1155/2013/649836

Hartley, L., Dyakova, M., Holmes, J., Clarke, A., Lee, M. S., Ernst, E., et al. (2014). Yoga for the primary prevention of cardiovascular disease. *Cochrane Database Syst. Rev.* 5:Cd010072. doi: 10.1002/14651858.CD010072.pub2

Hsieh, H. J., Liu, C. A., Huang, B., Tseng, A. H., and Wang, D. L. (2014). Shear-induced endothelial mechanotransduction: the interplay between reactive oxygen species (ROS) and nitric oxide (NO) and the pathophysiological implications. *J. Biomed. Sci.* 21:3. doi: 10.1186/1423-0127-21-3

Hunter, S. D., Dhindsa, M. S., Cunningham, E., Tarumi, T., Alkatan, M., Nualnim, N., et al. (2017). The effect of bikram yoga on endothelial function in young and middle-aged and older adults. *J. Bodyw. Mov. Ther.* 21, 30–34. doi: 10.1016/j.jbmt.2016.06.004

Hunter, S. D., Laosiripisan, J., Elmenshawy, A., and Tanaka, H. (2018). Effects of yoga interventions practised in heated and thermoneutral conditions on endothelium-dependent vasodilatation: the bikram yoga heart study. *Exp. Physiol.* 103, 391–396. doi: 10.1113/EP086725

Jerath, R., Edry, J. W., Barnes, V. A., and Jerath, V. (2006). Physiology of long pranayamic breathing: neural respiratory elements may provide a mechanism that explains how slow deep breathing shifts the autonomic nervous system. *Med. Hypotheses* 67, 566–571. doi: 10.1016/j.mehy.2006.02.042

Jorge, M. P., Santaella, D. F., Pontes, I. M., Shiramizu, V. K., Nascimento, E. B., Cabral, A., et al. (2016). Hatha yoga practice decreases menopause symptoms and improves quality of life: a randomized controlled trial. *Complement Ther. Med*. 26, 128–135. doi: 10.1016/j.ctim.2016.03.014

Kato, M., Masuda, T., Ogano, M., Hotta, K., Takagi, H., Tanaka, S., et al. (2017). Stretching exercises improve vascular endothelial dysfunction through attenuation of oxidative stress in chronic heart failure patients with an implantable cardioverter defibrillator. *J. Cardiopulm. Rehabil. Prev*. 37, 130–138. doi: 10.1097/HCR.0000000000000229

Kruse, N. T., and Scheuermann, B. W. (2017). Cardiovascular responses to skeletal muscle stretching: "stretching" the truth or a new exercise paradigm for cardiovascular medicine? *Sports Med*. 47, 2507–2520. doi: 10.1007/s40279-017-0768-1

Kruse, N. T., Silette, C. R., and Scheuermann, B. W. (2016). Influence of passive stretch on muscle blood flow, oxygenation and central cardiovascular responses in healthy young males. *Am. J. Physiol. Heart Circ. Physiol*. 310, H1210–H1221. doi: 10.1152/ajpheart.00732.2015

Laosiripisan, J., Parkhurst, K. L., and Tanaka, H. (2017). Associations of resting heart rate with endothelium-dependent vasodilation and shear rate. *Clin Exp Hypertens*. 39, 150–154. doi: 10.1080/10641963.2016.1226890

Laurent, S. (2012). Defining vascular aging and cardiovascular risk. *J. Hypertens*. 30, S3–S8. doi: 10.1097/HJH.0b013e328353e501

Limberg, J. K., Morgan, B. J., Schrage, W. G., and Dempsey, J. A. (2013). Respiratory influences on muscle sympathetic nerve activity and vascular conductance in the steady state. *Am. J. Physiol. Heart Circ. Physiol*. 304, H1615–H1623. doi: 10.1152/ajpheart.00112.2013

Lowry, O. H., Rosebrough, N. J., Farr, A. L., and Randall, R. J. (1951). Protein measurement with the folin phenol reagent. *J. Biol. Chem*. 193, 265–275.

Miller, J. D., Pegelow, D. F., Jacques, A. J., and Dempsey, J. A. (2005). Skeletal muscle pump versus respiratory muscle pump: modulation of venous return from the locomotor limb in humans. *J Physiol.* 563, 925–943. doi: 10.1113/jphysiol.2004.076422

Mitchell, G. F. (2009). Arterial stiffness and wave reflection: biomarkers of cardiovascular risk. *Artery Res*. 3, 56–64. doi: 10.1016/j.artres.2009.02.002

Modena, M. G. (2014). Hypertension in postmenopausal women: how to approach hypertension in menopause. *High Blood Press Cardiovasc. Prev*. 21, 201–204. doi: 10.1007/s40292-014-0057-0

Muka, T., Oliver-Williams, C., Colpani, V., Kunutsor, S., Chowdhury, S., Chowdhury, R., et al. (2016). Association of vasomotor and other menopausal symptoms with risk of cardiovascular disease: a systematic review and meta-analysis. *PLoS ONE* 11:e0157417. doi: 10.1371/journal.pone.0157417

Patil, S. G., Aithala, M. R., and Das, K. K. (2015). Effect of yoga on arterial stiffness in elderly subjects with increased pulse pressure: a randomized controlled study. *Complement Ther. Med*. 23, 562–569. doi: 10.1016/j.ctim.2015.06.002

Patil, S. G., Dhanakshirur, G. B., Aithala, M. R., Naregal, G., and Das, K. K. (2014). Effect of yoga on oxidative stress in elderly with grade-I hypertension: a randomized controlled study. *J. Clin. Diagn. Res.* 8, BC04–BC07. doi: 10.7860/JCDR/2014/9498.4586

Patil, S. G., Patil, S. S., Aithala, M. R., and Das, K. K. (2017). Comparison of yoga and walking-exercise on cardiac time intervals as a measure of cardiac function in elderly with increased pulse pressure. *Indian Heart J*. 69, 485–490. doi: 10.1016/j.ihj.2017.02.006

Pick, E., and Keisari, Y. (1980). A simple colorimetric method for the measurement of hydrogen peroxide produced by cells in culture. *J. Immunol. Methods* 38, 161–170. doi: 10.1016/0022-1759(80)90340-3

Pinheiro, C. H., Medeiros, R. A., Pinheiro, D. G., and Marinho M. D. E. J. (2007). Spontaneous respiratory modulation improves cardiovascular control in essential hypertension. *Arq. Bras. Cardiol*. 88, 651–659. doi: 10.1590/S0066-782X2007000600005

Reznick, A. Z., and Packer, L. (1994). Oxidative damage to proteins: spectrophotometric method for carbonyl assay. *Meth. Enzymol* 233, 357–363. doi: 10.1016/S0076-6879(94)33041-7

Sanchez-Barajas, M., Ibarra-Reynoso, L. D. R., Ayala-Garcia, M. A., and Malacara, J. M. (2018). Flow mediated vasodilation compared with carotid intima media thickness in the evaluation of early cardiovascular damage in menopausal women and the influence of biological and psychosocial factors. *BMC Womens Health* 18:153. doi: 10.1186/s12905-018-0648-3

Sankaralingam, S., Jiang, Y., Davidge, S. T., and Yeo, S. (2011). Effect of exercise on vascular superoxide dismutase expression in high-risk pregnancy. *Am. J. Perinatol*. 28, 803–810. doi: 10.1055/s-0031-1284230

Satin, J. R., Linden, W., and Millman, R. D. (2014). Yoga and psychophysiological determinants of cardiovascular health: comparing yoga practitioners, runners, and sedentary individuals. *Ann. Behav. Med*. 47, 231–241. doi: 10.1007/s12160-013-9542-2

Shibata, S., Zhang, R., Hastings, J., Fu, Q., Okazaki, K., Iwasaki, K., et al. (2006). Cascade model of ventricular-arterial coupling and arterial-cardiac baroreflex function for cardiovascular variability in humans. *Am. J. Physiol. Heart Circ. Physiol*. 291, H2142–H2151. doi: 10.1152/ajpheart.00157.2006

Somani, Y. B., Pawelczyk, J. A., De Souza, M. J., Kris-Etherton, P. M., and Proctor, D. N. (2019). Aging women and their endothelium: probing the relative role of estrogen on vasodilator function. *Am. J. Physiol. Heart Circ. Physiol*. 317, H395–H404. doi: 10.1152/ajpheart.00430.2018

Thijssen, D. H., Carter, S. E., and Green, D. J. (2016). Arterial structure and function in vascular ageing: are you as old as your arteries? *J. Physiol.* 594, 2275–2284. doi: 10.1113/JP270597

Thijssen, D. H. J., Bruno, R. M., van Mil, A., Holder, S. M., Faita, F., Greyling, A., et al. (2019). Expert consensus and evidence-based recommendations for the assessment of flow-mediated dilation in humans. *Eur. Heart J*. 40, 2534–2547. doi: 10.1093/eurheartj/ehz350

Townsend, R. R., Wilkinson, I. B., Schiffrin, E. L., Avolio, A. P., Chirinos, J. A., Cockcroft, J. R., et al. (2015). Recommendations for improving and standardizing vascular research on arterial stiffness: a scientific statement from the american heart association. *Hypertension* 66, 698–722. doi: 10.1161/HYP.0000000000000033

Wei, Y., Sowers, J. R., Nistala, R., Gong, H., Uptergrove, G. M., Clark, S. E., et al. (2006). Angiotensin II-induced NADPH oxidase activation impairs insulin signaling in skeletal muscle cells. *J. Biol. Chem*. 281, 35137–35146. doi: 10.1074/jbc.M601320200

Witkowski, S., and Serviente, C. (2018). Endothelial dysfunction and menopause: is exercise an effective countermeasure? *Climacteric* 21, 267–275. doi: 10.1080/13697137.2018.1441822

Wong, A., and Figueroa, A. (2014). Eight weeks of stretching training reduces aortic wave reflection magnitude and blood pressure in obese postmenopausal women. *J. Hum. Hypertens*. 28, 246–250. doi: 10.1038/jhh.2013.98

Yamamoto, K., Kawano, H., Gando, Y., Iemitsu, M., Murakami, H., Sanada, K., et al. (2009). Poor trunk flexibility is associated with arterial stiffening. *Am. J. Physiol. Heart Circ. Physiol*. 297, H1314–H1318. doi: 10.1152/ajpheart.00061.2009

Yanes, L. L., and Reckelhoff, J. F. (2011). Postmenopausal hypertension. *Am. J. Hypertens*. 24, 740–749. doi: 10.1038/ajh.2011.71

Conflict of Interest: The authors declare that the research was conducted in the absence of any commercial or financial relationships that could be construed as a potential conflict of interest.

frontiers in Physiology

REVIEW
published: 31 August 2020
doi: 10.3389/fphys.2020.00937

Metabolic Imaging and Biological Assessment: Platforms to Evaluate Acute Lung Injury and Inflammation

*Mehrdad Pourfathi[1], Stephen J. Kadlecek[1], Shampa Chatterjee[2] and Rahim R. Rizi[1]**

[1] Department of Radiology, University of Pennsylvania, Philadelphia, PA, United States, [2] Department of Physiology, University of Pennsylvania, Philadelphia, PA, United States

Pulmonary inflammation is a hallmark of several pulmonary disorders including acute lung injury and acute respiratory distress syndrome. Moreover, it has been shown that patients with hyperinflammatory phenotype have a significantly higher mortality rate. Despite this, current therapeutic approaches focus on managing the injury rather than subsiding the inflammatory burden of the lung. This is because of the lack of appropriate non-invasive biomarkers that can be used clinically to assess pulmonary inflammation. In this review, we discuss two metabolic imaging tools that can be used to non-invasively assess lung inflammation. The first method, Positron Emission Tomography (PET), is widely used in clinical oncology and quantifies flux in metabolic pathways by measuring uptake of a radiolabeled molecule into the cells. The second method, hyperpolarized ^{13}C MRI, is an emerging tool that interrogates the branching points of the metabolic pathways to quantify the fate of metabolites. We discuss the differences and similarities between these techniques and discuss their clinical applications.

Keywords: lung inflammation, lung injury, ARDS, FDG-PET, HP-MRI

OPEN ACCESS

Edited by:
Antonio Colantuoni, University of Naples Federico II, Italy

Reviewed by:
Dominga Lapi, University of Naples Federico II, Italy
Romeo Martini, University Hospital of Padua, Italy

****Correspondence:***
Rahim R. Rizi
rahim.rizi@uphs.upenn.edu

Specialty section:
This article was submitted to Vascular Physiology, a section of the journal Frontiers in Physiology

Received: *07 May 2020*
Accepted: *13 July 2020*
Published: *31 August 2020*

Citation:
Pourfathi M, Kadlecek SJ, Chatterjee S and Rizi RR (2020) Metabolic Imaging and Biological Assessment: Platforms to Evaluate Acute Lung Injury and Inflammation. Front. Physiol. 11:937. doi: 10.3389/fphys.2020.00937

INTRODUCTION

Acute respiratory distress syndrome (ARDS) and acute lung injury (ALI) are an acute conditions characterized by pulmonary infiltrates (visible in a chest radiograph) arising from pulmonary inflammation, decreased lung compliance, increased vascular permeability and edema (Ards Definition Task Force Ranieri et al., 2012; Pham and Rubenfeld, 2017). Approximately 200,000 patients each year in the US are diagnosed with ALI/ARDS, of which ˜10% of patients admitted to the intensive care unit (ICU) (Johnson and Matthay, 2010; Ards Definition Task Force Ranieri et al., 2012). Despite being defined over fifty years ago (Ashbaugh et al., 2005), ARDS remains a significant source of mortality in critically ill patients (Steinberg et al., 1994; Miller et al., 1996).

Respiratory failure from ARDS secondary to coronavirus disease 2019 (COVID-19) is a significant clinical challenge. What is more is that the number of patients and mortalities are anticipated to significantly rise in immediate future (Gattinoni et al., 2020; Ramanathan et al., 2020). As such, it is timely to focus our attention toward acute lung injury and tools that can provide additional insight into the biological mechanisms of ARDS and lung inflammation. Such techniques may not only enable earlier detection of lung injury but also can facilitate more effective strategies to monitor

patient's response to maneuvers and pharmacological interventions. The latter is crucial especially as identifying optimal interventions may alleviate the numerous difficulties of ARDS survivors including physical and psychological sequelae, exercise limitation, and increased use of health care services (Herridge, 2017; Thompson et al., 2017).

Pulmonary inflammation has been implicated in the pathogenesis and progression of ARDS and ALI. An important feature of lung inflammation, is the pivotal role of the vascular endothelium in the onset and amplification of inflammation. The endothelial layer is, by virtue of its location, an interface between flowing blood and the tissue and is thus a converging site of inflammation whereby immune cells adhere to the vessel wall, followed by their transmigration into tissue.

The severity of inflammation and cellular changes during early stages of ARDS, is shown to be predictive of progression of injury and eventual outcome (Miller et al., 1996; Shankar-Hari and McAuley, 2017). Indeed ˜33% of ARDS patients have a "hyper-inflammatory" sub-phenotype with a significantly higher mortality rate (Shankar-Hari and McAuley, 2017). Currently ARDS is managed in the ICU through careful optimization of mechanical ventilation to protect the lungs from ventilator-induced injury (Johnson and Matthay, 2010; Fanelli and Ranieri, 2015; Cereda et al., 2016; Tabuchi et al., 2016). However, these protocols do not limit the spread of inflammation (Johnson and Matthay, 2010; Fanelli and Ranieri, 2015).

Currently assessment of pulmonary dysfunction primarily relies on global functional parameters, such as pulmonary function test (PFT) or anatomical imaging tools. These do not provide cellular or molecular information. Histological and biological assessment of the tissue or bronchoalveolar lavage can provide information on inflammatory and injury biomarkers in lung tissue but do not provide regional information and cannot be used for longitudinal monitoring of the severity of lung inflammation and disease. Therefore, tools that enable early detection of pulmonary inflammation followed by its longitudinal assessment can help physicians identify ARDS patients with hyperinflammatory phenotype and monitor their response to pharmacological interventions to select a therapeutic strategy that works best for those patients to ultimately improve outcome.

There are a number of imaging modalities used for diagnosis and clinical management of ARDS (Mills, 2003; Mistry et al., 2008; Cereda et al., 2016; Thompson et al., 2017). Chest X-ray radiography and computed tomography (CT) are extensively used imaging techniques to assess lung inflammation, injury and progression, where edema and immune cell infiltrates appear as opacities (**Figure 1**). However it is not trivial to distinguish opacities caused by infiltration, edema, or atelectasis (Cereda et al., 2019). Moreover, these approaches focus on examining the secondary effects of inflammation rather than directly targeting the metabolic processes that are the underlying drivers of inflammation-induced change.

Molecular imaging tools enable non-invasive interrogation of lung cellularity, and therefore can assess inflammatory activity providing critical information about disease progression, response to therapy and prognosis in real time. The purpose of this review article is to provide a brief overview of two state-of-the-art molecular imaging techniques that are currently used pre-clinically. Both methods exploit alterations in lung metabolism as a result of inflammation to visualize regions with active inflammation. These non-invasive molecular imaging techniques can be used as novel platforms to evaluate pulmonary signaling associated with ARDS/ALI and be integrated with functional and physiological parameters obtained by from patients to improve patient prognosis and outcome.

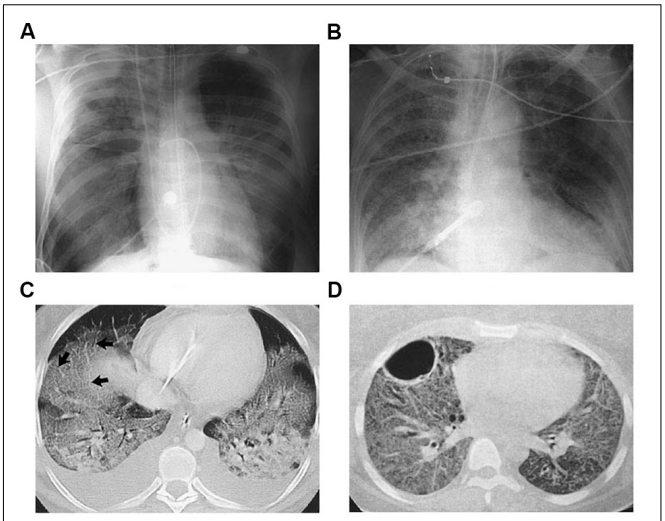

FIGURE 1 | Radiographic and Computed Tomographic (CT) Findings in the Acute, or Exudative, Phase (Panels **A,C**) and the Fibrosing-Alveolitis Phase (Panels **B,D**) of Acute Lung Injury and the Acute Respiratory Distress Syndrome (ARDS). Panel **(A)** shows a chest radiograph from a patient with the ARDS associated with gram-negative sepsis who was receiving mechanical ventilation. There are diffuse bilateral alveolar opacities consistent with the presence of pulmonary edema. Panel **(B)** shows an anteroposterior chest radiograph from another patient with ARDS who had been receiving mechanical ventilation for seven days. Reticular opacities are present throughout both lung fields, a finding suggestive of the development of fibrosing alveolitis. Panel **(C)** shows a CT scan of the chest obtained during the acute phase. The bilateral alveolar opacities are denser in the dependent, posterior lung zones, with sparing of the anterior lung fields. The arrows indicate thickened interlobular septa, consistent with the presence of pulmonary edema. Panel **(D)** shows a CT scan of the chest obtained during the fibrosing-alveolitis phase. There are reticular opacities and diffuse ground-glass opacities throughout both lung fields, and a large bulla is present in the left anterior hemithorax. Reproduced with permission from Ware and Matthay (2000).

The two state of art molecular imaging discussed here are Positron Emission Tomography (PET) and Hyperpolarized ^{13}C Magnetic Resonance Spectroscopic Imaging (HP ^{13}C-MRSI), a method recently developed that provides similar information to PET imaging using MRI.

PATHOGENESIS OF ARDS AND PULMONARY INFLAMMATION

Acute respiratory distress syndrome and acute lung injury (ARDS/ALI) is characterized by sudden onset of respiratory

failure, pulmonary edema, diffused alveolar damage and widespread inflammation of the lung (Thompson et al., 2017). There are two pathogenetic pathways leading to ARDS; pulmonary and extra pulmonary ARDS (Pelosi et al., 2003). In pulmonary ARDS, primary lungs injury occurs by a direct insult (e.g., pneumonia, gastric aspiration, or toxin inhalation). In extrapulmonary ARDS, widespread inflammation occurs as a result of a systemic injury (e.g., sepsis, burn injury, or cardiopulmonary bypass), which results in secondary lung injury. In both scenarios, lung injury may progress to ARDS, as shown in **Figure 2**. Such progression is followed by resolution of ARDS/ALI in response to treatment or further progression into severe respiratory and multi-organ failure.

In both types of ARDS, the endothelium plays a key role in the onset of inflammation. In pulmonary ARDS, local alveolar inflammatory response affects the alveolar endothelium. On the other hand, in systemic ARDS, the inflammatory mediators present in the bloodstream damage the microvascular endothelium. Subsequently, the alveolar or the microvascular endothelium layer is activated, which leads lead to production of cellular adhesion molecule (CAM) and proinflammatory cytokines. The elevation of inflammatory mediators leads to recruitment and adherence of polymorphonuclear neutrophils. In the acute, or exudative, phase of ARDS/ALI (**Figure 3**), the alveoli become filled with protein-rich edema fluid and resident macrophages (a type of white blood cell) secrete pro-inflammatory proteins and cytokines [e.g., interleukin-8 (IL-8)], which recruit the innate immune cells (primarily neutrophils). Neutrophils adhere to the endothelial lining of the vessels and roll on this lining until they migrate through the alveolar-capillary membrane into the airspace, thereby damaging it. Neutrophil adherence to the endothelial wall can be measured via markers of endothelial injury such as soluble intercellular adhesion molecule-1 (sICAM-1 and ICAM-1) (Jochen Grommes, 2011). Neutrophils are activated in the alveolar space, which release granula proteins and reactive oxygen species (ROS) into this space. These proteases and oxidants cause further epithelial and alveolar injury and subsequent formation of hyaline membranes. Neutrophil activity can be measured by the expression of enzymes and proteins released by activated neutrophils, such as elastase or myeloperoxidase (MPO) (Johnson and Matthay, 2010; Fanelli and Ranieri, 2015).

Pulmonary Metabolism

Healthy lung tissue predominantly relies on glucose utilization to sustain function, although its energy and metabolic needs are relatively modest compared to other organs such as the heart and liver (Fisher et al., 1974). Approximately 50% of the glucose utilized by the lung tissue converts to lactate (Fisher, 1984). The lungs typically maintain the glycolytic intermediary balance (lactate-to-pyruvate ratio) in the blood by utilizing the excess blood lactate, which results in a negligible difference in transpulmonary lactate concentration (Johnson, 2011). However, this function of the lung is compromised in many lung pathologies – especially in ARDS/ALI (Iscra et al., 2002). **Figure 4** demonstrates lung lactate production measured by the difference in the lactate concentration across the lungs (arteriovenous difference in lactate) in 122 patients with a variety of lung disorders (De Backer et al., 1997). Lungs of patients with ALI (N = 43) produce significantly more lactate than other pathologies. What is more is that lactate production in ALI patients was strongly correlated with lung injury score as shown in **Figure 4B**. The injury score is representative of the severity of opacities observed in chest radiographs and computed tomography

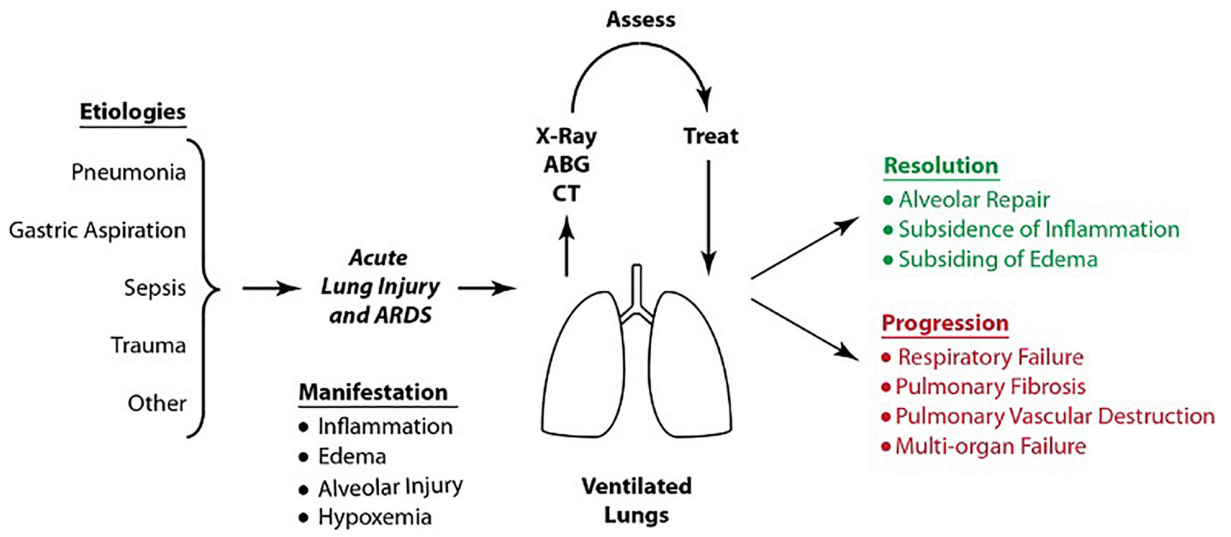

FIGURE 2 | Etiologies, manifestations and sequelae of ARDS/ALI. Upon diagnosis, patients undergo supportive therapy using protective ventilation. The patient's overall condition is assessed by chest radiography, computed tomography, ventilatory parameters and ABG. Treatment either results in resolution of ARDS/ALI or in the syndrome's progression into severe respiratory failure, pulmonary fibrosis and eventual multi-organ failure. Reproduced with permission from Pourfathi (2019).

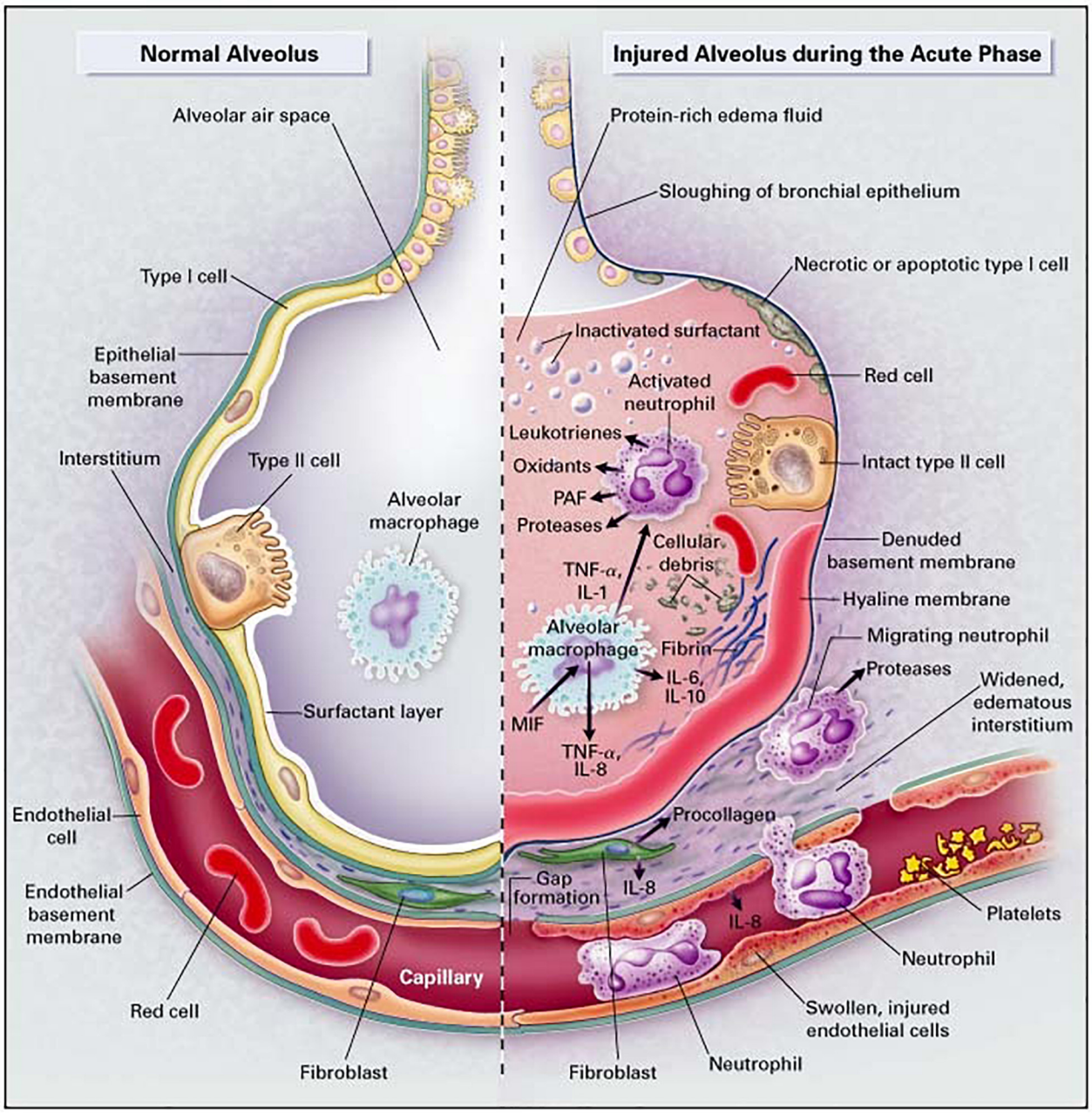

FIGURE 3 | The healthy lung (left), and the acute phase of ARDS/ALI (right). In ARDS/ALI, injury is initiated by either direct or indirect insults to the delicate alveolar structure of the distal lung and associated micro-vasculature. In the acute phase of the injury, resident alveolar macrophages are activated, leading to the release of potent pro-inflammatory mediators and chemokines that promote the accumulation of neutrophils and monocytes. Reproduced with permission from Ware and Matthay (2000).

images, as well as the severity of overall respiratory failure measured by P_aO_2/F_iO_2 ratio and loss of pulmonary compliance (Murray et al., 1988).

Although increased glycolysis and lactate production by the lung tissue may reflect the presence of hypoxia due to elevated anaerobic metabolism, several studies suggest that the elevated lactate production by the lungs in ARDS/ALI is primarily associated with increased lung inflammation and neutrophil activity, and can occur even in the absence of tissue hypoxia. This suggests that increased lactate concentration and lactate-to-pyruvate ratio in the lung tissue may be a surrogate for lung injury and inflammation (De Backer et al., 1997; Kellum et al., 1997; Iscra et al., 2002).

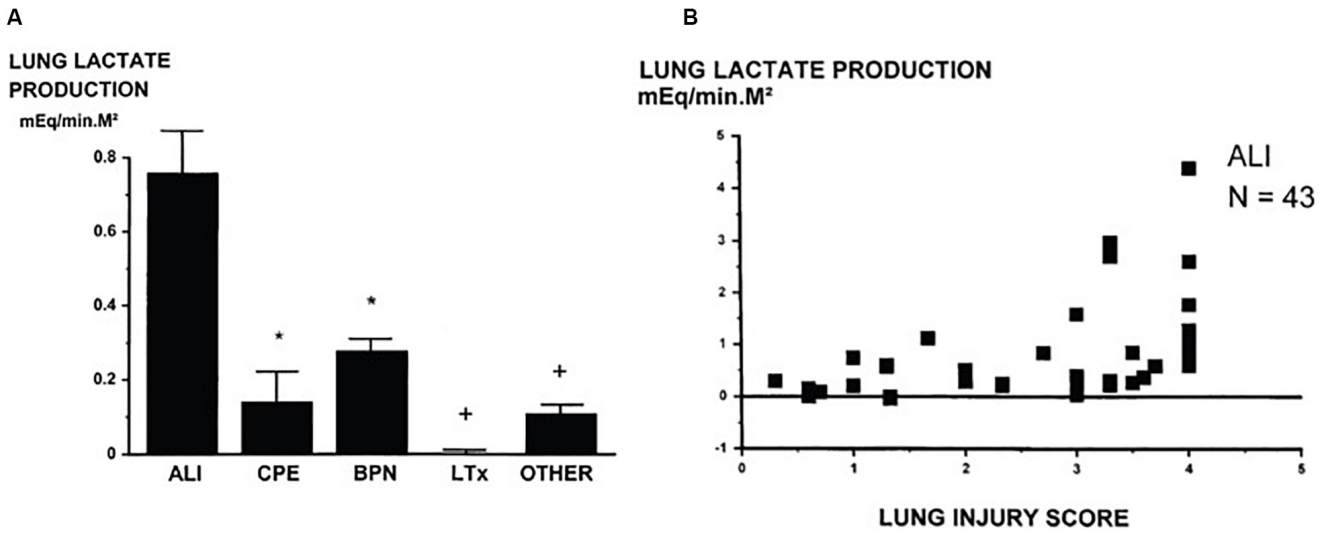

FIGURE 4 | (A) Lung lactate production measured by the difference in the lactate concentration across the lungs (arteriovenous difference in lactate) in various groups of patients shows that lungs of ALI patients produce significant amounts of lactate. **(B)** Lung lactate production measured in 43 patients with acute injury showed that it is proportional to injury severity as determined by Murray's lung injury score (Murray et al., 1988). (ALI, acute lung injury; CPE, acute pulmonary edema; BPN, bronchopneumonia; LTx, lung transplantation; Other, other types of respiratory failure, mEq/min.M^2: mmoles per minute per square meter). Reprinted with permission of the American Thoracic Society. Copyright © 2019 American Thoracic Society from De Backer et al. (1997). The *American Journal of Respiratory and Critical Care Medicine* is an official journal of the American Thoracic Society. $^*p < 0.05$ versus ALI, $^+p < 0.01$ versus ALI.

POSITION EMISSION TOMOGRAPHY

Positron emission tomography (PET) is a molecular imaging technique that enables visualization of metabolic and molecular processes by using a radiolabeled analog of a substance to interrogate specific pathways.

Principles

The radiolabeled analog is first synthesized at a cyclotron facility by bombarding a radioligands with accelerated protons to produce unstable radioactive isotopes e.g., ^{18}F and ^{11}C that are then used in a biosynthesizer unit to produce radio tracers. The tracer is then injected intravenously into the patient. The nucleolus of the radiolabeled atom then undergoes β radioactive decay, in which a positron is released and travels for a short distance in the tissue (< 1 mm) before colliding with an electron to produce two γ-ray photons that travel in opposite directions (Pauwels et al., 2000), which are detected using a ring-shaped array of sensor around the patient. By resolving the time difference between the arrival of photons at sensors in the opposite direction, using the time-of-flight algorithm, 2D or 3D images can be tomographically generated (Gambhir et al., 2001). Data acquisition is often performed over a period of 30–60 min, providing temporal information as well. The raw data obtained from the scanner can be converted to markers of metabolic activity using timed-blood sampling to measure overall radioactivity combined with kinetic approaches that fit temporal changes of data to multi-compartmental models to decompose relative contributions of signal intensity from solid organs, blood and extracellular matrix (Chen et al., 2017).

PET scanners do not obtain anatomical information and thus are often combined with CT scanners (PET/CT scanners) to overlay the functional information on the anatomical images.

Insights and Contributions

The most commonly used tracer for PET imaging is [^{18}F]-fluorodeoxyglucose (^{18}F-FDG). ^{18}F-FDG is glucose analog and is similarly transported into the cell by glucose transporter 1 (GLUT-1) and subsequently phosphorylated. ^{18}F-FDG cannot progress through the Krebs cycle and thus remains trapped in cells. Therefore, it can specifically be used to assess glucose uptake as a surrogate for overall glycolytic activity.

While ^{18}F-FDG-PET is routinely used in neuro-radiology (Gambhir et al., 2001) and oncology (Pastorino, 2010; Heusch et al., 2014; Miles et al., 2018), it is not clinically used for the management of ARDS/ALI. However, several studies have demonstrated its capability as a powerful molecular imaging tool to delineate regions in the injured lungs with elevated glycolysis. As activated neutrophils are largely responsible for the uptake of glucose, elevated glycolysis can be used as a surrogate for inflammation. This has been validated in other studies that used autoradiography of the lung tissue in animals after administration of ^{18}F-FDG showing that radioactivity was localized to neutrophils in the lung tissue.

Neutrophil recruitment and activation are heightened in ARDS, leading to elevated glycolysis, which can be regionally measured using ^{18}F-FDG-PET. The ability of this molecular imaging technique to regionally highlight alterations in metabolic activity has made ^{18}F-FDG-PET an invaluable research tool to non-invasively and quantitatively assess the severity lung inflammation. ^{18}F-FDG-PET has been employed in both animal

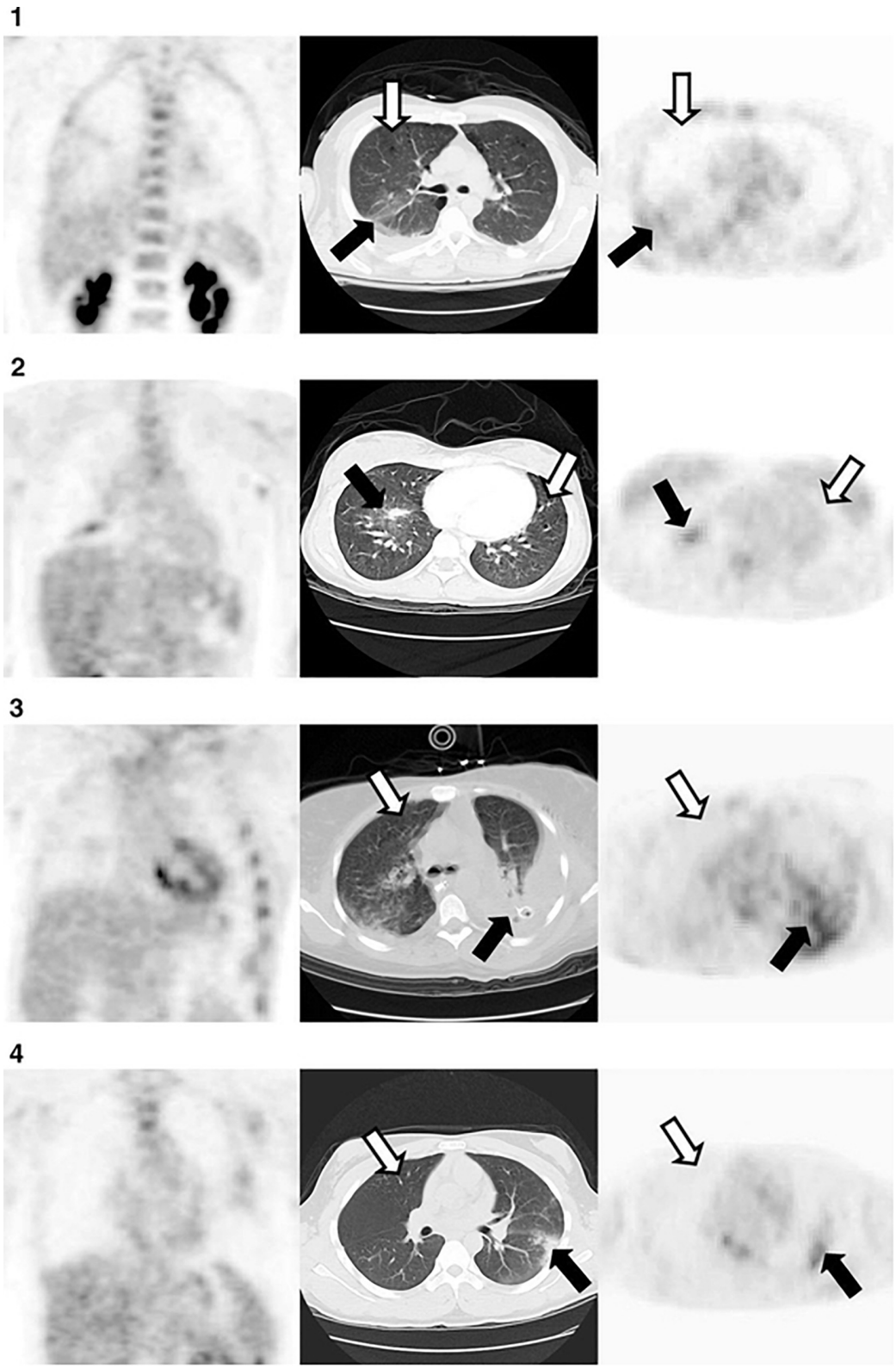

FIGURE 5 | Representative axial computed tomography (CT) in the middle panel, and coronal (left) and axial (right) [18F] fluorodeoxyglucose (18F-FDG) positron emission tomography (PET) at the obtained from 4 patients, 72 hours after diagnosis with acute lung injury. Moderate uptake of FDG was observed in non/poorly aerated regions (black arrows). In contrast, uptake of FDG was low in normally aerated lung (white arrow). Reproduced with permission from Rodrigues et al. (2008).

models of lung injury (de Prost et al., 2014) and in preclinical studies (Chen et al., 2006b; Bellani et al., 2012), and has provided valuable insight about the progression of lung injury (de Prost et al., 2014) as well as the importance of inflammation in patient outcome (Bellani et al., 2009, 2012).

In a preclinical study by de Prost et al. the authors assessed the impact of ventilation strategy on distribution and progression of lung inflammation using ^{18}F FDG-PET (de Prost et al., 2013) in an endotoxemia model of lung injury in sheep. They found that primary inflammatory injury progressed rapidly in sheep ventilated with a non-protective strategy, while the inflammation was contained in animals ventilated with protective ventilation. Furthermore, the study demonstrated that metabolic activity was significantly higher in the dependent regions of the lungs.

In patients, ^{18}F FDG-PET has been shown to be capable of localizing areas with higher neutrophilic activity the lung tissue as well. Chen et al. (2006b) showed that glucose uptake was significantly elevated in lungs of human subjects 24 h after instillation of 1–4 ng/kg endotoxin in airways using bronchoscopy. In a different study, Rodrigues et al. demonstrated the use of ^{18}F-FDG-PET at early stages of ARDS (1–3 days after admission) to predict outcome (**Figure 5**); patients with significantly higher glycolysis in the lung tissue hard poorer outcome that others (Rodrigues et al., 2008). Bellani et al. (2009, 2011) showed the use of ^{18}F FDG-PET to investigate the regional distribution of inflammatory activity in lungs of mechanically ventilated ARDS patients. Their work suggests that active inflammation is localized to non-dependent regions of the lungs at early stages. However, the inflammation spreads throughout the entire lung after days of ventilation. This data is supported by older work using localized biopsy that demonstrated similar destitution of inflammation (Papazian et al., 1998).

^{18}F-FDG-PET have been used to localize inflammatory activity in other lung pathologies as well. Chen et al. (2006a) showed elevated FDG uptake in lungs of patients suffering from cystic fibrosis (CF) compared to healthy subjects (Chen et al., 2006a). The uptake rate correlated strongly with the number of neutrophils present in the bronchoalveolar lavage. What was more interesting was that the glucose uptake rate was especially higher in patients with rapidly declining pulmonary function. In a different study, the authors assessed FDG uptake in lungs of patients with chronic obstructive pulmonary disease (COPD) patients with and without chronic bronchitis (Scherer and Chen, 2016). They showed increased average uptake of FDG in lungs with patients with chronic bronchitis. The CT scans of the same patients also showed more heterogeneously distributed emphysema.

Although these studies suggest a strong link between neutrophilic inflammation and increased FDG uptake, other inflammatory cells such as macrophages and eosinophils are also capable of accumulating FDG (Scherer and Chen, 2016). Nevertheless, FDG uptake can represent a measure of overall inflammatory response in the lungs. Given that inflammation and inflammatory burden is associated with decline in lung function, disease severity and lung tissue destruction in many lung pathologies, ^{18}F FDG-PET be used to classify patients with various disease severities to predict and assess response to treatments in these patients (Scherer and Chen, 2016).

There are a number of other less commonly used PET tracers that can provide more specific information about the inflammatory process. For instance, ^{68}Ga-citrate has been shown to bind to the lactoferrin within the neutrophil, therefore localizing specifically neutrophilic inflammation (Scherer and Chen, 2016). 18F-nitric oxide synthase (18F-NOS) can assess expression of nitric oxide synthase in lung epithelium, which has been shown to be elevated in patients with progressive asthma, COPD, ARDS, and emphysema (Huang et al., 2015). Lastly, Summers et al. (2014) administered a bolus of ^{111}Indium-tropolonate-labeled neutrophils to healthy subjects and ARDS patients and showed increased retention of neutrophils in and their delayed clearance in the ARDS patients.

Challenges and Limitations

The first principal limitations for clinical use of PET imaging is the cost of preparing the radiolabeled compound, which is done at a cyclotron facility followed by an on-site chemical synthesis apparatus to produce the final compound. Such facilities are expensive to maintain and thus are available only at a few universities and hospitals. Therefore, radio tracers that have a long-half life, such as ^{18}F-FDG (109.8 min) are often produced remotely at a cyclotron facility and transported to near-by locations. Since samples are radioactive, they need to be delivered via specially licensed road transport, or, for longer distances, via dedicated small commercial jet services, thereby making the scans costly. Another limitation is the long scan time (10–50 min) (Cereda et al., 2019) that is can be difficult for critically ill patients or patients with lung injury. Additionally, PET tracers expose patients to ionizing radiation, which limits use of this technique to monitor patient's response to interventions through repeated measurements.

Another potential disadvantage of ^{18}F-FDG-PET is that while it enables examining abnormalities in the uptake of the glucose analog fluorodeoxyglucose, it is unable to reveal changes in downstream metabolism as it cannot progress through the Kerbs cycle. Such information may be crucial to the evolution of inflammation and injury (Fisher and Dodia, 1984; De Backer et al., 1997). Lastly, given the long half-life of ^{18}F-FDG-PET, the radioactivity of the probe from a single injection can last for hours, which limits the possibility of repeated scans as frequently as needed. This is especially important in small animal research, where lung injury progression occurs on a time scale that is significantly shorter than in human patients.

HYPERPOLARIZED ^{13}C MAGNETIC RESONANCE SPECTROSCOPIC IMAGING

Hyperpolarized ^{13}C magnetic resonance spectroscopic imaging (MRSI) is a non-invasive emerging modality that enables delineation of different compounds via their distinct chemical

shift, thereby making it suitable to assess flux critical branching points in metabolic pathways.

Principles

^{13}C MRSI enables study of metabolic flux in the tissue due to its unique ability to distinguish metabolites through their distinct resonance frequencies (chemical shifts). Due to low natural abundance of ^{13}C nuclei, the MRI scan is performed after administration of an exogenous non-radioactive ^{13}C-labeled compound. Subsequently, spectroscopic imaging methods can be used to highlight changes in cellularity and metabolic pathways. Although this method has been shown to be insightful for tumor and neuroimaging it is limited as it requires a long scan time due to low intrinsic nuclear spin of the ^{13}C nuclei (Kurhanewicz et al., 2011, 2019). To overcome these challenges the signal can be increase through nuclear hyperpolarization.

Hyperpolarization is a process to temporarily enhance the sensitivity of the MRI signal by over 10,000-fold over conventional MRI (Kurhanewicz et al., 2011). Hyperpolarization of the ^{13}C nuclei is typically achieved through a process called dynamic nuclear polarization (DNP), which transfers spin alignment from the sparse unpaired electrons of an electron paramagnetic agent (EPA) to the adjacent ^{13}C labeled nuclei using resonant microwave irradiation at high magnetic fields (∼3.3T) at ∼1 K temperature (Ardenkjaer-Larsen et al., 2003). Once the sample reaches the desired polarization level (usually within 1–3 h), it is dissolved rapidly using a hot isotonic buffer to yield a highly polarized neutralized solution, which is then administered intravenously to the subject.

Upon injection, spectroscopic imaging must be carried out quickly and efficiently for two reasons; first, given the short life-time (T_1 relaxation time constant) of the probes (10–120 s depending on the probe), the data must be acquired quickly. Second, in conventional MRI 2D or 3D images are acquired, whereas HP ^{13}C MRSI requires data acquisition in the spectral dimension as well, which adds further complexity to the criteria for pulse sequence development. What is more is that any RF excitation causes additional irreversible signal loss. Several imaging and spectroscopic pulse sequences have been developed to address these challenges by limiting the number of excitations and exploiting the long T_2, and T_2* relaxation times of ^{13}C species in many organs (Yen et al., 2009), as well as ^{13}C species' large range of the chemical shift (Kurhanewicz et al., 2011).

Insights and Contributions

The most widely used hyperpolarized DNP probe is [1-^{13}C] pyruvate, a small and highly soluble molecule with high polarizability (up to 60% polarization reported) and a long T_1 relaxation time constant (40–60s). Because pyruvate is at a central branching point in several key metabolic pathways in cancer and inflammatory diseases, it be used to study a wide variety of metabolic perturbations in tissues and presents unique opportunities to characterize metabolic flux in various metabolic, Therefore [1-^{13}C] pyruvate is perhaps the most attractive HP ^{13}C imaging probe to date (**Figure 6**).

HP [1-^{13}C] pyruvate has been used extensively to study metabolic alterations in heart (Lau et al., 2010), liver (Lee et al., 2013), kidneys (Laustsen et al., 2015), and tumors (Day et al., 2007) in intact animals and has more recently been used in a number of human studies (Nelson et al., 2013; Cunningham et al., 2016; Park et al., 2018). Nevertheless, given that the lungs receive the full blood supply during each circulation, and therefore, play a major role in maintaining body's homeostasis and whole body's metabolic status, HP ^{13}C MRSI can be used as valuable tool for evaluating lung metabolism and pathology. In the context of lung injury, HP [1-^{13}C] pyruvate MRSI can be used to regionally measure lactate-to-pyruvate ratio as a surrogate for lactate labeling, which is significantly elevated in inflamed lungs (**Figure 7**; Pourfathi et al., 2018; Pourfathi, 2019).

In an *ex-vivo* perfused lung study with an experimental model of bleomycin-induced lung inflammation in rats, Shaghaghi et al. (2014) showed a significantly increased rate of hyperpolarized lactate labeling after injection of hyperpolarized [1-^{13}C] pyruvate in inflamed lungs. The lactate-to-pyruvate ratio declined but remained higher than healthy lungs even after fibrotic remodeling of the tissue at later stages of the injury. The study also showed a strong correlation between the lactate-to-pyruvate ratio and neutrophil scores derived from histological assessment of the lung samples. Interestingly there was no correlation between the macrophage count and the lactate signal suggesting that the primary source of the lactate is from neutrophils.

This technique has also been used for in-vivo imaging in small animals; Thind et al. (2012) showed elevated HP lactate-to-pyruvate ratio thus lactate labeling in irradiated lungs after radiation induced lung injury (RILI) compared to healthy animals. The authors showed a strong correlation between the lactate-to-pyruvate ratio and inflammatory markers measured from bronchoalveolar lavage. Pourfathi et al., showed that in an experimental model of aspiration pneumonia, HP lactate-to-pyruvate ratio was significantly elevated in mildly injured rats that received (intratracheally) a low volume of hydrochloric acid (HCl). Interestingly, the authors report a decline in the lactate-to-pyruvate ratio in more severely injured rats that received a larger volume of HCl. The authors showed that the although the lactate signal appeared to increase in the posterior regions of the injured lungs, the skewed measurement was in fact caused by a dramatic increase in the blood volume in the injured lungs.

Another study with HP [1-^{13}C] pyruvate MRSI by Pourfathi et al. showed that this technique can be used to mechanisms of injury progression by secondary ventilator-induced lung injury; the authors assessed the impact of recruiting atelectasis on the trajectory of lung injury and inflammation in ventilated rats with primary aspiration pneumonitis, and reported that positive end-expiratory pressure (PEEP) and recruitment contains regional pulmonary lactate production and inflammation. The study supported a direct relationship between pulmonary inflammation and increased HP lactate-to-pyruvate ratio, consistent with the link between increased glycolysis caused by recruitment and activation of neutrophils as part of an innate inflammatory cascade, that was proposed by previous FDG-PET studies (Jones et al., 1994), and showed a strong correlation between the lactate-to-pyruvate and inflammatory markers of neutrophilic activity (MPO) and adherence (ICAM-1).

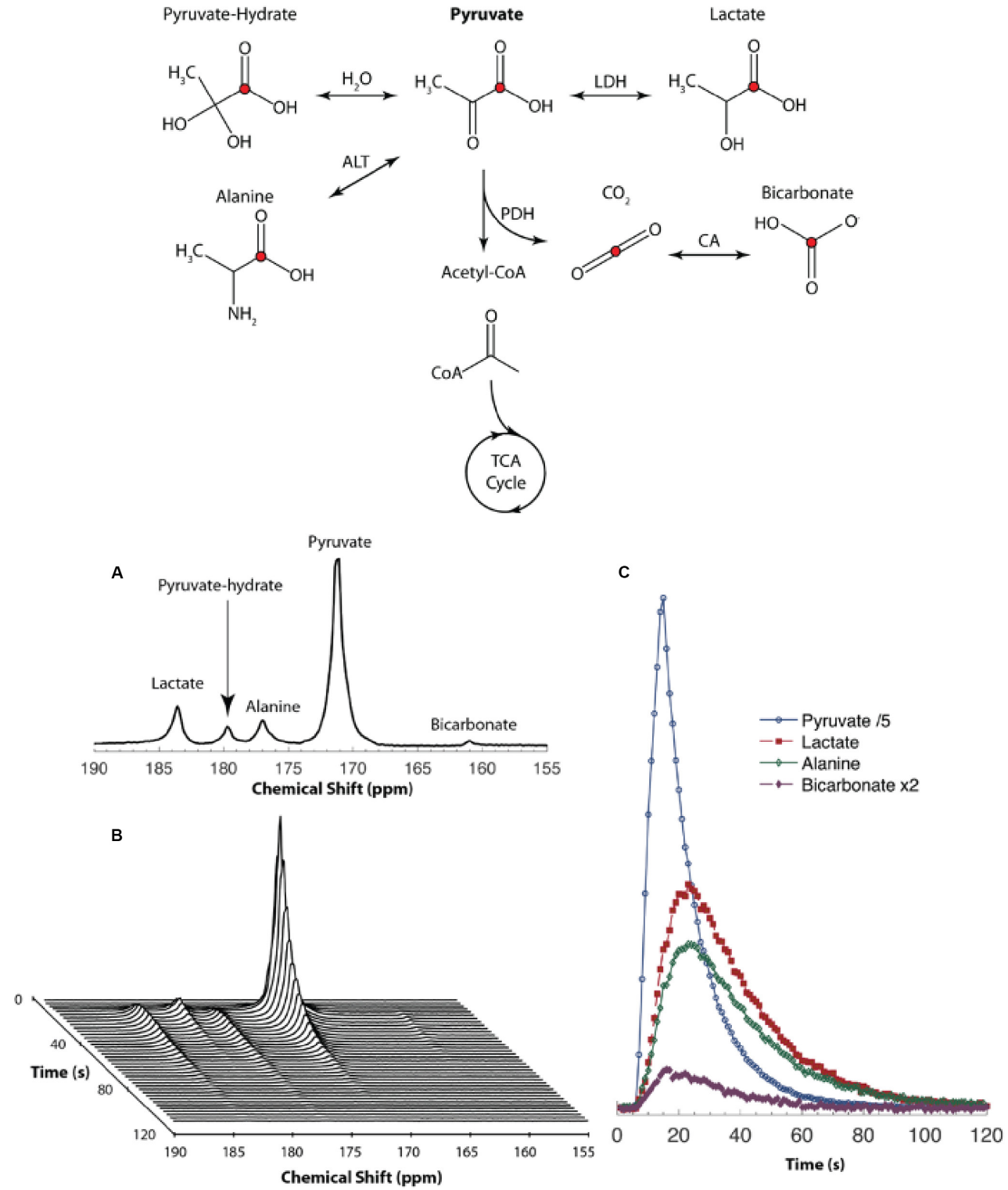

FIGURE 6 | (Top) Metabolites and their biochemical pathways that can be interrogated using [1-^{13}C] pyruvate. MRI. The red circle indicates atoms with ^{13}C labeled nuclei. The fate of the pyruvate beyond Acetyl-CoA into the Tricarboxylic Acid (TCA) cycle cannot be probed using [1-^{13}C] pyruvate as the ^{13}C labeled nucleolus remains on the $^{13}CO_2$ molecule. Cofactors are not shown in this diagram for simplicity (LDH, lactate dehydrogenase; ALT, alanine transaminase; PDH, pyruvate dehydrogenase; CA, carbonic anhydrase). **(Bottom) (A)** NMR spectrum obtained from a mouse after administration of hyperpolarized [1-^{13}C] pyruvate via the tail-vein. **(B)** Spectra obtained every second shows how different peaks vary over time. **(C)** Area under each peak depicted as a function of time to represent the relative concentration of each peak. Reproduced with permission from Pourfathi (2019).

Finally, Siddiqui et al. showed that HP [1-^{13}C] pyruvate MRI has the potential to be used as predictor for lung rejection. In a direct comparison between this technique and microCT in a lung allograft rejection rat model, the authors observed elevated lactate-to-pyruvate ratio prior to observing features in the microCT that are indicative of rejection. The authors also showed a strong relationship between the presence of markers of adaptive immunity CD4+ and CD8+, and the elevated lactate-to-pyruvate ratio in the transplanted lung (Siddiqui et al., 2019).

The preliminary results of these studies demonstrates the potential of HP [1-^{13}C] pyruvate MRSI to detect elevated pulmonary lactate-to-pyruvate ratio. This imaging marker can serve as a surrogate to regionally assess increased glycolysis and subsequent lactate production by injured lungs as a result of inflammation (Pourfathi et al., 2017). While lactate mapping can be a marker of neutrophilic infiltration, it may be used to assess other biological changes in the lung related to lung injury that promote lactate production as well, such as fibrosis (Kottmann et al., 2012). The ability to interrogate alterations in critical downstream metabolic pathways such as glycolysis, may enable non-invasive and. frequent assessment of patients' response to therapies early after treatment. This opens up opportunities to assess the response of various therapeutic apaches to select optimal strategy to attenuate lung injury and its consequences in the early stages (Shankar-Hari and McAuley, 2017).

Challenges and Limitations

The most critical limitation of HP ^{13}C MRSI is the very short lifetime of the hyperpolarization that limits the available "window-of-opportunity" to acquire data. Another limitation is the need for a clinical hyperpolarizer that is currently available at around 30 sites across the world. Unlike PET tracers, HP ^{13}C agents cannot be produced remotely and delivered to the site-of-interest given that the lifetime of the hyperpolarization is significantly shorter than that of the half-life of PET tracers. Therefore, clinical dissemination of this HP ^{13}C MRSI technology requires a polarizer at every site.

Other technical limitations of this technology for lung imaging in clinical studies are the field inhomogeneity in the lung tissue causing rapid spin dephasing at air-tissue interfaces and lung's overall low tissue density. This difficulty is further exacerbated in the case of metabolic imaging by lung's modest overall energy needs. These challenges limit both signal-to-noise ratio (SNR) and the suitability of rapid pulse sequences that are useful for imaging other organs. While many studies suggest that these challenges can be addressed (Pourfathi et al., 2017, 2018) the clinical utility of ^{13}C HP MRSI in critically ill patients raises safety concerns primarily because of the need to use MRI–compatible monitoring and ventilation equipment.

Lastly, quantification of the absolute concentration of metabolites using HP ^{13}C MRSI is non-trivial, as the absolute signal level is subject to variability due to polarization level and physiological conditions (Pourfathi et al., 2017). Although the use of hyperpolarized lactate-to-pyruvate ratio as a surrogate for endogenous lactate concentration (De Backer et al., 1997) and glycolysis (Siddiqui et al., 2016) can mitigate this variability, it can still be subject to bias caused by excess fluid in the extracellular space resulting from capillary bed leakage (Musch et al., 2007); the presence of such excess fluid can increase

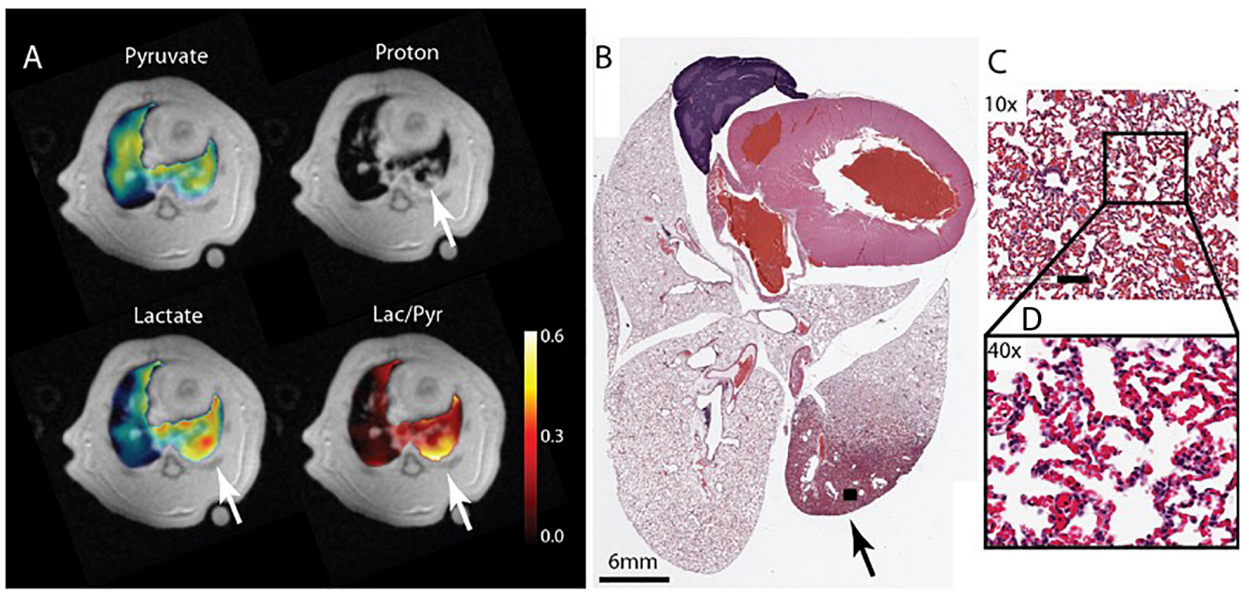

FIGURE 7 | (A) Pyruvate, lactate and lactate -to-pyruvate segmented maps overlaid on their corresponding proton image of a ZEEP rat 4 h after the acid instillation shows injury to the posterior right lung marked by increased intensity in the proton image (white arrow). The metabolite maps show increased lactate signal intensity and lactate-to-pyruvate ratio colocalized with the injured area. **(B)** Hematoxylin and Eosin (H&E) axial slide of the whole lung clearly shows damaged lung tissue in the same area (black arrow). Magnified images taken from the injured area (black box) with **(C)** 10× and **(D)** 40× magnifications show severe damage and inflammatory infiltrates in the tissue. The bar in **(C)** is 100 μm. Reproduced with permission from Pourfathi (2019).

pyruvate concentration or limit its uptake, thereby reducing the lactate-to-pyruvate ratio and the sensitivity of the method (Pourfathi et al., 2017). PET imaging studies have addressed similar challenges by using compartment models to pinpoint the local source of signal (Chen et al., 2017). In the case of MRI, this bias may be corrected for by using rapid MRI pulse sequences that allow the acquisition of multiple images to characterize metabolic flux in various tissues (Siddiqui et al., 2016).

FUTURE DEVELOPMENT

The pathophysiology of lung injury is complicated and entails changes in lung anatomy that arise from alterations at the cellular level and that compromise lung function. The molecular imaging techniques discussed here focus on the cellular changes which precede changes in the lung anatomy and function, thereby providing tools to detect inflammatory injury early and assess early response to treatment. Therefore, molecular imaging techniques may provide additional context to currently clinical tools to improve diagnostics and therapeutic approaches. Nevertheless, there are opportunities for improvement and further dissemination of either techniques to assess lung injury in a clinical setting.

Current research on PET imaging entails development of new hardware and analytical tools and algorithms, to improve spatial and temporal resolution. PET is often coupled with CT to capture an anatomical overlay of the metabolic maps. However, recent advancements in PET and MRI hardware technology and MRI pulse sequence development have created opportunities to combine PET and MRI together, that can potentially limit the ionizing radiation received by the patient. Additionally, in the case of lung injury, given the heterogeneity of tissue types with various disease, i.e., absence of solid tissue in healthy lungs and presence of edema or alveolar thickening in injured lungs, additional research is being performed to improve quantification of substrate uptake and flux (Chen et al., 2017).

Another potential area for future development is the use of deep learning methods to find spatial patterns that enables better classification of disease categories. While several studies have employed deep learning algorithms to classify CT images and to predict outcome (Merkow et al., 2017), its use has been much more limited with PET imaging (Singh et al., 2017). Nevertheless, addition of PET data to CT and other clinical markers can provide critical information about the severity of injury and its subsequent progression. However, a major limitation at this time is the absence of a large dataset of PET images obtained from the lungs of ARDS patients.

Hyperpolarized ^{13}C MRI technology is at its infancy, yet it is showing tremendous potential to characterize branching points of the metabolic pathways in the presence of diseases. One major advantage of this technology is that it can potentially be coupled with other informative MRI methods, such HP ^{129}Xe MRI. The latter is a non-invasive MRI technique that is capable of regionally quantifying lung function by measuring ventilation, oxygen uptake and apparent diffusion of gas in the alveolar airspace (Ruppert, 2014), thereby providing additional insight. Combined together, HP ^{129}Xe and ^{13}C MRI can obtain spatially correlated measurements of metabolism and function to provide a comprehensive insight into the pathology of the diseased lungs. Lastly, there has been significant progress in constructing inexpensive commercial and portable MRI machines. This can potentially make the use of MR-based molecular imaging methods to assess inflammation more accessible. This is particular important for imaging critically ill patients in the ICUs, where patient transport to the scanner is a major challenge. Despite the advantages, HP ^{13}C MRI, generally suffers from hyperpolarization lifetime and challenges associated with lung MRI. While the use of T_2-based pulse sequences may address some of these challenges (Pourfathi, 2019), there are several considerations that are required to address limitations with data acquisition and quantification (Yen et al., 2009).

Lastly, both methods exploit elevated glycolysis in activated inflammatory cells to localize pulmonary inflammation. As previously stated, while this provides a measure of integrated inflammatory activity in the lungs, it does not specify the type of cells present in the tissue. Future development for PET imaging can entail development of other substrates, similar to what was discussed earlier, to more specifically characterize the type of inflammation in the tissue. Moreover, additional novel tracers that are functionalized ligands that can bind to specific receptors may be synthesized to provide additional insight into the immune-pathogenesis of the disease (Kim et al., 2017).

Developing specific substrates for HP ^{13}C MRI will be significantly more challenging that PET. This is because the life-time of hyperpolarization shortens significantly for larger and more complex molecules that can provide more specific information, thereby making imaging impossible. However, a number of substrates may be potentially useful; [6-^{13}C] arginine has shown to be capable of reliably detecting the presence of myeloid-derived suppressor cells in bone-marrow (Najac et al., 2016). This substrate may be useful to study asthma as arginase, the enzyme that produces arginine, has shown to have a higher expression after allergen challenge in samples derived from asthmatic patients than healthy subjects (Arginine metabolism: enzymology, nutrition, and clinical significance. Proceedings of a symposium dedicated to the memory of Vernon R. Young. April 5-6, 2004; Bermuda, 2004). Another potentially useful substrate that may be polarizable is [1-^{13}C] proline, which may be used to assess presence of fibrosis at later stages of lung injury (Wallace et al., 2002).

SUMMARY

In this article, we briefly discussed the critical role of lung inflammation in the outcome of patients with lung injury. We then provided an overview of two novel molecular imaging tools to regionally assess lung inflammation in the context of lung injury. Both exploit the elevated glycolysis and energy demand of activated immune cells that are present in the inflamed lung tissue; ^{18}FDG-PET characterizes the uptake of glucose into the cell and its utilization, while HP ^{13}C MRI quantifies the

conversion of pyruvate to lactate thereby characterizing the fate of the glucose. Both techniques are valuable and can and can be used to assess lung inflammation or can combined together to provide a complementary picture of lungs bioenergetics. Such information could ultimately provide additional insight for clinical diagnosis and management of lung injury and ARDS and its trajectory. However, there are several technical challenges associated with either technique that requires to be addressed before their dissemination and ultimate clinical utility.

AUTHOR CONTRIBUTIONS

MP, SK, SC, and RR prepared the manuscript. All authors contributed to the article and approved the submitted version.

FUNDING

This study was supported by the National Heart, Lung, and Blood Institute, NIH (Grant/Award Number: R01-HL139066).

REFERENCES

Ardenkjaer-Larsen, J. H., Fridlund, B., Gram, A., Hansson, G., Hansson, L., Lerche, M. H., et al. (2003). Increase in signal-to-noise ratio of > 10,000 times in liquid-state NMR. *Proc. Natl. Acad. Sci. U.S.A.* 100, 10158–10163. doi: 10.1073/pnas.1733835100

Ards Definition Task Force, Ranieri V. M., Rubenfeld, G. D., Thompson, B. T., Ferguson, N. D., Caldwell, E., et al. (2012). Acute respiratory distress syndrome: the berlin definition. *JAMA* 307, 2526–2533. doi: 10.1001/jama.2012.5669

Ashbaugh, D. G., Bigelow, D. B., Petty, T. L., and Levine, B. E. (2005). Acute respiratory distress in adults. the lancet, saturday 12 august 1967. *Crit. Care Resusc* 7, 60–61.

Bellani, G., Guerra, L., Musch, G., Zanella, A., Patroniti, N., Mauri, T., et al. (2011). Lung regional metabolic activity and gas volume changes induced by tidal ventilation in patients with acute lung injury. *Am. J. Respir. Crit. Care Med.* 183, 1193–1199. doi: 10.1164/rccm.201008-1318OC

Bellani, G., Mauri, T., and Pesenti, A. (2012). Imaging in acute lung injury and acute respiratory distress syndrome. *Curr. Opin. Crit. Care* 18, 29–34. doi: 10.1097/MCC.0b013e32834eb47d

Bellani, G., Messa, C., Guerra, L., Spagnolli, E., Foti, G., Patroniti, N., et al. (2009). Lungs of patients with acute respiratory distress syndrome show diffuse inflammation in normally aerated regions: a [18F]-fluoro-2-deoxy-D-glucose PET/CT study. *Crit. Care Med.* 37, 2216–2222. doi: 10.1097/CCM.0b013e3181aab31f

Bermuda (2004). "Arginine metabolism: enzymology, nutrition, and clinical significance," in *Proceedings of a Symposium Dedicated to the Memory of Vernon R. Young. April 5-6, 2004*, Bermuda.

Cereda, M., Xin, Y., Goffi, A., Herrmann, J., Kaczka, D. W., Kavanagh, B. P., et al. (2019). Imaging the injured lung: mechanisms of action and clinical use. *Anesthesiology* 131, 716–749. doi: 10.1097/ALN.0000000000002583

Cereda, M., Xin, Y., Meeder, N., Zeng, J., Jiang, Y., Hamedani, H., et al. (2016). Visualizing the propagation of acute lung injury. *Anesthesiology* 124, 121–131. doi: 10.1097/ALN.0000000000000916

Chen, D. L., Cheriyan, J., Chilvers, E., Choudoury, G., Coello, C., Connell, M., et al. (2017). Quantification of lung PET images: challenges and opportunities. *J. Nucl. Med.* 58, 201–207. doi: 10.2967/jnumed.116.184796

Chen, D. L., Ferkol, T. W., Mintun, M. A., Pittman, J. E., Rosenbluth, D. B., and Schuster, D. P. (2006a). Quantifying pulmonary inflammation in cystic fibrosis with positron emission tomography. *Am. J. Respir. Crit. Care Med.* 173, 1363–1369. doi: 10.1164/rccm.200506-934OC

Chen, D. L., Rosenbluth, D. B., Mintun, M. A., and Schuster, D. P. (2006b). FDG-PET imaging of pulmonary inflammation in healthy volunteers after airway instillation of endotoxin. *J. Appl. Physiol.* 100, 1602–1609. doi: 10.1152/japplphysiol.01429.2005

Cunningham, C. H., Lau, J. Y. C., Chen, A. P., Geraghty, B. J., Perks, W. J., Roifman, I., et al. (2016). Hyperpolarized 13C metabolic MRI of the human heart: initial experience. *Circ. Res.* 119, 1177–1182. doi: 10.1161/CIRCRESAHA.116.309769

Day, S. E., Kettunen, M. I., Gallagher, F. A., Hu, D.-E., Lerche, M., Wolber, J., et al. (2007). Erratum: detecting tumor response to treatment using hyperpolarized 13C magnetic resonance imaging and spectroscopy. *Nat. Med.* 13, 1521–1521. doi: 10.1038/nm1207-1521

De Backer, D., Creteur, J., Zhang, H., Norrenberg, M., and Vincent, J. L. (1997). Lactate production by the lungs in acute lung injury. *Am. J. Respir. Crit. Care Med.* 156, 1099–1104. doi: 10.1164/ajrccm.156.4.9701048

de Prost, N., Costa, E. L., Wellman, T., Musch, G., Tucci, M. R., Winkler, T., et al. (2013). Effects of ventilation strategy on distribution of lung inflammatory cell activity. - PubMed - NCBI. *Crit. Care* 17:R175. doi: 10.1186/cc12854

de Prost, N., Feng, Y., Wellman, T., Tucci, M. R., Costa, E. L., Musch, G., et al. (2014). 18F-FDG kinetics parameters depend on the mechanism of injury in early experimental acute respiratory distress syndrome. *J. Nucl. Med.* 55, 1871–1877. doi: 10.2967/jnumed.114.140962

Fanelli, V., and Ranieri, V. M. (2015). Mechanisms and clinical consequences of acute lung injury. *Ann. ATS* 12, S3–S8. doi: 10.1513/AnnalsATS.201407-340MG

Fisher, A. B. (1984). Intermediary metabolism of the lung. *Environ. Health Perspect.* 55, 149–158. doi: 10.1289/ehp.8455149

Fisher, A. B., and Dodia, C. (1984). Lactate and regulation of lung glycolytic rate. *Am. J. Physiol.* 246, E426–E429. doi: 10.1152/ajpendo.1984.246.5.E426

Fisher, A. B., Steinberg, H., and Bassett, M. D. D. (1974). Energy utilization by the lung. *Symp. Lung Pulmon. Circ.* 57, 437–446.

Gambhir, S. S., Czernin, J., Schwimmer, J., Silverman, D. H., Coleman, R. E., and Phelps, M. E. (2001). A tabulated summary of the FDG PET literature. *J. Nucl. Med.* 42, 1S–93S.

Gattinoni, L., Chiumello, D., and Rossi, S. (2020). COVID-19 pneumonia: ARDS or not? *Crit. Care* 24, 1–3. doi: 10.1186/s13054-020-02880-z

Herridge, M. S. (2017). 50 years of research in ARDS. Long-term follow-up after ARDS: insights for managing medical complexity after critical illness. *Am. J. Respir. Crit. Care Med.* 196, 1380–1384. doi: 10.1164/rccm.201704-0815ED

Heusch, P., Buchbender, C., Kohler, J., Nensa, F., Gauler, T., Gomez, B., et al. (2014). Thoracic staging in lung cancer: prospective comparison of 18F-FDG PET/MR imaging and 18F-FDG PET/CT. *J. Nucl. Med.* 55, 373–378. doi: 10.2967/jnumed.113.129825

Huang, H. J., Isakow, W., Byers, D. E., Engle, J. T., Griffin, E. A., Kemp, D., et al. (2015). Imaging pulmonary inducible nitric oxide synthase expression with PET. *J. Nucl. Med.* 56, 76–81. doi: 10.2967/jnumed.114.146381

Iscra, F., Gullo, A., and Biolo, G. (2002). Bench-to-bedside review: lactate and the lung. *Crit. Care* 6, 327–329. doi: 10.1186/cc1519

Jochen Grommes, O. S. (2011). Contribution of neutrophils to acute lung injury. *Mol. Med.* 17, 293–307. doi: 10.2119/molmed.2010.00138

Johnson, E. R., and Matthay, M. A. (2010). Acute lung injury: epidemiology, pathogenesis, and treatment. *J. Aerosol. Med. Pulmon. Drug Deliv.* 23, 243–252. doi: 10.1089/jamp.2009.0775

Johnson, M. L. (2011). Transpulmonary lactate and pyruvate kinetics. *Am. J. Physiol. Regul. Integr. Comp. Physiol.* 301, R769–R774.

Jones, H. A., Clark, R. J., Rhodes, C. G., Schofield, J. B., Krausz, T., and Haslett, C. (1994). In vivo measurement of neutrophil activity in experimental lung inflammation. *Am. J. Respir. Crit. Care Med.* 149, 1635–1639. doi: 10.1164/ajrccm.149.6.7516252

Kellum, J. A., Kramer, D. J., Lee, K., Mankad, S., Bellomo, R., and Pinsky, M. R. (1997). Release of lactate by the lung in acute lung injury. *Chest* 111, 1301–1305. doi: 10.1378/chest.111.5.1301

Kim, J., Moon, B. S., Lee, B. C., Lee, H.-Y., Kim, H.-J., Choo, H., et al. (2017). A potential PET radiotracer for the 5-HT2C receptor: synthesis and in vivo evaluation of 4-(3-[18F]fluorophenethoxy)pyrimidine. *ACS Chem. Neurosci.* 8, 996–1003. doi: 10.1021/acschemneuro.6b00445

Kottmann, R. M., Kulkarni, A. A., Smolnycki, K. A., Lyda, E., Dahanayake, T., Salibi, R., et al. (2012). Lactic Acid Is Elevated in Idiopathic Pulmonary Fibrosis

and Induces Myofibroblast Differentiation via pH-Dependent Activation of Transforming Growth Factor-β. *Am. J. Respir. Crit. Care Med.* 186, 740–751. doi: 10.1164/rccm.201201-0084OC

Kurhanewicz, J., Vigneron, D. B., Ardenkjaer-Larsen, J. H., Bankson, J. A., Brindle, K., Cunningham, C. H., et al. (2019). Hyperpolarized 13C MRI: path to clinical translation in oncology. *Neoplasia* 21, 1–16. doi: 10.1016/j.neo.2018.09.006

Kurhanewicz, J., Vigneron, D. B., Brindle, K., Chekmenev, E. Y., Comment, A., Cunningham, C. H., et al. (2011). Analysis of cancer metabolism by imaging hyperpolarized nuclei: prospects for translation to clinical research. *Neoplasia* 13, 81–97. doi: 10.1593/neo.101102

Lau, A. Z., Chen, A. P., Ghugre, N. R., Ramanan, V., Lam, W. W., Connelly, K. A., et al. (2010). Rapid multislice imaging of hyperpolarized 13C pyruvate and bicarbonate in the heart. *Magn. Reson. Med.* 64, 1323–1331. doi: 10.1002/mrm.22525

Laustsen, C., Stokholm Nørlinger, T., Christoffer Hansen, D., Qi, H., Mose Nielsen, P., Bonde Bertelsen, L., et al. (2015). Hyperpolarized 13C urea relaxation mechanism reveals renal changes in diabetic nephropathy. *Magn. Reson. Med.* 75, 515–518. doi: 10.1002/mrm.26036

Lee, P., Leong, W., Tan, T., Lim, M., Han, W., and Radda, G. K. (2013). In Vivo hyperpolarized carbon-13 magnetic resonance spectroscopy reveals increased pyruvate carboxylase flux in an insulin-resistant mouse model. *Hepatology* 57, 515–524. doi: 10.1002/hep.26028

Merkow, J., Lufkin, R., Nguyen, K., Soatto, S., Tu, Z., and Vedaldi, A. (2017). DeepRadiologyNet: radiologist level pathology detection in CT head images. *arXiv* [Preprint]. Available online at: https://arxiv.org/abs/1711.09313 (accessed January 5, 2020).

Miles, K. A., Voo, S. A., and Groves, A. M. (2018). Additional clinical value for PET/MRI in oncology: moving beyond simple diagnosis. *J. Nucl. Med.* 59, 1028–1032. doi: 10.2967/jnumed.117.203612

Miller, E. J., Cohen, A. B., and Matthay, M. A. (1996). Increased interleukin-8 concentrations in the pulmonary edema fluid of patients with acute respiratory distress syndrome from sepsis. *Crit. Care Med* 24, 1448–1454. doi: 10.1097/00003246-199609000-00004

Mills, G. H. (2003). Functional magnetic resonance imaging of the lung. *Br. J. Anaesth.* 91, 16–30. doi: 10.1093/bja/aeg149

Mistry, N. N., Pollaro, J., Song, J., De Lin, M., and Johnson, G. A. (2008). Pulmonary perfusion imaging in the rodent lung using dynamic contrast-enhanced MRI. *Magn. Reson. Med.* 59, 289–297. doi: 10.1002/mrm.21353

Murray, J. F., Matthay, M. A., Luce, J. M., and Flick, M. R. (1988). An expanded definition of the adult respiratory distress syndrome. *Am. Rev. Respir. Dis.* 138, 720–723. doi: 10.1164/ajrccm/138.3.720

Musch, G., Venegas, J. G., Bellani, G., Winkler, T., Schroeder, T., Petersen, B., et al. (2007). Regional gas exchange and cellular metabolic activity in ventilator-induced lung injury. *Anesthesiology* 106, 723–735. doi: 10.1097/01.anes.0000264748.86145.ac

Najac, C., Chaumeil, M. M., Kohanbash, G., Guglielmetti, C., Gordon, J. W., Okada, H., et al. (2016). Detection of inflammatory cell function using 13C magnetic resonance spectroscopy of hyperpolarized [6-13C]-arginine. *Sci. Rep.* 6, 1–10. doi: 10.1038/srep31397

Nelson, S. J., Kurhanewicz, J., Vigneron, D. B., Larson, P. E. Z., Harzstark, A. L., Ferrone, M., et al. (2013). Metabolic imaging of patients with prostate cancer using hyperpolarized [1-13C]pyruvate. *Sci. Transl. Med.* 5:198ra108. doi: 10.1126/scitranslmed.3006070

Papazian, L., Thomas, P., Bregeon, F., Garbe, L., Zandotti, C., Saux, P., et al. (1998). Open-lung biopsy in patients with acute respiratory distress syndrome. *Anesthesiology* 88, 935–944. doi: 10.1097/00000542-199804000-00013

Park, I., Larson, P. E. Z., Gordon, J. W., Carvajal, L., Chen, H.-Y., Bok, R., et al. (2018). Development of methods and feasibility of using hyperpolarized carbon-13 imaging data for evaluating brain metabolism in patient studies. *Magn. Reson. Med.* 100:10158. doi: 10.1002/mrm.27077

Pastorino, U. (2010). Lung cancer screening. *Br. J. Cancer* 12, 1681–1686. doi: 10.1038/sj.bjc.6605660

Pauwels, E. K., Sturm, E. J., Bombardieri, E., Cleton, F. J., and Stokkel, M. P. (2000). Positron-emission tomography with [18F]fluorodeoxyglucose. Part I. Biochemical uptake mechanism and its implication for clinical studies. *J. Cancer Res. Clin. Oncol.* 126, 549–559. doi: 10.1007/pl00008465

Pelosi, P., D'Onofrio, D., Chiumello, D., Paolo, S., Chiara, G., Capelozzi, V. L., et al. (2003). Pulmonary and extrapulmonary acute respiratory distress syndrome are different. *Eur. Respir. J.* 22, 48s–56s. doi: 10.1183/09031936.03.00420803

Pham, T., and Rubenfeld, G. D. (2017). F iftyY ears ofR esearch inARDS. The epidemiology of acute respiratory distress syndrome. A 50th birthday review. *Am. J. Respir. Crit. Care Med.* 195, 860–870. doi: 10.1164/rccm.201609-1773cp

Pourfathi, M. (2019). Metabolic imaging of acute lung injury using hyperpolarzied 13C magnetic resonance imaging. *Magn. Reson. Med.* 78, 2106–2115. doi: 10.1002/mrm.26604

Pourfathi, M., Cereda, M., Chatterjee, S., Xin, Y., Kadlecek, S., Duncan, I., et al. (2018). Lung metabolism and inflammation during mechanical ventilation; an imaging approach. *Sci. Rep.* 8:3525. doi: 10.1038/s41598-018-21901-0

Pourfathi, M., Xin, Y., Kadlecek, S. J., Cereda, M. F., Profka, H., Hamedani, H., et al. (2017). In vivo imaging of the progression of acute lung injury using hyperpolarized [1-13 C] pyruvate. *Magn. Reson. Med.* 78, 2106–2115.

Ramanathan, K., Antognini, D., Combes, A., Paden, M., Zakhary, B., Ogino, M., et al. (2020). Planning and provision of ECMO services for severe ARDS during the COVID-19 pandemic and other outbreaks of emerging infectious diseases. *Lancet Respir. Med.* 8, 518–526. doi: 10.1016/S2213-2600(20)30121-1

Rodrigues, R. S., Miller, P. R., Bozza, F. A., Marchiori, E., Zimmerman, G. A., Hoffman, J. M., et al. (2008). FDG-PET in patients at risk for acute respiratory distress syndrome: a preliminary report. *Intensive Care Med.* 34, 2273–2278. doi: 10.1007/s00134-008-1220-7

Ruppert, K. (2014). Biomedical imaging with hyperpolarized noble gases. *Rep. Prog. Phys.* 77, 116701–116735. doi: 10.1088/0034-4885/77/11/116701

Scherer, P. M., and Chen, D. L. (2016). Imaging Pulmonary Inflammation. *J. Nucl. Med.* 57, 1764–1770. doi: 10.2967/jnumed.115.157438

Shaghaghi, H., Kadlecek, S., Deshpande, C., Siddiqui, S., Martinez, D., Pourfathi, M., et al. (2014). Metabolic spectroscopy of inflammation in a bleomycin-induced lung injury model using hyperpolarized 1-13C pyruvate. *NMR Biomed.* 27, 939–947. doi: 10.1002/nbm.3139

Shankar-Hari, M., and McAuley, D. F. (2017). Acute Respiratory Distress Syndrome Phenotypes and Identifying Treatable Traits The Dawn of Personalized Medicine for ARDS. *Am. J. Respir. Crit. Care Med.* 195, 280–281. doi: 10.1164/rccm.201608-1729ED

Siddiqui, S., Habertheuer, A., Xin, Y., Pourfathi, M., Tao, J. Q., Hamedani, H., et al. (2019). Detection of lung transplant rejection in a rat model using hyperpolarized [1-13 C] pyruvate-based metabolic imaging. *NMR Biomed.* 32:e4107. doi: 10.1002/nbm.4107

Siddiqui, S., Kadlecek, S., Pourfathi, M., Xin, Y., Mannherz, W., Hamedani, H., et al. (2016). The use of hyperpolarized carbon-13 magnetic resonance for molecular imaging. *Adv. Drug Deliv. Rev.* 113, 3–23. doi: 10.1016/j.addr.2016.08.011

Singh, S., Srivastava, A., Mi, L., Caselli, R. J., Chen, K., Goradia, D., et al. (2017). Deep learning based classification of FDG-PET data for alzheimers disease categories. *Proc. SPIE Int. Soc. Opt. Eng.* 10572:10572J. doi: 10.1117/12.2294537

Steinberg, K. P., Milberg, J. A., Martin, T. R., Maunder, R. J., Cockrill, B. A., and Hudson, L. D. (1994). Evolution of bronchoalveolar cell populations in the adult respiratory distress syndrome. *Am. J. Respir. Crit. Care Med.* 150, 113–122. doi: 10.1164/ajrccm.150.1.8025736

Summers, C., Singh, N. R., White, J. F., Mackenzie, I. M., Johnston, A., Solanki, C., et al. (2014). Pulmonary retention of primed neutrophils: a novel protective host response, which is impaired in the acute respiratory distress syndrome. *Thorax* 69, 623–629. doi: 10.1136/thoraxjnl-2013-204742

Tabuchi, A., Nickles, H. T., Kim, M., Semple, J. W., Koch, E., Brochard, L., et al. (2016). Acute lung injury causes asynchronous alveolar ventilation that can be corrected by individual sighs. *Am. J. Respir. Crit. Care. Med.* 193, 396–406. doi: 10.1164/rccm.201505-0901OC

Thind, K., Chen, A., Friesen-Waldner, L., Ouriadov, A., Scholl, T. J., Fox, M., et al. (2012). Detection of radiation-induced lung injury using hyperpolarized 13C magnetic resonance spectroscopy and imaging. *Magn. Reson. Med.* 185:A5582. doi: 10.1002/mrm.24525

Thompson, B. T., Chambers, R. C., and Liu, K. D. (2017). Acute respiratory distress syndrome. *N. Engl. J. Med.* 377, 562–572. doi: 10.1056/NEJMra1608077

Wallace, W. E., Gupta, N. C., Hubbs, A. F., Mazza, S. M., Bishop, H. A., Keane, M. J., et al. (2002). Cis-4-[(18)F]fluoro-L-proline PET imaging of pulmonary fibrosis in a rabbit model. *J. Nucl. Med.* 43, 413–420.

Ware, L. B., and Matthay, M. A. (2000). The Acute Respiratory Distress Syndrome. *N. Engl. J. Med.* 342, 1334–1349. doi: 10.1056/NEJM20000504342 1806

Yen, Y. F., Kohler, S. J., Chen, A. P., Tropp, J., Bok, R., Wolber, J., et al. (2009). Imaging considerations for in vivo 13C metabolic mapping using hyperpolarized 13C-pyruvate. *Magn. Reson. Med.* 62, 1–10. doi: 10.1002/mrm. 21987

Conflict of Interest: The authors declare that the research was conducted in the absence of any commercial or financial relationships that could be construed as a potential conflict of interest.

frontiers in Physiology

ORIGINAL RESEARCH
published: 16 September 2020
doi: 10.3389/fphys.2020.533683

Oxygen Glucose Deprivation Induced Prosurvival Autophagy Is Insufficient to Rescue Endothelial Function

Venkateswaran Natarajan[1†], Tania Mah[1†], Chen Peishi[1], Shu Yi Tan[1], Ritu Chawla[1], Thiruma Valavan Arumugam[2], Adaikalavan Ramasamy[3] and Karthik Mallilankaraman[1,4]*

[1] Mitochondrial Physiology and Metabolism Lab, Department of Physiology, Yong Loo Lin School of Medicine, National University of Singapore, Singapore, Singapore, [2] Department of Physiology, Anatomy and Microbiology School of Life Sciences, La Trobe University, Melbourne, VIC, Australia, [3] Genome Institute of Singapore, A*STAR, Singapore, Singapore, [4] Center for Healthy Longevity, NUHS, Singapore, Singapore

OPEN ACCESS

Edited by:
Shampa Chatterjee, University of Pennsylvania, United States

Reviewed by:
Vikas Anathy, The Robert Larner, M.D. College of Medicine at The University of Vermont, United States
Salvatore Mancarella, University of Tennessee Health Science Center (UTHSC), United States

***Correspondence:**
Karthik Mallilankaraman
phsmkb@nus.edu.sg

[†] These authors have contributed equally to this work

Specialty section:
This article was submitted to Vascular Physiology, a section of the journal Frontiers in Physiology

Received: 09 February 2020
Accepted: 12 August 2020
Published: 16 September 2020

Citation:
Natarajan V, Mah T, Peishi C, Tan SY, Chawla R, Arumugam TV, Ramasamy A and Mallilankaraman K (2020) Oxygen Glucose Deprivation Induced Prosurvival Autophagy Is Insufficient to Rescue Endothelial Function. Front. Physiol. 11:533683. doi: 10.3389/fphys.2020.533683

Endothelial dysfunction, referring to a disturbance in the vascular homeostasis, has been implicated in many disease conditions including ischemic/reperfusion injury and atherosclerosis. Endothelial mitochondria have been increasingly recognized as a regulator of calcium homeostasis which has implications in the execution of diverse cellular events and energy production. The mitochondrial calcium uniporter complex through which calcium enters the mitochondria is composed of several proteins, including the pore-forming subunit MCU and its regulators MCUR1, MICU1, and MICU2. Mitochondrial calcium overload leads to opening of MPTP (mitochondrial permeability transition pore) and results in apoptotic cell death. Whereas, blockage of calcium entry into the mitochondria results in reduced ATP production thereby activates AMPK-mediated pro-survival autophagy. Here, we investigated the expression of mitochondrial calcium uniporter complex components (MCU, MCUR1, MICU1, and MICU2), induction of autophagy and apoptotic cell death in endothelial cells in response to oxygen-glucose deprivation. Human pulmonary microvascular endothelial cells (HPMVECs) were subjected to oxygen-glucose deprivation (OGD) at 3-h timepoints up to 12 h. Interestingly, except MCUR1 which was significantly downregulated, all other components of the uniporter (MCU, MICU1, and MICU2) remained unchanged. MCUR1 downregulation has been shown to activate AMPK mediated pro-survival autophagy. Similarly, MCUR1 downregulation in response to OGD resulted in AMPK phosphorylation and LC3 processing indicating the activation of pro-survival autophagy. Despite the activation of autophagy, OGD induced Caspase-mediated apoptotic cell death. Blockade of autophagy did not reduce OGD-induced apoptotic cell death whereas serum starvation conferred enough cellular and functional protection. In conclusion, the autophagic flux induced by MCUR1 downregulation in response to OGD is insufficient in protecting endothelial cells from undergoing apoptotic cell death and requires enhancement of autophagic flux by additional means such as serum starvation.

Keywords: MCUR1, endothelial dysfunction, oxygen-glucose deprivation, autophagy, apoptotic cell death

INTRODUCTION

Endothelial cells are essential regulators of vascular function. Endothelial dysfunction is widely implicated in the development and progression of many vascular diseases (Deedwania, 2003; Gutierrez et al., 2013). Endothelial mitochondria plays an important role as a key regulator of endothelial function (Groschner et al., 2012). Defects in mitochondrial function could potentially contribute to development and progression of endothelial dysfunction (Tang et al., 2014). Endothelial mitochondria, beyond its role in providing support in energy production, also aid in shaping cytosolic Ca^{2+} signals and redox regulation (Dedkova and Blatter, 2005; Wilson et al., 2019). Ca^{2+} is an important second messenger that determines both cellular bioenergetics and the initiation of cell death mechanisms (Groschner et al., 2012; Williams et al., 2013; Natarajan et al., 2020). Mitochondrial matrix calcium regulates important cofactors for enzymes involved in the Krebs cycle – namely pyruvate dehydrogenase, isocitrate dehydrogenase and α-ketoglutarate dehydrogenase (Mallilankaraman et al., 2012a; Tarasov et al., 2012; Vatrinet et al., 2017). These enzymes are essential players of Krebs cycle which provides reducing equivalents to the electron transport chain (ETC), thereby contributing to the majority of mitochondrial ATP production (Quijano et al., 2016). Although the role of oxidative phosphorylation as an energy source in endothelial cells remains questionable (Quintero et al., 2006), it is still a major source of ROS (Murphy, 2009) that contributes to the pathophysiology of many cardiovascular diseases (Madamanchi and Runge, 2007). Furthermore, mitochondrial Ca^{2+} signaling has been shown to regulate NO production in endothelial cells (Williams et al., 2013; Park and Park, 2015).

Ca^{2+} enters the mitochondria through a highly calcium selective ion channel, the mitochondrial calcium uniporter (Kirichok et al., 2004). Mitochondrial calcium uniporter is a multiprotein complex comprising of, the pore forming subunit MCU (Baughman et al., 2011; De Stefani et al., 2011; Chaudhuri et al., 2013), regulatory subunits MCUR1 (Mallilankaraman et al., 2012a; Vais et al., 2015), MICU1 (Perocchi et al., 2010; Mallilankaraman et al., 2012b; Logan et al., 2014), MICU2 (Payne et al., 2017), MICU3 (Patron et al., 2019), MCUb (Raffaello et al., 2013) and EMRE (Sancak et al., 2013; Vais et al., 2016; Payne et al., 2020), of which MCU, MCUR1, MICU1, and MICU2 are well characterized. Despite the discovery of the components of mitochondrial calcium uniporter in the last decade, the role of these components in endothelial mitochondrial dysfunction during ischemic vascular injury remains poorly understood.

Mitochondrial calcium overload has been implicated in endothelial cells subjected to ischemic stress leading to deregulated NO signaling and ROS production (Choy et al., 2001). Mitochondrial Ca^{2+} overload and ROS overproduction are known to trigger the opening of mitochondrial permeability transition pore (mPTP), a large non-selective pore that spans across the IMM and OMM, leading to cell death (Bernardi, 1999; Duchen, 2000). On the other hand, loss of calcium transfer to mitochondria or defects in mitochondrial calcium uptake leads to ATP depletion resulting in activation of AMPK-mediated macro autophagy (Cardenas et al., 2010; Mallilankaraman et al., 2012a).

Here, we employed human pulmonary endothelial cells subjected to oxygen-glucose deprivation (OGD) to study the status of mitochondrial calcium uniporter components. Our results suggest that MCUR1 alone is downregulated under OGD conditions, whereas the other uniporter components tested namely MCU, MICU1 and MICU2 remains unchanged. Downregulation of MCUR1 activated pro-survival autophagy, which was still insufficient to rescue endothelial function. Blockade of autophagic flux did not confer protection against OGD-induced cell death, indicating a need for additional autophagy inducers to enhance autophagic flux. In the current study, we show the modulation of mitochondrial calcium uniporter and its downstream autophagic induction is insufficient and requires additional induction of autophagy to rescue endothelial function under OGD conditions.

MATERIALS AND METHODS

Cell Line

Wild type Human Pulmonary Micro Vascular Endothelial Cells (HPMVECs) were grown in low glucose Dulbecco's modified Eagle's medium (DMEM) supplemented with 10% fetal bovine serum (FBS), 100 U/ml penicillin, and 100 μg/ml streptomycin at 37°C and 5% CO_2.

Oxygen-Glucose-Deprivation (OGD) Treatment

Wild type HPMVECs were seeded at a density of 3.0×10^6 cells/plate in 10 cm plates 1 day before the experiments. Media in wild type HPMVECs were replaced with glucose-free Locke's buffer (154 mM NaCl, 5.6 mM KCl, 2.3 mM $CaCl_2$, 1 mM $NaHCO_3$ 5 mM HEPES at pH 7.2, supplemented with 5 mg/L gentamicin) and incubated in oxygen-deprivation chamber (Billups-Rothenberg, San Diego, CA, United States). For oxygen deprivation the chambers were flushed with a gaseous mix of 95% Nitrogen (N_2) and 5% CO_2 for 10 min. The oxygen-deprivation chamber was sealed and kept in an incubator at 37°C. Controls were incubated with low glucose DMEM supplemented with 10% FBS, 100 U/ml penicillin, and 100 μg/ml streptomycin at 37°C and 5% CO_2. The length of incubation in oxygen-glucose deprived conditions were 3, 6, 9, and 12 h, and referred to as OGD3, OGD6, OGD9, and OGD12, respectively. For chloroquine (CQ) or Metformin (Met) treatment studies, CQ or Met was added into the glucose-free Locke's buffer prior to incubation of the cells for 3, 6, 9, or 12 h of OGD. Controls were treated with CQ or Met 3 h prior before collection. For serum starvation studies, the cells were grown with 10% serum for 24 h. The medium was removed, washed and incubated with low glucose DMEM supplemented with 0.2% serum 24 h prior to OGD. Controls were incubated with low glucose DMEM

supplemented with 0.2% serum throughout the experiment until cell lysate collection.

Cell Lysate Preparation

Following OGD treatments, cell culture dishes were kept on ice, the cells scraped and collected into tubes. The cell pellets were then washed with cold PBS and centrifuged at 1500 × *g* for 5 min at 4°C. Cells were lysed by resuspending the pellet with RIPA lysis buffer (Thermo Scientific, #89900) containing protease inhibitor and phosphatase inhibitor cocktail (Thermo Scientific, #1860932). After sonication, cell lysates were centrifuged at 13,000 × *g* for 15 min at 4°C and the collected supernatant from each sample was stored at −80°C. Total protein concentration present in the collected supernatant was quantified using the Thermo Scientific Pierce™ bicinchoninic acid (BCA) Protein Assay Kit (Thermo Scientific, #23225). Each sample containing 30 μg of protein was denatured by boiling at 95°C for 10 min in 2 X Laemmli buffer (Bio-Rad Laboratories, #1610737) and β-mercaptoethanol (Sigma Aldrich) at 1:1 ratio before being subjected to Western blot analysis.

Western Blot

Protein samples were separated on a sodium dodecyl sulfate (SDS) polyacrylamide gel. 10% SDS-polyacrylamide gels (resolving gel: 8 ml of H_2O, 4 ml of 40% acrylamide, 4 ml of Tris buffer pH 8.5, 150 μl of APS and 13 μl of TEMED; stacking gel: 5.75 ml of H_2O, 0.75 ml of 40% acrylamide, 1 ml of Tris buffer pH 6.5, 77 μl of APS and 7.7 μl of TEMED) were used to separate MCU, MCUR1, MICU1, MICU2, AMPK, and phospho-AMPK (pAMPK). 15% SDS-polyacrylamide gels (resolving gel: 6 ml of H_2O, 6 ml of 40% acrylamide, 4 ml of Tris buffer pH 8.5, 150 μl of APS and 13 μl of TEMED; stacking gel: 5.75 ml of H_2O, 0.75 ml of 40% acrylamide, 1 ml of Tris buffer pH 6.5, 77 μl of APS and 7.7 μl of TEMED) were used to separate full-length Caspase 3, cleaved Caspase 3, and LC3B. Gel electrophoresis was run at 75 V for the first 30 min, then increased to 100 V for 90 min in 1 X Tris/Glycine/SDS running buffer (25 mM Tris, 192 mM glycine, 0.1% SDS, pH 8.3; Bio-Rad Laboratories, #1610772). The separated proteins on the gel were then transferred onto nitrocellulose membranes (Bio-Rad Laboratories, #1620112) using a wet transfer apparatus. The electroblotting was run at 350 mA for 100 min in chilled 1 X Tris/Glycine transfer buffer (25 mM Tris, 192 mM glycine, 20% (v/v) methanol, pH 8.3; Bio-Rad Laboratories, #161-0771). After transfer, membranes were subjected to blocking in 5% non-fat dry milk diluted in 1 X Tris–buffered saline containing 0.1% Tween-20 (1xTBST) for 1 h at room temperature and incubated with primary antibody overnight at 4°C with gentle shaking. Membranes were washed with 1xTBST three times, 10 min per wash, to remove excess primary antibody before incubation with horseradish peroxidase (HRP)-conjugated anti-rabbit or anti-mouse secondary antibody for 1 h at room temperature. Anti-rabbit secondary antibodies were used in the detection of MCU, MCUR1, MICU1, MICU2, AMPK, pAMPK, Caspase 3, cleaved Caspase 3, and LC3B, while anti-mouse secondary antibodies were used in the detection of β-actin. Membranes were again washed with 1xTBST three times, 10 min per wash, to remove excess secondary antibody. To visualize bands representing protein-of-interest, the membranes were incubated with chemiluminescent ECL reagent (BioRad, #1705061) for 3 min and specific bands were then detected on X-ray films (Research Instruments). To ensure equal protein loading across gels, membranes were stripped using Restore Western Blot Stripping Buffer (ThermoFisher Scientific, #21059) and probed with a loading control antibody. Antibodies for MCU (Sigma-Aldrich, HPA016480; 1:250); MCUR1 (Proteintech, 24948-1-AP; 1:500); MICU1 (Sigma-Aldrich, HPA037479; 1:500); MICU2 (Abcam, ab101465; 1:1000); Caspase 3 (Cell Signalling, 9662S; 1:1000); AMPK (Merck, 07-350; 1:1000); pAMPK (Cell Signaling, 40H9; 1:1000); LC3B (Cell Signalling, 2775S; 1:1000); anti-actin (Sigma-Aldrich, A2228; 1:5000); anti-mouse IgG-HRP (BBI Life Sciences, D110085-0100; 1:10,000); and anti-rabbit IgG-HRP (Amersham, NA934V; 1:2000) were used in the study. Relative band intensities were measured using ImageJ Imaging Software and expressed as a value normalized by the intensity of β-actin signal.

Migration Assay

Wild type HPMVECs were seeded at a density of 0.5×10^6 cells/well in six-well plates and incubated overnight at 37°C. A uniform 1.8 mm scratch running the entire length of the well was created using a sterile 200 μl tip. For the "Normal" condition, the wells were washed thrice with PBS to remove cell debris after making the scratch and then bathed in 2 ml low glucose DMEM supplemented with 10% FBS, 100 U/ml penicillin, and 100 μg/ml streptomycin. For endothelial cells subjected to 8 h of OGD, the wells were washed thrice with PBS to remove cell debris after making the scratch and then bathed in 2 ml glucose-free Locke's Buffer. For endothelial cells subjected to 8 h of OGD with serum starvation, the cells were pre-starved overnight prior to OGD treatment. Similar to the 8 h of OGD treatment, the wells were washed thrice with PBS to remove cell debris after making the scratch and then bathed in 2 ml of glucose-free Locke's Buffer. the cells were incubated at 37°C and 5% CO_2. The time-lapse of the cell migration within each well was captured using EVOS live cell imaging system equipped with on-stage incubation system by capturing images every 15 min for 8 h. Similarly, for OGD conditions the imaging was performed but gas mixture was set to 95% N_2 and 5% O_2.

Statistical Data Analysis

Data from multiple experiments were quantified and expressed as mean ± SEM. In order to analyze the differences between two groups, the two-tailed unpaired Student's *t*-test was used. All experiments were repeated n number of times as indicated in figure legends. Data were computed with GraphPad Prism software version 8.0.1, where *p*-values measuring the level of significance in differences observed between two groups were obtained. Any significant difference between the two groups were then indicated by either an asterisk * or ns, where ns represents non-significant, *represents

$p < 0.05$; **represents $p < 0.01$; ***represents $p < 0.001$ and ****represents $p < 0.0001$.

RESULTS

Modulation of Mitochondrial Calcium Uniporter Complex in Human Pulmonary Microvascular Endothelial Cells (HPMVECs) in Response to Oxygen-Glucose Deprivation (OGD)

To determine the expression pattern of the mitochondrial calcium uniporter complex components in HPMVECs in normal and OGD conditions, protein levels of MCU, MCUR1, MICU1, and MICU2 were assessed by western blot analysis (**Figure 1A**). Quantitative analyses showed no significant changes in MCU (**Figure 1B**), MICU1 (**Figure 1D**), and MICU2 (**Figure 1E**) expression across the OGD timepoints, but significant reduction in MCUR1 (**Figure 1C**) levels at 12 h of OGD. These findings suggest that OGD results in downregulation of MCUR1, the positive regulator of the mitochondrial calcium uniporter complex.

OGD Induces Endothelial Cell Death Despite the Induction of Autophagic Flux

MCUR1 downregulation is known to activate pro-survival autophagy (Mallilankaraman et al., 2012a). Since we observed a decrease in MCUR1 levels following OGD (**Figures 1A,C**), we sought to verify the status of autophagic flux. As expected, significant increase in autophagic markers phospho-AMPK (pAMPK)/AMPK ratio and LC3 processing was observed, which correlates with the significant decrease in MCUR1 observed over the same duration of OGD (**Figures 2A–D**). OGD has also been known to cause cell death in many cell types including endothelial cells (Xu et al., 2000; Plesnila et al., 2001). Therefore, we wanted to determine the expression level of apoptotic cell death markers during OGD. We observed significant increase in cleaved caspase 3 during OGD (**Figures 2E,F**), suggesting the activation of apoptotic cell death. Altogether, this suggests that despite the induction of autophagy which plays a protective role, HPMVECs still undergo apoptotic cell death induced by OGD.

Blockade of Autophagic Flux Has no Effect on OGD-Induced Cell Death

Autophagy is known to have a close connection with caspase-mediated cell death, despite its well accepted pro-survival role. To verify whether the observed OGD-induced cell death is triggered by autophagy, we blocked the autophagic flux using a widely used inhibitor Chloroquine (CQ) and assessed the cell death under different OGD conditions. Chloroquine inhibits autophagosome-lysosome fusion and there by enhances accumulation of LC3-II. Cells treated with CQ showed an increased LC3-II accumulation compared to untreated ones in both normoxic and OGD conditions (**Figures 3A,B**). Interestingly, CQ treatment did not alter OGD-induced caspase-mediated cell death (**Figures 3C,D**). Chloroquine has been reported to have additional effects on mitochondrial function and whether it affects MCUR1 expression remains unstudied. Like untreated cells, MCUR1 was significantly reduced in CQ-treated HPMVECs over 12 h of OGD (**Figures 3E,F**) suggesting CQ has no effect on MCUR1 expression. Taken together, these data suggest that autophagy induction is not responsible for caspase-mediated cell death in OGD conditions.

Serum Starvation Attenuates OGD-Induced Cell Death

Autophagic flux in OGD conditions neither have any protective effects nor causes cell death. Therefore, we speculated insufficient autophagic flux as a cause for lack of protection wherein enhancement of autophagic flux could rescue the cells from OGD-induced cell death. For induction of higher autophagic flux in endothelial cells under hypoxic conditions, we attempted using a previously reported activator of autophagy Metformin. However, good autophagic induction was not observed after treatment of cells with Metformin (**Supplementary Figure 1**), possibly due to the similar route these drugs take to activate autophagy as OGD (Meng et al., 2015; Kim et al., 2016). While Metformin failed to protect the cells from cell death at 3 and 6-h post OGD, it significantly reduced cell death at OGD 9 and 12 h (**Supplementary Figure 1**). This could possibly due to delayed induction of autophagy. Therefore we sought to attempt serum starvation, a widely used potent physiological inducer of autophagy (Mizushima and Klionsky, 2007; Mizushima et al., 2010). A recent study has shown short term serum starvation (12–48 h) induced autophagy via Akt-mTOR-p70S6K inhibition offered protection against endothelial blood brain barrier impairment (Yang et al., 2019). Therefore, we attempted to test the protective effect of serum starvation induced autophagy against OGD induced cell death.

Cells that were serum-starved for 24 h before OGD treatment showed increased levels of pAMPK/AMPK ratio and LC3 processing under normoxic conditions indicating an increase in autophagic flux. But the pAMPK/AMPK ratio in serum-starved cells did not increase during OGD (**Figures 4A,B**). Interestingly, LC3-II/I ratio decreased over different time points of OGD (**Figures 4C,D**) indicating the degradation of autophagosomes as seen in the final stages of autophagic process. To verify whether the serum starvation-induced enhancement of autophagic flux has any protective role during OGD, we assessed the Caspase 3 cleavage. The ratio of cleaved caspase 3 to full-length caspase 3 was significantly reduced in serum-starved group compared to during OGD (**Figures 4E,F**). Interestingly, Serum starvation was able to rescue the MCUR1 expression at OGD 12 (**Figures 4G,H**). Overall, these data suggest that serum starvation mediated enhanced induction of autophagy serves as a mechanism that confers protection of HPMVECs against cell death under OGD stress. To understand whether serum starvation-induced increase in autophagic flux is due to further decrease in MCUR1 during OGD, we verified the MCUR1 expression in serum-starved cells undergoing OGD treatment. Surprisingly, except OGD12 time point in which MCUR1 expression was increased, all other time

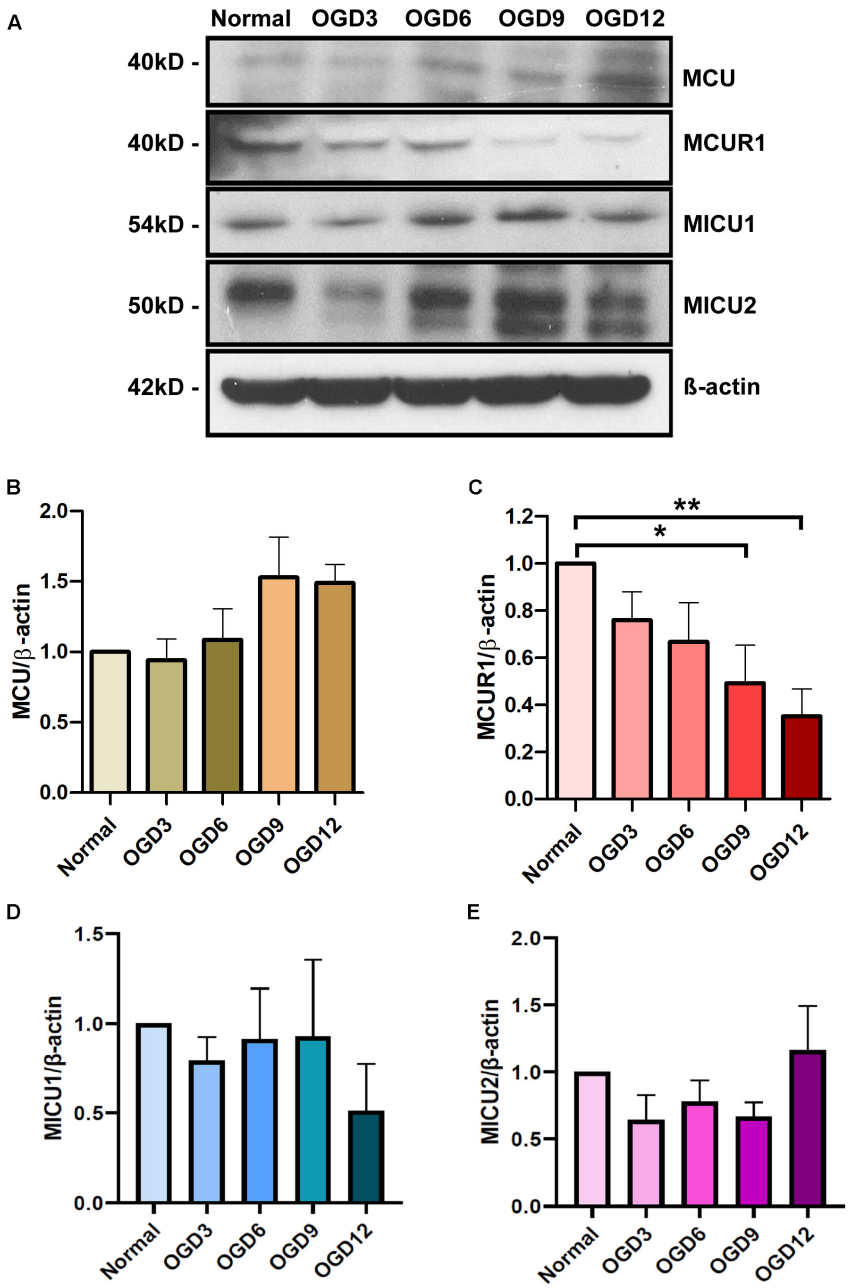

FIGURE 1 | (A) Representative western blots and **(B–E)** quantification showing the expression levels of **(B)** MCU, **(C)** MCUR1, **(D)** MICU1, and **(E)** MICU2 in human endothelial cells under in vitro OGD conditions at different time points as indicated. β-action was used as a loading control. mean ± SEM, $n = 5$, ns = non-significant; $^{*}P < 0.05$; $^{**}P < 0.01$.

points did not have significant change in MCUR1 expression levels indicating the increase in autophagic flux during serum starvation was independent of MCUR1 pathway (**Figures 4G,H**).

Serum Starvation Rescues Endothelial Migration Despite the OGD Treatment

To assess the functional status of endothelial cells under OGD conditions, we employed a widely used *in vitro* wound-healing scratch assay which implies the migratory potential. Endothelial cells migrated to cover the scratch area under normoxic conditions. However, this migration was significantly reduced under OGD condition. Since serum starvation had effectively reduced OGD-induced cell death, we sought to understand whether this could rescue the endothelial function. Interestingly, serum-starved endothelial cells under OGD conditions migrated similar to cells under normoxic conditions (**Figures 5A,B**). Overall, these data indicate that the

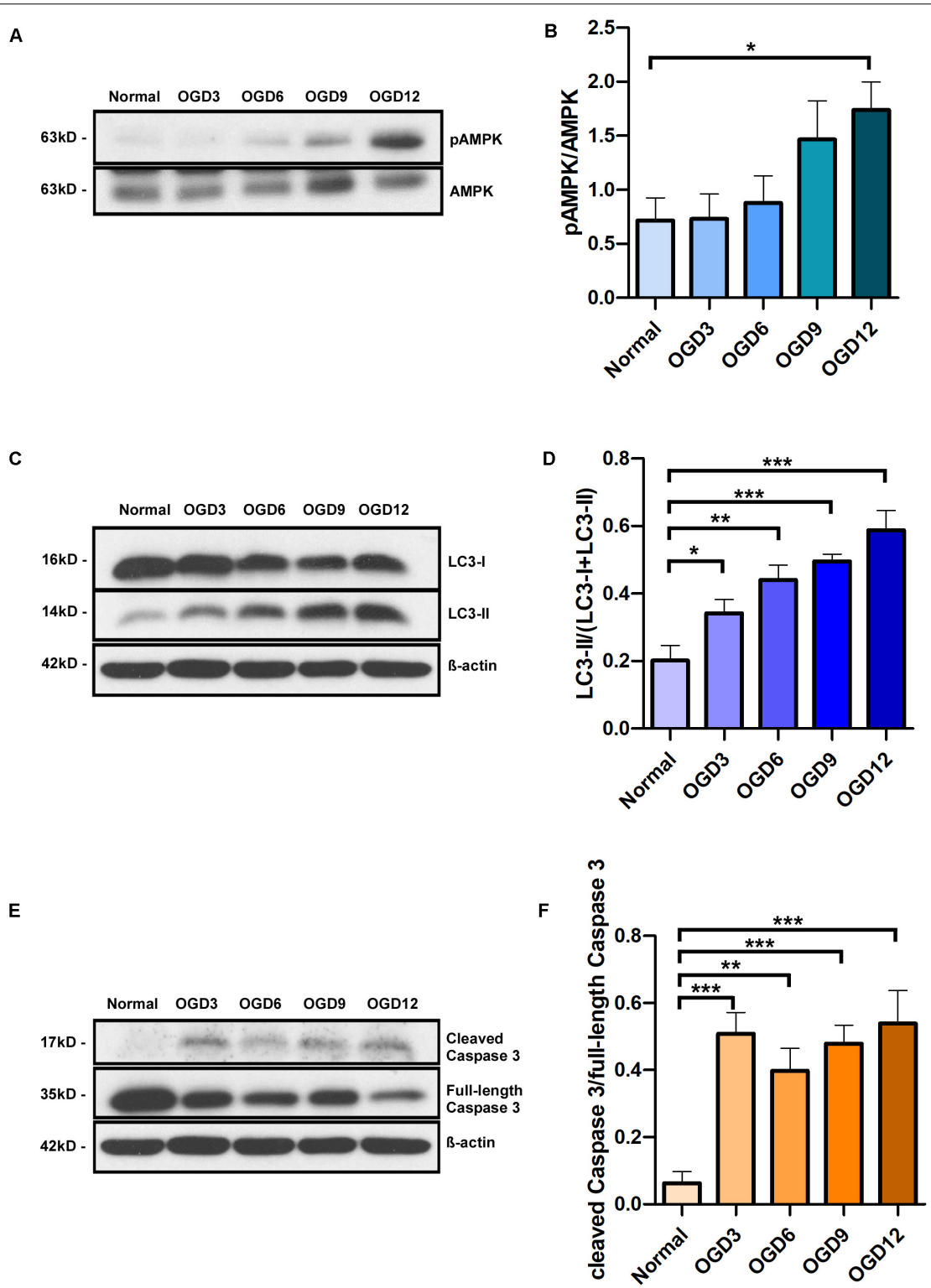

FIGURE 2 | Representative western blots and quantification of **(A,B)** Phospho-AMPK and total AMPK, **(C,D)** LC3-I and LC3-II, in human endothelial cells, **(E,F)** cleaved Caspase 3 and full-length Caspase 3 under in vitro OGD conditions at different time points as indicated. β-action was used as a loading control. mean ± SEM, $n = 4$; $^{*}P < 0.05$; $^{**}P < 0.01$; $^{***}P < 0.001$.

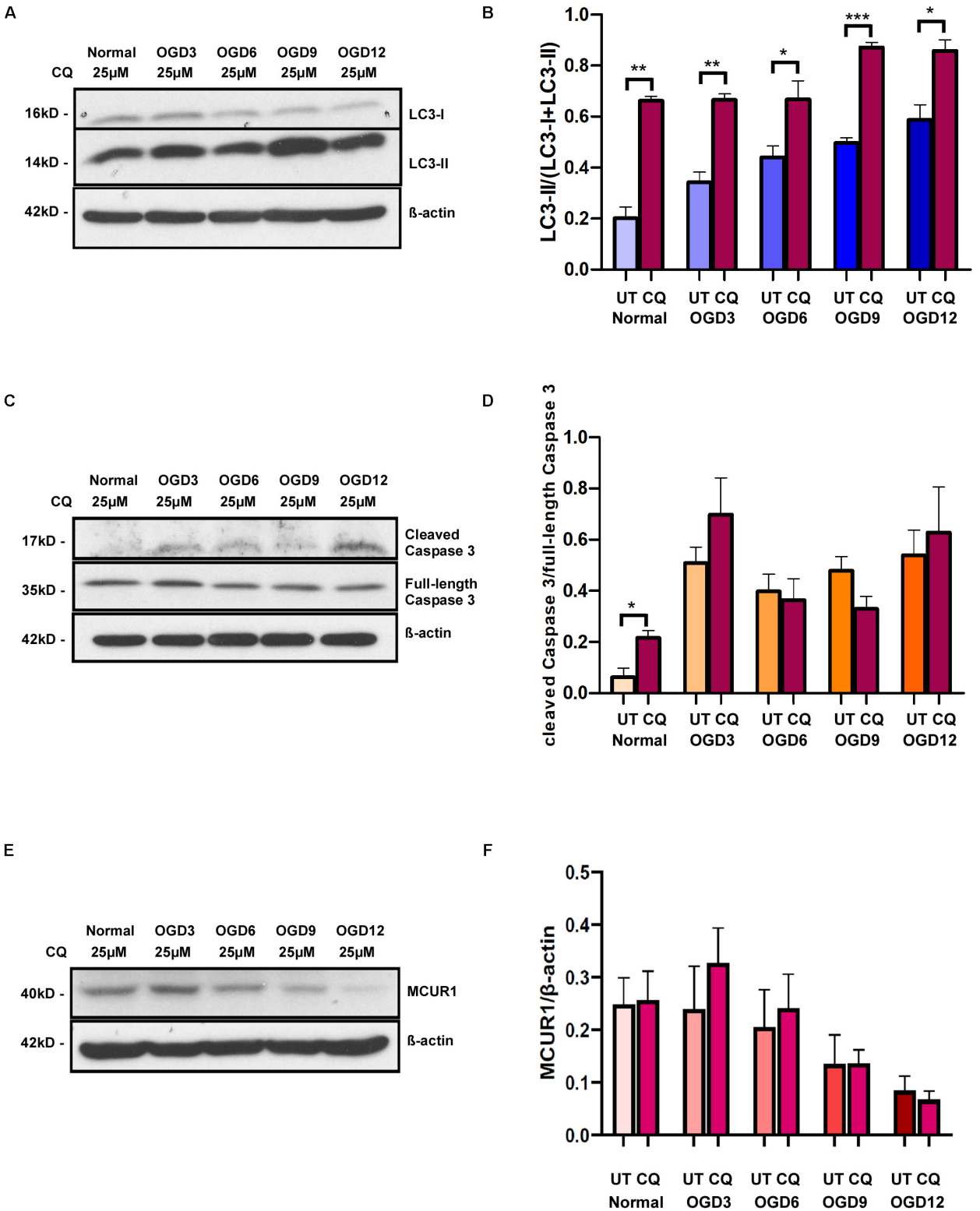

FIGURE 3 | Representative western blots and quantification showing the expression levels of **(A,B)** LC3-I and LC3-II **(C,D)** cleaved Caspase 3 and full-length Caspase 3 **(E,F)** MCUR1 in human endothelial cells under in vitro OGD conditions with (+) or without (–) chloroquine (CQ) at different time points as indicated. β-action was used as a loading control. mean ± SEM, $n = 4$; $^{*}P < 0.05$; $^{**}P < 0.01$; $^{***}P < 0.001$.

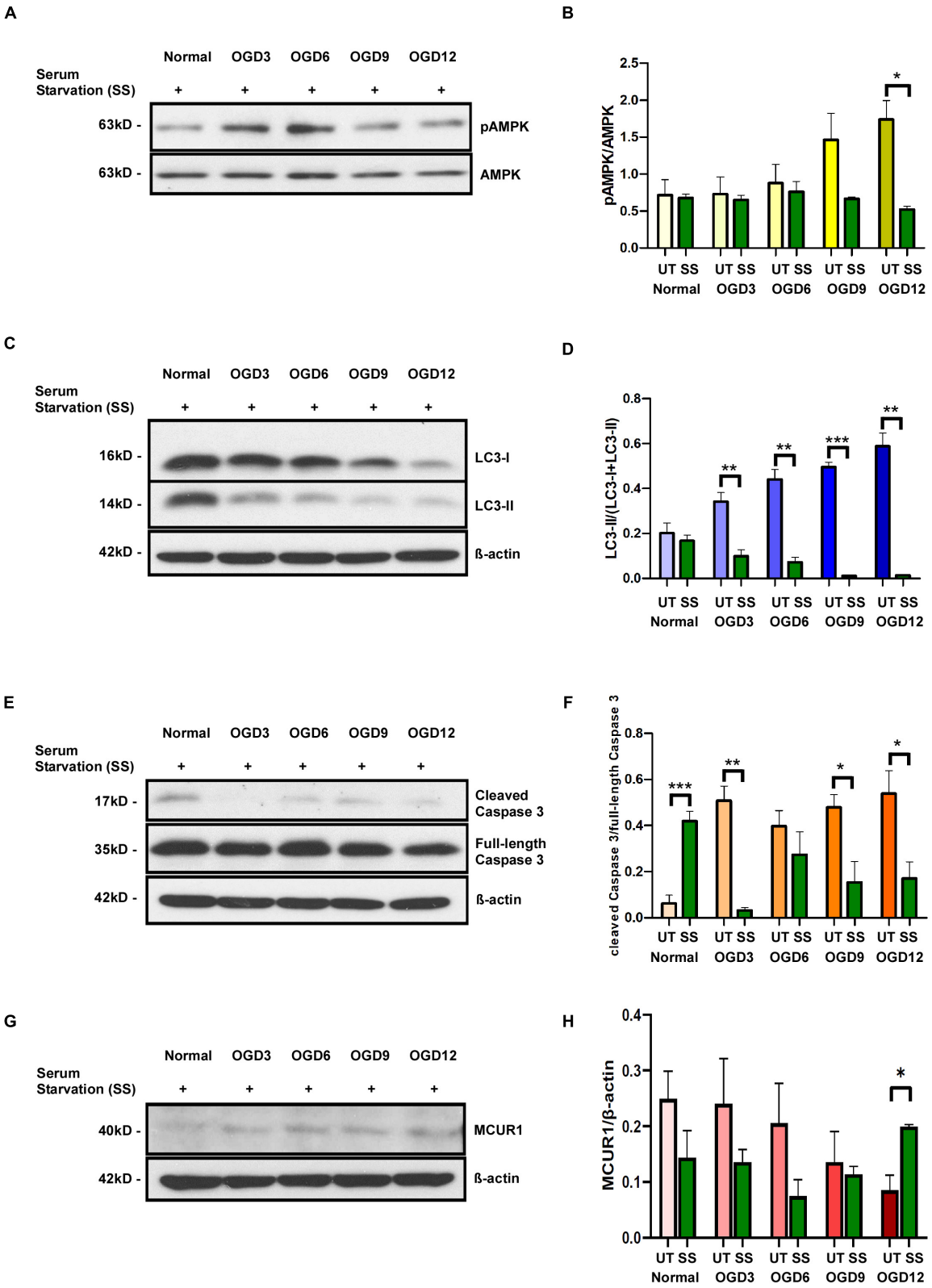

FIGURE 4 | Representative western blots and quantification of **(A,B)** Phospho-AMPK and total AMPK, **(C,D)** LC3-I and LC3-II **(E,F)** cleaved Caspase 3 and full-length Caspase 3, **(G,H)** MCUR1 in serum-starved in human endothelial cells under in vitro OGD conditions at different time points as indicated. β-action was used as a loading control. mean ± SEM, $n = 4$; $^{*}P < 0.05$; $^{**}P < 0.01$; $^{***}P < 0.001$.

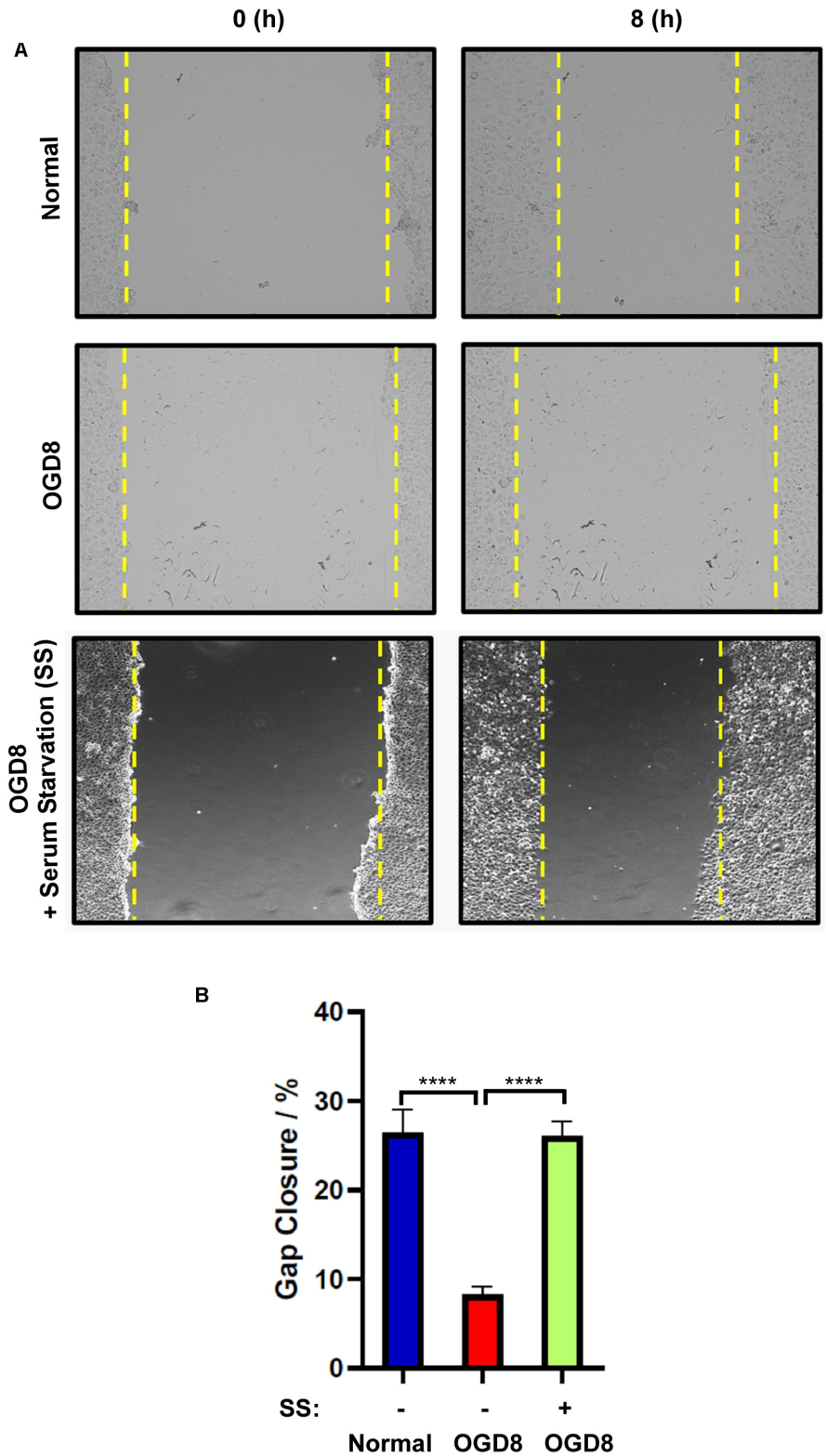

FIGURE 5 | (A) Representative images and **(B)** quantification of endothelial cell migration and normal, or OGD conditions with (+) or without (–) serum-starvation 8 h post-scratch using EVOS live cell imaging system. mean ± SEM, $n = 4$; $^{****}P < 0.0001$.

serum starvation-induced autophagic flux rescues endothelial function despite OGD treatment.

DISCUSSION

Ischemic injury causes endothelial dysfunction leading to functional decline of the vasculature. Role of endothelial mitochondria in response to ischemic insults have long been known but the underlying mechanisms are poorly understood. Here, we show MCUR1, a positive regulator of mitochondrial calcium uniporter is downregulated in response to *in vitro* ischemic conditions leading to activation of AMPK-mediated pro survival autophagy. Despite this autophagic flux, endothelial cells continue to activate apoptotic cell death suggesting a distinct pathway that surpasses pro survival autophagy. Nonetheless, activation of autophagic flux by serum starvation confers protection against OGD-induced endothelial cell death. Therefore, targeting mitochondrial calcium uniporter components to activate autophagy is insufficient in protecting from ischemic injury and requires a stronger inducer of autophagy. Our study clarifies the level of autophagic flux determining the protective function in ischemic injury.

Mitochondrial calcium overload has been implicated in ischemic injury of many cell types. Nonetheless, the status of the major ion channel through which calcium enters the mitochondria remains mysterious. This study shows the modulation of the positive regulator of mitochondrial calcium uniporter, MCUR1 (**Figure 1**), suggesting a defect in mitochondrial calcium uptake during OGD conditions. Further, the activity of calcium-dependent enzymes in the mitochondrial matrix that contributes the reducing equivalents to ETC decreases, leading to an energy crisis. Previous studies have shown that blockade of Ca^{2+} transfer from ER to mitochondria or defects in mitochondrial calcium uptake leads to activation of prosurvival autophagy (Cardenas et al., 2010). Interestingly, loss of MCUR1 has been reported to trigger the AMPK-mediated prosurvival autophagy (Mallilankaraman et al., 2012a). AMPK is well-recognized as an energy sensor that is typically activated allosterically by AMP (Langendorf et al., 2016). Reversal of AMP to ATP ratio happens during MCUR1 loss that leads to phosphorylation of AMPK (Mallilankaraman et al., 2012a). This instigated us to propose MCUR1 downregulation as a protective mechanism that sets in during OGD conditions in activating AMPK-mediated prosurvival autophagy. To further support the activation of autophagic flux data, LC3 processing was also observed in endothelial cells undergoing OGD. The increased processing of LC3-I to LC3-II, promotes the formation of autophagosomes that will eventually be degraded in the autophagic process (Tamargo-Gomez and Marino, 2018). Thus, the increase in the ratio of pAMPK to total AMPK together with the increase in LC3 processing suggests the induction of prosurvival autophagy (**Figure 2**). Nonetheless, our data supplements the few studies reporting OGD-induced apoptotic cell death in cells such as neurons and cerebral endothelial cells (Xu et al., 2000; Plesnila et al., 2001).

Surprisingly, caspase-mediated apoptotic cell death was increased despite the activation of prosurvival autophagy (**Figure 2**). Previous studies have shown AMPK-mediated autophagy as a pro-survival mechanism (Borger et al., 2008; Cardenas et al., 2010; Mallilankaraman et al., 2012a), implying that cell death should be reduced upon activation of AMPK-mediated autophagy. Whereas we observed both apoptosis and autophagic induction occurring simultaneously in endothelial cells subjected to OGD. This raised a concern whether AMPK-mediated autophagy induced in these cells under OGD stress, is serving as a protective mechanism or one that is promoting cell death. It must be noted that the paradoxical role of AMPK in autophagy and apoptotic cell death has been reported (Paz et al., 2016). While the accumulation of LC3-II demonstrates the induction of autophagy, it could also indicate the inhibition of autophagic flux, whereby autophagic flux measures the degradation activity of autophagic cargo. Therefore, we determined the autophagic flux induced in endothelial cells subjected to OGD by using a widely used inhibitor of autophagy, Chloroquine (CQ). CQ impairs the fusion of autophagosomes with lysosomes (Mauthe et al., 2018), thereby reduces the degradation of autophagic cargo, and inhibits autophagic flux (Mauthe et al., 2018). Our study showed a significant increase in LC3-II levels in the CQ-treated group compared to the corresponding untreated group, suggesting that the accumulation of LC3-II over time of OGD in untreated cells is not due to inhibition of autophagic flux, but rather a flux that is occurring at low and inefficient levels. Furthermore, since LC3-II is a marker of autophagosomes, significantly higher level of LC3-II in CQ-treated cells under normoxic conditions also indicates the accumulation of autophagosomes and thus the successful blockade of autophagic flux by CQ (**Figure 3**).

While the autophagic flux is inhibited by CQ treatment, OGD-induced cell death in CQ-treated group remained similar to untreated group (**Figure 3**). This suggests that the induction of AMPK-mediated autophagy in endothelial cells under OGD stress is playing a protective role as inhibition of pro-death autophagy should have reduced cell death. Moreover, the MCUR1 levels in both the untreated and CQ-treated groups remain unchanged suggesting that the downregulation of MCUR1 is upstream of autophagic flux. These data suggest that the endogenous induction of autophagic flux is insufficient in conferring protection against OGD-induced apoptotic cell death. The extent of autophagic flux seems to be the factor deciding whether cells survive or undergo apoptotic cell death. Therefore, we attempted to increase the autophagic flux in endothelial cells by other means and assess the degree of protection against OGD-induced cell death. Attempts with chemical activators such as Metformin induced autophagy like untreated group. However, Metformin reduced cell death only at 9 and 12 h of OGD compared untreated group (**Supplementary Figure 1**). This delay in protection could be due to the similarity in pathways that OGD and the chemical activators use to activate autophagy (Meng et al., 2015; Kim et al., 2016). Therefore, we decided to attempt serum starvation, which is a widely used and potent physiological inducer of autophagy (Mizushima and Klionsky, 2007; Mizushima et al., 2010). Further, Serum starvation was

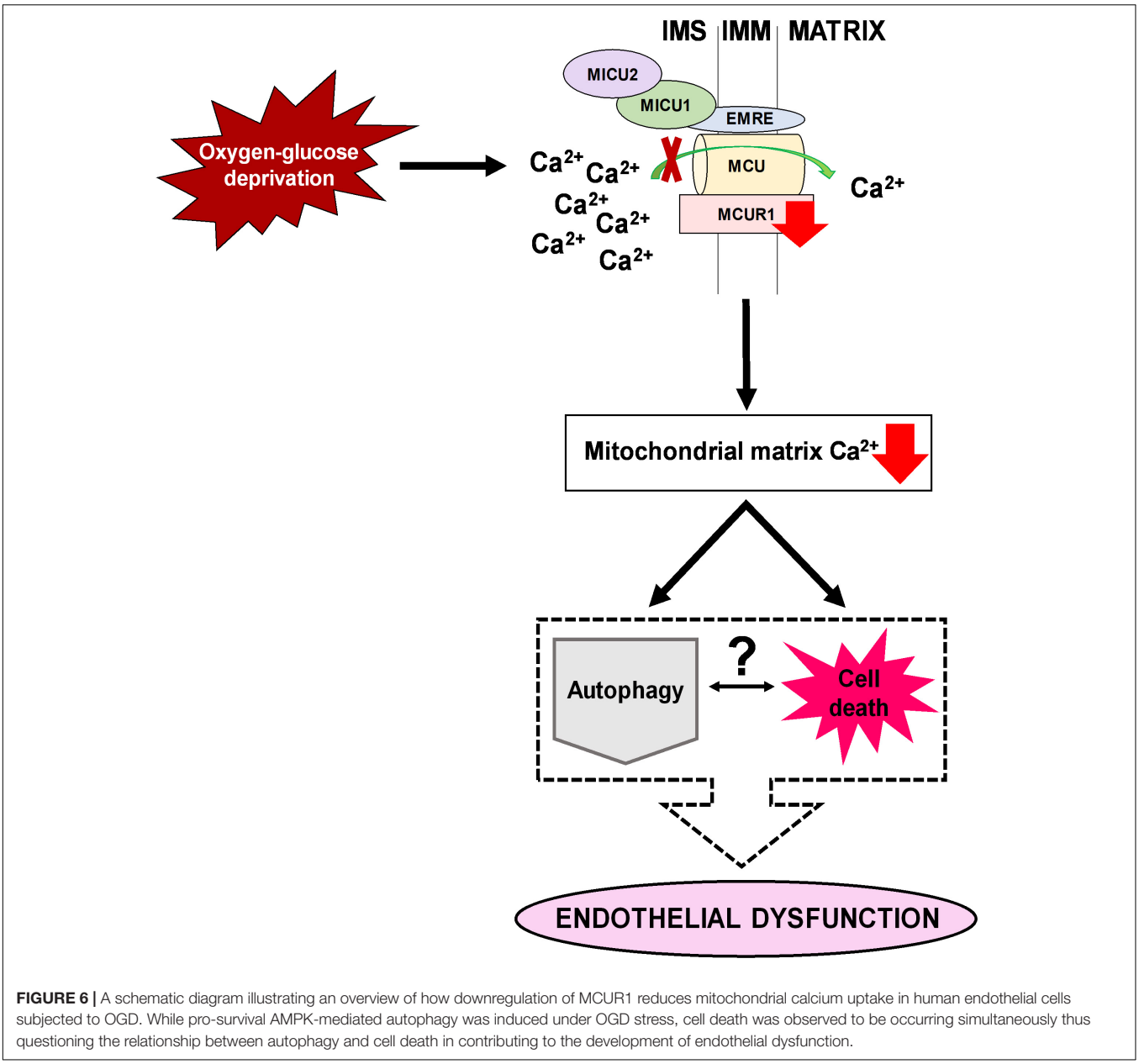

FIGURE 6 | A schematic diagram illustrating an overview of how downregulation of MCUR1 reduces mitochondrial calcium uptake in human endothelial cells subjected to OGD. While pro-survival AMPK-mediated autophagy was induced under OGD stress, cell death was observed to be occurring simultaneously thus questioning the relationship between autophagy and cell death in contributing to the development of endothelial dysfunction.

recently shown to induce autophagy in endothelial cells via Akt-mTOR-p70S6K pathway.

Serum-starved cells showed significantly reduced pAMPK levels indicating the cell's attempt to prevent excessive and constitutive AMPK activation, which could induce a "metabolic failure-like" state (Ramamurthy and Ronnett, 2006). While this finding suggests an increase in autophagic flux in serum-starved endothelial cells under OGD stress, the decrease in LC3-II levels further supports the enhancement of autophagic flux. LC3-II, a marker of autophagosomes, is expected to decrease as autophagosomes get degraded in the final stages of the autophagic process (Tamargo-Gomez and Marino, 2018). Interestingly, serum starvation-induced increase in autophagic flux correlated with significant decrease in caspase-mediated cell death, suggesting that the increase in autophagic flux could offer protection against OGD-induced cell death. An increase in autophagic flux by serum starvation in OGD conditions increases the amino acid availability through efficient degradation of autophagic cargo, thereby increasing protein synthesis (Herzig and Shaw, 2018). These amino-acids as well as the fatty acids liberated from bulk autophagic degradation can be recycled in a cell autonomous fashion and utilized by TCA cycle to maintain ATP production (Kuma et al., 2004; Lum et al., 2005; Mizushima, 2007; Mizushima and Klionsky, 2007). To further support the serum starvation-induced enhancement of autophagic flux, MCUR1 levels were rescued despite the OGD conditions in serum-starved endothelial cells presumably from the amino acids generated by autophagic degradation.

Endothelial cells migrate during angiogenesis, but they do migrate under pathophysiological conditions to restore vascular integrity (Michaelis, 2014). The ability of endothelial cells to migrate requires an enhancement in glycolysis, a process which is greatly reduced in cells subjected to OGD (Diebold et al., 2019). Besides requiring energy to drive the migration of endothelial cells, the role of mitochondrial Ca^{2+} homeostasis has been recently implicated in actin cytoskeleton dynamics and cell migration in mammals (Prudent et al., 2016). Specifically, endothelial cell migration is regulated by intracellular Ca^{2+} signaling, whereby Ca^{2+} acts on cytoskeleton architecture, migration direction, and focal adhesion dynamics (Prudent et al., 2016). We also observed defective migration in cells undergoing OGD. This is most likely attributed to the compromised energy production as the glycolytic process is less efficient in producing ATP in the absence of exogenous glucose supply. In addition, the reduced mitochondrial Ca^{2+} uptake resulting from MCUR1 downregulation is unable to sufficiently fuel oxidative phosphorylation to generate ATP. Interestingly, serum starvation rescued the defects in migration caused by OGD suggesting that serum starvation-induced autophagic flux rescued the migratory ability of the endothelial cells under OGD. Serum starvation induced autophagic degradation liberates amino acids and fatty acids that fuels the TCA cycle for energy production. The energy required for the endothelial migration is derived from the autophagic degradation and thereby rescues OGD induced impairment of endothelial migration. Further, restoration of MCUR1 expression by serum starvation could have rescued the mitochondrial Ca^{2+} uptake which inturn is essential for ATP production (Glitsch et al., 2002; Prudent et al., 2016).

Overall, our study identified perturbation in expression of MCUR1, the positive regulator of mitochondrial calcium uniporter in OGD conditions, resulting in the activation of pro-survival autophagy. While the autophagic flux that normally occurs during OGD conditions are insufficient to confer protection against apoptotic cell death, serum starvation induces autophagy and multiple pathways to offer protection and restore endothelial function.

CONCLUSION

In conclusion, our study has demonstrated the downregulation of mitochondrial calcium uniporter component MCUR1, leading to activation of both autophagic flux and OGD induced endothelial cell death. Careful analysis showed that the induced autophagic flux due to MCUR1 loss was insufficient to offer protection and required additional activators of autophagy to protect from cell death and rescue endothelial function (**Figure 6**). Serum starvation, a potent physiological activator of autophagy enhanced the autophagic flux, reversed the loss of MCUR1, and rescued endothelial function despite the presence of OGD stress. Our study suggests that targeting the mitochondrial calcium uniporter components in ischemic vascular diseases does not confer sufficient protection against endothelial dysfunction.

DATA AVAILABILITY STATEMENT

All datasets generated for this study are included in the article/**Supplementary Material**.

AUTHOR CONTRIBUTIONS

TM, VN, and KM participated in the design of the study. TM, VN, CP, RC, and KM conducted the experiments. AR, TV, and KM contributed with reagents or analytical tools. CP and ST prepared reagents for the study. TM, VN, CP, and KM performed the data analysis. AR performed the statistical analysis. TM, VN, and KM wrote the manuscript. All authors discussed and reviewed the manuscript.

FUNDING

This work was supported by funding from Ministry of Education (MOE) Tier 1, MOE Tier 2 (MOE2016-T2-2-105), from National Medical Research Council (NMRC) NIG (NMRC/BNIG/2042/2015), YIRG (OFYIRG15nov079), and start-up funds from NUS Yong Loo Lin School of Medicine to KM.

ACKNOWLEDGMENTS

The authors would like to express their special thanks to Prof. Shen Han Ming, Prof. Lim Kah Leong, and Prof. Brian Kennedy for their timely support with reagents and advice for the study.

SUPPLEMENTARY MATERIAL

The Supplementary Material for this article can be found online at: https://www.frontiersin.org/articles/10.3389/fphys.2020.533683/full#supplementary-material

REFERENCES

Baughman, J. M., Perocchi, F., Girgis, H. S., Plovanich, M., Belcher-Timme, C. A., Sancak, Y., et al. (2011). Integrative genomics identifies MCU as an essential component of the mitochondrial calcium uniporter. *Nature* 476, 341–345. doi: 10.1038/nature10234

Bernardi, P. (1999). Mitochondrial transport of cations: channels, exchangers, and permeability transition. *Physiol. Rev.* 79, 1127–1155. doi: 10.1152/physrev.1999.79.4.1127

Borger, D. R., Gavrilescu, L. C., Bucur, M. C., Ivan, M., and Decaprio, J. A. (2008). AMP-activated protein kinase is essential for survival in chronic hypoxia. *Biochem. Biophys. Res. Commun.* 370, 230–234. doi: 10.1016/j.bbrc.2008.03.056

Cardenas, C., Miller, R. A., Smith, I., Bui, T., Molgo, J., Muller, M., et al. (2010). Essential regulation of cell bioenergetics by constitutive InsP3 receptor Ca2+ transfer to mitochondria. *Cell* 142, 270–283. doi: 10.1016/j.cell.2010.06.007

Chaudhuri, D., Sancak, Y., Mootha, V. K., and Clapham, D. E. (2013). MCU encodes the pore conducting mitochondrial calcium currents. *eLife* 2:e00704.

Choy, J. C., Granville, D. J., Hunt, D. W., and McManus, B. M. (2001). Endothelial cell apoptosis: biochemical characteristics and potential implications for atherosclerosis. *J. Mol. Cell Cardiol.* 33, 1673–1690. doi: 10.1006/jmcc.2001.1419

De Stefani, D., Raffaello, A., Teardo, E., Szabo, I., and Rizzuto, R. (2011). A forty-kilodalton protein of the inner membrane is the mitochondrial calcium uniporter. *Nature* 476, 336–340. doi: 10.1038/nature10230

Dedkova, E. N., and Blatter, L. A. (2005). Modulation of mitochondrial Ca2+ by nitric oxide in cultured bovine vascular endothelial cells. *Am. J. Physiol. Cell Physiol.* 289, C836–C845.

Deedwania, P. C. (2003). Mechanisms of endothelial dysfunction in the metabolic syndrome. *Curr. Diab. Rep.* 3, 289–292. doi: 10.1007/s11892-003-0019-8

Diebold, L. P., Gil, H. J., Gao, P., Martinez, C. A., Weinberg, S. E., and Chandel, N. S. (2019). Mitochondrial complex III is necessary for endothelial cell proliferation during angiogenesis. *Nat. Metab.* 1, 158–171. doi: 10.1038/s42255-018-0011-x

Duchen, M. R. (2000). Mitochondria and calcium: from cell signalling to cell death. *J. Physiol.* 529(Pt. 1), 57–68. doi: 10.1111/j.1469-7793.2000.00057.x

Glitsch, M. D., Bakowski, D., and Parekh, A. B. (2002). Store-operated Ca2+ entry depends on mitochondrial Ca2+ uptake. *EMBO J.* 21, 6744–6754. doi: 10.1093/emboj/cdf675

Groschner, L. N., Waldeck-Weiermair, M., Malli, R., and Graier, W. F. (2012). Endothelial mitochondria–less respiration, more integration. *Pflugers Arch.* 464, 63–76. doi: 10.1007/s00424-012-1085-z

Gutierrez, E., Flammer, A. J., Lerman, L. O., Elizaga, J., Lerman, A., and Fernandez-Aviles, F. (2013). Endothelial dysfunction over the course of coronary artery disease. *Eur. Heart J.* 34, 3175–3181. doi: 10.1093/eurheartj/eht351

Herzig, S., and Shaw, R. J. (2018). AMPK: guardian of metabolism and mitochondrial homeostasis. *Nat. Rev. Mol. Cell Biol.* 19, 121–135. doi: 10.1038/nrm.2017.95

Kim, J., Yang, G., Kim, Y., Kim, J., and Ha, J. (2016). AMPK activators: mechanisms of action and physiological activities. *Exp. Mol. Med.* 48:e224. doi: 10.1038/emm.2016.16

Kirichok, Y., Krapivinsky, G., and Clapham, D. E. (2004). The mitochondrial calcium uniporter is a highly selective ion channel. *Nature* 427, 360–364. doi: 10.1038/nature02246

Kuma, A., Hatano, M., Matsui, M., Yamamoto, A., Nakaya, H., Yoshimori, T., et al. (2004). The role of autophagy during the early neonatal starvation period. *Nature* 432, 1032–1036. doi: 10.1038/nature03029

Langendorf, C. G., Ngoei, K. R., Scott, J. W., Ling, N. X., Issa, S. M., Gorman, M. A., et al. (2016). Structural basis of allosteric and synergistic activation of AMPK by furan-2-phosphonic derivative C2 binding. *Nat. Commun.* 7:10912.

Logan, C. V., Szabadkai, G., Sharpe, J. A., Parry, D. A., Torelli, S., Childs, A. M., et al. (2014). Loss-of-function mutations in MICU1 cause a brain and muscle disorder linked to primary alterations in mitochondrial calcium signaling. *Nat. Genet.* 46, 188–193. doi: 10.1038/ng.2851

Lum, J. J., Bauer, D. E., Kong, M., Harris, M. H., Li, C., Lindsten, T., et al. (2005). Growth factor regulation of autophagy and cell survival in the absence of apoptosis. *Cell* 120, 237–248. doi: 10.1016/j.cell.2004.11.046

Madamanchi, N. R., and Runge, M. S. (2007). Mitochondrial dysfunction in atherosclerosis. *Circ. Res.* 100, 460–473. doi: 10.1161/01.res.0000258450.44413.96

Mallilankaraman, K., Cardenas, C., Doonan, P. J., Chandramoorthy, H. C., Irrinki, K. M., Golenar, T., et al. (2012a). MCUR1 is an essential component of mitochondrial Ca2+ uptake that regulates cellular metabolism. *Nat. Cell Biol.* 14, 1336–1343. doi: 10.1038/ncb2622

Mallilankaraman, K., Doonan, P., Cardenas, C., Chandramoorthy, H. C., Muller, M., Miller, R., et al. (2012b). MICU1 is an essential gatekeeper for MCU-mediated mitochondrial Ca(2+) uptake that regulates cell survival. *Cell* 151, 630–644. doi: 10.1016/j.cell.2012.10.011

Mauthe, M., Orhon, I., Rocchi, C., Zhou, X., Luhr, M., Hijlkema, K. J., et al. (2018). Chloroquine inhibits autophagic flux by decreasing autophagosome-lysosome fusion. *Autophagy* 14, 1435–1455. doi: 10.1080/15548627.2018.1474314

Meng, S., Cao, J., He, Q., Xiong, L., Chang, E., Radovick, S., et al. (2015). Metformin activates AMP-activated protein kinase by promoting formation of the αβγ heterotrimeric complex. *J. Biol. Chem.* 290, 3793–3802. doi: 10.1074/jbc.m114.604421

Michaelis, U. R. (2014). Mechanisms of endothelial cell migration. *Cell Mol. Life. Sci.* 71, 4131–4148. doi: 10.1007/s00018-014-1678-0

Mizushima, N. (2007). The role of mammalian autophagy in protein metabolism. *Proc. Jpn. Acad. Ser. B Phys. Biol. Sci.* 83, 39–46. doi: 10.2183/pjab.83.39

Mizushima, N., and Klionsky, D. J. (2007). Protein turnover via autophagy: implications for metabolism. *Annu. Rev. Nutr.* 27, 19–40. doi: 10.1146/annurev.nutr.27.061406.093749

Mizushima, N., Yoshimori, T., and Levine, B. (2010). Methods in mammalian autophagy research. *Cell* 140, 313–326. doi: 10.1016/j.cell.2010.01.028

Murphy, M. P. (2009). How mitochondria produce reactive oxygen species. *Biochem. J.* 417, 1–13. doi: 10.1042/bj20081386

Natarajan, V., Chawla, R., Mah, T., Vivekanandan, R., Tan, S. Y., Sato, P. Y., et al. (2020). Mitochondrial dysfunction in age-related metabolic disorders. *Proteomics* 20:e1800404.

Park, K. H., and Park, W. J. (2015). Endothelial dysfunction: clinical implications in cardiovascular disease and therapeutic approaches. *J. Korean Med. Sci.* 30, 1213–1225. doi: 10.3346/jkms.2015.30.9.1213

Patron, M., Granatiero, V., Espino, J., Rizzuto, R., and De Stefani, D. (2019). MICU3 is a tissue-specific enhancer of mitochondrial calcium uptake. *Cell Death. Differ.* 26, 179–195. doi: 10.1038/s41418-018-0113-8

Payne, R., Hoff, H., Roskowski, A., and Foskett, J. K. (2017). MICU2 restricts spatial crosstalk between InsP3R and MCU channels by regulating threshold and gain of MICU1-mediated inhibition and activation of MCU. *Cell Rep.* 21, 3141–3154. doi: 10.1016/j.celrep.2017.11.064

Payne, R., Li, C., and Foskett, J. K. (2020). Variable assembly of EMRE and MCU Creates functional channels with distinct gatekeeping profiles. *Science* 23:101037. doi: 10.1016/j.isci.2020.101037

Paz, M. V., Cotan, D., Maraver, J. G., Oropesa-Avila, M., de la Mata, M., Pavon, A. D., et al. (2016). Erratum to: AMPK regulation of cell growth, apoptosis, autophagy, and bioenergetics. *Exp. Suppl.* 107:E1.

Perocchi, F., Gohil, V. M., Girgis, H. S., Bao, X. R., McCombs, J. E., Palmer, A. E., et al. (2010). MICU1 encodes a mitochondrial EF hand protein required for Ca(2+) uptake. *Nature* 467, 291–296. doi: 10.1038/nature09358

Plesnila, N., Zinkel, S., Le, D. A., Amin-Hanjani, S., Wu, Y., Qiu, J., et al. (2001). BID mediates neuronal cell death after oxygen/ glucose deprivation and focal cerebral ischemia. *Proc. Natl. Acad. Sci. U.S.A.* 98, 15318–15323. doi: 10.1073/pnas.261323298

Prudent, J., Popgeorgiev, N., Gadet, R., Deygas, M., Rimokh, R., and Gillet, G. (2016). Mitochondrial Ca(2+) uptake controls actin cytoskeleton dynamics during cell migration. *Sci. Rep.* 6:36570.

Quijano, C., Trujillo, M., Castro, L., and Trostchansky, A. (2016). Interplay between oxidant species and energy metabolism. *Redox Biol.* 8, 28–42. doi: 10.1016/j.redox.2015.11.010

Quintero, M., Colombo, S. L., Godfrey, A., and Moncada, S. (2006). Mitochondria as signaling organelles in the vascular endothelium. *Proc. Natl. Acad. Sci. U.S.A.* 103, 5379–5384. doi: 10.1073/pnas.0601026103

Raffaello, A., De Stefani, D., Sabbadin, D., Teardo, E., Merli, G., Picard, A., et al. (2013). The mitochondrial calcium uniporter is a multimer that can include a dominant-negative pore-forming subunit. *EMBO J.* 32, 2362–2376. doi: 10.1038/emboj.2013.157

Ramamurthy, S., and Ronnett, G. V. (2006). Developing a head for energy sensing: AMP-activated protein kinase as a multifunctional metabolic sensor in the brain. *J. Physiol.* 574, 85–93. doi: 10.1113/jphysiol.2006.110122

Sancak, Y., Markhard, A. L., Kitami, T., Kovacs-Bogdan, E., Kamer, K. J., Udeshi, N. D., et al. (2013). EMRE is an essential component of the mitochondrial calcium uniporter complex. *Science* 342, 1379–1382. doi: 10.1126/science.1242993

Tamargo-Gomez, I., and Marino, G. (2018). AMPK: regulation of metabolic dynamics in the context of autophagy. *Int. J. Mol. Sci.* 19, 1–16.

Tang, X., Luo, Y. X., Chen, H. Z., and Liu, D. P. (2014). Mitochondria, endothelial cell function, and vascular diseases. *Front. Physiol.* 5:175. doi: 10.3389/fphys.2014.00175

Tarasov, A. I., Griffiths, E. J., and Rutter, G. A. (2012). Regulation of ATP production by mitochondrial Ca(2+). *Cell Calcium* 52, 28–35. doi: 10.1016/j.ceca.2012.03.003

Vais, H., Mallilankaraman, K., Mak, D. D., Hoff, H., Payne, R., Tanis, J. E., et al. (2016). EMRE is a matrix Ca(2+) sensor that governs gatekeeping of the mitochondrial Ca(2+) uniporter. *Cell Rep.* 14, 403–410. doi: 10.1016/j.celrep.2015.12.054

Vais, H., Tanis, J. E., Muller, M., Payne, R., Mallilankaraman, K., and Foskett, J. K. (2015). MCUR1 CCDC90A, is a regulator of the mitochondrial calcium uniporter. *Cell Metab.* 22, 533–535. doi: 10.1016/j.cmet.2015.09.015

Vatrinet, R., Leone, G., De Luise, M., Girolimetti, G., Vidone, M., Gasparre, G., et al. (2017). The alpha-ketoglutarate dehydrogenase complex in cancer metabolic plasticity. *Cancer Metab.* 5:3.

Williams, G. S., Boyman, L., Chikando, A. C., Khairallah, R. J., and Lederer, W. J. (2013). Mitochondrial calcium uptake. *Proc. Natl. Acad. Sci. U.S.A.* 110, 10479–10486.

Wilson, C., Lee, M. D., Heathcote, H. R., Zhang, X., Buckley, C., Girkin, J. M., et al. (2019). Mitochondrial ATP production provides long-range control of endothelial inositol trisphosphate-evoked calcium signaling. *J. Biol. Chem.* 294, 737–758. doi: 10.1074/jbc.ra118.005913

Xu, J., He, L., Ahmed, S. H., Chen, S. W., Goldberg, M. P., Beckman, J. S., et al. (2000). Oxygen-glucose deprivation induces inducible nitric oxide synthase and nitrotyrosine expression in cerebral endothelial cells. *Stroke* 31, 1744–1751. doi: 10.1161/01.str.31.7.1744

Yang, Z., Huang, C., Wu, Y., Chen, B., Zhang, W., and Zhang, J. (2019). Autophagy protects the blood-brain barrier through regulating the dynamic of Claudin-5 in short-term starvation. *Front. Physiol.* 10:2. doi: 10.3389/fphys.2019.00002

Conflict of Interest: The authors declare that the research was conducted in the absence of any commercial or financial relationships that could be construed as a potential conflict of interest.

frontiers in Physiology

REVIEW
published: 22 October 2020
doi: 10.3389/fphys.2020.511391

Imaging Atherosclerosis by PET, With Emphasis on the Role of FDG and NaF as Potential Biomarkers for This Disorder

Michael Mayer[1†], Austin J. Borja[1,2†], Emily C. Hancin[1,3], Thomas Auslander[1], Mona-Elisabeth Revheim[1,4,5], Mateen C. Moghbel[6], Thomas J. Werner[1], Abass Alavi[1] and Chamith S. Rajapakse[1,7]*

[1] Department of Radiology, Hospital of the University of Pennsylvania, Philadelphia, PA, United States, [2] Perelman School of Medicine at the University of Pennsylvania, Philadelphia, PA, United States, [3] Lewis Katz School of Medicine at Temple University, Philadelphia, PA, United States, [4] Division of Radiology and Nuclear Medicine, Oslo University Hospital, Oslo, Norway, [5] Institute of Clinical Medicine, Faculty of Medicine, University of Oslo, Oslo, Norway, [6] Department of Radiology, Massachusetts General Hospital, Boston, MA, United States, [7] Department of Orthopaedic Surgery, Hospital of the University of Pennsylvania, Philadelphia, PA, United States

OPEN ACCESS

Edited by:
Silvia Lacchini,
University of São Paulo, Brazil

Reviewed by:
Robert Feil,
University of Tübingen, Germany
David Newby,
University of Edinburgh,
United Kingdom

***Correspondence:**
Chamith S. Rajapakse
chamith@pennmedicine.upenn.edu;
chamith@mail.med.upenn.edu

[†] These authors have contributed equally to this work and share first authorship

Specialty section:
This article was submitted to Vascular Physiology, a section of the journal Frontiers in Physiology

Received: 11 November 2019
Accepted: 08 September 2020
Published: 22 October 2020

Citation:
Mayer M, Borja AJ, Hancin EC, Auslander T, Revheim M-E, Moghbel MC, Werner TJ, Alavi A and Rajapakse CS (2020) Imaging Atherosclerosis by PET, With Emphasis on the Role of FDG and NaF as Potential Biomarkers for This Disorder. Front. Physiol. 11:511391. doi: 10.3389/fphys.2020.511391

Molecular imaging has emerged in the past few decades as a novel means to investigate atherosclerosis. From a pathophysiological perspective, atherosclerosis is characterized by microscopic inflammation and microcalcification that precede the characteristic plaque buildup in arterial walls detected by traditional assessment methods, including anatomic imaging modalities. These processes of inflammation and microcalcification are, therefore, prime targets for molecular detection of atherosclerotic disease burden. Imaging with positron emission tomography/computed tomography (PET/CT) using 18F-fluorodeoxyglucose (FDG) and 18F-sodium fluoride (NaF) can non-invasively assess arterial inflammation and microcalcification, respectively. FDG uptake reflects glucose metabolism, which is particularly increased in atherosclerotic plaques retaining macrophages and undergoing hypoxic stress. By contrast, NaF uptake reflects the exchange of hydroxyl groups of hydroxyapatite crystals for fluoride producing fluorapatite, a key biochemical step in calcification of atherosclerotic plaque. Here we review the existing literature on FDG and NaF imaging and their respective values in investigating the progression of atherosclerotic disease. Based on the large volume of data that have been introduced to the literature and discussed in this review, it is clear that PET imaging will have a major role to play in assessing atherosclerosis in the major and coronary arteries. However, it is difficult to draw definitive conclusions on the potential role of FDG in investigating atherosclerosis given the vast number of studies with different designs, image acquisition methods, analyses, and interpretations. Our experience in this domain of research has suggested that NaF may be the tool of choice over FDG in assessing atherosclerosis, especially in the setting of coronary artery disease (CAD). Specifically, global NaF assessment appears to be superior in detecting plaques in tissues with high background FDG activity, such as the coronary arteries.

Keywords: atherosclerosis, molecular imaging, PET, fluorodeoxyglucose, sodium fluoride

INTRODUCTION

Atherosclerosis is a vascular disease characterized by the formation of plaques and their eventual rupture. The endothelial layer plays a crucial role in the atherosclerotic process. Indeed, endothelial cell dysfunction (ECD) is pivotal in the onset and progression of the events that cause atherosclerosis (Gimbrone and Garcia-Cardena, 2016). ECD occurs via a sequence of signaling events that are part of a complex inflammatory cascade and involves the recruitment of circulating monocytes from the blood into the vessel wall (intima), where they differentiate into macrophages and internalize oxidized low-density lipoproteins to become foam cells. Foam cells are key components of atherosclerotic plaque. Structural remodeling of dead foam cells occurs by their encapsulation by a thin fibrous cap, the rupture of which results in thrombosis and vessel occlusion.

Currently, atherosclerosis and the increasing burden of resulting cardiovascular events constitute a global epidemic (Hansson, 2005; Lozano et al., 2012). Atherosclerosis represents the number one cause of death and disability in the developed world. The characteristic build-up and rupture of arterial plaque is a direct precursor of most cardiovascular and cerebrovascular events, which result in 7.0 and 2.8 million deaths every year, respectively. The economic burden of atherosclerosis is enormous, with annual aggregate inpatient hospital costs of over 10 billion dollars.

The initiation, progression, and complications of atherosclerotic plaque follow slow and gradual sequential events that occur over a lifetime (Mallika et al., 2007; Weber and Noels, 2011). Currently, early identification of at-risk patients poses a challenge for the medical community given the limitations of traditionally utilized assessment tools, such as risk-stratification surveys and mainstay imaging. For example, the Framingham Risk Score quantifies the 10-year risk of developing atherosclerotic disease as a function of risk factors such as dyslipidemia, hypertension, and diabetes, but it offers no means to visualize or predict plaque development. Conventional imaging modalities such as CT and MRI angiography allow physicians to visualize changes that occur in the later stages of atherosclerosis, such as plaque morphology and stenosis, but provide no insight into early detection of plaque formation. Locating and preventing the rupture of "vulnerable" plaques is challenging, as the plaques that are most prone to acute rupture often do not cause clinical symptoms before they rupture (Falk, 1992; Shah, 2003).

Molecular imaging has emerged as an entirely novel means to image and study atherosclerosis very early in the course of disease progression. From a pathophysiological perspective, atherosclerosis is characterized by microscopic processes of inflammation and microcalcification that precede the characteristic plaque buildup in arterial walls detected by traditional assessment methods discussed above. Moreover, the fibrous cap that lies on a lipid-rich necrotic core of oxidized lipoproteins, cholesterol crystals, and cellular debris also comprises calcified deposits. These processes of inflammation and microcalcification are, therefore, prime targets for molecular detection of cardiovascular disease risk.

The two most widely used and studied tracers to detect and characterize atherosclerosis are 18F-sodium fluoride (NaF) and 18F-fluorodeoxyglucose (FDG), which can non-invasively assess microcalcification and arterial inflammation, respectively (**Table 1**). NaF uptake reflects the exchange of hydroxyl groups of hydroxyapatite crystals for fluoride producing fluorapatite, a key biochemical step in the calcification of atherosclerotic plaque. FDG, an analog of glucose, is used as a surrogate marker for glucose metabolism at the target tissues. FDG is taken up by the cells via transporters and phosphorylated by the hexokinase enzyme inside the cell as FDG-phosphate which cannot be metabolized further. FDG is of particular interest in detecting atherosclerosis due to high metabolic activity of macrophages that reside in plaques and are undergoing hypoxic stress. Furthermore, smooth muscle cells, which have recently been implicated as playing a role in atherogenesis, are highly glycolytic and contribute to visualizing plaques by FDG-PET/CT (Feil et al., 2014; Basatemur et al., 2019; Liu and Gomez, 2019).

There have been many reviews regarding the importance of FDG-PET/CT and NaF-PET/CT in the diagnosis of atherosclerosis in various settings. In this review, we discuss the role of these two radiotracers in identifying atherosclerotic plaques at the molecular level and before they lead to clinically detectable symptoms. In addition, we examine current published literature and compare the strengths and weaknesses of the existing techniques.

MOLECULAR IMAGING IN ATHEROSCLEROSIS

Early Attempts to Employ Molecular Imaging Techniques as Correlates to Risk Factors and Prognosis

A study by Yun et al. (2001) represented the first investigation of the association of FDG uptake with atherosclerotic disease. Of 132 patients undergoing whole-body scans, approximately half demonstrated increased FDG uptake in at least one major artery (the abdominal aorta, iliac artery, proximal femoral arteries in whole-body scans and the femoral and popliteal arteries on lower extremity scans), with an increased uptake prevalence in older populations (34% of patients aged 20–40 years, 50% of patients aged 41–60 years, and 61% of patients aged 61–80 years). This result has been replicated in numerous studies in expanded age ranges and in the assessment of additional vasculature. A study by Bural et al. (2008) evaluated FDG uptake in 149 subjects ranging in age from 5 to 83 years. FDG uptake was noted in the major arteries in 145 of the patients, and both prevalence and intensity of FDG uptake in the thoracic aorta, abdominal aorta, iliac arteries, and femoral arteries increased with age. A more recent study by Bural et al. (2016) confirmed this finding. They determined that, in the femoral arteries of 38 patients of varying ages, the uptake ratio of FDG to the adjacent background was significantly increased with age, which suggests that the inflammation associated with atherosclerotic plaques becomes more severe as patients age

TABLE 1 | Comparison of the utility and limitations between FDG and NaF-PET/CT.

Clinical utility		Limitations	
FDG	**NaF**	**FDG**	**NaF**
Inflammatory processes and infections	Osseous processes due to high bone-to-background ratio	Inaccurate target-to-background measurements in highly metabolic tissues (i.e., heart)	Partial volume effects in small volume bones or intimal plaques
Brain metabolism and MCI/AD	Atherosclerosis, especially in the coronary arteries	Delayed-timepoint imaging may be logistically difficult to achieve	Fewer clinical studies regarding its utility in atherosclerosis
Cancer and neoplasms			

(Bural et al., 2016). Additionally, Emamzadehfard and colleagues observed an increase FDG uptake in the descending aorta in older (aged 60–75) subjects, when compared to younger (aged 20–30) individuals, in both healthy adults and in those exhibiting cardiovascular risk factors (Emamzadehfard et al., 2017).

While age has been consistently correlated with FDG uptake, association with other conventional risk factors has been less consistent. A further study by Yun et al. (2002) evaluated the frequency of FDG uptake in three major arteries (the abdominal aorta, iliac arteries, and proximal femoral arteries) in 156 patients and its relation to atherogenic risk factors (age, cigarette smoking, hypertension, diabetes, elevated cholesterol, and obesity) and known CAD. Only age and high cholesterol consistently demonstrated a significant correlation with FDG uptake in all three arteries. Additionally, patients with known CAD showed increased FDG uptake in the proximal femoral arteries compared to healthy patients. A study by Strobl et al. (2013) investigated the correlation between FDG uptake in the thoracic aorta, abdominal aorta, common carotid arteries, and iliac arteries with conventional cardiovascular disease risk factors. Different vascular regions demonstrated different correlations. In the thoracic and abdominal aorta, FDG uptake was associated with age greater than 65 and male sex. In the carotid arteries, FDG uptake was associated with age greater than 65, male subjects, and BMI greater than 30. In the iliac arteries, FDG uptake was associated with age greater than 65. Pasha et al. (2015) investigated the correlation between FDG uptake in 76 patients in the aorta and in the peripheral arteries with conventional cardiovascular risk factors. As expected, increased FDG uptake was observed in the peripheral arteries and aorta with increasing age. Cardiovascular risk factors were associated with FDG uptake in the aorta, but not the peripheral arteries. The study by Emamzadehfard et al. (2017) also determined that, in addition to the descending aorta, increased mean FDG uptake was also observed in the aortic arch and ascending aorta in patients with cardiovascular risk factors.

Soon after the early reports appeared in the literature, investigators began exploring the potential role of FDG in detection and characterization of atherosclerosis in various settings. A study by Rudd et al. (2002) investigated FDG uptake in 8 patients who had recently experienced a carotid-territory transient ischemic attack and had severe internal carotid artery stenosis of at least 70 percent. FDG uptake was quantified in plaques in the affected carotid artery and in plaques in the contralateral asymptomatic side. This analysis showed that FDG accumulation was 27% higher in the symptomatic lesions in comparison to the contralateral asymptomatic plaques. Following imaging studies, plaque histology was determined on carotid endarterectomy samples from all 8 patients. Plaque autoradiography demonstrated FDG uptake in macrophage-rich areas of the plaques, notably at the lipid core and fibrous cap border of the lesions, suggesting a potential role for FDG-PET in the assessment of intimal inflammatory response in atherosclerosis.

A study by Paulmier et al. (2008) determined the rate of cardiovascular events in two groups of stable patients with either increased FDG uptake or unremarkable FDG uptake on PET/CT which was performed for cancer staging and follow-up. A calcium index score was calculated for each patient, and subjects from both groups were matched for age, conventional risk factors, and type of cancer. The rates of both remote cardiovascular events (defined as 6 months prior to PET/CT study) and recent cardiovascular events (defined as less than 6 months before or after the PET study) were tracked. In brief, the study revealed that calcium index was the single factor related to remote cardiovascular events, and the extent of FDG uptake was the single factor significantly related to the occurrence of a recent event.

A study by Rominger et al. (2009) evaluated the association of FDG uptake in large arteries of 932 asymptomatic cancer patients with the subsequent occurrence of a vascular event, defined as an ischemic stroke, myocardial infarction, or revascularization. In the 15 of 932 patients (1.6%) who experienced a vascular event, increased FDG uptake was the strongest predictor of said event, more so than conventional risk factors. A study by Marnane et al. (2012) investigated the relationship between FDG uptake and stroke recurrence in 60 patients with a recent stroke, transient ischemic attack, or retinal embolism with ipsilateral carotid plaque stenosis greater than 50%. In 13 of the 60 patients (22%) who suffered from another stroke within 90 days, the FDG uptake in the ipsilateral carotid artery was greater in than those who remained stable. Further analysis in a Cox regression model revealed plaque FDG uptake as one independent predictor of stroke recurrence over conventional risk factors such as age or degree of stenosis. A study by Figueroa et al. (2013) retrospectively identified 513 patients over the age of 30 without a prior history of cardiovascular disease or cancer who had undergone PET/CT. During a follow-up period (median 4.2 years), 44 patients developed cardiovascular disease. Three main findings were observed from the study. First, the degree of FDG uptake and cardiovascular disease incidence were significantly correlated. Second, the inclusion of

FDG uptake along with the Framingham Risk Score models of cardiovascular risk improved risk discrimination. Finally, increasing FDG uptake was inversely correlated with the timing of cardiovascular disease defining events.

More recent studies have continued to support the importance of FDG as a molecular indicator of adverse cardiovascular events. Kim et al. (2016) used a cohort of cancer patients to show that arterial FDG uptake, metabolically active malignancy, and the visceral adipose tissue seen on CT scans might have the capacity to predict future ischemic strokes. A study conducted by Iwatsuka et al. (2018) reviewed the medical records of 309 patients age 65 and older who did not have coronary artery disease but had previously undergone FDG-PET/CT imaging to determine the presence of cancer (all patients' scans were cancer-free). After a median follow-up period of 3.9 years, the authors noted that a high target to background ratio in the arteries was associated with a high likelihood of a coronary heart disease event. Similarly, Tuominen et al. (2019) examined the relationship between pathological FDG uptake and future cardiovascular events in patients who exhibited symptoms of cardiac sarcoidosis. They determined that both total cardiac metabolic activity, as well as right ventricular FDG uptake, were significantly associated with the occurrence of cardiovascular events during a mean follow-up period of 54.7 months following initial FDG-PET scans. Taken together, these recent data demonstrate that FDG-PET has the potential to identify patients who are at risk for cardiovascular events. The data published in the literature indicate that FDG-PET may change the landscape for early identification of patients at-risk for cardiovascular events and may contribute to the development of preventative measures to avoid vascular damage and improve patient outcomes.

Whereas FDG-PET imaging has been shown to be of value in detecting inflammatory processes in the arteries in several studies, NaF has emerged as a superior radiotracer for assessing and quantifying atherosclerosis in the aorta, carotids, and coronary arteries. Derlin et al. (2010) demonstrated in 2010 the feasibility of NaF-PET/CT for detecting vascular microcalcification. The authors performed visual and semi-quantitative methods to quantify NaF uptake. They observed vascular NaF uptake at 254 sites in 57 of the 75 subjects (76%) compared to vascular CT-based calcification at 1,930 sites in 63 patients (84%). Moreover, only 12% of subjects with arterial wall NaF uptake demonstrated corresponding CT calcification, suggesting the high sensitivity of this imaging modality. The same group (Derlin et al., 2011) was able to reproduce their original observation and also demonstrated that common carotid artery NaF uptake is significantly associated with age, male gender, hypertension, and hypercholesterolemia. Morbelli et al. (2014) reached similar conclusions by observing that large vessel NaF uptake in 80 patients with either breast or prostate malignancies (age 65.3 $\pm$ 8.2, 20 males) was correlated with Framingham Risk Score and several cardiovascular risk factors including gender, hypertension, smoking, diabetes, and age. Additionally, visible structural changes due to calcified atherosclerosis were not correlated with increased NaF uptake, suggesting that NaF as a molecular calcification marker provides certain specific inflammation about the process.

Blomberg et al. (2017a) demonstrated that thoracic aorta microcalcifications as quantified by NaF-PET/CT revealed a significantly increased risk for cardiovascular disease. This prospective project known as CAMONA determined the role of FDG and NaF imaging in detecting atherosclerosis in 139 subjects, which included healthy controls and individuals at increased risk for fatal cardiovascular disease estimated by the Systematic Coronary Risk Evaluation tool (using gender, age, smoking, systolic blood pressure, and total cholesterol). There was no correlation between FDG uptake and cardiovascular disease risk. The same group also demonstrated that NaF uptake within the coronary arteries is similarly associated with cardiovascular disease risk (Blomberg et al., 2017b). Further analysis of the CAMONA dataset by Arani et al. (2018) and Castro et al. (2017) found a correlation between NaF uptake in the abdominal aorta and common carotid arteries and cardiovascular risk and age. A similar correlation was not found for FDG. Because the carotid arteries are the primary source of blood flow to the brain, NaF-PET/CT may play a major role in detecting atherosclerosis in the vasculature and therefore in the management of patients with cognitive impairment (Borja et al., 2020).

Several recently published studies have demonstrated convincing results by employing NaF as a tracer for detecting molecular calcification, which is indicative of its expanding clinical applications. For example, NaF showed utility in measuring both plaque size and calcification in the arterial beds of transgenic Yucutan minipigs (Nogales et al., 2019). Nogales et al. noted that NaF-PET/CT can reliably detect microcalcifications in the vessels, particularly those in the abdominal aorta, in these animals, suggesting that this methodology can be used to assess plaque burden in entire body. Similarly, Hayrapetian et al. (2019) investigated the utility of NaF-PET in monitoring coronary artery calcifications that are potentially at risk for rupture. They found that NaF uptake can be used as a predictive indicator of the progression of coronary artery atherosclerosis, as well as the degree of coronary stenosis.

Molecular and Conventional Diagnostic Imaging Modalities

Calcification is a highly specific feature of coronary atherosclerosis. As such, the coronary artery calcium (CAC) score has been widely used as a diagnostic tool for assessing cardiovascular disease risk. However, despite the established association between FDG uptake and conventional cardiovascular risk factors, the relationship between FDG and arterial calcification detected on CT has consistently failed to show any significant correlation. A study by Tatsumi et al. (2003) investigated the relationship between FDG uptake as detected on PET/CT with aortic wall calcification. In a cohort of 85 cancer patients who underwent FDG PET/CT, sites of FDG uptake in the thoracic aortic wall were almost entirely distinct from sites of thoracic aortic wall calcification. FDG uptake was higher in patients older than 65, in those with hyperlipidemia, and in subjects with a prior history of cardiovascular disease.

A study by Ben-Haim et al. (2004) assessed the distribution of both vascular FDG uptake and CT calcifications using PET/CT in 122 patients. A total of 349 vascular sites were identified as abnormal by demonstrating increased FDG uptake, calcification, or both. CT calcification and increased FDG uptake both demonstrated a positive correlation with cardiovascular risk factors and age. CT calcifications were found in 92% of sites and increased FDG uptake was found in 15% of sites, although concomitantly increased FDG uptake and CT calcification was noted in only 7% of sites. Comparable results were described in similarly designed studies by Dunphy et al. (2005), who observed the colocalization between increased FDG uptake and calcification in less than 2% of cases, and by Derlin et al. (2010), who found colocalization in only 12% of cases. A study by Meirelles et al. (2011) examined FDG-PET/CT scans of 100 cancer patients who had undergone at least two PET/CT studies and in whom sites of aortic FDG uptake and calcification were identified. These two image sets (baseline and repeat scans) demonstrated FDG uptake in 70% of the initial scans, which changed in 55% on the second scan. Furthermore, calcification and FDG uptake only overlapped in two cases.

An important study was initiated by Abdelbaky et al. (2013) to demonstrate the relationship between FDG uptake and arterial calcium deposition. They retrospectively identified 137 patients from a single hospital database who had undergone serial PET/CT scans 1–5 years apart. Based on this research, focal FDG uptake was found to be the strongest predictor of future arterial calcification within the same locations after adjusting for risk factors. In other words, localized FDG uptake preceded subsequent calcification over the years. A similar study by Cho et al. (2017) followed 96 patients over 1 year and demonstrated that FDG uptake in the aorta predicted the progression of coronary artery calcification. Enhanced FDG uptake was associated with coronary artery calcification progression in patients without any baseline coronary artery calcification but was not seen in patients with baseline coronary artery calcification.

Based on the data that have been published in the literature, it is clear that sites of CT calcification consistently demonstrate no or very minimal uptake of FDG. This indicates that by the time CT calcification is noted, inflammation is no longer an active component of atherosclerotic plaques (McKenney-Drake et al., 2018; Moghbel et al., 2018). The degree of uptake of NaF in the calcified lesions on CT varies considerably (Blomberg et al., 2014b; **Figure 1**). While some lesions show no uptake, others reveal varying degrees of active molecular calcification (Blomberg et al., 2015b, 2017a,b). These observations indicate that atherosclerotic plaques may be classified as active or inactive based on NaF-PET findings, suggesting the potential clinical utility of NaF uptake in the assessment of atherosclerotic disease burden. Additionally, NaF-PET imaging may be used for the early detection and characterization of patients with atherosclerosis (George, 2012; McKenney-Drake et al., 2018). Animal research studies from our group have validated the reliability of global NaF assessment techniques for early evidence of coronary artery calcification (McKenney-Drake et al., 2018). We have also applied this approach in human studies and have shown significant correlation between NaF uptake and cardiovascular risk factors (Blomberg et al., 2017b; **Figure 2**). Therefore, we believe NaF-PET will continue to play a major role in assessing atherosclerosis in the major and coronary arteries in the future.

Investigations Into Plaque Morphology, Histology, and Pharmacotherapy

The early stages of atherosclerosis are characterized by increased endothelial permeability resulting in the buildup of LDL in the arterial intima (van der Wal and Becker, 1999). The exact mechanisms are not completely understood, but subsequent activation of endothelial cells and smooth muscle cells release chemo-attractants, mobilizing monocytes. Monocytes differentiate into macrophages that engulf LDL, transforming into cholesterol-laden apoptotic foam cells, which induce a self-sustaining inflammatory response.

The hallmark of atherosclerosis is plaque formation. "Stable" plaques are unlikely to rupture and are characterized by a thick fibrous cap, a small lipid pool, few inflammatory cells, and a dense extracellular matrix. The continuous cycle of arterial damage and repair in atherosclerosis results in the formation of "vulnerable" plaques (Spacek et al., 2018). In contrast to stable plaques, they are characterized by a thin fibrous cap, a large lipid pool, many inflammatory cells, and few smooth muscle cells. Vulnerable plaques are at an increased risk of rupture. In response, calcification is thought to stabilize vulnerable plaque and reduce the risk of rupture. Initially, apoptotic foam cells are phagocytized by adjacent arterial smooth muscle cells. However, at a certain threshold, apoptotic cells are too numerous to be cleared, giving rise to a necrotic core (Gonzalez and Trigatti, 2017). Vesicles in the necrotic core serve as nucleation sites for microcalcification, which accumulate to form calcifications large enough to be visualized by CT.

The identification of which plaques are "vulnerable" remains a highly desirable goal since the subsequent formation of a thrombus predisposes patients to cardiovascular and cerebrovascular events such as myocardial infarction and stroke. As a marker of inflammation, FDG represents a key component of the atherosclerotic disease process. It is relatively well established that FDG uptake in the setting of atherosclerosis is related to the inflammatory process of the activated macrophages within plaques.

A study by Tawakol et al. (2006) examined 17 patients with severe carotid artery stenosis who underwent PET/CT prior to endarterectomy. Following surgery, immunohistochemistry was performed on the excised plaque extracts. The study specifically examined the association of FDG uptake with CD68 level, serving as a measure of macrophage content, and demonstrated a strong correlation between these two variables. A similar study by Myers et al. (2012) resulted in significantly different results. The study investigated the correlation between FDG uptake in the aorta, carotid arteries, and femoral arteries in 30 patients who underwent an atherectomy procedure for symptomatic common or superficial femoral arterial disease. After the procedure, immunohistochemistry was performed on the excised plaque extracts to quantify CD68 uptake, once again serving as a measure

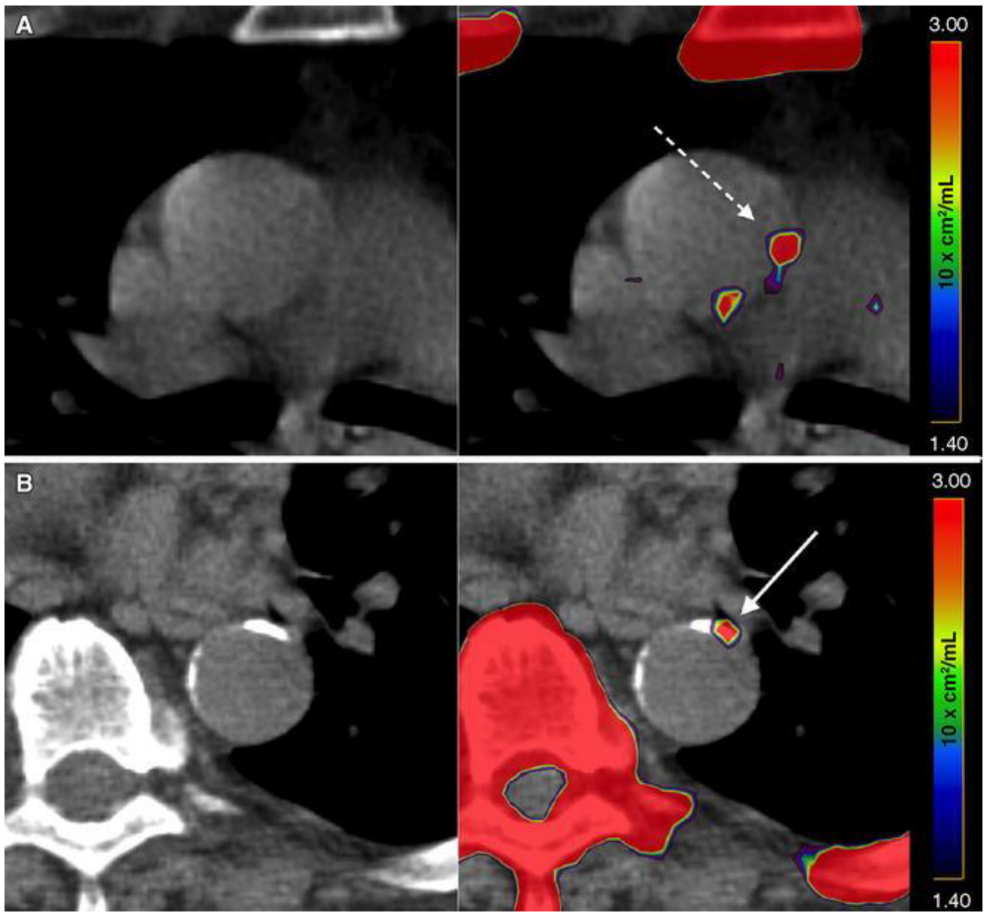

FIGURE 1 | Active and indolent molecular vascular calcification. **(A)** Patient without structural vascular calcification. A positive NaF PET signal, representing molecular vascular calcification, was observed in the ascending aorta (interrupted arrow). **(B)** Patient with active (arrow) and indolent vascular calcification in the descending aorta. Note the intense uptake of NaF in the sternum, vertebra, and ribs (Reproduced from Blomberg et al. (Castro et al., 2017) with permission).

of macrophage content. In 34 plaque specimens obtained, no correlation was noted between FDG uptake and CD68 level. Finally, a study by Figueroa et al. (2012) designed a similar study but used investigators blinded to the clinical, PET, and histological data to characterize plaque morphology as a risk factor in 34 patients scheduled for endarterectomy, 10 of whom had plaque histologically assessed for CD68 staining. Both FDG uptake and CD68 staining were higher in vascular segments that contained plaque and in plaques characterized as possessing high-risk morphology.

A more recent study by van der Valk et al. (2016) investigated the relationship between FDG uptake and atherogenic lipoprotein(a), a proinflammatory oxidized phospholipid transporter associated with accelerated arterial inflammation. In 30 subjects with elevated lipoprotein(a) levels, FDG uptake was significantly elevated compared to 30 control subjects with normal lipoprotein(a) levels.

Other studies have taken advantage of animal models to investigate the biological characteristics of atherosclerotic plaques. Ogawa et al. (2004) studied FDG uptake in an animal model of atherosclerosis, Watanabe heritable hyperlipidemic (WHHL) rabbits. Eleven WHHL and 3 control rabbits were injected with FDG and imaged with PET/CT, followed by the removal of both the thoracic and abdominal aortas 4 h later. Histologic analysis was performed to quantify macrophage content. In the control rabbits, the aortas were devoid of plaque and no macrophages were seen on histological examination. In the WHHL rabbits, a thick intima representing plaque content as well as significant macrophage content were observed. FDG uptake in the WHHL rabbits was strongly correlated with atherosclerotic lesions and macrophage content. Of note, FDG may have the potential to be used in drug development studies. As indicated by Plana et al. (2018), FDG-PET imaging can identify patients at risk for doxorubicin-mediated cardiotoxicity following chemotherapy treatments, though this has only been determined in mice models and has not yet been widely clinically tested.

Joshi et al. (2014) compared coronary NaF uptake in areas of culprit and non-culprit plaques in 40 patients with myocardial infarction and compared NaF uptake to intravascular ultrasound examination in 40 patients with stable angina. In patients with myocardial infarction, culprit plaques and sites

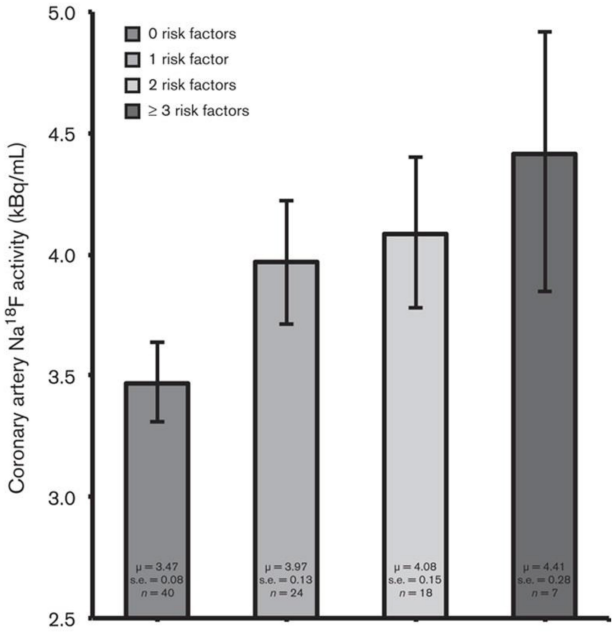

FIGURE 2 | NaF uptake in relation to cardiovascular risk factors. Bar graph showing coronary artery NaF uptake (kBq/ml), adjusted for blood NaF activity, injected NaF dose, and PET/CT technology, in relation to the number of cardiovascular risk factors (i.e., BMI, systolic blood pressure, serum triglyceride concentration, and serum low-density lipoprotein-cholesterol concentration) present. Coronary NaF uptake increased linearly according to the number of risk factors present ($P < 0.001$ for a linear trend). Coronary NaF uptake was significantly lower in the absence of risk factors compared with the presence of one or more risk factors (3.47 vs. 3.97, 4.08, and 4.41 kBq/ml, respectively; $P < 0.001$). Error bars represent the 95% confidence interval of the mean (Reproduced from Blomberg et al. (Figueroa et al., 2013) with permission).

of atherosclerotic plaque ruptures demonstrated high focal NaF uptake. Moreover, histological examinations of focal regions of uptake showed active calcification and necrotic changes. On the other hand, patients with stable angina who demonstrated high NaF uptake also demonstrated high-risk characteristics on ultrasound, including vascular remodeling and calcification. A more recent study by Kim et al. (2019) performed FDG- and NaF-PET/CT imaging in 20 stroke patients with culprit and non-culprit carotid plaques. High radiotracer uptake was present in both groups, and the target-to-blood ratio demonstrated a significant increase in uptake in culprit atheromas. Vesey et al. (2017) used both FDG and NaF-PET/CT to determine the superior modality in identifying carotid plaques in 26 patients with recent ischemic strokes. They determined that, while both NaF and FDG uptake were significantly associated with predicted cardiovascular risk, only NaF was significantly correlated with plaque burden and associated plaque characteristics. Vesey et al. also used histologic and micro PET/CT to confirm the potential for NaF to be used as a tracer in the identification of microcalcifications. Similarly, Irkle et al. (2015) used sequential staining of carotid artery plaques to identify the specificity of binding of NaF to regions of carotid artery plaques. Using Alizarin Red, a calcification marker, along with macrophage and endothelial cell neovascularization markers, they determined that the NaF radioactivity signal was only significantly associated with the Alizarin Red stain, which is reflective of the ability of NaF to identify calcifications in the carotid artery and not the presence of infection or other related cellular processes. Taken together, these recent data suggest that NaF is a powerful indicator of the presence of microcalcifications, which may potentiate its role in the surveillance of plaque development in the vasculature.

A study by Beheshti et al. (2011) examined NaF-PET/CT images in 51 to determine cardiac and aortic uptake. The authors correlated NaF uptake to age, suggesting the potential for NaF in the assessment of atherosclerosis. Additionally, this study was the first to utilize global disease assessment with NaF-PET. Global disease assessment was first described by Alavi et al. (1993) by measuring FDG uptake in the brains of patients with mild cognitive impairment or Alzheimer's Disease. Recently, Sorci et al. (2019) adopted this approach in their 2019 study which compared NaF-PET/CT and Framingham Risk Score to CAD risk factors, including age and BMI, in 86 controls and 50 CAD patients. The authors observed that both NaF-PET/CT and Framingham Risk Score were increased in CAD patients. Moreover, NaF-PET/CT but not Framingham Risk Score could differentiate between patients and controls, and global NaF uptake was significantly correlated with both age and BMI. Taken together, these studies all suggest a major role for global NaF assessment in individuals at risk for atherosclerosis and CAD.

McKenney-Drake et al. (2018) demonstrate that early identification of vascular microcalcification by NaF-PET/CT has significant prognostic value. Coronary NaF uptake and histopathological and sonographic assessment were compared between 13 lean (control) Ossabaw swine and 11 animals with metabolic syndrome and early CAD. The researchers found that the animals with metabolic syndrome demonstrated both 2.5-times higher coronary vascular uptake and 100-times higher plaque burden as the control animals. Furthermore, a recent publication by Kwiecinski et al. (2011) investigated 293 patients with CAD to determine if NaF-PET/CT could be used as a predictor of future myocardial infarction. They found that only patients who experienced a myocardial infarction during the 42-month follow-up period demonstrated increased NaF uptake in the coronary arteries in the initial scans. Importantly, the authors concluded that NaF uptake in the coronary arteries could be used as an independent prognostic factor for myocardial infarction occurrence. These data suggest the prognostic potential of NaF PET/CT, in correlation with histological and pathological changes of atherosclerotic calcification in CAD.

FDG-PET/CT have been used with varying success to investigate the efficacy of potential atherosclerosis therapeutics. Kim et al. (2018) found that FDG-PET could not be used to evaluate statin efficacy. In their prospective study of 13 acute coronary symptom patients imaged before and after 1 month of 20 mg/day atorvastatin, they found no difference in FDG uptake within the carotid arteries. On the other hand, Choo et al. (2018) demonstrated in 2018 that atorvastatin and pioglitazone co-therapy is associated with decreased vessel inflammation as assessed by FDG-PET/CT relative to atorvastatin alone in 41

patients with coronary artery disease. This data suggest that FDG-PET should be applied toward therapies that alter vascular inflammation, such as tumor necrosis factor-alpha modulators or interleukin-6 blockers, rather than plaque development. Based on the limited utility of FDG-PET/CT in this domain, further studies should utilize NaF-PET over FDG to assess atherosclerotic disease and consequent response to treatment. For example, Moss et al. (2019) used NaF-PET to examine the effects of ticagrelor, a platelet adenosine diphosphate P2Y12 receptor antagonist, on troponin I levels in patients with multivessel coronary artery disease. Using NaF uptake in the coronary arteries to monitor the presence of plaques, the authors confirmed that ticagrelor did not significantly influence troponin I levels in patients with multivessel coronary artery disease, which suggests that this factor is not a reliable marker for monitoring antagonism to the P2Y12 receptor on platelets. This study demonstrates a potential role for NaF in pharmaceutical development, which may be of use to physicians in future clinical trials.

Limitations of Molecular Imaging in Assessing Atherosclerosis

A major limitation of FDG as a means to investigate atherosclerosis has been its non-specific uptake by myocardial tissue as well as the arterial wall. This is particularly of major concern in the coronary arteries, since spillover from the physiologic activity of the heart obscures detection of atherosclerotic inflammation (McKenney-Drake et al., 2018). A study by Williams and Kolodny (2008) proposed a method of circumventing this limitation in certain settings. In brief, myocardial glucose metabolism and undesired FDG uptake is suppressed by requiring subjects to consume a very high-fat, low-carbohydrate, protein-permitted diet (VHFLCPP) 3–6 h prior to image acquisition. In comparison to a fasting control group, the average FDG uptake in the VHFLCPP group was suppressed. The utility of the VHFLCPP diet protocol was replicated by Wykrzykowska et al. (2009), who demonstrated "good" or "adequate" myocardial suppression in 20 out of 32 patients. The cases of inadequate suppression were due to self-reported dietary non-adherence. Other than myocardial spillover, FDG uptake is also limited by its spatial resolution, as visualization of uptake in the millimeter range is past the physical limits of PET imaging (Bural et al., 2006).

Based on recent publications in the literature, it is apparent that FDG-PET possesses low sensitivity and specificity as a molecular probe for detecting inflammation in atherosclerotic plaques (McKenney-Drake et al., 2018; Moghbel et al., 2018; Arani et al., 2019; **Figure 3**). This is primarily because FDG is not

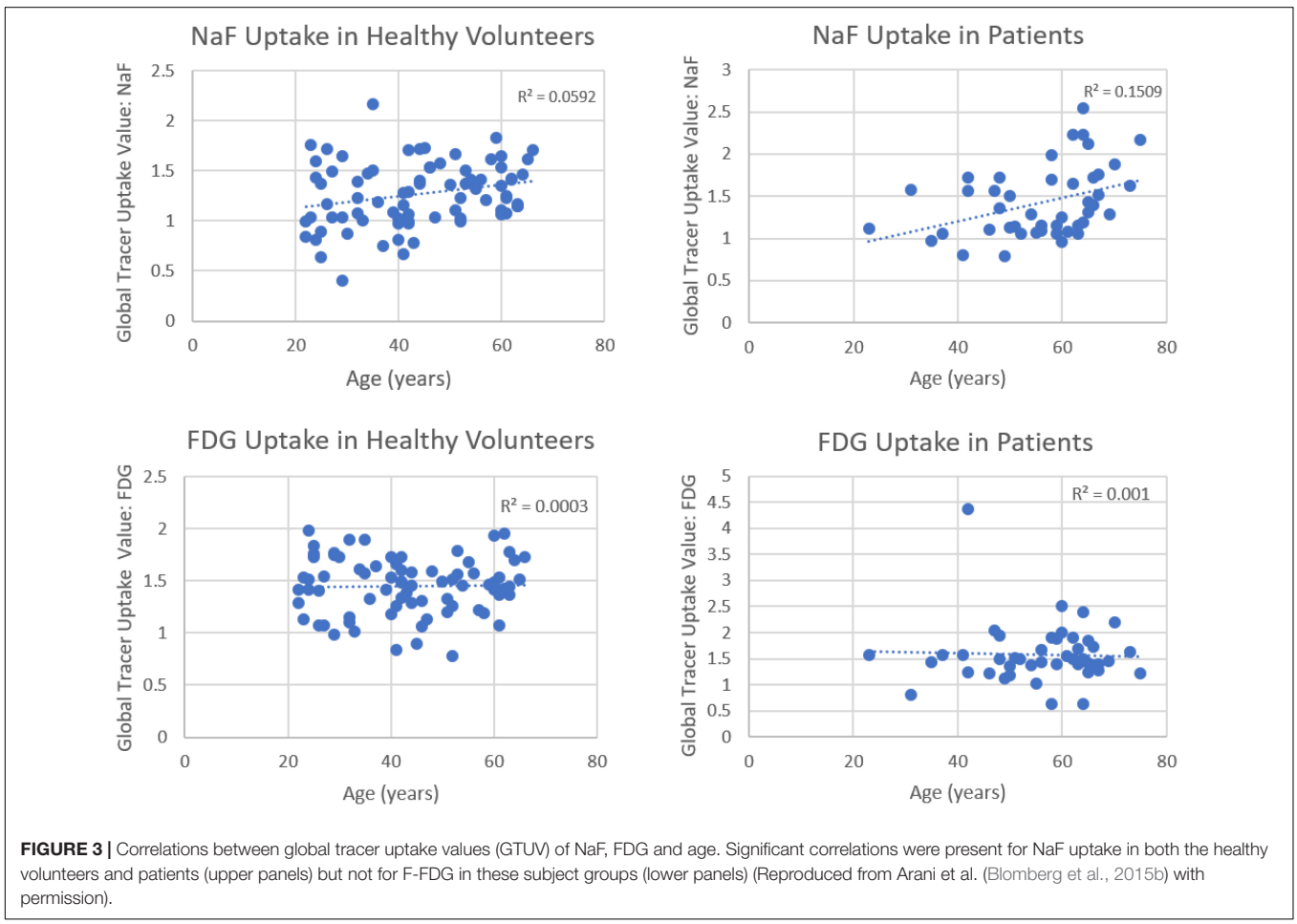

FIGURE 3 | Correlations between global tracer uptake values (GTUV) of NaF, FDG and age. Significant correlations were present for NaF uptake in both the healthy volunteers and patients (upper panels) but not for F-FDG in these subject groups (lower panels) (Reproduced from Arani et al. (Blomberg et al., 2015b) with permission).

only taken up by inflammatory cells, but also by other cellular structures in the vessel wall. In other words, smooth muscle cells in the arterial wall, which are known to be highly glycolytic, may have high levels of FDG uptake and this decreases the specificity of FDG-PET imaging for detection of atherosclerotic plaques. Furthermore, the suboptimal spatial resolution of PET (in the range of 5–8 mm) results in substantial underestimation of the degree of uptake in the plaques. Efforts have been made to correct for partial volume effects to accurately quantify the degree of inflammation in plaques (Blomberg et al., 2015a). This would require administering contrast agents along with PET, which is not routinely employed for the assessment of cardiovascular imaging with PET/CT (Blomberg et al., 2015a). Furthermore, the majority of reports in the literature regarding the detection of inflammation in atherosclerotic plaque is based on FDG-PET imaging only 60 min following administration of the tracer. The degree of clearance of FDG is relatively slow, and substantially high levels of the tracer that remain in the circulation affect the accuracy of measurements made with this approach (Cheng et al., 2013). In other words, spillover from the high levels of intravascular tracer activity results in an overestimation of inflammatory reaction in plaques. Efforts have been made to minimize this undesirable effect on optimal quantification of atherosclerosis by imaging at delayed time points of up to 3 h (Blomberg et al., 2013, 2014a, 2015a; Moghbel et al., 2018; **Figure 4**). Therefore, the results from existing literature that are based on 60-min imaging are somewhat inaccurate and need to be verified by optimally delayed imaging protocols. We should also emphasize that target-to-background ratio, which is commonly used for assessing atherosclerosis, is of questionable value for overcoming blood pool activity effect on accurate quantification of atherosclerosis (**Figure 5**). Based on studies that have been performed at 1, 2, and 3 h post-injection and TBR quantification, it is clear that target-to-background ratio provides unreliable numbers for the presence and degree of inflammation in plaques (Blomberg et al., 2013, 2015a). Finally, a number of FDG-PET/CT studies have been performed in patients with numerous co-morbidities, such as cancer, subsequent chemotherapy/radiation therapy, and other inflammatory conditions. Upregulation of proinflammatory cytokines due to these abnormalities may therefore, influence FDG uptake in other structures, similarly suggesting that NaF-PET/CT may be the tool of choice for the clinical assessment for atherogenic microcalcifications.

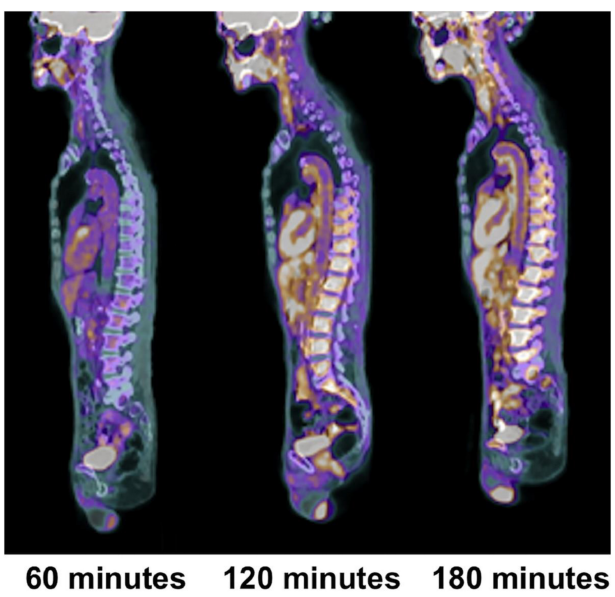

FIGURE 4 | Changes in aortic wall and luminal blood FDG activity at different imaging time-points as seen on sagittal FDG PET images of the thoracic aorta. With time, luminal blood activity decreases while the aortic wall activity increases, which improves the arterial wall-to-blood contrast (superior target-to-background ratio) (Reproduced from Moghbel et al. (Gonzalez and Trigatti, 2017)with permission).

The clinical utility of NaF in the assessment of atherosclerosis is still being evaluated. While microcalcifications may be detected by NaF-PET/CT and are believed to precede macroscopic plaque buildup in arterial walls, the mechanistic relationship of microcalcifications toward the overall pathobiology of atherosclerosis has yet to be elucidated. Additionally, the small size of atherosclerotic plaques is comparable to the typical spatial resolution of PET, leading to potential inaccuracies in NaF quantification due to partial volume effects. Recently, Cal-Gonzalez et al. (2018) developed partial volume correction techniques to improve NaF-PET quantification of atherosclerotic plaques to help mitigate this issue. Also, global assessment of NaF uptake in the coronaries and major arteries may overcome this limitation. Uptake of NaF in the bony structures may adversely affect the results in the arteries adjacent to the skeleton. We believe that further translational and clinical research using NaF-PET/CT will answer these questions and provide a more definitive review for the role of this imaging modality.

PET-based imaging modalities may further aid in the assessment of atherosclerosis and cardiac disease. Specifically, radiolabeled nanoparticles may be used to assess macrophage activity (de Barros et al., 2012). de Barros et al. (2014) utilized dextran-coated iron oxide nanoparticles to assess the macrophage burden in the coronary arteries of apolipoprotein-E-deficient mice. They found the ApoE knockout mice demonstrated high cardiac uptake of radiotracer than controls. Additionally, among ApoE knockout mice, radiotracer was specifically localized to diseased hearts but not healthy hearts. This approach may allow detection of inflammation in the coronary arteries which is unachievable with FDG. Additionally, many studies have been performed using tracers other than NaF and FDG which have shown success in the study of cardiovascular pathology. For example, Thackeray et al. (2018) examined the effects of myocardial infarction on inflammation in the heart and brain in mice models using mitochondrial translocator protein (TSPO) as their PET ligand. They determined that TPSO uptake was significantly increased in the infarct region 1 week following infarction, as well as in remote cardiomyocytes 8 weeks later, correlating with left ventricular remodeling and heart failure. In the brain, TSPO uptake was increased in the microglia, which reflects the presence of neuroinflammation occurring alongside the

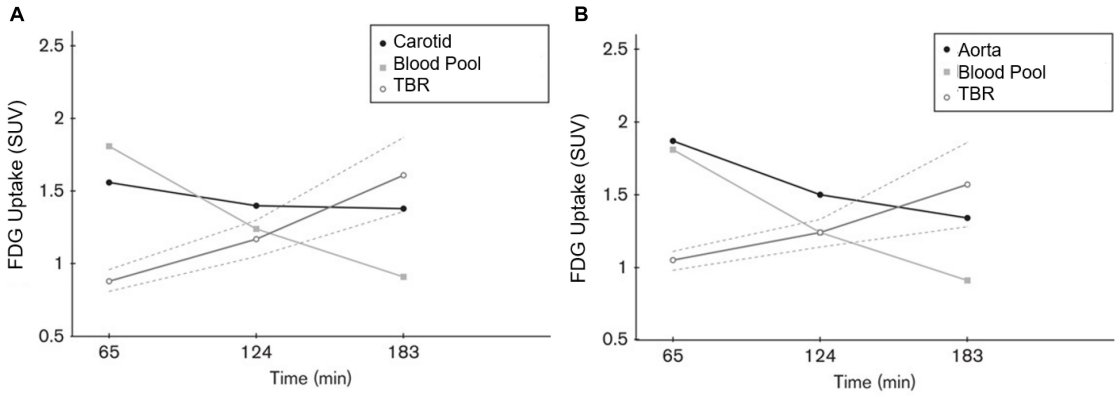

FIGURE 5 | Graph plotting the FDG activity (SUV) in the carotid arteries **(A)**, aorta **(B)** and the right atrial blood pool at 65, 124, and 183 min after FDG administration. The ratio between the arterial and blood pool activity increased with time. The interrupted lines represent the 95% confidence interval of TBR values. We would like to emphasize the TBR measurements differ at 1, 2, and 3 h. This indicates the lack of reliability of TBR for accurate quantification of uptake in the atherosclerotic plaques (Reproduced from Blomberg et al. (van der Wal and Becker, 1999) with permission).

infarction. This suggests that using TSPO as a PET ligand may be of interest in future large-scale studies, as it has the potential to identify multiple areas of cellular and tissue damage. Additionally, Tarkin et al. (2019) used 68Ga-DOTATATE, a somatostatin receptor subtype-2 PET ligand, alongside FDG to examine residual myocardial inflammation following myocardial infarction. They determined that, not only was 68Ga-DOTATATE uptake significantly correlated with post-infarction myocardial inflammation, but it also had less background signal than the FDG scans, which may point to its superiority over FDG as a PET tracer.

Both NaF and FDG have been used as proxies for the detection of early stage CVD. We may see refinement in the specific processes captured by each radiotracer, and how exactly they relate to large-scale pathology. Given that NaF is an effective tool for the detection of microcalcification, and that FDG is only proven as an inflammatory marker, more research with standardized protocols and methods is needed to assess FDG's utility as a diagnostic tool for cardiovascular illness. A literature search by Huet et al. (2015) identified 46 different quantification methods for the quantification of FDG uptake in atherosclerotic plaques used in 49 studies. Since inflammation is a critical risk factor for plaque rupture, likely, there is still potential for this radiotracer in the area of cardiovascular health, which will be better understood as its relationship with CVD and acute cardiac events is increasingly quantified. A recent example of the potential benefits of using NaF and FDG concurrently is demonstrated by recent data from Chowdhury et al. (2019), which sought to predict the development of restenosis following percutaneous transluminal angioplasty in individuals with peripheral artery disease. The authors identified significantly increased femoral artery inflammation using FDG, as well as a significant increase in the degree of microcalcification present using NaF, in patients with restenosis as compared to individuals without restenosis. This study demonstrates one of many possibilities in the future of using NaF and FDG together, which will help clinicians evaluate diseases with complex presentations involving both microcalcification and inflammation.

Future Directions in PET Imaging

Based on the large volume of data that have been introduced to the literature and discussed in this review, it is clear that PET imaging will have a major role to play in assessing atherosclerosis in the major and coronary arteries. Recent evidence demonstrates the feasibility of NaF in assessing atherosclerosis in the aorta, carotid arteries, and coronary arteries. This agent is rapidly cleared from the circulation and therefore the degree of background activity, which is a major source of error for such measurements, no longer interferes with accurate quantification of atherosclerotic plaques. In other words, significant clearance of NaF by the bony skeleton and the kidneys over a short period of time results in very minimal activity remaining in the blood even after 1 h. Therefore, the need for target-to-background ratio measurements is obviated by using NaF-PET. Furthermore, the specificity of microcalcification to the atherosclerotic plaques allows measurements of CAD which is almost impossible to achieve by FDG. Since coronary artery atherosclerosis is a serious and potentially fatal predisposing risk factor in patients with CAD, NaF imaging has great promise for becoming the study of choice for early detection and accurate quantification of the disease process. We believe NaF-PET imaging will obviate the need for CT calcification assessment which reveals irreversible disease process in the coronary arteries and therefore is of limited value in the management of these patients. Large multi-center trials are necessary to further confirm the role of PET in this disease (McKenney-Drake et al., 2018; Moghbel et al., 2018; Hoilund-Carlsen et al., 2019).

AUTHOR CONTRIBUTIONS

All authors made a substantial contribution to this review, and approved it for publication.

REFERENCES

Abdelbaky, A., Corsini, E., Figueroa, A. L., Fontanez, S., Subramanian, S., Ferencik, M., et al. (2013). Focal arterial inflammation precedes subsequent calcification in the same location: a longitudinal FDG-PET/CT study. *Cir. Cardiovasc. Imaging* 6, 747–754. doi: 10.1161/CIRCIMAGING.113.000382

Alavi, A., Newberg, A. B., Souder, E., and Berlin, J. A. (1993). Quantitative analysis of PET and MRI data in normal aging and Alzheimer's disease: atrophy weighted total brain metabolism and absolute whole brain metabolism as reliable discriminators. *J. Nucl. Med.* 34, 1681–1687.

Arani, L., Gharavi, M., Saboury, B., Al-Zaghal, A., Jahangiri, P., Khosravi, M., et al. (2018). Assessment of the role of age and cardiovascular risk factors on 18F-Fluorodeoxyglucose (18F-FDG) and 18F-Sodium Fluoride (NaF) uptake in abdominal aortic artery. *J. Nucl. Med.* 59(Suppl. 1), 1539–1539.

Arani, L. S., Gharavi, M. H., Zadeh, M. Z., Raynor, W. Y., Seraj, S. M., Constantinescu, C. M., et al. (2019). Association between age, uptake of (18)F-fluorodeoxyglucose and of (18)F-sodium fluoride, as cardiovascular risk factors in the abdominal aorta. *Hell J. Nucl. Med.* 22, 14–19.

Basatemur, G. L., Jorgensen, H. F., Clarke, M. C. H., Bennett, M. R., and Mallat, Z. (2019). Vascular smooth muscle cells in atherosclerosis. *Nat. Rev. Cardiol.* 16, 727–744. doi: 10.1038/s41569-019-0227-9

Beheshti, M., Saboury, B., Mehta, N. N., Torigian, D. A., Werner, T., Mohler, E., et al. (2011). Detection and global quantification of cardiovascular molecular calcification by fluoro18-fluoride positron emission tomography/computed tomography–a novel concept. *Hell J. Nucl. Med.* 14, 114–120.

Ben-Haim, S., Kupzov, E., Tamir, A., and Israel, O. (2004). Evaluation of 18F-FDG Uptake and arterial wall calcifications using 18F-FDG PET/CT. *J. Nucl. Med.* 45, 1816–1821.

Blomberg, B., Thomassen, A., Takx, R., Hildebrandt, M., Simonsen, J., Buch-Olsen, K., et al. (2014a). Delayed 18F-fluorodeoxyglucose PET/CT imaging improves quantitation of atherosclerotic plaque inflammation: results from the CAMONA study. *J. Nucl. Cardiol.* 21, 588–597. doi: 10.1007/s12350-014-9884-6

Blomberg, B. A., Thomassen, A., Takx, R. A., Vilstrup, M. H., Hess, S., Nielsen, A. L., et al. (2014b). Delayed sodium 18F-fluoride PET/CT imaging does not improve quantification of vascular calcification metabolism: results from the CAMONA study. *J. Nucl. Cardiol.* 21, 293–304. doi: 10.1007/s12350-013-9829-5

Blomberg, B. A., Akers, S. R., Saboury, B., Mehta, N. N., Cheng, G., Torigian, D. A., et al. (2013). Delayed time-point 18F-FDG PET CT imaging enhances assessment of atherosclerotic plaque inflammation. *Nucl. Med. Commun.* 34, 860–867. doi: 10.1097/MNM.0b013e3283637512

Blomberg, B. A., Bashyam, A., Ramachanan, A., Gholami, S., Houshmand, S., Salavati, A., et al. (2015a). Quantifying [F-18]fluorodeoxyglucose uptake in the arterial wall: the effects of dual time-point imaging and partial volume effect correction. *Eur. J. Nucl. Med. Mol. Imaging* 42, 1414–1422. doi: 10.1007/s00259-015-3074-x

Blomberg, B. A., Thomassen, A., de Jong, P. A., Simonsen, J. A., Lam, M. G., Nielsen, A. L., et al. (2015b). Impact of personal characteristics and technical factors on quantification of sodium 18F-fluoride uptake in human arteries: prospective evaluation of healthy subjects. *J. Nucl. Med.* 56, 1534–1540. doi: 10.2967/jnumed.115.159798

Blomberg, B. A., de Jong, P. A., Thomassen, A., Lam, M. G. E., Vach, W., Olsen, M. H., et al. (2017a). Thoracic aorta calcification but not inflammation is associated with increased cardiovascular disease risk : results of the CAMONA study. *Eur. J. Nucl. Med. Mol. Imaging* 44, 249–258. doi: 10.1007/s00259-016-3552-9

Blomberg, B. A., Thomassen, A., de Jong, P. A., Lam, M. G. E., Diederichsen, A. C. P., Olsen, M. H., et al. (2017b). Coronary fluorine-18-sodium fluoride uptake is increased in healthy adults with an unfavorable cardiovascular risk profile : results from the CAMONA study. *Nucl. Med. Commun.* 38, 1007–1014. doi: 10.1097/MNM.0000000000000734

Borja, A. J., Hancin, E. C., Zhang, V., Revheim, M. E., and Alavi, A. (2020). Potential of PET/CT in assessing dementias with emphasis on cerebrovascular disorders. *Eur. J. Nucl. Med. Mol. Imaging* doi: 10.1007/s00259-020-04697-y [Epub ahead of print].

Bural, G., Torigian, D., Chamroonrat, W., Houseni, M., Chen, W., Basu, S., et al. (2008). FDG-PET is an effective imaging modality to detect and quantify age-related atherosclerosis in large arteries. *Eur. J. Nucl. Med. Mol. Imaging* 35, 562–569. doi: 10.1007/s00259-007-0528-9

Bural, G. G., Torigian, D., Rubello, D., and Alavi, A. (2016). Atherosclerotic 18F-FDG and MDP uptake in femoral arteries, changes with age. *Nucl. Med. Commun.* 37, 833–836. doi: 10.1097/MNM.0000000000000515

Bural, G. G., Torigian, D. A., Chamroonrat, W., Alkhawaldeh, K., Houseni, M., El-Haddad, G., et al. (2006). Quantitative assessment of the atherosclerotic burden of the aorta by combined FDG-PET and CT image analysis: a new concept. *Nucl. Med. Biol.* 33, 1037–1043. doi: 10.1016/j.nucmedbio.2006.08.005

Cal-Gonzalez, J., Li, X., Heber, D., Rausch, I., Moore, S. C., Schafers, K., et al. (2018). Partial volume correction for improved PET quantification in (18)F-NaF imaging of atherosclerotic plaques. *J. Nucl. Cardiol.* 25, 1742–1756. doi: 10.1007/s12350-017-0778-2

Castro, S., Muser, D., Acosta-Montenegro, O., Emamzadehfard, S., Shamchi, S. P., Desjardins, B., et al. (2017). Common carotid artery molecular calcification assessed by 18F-NaF PET/CT is associated with increased cardiovascular disease risk: results from the CAMONA study. *J. Nucl. Med.* 58(Suppl. 1):34.

Cheng, G., Alavi, A., Lim, E., Werner, T. J., Dell Bello, C.V., and Akers, S. R. (2013). Dynamic changes of FDG uptake and clearance in normal tissues. *Mol. Imaging Biol.* 15, 345–352. doi: 10.1007/s11307-012-0600-0

Cho, S.-G., Park, K., Kim, J., Kang, S.-R., Kwon, S., Seon, H., et al. (2017). Prediction of coronary artery calcium progression by FDG uptake of large arteries in asymptomatic individuals. *Eur. J. Nucl. Med. Mol. Imaging* 44, 129–140. doi: 10.1007/s00259-016-3523-1

Choo, E. H., Han, E. J., Kim, C. J., Kim, S. H., Jh, O., Chang, K., et al. (2018). Effect of pioglitazone in combination with moderate dose statin on atherosclerotic inflammation: randomized controlled clinical trial using serial FDG-PET/CT. *Korean Circ. J.* 48, 591–601. doi: 10.4070/kcj.2017.0029

Chowdhury, M. M., Tarkin, J. M., Albaghdadi, M. S., Evans, N. R., Le, E. P. V., Berrett, T. B., et al. (2019). Vascular positron emission tomography and restenosis in symptomatic peripheral arterial disease: a prospective clinical study. *JACC Cardiovasc. Imaging* 13, 1008–1017. doi: 10.1016/j.jcmg.2019.03.031

de Barros, A. B., Tsourkas, A., Saboury, B., Cardoso, V. N., and Alavi, A. (2012). Emerging role of radiolabeled nanoparticles as an effective diagnostic technique. *EJNMMI Res.* 2:39. doi: 10.1186/2191-219X-2-39

de Barros, A. L., Chacko, A. M., Mikitsh, J. L., Zaki, A. Al, Salavati, A., Saboury, B., et al. (2014). Assessment of global cardiac uptake of radiolabeled iron oxide nanoparticles in apolipoprotein-E-deficient mice: implications for imaging cardiovascular inflammation. *Mol. Imaging Biol.* 16, 330–339. doi: 10.1007/s11307-013-0709-9

Derlin, T., Richter, U., Bannas, P., Begemann, P., Buchert, R., Mester, J., et al. (2010). Feasibility of 18F-sodium fluoride PET/CT for imaging of atherosclerotic plaque. *J. Nucl. Med.* 51, 862–865. doi: 10.2967/jnumed.110.076471

Derlin, T., Wisotzki, C., Richter, U., Apostolova, I., Bannas, P., Weber, C., et al. (2011). In vivo imaging of mineral deposition in carotid plaque using 18F-sodium fluoride PET/CT: correlation with atherogenic risk factors. *J. Nucl. Med.* 52, 362–368. doi: 10.2967/jnumed.110.081208

Dunphy, M. P. S., Freiman, A., Larson, S. M., and Strauss, H. W. (2005). Association of vascular 18F-FDG uptake with vascular calcification. *J. Nucl. Med.* 46, 1278–1284.

Emamzadehfard, S., Raynor, W., Paydary, K., Shamchi, S. P., Werner, T., Hoilund-Carlsen, P. F., et al. (2017). Evaluation of the role of age and cardiovascular risk factors on FDG-PET/CT quantification of atherosclerosis in the thoracic aorta. *J. Nucl. Med.* 58(Suppl. 1):1181.

Falk, E. (1992). Why do plaques rupture? *Circulation* 86(6 Suppl.), III30–III42.

Feil, S., Fehrenbacher, B., Lukowski, R., Essmann, F., Schulze-Osthoff, K., Schaller, M., et al. (2014). Transdifferentiation of vascular smooth muscle cells to macrophage-like cells during atherogenesis. *Circ. Res.* 115, 662–667. doi: 10.1161/CIRCRESAHA.115.304634

Figueroa, A. L., Abdelbaky, A., Truong, Q. A., Corsini, E., MacNabb, M. H., Lavender, Z. R., et al. (2013). Measurement of arterial activity on routine FDG PET/CT images improves prediction of risk of future CV events. *JACCCardiovasc. Imaging* 6, 1250–1259. doi: 10.1016/j.jcmg.2013.08.006

Figueroa, A. L., Subramanian, S. S., Cury, R. C., Truong, Q. A., Gardecki, J. A., Tearney, G. J., et al. (2012). Distribution of inflammation within carotid atherosclerotic plaques with high-risk morphological features:

a comparison between positron emission tomography activity, plaque morphology, and histopathology. *Circ. Cardiovas. Imaging* 5, 69–77. doi: 10.1161/CIRCIMAGING.110.959478

George, R. T. (2012). 18F-sodium fluoride positron emission tomography: an in vivo window into coronary atherosclerotic plaque biology. *J. Am. Coll Cardiol.* 59, 1549–1550. doi: 10.1016/j.jacc.2012.01.029

Gimbrone, M. A. Jr., and Garcia-Cardena, G. (2016). Endothelial cell dysfunction and the pathobiology of atherosclerosis. *Circ. Res.* 118, 620–636. doi: 10.1161/CIRCRESAHA.115.306301

Gonzalez, L., and Trigatti, B. L. (2017). Macrophage apoptosis and necrotic core development in atherosclerosis: a rapidly advancing field with clinical relevance to imaging and therapy. *Can. J. Cardiol.* 33, 303–312. doi: 10.1016/j.cjca.2016.12.010

Hansson, G. K. (2005). Inflammation, atherosclerosis, and coronary artery disease. *N. Engl. J. Med.* 352, 1685–1695. doi: 10.1056/NEJMra043430

Hayrapetian, A., Berenji, G., and Li, Y. (2019). Coronary 18F-sodium fluoride uptake is associated with increased stenosis in calcified coronary atherosclerosis. *J. Nucl. Med.* 60(Suppl. 1):452.

Hoilund-Carlsen, P. F., Moghbel, M. C., Gerke, O., and Alavi, A. (2019). Evolving role of PET in detecting and characterizing atherosclerosis. *PET Clin.* 14, 197–209. doi: 10.1016/j.cpet.2018.12.001

Huet, P., Burg, S., Guludec, D. Le, Hyafil, F., and Buvat, I. (2015). Variability and uncertainty of 18F-FDG PET imaging protocols for assessing inflammation in atherosclerosis: suggestions for improvement. *J. Nucl. Med.* 56, 552–559. doi: 10.2967/jnumed.114.142596

Irkle, A., Vesey, A. T., Lewis, D. Y., Skepper, J. N., Bird, J. L., Dweck, M. R., et al. (2015). Identifying active vascular microcalcification by (18)F-sodium fluoride positron emission tomography. *Nat. Commun.* 6:7495. doi: 10.1038/ncomms8495

Iwatsuka, R., Matsue, Y., Yonetsu, T., O'Uchi, T., Matsumura, A., Hashimoto, Y., et al. (2018). Arterial inflammation measured by (18)F-FDG-PET-CT to predict coronary events in older subjects. *Atherosclerosis* 268, 49–54. doi: 10.1016/j.atherosclerosis.2017.11.016

Joshi, N. V., Vesey, A. T., Williams, M. C., Shah, A. S., Calvert, P. A., Craighead, F. H., et al. (2014). 18F-fluoride positron emission tomography for identification of ruptured and high-risk coronary atherosclerotic plaques: a prospective clinical trial. *Lancet* 383, 705–713. doi: 10.1016/S0140-6736(13)61754-7

Kim, C. J., Han, E. J., Chu, E. H., Hwang, B. H., Kim, J. J., Seung, K. B., et al. (2018). Effect of moderate-intensity statin therapy on plaque inflammation in patients with acute coronary syndrome: a prospective interventional study evaluated by 18F-FDG PET/CT of the carotid artery. *Cardiol. J.* doi: 10.5603/CJ.a2018.0069 [Epub ahead of print].

Kim, J., Choi, K. H., Song, H. C., Kim, J. T., Park, M. S., and Cho, K. H. (2016). (18)F-FDG PET/CT imaging factors that predict ischaemic stroke in cancer patients. *Eur. J. Nucl. Med. Mol. Imaging* 43, 2228–2235. doi: 10.1007/s00259-016-3460-z

Kim, J. M., Lee, E. S., Park, K. Y., Seok, J. W., and Kwon, O. S. (2019). Comparison of [(18)F]-FDG and [(18)F]-NaF positron emission tomography on culprit carotid atherosclerosis: a prospective study. *JACC Cardiovasc. Imaging* 12, 370–372. doi: 10.1016/j.jcmg.2018.07.026

Kwiecinski, J., Tzolos, E., Adamson, P. D., Cadet, S., Moss, A. J., Joshi, N., et al. (2011). Coronary 18F-sodium fluoride uptake predicts outcomes in patients with coronary artery disease. *J. Am. Coll Caridol.* 75, 3061–3074. doi: 10.1016/j.jacc.2020.04.046

Liu, M., and Gomez, D. (2019). Smooth muscle cell phenotypic diversity. *Arterioscler Thromb. Vasc. Biol.* 39, 1715–1723. doi: 10.1161/ATVBAHA.119.312131

Lozano, R. P., Naghavi, M., Foreman, K., Lim, S., Shibuya, K., Aboyans, V., et al. (2012). Global and regional mortality from 235 causes of death for 20 age groups in 1990 and 2010: a systematic analysis for the global burden of disease study 2010. *Lancet* 380, 2095–2128. doi: 10.1016/S0140-6736(12)61728-0

Mallika, V., Goswami, B., and Rajappa, M. (2007). Atherosclerosis pathophysiology and the role of novel risk factors: a clinicobiochemical perspective. *Angiology* 58, 513–522. doi: 10.1177/0003319707303443

Marnane, M., Merwick, A., Sheehan, O. C., Hannon, N., Foran, P., Grant, T., et al. (2012). Carotid plaque inflammation on 18F—fluorodeoxyglucose positron emission tomography predicts early stroke recurrence. *Ann. Neurol.* 71, 709–718. doi: 10.1002/ana.23553

McKenney-Drake, M., Moghbel, M., Paydary, K., Alloosh, M., Houshmand, S., Moe, S., et al. (2018). 18F-NaF and 18F-FDG as molecular probes in the evaluation of atherosclerosis. *Eur. J. Nucl. Med. Mol. Imaging* 45, 2190–2200. doi: 10.1007/s00259-018-4078-0

Meirelles, G. S., Gonen, M., and Strauss, H. (2011). 18F-FDG uptake and calcifications in the thoracic aorta on positron emission tomography/computed tomography examinations: frequency and stability on serial scans. *J. Thoracic Imaging* 26, 54–62. doi: 10.1097/RTI.0b013e3181d9c9f9

Moghbel, M., Al-Zaghal, A., Werner, T. J., Constantinescu, C. M., Hoilund-Carlsen, P. F., and Alavi, A. (2018). The Role of PET in evaluating atherosclerosis: a critical review. *Semin. Nucl. Med.* 48, 488–497. doi: 10.1053/j.semnuclmed.2018.07.001

Morbelli, S., Fiz, F., Piccardo, A., Picori, L., Massollo, M., Pestarino, E., et al. (2014). Divergent determinants of 18F-NaF uptake and visible calcium deposition in large arteries: relationship with Framingham risk score. *Int. J. Cardiovasc. Imaging* 30, 439–447. doi: 10.1007/s10554-013-0342-3

Moss, A. J., Dweck, M. R., Doris, M. K., Andrews, J. P. M., Bing, R., Forsythe, R. O., et al. (2019). Ticagrelor to reduce myocardial injury in patients with high-risk coronary artery plaque. *JACC Cardiovasc. Imaging* 13, 1549–1560. doi: 10.1016/j.jcmg.2019.05.023

Myers, K. S., Rudd, J. H., Hailman, E. P., Bolognese, J. A., Burke, J., Pinto, C. A., et al. (2012). Correlation between arterial fdg uptake and biomarkers in peripheral artery disease. *JACC Cardiovasc. Imaging* 5, 38–45. doi: 10.1016/j.jcmg.2011.08.019

Nogales, P., Velasco, C., González-Cintado, L. R., Mota-Cobián, A., Mateo, J., España, S., et al. (2019). Abstract 191: 18F-sodium fluoride PET-CT measures plaque burden in gene modified minipigs with atherosclerosis. *Arterioscler. Thromb. Vasc. Biol.* 39(Suppl._1), A191–A191.

Ogawa, M., Ishino, S., Mukai, T., Asano, D., Teramoto, N., Watabe, H., et al. (2004). (18)F-FDG accumulation in atherosclerotic plaques: immunohistochemical and PET imaging study. *J. Nucl. Med.* 45, 1245–1250.

Pasha, A. K., Moghbel, M., Saboury, B., Gharavi, M. H., Blomberg, B. A., Torigian, W. A., et al. (2015). Effects of age and cardiovascular risk factors on 18F-FDG PET/CT quantification of atherosclerosis in the aorta and peripheral arteries. *Hell. J. Nucl. Med.* 18, 5–10.

Paulmier, B., Duet, M., Khayat, R., Pierquet-Ghazzar, N., Laissy, J.-P., Maunoury, C., et al. (2008). Arterial wall uptake of fluorodeoxyglucose on PET imaging in stable cancer disease patients indicates higher risk for cardiovascular events. *J. Nucl. Cardiol.* 15, 209–217. doi: 10.1016/j.nuclcard.2007.10.009

Plana, J. C., Thavendiranathan, P., Bucciarelli-Ducci, C., and Lancellotti, P. (2018). Multi-modality imaging in the assessment of cardiovascular toxicity in the cancer patient. *JACC Cardiovasc. Imaging* 11, 1173–1186. doi: 10.1016/j.jcmg.2018.06.003

Rominger, A., Saam, T., Wolpers, S., Cyran, C. C., Schmidt, M., Foerster, S., et al. (2009). 18F-FDG PET/CT identifies patients at risk for future vascular events in an otherwise asymptomatic cohort with neoplastic disease. *J. Nuc. Med.* 50, 1611–1620. doi: 10.2967/jnumed.109.065151

Rudd, J. H. F., Warburton, E. A., Fryer, T. D., Jones, H. A., Clark, J. C., Antoun, N., et al. (2002). Imaging atherosclerotic plaque inflammation With [18F]-Fluorodeoxyglucose positron emission tomography. *Circulation* 105, 2708–2711. doi: 10.1161/01.CIR.0000020548.60110.76

Shah, P. K. (2003). Mechanisms of plaque vulnerability and rupture. *J. Am. College Cardiol.* 41, S15–S22. doi: 10.1016/S0735-1097(02)02834-6

Sorci, O., Batzdorf, A. S., Mayer, M., Rhodes, S., Peng, M., Jankelovits, A. R., et al. (2019). (18)F-sodium fluoride PET/CT provides prognostic clarity compared to calcium and Framingham risk scoring when addressing whole-heart arterial calcification. *Eur. J. Nucl. Med. Mol. Imaging* 47, 1678–1687. doi: 10.1007/s00259-019-04590-3

Spacek, M., Zemanek, D., Hutyra, M., Sluka, M., and Taborsky, M. (2018). Vulnerable atherosclerotic plaque - a review of current concepts and advanced imaging. *Biomed. Pap. Med. Fac. Univ. Palacky Olomouc. Czech Repub.* 162, 10–17. doi: 10.5507/bp.2018.004

Strobl, F., Rominger, A., Wolpers, S., Rist, C., Bamberg, F., Thierfelder, K., et al. (2013). Impact of cardiovascular risk factors on vessel wall inflammation and calcified plaque burden differs across vascular beds: a PET-CT study. *Int. J. Cardiovasc. Imaging* 29, 1899–1908. doi: 10.1007/s10554-013-0277-8

Tarkin, J. M., Calcagno, C., Dweck, M. R., Evans, N. R., Chowdhury, M. M., Gopalan, D., et al. (2019). 68Ga-DOTATATE PET identifies residual myocardial inflammation and bone marrow activation after myocardial infarction. *J. Am. College Cardiol.* 73, 2489–2491. doi: 10.1016/j.jacc.2019.02.052

Tatsumi, M., Cohade, C., Nakamoto, Y., and Wahl, R. L. (2003). Fluorodeoxyglucose uptake in the aortic wall at PET/CT: possible finding for active atherosclerosis. *Radiology* 229, 831–837. doi: 10.1148/radiol.2293021168

Tawakol, A., Migrino, R. Q., Bashian, G. G., Bedri, S., Vermylen, D., Cury, R. C., et al. (2006). In Vivo 18F-fluorodeoxyglucose positron emission tomography imaging provides a noninvasive measure of carotid plaque inflammation in patients. *J. Am. College Cardiol.* 48, 1818–1824. doi: 10.1016/j.jacc.2006.05.076

Thackeray, J. T., Hupe, H. C., Wang, Y., Bankstahl, J. P., Berding, G., Ross, T. L., et al. (2018). Myocardial inflammation predicts remodeling and neuroinflammation after myocardial infarction. *J. Am. College Cardiol.* 71, 263–275. doi: 10.1016/j.jacc.2017.11.024

Tuominen, H., Haarala, A., Tikkakoski, A., Kahonen, M., Nikus, K., and Sipila, K. (2019). FDG-PET in possible cardiac sarcoidosis: right ventricular uptake and high total cardiac metabolic activity predict cardiovascular events. *J. Nucl. Cardiol.* 1–7. doi: 10.1007/s12350-019-01659-2

van der Valk, F. M., Verweij, S. L., Zwinderman, K. A., Strang, A. C., Kaiser, Y., Marquering, H. A., et al. (2016). Thresholds for arterial wall inflammation quantified by (18)F-FDG PET imaging: implications for vascular interventional studies. *JACC Cardiovasc. Imaging* 9, 1198–1207. doi: 10.1016/j.jcmg.2016.04.007

van der Wal, A. C., and Becker, A. E. (1999). Atherosclerotic plaque rupture–pathologic basis of plaque stability and instability. *Cardiovasc. Res.* 41, 334–344. doi: 10.1016/S0008-6363(98)00276-4

Vesey, A. T., Jenkins, W. S., Irkle, A., Moss, A., Sng, G., Forsythe, R. O., et al. (2017). 18)F-Fluoride and (18)F-Fluorodeoxyglucose positron emission tomography after transient ischemic attack or minor ischemic stroke: case-control study. *Circ. Cardiovasc. Imaging* 10:e004976. doi: 10.1161/CIRCIMAGING.116.004976

Weber, C., and Noels, H. (2011). Atherosclerosis: current pathogenesis and therapeutic options. *Nat. Med.* 17, 1410–1422. doi: 10.1038/nm.2538

Williams, G., and Kolodny, G. M. (2008). Suppression of myocardial 18F-FDG uptake by preparing patients with a high-fat, low-carbohydrate diet. *Am. J. Roentgenol.* 190, W151–W156. doi: 10.2214/AJR.07.2409

Wykrzykowska, J., Lehman, S., Williams, G., Parker, J. A., Palmer, M. R., Varkey, S., et al. (2009). Imaging of inflamed and vulnerable plaque in coronary arteries with 18F-FDG PET/CT in patients with suppression of myocardial uptake using a low-carbohydrate, high-fat preparation. *J. Nucl. Med.* 50, 563–568. doi: 10.2967/jnumed.108.055616

Yun, M., Jang, S., Cucchiara, A., Newberg, A. B., and Alavi, A. (2002). 18F FDG uptake in the large arteries: a correlation study with the atherogenic risk factors. *Semin. Nucl. Med.* 32, 70–76. doi: 10.1053/snuc.2002.29279

Yun, M., Yeh, D., Araujo, L., Jang, S., Newberg, A., and Alavi, A. (2001). F-18 FDG uptake in the large arteries: a new observation. *Clin. Nucl. Med.* 26, 314–319. doi: 10.1097/00003072-200104000-00007

Conflict of Interest: The authors declare that the research was conducted in the absence of any commercial or financial relationships that could be construed as a potential conflict of interest.

frontiers in Physiology

MINI REVIEW
published: 18 December 2020
doi: 10.3389/fphys.2020.581420

Novel Strategies for Endothelial Preservation in Lung Transplant Ischemia-Reperfusion Injury

Wolfgang Jungraithmayr[1,2,3]*

[1] Department of Thoracic Surgery, University Hospital Freiburg, Freiburg, Germany, [2] Department of Thoracic Surgery, University Hospital Zurich, Zurich, Switzerland, [3] Department of Thoracic Surgery, University Hospital Rostock, Rostock, Germany

Lung ischemia reperfusion (IR) injury inevitably occurs during lung transplantation. The pulmonary endothelium is the primary target of IR injury that potentially results in severe pulmonary dysfunction. Over the last decades, various molecules, receptors, and signaling pathways were identified in order to develop treatment strategies for the preservation of the pulmonary endothelium against IR injury. We here review the latest and most promising therapeutic strategies for the protection of the endothelium against IR injury. These include the stabilization of the endothelial glycocalyx, inhibition of endothelial autophagy, inhibition of adhesion molecules, targeting of angiotensin-converting enzyme, and traditional viral and novel non-viral gene transfer approaches. Though some of these strategies proved to be promising in experimental studies, very few of these treatment concepts made the transfer into clinical application. This dilemma underscores the need for more experimental evidence for the translation into clinical studies to invent therapeutic concepts against IR injury-mediated endothelial damage.

Keywords: lung, transplantation, ischemia-reperfusion injury, endothelium, strategies

OPEN ACCESS

Edited by:
Jing-Yan Han,
Peking University, China

Reviewed by:
Prasad V. Katakam,
Tulane University, United States
Swapnil K. Sonkusare,
University of Virginia, United States

***Correspondence:**
Wolfgang Jungraithmayr
wolfgang.jungraithmayr@uniklinik-freiburg.de

Specialty section:
This article was submitted to Vascular Physiology, a section of the journal Frontiers in Physiology

Received: *08 July 2020*
Accepted: *10 November 2020*
Published: *18 December 2020*

Citation:
Jungraithmayr W (2020) Novel Strategies for Endothelial Preservation in Lung Transplant Ischemia-Reperfusion Injury. Front. Physiol. 11:581420. doi: 10.3389/fphys.2020.581420

INTRODUCTION

Ischemia reperfusion (IR) injury in lung transplantation (Tx) is associated with an increased rate of delayed graft function, but also acute and chronic graft rejection. As IR injury is unavoidably correlated with Tx, treatment strategies for the attenuation of IR injury should aim at protecting target compartments that are primarily affected by IR injury.

The pulmonary endothelium is the first site of IR injury. Already during organ ischemia, multiple donor-associated changes can alter the status of the pulmonary vasculature, that is e.g., the loss of surfactant, hypovolemia resulting in platelet occlusion of the vascular bed, an increase of pro-inflammatory mediators due to brain death, and an increase of adhesion molecules (Porteous and Lee, 2017). Upon reperfusion, the endothelial layer of the pulmonary vasculature produces reactive oxygen species (ROS) and other damaging agents (Preissler et al., 2011) which in turn results in endothelium swelling and detachment from the basement membrane (Pickford et al., 1990). This process results in a damage of the vascular permeability thereby facilitating leukocyte adherence and transmigration, the key step in mediating IR injury (Soroush et al., 2018). The interaction between leukocytes and endothelium depends on and involves a complex network of various proteins.

Over the last decades, a wide range of those proteins have been identified that mediate the differential steps necessary for the interaction between white blood cells and endothelium. Among them, selectins are responsible for a first contact and weak adhesion of leukocytes (Kawut et al., 2009), different adhesion molecules create a firmer contact of leukocytes on the endothelium and leukocyte extravasation across the endothelial wall (Muller, 2016), and finally the migration of leukocytes into the tissue is mediated by IL-8 and other mediators (Allen and Kurdowska, 2014). A number of other mediators such as TNFα, IL-1, IL-6, leukotriene B4, proteases, and elastases that are in part released from activated neutrophils, indirectly or directly, contribute to endothelial dysfunction and injury (Porteous and Lee, 2017).

Another target of IR that contributes to endothelial damage and tissue dysfunction after IR is the endothelial glycocalyx. This layer consists of proteoglycans and glycoproteins at the surface of the endothelium and harbors various chemokines, receptors, growth factors, and enzymes that play a central role in endothelial function. The endothelial glycocalyx has a pivotal importance in lung injury which has been shown during edema formation after lung IR injury when the integrity of the glycocalyx was damaged (Brettner et al., 2017).

During the last decades of research, many of these proteins, receptors, mediators, and inflammatory cascades participating in endothelial injury upon IR injury have been targeted by treatment strategies, either by antibodies, inhibitors, or modulators of the inflammatory milieu. Among these, older agents include the phosphodiesterase inhibitor cyclic AMP analog or nitride oxide.

We here will present and discuss the most recent and promising developments on strategies how to efficiently preserve the endothelium from lung IR injury.

An Ambiguous Role for Autophagy Inhibition on Pulmonary Endothelium During IR Injury

Autophagy allows for the regular degradation and recycling of cellular components and thus promotes cell survival. However, upon injury, an imbalance in endosomal and autophagic pathways can enhance macromolecular or organelle degradation thereby causing cell death. Inhibition of autophagy was shown to result in reduced apoptosis indicating that the process of autophagy as a cell survival mechanism is rather endangering the lung during IR injury (Zhang et al., 2013). On the other hand, recent analyses on pulmonary microvascular endothelial cells exposed to hypoxia-reoxygenation revealed that the suppression of mitochondrial autophagy by 3-Methyladenine (3-MA), a selective PI3K inhibitor, inhibited the apoptosis of endothelial cells and enhanced its proliferation via the mechanistic Target of Rapamycin-pathway (Liu et al., 2019). Another study in human and mouse pulmonary microvascular endothelial cells convincingly showed that promoting autophagy with rapamycin ameliorated IR-induced lung edema and tissue inflammation due to injured endothelium (Zhang et al., 2015).

Taken together, research on targeting autophagy has so far been scarce and results presented seem to be ambiguous, so there is a clear need for more studies that proves an either endothelial-preserving or endothelial-damaging effect of autophagy.

Stabilization of the Endothelial Glycocalyx From Degradation by Lung I/R Injury

The luminal surface of vascular endothelial cells is lined with a glycocalyx, comprising of membrane-bound proteoglycans, glycosaminoglycans, and sialic acid–containing glycoproteins. This layer is pivotal for the integrity and functionality of the endothelium, as it modulates the interaction of the endothelium with the components of the circulating blood. The glycocalyx harbors a variety of chemokines, receptors, growth factors, and enzymes that play a central role in endothelial function. This layer protects the endothelium from shear stress which is caused by blood flow and serves as a vascular permeability barrier. Glycocalyx damage during IR can be detected by elevated plasma levels of e.g., heparan sulfate and syndecan-1, which suggests their use as biomarkers of endothelial integrity (Abassi et al., 2020) (**Figure 1**).

The glycocalyx of the pulmonary vasculature is thicker than that of other organs (Yang and Schmidt, 2013) which might be owed to the complex lung defense against internal and external antigens. During and after lung IR, the glycocalyx is degraded and leads to leukocyte activation and adhesion with subsequent pulmonary edema and lung injury. Experimental studies showed that the integrity of the glyocalyx layer could be preserved: e.g., in an auto-transplantation model, Rancan et al. (2018) could show that IR itself causes glycocalyx alterations with an increase in pulmonary edema and expression of adhesion molecules, and that by the administration of lidocaine, the described alterations of glycocalyx degradation could be abolished (**Figure 1**). The same research group proved in an *in vivo* auto-transplantation model of pulmonary IR that by preconditioning with sevoflurane, the pulmonary glycocalyx could be protected and the expression of leukocyte chemokines could be reduced (Casanova et al., 2016). In this study, authors compared the effects of sevoflurane with propofol on IR-injured endothelium and found that propofol, but not sevoflurane, induced glycocalyx destruction and a higher chemokine and adhesion molecule expression with also an increase of the glycocalyx components heparan sulfate and serum syndecan levels (Casanova et al., 2016). Work from Chappell et al. also revealed less shedding and a reduced leukocyte adhesion after sevoflurane pre-treatment in an isolated organ model (Chappell et al., 2010). In contrast, another group analyzed those endothelial glycocalyx-injuring markers heparan sulfate and human syndecan-1 in patients undergoing pulmonary resection with one lung ventilation, however, they could not find any difference in outcome between sevoflurane and propofol (Kim et al., 2018).

As reflected by increased research activity in recent years, the glycocalyx has gained more attention taking a pivotal role in the regulation of endothelial function and vascular permeability. Though the number of studies is limited, glycocalyx components such as syndecan-1 and heparan sulfate have the potential to serve as circulatory biomarkers

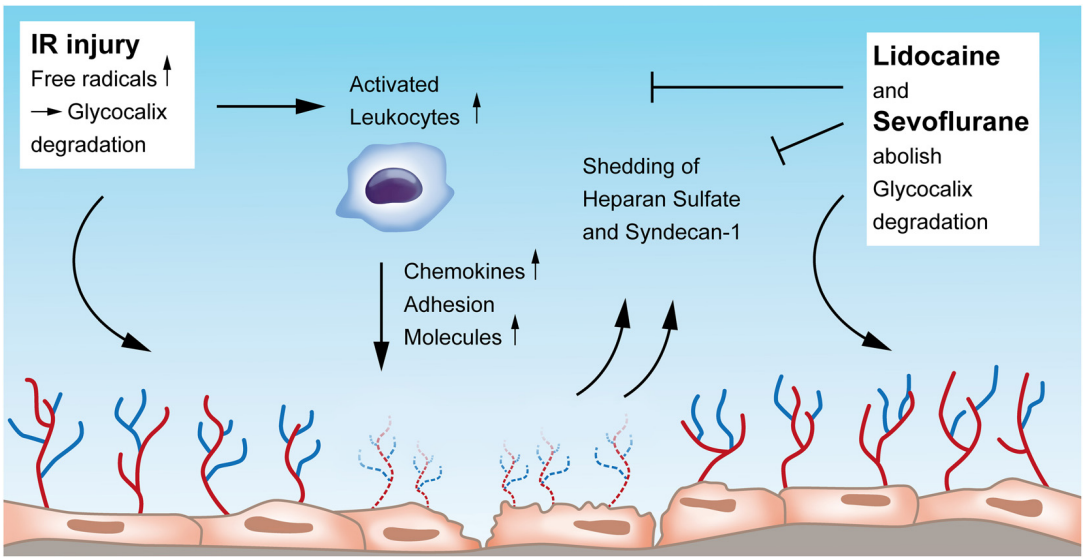

FIGURE 1 | Endothelial glycocalyx degradation induced by ischemia-reperfusion injury and its restoration by Lidocaine and Sevoflurane. Upon IR injury, free radicals, among others, contribute to glycocalyx erosion. IR injury also leads to activation of leukocytes that in turn increase the secretion of chemokines and adhesion molecules, all damaging the endothelial layer. Heparan sulfate and syndecan-1 are shed into the blood when the glycocalyx is damaged by IR and could function as biomarkers of endothelial integrity. Both Lidocaine and Sevoflurane can restore and preserve damaged glycocalyx. IR, ischemia-reperfusion.

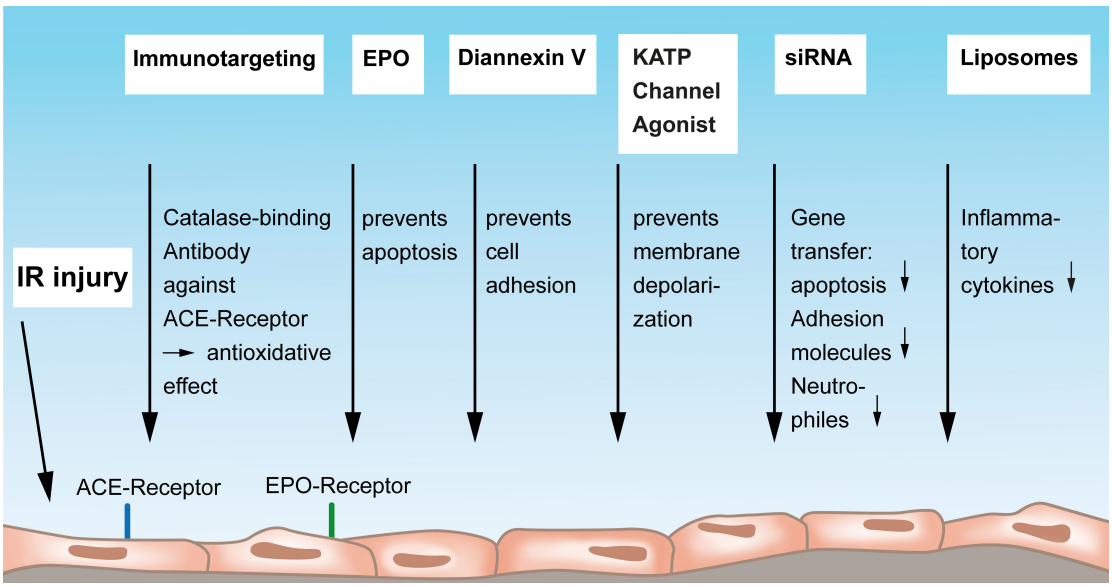

FIGURE 2 | Mediators and strategies to protect the vascular endothelium from lung IR injury. Endothelial immunotargeting by a catalase-binding antibody to the angiotensin-converting-receptor on endothelium can reduce IR-reactive oxygen species. Erythropoietin exerts protective functions on endothelial cells by preventing apoptosis via endothelium-bound EPO receptors. Diannexin V mainly acts via preventing endothelial cell adhesion, and Kalium ATP-sensitive (ATP-sensitive potassium channels, KATP) channel agonists have the potential to prevent membrane depolarization thereby protecting the endothelium. Gene transfer of siRNA to the endothelium can reduced apoptosis, less production of adhesion molecules, and a reduced attraction of neutrophils. Finally, antibody-conjugated endothelial-targeted liposomes can inhibit the cytokine-induced inflammatory activation of the endothelium. IR, ischemia-reperfusion; ACE, angiotensin-converting enzyme; EPO, Erythropoetin; KATP, Kalium ATP-sensitive; siRNA, small interfering ribonucleic acid.

for monitoring the severity of vascular endothelial damage during lung IR injury. Moreover, future research on glycocalyx protection and restoration has so far received a solid base, and pharmacologic and non-pharmacologic maneuvers on this topic should be promoted. **Figure 1** provides an overview of the current understanding of the glycocalyx in the context of IR injury and its preservation by Lidocaine and Sevoflurane.

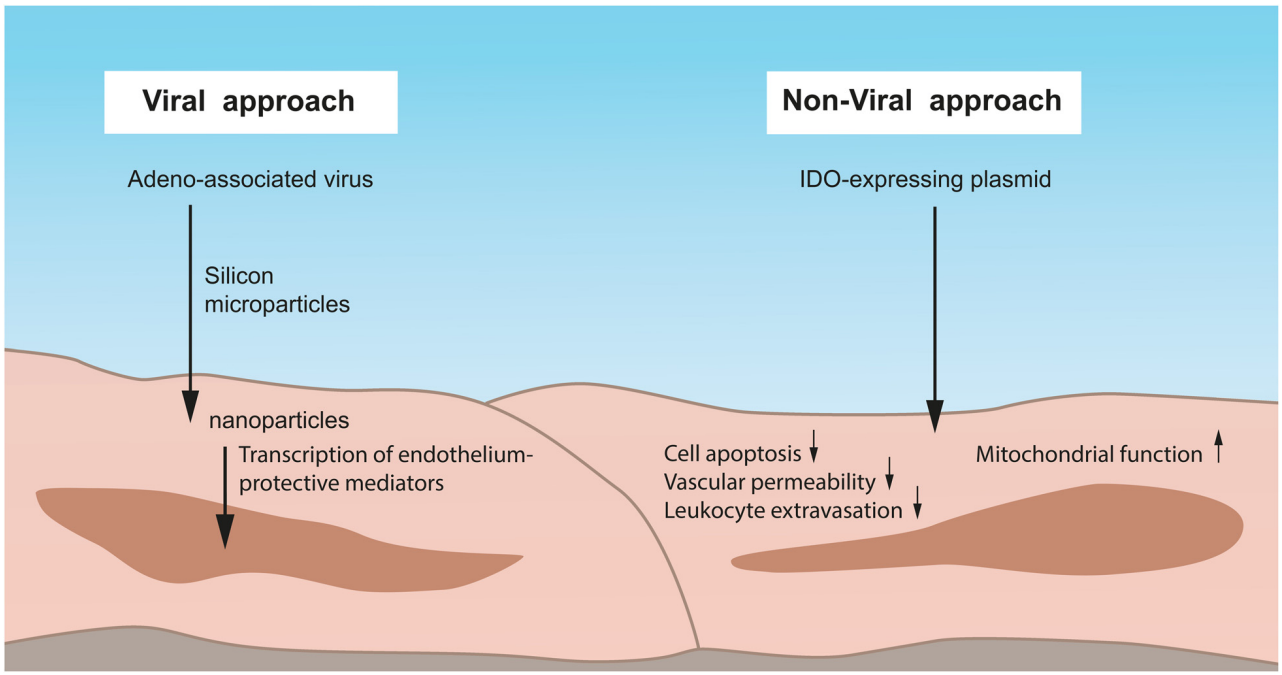

FIGURE 3 | Viral and non-viral approaches to preserve IR-injured lung endothelium. One of the most commonly employed viral vectors is the adeno-associated virus. By such a virus, silicon microparticles can be delivered into inflammation-associated endothelium where it is internalized with the subsequent release of therapeutic nanoparticles. The virus becomes free within the cytoplasm, undergoes genetic cargo, and transfers into the nucleus for the transcription of endothelium-protective mediators. In contrast, non-viral approaches have advantages over the commonly used viral systems such as lower immunogenicity, reduced inflammation, and an overall better safety. A human Indoleamine-2,3-dioxygenase (IDO)–expressing plasmid can be delivered by a specific promoter into the endothelium and reduces cell apoptosis, vascular permeability, and leukocyte extravasation. Moreover, the mitochondrial function and ultrastructure of the endothelium is protected from oxidative stress. IDO, Indoleamine-2,3-dioxygenase.

Targeting P-selectin on I/R-Injured Pulmonary Endothelium

Selectins are molecules involved in the initial process of adhesion of activated neutrophils on the pulmonary endothelium. Early work has shown that when selectively blocking selectins with a monoclonal antibody, reperfusion-induced hyperpermeability was ameliorated (Demertzis et al., 1999; Levine et al., 2002). More recently, a particular role has been assigned to P-selectin in IR injury (Moore et al., 1985; Scalia et al., 1999). As a key endothelial cell rolling factor, P-selectin mediates the adhesion of leukocytes on the endothelium and binds to glycoprotein ligand-1 (PSGL-1) on leukocytes. Moore et al. (1985) showed that when inhibiting P-selectin by a monoclonal antibody, the increase of IR-induced permeability, lung sequestration of neutrophils, mononuclear leukocytes, and eosinophils could be significantly attenuated. But also the rolling and adhesion of platelets along arteriolar walls depends on P-selectin, suggesting that platelets are also responsible for contributing to the development of pulmonary IR injury (Roberts et al., 2004). In line with these data, recent work from Lam et al. (2018) confirmed the role of P-Selectin in interaction with PSGL-1 in the attenuation of pulmonary IR injury: when using recombinant human vimentin, leukocyte adhesion to endothelial and platelet monolayers where blocked on P-selectin-coated surfaces *in vitro*. *In vivo*, histologic findings of acute lung injury decreased.

These data underscore the relevant role of the adhesion molecule P-Selectin and its inhibition on pulmonary endothelium for the attenuation of IR injury.

Immunotargeting of Angiotensin-Converting Enzyme and Antioxidant Enzymes Against Oxidative Injury

Angiotensin-converting enzyme (ACE) was previously identified as a cell-specific marker of endothelial injury (Atochina et al., 1997). Atochina et al. (1997) showed that IR induces significant elevation of ACE activity in the perfusate of isolated rat lungs. In this context, ACE serves as a surface endothelial antigen that drives leukocyte-mediated oxidative injury to endothelial cells. Muzykantov (2000) have shown that applying a monoclonal antibody against ACE serves as an affinity carrier for targeting of catalase to the pulmonary endothelial cells for specific augmentation of their anti-oxidative defense. The antioxidative effect of the conjugation of this ACE antibody to catalase has also been investigated and confirmed *in vivo* by Nowak and co-workers in a rat lung ischemia model (Nowak et al., 2007). They used the ACE monoclonal antibody (MAb) 9B9 and showed a better function of the affected lung but also decreased serum levels of endothelin-1 and less levels of inducible nitric oxide synthase. The same group

evaluated the treatment of IR-injured lung allografts with conjugates of anti-ACE antibody with catalase (9B9-CAT) in an experimental set up of hypothermic preservation. Lungs that were conditioned with this antibody showed a significantly higher catalase activity and an anti-oxidative status after cold storage compared to the catalase treatment alone (Nowak et al., 2010). Finally, these authors extended their research on an anti-ACE catalase-binding antibody in a human model of isolated perfused and ventilated lung resection (Nowak et al., 2013) and thus provided a possibility of immunotargeting of human pulmonary endothelium toward a therapeutic approach in patients. Of note, in the research of antioxidant therapeutics against endothelial injury by reactive oxygen species, catalase was also conjugated to platelet/endothelial cell adhesion molecule-1 and was demonstrated *in vitro* as well as *in vivo* to have good protective effects against endothelial oxidative stress, injury, and lethality (Christofidou-Solomidou et al., 2003) (**Figure 2**). This approach could be confirmed by Kozower et al. (2003). The entire concept of vascular immunotargeting by a specific delivery of therapeutic agents to endothelial cells and by modulating enzymes conjugated with antibodies to endothelial surface molecules has been nicely summarized in a review by Shuvaev and Muzykantov (2011).

Taken together, these studies show that vascular immunotargeting of anti-oxidative enzymes, specifically conjugates to ACE, can effectively limit reactive oxygen species–mediated IR injury of the lung.

Other Strategies to Protect the Vascular Endothelium From Lung IR Injury

This subsection will consider more therapeutic strategies on how to preserve and protect the vascular endothelium from IR injury that do not fall into the scope of the above described approaches (**Figure 2**). Erythropoietin (EPO) has been shown to positively influence acute lung injury caused by renal IR injury (Janmaat et al., 2010). EPO acts as the major regulator of erythropoiesis by stimulating growth, preventing apoptosis, and inducing differentiation of blood precursor cells. An explanation for a beneficial effect on lung injury could lie in the fact that endothelial cells express EPO receptors and thereby respond to EPO. Zhu et al. (2019) found in a model of remote lung injury induced by mouse renal injury that EPO exerts protective functions by promoting endothelial cell proliferation via the Janus Kinase-Signal Transducer and Activator of Transcription 3 pathway, rather than exerting antiapoptotic or anti-inflammatory mechanisms.

Sharma et al. (2018) analyzed the role of pannexin-1 (Panx1), a channel-forming glycoprotein that mediates signaling in vascular endothelium and plays a major role in the initiation of endothelial permeability, edema, leukocyte trafficking, and inflammation during lung IR injury. In an *in vivo* mouse lung hilar ligation model, authors found that endothelial pannexin 1 contributes to IR of the lung. Moreover, their results demonstrate a novel role of endothelial Panx1 channels in the regulation of vascular inflammation after lung IR: when blocking Panx1-mediated ATP release by Panx1 inhibitors, lung IR injury could be attenuated.

The inhibition of the adhesion of leukocytes and platelets to the endothelium was targeted in a study by Hashimoto and the thoracic research group at Toronto General Hospital. Their report in a rat lung transplant model says that Diannexin V, which is a homodimer of annexin V, ameliorates IR injury. Authors administered Diannexin V to the donor before procuring the lung and also to the recipient shortly after reperfusion and could prove a significantly enhanced graft function and an improved oxygenation. A mechanistic explanation for the observed benefits was that Diannexin is designed to shield phosphatidylserine, to prevent cell adhesion, to improve blood flow and to diminish subsequent tissue injury (Hashimoto et al., 2016). Practically, authors concluded to employ this compound at an early phase after transplantation to the recipient.

The group around Chatterjee, Christy and Fisher, all renowned scientists in shear stress-related mechanosignaling research in lung ischemia provided an excellent review article showing that the mechanosignaling cascade during lung IR injury is initiated by a mechanosensing complex, transmitted by endothelial cell membrane depolarization due to closure of KATP (ATP-sensitive potassium channels) channels, resulting in activation of NADPH oxidase, NOX2 with generation of ROS and increased intracellular $Ca2^{+}$ (Chatterjee et al., 2014). Authors point to an approach to prevent the mechanosignaling cascade by using a KATP channel agonist to prevent endothelial cell membrane depolarization. Although these agents are available for this purpose, they have not yet been trialed clinically (Chatterjee et al., 2014).

Viruses are used since long as gene delivery vectors to treat diseases by therapeutic gene expression (Waehler et al., 2007) (**Figure 3**). One of the most commonly investigated viral vectors is the adeno-associated virus. As an immunotherapeutic approach, McConnell et al. (2014) took advantage of such a virus as a "trojan horse" that delivers silicon microparticles into inflammation-associated endothelium where it is internalized and subsequently releases therapeutic nanoparticles. The virus than becomes free within the cytoplasm undergoing genetic cargo to successfully transfer into the nucleus for transcription. This kind of uptake is independent from cell receptors, enabling access to not only endothelial cells. Authors, thus, showed that whole organs can be genetically modified using this particle platform as a technique for improving organ or vessel transplant.

But also a non-viral gene transfer approach for the preservation of IR-injured endothelium is possible and, beyond that, provides several advantages over the commonly used viral systems, such as lower immunogenicity, reduced inflammation, and an overall better safety. Using this approach, Liu and colleagues analyzed the role of Indoleamine-2,3-dioxygenase (IDO) as a cytosolic enzyme possessing both immune modulating and antioxidant properties against lung transplant IR injury (**Figure 3**). They delivered a human IDO (hIDO)-expressing plasmid driven by an endothelial cell-specific endothelin-1 promoter into rat donor lungs and found that hIDO expression specifically enhanced in endothelial cells within lung grafts and prevented endothelial cell apoptosis, reduced vascular permeability and leukocyte extravasation *in vivo* (Liu et al., 2019). *In vitro*, they showed that increased IDO activity in endothelial cells protected its mitochondrial function and ultrastructure from

oxidative stress through stabilization of the intracellular redox status (Liu et al., 2019) (**Figure 3**). Authors, thus, presented a strategy of non-viral gene transfer for the protection of lung endothelium, at the same time avoiding the toxic effects of a traditional viral therapy.

Another promising treatment tool is siRNA (**Figure 2**). By using this highly specific technology, an organ-specific gene transfer can be achieved even without the need of viral vectors or other transfection agents. Zhang et al. (2004) showed that by intranasal delivery of siRNA into mouse IR-injured endothelial cells, apoptosis can be attenuated via an overexpression of Heme oxygenase-1 (HO-1), an important cytoprotective enzyme in IR injury. This concept contributes to the identification of genes that modulate IR-induced apoptosis with potential therapeutic relevance. siRNA was also used to target adhesion molecules in an *in vitro* work by Walker et al. (2011). They transfected human lung microvascular endothelial cells with specific siRNA and found that not only adhesion molecules on the endothelium were decreased but also the adhering neutrophils were diminished (Walker et al., 2011) (**Figure 2**).

Another drug delivery system to target IR-injury–mediated reactive oxygen species in the vascular endothelium are liposomes. Howard et al. (2014) designed endothelial-targeted liposomes carrying a potent superoxide dismutase (SOD)/catalase mimetic, EUK-134, antibody-targeted against PECAM. The Ab/EUK/liposome conjugates bound to endothelial cells and inhibited cytokine-induced inflammatory activation *in vitro* (**Figure 2**); *in vivo*, they accumulated in lungs after intravascular injection and protected against pulmonary edema in endotoxin-challenged mice (Howard et al., 2014). The advantage of this compound is that it is already in clinical use.

Oxidized phospholipids are known to enhance the endothelial barrier by maintaining the endothelial cell-cell junctions. Such a compound, OxPAPC, was shown to directly bind to different cytoskeletal proteins thereby stabilizing the cytoskeletal reorganization and endothelial cell barrier enhancement and, thus, the vascular integrity (Birukova et al., 2014).

SUMMARY AND CONCLUSION

Maintenance of the integrity of the pulmonary vascular endothelium is pivotal in order to protect from IR injury in lung transplantation. A number of therapeutic strategies with strong impact have been developed, among them are mediators against ROS and inhibition of endothelial-related adhesion molecules to mainly attenuate neutrophil transmigration into the pulmonary tissue. But also very promising recent approaches, e.g., the stabilization of the endothelial glycocalyx seems to be important as this layer is the prominent interface between the blood stream, its constituents, and the vascular endothelium. On the other hand, novel developments such as the concept of the inhibition of endothelial autophagy are promising, but need more experimental work in order to gain solid scientific evidence. Finally, viral as well as non-viral strategies and siRNA treatment approaches are emerging and seem fascinating. At the same time, they have fewer side effects in contrast to immunotargeting approaches. While the concept of liposome release is already in clinical use, the majority of the other approaches did not translate into clinics up to now. We can only speculate why these approaches did not reach clinical application. One reason is certainly that there is a clear need for more translational research to clarify a definite role for these therapeutic tools in endothelial preservation. Another reason could lie in the fact that there is more support needed from respective pharmacological industrial partners to apply these measures broadly into the clinic. The future, in my eyes, lies in making major efforts in the prevention of the initiating damaging effects of IR injury such as preserving the glycocalyx, rather than the treatment of the endothelium that is already IR-injured. The impact of lung endothelium IR-injury on the development and incidence of transplant rejection and overall transplant outcome is undoubted, therefore, major efforts need to be taken to strengthen those promising experimental therapeutic approaches and translate them into clinical trials.

AUTHOR CONTRIBUTIONS

The author confirms being the sole contributor of this work and has approved it for publication.

ACKNOWLEDGMENTS

Special thanks are owed to Carol De Simio-Hilton for her valuable support in creating the artwork.

REFERENCES

Abassi, Z., Armaly, Z., and Heyman, S. N. (2020). Glycocalyx Degradation in Ischemia-Reperfusion Injury. *Am. J. Pathol.* 190, 752–767. doi: 10.1016/j.ajpath.2019.08.019

Allen, T. C., and Kurdowska, A. (2014). Interleukin 8 and acute lung injury. *Arch. Pathol. Lab Med.* 138, 266–269. doi: 10.5858/arpa.2013-0182-ra

Atochina, E. N., Muzykantov, V. R., Al-Mehdi, A. B., et al. (1997). Normoxic lung ischemia/reperfusion accelerates shedding of angiotensin converting enzyme from the pulmonary endothelium. *Am. J. Respir. Crit. Care Med.* 156, 1114–1119. doi: 10.1164/ajrccm.156.4.96-12116

Birukova, A. A., Singleton, P. A., Gawlak, G., et al. (2014). GRP78 is a novel receptor initiating a vascular barrier protective response to oxidized phospholipids. *Mol. Biol. Cell* 25, 2006–2016. doi: 10.1091/mbc.e13-12-0743

Brettner, F., von Dossow, V., and Chappell, D. (2017). The endothelial glycocalyx and perioperative lung injury. *Curr. Opin. Anaesthesiol.* 30, 36–41.

Casanova, J., Simon, C., Vara, E., et al. (2016). Sevoflurane anesthetic preconditioning protects the lung endothelial glycocalyx from ischemia reperfusion injury in an experimental lung autotransplant model. *J. Anesth.* 30, 755–762. doi: 10.1007/s00540-016-2195-0

Chappell, D., Dorfler, N., Jacob, M., et al. (2010). Glycocalyx protection reduces leukocyte adhesion after ischemia/reperfusion. *Shock* 34, 133–139. doi: 10.1097/shk.0b013e3181cdc363

Chatterjee, S., Nieman, G. F., Christie, J. D., and Fisher, A. B. (2014). Shear stress-related mechanosignaling with lung ischemia: lessons from basic research can inform lung transplantation. *Am. J. Physiol. Lung Cell Mol. Physiol.* 307, L668–L680.

Christofidou-Solomidou, M., Scherpereel, A., Wiewrodt, R., et al. (2003). PECAM-directed delivery of catalase to endothelium protects against pulmonary vascular oxidative stress. *Am. J. Physiol. Lung Cell Mol. Physiol.* 285, L283–L292.

Demertzis, S., Langer, F., Graeter, T., et al. (1999). Amelioration of lung reperfusion injury by L- and E- selectin blockade. *Eur. J. Cardiothorac. Surg.* 16, 174–180. doi: 10.1016/s1010-7940(99)00206-7

Hashimoto, K., Kim, H., Oishi, H., et al. (2016). Annexin V homodimer protects against ischemia reperfusion-induced acute lung injury in lung transplantation. *J. Thorac. Cardiovasc. Surg.* 151, 861–869. doi: 10.1016/j.jtcvs.2015.10.112

Howard, M. D., Greineder, C. F., Hood, E. D., and Muzykantov, V. R. (2014). Endothelial targeting of liposomes encapsulating SOD/catalase mimetic EUK-134 alleviates acute pulmonary inflammation. *J. Control Release* 177, 34–41. doi: 10.1016/j.jconrel.2013.12.035

Janmaat, M. L., Heerkens, J. L., de Bruin, A. M., et al. (2010). Erythropoietin accelerates smooth muscle cell-rich vascular lesion formation in mice through endothelial cell activation involving enhanced PDGF-BB release. *Blood* 115, 1453–1460. doi: 10.1182/blood-2009-07-230870

Kawut, S. M., Okun, J., Shimbo, D., et al. (2009). Soluble p-selectin and the risk of primary graft dysfunction after lung transplantation. *Chest* 136, 237–244. doi: 10.1378/chest.08-2697

Kim, H. J., Kim, E., Baek, S. H., et al. (2018). Sevoflurane did not show better protective effect on endothelial glycocalyx layer compared to propofol during lung resection surgery with one lung ventilation. *J. Thorac. Dis.* 10, 1468–1475. doi: 10.21037/jtd.2018.03.44

Kozower, B. D., Christofidou-Solomidou, M., Sweitzer, T. D., et al. (2003). Immunotargeting of catalase to the pulmonary endothelium alleviates oxidative stress and reduces acute lung transplantation injury. *Nat. Biotechnol.* 21, 392–398. doi: 10.1038/nbt806

Lam, F. W., Da, Q., Guillory, B., and Cruz, M. A. (2018). Recombinant Human Vimentin Binds to P-Selectin and Blocks Neutrophil Capture and Rolling on Platelets and Endothelium. *J. Immunol.* 200, 1718–1726.

Levine, A. J., Parkes, K., Rooney, S. J., and Bonser, R. S. (2002). The effect of adhesion molecule blockade on pulmonary reperfusion injury. *Ann. Thorac. Surg.* 73, 1101–1106. doi: 10.1016/s0003-4975(01)03380-x

Liu, W. C., Chen, S. B., Liu, S., et al. (2019). Inhibition of mitochondrial autophagy protects donor lungs for lung transplantation against ischaemia-reperfusion injury in rats via the mTOR pathway. *J. Cell Mol. Med.* 23, 3190–3201. doi: 10.1111/jcmm.14177

McConnell, K. I., Rhudy, J., Yokoi, K., et al. (2014). Enhanced gene delivery in porcine vasculature tissue following incorporation of adeno-associated virus nanoparticles into porous silicon microparticles. *J. Control Release* 194, 113–121. doi: 10.1016/j.jconrel.2014.08.020

Moore, T. M., Khimenko, P., Adkins, W. K., et al. (1985). Adhesion molecules contribute to ischemia and reperfusion-induced injury in the isolated rat lung. *J. Appl. Physiol.* 1995, 2245–2252. doi: 10.1152/jappl.1995.78.6.2245

Muller, W. A. (2016). Transendothelial migration: unifying principles from the endothelial perspective. *Immunol. Rev.* 273, 61–75. doi: 10.1111/imr.12443

Muzykantov, V. R. (2000). 14 immunotargeting of catalase to the pulmonary vascular endothelium. *Methods Mol. Med.* 25, 241–254. doi: 10.1385/1-59259-075-6:241

Nowak, K., Hanusch, C., Nicksch, K., et al. (2010). Pre-ischaemic conditioning of the pulmonary endothelium by immunotargeting of catalase via angiotensin-converting-enzyme antibodies. *Eur. J. Cardiothorac. Surg.* 37, 859–863. doi: 10.1016/j.ejcts.2009.10.029

Nowak, K., Kolbel, H. C., Metzger, R. P., et al. (2013). Immunotargeting of the pulmonary endothelium via angiotensin-converting-enzyme in isolated ventilated and perfused human lung. *Adv. Exp. Med. Biol.* 756, 203–212. doi: 10.1007/978-94-007-4549-0_26

Nowak, K., Weih, S., Metzger, R., et al. (2007). Immunotargeting of catalase to lung endothelium via anti-angiotensin-converting enzyme antibodies attenuates ischemia-reperfusion injury of the lung in vivo. *Am. J. Physiol. Lung. Cell Mol. Physiol.* 293, L162–L169.

Pickford, M. A., Green, C. J., Sarathchandra, P., and Fryer, P. R. (1990). Ultrastructural changes in rat lungs after 48 h cold storage with and without reperfusion. *Int. J. Exp. Pathol.* 71, 513–528.

Porteous, M. K., and Lee, J. C. (2017). Primary Graft Dysfunction After Lung Transplantation. *Clin. Chest Med.* 38, 641–654.

Preissler, G., Loehe, F., Huff, I. V., et al. (2011). Targeted endothelial delivery of nanosized catalase immunoconjugates protects lung grafts donated after cardiac death. *Transplantation* 92, 380–387. doi: 10.1097/tp.0b013e318226bc6b

Rancan, L., Simon, C., Sanchez Pedrosa, G., et al. (2018). Glycocalyx Degradation after Pulmonary Transplantation Surgery. *Eur. Surg. Res.* 59, 115–125. doi: 10.1159/000489492

Roberts, A. M., Ovechkin, A. V., Mowbray, J. G., et al. (2004). Effects of pulmonary ischemia-reperfusion on platelet adhesion in subpleural arterioles in rabbits. *Microvasc. Res.* 67, 29–37. doi: 10.1016/j.mvr.2003.09.003

Scalia, R., Armstead, V. E., Minchenko, A. G., and Lefer, A. M. (1999). Essential role of P-selectin in the initiation of the inflammatory response induced by hemorrhage and reinfusion. *J. Exp. Med.* 189, 931–938. doi: 10.1084/jem.189.6.931

Sharma, A. K., Charles, E. J., Zhao, Y., et al. (2018). Pannexin-1 channels on endothelial cells mediate vascular inflammation during lung ischemia-reperfusion injury. *Am. J. Physiol. Lung Cell Mol. Physiol.* 315, L301–L312.

Shuvaev, V. V., and Muzykantov, V. R. (2011). Targeted modulation of reactive oxygen species in the vascular endothelium. *J. Control Release* 153, 56–63. doi: 10.1016/j.jconrel.2011.03.022

Soroush, F., Tang, Y., Zaidi, H. M., et al. (2018). PKCdelta inhibition as a novel medical countermeasure for radiation-induced vascular damage. *FASEB J.* 2018: fj201701099.

Waehler, R., Russell, S. J., and Curiel, D. T. (2007). Engineering targeted viral vectors for gene therapy. *Nat. Rev. Genet.* 8, 573–587.

Walker, T., Siegel, J., Nolte, A., et al. (2011). Small interfering RNA efficiently suppresses adhesion molecule expression on pulmonary microvascular endothelium. *J. Nucleic. Acids* 2011:694789.

Yang, Y., and Schmidt, E. P. (2013). The endothelial glycocalyx. *Tissue Barriers* 1:e23494.

Zhang, D., Li, C., Zhou, J., et al. (2015). Autophagy protects against ischemia/reperfusion-induced lung injury through alleviating blood-air barrier damage. *J. Heart Lung Transplant.* 34, 746–755. doi: 10.1016/j.healun.2014.12.008

Zhang, J., Wang, J. S., Zheng, Z. K., et al. (2013). Participation of autophagy in lung ischemia-reperfusion injury in vivo. *J. Surg. Res.* 182, e79–e87.

Zhang, X., Shan, P., Jiang, D., et al. (2004). Small interfering RNA targeting heme oxygenase-1 enhances ischemia-reperfusion-induced lung apoptosis. *J. Biol. Chem.* 279, 10677–10684. doi: 10.1074/jbc.m312941200

Zhu, M., Wang, L., Yang, J., et al. (2019). Erythropoietin Ameliorates Lung Injury by Accelerating Pulmonary Endothelium Cell Proliferation via Janus Kinase-Signal Transducer and Activator of Transcription 3 Pathway After Kidney Ischemia and Reperfusion Injury. *Transplant. Proc.* 51, 972–978. doi: 10.1016/j.transproceed.2019.01.059

Conflict of Interest: The author declares that the research was conducted in the absence of any commercial or financial relationships that could be construed as a potential conflict of interest.

frontiers in Physiology

REVIEW
published: 05 January 2021
doi: 10.3389/fphys.2020.511799

The Effect of Inflammation on Bone

Scott Epsley[1†], Samuel Tadros[2], Alexander Farid[2], Daniel Kargilis[2], Sameer Mehta[3] and Chamith S. Rajapakse[2]*

[1] Philadelphia 76ers, Philadelphia, PA, United States, [2] Department of Radiology and Orthopaedic Surgery, University of Pennsylvania, Philadelphia, PA, United States, [3] Orlando Magic, Orlando, FL, United States

Bone remodeling is the continual process to renew the adult skeleton through the sequential action of osteoblasts and osteoclasts. Nuclear factor RANK, an osteoclast receptor, and its ligand RANKL, expressed on the surface of osteoblasts, result in coordinated control of bone remodeling. Inflammation, a feature of illness and injury, plays a distinct role in skewing this process toward resorption. It does so via the interaction of inflammatory mediators and their related peptides with osteoblasts and osteoclasts, as well as other immune cells, to alter the expression of RANK and RANKL. Such chemical mediators include TNFα, glucocorticoids, histamine, bradykinin, PGE2, systemic RANKL from immune cells, and interleukins 1 and 6. Conditions, such as periodontal disease and alveolar bone erosion, aseptic prosthetic loosening, rheumatoid arthritis, and some sports related injuries are characterized by the result of this process. A thorough understanding of bone response to injury and disease, and ability to detect such biomarkers, as well as imaging to identify early structural and mechanical property changes in bone architecture, is important in improving management and outcomes of bone related pathology. While gut health and vitamin and mineral availability appear vitally important, nutraceuticals also have an impact on bone health. To date most pharmaceutical intervention targets inflammatory cytokines, although strategies to favorably alter inflammation induced bone pathology are currently limited. Further research is required in this field to advance early detection and treatments.

Keywords: bone, inflammation, osteoblasts, osteoclasts, cytokines

OPEN ACCESS

Edited by:
Silvia Lacchini,
University of São Paulo, Brazil

Reviewed by:
Stuart Warden,
Indiana University, Purdue University Indianapolis, United States
Craig Purdam,
La Trobe University, Australia

****Correspondence:***
Chamith S. Rajapakse
chamith@mail.med.upenn.edu

†Present address:
Scott Epsley,
Private Consultant, Washington, DC, United States

Specialty section:
This article was submitted to Vascular Physiology, a section of the journal Frontiers in Physiology

Received: *13 November 2019*
Accepted: *30 November 2020*
Published: *05 January 2021*

Citation:
Epsley S, Tadros S, Farid A, Kargilis D, Mehta S and Rajapakse CS (2021) The Effect of Inflammation on Bone. Front. Physiol. 11:511799. doi: 10.3389/fphys.2020.511799

Abbreviations: RANK, receptor activator of nuclear factor-kappa B; RANKL, RANK ligand; TNFα, tumor necrosis factor alpha; PGE2, prostaglandin E2; OPG, osteoprotegerin; M-CSF, macrophage colony-stimulating factor; MMPs, matrix metalloproteinases; IL, interleukin; MCP 1, monocyte chemoattractant protein 1; COX2, cyclooxygenase-II; GM-SF, granulocyte macrophage-colony stimulating factor; VIP, vasoactive intestinal peptide; MRI, magnetic resonance imaging; uCT, micro-computed tomography; UTE MRI, ultrashort echo time MRI; PET, positron emission tomography; TRAF6, TNF receptor-associated factor 6; NF-kB, nuclear factor kappa-light-chain-enhancer of activated B cells; NFAT, nuclear factor of activated T-cells; Th17, T-helper cell 17; DKK1, dickkopf WNT signaling pathway inhibitor 1; IFN-gamma, interferon gamma; TGB-beta, transforming growth factor beta; IGF-1, insulin-like growth factor 1; AS, ankylosing spondylitis; MTSS, medial tibial stress syndrome; RA, rheumatoid arthritis; BME, bone marrow edema; VDR, vitamin D receptor; GM, gut microbiota; NCDs, non-communicable human diseases; GLP-1, glucagon-like peptide-1; CTX, C-terminal telopeptide; GIP, glucose dependent insulinotropic polypeptide; miRNAs, Micro Ribonucleic Acids; VMH, ventromedial hypothalamus; CNO, chronic non-bacterial osteomyelitis; FDG-PET, fluorodeoxyglucose-positron emission tomography; CRP, C-reactive protein; BMD, bone mineral density.

INTRODUCTION

Inflammation is generally understood to promote resorption in bone (Boyce et al., 2005; Tanaka et al., 2005; Hardy and Cooper, 2009). A number of local and systemic mechanisms, particularly those involving inflammatory cytokines, have been elucidated (Adamopoulos, 2018). Inflammatory signaling pathways and chemical messengers that participate in bone remodeling will be discussed in depth, as well as a review of the OPG/RANKL system that regulates bone remodeling.

Much has been learned from studying the effects of periodontitis on alveolar bone loss in contributing to our understanding of immune and inflammatory mediated pathways in bone remodeling (Hienz et al., 2015), as has research into bone erosion secondary to rheumatoid arthritis (Wong et al., 2006). However, there is a paucity of information on the effects of local inflammation in the appendicular skeleton. A theoretical framework for the link between local inflammation and bone changes, termed here as the Outside-In and Inside-Out models, will be presented using an exertional leg pain model and drawing on what is already known about rheumatoid induced bone erosion.

Gastrointestinal mechanisms in inflammatory auto-immune disease that impact nutritional state and nutrient absorption have also been implicated. We will touch on the effects of calcium and vitamin D on bone health, as well as introduce the Gut-Bone Axis concept that has gained significant attention in recent years. Various nutraceuticals with evidence for impacting bone turnover will be explored.

Despite this knowledge, identification and targeted interventions for inflammatory induced bone resorption remain limited. The role of radiologic testing and blood chemistry markers in monitoring bone in inflammatory states will be reviewed in the context that an improved understanding of these mechanisms and early detection may lead to earlier intervention and improved patient outcomes. This paper seeks to raise clinician awareness and the need for further research to advance this area.

BONE AND ITS REMODELING

Bone remodeling is a continuous process that renews the adult skeleton. It is distinct from bone modeling which is responsible for skeletal development, growth, and the shaping of bones, by the coordinated sequential action of osteoblasts and osteoclasts (Langdahl et al., 2016). The process is regulated both locally and systemically and is characterized by a resorption period lasting 30–40 days, and a formation period as long as 150 days (Eriksen, 2010). This cellular coordination is carried out by basic multicellular units (BMUs) (Khosla, 2001; Jilka, 2003) and forms resorption pits or lacunae (Everts et al., 2002; Eriksen, 2010). Bone lining cells then remove remaining collagen prior to new collagen matrix deposition and filling of the lacunae with new bone (Everts et al., 2002).

Bone remodeling is mediated by osteoclasts, osteoblasts, bone lining cells and osteocytes. Osteoclasts are large multiple nucleated cells that are responsible for breaking down bone tissue. They digest bone mineral by creating an acid compartment by acting as a proton pump and then release proteases, such as Tartrate-resistant Acid Phosphatase (TRAP) to degrade both inorganic and bone components, respectively (Boyle et al., 2003; Halleen et al., 1999; Owen and Reilly, 2018). Osteoclasts arise from hematopoeitc progenitors as osteoclast pre-cursors (Jilka, 2003) and are chemotactically attracted to resorption sites, where they fuse into mature osteoclasts (Pfeilschifter et al., 1989). Bone lining cells then remove any remaining debris via matrix metalloproteinases (MMP's) (Everts et al., 2002). Various chemotactic agents including Parathyroid Hormone (PTH), TNFα, and Prostaglandin E2 (PGE2) upregulate RANKL expression which binds to its receptor RANK on osteoclast pre-cursors, leading to fusion and mature osteoclast formation (Roux and Orcel, 2000). RANKL is a Tumor Necrosis Factor (TNF) related ligand expressed on the surface membrane of osteoblasts that regulate their function (Roux and Orcel, 2000; Khosla, 2001). Osteoblasts are cells that work to synthesis bone. During bone formation, osteoblasts work as a group of connected cells within a functional unit called the osteon. Osteoblasts originate as mesenchymal stem cells (Jilka, 2003). Osteocytes are cells that originate from osteoblasts and become lodged in mineralized bone matrix. They participate in formation of bone, and the maintenance of matrix. Osteocyte apoptosis has been associated with bone fatigue, microcracks, and osteoclastic resorption indicative of early bone remodeling (Verborgt et al., 2000).

The attraction of pre-osteoclasts to a remodeling site is also chemotactically controlled by the osteoblast. Macrophage Colony Stimulating Factor (M-CSF) and Monocyte Chemoattractant Protein 1 (MCP 1) is secreted by osteoblasts in response to cytokines, such as TNFα and IL-1 and attracts osteoclast pre-cursors to the area (Graves et al., 1999). Various other important bone proteins include Osteoprotegerin (OPG) which binds to the RANK ligand (RANKL), blocking its interaction with RANK on the osteoclast pre-cursor cell, thereby inhibiting mature osteoclast formation (Roux and Orcel, 2000; Khosla, 2001; Boyce and Xing, 2008). Proteases released by resorbing osteoclasts activate transforming growth factor beta-1. (TGF-β1). TGF-β1 attracts osteoblasts and enhances proliferation and differentiation, proteoglycan synthesis, and type II collagen production. Thus, the process of resorption and formation is closely coupled to maintain bone homeostasis (Janssens et al., 2005).

INFLAMMATORY FACTORS THAT PARTICIPATE IN BONE REMODELING

Inflammatory cytokines, including interleukins (IL), IL-1, IL-6, and TNFα, have been found to have a significant effect on the bone remodeling process, mostly driving the system in the direction of resorption. Various neuropeptides have also been implicated.

Described below are some of the participants of inflammation signaling that also facilitate the bone remodeling processes:

Cytokines

As well as stimulating M-CSF and MCP-1 to attract osteoclasts, TNFα and IL-1 stimulate the activity of mature osteoclasts, and attract other monocytes (Pfeilschifter et al., 1989). Macrophages between bone lining cells of the endosteum and periosteum have been shown to release TNFα (Chang et al., 2008). Furthermore, TNFα promotes systemic RANKL production by lymphocytes and endothelial cells (Boyce et al., 2005), while IL-1 acts on osteoblasts to induce Prostaglandin E2 (PGE2) synthesis, both indirectly inducing osteoclast formation. IL-1 also has an effect on RANKL expression that appears dependent on PGE2 (Miyaura et al., 2003; Tanaka et al., 2005). TNFα and prostaglandins play a pivotal role in osteoclast maturation. Osteoclast precursors require TNFα in the presence of small amounts of RANKL in order to differentiate into mature osteoclasts (Lam et al., 2000). Furthermore, when prostaglandin production is inhibited in cyclooxygenase-II (COX2) knockout mice, upregulation of Granulocyte Macrophage-Colony Stimulating Factor (GM-SF) occurs which inhibits osteoclast formation from pre-cursors (Tanaka et al., 2005). The use of a TNFα inhibitor (Etanercept), when combined with Methotrexate, were shown to reduce radiographic disease progression in those with rheumatoid arthritis despite high circulating inflammatory markers. This would imply that TNFα, independent of other systemic factors, has a significant effect on bone resorption, and that it may be possible to interrupt this process (Landewe et al., 2006).

IL-6 concentrations have been found to correlate with levels of joint erosion in rheumatoid arthritis sufferers, indicating a role in bone resorption (Kotake et al., 1996). Much like other inflammatory cytokines, it acts on osteoblasts and T-lymphocytes to increase RANKL production. In experimentally induced arthritis, IL-6 deficient mice show significantly less bone erosion (Wong et al., 2006). Much like IL-1, IL-6 also induces PGE2 production (Liu et al., 2005).

Mast Cells

Mast cells may also contribute to the release of IL-6 and TNFα (Konttinen et al., 1996). They have further been implicated in studies investigating the effects of histamine 1 and histamine 2 receptor antagonists, in which they were shown to decrease the size of the osteoclast population (Dobigny and Saffar, 1997). This would suggest that mast cells are intricately linked with the osteoclastic bone resorption cascade.

Neuropeptides

Neuropeptides have been implicated in bone resorption. Bradykinin, a vasoactive peptide with effects on vessel permeability and associated with inflammation, was found to stimulate the release of calcium from mice bones 24 h after administration. This process was inhibited by non-steroidal anti-inflammatories. Combined with the delayed response it is thought that bradykinin acts in bone resorption by mediating prostaglandin synthesis (Lerner et al., 1987). Other neuropeptides, such as Substance P and Vasoactive Intestinal Peptide (VIP) may also contribute to bone resorption (Konttinen et al., 1996).

SIGNALING PATHWAYS THAT LEAD TO BONE LOSS

A relationship between inflammation and bone disease has been observed in a variety of clinical and laboratory settings, but the pathophysiology underlying this has yet to be fully appreciated. Diseases, such as chronic joint diseases, inflammatory bowel disease, lung inflammation, and renal diseases share many of the same mechanisms that can lead to bone loss, driven by immune signals that can tip the balance of bone homeostasis toward bone resorption (Hardy and Cooper, 2009). The bone remodeling cycle refers to this coordinated process, described earlier as osteoclasts removing bone at the microscopic level and osteoblasts replacing this matrix which ultimately re-mineralizes. The link between inflammation and the signaling pathways involved in this process will now be outlined.

OPG/RANKL System

One of the major breakthroughs in understanding bone homeostasis at the molecular level was the discovery of the OPG/RANKL system. Osteoblasts express RANKL on their cell surface, the expression of which is upregulated in response to proinflammatory cytokines, glucocorticoids, estrogen deficiency and hyperparathyroidism (Hofbauer et al., 2000). RANKL then binds to the RANK receptor on the surface of osteoclasts and their precursors. Osteoprotegerin (OPG) is produced by osteoblasts and B lymphocytes and inhibits osteoclastogenesis. It acts as a decoy receptor, binding with RANKL to block its activation with RANK (Chen et al., 2018). Osteoclast precursors are cells that express a monocyte lineage marker (usually CD14, the M-CSF receptor, or CD11b) as well as RANK. The binding of RANKL to RANK induces a series of signal transduction pathways mediated through TNF receptor-associated factor 6 (TRAF6), which includes Nuclear Factor kappa-light-chain-enhancer of activated B cells (NF-kB) and Nuclear factor of activated T-cells (NFAT), that initiates the differentiation of the early osteoclast progenitor into a preosteoclast. Continued stimulation promotes the fusion of these preosteoclasts into the mature, multinucleated bone resorbing osteoclasts which can be recognized by any number of molecular markers (Weitzmann, 2013). Thus, balancing RANKL and OPG determines bone homeostasis, and if there will be net bone formation or resorption (Agrawal et al., 2011). Inflammatory cytokines like IL-1, TNF-α, and M-CSF have previously been shown to have associations with osteoclastic bone loss, by either promoting RANKL production by bone marrow stromal cells (osteoblast precursors) or mature osteoblasts (Hofbauer et al., 1999); by reducing OPG production (Weitzmann et al., 2002); or by promoting RANK on osteoclast precursors and thereby increasing their sensitivity to RANKL (Arai et al., 1999).

TNF-a has a particularly potent osteoclastic effect, likely due to the fact that RANKL is itself a TNF-superfamily member and functions through many of the same signal transduction pathways that TNF-a induces. TNF-a has been shown to act

synergistically with IL-1 to upregulate RANKL expression on stromal cells and cause osteoclastogenesis (Wei et al., 2005). Against the background of inflammation, other cell types can supply RANKL in addition to stromal cells and osteoblasts. These include lymphocytes and fibroblasts, which constitute a large portion of the cells present in an inflamed synovium. The presence of this non-osteoblastic RANKL stimulates osteoclastogenesis independent of osteoblastic negative feedback, likely playing a role in the observed pathology. The recently identified T-helper cell 17 (Th17) subset of T-cells, which secrete the particularly osteoclastic cytokine IL-17, have been observed in inflammatory arthritis, and may explain the bone destruction that is commonly seen in that disease (Lundy et al., 2007).

Not all inflammatory cytokines demonstrate this effect. Some cytokines, such as IL-4, IFN-gamma, and TFG-β, have an inhibitory effect on osteoclastogenesis (Lorenzo et al., 2008). In the setting of bone disease however, the effect of these inhibitory cytokines is outweighed by those favoring osteoclastogenesis and the balance skews in favor of resorption. Another hypothesis is that osteoclastic cytokines can uncouple bone formation from bone resorption. Some studies have found that TNF-a can disrupt the differentiation of osteoblasts (Gilbert et al., 2000), and the presence of inflammatory cells may directly interrupt the signaling that couples these two processes, although the details of how this happens remains to be elucidated completely. A likely mechanism involves proteins synthesized by Wingless (Wnt) genes that mediate osteoblastogenesis. TNFα has been shown to upregulate production of Dickkopf-1 (DKK-1) which bind to and block Wnt receptors LPR5/6, suppressing osteoblast development. This system is integrated with the RANKL/OPG system whereby increased circulating levels of DKK-1 decreased levels of OPG, ultimately leading to bone resorption, and DKK-1 inhibition has been shown to increase OPG levels (Diarra et al., 2007; Baker-LePain et al., 2011).

Glucocorticoid Signaling

It is also worth mentioning the role of glucocorticoids in bone diseases. Glucocorticoid excess has a negative impact on bone by uncoupling bone formation from resorption. Glucocorticoids downregulate a number of important signaling pathways in osteoblasts, especially the IGF-1 and WNT signaling pathways (Wang et al., 2008), and also decrease osteoblast proliferation and osteoblast specific protein production (Eijken et al., 2006). Glucocorticoid excess can also lead to inappropriate bone resorption due to decreases in OPG, although long term glucocorticoid use may actually inhibit osteoclast differentiation and thus decrease bone resorption (Weinstein et al., 2002), the dominant effects are thought to be through decreased bone deposition and bone quality (Chiodini et al., 2016). Dexamethasone has been shown to interrupt NF-kB signaling, inhibiting osteoclast maturation, leading to osteopetrosis (Unlap and Jope, 1997).

The role of endogenous glucocorticoids in bone disease is evident from patients with Cushing's syndrome and other pathologies characterized by increased cortisol release who demonstrate a higher prevalence of vertebral fractures. Trabecular bone appears to be more sensitive to the effects of endogenous glucocorticoids than cortical bone (Wetzsteon et al., 2009), with changes in cortical bone equivocal (Chiodini et al., 2016).

While chronic exogenous glucocorticoid therapy is well-known to have deleterious effects on bone health as evidenced by 30–50% increased fracture risk (Canalis et al., 2007), chronic inflammatory disease itself may detrimentally impact bone, with Chronic Obstructive Pulmonary Disease associated with a higher risk of osteoporosis independent of glucocorticoid use (Chen et al., 2015). In fact, treatment of chronic inflammatory disease with glucocorticoids may have a beneficial effect on bone in some cases. Bone mineral density was not correlated to the cumulative dose of corticosteroid therapy in a study of children with Inflammatory Bowel Disease but was inversely related to the cytokine IL-6. This would suggest more research is required to understand the exact way in which glucocorticoids affect bone modeling (Paganelli et al., 2007).

IMMUNOLOGICALLY DRIVEN BONE LOSS PATHOLOGIES

Several pathological models have been utilized to better understand the local tissue inflammatory mediated bone response. Periodontitis, rheumatoid arthritis, and aseptic prosthesis loosening will be discussed below:

Periodontitis

Periodontitis is a dysbiotic disease in which the oral microbiota become dysregulated and lead to an increased risk of systemic inflammatory diseases, such as Rheumatoid arthritis (RA) (Hajishengallis, 2015). There has been increasing interest in understanding the pathophysiology of periodontitis due to its rising prevalence and its potential use as a model to study bone resorption (Hienz et al., 2015). While it is known that both the microbial infection and inflammatory immune responses play a role in bone resorption due to periodontitis, the specific mechanism underlying this has not been clearly defined (Nanci and Bosshardt, 2006; Abusleme et al., 2013). One obstacle in identifying the precise role of the various factors involved is the overlapping nature of their effects. For example, many cytokines have multiple roles throughout the body. The field of osteoimmunology has been helpful in defining the complex interactions between bone, surrounding tissue, and the resulting inflammatory response (Hienz et al., 2015). Bacterial infection of the tissue surrounding and supporting the tooth is also known to trigger an inflammatory response, and it is worth noting that this response is dependent on the specific tissue type and its function (Nanci and Bosshardt, 2006).

Helper T-cells have been implicated in the immunopathogenesis of bone resorption. These cells are generally classified into two subsets; Th1 cells (involved in cell-mediated response to intracellular infection), and Th2 cells (involved in response to extracellular infection). RANKL expression on the surface of Th1 cells has been associated with bone loss in periodontitis (Taubman et al., 2005). Suppression of Th1 cells in rat models have resulted in a decrease in bone resorption and RANKL expression (Valverde et al., 2004).

Interestingly, RANKL-expressing B lymphocytes have been shown to increase bone resorption even in the absence of RANKL-expressing helper T cells (Taubman et al., 2005). Conversely, T cells promote OPG production by B lymphocytes, and thus this interaction between lymphocytes is critical for bone homeostasis (Li et al., 2007).

Rheumatoid Arthritis (RA)

Rheumatoid arthritis (RA) is another systemic inflammatory disease primarily caused by an excess of pro-inflammatory cytokines resulting in inappropriate immune response. The disease is characterized by inflammation of the synovial membrane, surrounding cartilage, and bone (McInnes and Schett, 2007), and affects approximately 1% of people worldwide (Gabriel, 2001).

An autoimmune inflammatory response can last for years before bone and cartilage loss accelerates (Dekkers et al., 2016; Weyand and Goronzy, 2017). Synovial macrophages in RA produce inflammatory cytokines previously described to induce bone resorption including TNF-a, IL-1, and IL-6 (Li et al., 2012). Furthermore, RANKL is expressed in RA synovial fibroblasts (Kim et al., 2007) promoting differentiation of synovial macrophages into osteoclasts (Takayanagi et al., 1997).

The development of the disease has a genetic component, as evidenced by concordance rates of around 15% for monozygotic twins and 3% for dizygotic twins (Silman et al., 1993). It has been proposed that genetic factors may account for as much as 60% of the liability to the disease (MacGregor et al., 2000). There are also significant associations with immunological regulatory genes as demonstrated by genome-wide association study (GWAS) analysis, providing further evidence for a genetic predisposition to developing RA. It has been suggested that the gastrointestinal microbiota plays a role in onset of RA as well (Scher et al., 2010).

While the mechanism of immune response and eventually bone loss are still to be well elucidated it is likely that glucocorticoids play a significant role. As previously stated, glucocorticoids stimulate the process of bone resorption, increase the expression of RANK, and decrease the expression of OPG (Canalis and Delany, 2002). Treatment with glucocorticoids have played a role in the clinical management of patients with RA for some time due to symptomatic relief, however, adverse effects have led to their use in low dosages as a "bridge therapy" to anti-rheumatic drugs (Van Gestel et al., 1995). Also of interest is the relationship between stress and bone resorption for patients with chronic inflammatory diseases. Continual stress is consistently associated with increased inflammation and bone resorption for patients with RA (Straub et al., 2005).

Aseptic Prosthesis Loosening

Several groups have found that it is possible for macrophages themselves to induce a low-grade kind of bone resorption. Aseptic loosening of the prosthetic is one of the major reasons for joint replacement failure. Inflammatory cells, such as foreign-body macrophage polykaryons are known to aggregate at the border of the native bone and cemented prosthesis and can be characterized histologically. The resorptive pits that these cells create can be seen microscopically (Athanasou et al., 1991). Macrophages found in pseudo-synovial tissue surrounding joint replacements have been shown to be accompanied by T-cells and demonstrated high levels of inflammatory cytokines (Perry et al., 1995). RANKL has also been identified in this tissue providing further impetus for osteoclastogenesis and resorption (Horiki et al., 2004).

That macrophages can engage in bone resorptive behavior challenged a previous paradigm that only osteoclasts could resorb bone, although the character of macrophage resorption was noticeably different. Bone resorption done by macrophages is typically low-grade, with fewer pits and smaller diameter. The major implication of this is that anywhere in the body that may excite macrophages, such as areas with a lot of cellular death products, or bacterial and foreign particulate matter, may be prone to low-grade bone resorption. This has to be considered clinically, especially with regard to joint replacements, because this resorption could lead to loosening of the prosthesis (Horowitz and Purdon, 1995).

OUTSIDE IN AND INSIDE OUT MODELS

While there is an established body of literature linking chronic and systemic inflammatory responses to bone resorption, there is paucity with respect to local inflammation. The pathophysiology of conditions, such as medial tibial stress syndrome (MTSS) has been theorized to comprise either a periostitis secondary to fascial traction (Michael and Holder, 1985; Bouché and Johnson, 2007; Stickley et al., 2009) or a distinctly bony etiology characterized by decreased regional bone density and high resolution CT abnormalities (Magnusson et al., 2001; Gaeta et al., 2006).

Histology from biopsies of the painful regions of MTSS patients that failed conservative treatment demonstrated active osteoblasts, inflammatory changes in the crural fascia, and in one case inflammatory infiltrate into the lymphatics of the periosteum (Johnell et al., 1982). Furthermore, inflammatory cells were noted in the fascia of those suffering from chronic exertional compartment syndrome (Barbour et al., 2004). Periosteal osteoblasts have been shown to be sensitive to physiological traction strains, responding with an increased production of PGE2 (Forwood et al., 1998; Jones et al., 1991). Given the established local inflammatory environment, increased PGE2 production from fascial traction, and previously discussed effects of both (Tanaka et al., 2005), it is not inconceivable that a bony response could follow. This model, in which the presence of an inflammatory infiltrate in the local environment inhibits the formation of new bone, has been described as the "outside-in" model. Although induced by an acute local inflammatory response, this is analogous to bone resorption secondary to autoimmune mediated synovial inflammation in RA (Li et al., 2012).

In contradiction to this theory biopsies of 6 symptomatic MTSS patients, only noted one associated bone remodeling front from 3/6 tibiae that exhibited microcracks. However, that signifies a remodeling response in one third of samples exhibiting bone micro-trauma (Winters et al., 2019).

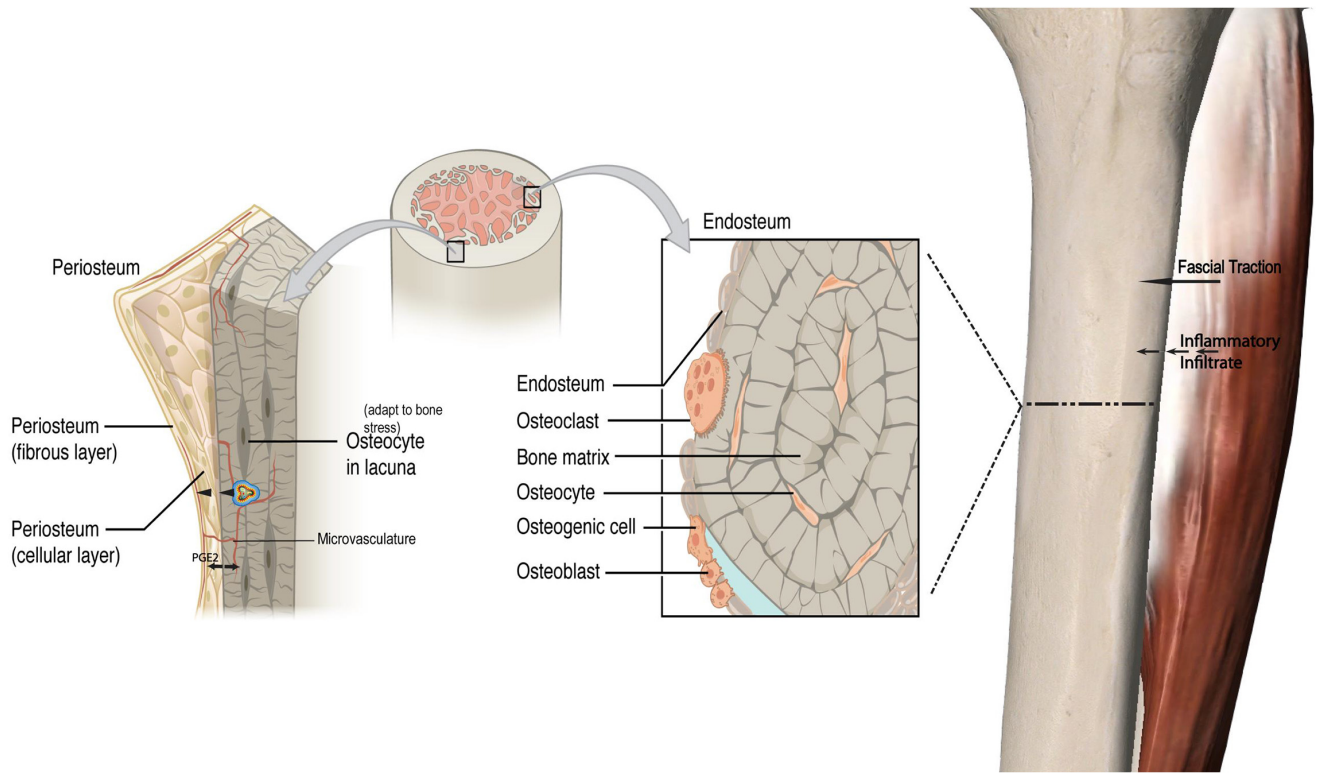

FIGURE 1 | Fascial-bone stress model. A visual framework depicting a proposed pathway of an outside-in model for bone remodeling with a local inflammatory response via fascial traction and resultant bony response with impact on periosteal osteoblasts and increased production of PGE2. Similar to the outside-in model with cascade of inflammatory processes coming from fascial layers into periosteum and endocortex, a proposed inside-out mechanism is illustrated. This load induced bone stress response along with increased vasculature and inflammatory cytokines originating from the endocortex drives periosteal change in addition to crosstalk between the endocortical and periosteal layers. *PGE2* Prostaglandin E2. The cell in cocentric multicolor lines represent an inflammatory cytokine (not to scale). Adapted from https://openstax.org/books/anatomy-and-physiology/pages/6-3-bone-structure.

While an outside-in model for bone remodeling is proposed, this could be extended to an "inside-out" model as well. Transcortical vessels, capillaries in long bones linking the marrow and traversing vertically and horizontally to connect to the periosteum have recently been described. Proliferation of these vessels has been observed within weeks in chronic arthritic bone inflammation (Grüneboom et al., 2019). These vessels express arterial or venous markers and transport neutrophils. Given that periosteal osteoblasts make direct contact with the bone cortex (Squier et al., 1990) and have cytoplasmic projections into the osteoid (Ellender et al., 1988), and that there is now an established vascular connection, this may be a pathway by which chemotactic agents and even monocytes induce periosteal changes secondary to an endocortical response. In keeping with this, mechanical loading has been demonstrated to induce significant and rapid PGE2 release in the metaphysis (Thorsen et al., 1996). This type of response may be represented in non-invasive modalities, such as MRI's where both endocortical and periosteal signal co-exist to represent a bone stress response (Batt et al., 1998). Increased microvasculature density has been correlated with local histological inflammatory changes in facets joints of Ankylosing Spondylitis patients who also demonstrate bone marrow edema, strengthening the argument for a link between endocortical and superficial cortical bone (Appel et al., 2006a). **Figure 1** illustrates the fascial-bone stress model.

NUTRITION, MICROBIOTA, AND BONE HEALTH

In addition to inflammatory processes, nutritional status is also important for bone health. Inflammation and nutritional status are not mutually exclusive. Chronic inflammatory conditions of the gastrointestinal tract are frequently associated with poor nutritional status, largely having to do with a reduction in caloric intake and difficulty in absorbing nutrients important to bone metabolism (Corazza et al., 2005). Moreover, the gut microbiota plays a role in systemic inflammation via the immune system (D'Amelio and Sassi, 2018), and meal ingestion can influence bone remodeling (Villa et al., 2017).

Calcium

Coelic disease is a chronic inflammatory disease of the gastrointestinal tract that can impact the absorption of calcium and vitamin D (Corazza et al., 2005). These nutrients are crucial in maintaining adequate mineralization of bone, and the

body responds to deficiency by increasing parathyroid hormone (PTH) secretion. PTH receptors expressed on osteoblasts provide increased signaling that results in increased RANKL expression. This elevated RANKL increases osteoclastogenesis and leads to bone resorption in order to increase serum calcium levels to compensate for the deficiency. However, if calcium absorption is limited because of impaired gut absorption this cycle will continue. Bone will continue to be resorbed and remineralization will be impaired. As such a lack of calcium and vitamin D can adversely affect bone mineralization independent of the bone remodeling cycle.

Vitamin D

Vitamin D has an additional physiologic role in that it can also modulate the immune system. Vitamin D has demonstrated an anti-inflammatory role in diseases, such as kidney disease, rheumatoid arthritis, and inflammatory bowel disease (Zehnder et al., 2008). Low levels of vitamin D are correlated with a greater degree of inflammation in these conditions. Immune cells have the capacity to convert the precursor to active vitamin D, 25-hydroxyvitamin D, to the active form, 1,25-hydroxyvitamin D (Adams and Hewison, 2008). This active form of vitamin D functions as a steroid hormone and binds to the nuclear vitamin D receptor (VDR), of which there are particularly high levels in macrophages, dendritic cells, and lymphocytes (Mousa et al., 2016). This VDR suppresses the proliferation of lymphocytes and downregulates pro-inflammatory cytokines like TNF-α, IL-1, IL-6, and IL-8, while upregulating IL-10 which is an anti-inflammatory cytokine. VDR also seems to promote the differentiation of monocytes into macrophages and inhibits their ability to secrete inflammatory cytokines and express MHC-II molecules at their surface, thereby reducing their inflammatory profile (Guillot et al., 2010). VDR also appears to downregulate NF-kB, an important proinflammatory transcription factor (Harant et al., 1997). Despite this, supplementation with vitamin D has not been shown to be effective in treating inflammatory diseases in a clinical setting.

It is clear that poor nutrient intake as the result of an inflammatory disease may affect the bone remodeling process as we have just detailed. Other conditions characterized by poor nutrient intake without an inflammatory environment, such as anorexia nervosa display a similar uncoupling of bone formation and resorption (Soyka et al., 1999). The reason for this is not well understood, but at least part of this bone remodeling is governed by central inputs (Karsenty, 2006).

Gut Bone Axis

The gut microbiota (GM) is defined as the whole system of symbiotic and pathogenic microorganisms inhabiting our intestines (Quach and Britton, 2017; Villa et al., 2017; D'Amelio and Sassi, 2018). The GM has a complex relationship with its host aiding in digestion, battling pathogens, and maturation of the immune system in the first years of life. These constant interactions between GM and the host contribute to the variation of gut and systemic immunity throughout life (D'Amelio and Sassi, 2018). However, disturbances in immune homeostasis can serve as a contributing factor for chronic non-communicable human diseases (NCDs) like allergies, asthma, some autoimmune, cardiovascular and metabolic diseases, and neurodegenerative disorders (D'Amelio and Sassi, 2018). Alterations in GM and host interaction has been associated with a possible cause of immune disruption and increased inflammation associated with several NCDs (Peterson et al., 2015).

The GM-Bone axis is defined as the effect of the GM, or the molecules they synthesize, on bone health (Villa et al., 2017). A symbiotic interplay between immune and bone cells, leads the GM to have a central role in maintaining bone health along with influencing bone turnover and density (Mori et al., 2015). GM can improve bone health by increasing calcium absorption and modulating the production of gut serotonin, a molecule that interacts with bone cells and has been suggested to act as a bone mass regulator (D'Amelio and Sassi, 2018). Manipulation of GM with changes in dietary habits, consumption of antibiotics, and probiotic use may positively influence bone health.

Similarly, glucagon-like peptide-1 (GLP-1) is a peptide hormone secreted from entero-endocrine L-cells post meal ingestion (Nissen et al., 2019). In a recent study on healthy, young male and female human subjects, CTX along with other bone markers were analyzed via blood sampling (Nissen et al., 2019). It concluded GLP-1 plays a role in the gut-bone axis since GLP-1 has an inhibitory effect on the bone resorption marker CTX. GLP-1 is known primarily as an insulinotropic hormone and together with glucose dependent insulinotropic polypeptide (GIP), both are responsible for increased insulin secretion after oral ingestion of glucose (Nissen et al., 2019). Bone remodeling can vary daily with a decrease in bone resorption postprandially, whereas the opposite is true when fasting. Thus, GLP-1 contributes to the regulation of bone turnover as part of the gut-bone axis. In summary, the gut-bone axis has become an emerging topic and GM plays a multi-faceted role in bone turnover, modulating the immune system, controlling inflammation, interacting with key hormones, and ensuring appropriate absorption of calcium and vitamin D levels (Quach and Britton, 2017; Villa et al., 2017).

MicroRNA and Bone Remodeling

In addition, the activity of bone cells is controlled by a variety of factors, such as their own intracellular molecular processes. Any impairment of these intracellular processes can affect bone homeostasis. MicroRNAs (miRNAs) are a type of RNA that regulate biological processes, like posttranscriptional intracellular protein expression (Liu et al., 2019; Zhao et al., 2019). Studies have found that miRNA play a key role in mediating osteoblast, osteoclast, and osteocyte activity while any miRNA deregulation can result in impaired bone remodeling (Sugatani and Hruska, 2009; Zhao et al., 2019). Also, the proinflammatory cytokine TNF-a is involved in the pathogenesis of chronic inflammatory diseases and ultimately plays a role in osteoclastic activity (Liu et al., 2019). Suppression of certain miRNAs supports the mechanism to restrain TNF-a induced bone resorption. Relocating to outside the cell, miRNA can also control exosomes serving as intercellular signals to facilitate cell to cell crosstalk among bone cells (Liu et al., 2019). **Figure 2** illustrates the integrated inflammatory model.

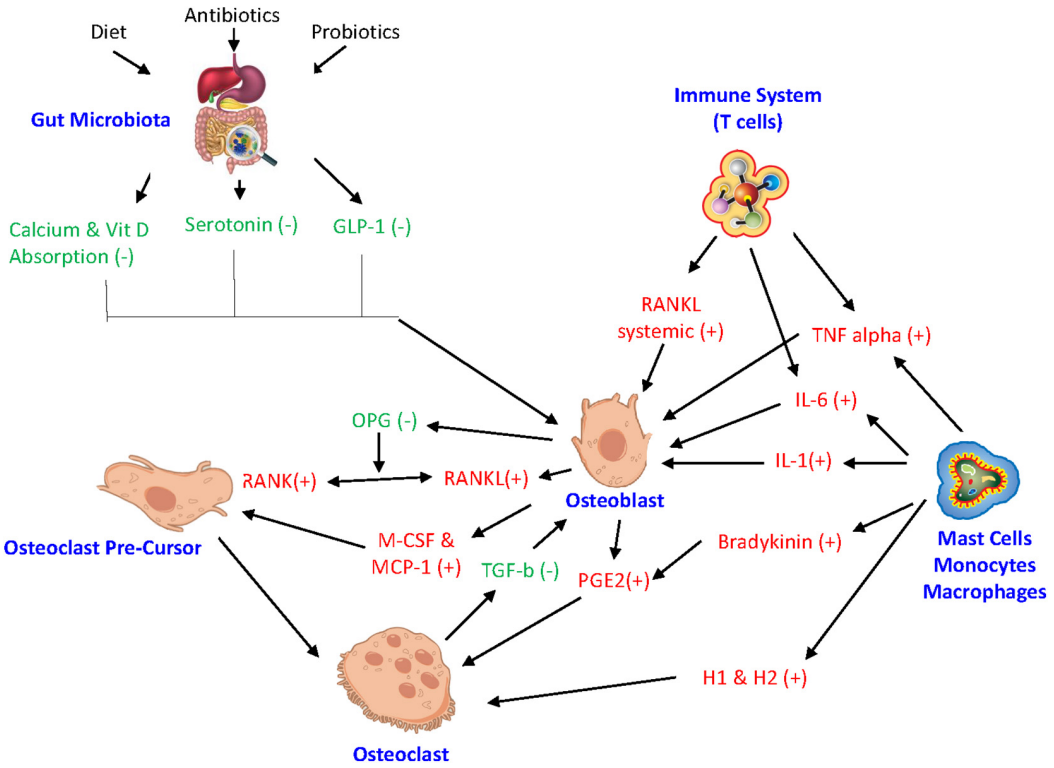

FIGURE 2 | Integrated inflammatory model. The complex link between gut microbiota, hormonal pathways, immune system, and bone turnover. *GLP-1* glucagon-like peptide, *miRNA* microRNA, *IL-6* interleukin-6, *IL-1* interleukin-1, *RANKL* receptor activator of NF-kB ligand, *RANK* receptor activator of nuclear factor-kB, *OPG* Osteoprotegrin, TNF *alpha* tumor necrosis factor-alpha, *M-CSF* macrophage colony stimulating factor, *MCP-1* monocyte chemoattractant protein 1, *H1* histamine 1, *H2* histamine 2, *PGE2* Prostaglandin E2. (+) drive osteoclastogenesis or resorption. (–) inhibit resorption.

ENDOCRINE FACTORS IN INFLAMMATION AND BONE HEALTH

Another important factor to consider in bone health is the role of hormonal signals. Endocrine factors, such as leptin signal in the central nervous system and mediate their effects on bone through the sympathetic nervous system. Mature osteoblasts and chondrocytes both have leptin receptors on their cell surface, suggesting leptin may be directly affecting these cells, potentially through activity of Fibroblast growth factor 23 (FGF-23) (Upadhyay et al., 2015). However, it is more likely that leptin's effects on bone mass are indirect. One potential mechanism is that the ventromedial hypothalamus (VMH) activates local noradrenergic signaling in osteoblasts in response to leptin, stimulating them to form bone (Takeda et al., 2002). Leptin also works by downregulating serotonin and inhibiting serotonergic receptors in the VMH. Serotonin has the opposite effect of leptin and inhibits osteoblasts, thus decreasing bone growth (Yadav et al., 2009). Leptin is involved in the regulatory networks of several important endocrine hormones, such as cortisol, thyroid and parathyroid hormone, IGF-1 and growth hormone, and estrogen, all of which can impact the bone remodeling cycle. Therefore, leptin secreted from the central nervous system could affect bone directly or indirectly through a wide range of secondary endocrine mediators (Khan et al., 2012).

In humans it has been demonstrated that estrogen deficiency affects the number of bone cells, and bone turnover partially through its effect on the immune system. During estrogen deficiency, T cells increase their production of pro-inflammatory and pro-osteoclastogenic cytokines, TNF-α and RANKL (D'Amelio and Sassi, 2018). Estrogen therapy may also help prevent bone loss in post-menopausal women by altering the balance between IL-1 and its receptor agonist (Rogers and Eastell, 1998), providing further evidence for a link between the endocrine system and cytokine mechanisms of bone remodeling.

THE ROLE OF IMMOBILITY ON BONE HEALTH

Another mechanism affecting bone health that remains poorly understood is immobility. Several groups have shown that bedridden patients display poorer bone health and are at an increased risk of fracture (Eimori et al., 2016). It has been speculated that osteocytes, embedded within the bone matrix, may be involved in mechanosensing. These cells likely work by modulating signaling, such as the wnt pathway which involves both bone formation and resorption, making them crucial for coupling these processes (Bonewald and Johnson, 2008). One study demonstrated that osteoblasts displaying

estrogen receptor alpha, whose expression is upregulated in the presence of estrogen, responded to load via wnt pathway gene upregulation. They concluded that estrogen decline in both men and women may in part lead to failure to maintain appropriate bone mass via this decreased sensitivity to load (Armstrong et al., 2007). Immobility also typically restricts time spent outdoors thus limiting exposure to sunlight, decreasing vitamin D synthesis in the skin. Therefore, immobility can lead to decreased vitamin D levels which can negatively affect the mineralization of bone (Cooper and Gittoes, 2008). Furthermore, in rheumatoid arthritis immobility may compound bone loss due to inflammatory disease activity (Haugeberg et al., 2002). It would appear, however, that increasing mobility has the propensity to reverse these changes, with strength training demonstrating increased levels of osteocalcin and alkaline phosphatase, markers of bone deposition, as well as improved bone mineral density (Menkes et al., 1993).

INTERVENTIONS

Treatment for inflammatory disease affecting bone has progressed to specifically address inflammatory cytokines and their pathways in various different ways. Infliximab, a TNF-α antibody that blocks TNF-α receptor interactions has shown promise in the treatment of rheumatoid arthritis, as has Etanercept, an agent that binds with TNF-α preventing from interacting with its receptor. While successful in reducing joint erosion they are not without adverse effects and should be avoided in the presence of chronic infection and heart failure (Scott and Kingsley, 2006). Estrogen therapy may have an indirect effect on IL-1 and thus its negative influence on bone, by altering the balance between IL-1 and its receptor agonist (Rogers and Eastell, 1998). Gene therapy, specifically aimed at upregulating OPG, showed early promise in decreasing inflammation and bone resorption in aseptic prosthesis loosening (Wooley and Schwarz, 2004). More recently the influence of MMP inhibitor alpha-2-macroglobulin has been shown to decrease IL-1 beta and TNF-α resulting in lower osteoarthritis scores, although the direct influence on bone resorption is yet to be studied (Wang et al., 2014).

Monoclonal antibodies are now playing a role in management also. Rituximab is a monoclonal antibody that depletes B cell population by targeting their CD20 surface antigen, showing up to 20% improvement in RA symptoms (Edwards et al., 2004), while Tocilizumab, an anti-IL-6 monoclonal antibody demonstrated a decrease in bone degradation markers when combined with methotrexate (Garnero et al., 2010).

As previously stated, nutrition has an impact on bone health, and the influence of nutraceuticals should not go unmentioned. Green tea polyphenol supplementation, of which epigallocatechins are the active component, inhibited TNF-α and suppressed osteoclast activity (Shen et al., 2011), inhibited IL-6 expression and downregulated bone resorption (Wu et al., 2018), while 500 mg daily when combined with Tai Chi shifted the ratio of bone formation to resorption in a net positive direction (Shen et al., 2012). Curcumin has also been shown to inhibit RANKL induced NF-kB osteoclastogenesis *in vitro* in a dose dependent manner (Bharti et al., 2004).

CONTEMPORARY IMAGING IN INFLAMMATION AND BONE HEALTH

Lastly, we will discuss imaging and blood based methods to monitor inflammation and its effect on bone health that are currently in use today.

Micro-Computed Tomography

Micro-computed tomography (uCT) has been used extensively to measure bone resorption in inflammation studies on animals (Lopes et al., 2018; Kuraji et al., 2018; Yoshihara-Hirata et al., 2018). uCT has been used to confirm that bone resorption was positively associated with levels of inflammation following administration of a 5-Lipoxygenase (5-LO) inhibitor; 5-LO has been implicated in inflammatory processes (Lopes et al., 2018). uCT has been used to confirm similar findings following administration of theaflavins, which are thought to reduce inflammation and subsequently reduce bone resorption (Kuraji et al., 2018). uCT used in a study on anti-HMGB1 neutralizing antibody and its effect on inflammation and bone resorption also demonstrated a positive correlation between levels of inflammation and bone resorption (Yoshihara-Hirata et al., 2018). It should be acknowledged that uCT administers a dose of ionizing radiation too aggressive and damaging for regular clinical use (Willekens et al., 2010).

Magnetic Resonance Imaging

Magnetic resonance imaging (MRI) is a safer and ubiquitous imaging option in a clinical setting. Several studies have determined its efficacy in measuring bone resorption in response to inflammation. One study compared bone marrow edema (BME)—inflammation of bone marrow—seen on MR images to levels of inflammation and BMD in patients with ankylosing spondylitis (AS), a chronic systemic inflammatory disease (Wang et al., 2017). From this study, it was determined that MRI-based imaging was effective in showing high BME in areas of low BMD and high inflammation. However, in another study on similar patients the amount of BME on MRI was only well-correlated to mononuclear cell infiltrates and other histopathologic measures of inflammation when high levels of inflammation were present. These authors concluded that signal identified on T2 weighted MRI imaging likely represents water as a correlate of BME and inflammation, but not inflammation itself (Appel et al., 2006b).

Positron Emission Tomography

Positron Emission Tomography (PET) is an effective method of detecting inflammation markers and visualizing the biological process of inflammation in a specific and sensitive fashion (Wu et al., 2013). PET tracers were able to more sensitively detect inflammation in the gastrointestinal tract, when compared to MRI (Dmochowska et al., 2019). In a study designed to investigate the bone metabolism and inflammatory characteristics of chronic non-bacterial osteomyelitis (CNO),

fluorodeoxyglucose (FDG)-PET was utilized to locate regions of inflammation, even where symptoms of CNO were not present (Ata et al., 2017). PET could theoretically be used to help accurately and visually trace the inflammation process and its interaction with bone resorption.

Ultrashort Echo Time MRI

Ultrashort echo time (UTE) MRI is another imaging technique utilized regularly today. This method allows for unprecedented imaging of microstructure and composition of cortical bone. More specifically, it can more accurately discern between different regions of bone, such as bone bound to the collagen matrix vs. perforations within the bone cortex vs. the water content of the bone (Siriwanarangsun et al., 2016). While it may be unable to detect inflammation directly, it can depict how the bone is being affected as a result of inflammation. Use of UTE-MRI in determining the interplay between inflammation and bone resorption has not yet been extensively studied. However, due to its uniquely detailed imaging of cortical bone, UTE-MRI may become an important tool in the future in determining the mechanism of remodeling bone.

BLOOD BIOMARKERS

Blood chemistries focusing on inflammatory biomarkers have also demonstrated clinical utility. For example, it has been shown that higher levels of C-reactive protein (CRP), a marker of inflammation, is associated with lower bone mineral density (BMD), suggesting that bone resorption is increased in the inflammatory setting (Koh et al., 2005; Lim et al., 2016). Similarly, another study measured blood levels of various inflammatory markers—CRP, interleukin (IL)-1β, and IL-6, among others—with BMD and bone mineral content (BMC) over 6 and 12 months in postmenopausal women. It found that these markers accounted for 1.1–6.1% of variation in bone loss amongst their subjects, and suggests that altering inflammatory markers may lead to decreased bone loss (Gertz et al., 2010).

CONCLUSION

It is clear that inflammation drives bone toward a resorption state. Osteoblasts have been highlighted as a central player, responding to inflammatory cytokines including TNFα and IL-1 by releasing MCS-F and MCP 1 to attract osteoclast pre-cursors. Systemic inflammation may also contribute, both chemotactically and via decreased mobility. Inflammatory mediators, such as TNFα stimulate RANKL production by lymphocytes and endothelial cells, and IL-1 and IL-6 induces PGE2 production by osteoblasts. Both mechanisms indirectly induce osteoclast formation and lead to bone resorption. Similarly, immune mediated responses via helper T cells and B lymphocytes appear to increase resorption. The discovery that macrophages play a role in bone resorption in aseptic prosthesis loosening has challenged the notion that only osteoclasts resorb bone. The effect of nutrition on bone status, specifically vitamin D and calcium is well-documented, however, the gut microbiota is less frequently considered but may be equally as important in both improving gut absorption and minimizing immune mediated systemic responses. The interplay between periosteal and endosteal bone remodeling may in part be explained by local inflammatory mediators, such as PGE2, IL-1, and IL-6 acting bi-directionally through periosteal, endosteal and synovial cell surface contact, and the recently described microcirculation. uCT and UTE MRI are emerging imaging modalities that provide for improved monitoring and identification of bone resorption, while blood monitoring of inflammatory markers may give measures of inflammation which have been shown to contribute directly to bone loss.

Despite well-described pathways for the effect of inflammation on bone, interventions to directly impact these pathways remain limited. While cytokine inhibitors appear to uncouple the relationship between inflammation and bone erosion, glucocorticoids appear to have differing effects in different populations. Nutraceuticals may also play a role in influencing inflammation driven resorption. More research is needed in these areas in order to develop interventions that protect bone in the presence of inflammation.

Limitations of this paper include an original, theoretical framework around specific players and pathways of inflammation involved in bone remodeling. These models uncover mechanisms involved with achieving bone homeostasis and identify potential actionable areas. Future research is warranted in humans to bring understanding of methodology to clinical practice and to determine if specific radiologic testing and blood biomarkers are key players in monitoring inflammation, directly and indirectly. However, these limitations also serve as strengths since there is a paucity of evidence on impact of local inflammation in the appendicular skeleton.

Finally, by understanding the effect of local and systemic inflammation on bone remodeling and the precise mechanisms by which this occurs, research into interventions can be better directed at minimizing inflammatory mediated bone resorption, thereby improving outcomes and hastening recovery from injury.

AUTHOR CONTRIBUTIONS

All authors contributed substantially to the drafting and editing of the manuscript.

REFERENCES

Abusleme, L., Dupuy, A. K., Dutzan, N., Silva, N., Burleson, J. A., Strausbaugh, L. D., et al. (2013). The subgingival microbiome in health and periodontitis and its relationship with community biomass and inflammation. *ISME J.* 7, 1016–1025. doi: 10.1038/ismej.2012.174

Adamopoulos, I. E. (2018). Inflammation in bone physiology and pathology. *Curr. Opin. Rheumatol.* 30, 59–64. doi: 10.1097/BOR.0000000000000449

Adams, J. S., and Hewison, M. (2008). Unexpected actions of vitamin D: new perspectives on the regulation of innate and adaptive immunity. *Nat. Clin. Pract. Endocrinol. Metab.* 4, 80–90. doi: 10.1038/ncpendmet 0716

Agrawal, M., Arora, S., Li, J., Rahmani, R., Sun, L., Steinlauf, A. F., et al. (2011). Bone, inflammation, and inflammatory bowel disease. *Curr. Osteoporos. Rep.* 9, 251–257. doi: 10.1007/s11914-011-0077-9

Appel, H., Kuhne, M., Spiekermann, S., Ebhardt, H., Grozdanovic, Z., Köhler, D., et al. (2006a). Immunohistologic analysis of zygapophyseal joints in patients with ankylosing Spondylitis. *Arthritis Rheum.* 54, 2845–2851. doi: 10.1002/art.22060

Appel, H., Loddenkemper, C., Grozdanovic, Z., Ebhardt, H., Dreimann, M., Hempfing, A., et al. (2006b). Correlation of histopathological findings and magnetic resonance imaging in the spine of patients with ankylosing spondylitis. *Arthritis Res. Ther.* 8:R143. doi: 10.1186/ar2035

Arai, F., Miyamoto, T., Ohneda, O., Inada, T., Sudo, T., Brasel, K., et al. (1999). Commitment and differentiation of Osteoclast Precursor cells by the sequential expression of C-Fms and receptor activator of Nuclear Factor κb (Rank) receptors. *J. Exp. Med.* 190, 1741–1754. doi: 10.1084/jem.190.12.1741

Armstrong, V. J., Muzylak, M., Sunters, A., Zaman, G., Saxon, L. K., Price, J. S., et al. (2007). Wnt/β-Catenin signaling is a component of Osteoblastic bone cell early responses to load-bearing and requires Estrogen Receptor α. *J. Biol. Chem.* 282, 20715–20727. doi: 10.1074/jbc.M703224200

Ata, Y., Inaba, Y., Choe, H., Kobayashi, N., Machida, J., Nakamura, N., et al. (2017). Bone metabolism and inflammatory characteristics in 14 cases of chronic nonbacterial osteomyelitis. *Pediatr. Rheumatol. Online J.* 15, 56–56. doi: 10.1186/s12969-017-0183-z

Athanasou, N., Quinn, J., and Bulstrode, C. J. K. (1991). Resorption of bone inflammatory cells derived from the joint capsule of hip arthroplasty. *J. Bone Joint Surg. Br. Vol.* 74, 57–62. doi: 10.1302/0301-620X.74B1.1732267

Baker-LePain, J. C., Nakamura, M. C., and Lane, N. E. (2011). Effect of inflammation on bone: an update. *Curr. Opin. Rheumatol.* 23, 389–395. doi: 10.1097/BOR.0b013e3283474dbe

Barbour, T. D. A., Briggs, C. A., Bell, S. N., Bradshaw, C. J., Venter, D. J., and Brukner, P. D. (2004). Histology of the fascial-periosteal interface in lower limb chronic deep posterior compartment syndrome. *Br. J. Sports Med.* 38, 709–717. doi: 10.1136/bjsm.2003.007039

Batt, M., Ugalde, V., Anderson, M., and Shelton, D. (1998). A prospective controlled study of diagnostic imaging for acute shin splints. *Med. Sci. Sports Exerc.* 30, 1564–1571. doi: 10.1097/00005768-199811000-00002

Bharti, A. C., Takada, Y., and Aggarwal, B. B. (2004). Curcumin (Diferuloylmethane) inhibits receptor activator of NF-kB Ligand-Induced NF-kB activation in Osteoclast Precursors and Suppresses Osteoclastogenesis. *J. Immunol.* 172, 5940–5947. doi: 10.4049/jimmunol.172.10.5940

Bonewald, L. F., and Johnson, M. L. (2008). Osteocytes, mechanosensing and Wnt signaling. *Bone* 42, 606–615. doi: 10.1016/j.bone.2007.12.224

Bouché, R. T., and Johnson, C. H. (2007). Medial tibial stress syndrome (tibial fasciitis): a proposed pathomechanical model involving fascial traction. *J. Am. Podiatr. Med. Assoc.* 97, 31–36. doi: 10.7547/0970031

Boyce, B. F., and Xing, L. (2008). Functions of RANKL/RANK/OPG in bone modeling and remodeling. *Arch. Biochem. Biophys.* 473, 139–146. doi: 10.1016/j.abb.2008.03.018

Boyce, B. E., Li, P., Yao, Z., Zhang, Q., Badell, I. R., Schwarz, E. M., et al. (2005). TNF-alpha and pathologic bone resorption. *Keio J. Med.* 54, 127–131. doi: 10.2302/kjm.54.127

Boyle, W. J., Simonet, W. S., and Lacey, D. L. (2003). Osteoclast differentiation and activation. *Nature* 423, 337–342. doi: 10.1038/nature01658

Canalis, E., and Delany, A. M. (2002). Mechanisms of glucocorticoid action in bone. *Ann. N. Y. Acad. Sci.* 966, 73–81. doi: 10.1111/j.1749-6632.2002.tb04204.x

Canalis, E., Mazziotti, G., Giustina, A., and Bilezekian, J. P. (2007). Glucocorticoid-induced osteoporosis: pathophysiology and therapy. *Osteoporosis Int.* 18, 1319–1328. doi: 10.1007/s00198-007-0394-0

Chang, M. K., Raggatt, L. J., Alexander, K. A., Kuliwaba, J. S., Fazzalari, N. L., Schroder, K., et al. (2008). Osteal tissue macrophages are intercalated throughout human and mouse bone lining tissues and regulate osteoblast function in vitro and in vivo. *J. Immunol.* 181, 1232–1244. doi: 10.4049/jimmunol.181.2.1232

Chen, S. J., Liao, W. C., Huang, K. H., Lin, C. L., Tsai, W. C., Kung, P. T., et al. (2015). Chronic obstructive pulmonary disease and allied conditions is a strong independent risk factor for osteoporosis and pathologic fractures: a population-based cohort study. *QJM* 108, 633–640. doi: 10.1093/qjmed/hcv012

Chen, X., Wang, Z., Duan, N., Zhu, G., Schwarz, E. M., and Xie, C. (2018). Osteoblast-osteoclast interactions. *Connect. Tissue Res.* 59, 99–107. doi: 10.1080/03008207.2017.1290085

Chiodini, I., Vainicher, C. E., Morelli, V., Palmieri, S., Cairoli, E., Salcuni, A. S., et al. (2016). Mechanisms in endocrinology: endogenous subclinical hypercortisolism and bone: a clinical review. *Eur. J. Endocrinol.* 175, R265–R282. doi: 10.1530/EJE-16-0289

Cooper, M. S., and Gittoes, N. J. L. (2008). Diagnosis and management of hypocalcaemia. *BMJ* 336, 1298–1302. doi: 10.1136/bmj.39582.589433.BE

Corazza, G. R., Di Stefano, M., Mauriño, E., and Bai, J. C. (2005). Bones in coeliac disease: diagnosis and treatment. *Best Pract. Res. Clin. Gastroenterol.* 19, 453–465. doi: 10.1016/j.bpg.2005.01.002

D'Amelio, P., and Sassi, F. (2018). Gut microbiota, immune system, and bone. *Calcif. Tissue Int.* 102, 415–425. doi: 10.1007/s00223-017-0331-y

Dekkers, J., Toes, R. E., Huizinga, T. W., and van der Woude, D. (2016). The role of anticitrullinated protein antibodies in the early stages of rheumatoid arthritis. *Curr. Opin. Rheumatol.* 28, 275–281. doi: 10.1097/BOR.0000000000000277

Diarra, D., Stolina, M., Polzer, K., Zwerina, J., Ominsky, M. S., Dwyer, D., et al. (2007). Dickkopf-1 is a master regulator of joint remodeling. *Nat. Med.* 13:156. doi: 10.1038/nm1538

Dmochowska, N., Tieu, W., Keller, M. D., Wardill, H. R., Mavrangelos, C., Campaniello, M. A., et al. (2019). Immuno-PET of Innate Immune Markers CD11b and IL-1β detects inflammation in Murine Colitis. *J. Nuclear Med.* 60, 858–863. doi: 10.2967/jnumed.118.219287

Dobigny, C., and Saffar, J. L. (1997). H1 and H2 histamine receptors modulate osteoclastic resorption by different pathways: evidence obtained by using receptor antagonists in a rat synchronized resorption model. *J. Cell Physiol.* 173, 10–18. doi: 10.1002/(SICI)1097-4652(199710)173:1<10::AID-JCP2>3.0.CO;2-M

Edwards, J. C., Szczepański, L., Szechiński, J., Filipowicz-Sosnowska, A., Emery, P., Close, D. R., et al. (2004). Efficacy of B-cell-targeted therapy with rituximab in patients with rheumatoid arthritis. *New Engl. J. Med.* 350, 2572–2581. doi: 10.1056/NEJMoa032534

Eijken, M., Koedam, M., van Driel, M., Buurman, C. J., Pols, H. A., and van Leeuwen, J. P. (2006). The essential role of glucocorticoids for proper human osteoblast differentiation and matrix mineralization. *Mol. Cell. Endocrinol.* 248, 87–93. doi: 10.1016/j.mce.2005.11.034

Eimori, K., Endo, N., Uchiyama, S., Takahashi, Y., Kawashima, H., and Watanabe, K. (2016). Disrupted bone metabolism in long-term bedridden patients. *PLoS One* 11:e0156991. doi: 10.1371/journal.pone.0156991

Ellender, G., Feik, S. A., and Carach, B. J. (1988). Periosteal structure and development in a rat caudal vertebra. *J. Anat.* 158, 173–187.

Eriksen, E. F. (2010). Cellular mechanisms of bone remodeling. *Rev. Endocr. Metab. Disord.* 11, 219–227. doi: 10.1007/s11154-010-9153-1

Everts, V., Delaisse, J. M., Korper, W., Jansen, D. C., Tigchelaar-Gutter, W., Saftig, P., et al. (2002). The bone lining cell: its role in cleaning Howship's lacunae and initiating bone formation. *J. Bone Miner. Res.* 17, 77–90. doi: 10.1359/jbmr.2002.17.1.77

Forwood, M. R., Kelly, W. L., and Worth, N. F. (1998). Localisation of prostaglandin endoperoxide H synthase (PGHS)-1 and PGHS-2 in bone following mechanical loading in vivo. *Anat. Rec.* 252, 580–586. doi: 10.1002/(SICI)1097-0185(199812)252:4<580::AID-AR8>3.0.CO;2-S

Gabriel, S. E. (2001). The epidemiology of rheumatoid arthritis. *Rheum. Dis. Clin. North Am.* 27, 269–281. doi: 10.1016/S0889-857X(05)70201-5

Gaeta, M., Minutoli, F., Vinci, S., Salamone, I., D'Andrea, L., Bitto, L., et al. (2006). Grading of Tibial stress reactions in distance runners. *Am. J. of Roentgenol.* 187, 789–793. doi: 10.2214/AJR.05.0303

Garnero, P., Thompson, E., Woodworth, T., and Smolen, J. S. (2010). Rapid and sustained improvement in bone and cartilage turnover markers with the anti-interleukin-6 receptor inhibitor Tocilizumab plus Methotrexate in rheumatoid arthritis patients with an inadequate response to methotrexate: results from a substudy of the multicenter double-blind, placebo-controlled trial of Tocilizumab in inadequate responders to Methotrexate alone. *Arthrit. Rheum.* 62, 33–43. doi: 10.1002/art.25053

Gertz, E. R., Silverman, N. E., Wise, K. S., Hanson, K. B., Alekel, D. L., Stewart, J. W., et al. (2010). Contribution of serum inflammatory markers to changes in bone

mineral content and density in postmenopausal women: a 1-year investigation. *J. Clin. Densitometr* 13, 277–282. doi: 10.1016/j.jocd.2010.04.003

Gilbert, L., He, X., Farmer, P., Boden, S., Kozlowski, M., Rubin, J., et al. (2000). Inhibition of Osteoblast differentiation by tumor Necrosis Factor-α. *Endocrinology* 141, 3956–3964. doi: 10.1210/endo.141.11.7739

Graves, D. T., Jiang, Y., and Valente, A. J. (1999). The expression of monocyte chemoattractant protein-1 and other chemokines by osteoblasts. *Front. Biosci.* 4, D571–D580. doi: 10.2741/Graves

Grüneboom, A., Hawwari, I., Weidner, D., Culemann, S., Müller, S., Henneberg, S., et al. (2019). A network of trans-cortical capillaries as mainstay for blood circulation in long bones. *Nat. Metab.* 1, 236–250. doi: 10.1038/s42255-018-0016-5

Guillot, X., Semerano, L., Saidenberg-Kermanac'h, N., Falgarone, G., and Boissier, M. C. (2010). Vitamin D and inflammation. *Joint Bone Spine* 77, 552–557. doi: 10.1016/j.jbspin.2010.09.018

Hajishengallis, G. (2015). Periodontitis: from microbial immune subversion to systemic inflammation. *Nat. Rev. Immunol.* 15, 30–44. doi: 10.1038/nri3785

Halleen, J. M., Räisänen, S., Salo, J. J., Reddy, S. V., Roodman, G. D., Hentunen, T. A., et al. (1999). Intracellular fragmentation of bone resorption products by reactive oxygen species generated by Osteoclastic Tartrate-resistant Acid Phosphatase. *J. Biol. Chem.* 274, 22907–22910. doi: 10.1074/jbc.274.33.22907

Harant, H., Andrew, P. J., Reddy, G. S., Foglar, E., and Lindley, I. J. (1997). 1alpha,25-Dihydroxyvitamin D3 and a Variety of its Natural Metabolites Transcriptionally Repress Nuclear-Factor-kappaB-Mediated Interleukin-8 Gene Expression. *Eur. J. Biochem.* 250, 63–71. doi: 10.1111/j.1432-1033.1997.00063.x

Hardy, R., and Cooper, M. S. (2009). Bone loss in inflammatory disorders. *J. Endocrinol.* 201, 309–320. doi: 10.1677/JOE-08-0568

Haugeberg, G., Orstavik, R. E., Uhlig, T., Falch, J. A., Halse, J. I., and Kvien, T. K. (2002). Clinical decision rules in rheumatoid arthritis: do they identify patients at high risk for osteoporosis? Testing clinical criteria in a population based cohort of patients with rheumatoid arthritis recruited from the Oslo Rheumatoid Arthritis Register. *Ann. Rheum. Dis.* 61, 1085–1089. doi: 10.1136/ard.61.12.1085

Hienz, S. A., Paliwal, S., and Ivanovski, S. (2015). Mechanisms of bone resorption in periodontitis. *J. Immunol. Res.* 2015:615486. doi: 10.1155/2015/615486

Hofbauer, L. C., Khosla, S., Dunstan, C. R., Lacey, D. L., Boyle, W. J., and Riggs, B. L. (2000). The roles of Osteoprotegerin and Osteoprotegerin Ligand in the Paracrine regulation of bone resorption. *J. Bone Mineral Res.* 15, 2–12. doi: 10.1359/jbmr.2000.15.1.2

Hofbauer, L. C., Lacey, D. L., Dunstan, C. R., Spelsberg, T. C., Riggs, B. L., and Khosla, S. (1999). Interleukin-1beta and tumor necrosis factor-alpha, but not interleukin-6, stimulate osteoprotegerin ligand gene expression in human osteoblastic cells. *Bone* 25, 255–259. doi: 10.1016/S8756-3282(99)00162-3

Horiki, M., Nakase, T., Myoui, A., Sugano, N., Nishii, T., Tomita, T., et al. (2004). Localization of RANKL in osteolytic tissue around a loosened joint prosthesis. *J. Bone Mineral Res.* 22, 346–351. doi: 10.1007/s00774-003-0493-8

Horowitz, S. M., and Purdon, M. A. (1995). Mechanisms of cellular recruitment in aseptic loosening of prosthetic joint implants. *Calcif Tissue Int.* 57, 301–305. doi: 10.1007/BF00298886

Janssens, K., ten Dijke, P., Janssens, S., and van Hul, W. (2005). Transforming growth factor-β1 to the bone. *Endocr. Rev.* 26, 743–774. doi: 10.1210/er.2004-0001

Jilka, R. L. (2003). Biology of the basic multicellular unit and the pathophysiology of osteoporosis. *Med. Pediatr. Oncol.* 41, 182–185. doi: 10.1002/mpo.10334

Johnell, O., Rausing, A., Wendeberg, B., and Westlin, N. (1982). Morphological bone changes in shin splints. *Clin. Orthop. Relat. Res.* 167, 180–184. doi: 10.1097/00003086-198207000-00027

Jones, D. B., Nolte, H., Scholübbers, J. G., Turner, E., and Veltel, D. (1991). Biochemical signal transduction of mechanical strain in osteoblast-like cells. *Biomaterials* 12, 101–110. doi: 10.1016/0142-9612(91)90186-E

Karsenty, G. (2006). Convergence between bone and energy homeostases: Leptin regulation of bone mass. *Cell Metab.* 4, 341–348. doi: 10.1016/j.cmet.2006.10.008

Khan, S. M., Hamnvik, O. P. R., Brinkoetter, M., and Mantzoros, C. S. (2012). Leptin as a modulator of neuroendocrine function in humans. *Yonsei Med. J.* 53, 671–679. doi: 10.3349/ymj.2012.53.4.671

Khosla, S. (2001). Minireview: The OPG/RANKL/RANK system. *Endocrinology* 142, 5050–5055. doi: 10.1210/endo.142.12.8536

Kim, K. W., Cho, M. L., and Leetal, S. H. (2007). Human rheumatoid synovial fibroblasts promote osteoclastogenic activity by activating RANKL via TLR-2 and TLR-4 activation. *Immunol. Lett.* 110, 54–64. doi: 10.1016/j.imlet.2007.03.004

Koh, J. M., Khang, Y. H., Jung, C. H., Bae, S., Kim, D. J., Chung, Y. E., et al. (2005). Higher circulating hsCRP levels are associated with lower bone mineral density in healthy pre- and postmenopausal women: evidence for a link between systemic inflammation and osteoporosis. *Osteoporosis Int.* 16, 1263–1271. doi: 10.1007/s00198-005-1840-5

Konttinen, Y., Imai, S., and Suda, A. (1996). Neuropeptides and the puzzle of bone remodeling. State of the art. *Acta Orthop. Scand.* 67, 632–639. doi: 10.3109/17453679608997772

Kotake, S., Sato, K., Kim, K. J., Takahashi, N., Udagawa, N., Nakamura, I., et al. (1996). Interleukin-6 and soluble interleukin-6 receptors in the synovial fluids from rheumatoid arthritis patients are responsible for osteoclast-like cell formation. *J. Bone Mineral Res.* 11, 88–95. doi: 10.1002/jbmr.5650110113

Kuraji, R., Fujita, M., Ito, H., Hashimoto, S., and Numabe, Y. (2018). Effects of experimental periodontitis on the metabolic system in rats with diet-induced obesity (DIO): an analysis of serum biochemical parameters. *Odontology* 106, 162–170. doi: 10.1007/s10266-017-0322-5

Lam, J., Takeshita, S., Barker, J. E., Kanagawa, O., Ross, F. P., and Teitelbaum, S. L. (2000). TNF-α induces osteoclastogenesis by direct stimulation of macrophages exposed to permissive levels of RANK ligand. *J. Clin. Invest.* 106, 1481–1488. doi: 10.1172/JCI11176

Landewe, R., van der Heije, D., Klareskog, L., van Vollenhoven, R., and Fatenejad, S. (2006). Disconnect Between Inflammation and Joint Destruction After Treatment With Etanercept Plus Methotrexate. *Arthritis Rheum.* 54, 3119–3125. doi: 10.1002/art.22143

Langdahl, B., Ferrari, S., and Dempster, D. W. (2016). Bone modeling and remodeling: potential as therapeutic targets for the treatment of osteoporosis. *Ther. Adv Musculoskelet. Dis.* 8, 225–235. doi: 10.1177/1759720X16670154

Lerner, U. H., Jones, I. L., and Gustafson, G. T. (1987). Bradykinin, a new potential mediator of inflammation-induced bone resorption. *Arthritis Rheum.* 30, 530–540. doi: 10.1002/art.1780300507

Li, J., Hsu, H., and Mountz, J. D. (2012). Managing macrophages in rheumatoid arthritis by reform or removal. *Curr. Rheumatol. Rep.* 14, 445–454. doi: 10.1007/s11926-012-0272-4

Li, Y., Toraldo, G., Li, A., Yang, X., Zhang, H., Qian, W. P., et al. (2007). B cells and T cells are critical for the preservation of bone homeostasis and attainment of peak bone mass in vivo. *Blood* 109, 3839–3848. doi: 10.1182/blood-2006-07-037994

Lim, H. S., Park, Y. H., and Kim, S. K. (2016). Relationship between Serum Inflammatory Marker and Bone Mineral Density in Healthy Adults. *J. Bone Metab.* 23, 27–33. doi: 10.11005/jbm.2016.23.1.27

Liu, J., Dang, L., Wu, X., Li, D., Ren, Q., Lu, A., et al. (2019). MicroRNA-mediated regulation of bone remodeling: a brief review. *JBMR Plus* 3:e10213. doi: 10.1002/jbm4.10213

Liu, X.-H., Kirschenbaum, A., Yao, S., and Levine, A. C. (2005). Cross-Talk between the Interleukin-6 and Prostaglandin E2 Signaling Systems Results in Enhancement of Osteoclastogenesis through Effects on the Osteoprotegerin/Receptor Activator of Nuclear Factor-kB (RANK) Ligand/RANK System. *Endocrinology* 146, 1991–1998. doi: 10.1210/en.2004-1167

Lopes, D. E., Jabr, C. L., Dejani, N. N., Saraiva, A. C., de Aquino, S. G., Medeiros, A. I., et al. (2018). Inhibition of 5-Lipoxygenase attenuates inflammation and bone resorption in Lipopolysaccharide-induced periodontal disease. *J. Periodontol.* 89, 235–245.

Lorenzo, J., Horowitz, M., and Choi, Y. (2008). Osteoimmunology: interactions of the bone and immune system. *Endocrine Rev.* 29, 403–440. doi: 10.1210/er.2007-0038

Lundy, S. K., Sarkar, S., Tesmer, L. A., and Fox, D. A. (2007). Cells of the synovium in rheumatoid arthritis. *T lymphocytes. Arthritis Res. Ther.* 9:202. doi: 10.1186/ar2107

MacGregor, A. J., Snieder, H., Rigby, A. S., Koskenvuo, M., Kaprio, J., Aho, K., et al. (2000). Characterizing the quantitative genetic contribution to rheumatoid

arthritis using data from twins. *Arthritis Rheum.* 43, 30–37. doi: 10.1002/1529-0131(200001)43:1<30::AID-ANR5>3.0.CO;2-B

Magnusson, H. I., Westlin, N. E., Nyqvist, F., Gärdsell, P., Seeman, E., and Karlsson, M. K. (2001). Abnormally decreased regional bone density in Athletes with Medial Tibial stress syndrome. *Am. J. Sports Med.* 29, 712–715. doi: 10.1177/03635465010290060701

McInnes, I. B., and Schett, G. (2007). Cytokines in the pathogenesis of rheumatoid arthritis. *Nat. Rev. Immunol.* 7, 429–442. doi: 10.1038/nri2094

Menkes, A., Mazel, S., Redmond, R. A., Koffler, K., Libanati, C. R., Gundberg, C. M., et al. (1993). Strength training increases regional bone mineral density and bone remodeling in middle-aged and older men. *J. Appl. Physiol.* 74, 2478–2484. doi: 10.1152/jappl.1993.74.5.2478

Michael, R. H., and Holder, L. E. (1985). The soleus syndrome. A cause of medial tibial stress (shin splints). *Am. J. Sports Med.* 13, 87–94. doi: 10.1177/036354658501300202

Miyaura, C., Inada, M., Matsumoto, C., Ohshiba, T., Uozumi, N., Shimizu, T., et al. (2003). An Essential Role of Cytosolic Phospholipase A2α in Prostaglandin E2–mediated bone resorption associated with inflammation. *J. Exp. Med.* 197, 1303–1310. doi: 10.1084/jem.20030015

Mori, G., D'Amelio, P., Faccio, R., and Brunetti, G. (2015). Bone-immune cell crosstalk: bone diseases. *J. Immunol. Res.* 2015:108451. doi: 10.1155/2015/108451

Mousa, A., Misso, M., Teede, H., Scragg, R., and de Courten, B. (2016). Effect of vitamin D supplementation on inflammation: protocol for a systematic review. *BMJ Open* 6:e010804. doi: 10.1136/bmjopen-2015-010804

Nanci, A., and Bosshardt, D. D. (2006). Structure of periodontal tissues in health and disease. *Periodontology* 40, 11–28. doi: 10.1111/j.1600-0757.2005.00141.x

Nissen, A., Marstrand, S., Skov-Jeppesen, K., Bremholm, L., Hornum, M., Andersen, U. B., et al. (2019). A Pilot Study Showing Acute Inhibitory Effect of GLP-1 on the Bone Resorption Marker CTX in Humans. *JBMR Plus* 3:e10209. doi: 10.1002/jbm4.10209

Owen, R., and Reilly, G. C. (2018). In vitro models of bone remodelling and associated disorders. *Front. Bioeng. Biotechnol.* 6:134. doi: 10.3389/fbioe.2018.00134

Paganelli, M., Albanese, C., Borrelli, O., Civitelli, F., Canitano, F. V., Passariello, R., et al. (2007). Inflammation is the main determinant of low bone mineral density in pediatric inflammatory bowel disease. *Inflam. Bowel Dis.* 13, 416–423. doi: 10.1002/ibd.20039

Perry, M. J., Mortuza, F. Y., Ponsford, F. M., Elson, C. J., and Atkins, R. M. (1995). Tissues around loosening joint implants. *Rheumatology* 34, 1127–1134. doi: 10.1093/rheumatology/34.12.1127

Peterson, C. T., Sharma, V., Elmén, L., and Peterson, S. N. (2015). Immune homeostasis, dysbiosis and therapeutic modulation of the gut microbiota. *Clin. Exp. Immunol.* 179, 363–377. doi: 10.1111/cei.12474

Pfeilschifter, J., Chenu, C., Bird, A., Mundy, G. R., and Roodman, D. G. (1989). Interleukin-1 and tumor necrosis factor stimulate the formation of human osteoclastlike cells in vitro. *J. Bone Miner. Res.* 4, 113–118. doi: 10.1002/jbmr.5650040116

Quach, D., and Britton, R. A. (2017). *Gut Microbiota and Bone Health*. Berlin: Springer International Publishing, 47–58. doi: 10.1007/978-3-319-66653-2_4

Rogers, A., and Eastell, R. (1998). Effects of estrogen therapy in postmenopausal women on cytokines measured in peripheral blood. *J. Bone Mineral Res.* 13, 1577–1586. doi: 10.1359/jbmr.1998.13.10.1577

Roux, S., and Orcel, P. (2000). Bone loss. Factors that regulate osteoclast differentiation: an update. *Arthritis Res.* 2, 451–456. doi: 10.1186/ar127

Scher, J. U., Ubeda, C., Pillinger, M. H., Bretz, W., Buischi, Y., Rosenthal, P. B., et al. (2010). Characteristic oral and intestinal microbiota in rheumatoid arthritis: a trigger for autoimmunity. *Arthritis Rheum.* 62:S577.

Scott, D. L., and Kingsley, G. H. (2006). Tumor necrosis factor inhibitors for rheumatoid arthritis. *New Engl. J. Med.* 355, 704–712. doi: 10.1056/NEJMct055183

Shen, C. L., Chyu, M. C., Yeh, J. K., Zhang, Y., Pence, B. C., Felton, C. K., et al. (2012). Effect of green tea and Tai Chi on bone health in postmenopausal osteopenic women: a 6-month randomized placebo-controlled trial. *Osteoporosis Int.* 23, 1541–1552. doi: 10.1007/s00198-011-1731-x

Shen, C. L., Yeh, J. K., Samathanam, C., Cao, J. J., Stoecker, B. J., Dagda, R. Y., et al. (2011). Green tea polyphenols attenuate deterioration of bone microarchitecture in female rats with systemic chronic inflammation. *Osteoporosis Int.* 22, 327–337. doi: 10.1007/s00198-010-1209-2

Silman, A. J., MacGregor, A. J., Thomson, W., Holligan, S., Carthy, D., Farhan, A., et al. (1993). Twin concordance rates for rheumatoid arthritis: results from a nationwide study. *Br. J. Rheumatol.* 32, 903–907. doi: 10.1093/rheumatology/32.10.903

Siriwanarangsun, P., Statum, S., Biswas, R., Bae, W. C., and Chung, C. B. (2016). Ultrashort time to echo magnetic resonance techniques for the musculoskeletal system. *Quan. Imaging Med. Surg.* 6, 731–743. doi: 10.21037/qims.2016.12.06

Soyka, L. A., Grinspoon, S., Levitsky, L. L., Herzog, D. B., and Klibanski, A. (1999). The effects of Anorexia Nervosa on bone metabolism in Female Adolescents1. *J. Clin. Endocrinol. Metab.* 84, 4489–4496. doi: 10.1210/jcem.84.12.6207

Squier, C. A., Ghoneim, S., and Kremenak, C. R. (1990). Ultrastructure of the periosteum from membrane bone. *J. Anat.* 171, 233–239.

Stickley, C. D., Hetzler, R. K., Kimura, I. F., and Lozanoff, S. (2009). Crural fascia and muscle origins related to medial tibial stress syndrome symptom location. *Med. Sci. Sports Exerc.* 41, 1991–1996. doi: 10.1249/MSS.0b013e3181a6519c

Straub, R. H., Dhabhar, F. S., Bijlsma, J. W., and Cutolo, M. (2005). How psychological stress via hormones and nerve fibers may exacerbate rheumatoid arthritis. *Arthritis Rheum.* 52, 16–26. doi: 10.1002/art.20747

Sugatani, T., and Hruska, K. A. (2009). Impaired Micro-RNA pathways diminish Osteoclast differentiation and function. *J. Biol. Chem.* 284, 4667–4678. doi: 10.1074/jbc.M805777200

Takayanagi, H., Oda, H., Yamamoto, S., Kawaguchi, H., Tanaka, S., Nishikawa, T., et al. (1997). A new mechanism of bone destruction in rheumatoid arthritis: synovial fibroblasts induce osteoclastogenesis. *Biochem. Biophys. Res. Commun.* 240, 279–286. doi: 10.1006/bbrc.1997.7404

Takeda, S., Elefteriou, F., Levasseur, R., Liu, X., Zhao, L., Parker, K. L., et al. (2002). Leptin regulates bone formation via the sympathetic nervous system. *Cell* 111, 305–317. doi: 10.1016/S0092-8674(02)01049-8

Tanaka, Y., Nakayamada, S., and Okada, Y. (2005). Osteoblasts and osteoclasts in bone remodeling and inflammation. *Curr. Drug Targets Inflamm. Allergy* 4, 325–328. doi: 10.2174/1568010054022015

Taubman, M. A., Valverde, P., Han, X., and Kawai, T. (2005). Immune response: the key to bone resorption in periodontal disease. *J. Periodontol.* 76(11 Suppl.), 2033–2041. doi: 10.1902/jop.2005.76.11-S.2033

Thorsen, K., Kristoffersson, A. O., Lerner, U. H., and Lorentzon, R. P. (1996). In situ microdialysis in bone tissue. Stimulation of prostaglandin E2 release by weight-bearing mechanical loading. *J. Clin. Invest.* 98, 2446–2449. doi: 10.1172/JCI119061

Unlap, M. T., and Jope, R. S. (1997). Dexamethasone attenuates NF-κ B DNA binding activity without inducing I κ B levels in rat brain in vivo. *Mol. Brain Res.* 45, 83–89. doi: 10.1016/S0169-328X(96)00240-9

Upadhyay, J., Farr, O. M., and Mantzoros, C. S. (2015). The role of leptin in regulating bone metabolism. *Metabolism* 64, 105–113. doi: 10.1016/j.metabol.2014.10.021

Valverde, P., Kawai, T., and Taubman, M. A. (2004). Selective blockade of voltage-gated potassium channels reduces inflammatory bone resorption in experimental periodontal disease. *J. Bone Miner. Res.* 19, 155–164. doi: 10.1359/jbmr.0301213

Van Gestel, A. M., Laan, R. F. J. M., Haagsma, C. J., Van De Putte, L. B. A., and Van Riel, P. L. C. M. (1995). Oral steroids as bridge therapy in rheumatoid arthritis patients starting with parenteral gold a randomized double-blind placebo-controlled trial. *Br. J. Rheumatol.* 35, 347–351. doi: 10.1093/rheumatology/34.4.347

Verborgt, O., Gibson, G. J., and Schaffler, M. B. (2000). Loss of osteocyte integrity in association with microdamage and bone remodeling after fatigue in vivo. *J Bone Miner. Res.* 15, 60–67. doi: 10.1359/jbmr.2000.15.1.60

Villa, C. R., Ward, W. E., and Comelli, E. M. (2017). Gut microbiota-bone axis. *Crit. Rev. Food Sci. Nutr.* 57, 1664–1672. doi: 10.1080/10408398.2015.1010034

Wang, D., Hou, Z., Gong, Y., Chen, S., Lin, L., and Xiao, Z. (2017). Bone edema on magnetic resonance imaging is highly associated with low bone mineral density in patients with ankylosing spondylitis. *PLoS One* 12:e0189569. doi: 10.1371/journal.pone.0189569

Wang, F. S., Ko, J. Y., Yeh, D. W., Ke, H. C., and Wu, H. L. (2008). Modulation of Dickkopf-1 attenuates Glucocorticoid induction of Osteoblast Apoptosis

Adipocytic differentiation, and bone mass loss. *Endocrinology* 149, 1793–1801. doi: 10.1210/en.2007-0910

Wang, S., Wei, X., Zhou, J., Zhang, J., Li, K., Chen, Q., et al. (2014). Identification of a-2-Macroglobulin as a master inhibitor of Cartilage-Degrading factors That Attenuates the progression of Posttraumatic Osteoarthritis. *Arthritis Rheumatol.* 66, 1843–1853. doi: 10.1002/art.38576

Wei, S., Kitaura, H., Zhou, P., Ross, F. P., and Teitelbaum, S. L. (2005). IL-1 mediates TNF-induced osteoclastogenesis. *J. Clin. Invest.* 115, 282–290. doi: 10.1172/JCI200523394

Weinstein, R. S., Chen, J. R., Powers, C. C., Stewart, S. A., Landes, R. D., Bellido, T., et al. (2002). Promotion of osteoclast survival and antagonism of bisphosphonate-induced osteoclast apoptosis by glucocorticoids. *J. Clin. Invest.* 109, 1041–1048. doi: 10.1172/JCI0214538

Weitzmann, M. N. (2013). The Role of Inflammatory Cytokines, the RANKL/OPG Axis, and the immunoskeletal interface in physiological bone turnover and Osteoporosis. *Scientifica* 2013, 1–29. doi: 10.1155/2013/125705

Weitzmann, M. N., Roggia, C., Toraldo, G., Weitzmann, L., and Pacifici, R. (2002). Increased production of IL-7 uncouples bone formation from bone resorption during estrogen deficiency. *J. Clin. Invest.* 110, 1643–1650. doi: 10.1172/JCI0215687

Wetzsteon, R. J., Shults, J., Zemel, B. S., Gupta, P. U., Burnham, J. M., Herskovitz, R. M., et al. (2009). Divergent effects of glucocorticoids on cortical and trabecular compartment BMD in childhood nephrotic syndrome. *J. Bone Miner. Res.* 24, 503–513. doi: 10.1359/jbmr.081101

Weyand, C. M., and Goronzy, J. J. (2017). Immunometabolism in early and late stages of rheumatoid arthritis. *Nat. Rev. Rheumatol.* 13, 291–301. doi: 10.1038/nrrheum.2017.49

Willekens, I., Buls, N., Lahoutte, T., Baeyens, L., Vanhove, C., Caveliers, V., et al. (2010). Evaluation of the radiation dose in micro-CT with optimization of the scan protocol. *Contrast Media Mol. Imaging* 5, 201–207. doi: 10.1002/cmmi.394

Winters, M., Burr, D. B., van der Hoeven, H., Condon, K. W., Bellemans, J., and Moen, M. H. (2019). Microcrack-associated bone remodeling is rarely observed in biopsies from athletes with medial tibial stress syndrome. *J. Bone Miner. Metab.* 37, 496–502. doi: 10.1007/s00774-018-0945-9

Wong, P. K., Quinn, J. M., Sims, N. A., van Nieuwenhuijze, A., Campbell, I. K., and Wicks, I. P. (2006). Interleukin-6 modulates production of T lymphocyte-derived cytokines in antigen-induced arthritis and drives inflammation-induced osteoclastogenesis. *Arthritis Rheum.* 54, 158–168. doi: 10.1002/art.21537

Wooley, P. H., and Schwarz, E. M. (2004). Aseptic loosening. *Gene Ther.* 11, 402–407. doi: 10.1038/sj.gt.3302202

Wu, C., Li, F., Niu, G., and Chen, X. (2013). PET imaging of inflammation biomarkers. *Theranostics* 3, 448–466. doi: 10.7150/thno.6592

Wu, Y. H., Kuraji, R., Taya, Y., Ito, H., and Numabe, Y. (2018). Effects of theaflavins on tissue inflammation and bone resorption on experimental periodontitis in rats. *J. Period. Res.* 53, 1009–1019. doi: 10.1111/jre.12600

Yadav, V. K., Oury, F., Suda, N., Liu, Z. W., Gao, X. B., Confavreux, C., et al. (2009). A serotonin-dependent mechanism explains the leptin regulation of bone mass, appetite, and energy expenditure. *Cell* 138, 976–989. doi: 10.1016/j.cell.2009.06.051

Yoshihara-Hirata, C., Yamashiro, K., Yamamoto, T., Aoyagi, H., Ideguchi, H., Kawamura, M., et al. (2018). Anti-hmgb1 neutralizing antibody attenuates periodontal inflammation and bone resorption in a Murine Periodontitis model. *Infect. Immun.* 86:e00111-18. doi: 10.1128/IAI.00111-18

Zehnder, D., Quinkler, M., Eardley, K. S., Bland, R., Lepenies, J., Hughes, S. V., et al. (2008). Reduction of the vitamin D hormonal system in kidney disease is associated with increased renal inflammation. *Kidney Int.* 74, 1343–1353. doi: 10.1038/ki.2008.453

Zhao, J., Huang, M., Zhang, X., Xu, J., Hu, G., Zhao, X., et al. (2019). MiR-146a deletion protects from bone loss in OVX Mice by suppressing RANKL/OPG and M-CSF in Bone Microenvironment. *J. Bone Min. Res.* 34, 2149–2161. doi: 10.1002/jbmr.3832

Conflict of Interest: SE was employed by Philadelphia 76ers. SM was employed by Orlando Magic.

The remaining authors declare that the research was conducted in the absence of any commercial or financial relationships that could be construed as a potential conflict of interest.

frontiers in Physiology

MINI REVIEW
published: 14 January 2021
doi: 10.3389/fphys.2020.609614

Inflammation in Periodontal Disease: Possible Link to Vascular Disease

*Oindrila Paul[1], Payal Arora[2], Michael Mayer[3] and Shampa Chatterjee[1]**

[1] Institute for Environmental Medicine, Department of Physiology, University of Pennsylvania School of Medicine, Philadelphia, PA, United States, [2] Early-Research Oral Care, Colgate-Palmolive Company, Piscataway, NJ, United States, [3] Department of Radiology, University of Pennsylvania School of Medicine, Philadelphia, PA, United States

Inflammation is a well-organized protective response to pathogens and consists of immune cell recruitment into areas of infection. Inflammation either clears pathogens and gets resolved leading to tissue healing or remains predominantly unresolved triggering pathological processes in organs. Periodontal disease (PD) that is initiated by specific bacteria also triggers production of inflammatory mediators. These processes lead to loss of tissue structure and function. Reactive oxygen species and oxidative stress play a role in susceptibility to periodontal pathogenic bacterial infections. Periodontal inflammation is a risk factor for systemic inflammation and eventually cardiovascular disease (CVD). This review discusses the role of inflammation in PD and its two way association with other health conditions such as diabetes and CVD. Some of the mechanisms underpinning the links between inflammation, diabetes, CVD and PD are also discussed. Finally, we review available epidemiological data and other reports to assess possible links between oral health and CVD.

Keywords: vascular inflammation, cardiovascular disease, dental plaque, risk factors, oxidative stress, antioxidants, NLRP3 inflammasome, periodontal disease (PD)

OPEN ACCESS

Edited by:
John D. Imig, Medical College of Wisconsin, United States

Reviewed by:
Dorina Lauritano, University of Milano-Bicocca, Italy
Tomoko Kurita-ochiai, Nihon University School of Dentistry at Matsudo, Japan

***Correspondence:**
Shampa Chatterjee
shampac@pennmedicine.upenn.edu

Specialty section:
This article was submitted to Vascular Physiology, a section of the journal Frontiers in Physiology

Received: *24 September 2020*
Accepted: *21 December 2020*
Published: *14 January 2021*

Citation:
Paul O, Arora P, Mayer M and Chatterjee S (2021) Inflammation in Periodontal Disease: Possible Link to Vascular Disease. Front. Physiol. 11:609614. doi: 10.3389/fphys.2020.609614

INTRODUCTION

Periodontal disease (PD) is a chronic inflammatory disorder characterized by the destruction of the periodontium, or the supporting tissues of the teeth (gingival tissue, periodontal ligament, and alveolar bone). PD is highly prevalent, and approximately 50% of adults 30 years and older and 70% of adults 65 or older have a form of the disease (Eke et al., 2012). Clinically, the failure to treat PD leads to loss of teeth (Schultz-Haudt et al., 1954; Hajishengallis et al., 2011; Abusleme et al., 2013). Central to PD is dysregulation of the resolution of inflammation, resulting in characteristic chronic and progressive destruction.

Inflammation is a programmed signaling event initiated to protect organisms upon infection and/or injury. In general, infection-injury stimuli lead to release of pathogen or danger associated molecular patterns (PAMPs or DAMPs) followed by their binding to respective receptors in the host cells. Although there are multiple contributing factors to PD, one of the increasingly well-characterized triggers is the colonization of the oral cavity by pathogenic bacteria and their subsequent penetration into local epithelial lining (Darveau, 2010; Abusleme et al., 2013). This initiates an inflammatory cascade characterized by increased expression of various inflammatory mediators and adhesion molecules that collectively mobilize and recruit polymorphonuclear neutrophils (PMN), macrophages, natural killer (NK), dendritic cells (DC) etc. into the affected tissue. Under normal conditions, neutrophils and macrophages phagocytose the microbial organisms after which they undergo apoptosis at the inflamed site (Fox et al., 2010). The clearance of apoptotic

cells facilitates a switch from a pro- to an anti-inflammatory macrophage phenotype (Fadok et al., 1998; Michlewska et al., 2009) and initiates the onset of the resolution of inflammation, a coordinated signaling process that restores tissue integrity and function. However, failure to switch off the inflammation cascade once the pathogenic stimulus is removed, leads chronic inflammation (i.e., an uncontrolled inflammatory response that can culminate into damage to the host tissue) and is the hallmark of several inflammatory disorder related pathologies. In PD specifically, the inflammatory response becomes chronic when pathogenic bacteria continue to propagate and cannot be controlled by the acute immune response, resulting in unresolved inflammation, destruction of local bone and soft tissue, and fibrosis (Cochrane, 2008).

Importantly, reports have consistently highlighted a role for periodontal inflammation in acceleration of various vascular pathologies and other systemic implications (Humphrey et al., 2008; Ogrendik, 2013; Ketabi et al., 2016). The destruction of local epithelium by PD pathogens can result in release of local inflammatory mediators from the periodontal pocket into the systemic circulation thus facilitating immune cell recruitment elsewhere. Also, bacteria can either indirectly (within immune cells that have ingested them) or directly circulate in the bloodstream (Lockhart et al., 2009). Therefore, under conditions where there is disposition (e.g., genetic, lifestyle) toward cardiovascular disease (CVD), the bacterial components and systemic inflammatory mediators can potentially accelerate plaque formation. To this point, PD pathogens have been detected in distant tissues and organs, particularly in the cardiovascular system (Okuda et al., 2001; Kozarov et al., 2006; Nakano et al., 2006; Pessi et al., 2013; Moreno et al., 2017). The relationship between PD and systemic diseases such as CVD has been increasingly well-characterized. Importantly, two classic meta-analyses demonstrated the correlation between PD and CVD, highlighting PD as a potential risk factor for CVD processes such as coronary artery disease (Janket et al., 2003; Khader et al., 2004). Additionally, recent evidence suggests a major role for reactive oxygen species (ROS) and proteolytic enzymes (bacteria- and host-derived) in PD and CVD such as atherosclerosis (Chistiakov et al., 2016).

CVD is an umbrella term for a number of linked pathologies, commonly defined as coronary heart disease (CHD), cerebrovascular disease, peripheral arterial disease, rheumatic and congenital heart diseases, and venous thromboembolism (Lara-Pezzi et al., 2012; Mandviwala et al., 2016). The associated risk factors include ethnicity, age, and family history of CVD, dyslipidemia, hypertension, tobacco smoke, excess body weight, physical inactivity, and diabetes mellitus. It is well established that these classic risk factors interact with cellular immune-inflammatory signaling processes to lead to endothelial dysfunction and atheromatous plaque development (Lopez-Candales et al., 2017; Lazzerini et al., 2019). Thus chronic inflammation plays a crucial role in the long-term progression of atherosclerosis. About 35–50% of the world population suffers from periodontitis as reported by World Health Organization (Petersen and Ogawa, 2012); therefore understanding any correlation or link between PD and CVD is a question that has tremendous importance given the high incidences of both diseases. This review summarizes pathophysiology of PD and examines the possibility of its link with CVD.

PERIODONTAL DISEASE

The inflammation of tissues in gingivitis and periodontitis is caused by a host of bacteria (Schultz-Haudt et al., 1954). The bacterial species present in the gingival margin are *Porphyromonas gingivalis*, *Treponema denticola*, and *Tannnerella forsythia*, all of which are Gram negative. Also present are Gram positive bacteria like *Streptococcus sanguis*, *Streptococcus oralis*, *Streptococcus mutans*, *Actinomyces naeslundii*, and *Actinomyces odontolyticus (Abusleme et al., 2013)*. This is followed by appearance of secondary bacteria such as *Fusobacterium nucleatum* (Kolenbrander et al., 1989). Aggregates of bacterial colonies form and Gram-positive and Gram-negative bacilli become embedded in the extracellular matrix (Gibbons, 1989). Indeed more than 700 bacterial species have been reported to be detected in dental plaques (Moore, 1987; Gao et al., 2018). Bacterial species normally act as symbiotic communities with the host but shifts of the oral microbiome often associated with "poor" host health can lead to dysbiosis, an imbalance that is responsible for the development of microbe-related PD (Socransky et al., 1998; Darveau, 2010).

Several of these bacteria are also present in healthy individuals; however it is their relative abundance due to with poor oral hygiene (Hoare et al., 2019), tobacco consumption etc. that drives the selection and prevalence of pathogenic bacteria in subgingival margin that lead to the onset of periodontitis (Schultz-Haudt et al., 1954; Socransky et al., 1998). Increased oxidative stress with smoking, lifestyle diseases and aging also plays a role; indeed a strong association between oxidative stress and PD has been reported (Chapple and Matthews, 2007). This occurs either due to diminution of antioxidants or an exaggerated inflammatory response post periodontal infection. This is described in the next section. Bacterial plaque formation leads to increases in PAMPs causing a rise in local inflammation, causing increased flow of gingival crevicular fluid (GCF). This in turn provides protein rich nutrients that increase the proliferation of the Gram-negative bacteria. The dental plaque biofilm of bacteria in the periodontal crevice induces clinical signs of inflammation. The progression of PD is driven primarily by the proliferation of *P. gingivalis* which facilitates increase in harmful microbiota. The next step is the secondary bacteria *F. nucleatum's* role in the subgingival biofilm as this bacterium interacts with other bacterial species found in the biofilm. *F. nucleatum* serves as a bridge between the early colonizers like *Streptococcus* sp. and the late colonizers like *P. gingivalis*. The innate immune response is the recruitment of PMN and the NK cells that is driven by the subgingival bacterial community present in the periodontal pocket. As the microorganisms are abundant, PMN recruitment and phagocytosis is followed by extensive PMN apoptosis or necrosis. A cytokine rich proinflammatory environment consists of tumor necrosis factor (TNF)-α, interleukins (IL)-1, IL-4, IL-10, interferon (IFN-γ) and transforming growth factor (TGF-β).

These signaling molecules stimulate the activation of enzymes and transcription factors that in turn recruit more immune cells and degrade the surrounding tissues by maintaining a continual loop of local inflammation (Cekici et al., 2014; **Figure 1**). This is also accompanied by an adaptive immune response as antigen uptake and processing is carried out by DC and presented to naive T cells. DCs direct CD4+ T cells to differentiate to T-cell subsets such as T helper cells types 1, 2, and 17, and regulatory T cells (Song et al., 2018). CD4+ T cells produce the bone resorption promoting cytokine, Receptor activator of nuclear factor-κB (RANK-L; Tang et al., 2007) leading to bone loss.

OXIDATIVE STRESS IN PD and CVD

Reactive oxygen species and the resultant oxidative stress plays an important role in onset and progression of PD (Chapple and Matthews, 2007). This occurs via multiple mechanisms. First, is the ROS production that occurs with periodontal infection, as inflammatory cells are recruited to the infection site with chronic or aggressive periodontitis. Numerous reports have shown that PMN in the population diagnosed with PD generate significantly more ROS (upon stimulation) as compared to PMN of healthy controls (Aboodi et al., 2011; White et al., 2014; Ling et al., 2016). While this is indicative of a hyper-reactive phenotype of neutrophils in the PD affected, it also suggests that high oxidative stress arising from the excessive ROS could increase local gingival oxidative stress which in turn would drive more inflammation. Alteration of the gingival crevicular environment increase susceptibility to periodontal pathogenic bacteria. Second, is the antioxidant status of PD affected individuals; several studies have shown that the low levels of anti-oxidants (that may be associated with high levels of ROS) in the GCF activated the local periodontal inflammation and caused oxidative injury and destruction of the tissue (Tsai et al., 2005; Chapple and Matthews, 2007; Konopka et al., 2007). **Figure 2** shows the feed forward loop of infection induced ROS and oxidative stress that in turn drives more inflammation and changes the local gingival tissue environment making it more susceptible to infection. Lifestyle diseases also play a part in this ROS oxidative stress inflammation cascade.

As is well established, inflammation and oxidative stress are pivotal events that lead to CVD (Mandviwala et al., 2016; Cervantes Gracia et al., 2017) and seem to be the common link between the onset of tissue destruction in periodontitis and systemic inflammation (Wang et al., 2017). Indeed several lifestyle and age related conditions associated with CVD (such as diabetes, hypertension etc.) that lead to high oxidative stress (as assessed by markers of ROS and lipid peroxidation) can also increase susceptibility to PD (Dhadse et al., 2010). When periodontitis susceptible patients are exposed to the bacterial antigen, their main two immune responses in the form of neutrophil recruitment and proteolytic enzymes production further release ROS at the gingival site, thus perpetuating oxidative stress and tissue damage (Scott and Krauss, 2012; Cortes-Vieyra et al., 2016). As periodontitis progresses, periodontal inflammation produces ROS that diffuses into the blood stream (Sobaniec and Sobaniec-Lotowska, 2000; Tomofuji et al., 2007). As a result, various moieties in the blood get oxidized and induce an oxidative stress on other organs via the circulating blood causing circulating oxidative stress (Yagi, 1987; Tomofuji et al., 2007; **Figure 3**). Thus, it can be inferred that the bacteria present in the periodontal pocket suppress detoxification of ROS by consuming the antioxidants present in the pockets

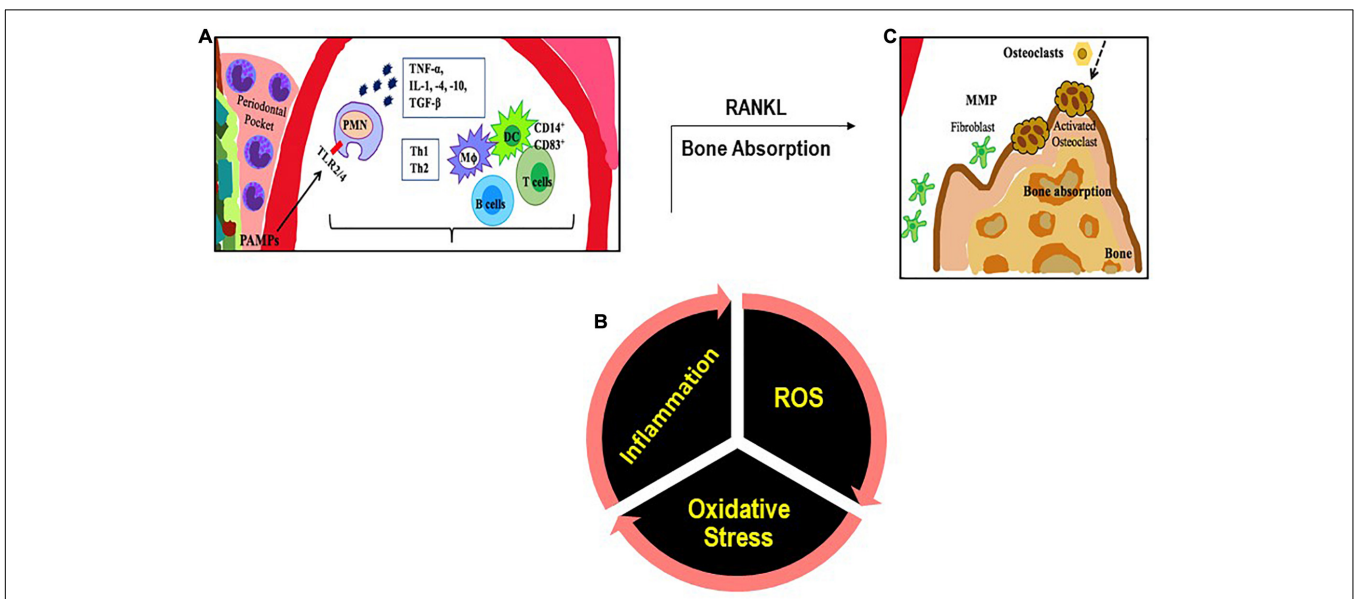

FIGURE 1 | An illustration of the inflammatory immune response with PD. **(A)** PAMPs (like LPS) are recognized by TLRs. The PAMP-TLR interaction triggers a proinflammatory signaling cascade that drives a chemokine and cytokine rich environment into which multiple immune cells [macrophages (MΦ), T and B lymphocytes, dendritic cells (DC)] are recruited. **(B)** Multiple immune cells produce ROS. **(C)** T cells produce the cytokine RANKL that participates in bone resorption.

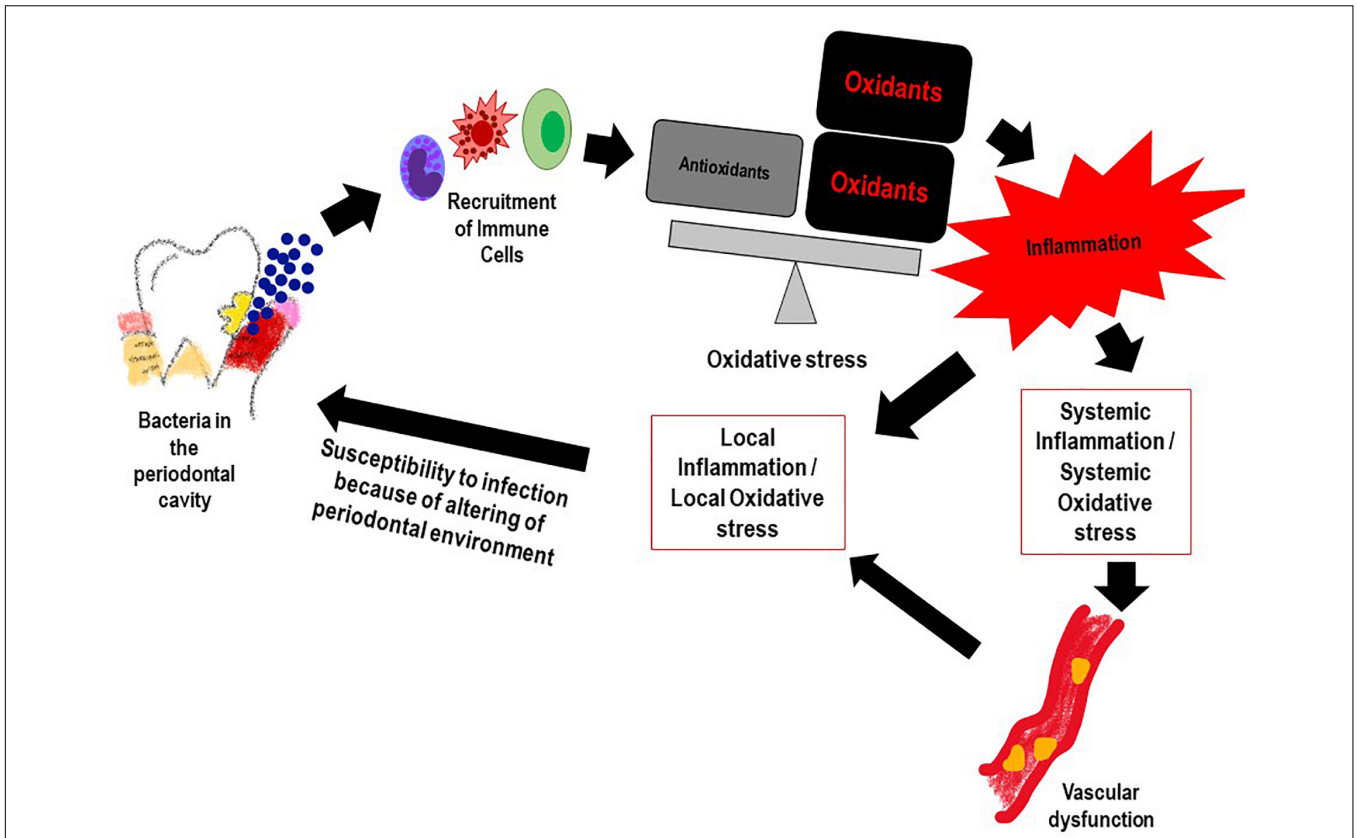

FIGURE 2 | The feed forward mechanism of the "Infection-ROS-Inflammation" triad that seems to accelerate susceptibility to infection, inflammation and oxidative stress.

of the oral cavity (Ekuni et al., 2009). The consequence of the lowered levels of antioxidants enables ROS to enter into systemic circulation from the periodontal tissues (Wang et al., 2017).

Regular smoking, diabetes mellitus, insufficient and appropriate nutrition, and aging have all been mentioned as risk factors for both PD and CVD (Yanbaeva et al., 2007; Graves and Kayal, 2008; Dhadse et al., 2010). All the above lifestyle diseases have been known to increase the circulating oxidative stress; indeed increase in levels of malondialdehyde (MDA) and 4-hydroxynonenal (HNE) locally and systemically with PD and with CVD have been observed, thus suggesting an association between local and systemic oxidative stress diseases (Celec et al., 2005; Guentsch et al., 2008; Hendek et al., 2015). Similarly, levels of antioxidants such as SOD and glutathione decrease in the (GCF) and saliva due to smoking in both, healthy individuals and patients with periodontitis (Guentsch et al., 2008; Agnihotri et al., 2009).

RISK FACTORS (PD AND VASCULAR INFLAMMATION)

Vascular inflammation involves the onset of a signaling cascade that is triggered by endothelial signaling which leads to increase in cellular adhesions molecules, cytokines and chemokines. This leads to recruitment and adherence of immune cells. The atherogenic process starts with endothelial dysfunction and the accumulation of several plasma low density lipoproteins (LDL) in the subendothelial space. The accumulation of LDL correlates with classical risk factors, such as smoking, hypertension, and metabolic dysregulation in obesity and diabetes mellitus (Gimbrone et al., 2000). As these risk factors are largely associated with PD too, it is reasonable to conclude that common biochemical signaling pathways play a role in vulnerability to both CVD and PD. All the major risk factors associated with PD either activate pathogen initiated inflammation signals (bacteria like *P. gingivalis* and *A. actinomycetemcomitans B. forsythus, P. intermedia, P. micros*, and *F. nucleatum* (Lovegrove, 2004; Saito et al., 2008) or a life style (diabetes mellitus, obesity, aging, smoking, vascular disease) driven inflammatory cascade (Jensen et al., 1991; Grossi and Genco, 1998; Cohen, 2000; Merchant et al., 2003; Humphrey et al., 2008; Hujoel, 2009; Kumar et al., 2011; Nakamura et al., 2011; Ozcaka et al., 2011). Nutrition and oral health are closely linked. This is because oxidative stress and antioxidant balance which drives ROS induced inflammation signals, can be regulated by diets rich in antioxidants (Muniz et al., 2015). Diets that lead to obesity such as high carbohydrates and sugars have been implicated in dental caries and PD as these drive plaque formation and

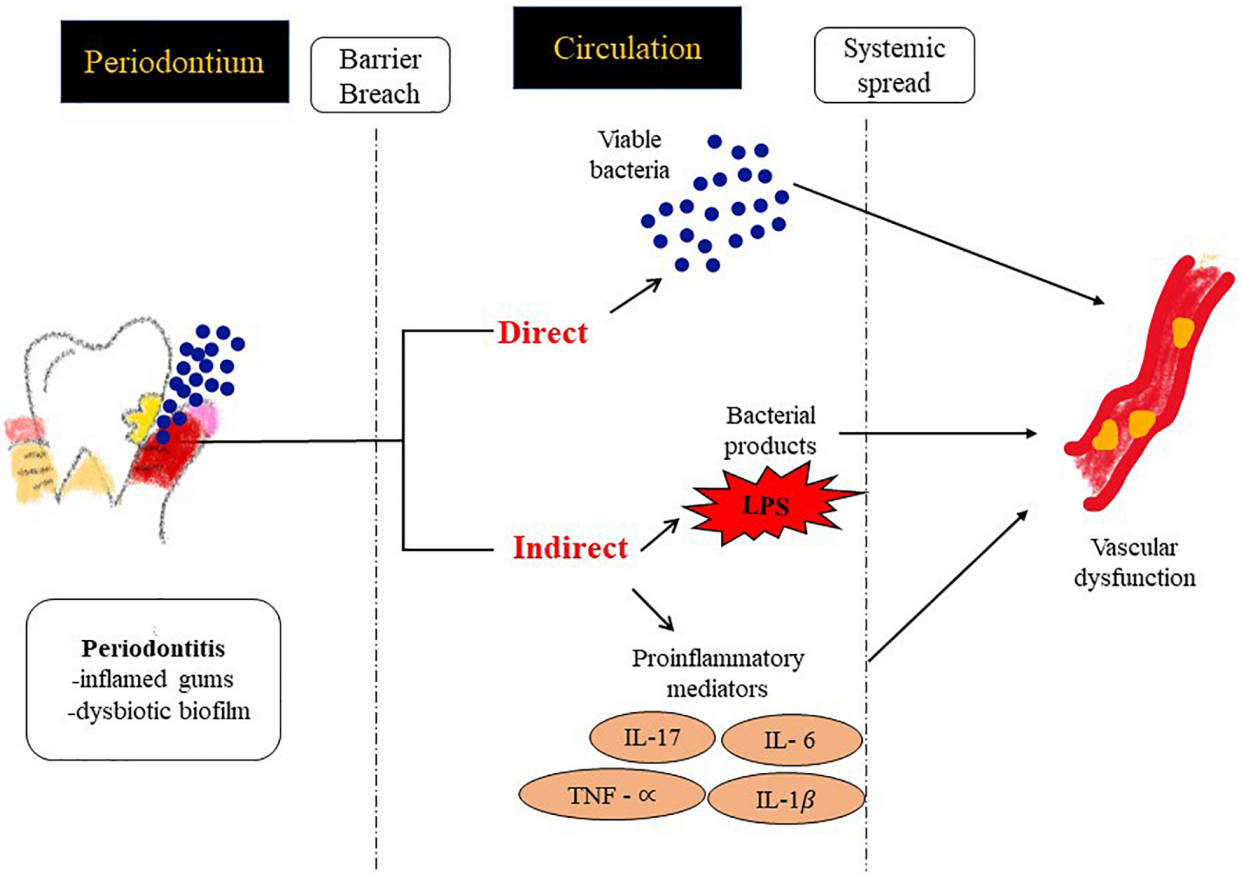

FIGURE 3 | Possible mechanisms by which PD contributes to inflammation at distal sites and thus drives an atherosclerotic phenotype. (1) Direct: vascular infection by periodontal bacterial pathogens and (2) Indirect: facilitating the passage of inflammatory modulators into the systemic circulation.

accelerate inflammation thus causing dental tissue oxidative damage and decay (Hujoel, 2009). Changes in dietary intake influence the extent of PD. As seen in the dietary intake of adolescents between 11 and 18 years old, the decrease in consumption of raw fruits and non-potato vegetables with concomitant increase in uptake of soft drinks, led to increased PD (Chaffee and Weston, 2010).

Indeed when all these risk factors are controlled, both PD and CVD show improvement (**Table 1**; Higashi et al., 2008; Bokhari et al., 2012; Montenegro et al., 2019; Lobo et al., 2020).

PD AND CVD: IS THERE A LINK?

It is not clear if there is a direct and common thread between PD and CVD; however the fact that people with PD have a two or three times higher risk of a cardiovascular event (stroke, heart attack etc.) seems to point to a cluster of shared risk factors between the two (Sanz et al., 2020). The "inflammation" link seems to be a key contributor to both.

For instance, when infected with *P. gingivalis*, the host innate immune system responds by activating inflammation consisting of the NLRP3 inflammasome (pro-inflammatory IL-1β, IL-18) (Lamkanfi and Dixit, 2009; Xue et al., 2015). Patients with chronic PD and aggressive PD expressed significantly higher levels of NLRP3 in gingiva (Xue et al., 2015; Ran et al., 2017). In wild type mice with *P. gingivalis* infection, the increase in expression of NLRP3 inflammation cascade in the gingival tissue was matched with a concomitant increase in caspase-1 activity in the macrophages found in peritoneum; this was not observed in NLRP3 deficient mice (Yamaguchi et al., 2017). This suggests that the NLRP3 inflammasome activated in periodontitis has effects on the systemic organs. NLRP3 inflammasome has also been shown to be highly expressed and activated with systemic vascular disease (Satoh et al., 2014) although it is not clear whether NLRP3 from *P. gingivalis* (Yamaguchi et al., 2017) is directly involved. However, excess ROS, glucose, ATP, ceramides, sphingosine, cholesterol crystals, uric acid and oxidized LDL (all of which are associated with CVD) have been known to activate NLRP3 inflammasome (Duewell et al., 2010; Jiang et al., 2012; Luheshi et al., 2012).

Epidemiologic data till date that suggest an association between PD and CVD (Humphrey et al., 2008; Blaizot et al., 2009; Tonetti, 2009) have monitored PD via indices of clinical

TABLE 1 | Clinical trials investigating relationship between periodontal disease and cardiovascular disease.

Citation	Aims	Patients	Cohorts	Outcomes
Elter et al., 2006	Effect of periodontal treatment on endothelium-dependent flow-mediated dilation and serum inflammatory biomarkers in patients with PD	Twent-two male patients with PD	All patients underwent periodontal treatment (scaling and root planning, periodontal flap surgery if indicated, and extraction of hopeless teeth)	Periodontal treatment resulted in significant improvements in flow-mediated dilation and decreased serum IL-6 (and a trend toward reduction in CRP)
D'Aiuto et al., 2006	Effects of intensive periodontal treatment on serum inflammatory biomarkers, serum lipid levels, and blood pressure in patients with PD	Forty patients with severe PD	- Experimental group: subject to intensive periodontal treatment (defined as standard treatment plus adjunctive use of a locally delivered antimicrobial) - Control group: standard periodontal treatment (scaling and root planning)	Intensive periodontal treatment resulted in significant reduction in IL-6, CRP, total cholesterol, and systolic blood pressure at 2-month follow-up
Tonetti et al., 2007	To investigate the effects of periodontal treatment on parameters of endothelial function in patients with PD	Hundred and twnety patients with severe PD	- Experimental group: subject to intensive PD treatment - Control group: subject to community-based periodontal care	Intensive periodontal treatment resulted in reduced brachial artery flow, reduced levels of CRP and IL-6, and elevated endothelial-activation markers.- Intensive treatment was associated with reduced indexes of periodontal disease severity and significantly better endothelial function at 6 month follow-up
Higashi et al., 2008	To evaluate endothelial function in patients with hypertension and PD	Sixty-four patients with hypertension (26 with PD and 38 without PD)	- Experimental group: subject to periodontal treatment - Control group: subject to community-based periodontal care	Periodontal treatment resulted in decreased serum CRP and IL-6 at 24-week follow-up Periodontal treatment resulted in reduced acetylcholine-stimulated vasodilation Delivery of a nitric oxide synthase inhibitor before and after PD treatment resulted in similar acetylcholine-stimulated vasodilation, suggesting role of nitric oxide bioavailability in mechanism of endothelial dysfunction in patients with PD
Higashi et al., 2009	To evaluate endothelial function and the effects of periodontal treatment on patients with CAD and PD	101 patients with CAD (48 with PD and 53 without PD)	- Experimental group: subject to periodontal treatment - Control group: subject to community-based periodontal care	- Periodontal treatment resulted in decreased serum CRP and IL-6 at follow-up - Periodontal treatment resulted in reduced acetylcholine-stimulated vasodilation - Delivery of a nitric oxide synthase inhibitor before and after PD treatment resulted in similar acetylcholine-stimulated vasodilation, suggesting role of nitric oxide bioavailability in mechanism of endothelial dysfunction in patients with PD
Offenbacher et al., 2009	Impact of periodontal treatment on serum CRP levels, clinical PD parameters, and cardiovascular endpoints in patients with PD	Three hundred three patients with PD and previous history of CVD	- Experimental group: subject to periodontal treatment (scaling and root planning - Control group: not subject to periodontal treatment	Periodontal treatment resulted in a significant improvement in PD status at 6 months as assessed by reduction of probing depth, but no difference in attachment levels, bleeding upon probing, or extent of subgingival calculus Periodontal treatment resulted in significant decrease of the odds of being in the high-risk (>3 mg/L) CRP group at 6 months, with obesity nullifying such effect

(Continued)

TABLE 1 | Continued

Citation	Aims	Patients	Cohorts	Outcomes
Vidal et al., 2009	Effects of non-surgical PD treatment on plasma levels of inflammatory markers (interleukin [IL]-6, C-reactive protein [CRP], and fibrinogen) in patients with severe PD and refractory arterial hypertension	Twenty-two patients with severe PD and refractory arterial hypertension	- Experimental group: subject to periodontal treatment at start of trial - Control group: subject to periodontal treatment delayed 3-months from start of trial	Periodontal treatment resulted in significant reduction in markers of PD severity (probing, probing depth, and clinical attachment loss) Periodontal treatment resulted in significant reduction of fibrinogen, CRP, and IL-6
Wehmeyer et al., 2013	Impact of periodontal treatment PD parameters and inflammatory biomarkers in patients with end-stage renal disease and PD	Three hundred forty-two dialysis patients with moderate/severe chronic PD	- Experimental group: subject to intensive periodontal treatment - Control group: subject to intensive periodontal treatment following study completion at 6 months	Intensive periodontal treatment resulted in significantly improved measures of periodontal health at 3 months, but only PD remained significantly different at 6 months No significant difference between the groups inflammatory biomarkers (serum albumin or high-sensitivity interleukin 6) at any time point
Bokhari et al., 2012	Effect of non-surgical periodontal treatment on systemic C-reactive protein, fibrinogen and white blood cells in coronary heart disease patients with PD	Three hundred seventeen patientswith angiographically proven coronary heart disease	- Experimental group: subject to on-surgical periodontal treatment (scaling, root planning and oral hygiene instructions) - Control group: not subject to periodontal treatment	Non−surgical periodontal treatment resulted in significant reduction of systemic levels of inflammatory markers (CRP, fibrinogen and WBCs) at 2-month follow-up
Caula et al., 2014	Influence of non−surgical mechanical PD treatment on c-reactive protein serum level, erythrocyte sedimentation rate (ESR), and lipid profile in patients with severe chronic periodontitis	Sixty-four patients with severe chronic PD	- Experimental group: Began non-surgical PD treatment - Control group: Withheld PD treatment during study period	PD treatment resulted in a significant reduction of ESR and triglycerides at 2 months PD treatment resulted in significant reduction in median values of C−reactive protein, ESR, total cholesterol, and triglycerides after 6 months
Zhou et al., 2017	To investigate if intensive periodontal treatment can lower blood pressure levels and endothelial microparticles (EMPs) in patients with prehypertension and PD without antihypertensive medication	Hundred and seven patients with prehypertension and PD	- Experimental group: Subject to intensive periodontal treatment - Control group: Subject to community−based periodontal care	Intensive periodontal treatment resulted in reduced clinical PD parameters, reduced systolic and diastolic blood pressures, and reduced endothelial microparticles
Montenegro et al., 2019	To assess the effect of periodontal treatment on clinical PD parameters and levels of cardiovascular risk biomarkers in stable coronary artery disease (CAD) patients (CRP, glycated hemoglobin, lipids, IL−1β, IL−6, IL−8, IL−10, IFN−γ and TNF−α)	88 patients with stable coronary artery disease and periodontitis	- Experimental group: Subject to non-surgical periodontal treatment - Control group: Subject to one session of plaque removal	Periodontal treatment resulted in significantly better periodontal parameters after 3 months without significant differences in blood biomarkers In patients with baseline high levels of CRP, periodontal treatment resulted in lower levels of CRP, IL−6 and IL−8
Lobo et al., 2020	To investigate the impact of periodontal treatment on the endothelial function of patients with a recent ST-segment elevation myocardial infarction (STEMI), specifically looking at variation of flow-mediated vasodilation (FMD) in the brachial artery, inflammatory biomarkers, and adverse CVD events	Forty-eight patients with PD and with recent admission for STEMI	- Experimental group: subject to periodontal treatment within 2 weeks of STEMI - Control group: not subject to periodontal treatment	Periodontal treatment significantly improved endothelial function of the brachial artery without adverse clinical effects over a period of 6 months Inflammatory biomarkers and cardiovascular events were not significantly different between both groups

attachment level, pocket depth, bleeding on probing and decayed-missing-filled teeth and CVD by degree and number of obstructed coronary arteries, observed an association between PD and CVDs (Ketabi et al., 2016). **Table 1** shows the clinical trials which investigated the relationship between the two diseases. While risk factors as discussed in the earlier section play a crucial role in the onset of CVD, increasing number of CVD patients do not harbor the classical risk factors. Low grade infection such as in periodontal infection could be a potential cause for CVD in these cases; indeed several studies show that PD as a risk factor for CVD and, in particular, atherosclerosis (Bartova et al., 2014; Toregeani et al., 2016).

Potential links between PD and CVD could be via two mechanisms (**Figure 3**).

1. Systemic Inflammation: Systemic inflammatory markers such as C-reactive protein (CRP), IL-6 etc. have shown direct correlation with specific indices of CVD such as carotid-intima media thickness, or MI (myocardial infarct size) (Ali et al., 2006). Chronic periodontal infection is characterized by elevation of CRP and inflammatory cytokines in the systemic circulation (Loos et al., 2000), so it is possible that systemic inflammation in patients with PD can potentially accelerate endothelial dysfunction, plaque buildup and CHD events.
2. Vascular Infection: There have been reports that identify bacterial species in blood after dental procedures suggesting gingiva as a portal via which oral bacterial pathogens can enter the systemic circulation (Bahrani-Mougeot et al., 2008; Lockhart et al., 2009). As a result bacteremia of dental origin seems to play a role in the appearance of bacterial endocarditis (Mang-de la Rosa et al., 2014) and periodontal bacterial components colonize human atheromatous plaques (Haraszthy et al., 2000; Fiehn et al., 2005).

CONCLUSION

While both PD and CVD have manifestations of classic inflammation, a causative link between them has not been established. However, oxidative stress arising from lifestyle diseases play a crucial role in progression of both PD and CVD, indicating that host influence in terms of an imbalance between ROS production and endogenous antioxidant levels can increase susceptibility in individuals.

Understanding how oxidative stress and inflammation overlap in PD and CVD for high risk and older populations is of great public health importance because of the high prevalence of PD. Although both these pathologies arise from the same risk factors and show a similar systemic inflammation profile, it is not clear how these diseases intersect. Therefore it cannot be concluded that therapeutic periodontal interventions can prevent heart disease or stroke. Nevertheless, controlling the overall inflammation status by implementing a good periodontal maintenance program could presumably control the progression of CVD in periodontitis patients.

AUTHOR CONTRIBUTIONS

OP drafted the article and prepared the figures. PA drafted the article. MM drafted the article and prepared the table. SC developed the concept and outline, drafted the article, and formalized the final version. All authors approved the submission.

FUNDING

Funding was provided by a Colgate Palmolive Grant (A-2019-592-OC) to SC.

REFERENCES

Aboodi, G. M., Goldberg, M. B., and Glogauer, M. (2011). Refractory periodontitis population characterized by a hyperactive oral neutrophil phenotype. *J. Periodontol.* 82, 726–733. doi: 10.1902/jop.2010.100508

Abusleme, L., Dupuy, A. K., Dutzan, N., Silva, N., Burleson, J. A., Strausbaugh, L. D., et al. (2013). The subgingival microbiome in health and periodontitis and its relationship with community biomass and inflammation. *ISME J.* 7, 1016–1025. doi: 10.1038/ismej.2012.174

Agnihotri, R., Pandurang, P., Kamath, S. U., Goyal, R., Ballal, S., Shanbhogue, A. Y., et al. (2009). Association of cigarette smoking with superoxide dismutase enzyme levels in subjects with chronic periodontitis. *J. Periodontol.* 80, 657–662. doi: 10.1902/jop.2009.080545

Ali, Y. S., Rembold, K. E., Weaver, B., Wills, M. B., Tatar, S., Ayers, C. R., et al. (2006). Prediction of major adverse cardiovascular events by age-normalized carotid intimal medial thickness. *Atherosclerosis* 187, 186–190. doi: 10.1016/j.atherosclerosis.2005.09.003

Bahrani-Mougeot, F. K., Paster, B. J., Coleman, S., Ashar, J., Barbuto, S., and Lockhart, P. B. (2008). Diverse and novel oral bacterial species in blood following dental procedures. *J. Clin. Microbiol.* 46, 2129–2132. doi: 10.1128/jcm.02004-07

Bartova, J., Sommerova, P., Lyuya-Mi, Y., Mysak, J., Prochazkova, J., Duskova, J., et al. (2014). Periodontitis as a risk factor of atherosclerosis. *J. Immunol. Res.* 2014:636893.

Blaizot, A., Vergnes, J. N., Nuwwareh, S., Amar, J., and Sixou, M. (2009). Periodontal diseases and cardiovascular events: meta-analysis of observational studies. *Int. Dent. J.* 59, 197–209.

Bokhari, S. A., Khan, A. A., Butt, A. K., Azhar, M., Hanif, M., Izhar, M., et al. (2012). Non-surgical periodontal therapy reduces coronary heart disease risk markers: a randomized controlled trial. *J. Clin. Periodontol.* 39, 1065–1074. doi: 10.1111/j.1600-051x.2012.01942.x

Caula, A. L., Lira-Junior, R., Tinoco, E. M., and Fischer, R. G. (2014). The effect of periodontal therapy on cardiovascular risk markers: a 6-month randomized clinical trial. *J. Clin. Periodontol.* 41, 875–882. doi: 10.1111/jcpe.12290

Cekici, A., Kantarci, A., Hasturk, H., and Van Dyke, T. E. (2014). Inflammatory and immune pathways in the pathogenesis of periodontal disease. *Periodontology* 2000, 57–80. doi: 10.1111/prd.12002

Celec, P., Hodosy, J., Celecova, V., Vodrazka, J., Cervenka, T., Halcak, L., et al. (2005). Salivary thiobarbituric acid reacting substances and malondialdehyde–their relationship to reported smoking and to parodontal status described by the papillary bleeding index. *Dis. Markers* 21, 133–137. doi: 10.1155/2005/693437

Cervantes Gracia, K., Llanas-Cornejo, D., and Husi, H. (2017). CVD and oxidative stress. *J. Clin. Med.* 6:22. doi: 10.3390/jcm6020022

Chaffee, B. W., and Weston, S. J. (2010). Association between chronic periodontal disease and obesity: a systematic review and meta-analysis. *J. Periodontol.* 81, 1708–1724. doi: 10.1902/jop.2010.100321

Chapple, I. L., and Matthews, J. B. (2007). The role of reactive oxygen and antioxidant species in periodontal tissue destruction. *Periodontology* 2000, 160–232. doi: 10.1111/j.1600-0757.2006.00178.x

Chistiakov, D. A., Orekhov, A. N., and Bobryshev, Y. V. (2016). Links between atherosclerotic and periodontal disease. *Exp. Mol. Pathol.* 100, 220–235. doi: 10.1016/j.yexmp.2016.01.006

Cochrane (2008). New cochrane systematic reviews — cochrane oral health group. *J. Evid. Based Dent. Pract.* 8, 258–260. doi: 10.1016/j.jebdp.2008.09.001

Cohen, D. W. (2000). Periodontal medicine in the next millennium. *Intl. J. Periodontics Restorative Dent.* 20, 6–7.

Cortes-Vieyra, R., Rosales, C., and Uribe-Querol, E. (2016). Neutrophil functions in periodontal homeostasis. *J. Immunol. Res.* 2016:1396106.

D'Aiuto, F., Parkar, M., Nibali, L., Suvan, J., Lessem, J., and Tonetti, M. S. (2006). Periodontal infections cause changes in traditional and novel cardiovascular risk factors: results from a randomized controlled clinical trial. *Am. Heart. J.* 151, 977–984. doi: 10.1016/j.ahj.2005.06.018

Darveau, R. P. (2010). Periodontitis: a polymicrobial disruption of host homeostasis. *Nat. Rev. Microbiol.* 8, 481–490. doi: 10.1038/nrmicro2337

Dhadse, P., Gattani, D., and Mishra, R. (2010). The link between periodontal disease and cardiovascular disease: how far we have come in last two decades? *J. Indian Soc. Periodontol.* 14, 148–154. doi: 10.4103/0972-124x.75908

Duewell, P., Kono, H., Rayner, K. J., Sirois, C. M., Vladimer, G., Bauernfeind, F. G., et al. (2010). NLRP3 inflammasomes are required for atherogenesis and activated by cholesterol crystals. *Nature* 464, 1357–1361. doi: 10.1038/nature08938

Eke, P. I., Dye, B. A., Wei, L., Thornton-Evans, G. O., and Genco, R. J. (2012). Prevalence of periodontitis in adults in the United States: 2009 and 2010. *J. Dent. Res.* 91, 914–920. doi: 10.1177/0022034512457373

Ekuni, D., Tomofuji, T., Sanbe, T., Irie, K., Azuma, T., Maruyama, T., et al. (2009). Periodontitis-induced lipid peroxidation in rat descending aorta is involved in the initiation of atherosclerosis. *J. Periodontal Res.* 44, 434–442. doi: 10.1111/j.1600-0765.2008.01122.x

Elter, J. R., Hinderliter, A. L., Offenbacher, S., Beck, J. D., Caughey, M., Brodala, N., et al. (2006). The effects of periodontal therapy on vascular endothelial function: a pilot trial. *Am. Heart. J.* 151:47.

Fadok, V. A., Bratton, D. L., Konowal, A., Freed, P. W., Westcott, J. Y., and Henson, P. M. (1998). Macrophages that have ingested apoptotic cells in vitro inhibit proinflammatory cytokine production through autocrine/paracrine mechanisms involving TGF-beta. PGE2, and PAF. *J. Clin. Invest.* 101, 890–898. doi: 10.1172/jci1112

Fiehn, N. E., Larsen, T., Christiansen, N., Holmstrup, P., and Schroeder, T. V. (2005). Identification of periodontal pathogens in atherosclerotic vessels. *J. Periodontol.* 76, 731–736. doi: 10.1902/jop.2005.76.5.731

Fox, S., Leitch, A. E., Duffin, R., Haslett, C., and Rossi, A. G. (2010). Neutrophil apoptosis: relevance to the innate immune response and inflammatory disease. *J. Innate Immunity* 2, 216–227. doi: 10.1159/000284367

Gao, L., Xu, T., Huang, G., Jiang, S., Gu, Y., and Chen, F. (2018). Oral microbiomes: more and more importance in oral cavity and whole body. *Protein Cell* 9, 488–500. doi: 10.1007/s13238-018-0548-1

Gibbons, R. J. (1989). Bacterial adhesion to oral tissues: a model for infectious diseases. *J. Dent. Res.* 68, 750–760. doi: 10.1177/00220345890680050101

Gimbrone, M. A. Jr., Topper, J. N., Nagel, T., Anderson, K. R., and Garcia-Cardena, G. (2000). Endothelial dysfunction, hemodynamic forces, and atherogenesis. *Ann. N. Y. Acad. Sci.* 902, 230–239. doi: 10.1111/j.1749-6632.2000.tb06318.x

Graves, D. T., and Kayal, R. A. (2008). Diabetic complications and dysregulated innate immunity. *Front. Biosci.* 13, 1227–1239. doi: 10.2741/2757

Grossi, S. G., and Genco, R. J. (1998). Periodontal disease and diabetes mellitus: a two-way relationship. *Ann. Periodontol.* 3, 51–61. doi: 10.1902/annals.1998.3.1.51

Guentsch, A., Preshaw, P. M., Bremer-Streck, S., Klinger, G., Glockmann, E., and Sigusch, B. W. (2008). Lipid peroxidation and antioxidant activity in saliva of periodontitis patients: effect of smoking and periodontal treatment. *Clin. Oral Investig.* 12, 345–352. doi: 10.1007/s00784-008-0202-z

Hajishengallis, G., Liang, S., Payne, M. A., Hashim, A., Jotwani, R., Eskan, M. A., et al. (2011). Low-abundance biofilm species orchestrates inflammatory periodontal disease through the commensal microbiota and complement. *Cell Host Microbe* 10, 497–506. doi: 10.1016/j.chom.2011.10.006

Haraszthy, V. I., Zambon, J. J., Trevisan, M., Zeid, M., and Genco, R. J. (2000). Identification of periodontal pathogens in atheromatous plaques. *J. Periodontol.* 71, 1554–1560. doi: 10.1902/jop.2000.71.10.1554

Hendek, M. K., Erdemir, E. O., Kisa, U., and Ozcan, G. (2015). Effect of initial periodontal therapy on oxidative stress markers in gingival crevicular fluid, saliva, and serum in smokers and non-smokers with chronic periodontitis. *J. Periodontol.* 86, 273–282. doi: 10.1902/jop.2014.140338

Higashi, Y., Goto, C., Hidaka, T., Soga, J., Nakamura, S., Fujii, Y., et al. (2009). Oral infection-inflammatory pathway, periodontitis, is a risk factor for endothelial dysfunction in patients with coronary artery disease. *Atherosclerosis* 206, 604–610. doi: 10.1016/j.atherosclerosis.2009.03.037

Higashi, Y., Goto, C., Jitsuiki, D., Umemura, T., Nishioka, K., Hidaka, T., et al. (2008). Periodontal infection is associated with endothelial dysfunction in healthy subjects and hypertensive patients. *Hypertension* 51, 446–453. doi: 10.1161/hypertensionaha.107.101535

Hoare, A., Soto, C., Rojas-Celis, V., and Bravo, D. (2019). Chronic Inflammation as a Link between periodontitis and carcinogenesis. *Mediators Inflamm.* 2019:1029857.

Hujoel, P. (2009). Dietary carbohydrates and dental-systemic diseases. *J. Dent. Res.* 88, 490–502. doi: 10.1177/0022034509337700

Humphrey, L. L., Fu, R., Buckley, D. I., Freeman, M., and Helfand, M. (2008). Periodontal disease and coronary heart disease incidence: a systematic review and meta-analysis. *J. Gen. Intern. Med.* 23, 2079–2086. doi: 10.1007/s11606-008-0787-6

Janket, S. J., Baird, A. E., Chuang, S. K., and Jones, J. A. (2003). Meta-analysis of periodontal disease and risk of coronary heart disease and stroke. *Oral Surg. Oral Med. Oral Pathol. Oral Radiol. Endod.* 95, 559–569. doi: 10.1067/moe.2003.107

Jensen, J. A., Goodson, W. H., Hopf, H. W., and Hunt, T. K. (1991). Cigarette smoking decreases tissue oxygen. *Arch. Surg.* 126, 1131–1134. doi: 10.1001/archsurg.1991.01410330093013

Jiang, Y., Wang, M., Huang, K., Zhang, Z., Shao, N., Zhang, Y., et al. (2012). Oxidized low-density lipoprotein induces secretion of interleukin-1beta by macrophages via reactive oxygen species-dependent NLRP3 inflammasome activation. *Biochem. Biophys. Res. Commun.* 425, 121–126. doi: 10.1016/j.bbrc.2012.07.011

Ketabi, M., Meybodi, F. R., and Asgari, M. R. (2016). The association between periodontal disease parameters and severity of atherosclerosis. *Dent. Res. J.* 13, 250–255. doi: 10.4103/1735-3327.182185

Khader, Y. S., Albashaireh, Z. S., and Alomari, M. A. (2004). Periodontal diseases and the risk of coronary heart and cerebrovascular diseases: a meta-analysis. *J. Periodontol.* 75, 1046–1053. doi: 10.1902/jop.2004.75.8.1046

Kolenbrander, P. E., Andersen, R. N., and Moore, L. V. (1989). Coaggregation of *Fusobacterium nucleatum*, *Selenomonas flueggei*, *Selenomonas infelix*, *Selenomonas noxia*, and selenomonas sputigena with strains from 11 genera of oral bacteria. *Infect. Immun.* 57, 3194–3203. doi: 10.1128/iai.57.10.3194-3203.1989

Konopka, T., Krol, K., Kopec, W., and Gerber, H. (2007). Total antioxidant status and 8-hydroxy-2'-deoxyguanosine levels in gingival and peripheral blood of periodontitis patients. *Arch. Immunol. Ther. Exp.* 55, 417–422. doi: 10.1007/s00005-007-0047-1

Kozarov, E., Sweier, D., Shelburne, C., Progulske-Fox, A., and Lopatin, D. (2006). Detection of bacterial DNA in atheromatous plaques by quantitative PCR. *Microbes Infect.* 8, 687–693. doi: 10.1016/j.micinf.2005.09.004

Kumar, P. S., Matthews, C. R., Joshi, V., De Jager, M., and Aspiras, M. (2011). Tobacco smoking affects bacterial acquisition and colonization in oral biofilms. *Infect. Immun.* 79, 4730–4738. doi: 10.1128/iai.05371-11

Lamkanfi, M., and Dixit, V. M. (2009). Inflammasomes: guardians of cytosolic sanctity. *Immunol. Rev.* 227, 95–105. doi: 10.1111/j.1600-065x.2008.00730.x

Lara-Pezzi, E., Dopazo, A., and Manzanares, M. (2012). Understanding cardiovascular disease: a journey through the genome (and what we found there). *Dis. Models Mech.* 5, 434–443. doi: 10.1242/dmm.009787

Lazzerini, P. E., Hamilton, R. M., and Boutjdir, M. (2019). Editorial: cardioimmunology: inflammation and immunity in cardiovascular disease. *Front. Cardiovasc. Med.* 6:181.

Ling, M. R., Chapple, I. L., and Matthews, J. B. (2016). Neutrophil superoxide release and plasma C-reactive protein levels pre- and post-periodontal therapy. *J. Clin. Periodontol.* 43, 652–658. doi: 10.1111/jcpe.12575

Lobo, M. G., Schmidt, M. M., Lopes, R. D., Dipp, T., Feijo, I. P., Schmidt, K. E. S., et al. (2020). Treating periodontal disease in patients with myocardial infarction: a randomized clinical trial. *Eur. J. Intern. Med.* 71, 76–80. doi: 10.1016/j.ejim.2019.08.012

Lockhart, P. B., Brennan, M. T., Thornhill, M., Michalowicz, B. S., Noll, J., Bahrani-Mougeot, F. K., et al. (2009). Poor oral hygiene as a risk factor for infective endocarditis-related bacteremia. *J. Am. Dent. Assoc.* 140, 1238–1244. doi: 10.14219/jada.archive.2009.0046

Loos, B. G., Craandijk, J., Hoek, F. J., Wertheim-Van Dillen, P. M., and Van Der Velden, U. (2000). Elevation of systemic markers related to cardiovascular diseases in the peripheral blood of periodontitis patients. *J. Periodontol.* 71, 1528–1534. doi: 10.1902/jop.2000.71.10.1528

Lopez-Candales, A., Hernandez Burgos, P. M., Hernandez-Suarez, D. F., and Harris, D. (2017). Linking chronic inflammation with cardiovascular disease: from normal aging to the metabolic syndrome. *J. Nat. Sci.* 3:e341.

Lovegrove, J. M. (2004). Dental plaque revisited: bacteria associated with periodontal disease. *J. N. Z. Soc. Periodontol.* 2004, 7–21.

Luheshi, N. M., Giles, J. A., Lopez-Castejon, G., and Brough, D. (2012). Sphingosine regulates the NLRP3-inflammasome and IL-1beta release from macrophages. *Eur. J. Immunol.* 42, 716–725. doi: 10.1002/eji.201142079

Mandviwala, T., Khalid, U., and Deswal, A. (2016). Obesity and cardiovascular disease: a risk factor or a risk marker? *Curr. Atheroscler. Rep.* 18:21.

Mang-de la Rosa, M. R., Castellanos-Cosano, L., Romero-Perez, M. J., and Cutando, A. (2014). The bacteremia of dental origin and its implications in the appearance of bacterial endocarditis. *Med. Oral Patol. Oral Cir. Bucal* 19, e67–e74.

Merchant, A. T., Pitiphat, W., Ahmed, B., Kawachi, I., and Joshipura, K. (2003). A prospective study of social support, anger expression and risk of periodontitis in men. *J. Am. Dent. Assoc.* 134, 1591–1596. doi: 10.14219/jada.archive.2003.0104

Michlewska, S., Dransfield, I., Megson, I. L., and Rossi, A. G. (2009). Macrophage phagocytosis of apoptotic neutrophils is critically regulated by the opposing actions of pro-inflammatory and anti-inflammatory agents: key role for TNF-alpha. *FASEB J.* 23, 844–854. doi: 10.1096/fj.08-121228

Montenegro, M. M., Ribeiro, I. W. J., Kampits, C., Saffi, M. A. L., Furtado, M. V., Polanczyk, C. A., et al. (2019). Randomized controlled trial of the effect of periodontal treatment on cardiovascular risk biomarkers in patients with stable coronary artery disease: preliminary findings of 3 months. *J. Clin. Periodontol.* 46, 321–331. doi: 10.1111/jcpe.13085

Moore, W. E. (1987). Microbiology of periodontal disease. *J. Periodontal Res.* 22, 335–341. doi: 10.1111/j.1600-0765.1987.tb01595.x

Moreno, S., Parra, B., Botero, J. E., Moreno, F., Vasquez, D., Fernandez, H., et al. (2017). Periodontal microbiota and microorganisms isolated from heart valves in patients undergoing valve replacement surgery in a clinic in Cali, Colombia. *Biomedica* 37, 516–525. doi: 10.7705/biomedica.v37i4.3232

Muniz, F. W., Nogueira, S. B., Mendes, F. L., Rosing, C. K., Moreira, M. M., De Andrade, G. M., et al. (2015). The impact of antioxidant agents complimentary to periodontal therapy on oxidative stress and periodontal outcomes: a systematic review. *Arch. Oral. Biol.* 60, 1203–1214. doi: 10.1016/j.archoralbio.2015.05.007

Nakamura, Y., Tagusari, O., Seike, Y., Ito, Y., Saito, K., Miyamoto, R., et al. (2011). Prevalence of periodontitis and optimal timing of dental treatment in patients undergoing heart valve surgery. *Interact. Cardiovasc. Thorac. Surg.* 12, 696–700. doi: 10.1510/icvts.2010.255943

Nakano, K., Inaba, H., Nomura, R., Nemoto, H., Takeda, M., Yoshioka, H., et al. (2006). Detection of cariogenic *Streptococcus mutans* in extirpated heart valve and atheromatous plaque specimens. *J. Clin. Microbiol.* 44, 3313–3317. doi: 10.1128/jcm.00377-06

Offenbacher, S., Beck, J. D., Moss, K., Mendoza, L., Paquette, D. W., Barrow, D. A., et al. (2009). Results from the Periodontitis and Vascular Events (PAVE) Study: a pilot multicentered, randomized, controlled trial to study effects of periodontal therapy in a secondary prevention model of cardiovascular disease. *J. Periodontol.* 80, 190–201. doi: 10.1902/jop.2009.080007

Ogrendik, M. (2013). Rheumatoid arthritis is an autoimmune disease caused by periodontal pathogens. *Intl. J. Gen. Med.* 6, 383–386. doi: 10.2147/ijgm.s45929

Okuda, K., Ishihara, K., Nakagawa, T., Hirayama, A., and Inayama, Y. (2001). Detection of *Treponema denticola* in atherosclerotic lesions. *J. Clin. Microbiol.* 39, 1114–1117. doi: 10.1128/jcm.39.3.1114-1117.2001

Ozcaka, O., Bicakci, N., Pussinen, P., Sorsa, T., Kose, T., and Buduneli, N. (2011). Smoking and matrix metalloproteinases, neutrophil elastase and myeloperoxidase in chronic periodontitis. *Oral Dis.* 17, 68–76. doi: 10.1111/j.1601-0825.2010.01705.x

Pessi, T., Karhunen, V., Karjalainen, P. P., Ylitalo, A., Airaksinen, J. K., Niemi, M., et al. (2013). Bacterial signatures in thrombus aspirates of patients with myocardial infarction. *Circulation* 127:e1-6.

Petersen, P. E., and Ogawa, H. (2012). The global burden of periodontal disease: towards integration with chronic disease prevention and control. *Periodontology* 60, 15–39. doi: 10.1111/j.1600-0757.2011.00425.x

Ran, S., Liu, B., Gu, S., Sun, Z., and Liang, J. (2017). Analysis of the expression of NLRP3 and AIM2 in periapical lesions with apical periodontitis and microbial analysis outside the apical segment of teeth. *Arch. Oral. Biol.* 78, 39–47. doi: 10.1016/j.archoralbio.2017.02.006

Saito, Y., Fujii, R., Nakagawa, K. I., Kuramitsu, H. K., Okuda, K., and Ishihara, K. (2008). Stimulation of *Fusobacterium nucleatum* biofilm formation by *Porphyromonas gingivalis*. *Oral Microbiol. Immunol.* 23, 1–6. doi: 10.1111/j.1399-302x.2007.00380.x

Sanz, M., Marco Del, Castillo, A., Jepsen, S., Gonzalez-Juanatey, J. R., D'aiuto, F., et al. (2020). Periodontitis and cardiovascular diseases: consensus report. *J. Clin. Periodontol.* 47, 268–288.

Satoh, M., Tabuchi, T., Itoh, T., and Nakamura, M. (2014). NLRP3 inflammasome activation in coronary artery disease: results from prospective and randomized study of treatment with atorvastatin or rosuvastatin. *Clin. Sci.* 126, 233–241. doi: 10.1042/cs20130043

Schultz-Haudt, S., Bibby, B. G., and Bruce, M. A. (1954). Tissue-destructive products of gingival bacteria from nonspecific gingivitis. *J. Dent. Res.* 33, 624–631. doi: 10.1177/00220345540330050601

Scott, D. A., and Krauss, J. (2012). Neutrophils in periodontal inflammation. *Front. Oral Biol.* 15, 56–83. doi: 10.1159/000329672

Sobaniec, H., and Sobaniec-Lotowska, M. E. (2000). Morphological examinations of hard tissues of periodontium and evaluation of selected processes of lipid peroxidation in blood serum of rats in the course of experimental periodontitis. *Med. Sci. Monit.* 6, 875–881.

Socransky, S. S., Haffajee, A. D., Cugini, M. A., Smith, C., et al. (1998). Microbial complexes in subgingival plaque. *J. Clin. Periodontol.* 25, 134–144. doi: 10.1111/j.1600-051x.1998.tb02419.x

Song, L., Dong, G., Guo, L., and Graves, D. T. (2018). The function of dendritic cells in modulating the host response. *Mol. Oral Microbiol.* 33, 13–21. doi: 10.1111/omi.12195

Tang, D., Shi, Y., Kang, R., Li, T., Xiao, W., Wang, H., et al. (2007). Hydrogen peroxide stimulates macrophages and monocytes to actively release HMGB1. *J. Leukoc. Biol.* 81, 741–747. doi: 10.1189/jlb.0806540

Tomofuji, T., Ekuni, D., Yamanaka, R., Kusano, H., Azuma, T., Sanbe, T., et al. (2007). Chronic administration of lipopolysaccharide and proteases induces periodontal inflammation and hepatic steatosis in rats. *J. Periodontol.* 78, 1999–2006. doi: 10.1902/jop.2007.070056

Tonetti, M. S. (2009). Periodontitis and risk for atherosclerosis: an update on intervention trials. *J. Clin. Periodontol.* 36(Suppl. 10), 15–19. doi: 10.1111/j.1600-051x.2009.01417.x

Tonetti, M. S., D'aiuto, F., Nibali, L., Donald, A., Storry, C., Parkar, M., et al. (2007). Treatment of periodontitis and endothelial function. *N. Engl. J. Med.* 356, 911–920.

Toregeani, J. F., Nassar, C. A., Nassar, P. O., Toregeani, K. M., Gonzatto, G. K., Vendrame, R., et al. (2016). Evaluation of periodontitis treatment effects on carotid intima-media thickness and expression of laboratory markers related to atherosclerosis. *Gen. Dent.* 64, 55–62.

Tsai, C. C., Chen, H. S., Chen, S. L., Ho, Y. P., Ho, K. Y., Wu, Y. M., et al. (2005). Lipid peroxidation: a possible role in the induction and progression of chronic periodontitis. *J. Periodontal Res.* 40, 378–384. doi: 10.1111/j.1600-0765.2005.00818.x

Vidal, F., Figueredo, C. M., Cordovil, I., and Fischer, R. G. (2009). Periodontal therapy reduces plasma levels of interleukin-6, C-reactive protein, and fibrinogen in patients with severe periodontitis and refractory arterial hypertension. *J. Periodontol.* 80, 786–791. doi: 10.1902/jop.2009.080471

Wang, Y., Andrukhov, O., and Rausch-Fan, X. (2017). Oxidative stress and antioxidant system in periodontitis. *Front. Physiol.* 8:910.

Wehmeyer, M. M., Kshirsagar, A. V., Barros, S. P., Beck, J. D., Moss, K. L., Preisser, J. S., et al. (2013). A randomized controlled trial of intensive periodontal therapy on metabolic and inflammatory markers in patients With ESRD: results of an exploratory study. *Am. J. Kidney Dis.* 61, 450–458. doi: 10.1053/j.ajkd.2012.10.021

White, P., Cooper, P., Milward, M., and Chapple, I. (2014). Differential activation of neutrophil extracellular traps by specific periodontal bacteria. *Free Radic. Biol. Med.* 75(Suppl. 1):S53.

Xue, F., Shu, R., and Xie, Y. (2015). The expression of NLRP3, NLRP1 and AIM2 in the gingival tissue of periodontitis patients: RT-PCR study and immunohistochemistry. *Arch. Oral. Biol.* 60, 948–958. doi: 10.1016/j.archoralbio.2015.03.005

Yagi, K. (1987). Lipid peroxides and human diseases. *Chem. Phys. Lipids* 45, 337–351. doi: 10.1016/0009-3084(87)90071-5

Yamaguchi, Y., Kurita-Ochiai, T., Kobayashi, R., Suzuki, T., and Ando, T. (2017). Regulation of the NLRP3 inflammasome in Porphyromonas gingivalis-accelerated periodontal disease. *Inflamm. Res.* 66, 59–65. doi: 10.1007/s00011-016-0992-4

Yanbaeva, D. G., Dentener, M. A., Creutzberg, E. C., Wesseling, G., and Wouters, E. F. (2007). Systemic effects of smoking. *Chest* 131, 1557–1566. doi: 10.1378/chest.06-2179

Zhou, Q. B., Xia, W. H., Ren, J., Yu, B. B., Tong, X. Z., Chen, Y. B., et al. (2017). Effect of intensive periodontal therapy on blood pressure and endothelial microparticles in patients with prehypertension and periodontitis: a randomized controlled trial. *J. Periodontol.* 88, 711–722. doi: 10.1902/jop.2017.160447

Conflict of Interest: The authors declare that the research was conducted in the absence of any commercial or financial relationships that could be construed as a potential conflict of interest.

frontiers in Physiology

ORIGINAL RESEARCH
published: 26 January 2021
doi: 10.3389/fphys.2020.514494

Osthole Alleviates Neointimal Hyperplasia in Balloon-Induced Arterial Wall Injury by Suppressing Vascular Smooth Muscle Cell Proliferation and Downregulating Cyclin D1/CDK4 and Cyclin E1/CDK2 Expression

*Yi-Qi Li[1,2], Ye-Li Li[1], Xiao-Tong Li[1], Jun-Yuan Lv[3], Yang Gao[1], Wen-Na Li[2], Qi-Hai Gong[1] and Dan-Li Yang[1]**

[1]Joint International Research Laboratory of Ethnomedicine of Ministry of Education, Key Laboratory of Basic Pharmacology of the Ministry of Education, The Key Laboratory of Basic Pharmacology of Guizhou Province, Department of Pharmacology, School of Pharmacy, Zunyi Medical University, Zunyi, China, [2]Department of Pharmacology, Zhuhai Campus of Zunyi Medical University, Zhuhai, China, [3]Department of Breast and Thyroid Surgery, Affiliated Hospital of Zunyi Medical University, Zunyi, China

OPEN ACCESS

Edited by:
Shampa Chatterjee, University of Pennsylvania, United States

Reviewed by:
Hai-Jian Sun, National University of Singapore, Singapore
Helen Williams, University of Bristol, United Kingdom

***Correspondence:**
Dan-Li Yang
yangdanlizmu@163.com

Specialty section:
This article was submitted to Vascular Physiology, a section of the journal Frontiers in Physiology

Received: *25 November 2019*
Accepted: *30 December 2020*
Published: *26 January 2021*

Citation:
Li Y-Q, Li Y-L, Li X-T, Lv J-Y, Gao Y, Li W-N, Gong Q-H and Yang D-L (2021) Osthole Alleviates Neointimal Hyperplasia in Balloon-Induced Arterial Wall Injury by Suppressing Vascular Smooth Muscle Cell Proliferation and Downregulating Cyclin D1/CDK4 and Cyclin E1/CDK2 Expression. Front. Physiol. 11:514494. doi: 10.3389/fphys.2020.514494

Percutaneous coronary intervention (PCI) is the most widely used therapy for treating ischemic heart disease. However, intimal hyperplasia and restenosis usually occur within months after angioplasty. Modern pharmacological researchers have proven that osthole, the major active coumarin of *Cnidium monnieri* (L.) Cusson, exerts potent antiproliferative effects in lung cancer cells, the human laryngeal cancer cell line RK33 and TE671 medulloblastoma cells, and its mechanism of action is related to cell cycle arrest. The goal of the present study was to observe the effect of osthole on vascular smooth muscle cell (VSMC) proliferation using platelet-derived growth factor-BB (PDGF-BB)-stimulated VSMCs isolated from rats and vascular balloon injury as models to further elucidate the molecular mechanisms underlying this activity. We detected the relative number of VSMCs by the MTT assay and EdU staining and examined cell cycle progression by flow cytometry. To more deeply probe the mechanisms, the protein expression levels of PCNA, the cyclin D1/CDK4 complex and the cyclin E1/CDK2 complex in balloon-treated rat carotid arteries and the mRNA and protein expression levels of the cyclin D1/CDK4 and cyclin E1/CDK2 complexes in VSMCs were detected by real-time RT-PCR and western blotting. The data showed that osthole significantly inhibited the proliferation of VSMCs induced by PDGF-BB. Furthermore, osthole caused apparent VSMC cycle arrest early in G0/G1 phase and decreased the expression of cyclin D1/CDK4 and cyclin E1/CDK2. Our results demonstrate that osthole can significantly inhibit PDGF-BB-induced VSMC proliferation and that its regulatory effects on cell cycle progression and proliferation may be related to the downregulation of cyclin D1/CDK4 and cyclin E1/CDK2 expression as well as the prevention of cell cycle progression from G0/G1 phase to S phase. The abovementioned mechanism may be responsible for the alleviation of neointimal hyperplasia in balloon-induced arterial wall injury by osthole.

Keywords: osthole, platelet-derived growth factor-BB, vascular smooth muscle cells, proliferation, cyclin D1, CDK4, cyclin E1, CDK2

INTRODUCTION

Percutaneous coronary intervention (PCI) is the most widely used therapy for treating ischemic heart disease. However, intimal hyperplasia and restenosis usually occur within months after angioplasty. Many studies have shown that the hallmark of intimal hyperplasia is the excessive proliferation of vascular smooth muscle cells (VSMCs), which is an early response to the arterial wall injury (Direnzo et al., 2016; Tang and Gerlach, 2017). In their quiescent state, these cells help to modulate the blood supply *via* vasoconstriction and vasodilatation. Upon activation, VSMCs proliferate at a very high rate and migrate from the media into the lumen of blood vessels (Qiu et al., 2013); meanwhile, a large number of cytokines and growth factors released from activated cells also contribute to this progression (Liu et al., 2009, 2013). Therefore, inhibiting VSMC proliferation may represent a potential therapeutic target for preventing and treating vascular proliferative diseases.

Cell proliferation occurs through the regulation of the cell cycle, a complex and tightly controlled process. The G0, G1, S, G2, and M phases are five sequential stages involved in this process. The correct progression of the cell cycle is guaranteed because activation of each phase is dependent on the successful completion of previous stages (Begum et al., 2011). Molecular analysis of the cell cycle has shown that regulatory molecules (cyclins) and catalytic molecules (cyclin-dependent kinases, CDKs) act as the master regulators in this process and determine whether a cell commits to division or leaves the cell cycle (Urrego et al., 2014). The cyclin D1/CDK4 complex is required to promote the progression of cells from G0/G1 phase to S phase. The inhibition of cyclin D1 can arrest cells in G0/G1 phase (Liu et al., 2009).

Cnidium monnieri (L.) Cusson has been used as a traditional Chinese medicine for the treatment of gynecological diseases, cutaneous pruritus, and nephritis (Li et al., 2015; Zhang et al., 2015). Osthole (7-methoxy-8-isopentenoxy-coumarin), one of the pharmacologically active coumarins of *Cnidium monnieri* (L.) Cusson, has been reported to have cardioprotective (Duan et al., 2016), anti-inflammatory (Li et al., 2014), and antihypertensive activities (Fusia et al., 2012). Previous studies demonstrated that osthole suppresses the proliferation of pulmonary arterial smooth muscle cells (Yue et al., 2020), lung cancer cells (Xu et al., 2011), the human laryngeal cancer cell line RK33, and TE671 medulloblastoma cells (Jarzab et al., 2014); specifically, the associated mechanism is related to cell cycle arrest. Interestingly, data have indicated that some characteristics of cardiovascular diseases, such as atherosclerosis and angiostenosis (Jiang et al., 2013), are similar to those of cancer. In our previous study, we found that inflammatory mediators affect the rat carotid artery after balloon injury and the antiproliferative effect of osthole are related to the NF-κB and TGF-β1/Smad2 signaling pathways (Li et al., 2017). Despite these observations, the exact mechanisms still require further investigation. In the present study, we aimed to observe the effect of osthole on VSMC proliferation using PDGF-BB-stimulated VSMCs isolated from rats and vascular balloon injury as models to further elucidate the molecular mechanisms underlying this activity.

MATERIALS AND METHODS

Animals and Materials

Male Sprague-Dawley rats were obtained from the Animal Center of the Research Institute of Surgery at the Third Military Medical University (Chongqing, China). Osthole (purity 98.0%) was purchased from Nanjing Zelang Medical Technology Co., Ltd. (Nanjing, China), dissolved to 160 mM (in dimethyl sulfoxide, DMSO) as a stock solution and stored at −20°C. Platelet-derived growth factor-BB (PDGF-BB) was purchased from Sigma-Aldrich Co (United States). A Cell Cycle Assay Kit was obtained from KeyGen BioTech (Nanjing, China). 2-F Fogarty balloon catheters were purchased from Edwards Lifesciences Co (United States). MTT (3-(4,5-dimethylthiazol-2-yl)-2,5-diphenyltetrazolium bromide) was obtained from Sigma Chemical Co (St. Louis, MO, United States). A mouse anti-rat monoclonal PCNA antibody and rabbit anti-rat polyclonal antibodies targeting cyclin D1, cyclin E1, CDK2, and CDK4 were purchased from Abcam Co (United States). The primers used in the study were designed and synthesized by TaKaRa Systems (Dalian, China), and IQ™ SYBR® Green Supermix was obtained from BIO-RAD (United States).

Vascular Balloon Injury Model

For balloon injury, 8-week-old male Sprague-Dawley rats (320 ± 20 g) were anesthetized *via* intraperitoneal administration of sodium pentobarbital (40 mg/kg), after which the left external carotid arteries were exposed, and a 2-F Fogarty balloon catheter was introduced into the left common carotid artery. The catheter was inflated and passed through the artery three times to ensure complete and reproducible removal of the endothelial lining. Finally, the wound was ligated and closed following the last passage of the balloon. In the sham group, animals were subjected to left external carotid artery exposure, but a balloon catheter was not inserted into the vessel. All animal experiments were performed in accordance with Animal Care and Use Guidelines of China and were approved by the Animal Use and Care Committee of Zunyi Medical University.

Arterial Harvest and Histological Examination

The rats were randomly divided into the following four groups (n = 6): the sham group, model group, 20 mg/kg/d osthole-treated (Osthole-20) group, and 40 mg/kg/d osthole-treated (Osthole-40) group. All treatments were administered daily *via* oral gavage on the first day following surgery. The rats in the sham and model groups were given normal saline, which is also used as vehicle in Osthole-20 and Osthole-40 groups. Fourteen days after balloon injury, the rats were euthanized to detect vascular injury and intimal thickening of the target arteries. The left common carotid arteries were harvested and fixed with a 4% formaldehyde solution. The tissues were embedded in paraffin, sectioned at a thickness of 4 µm, and stained with hematoxylin and eosin (H&E). The neointimal thickness and the ratio of tunica intima/media were analyzed using computer-assisted morphometry.

Vascular Smooth Muscle Cell Culture and Experimental Design

VSMCs were isolated from the thoracic aortas of 8-week-old male Sprague-Dawley rats (180 ± 20 g). The aortas were stripped of their endothelium and adventitia and were cut into small pieces, which were placed in cell culture flask containing Dulbecco's modified Eagle's medium supplemented with 20% fetal bovine serum and incubated at 37°C in a CO_2 incubator (95% air and 5% CO_2) for 10 days. The medium was changed every 3 days, and cells were removed by trypsinization and successively subcultured. Subcultured VSMCs between passages 3 and 6 were used for this experiment.

The cultured VSMCs were randomly divided into six groups: control group (control), no drug was added; DMSO group (DMSO), 0.5% DMSO was added in normal cells; PDGF-BB group: PDGF-BB 25 ng/ml was added in normal grown cells; osthole low-dose group (Osthole-20), middle-dose group (Osthole-40), and high-dose group (Osthole-80): osthole 20, 40, and 80 μM were added, respectively, to the cells treated with 25 ng/ml PDGF-BB (PDGF-BB was added at 60 min before the addition of osthole). The above concentrations of PDGF-BB or osthole used in each group were final concentration.

Assessment of VSMC Proliferation by the MTT Assay

Rat VSMCs were plated in 96-well plates at a density of 8×10^4 cells/ml and treated with PDGF-BB prior to osthole (PDGF-BB was added at 60 min before the addition of osthole). After the cells were cultured for 24 h, MTT assays were carried out as follows: VSMCs were grown in 100 μl of medium at 37°C under 5% CO_2 for 24 h, after which 10 μl of a 3-(4,5-dimethylthiazol-2-yl)-2,5-diphenyltetrazolium bromide (MTT) solution was added to each well for 4 h to allow MTT reduction. The resulting formazan crystals were dissolved in DMSO, and the absorbance values were measured at a wavelength of 490 nm on a microplate reader. Each condition was conducted in triplicate.

EdU Staining

Cell proliferation was analyzed using a Cell-light EdU Apollo488 Kit according to the manufacturer's protocol (RIBOBio. Co., Cat. No. C10310-3, Guangzhou, China). The logarithmic growth of VSMCs seeded in 96-well plates at a density of 8×10^4 cells/ml was determined. Following treatment with PDGF-BB and osthole, the cells in each well were incubated with 50 μM EdU for 3 h. The cells were permeabilized for 10 min with 0.5% Triton X-100 after being fixed in PBS containing 4% paraformaldehyde for 30 min at room temperature. After washing with PBS, the cells were stained with Hoechst 33342 in the dark, washed, and imaged using a fluorescence microscope.

Cell Cycle Analysis Using Flow Cytometry

VSMCs were treated with either PDGF-BB or different concentrations of osthole for 24 h, and cell cycle distribution was determined by flow cytometry. Briefly, cells were harvested by trypsinization, washed twice in PBS, and fixed in 70% ice-cold ethanol overnight. Then, the ethanol was removed, and the cells were resuspended in PBS. After they were treated with 100 μl RNase at 37°C for 30 min, the cells were stained with 100 μl of propidium iodide (PI) and incubated in the dark at 4°C. The cell cycle distribution was analyzed on a flow cytometer (Beckman Coulter, United States).

Real-Time Quantitative Reverse Transcription-PCR

Total RNA was extracted using RNAiso Plus and then reverse-transcribed in a reaction containing PrimeScript™ RT Enzyme Mix, oligodT primer, random 6-mers, and PrimeScript™ Buffer (5×). To detect the mRNA expression levels of cyclin D1, cyclin E1, CDK2, and CDK4, we performed a two-step RT-PCR using an iCycler iQ Real-Time PCR Detection System with IQ™ SYBR®GREEN Supermix. The following primers were used for this experiment: cyclin D1 (GenBank accession no. NM_171992.4), forward primer: (5'–3') TACCGCACAACGCACTTTC and reverse primer: (5'–3') AAGGGCTTCAATCTGTTCCTG; cyclin E1 (GenBank accession no. NM_001100821.1), forward primer: (5'–3') TTTGCAAGATCCGGATGAA and reverse primer: (5'–3') CGCTGAATCATCATCCCAAG; CDK2 (GenBank accession no. NM_199501.1), forward primer: (5'–3') CCTGCACCAGGAC CTCAAGAA and reverse primer: (5'–3') CGGTGAGAATGGC AGAATGCTA; CDK4 (GenBank accession no. NM_053593.2), forward primer: (5'–3') AGTCAGTGGTGCCGGAGATG and reverse primer: (5'–3') CAGCGTCCGGAAACTGGAA; and β-actin (GenBank accession no. NM_031144.2), forward primer: (5'–3') GGAGATTACT GCCCTGGCTCCTA and reverse primer: (5'–3') GACTCATCGTACTCCTGCTTGCTG. The threshold cycle (Ct) values of the target genes were normalized to those of β-actin in the same samples.

Western Blot Analysis

Carotid arteries were pulverized with an electric homogenizer in cold RIPA lysis buffer containing proteinase inhibitors. The dissolved proteins were prepared by centrifugation at 12,000 × *g* for 10 min at 4°C, after which the supernatant was collected. The protein concentrations were quantified by a Bicinchoninic Acid (BCA) Protein Assay Kit. After the VSMCs were subjected to their respective treatments for 24 h, they were washed with ice-cold PBS and homogenized in a lysis buffer. The protein concentration was determined by a Bicinchoninic Acid (BCA) Protein Assay Kit. For western blot analysis, equal quantities of protein were separated on SDS-polyacrylamide gel electrophoresis (SDS-PAGE) gels. After electrophoresis, the proteins were electroblotted to polyvinylidene difluoride (PVDF) membranes and subsequently incubated in 5% nonfat dry milk in tris-buffered saline containing Tween (TBST) for 1 h at room temperature. After the membranes were washed with TBST and incubated with anti-PCNA (1:1,000), anti-cyclin D1 (1:10,000), anti-cyclin E1 (1:1,000), anti-CDK2 (1:1,000), and anti-CDK4 (1:500) antibodies in 1% nonfat dry milk in TBST overnight at 4°C, they were washed with TBST for 10 min three times and

then incubated with horseradish peroxidase (HRP)-conjugated secondary antibodies for 2 h at room temperature. The immunoblots were visualized *via* enhanced chemiluminescence (ECL-Plus; Beyotime, P0018, Shanghai, China), and the band intensities were quantified using Quantity One® software.

Data Analysis

Data were analyzed using one-way ANOVA with SPSS 17.0 software, and all the results are presented as the mean ± S.E.M. *Post hoc* comparisons were performed using LSD with equal variances and with Dunnett's T3 with unequal variances, $p < 0.05$ was considered statistically significant.

RESULTS

Effects of Osthole on Neointimal Hyperplasia

Digital images were acquired with the Q Win image manipulation system. As shown in **Figure 1**, hematoxylin and eosin (H&E) staining showed that no neointima was found in the vessels not subjected to balloon angioplasty, and the model group showed bulky concentric neointimal hyperplasia as well as a disrupted elastic membrane after balloon injury ($p < 0.01$). However, The results from the image analysis system suggested that there was an obvious reduction in neointimal thickness and the ratio of tunica intima/media in balloon-injured sections from the osthole-treated animals, with 38% (Osthole-20) and 64% (Osthole-40) reductions in the neointimal thickness compared with that in the model group ($p < 0.01$).

Effects of Osthole on PCNA, Cyclin D1, CDK4, Cyclin E1, and CDK2 Protein Expression Levels in Balloon-Treated Rat Carotid Arteries

To understand the mechanisms underlying the protective effects of osthole on neointimal formation in rat carotid arteries, the protein expression of PCNA, cyclin D1, CDK4, cyclin E1, CDK2 in the carotid arteries was measured by western blotting. As shown in **Figure 2**, compared with that in the sham group, the protein expression of PCNA, cyclin D1, CDK4, cyclin E1, and CDK2 was significantly increased by 3.1, 2.9, 2.5, and 3.1 times, respectively ($p < 0.01$). However, compared with that in the model group, the

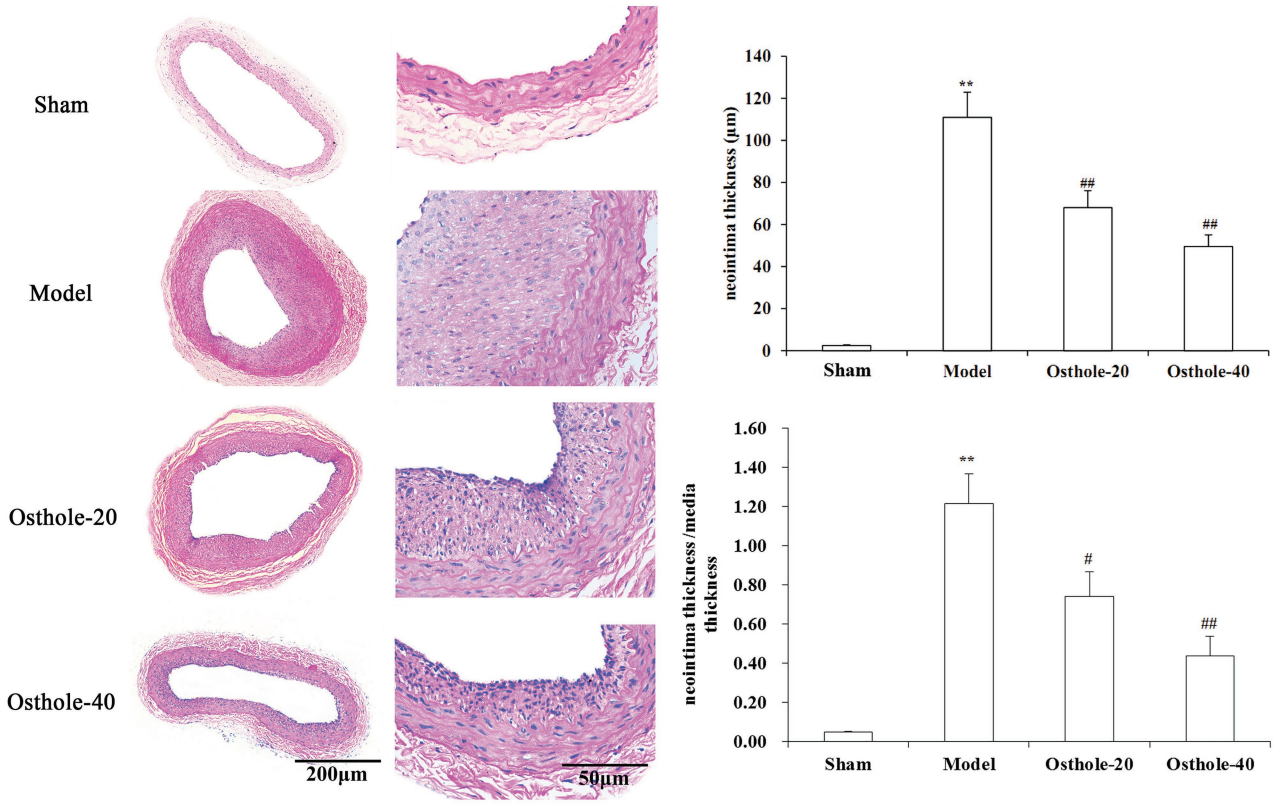

FIGURE 1 | Effects of osthole on neointimal formation in rat carotid arteries. Representative sections from the sham, model, Osthole-20, and Osthole-40 groups. The neointimal thickness and the ratio of tunica intima/media of each group is expressed as the mean ± SEM. Data are presented as the mean ± SEM, $n = 6$. **Significant difference compared to the sham group at $p < 0.01$, #Significant difference compared to the model group at $p < 0.05$, ##Significant difference compared to the model group at $p < 0.01$.

expression of these proteins was decreased by 19, 20, 27, and 15% respectively, upon treatment with osthole at a dosage of 20 mg/kg/day ($p < 0.01$), and the expression of these proteins was further downregulated by 40, 43, 50, and 43%, respectively, upon treatment with osthole at a dosage of 40 mg/kg/day ($p < 0.01$).

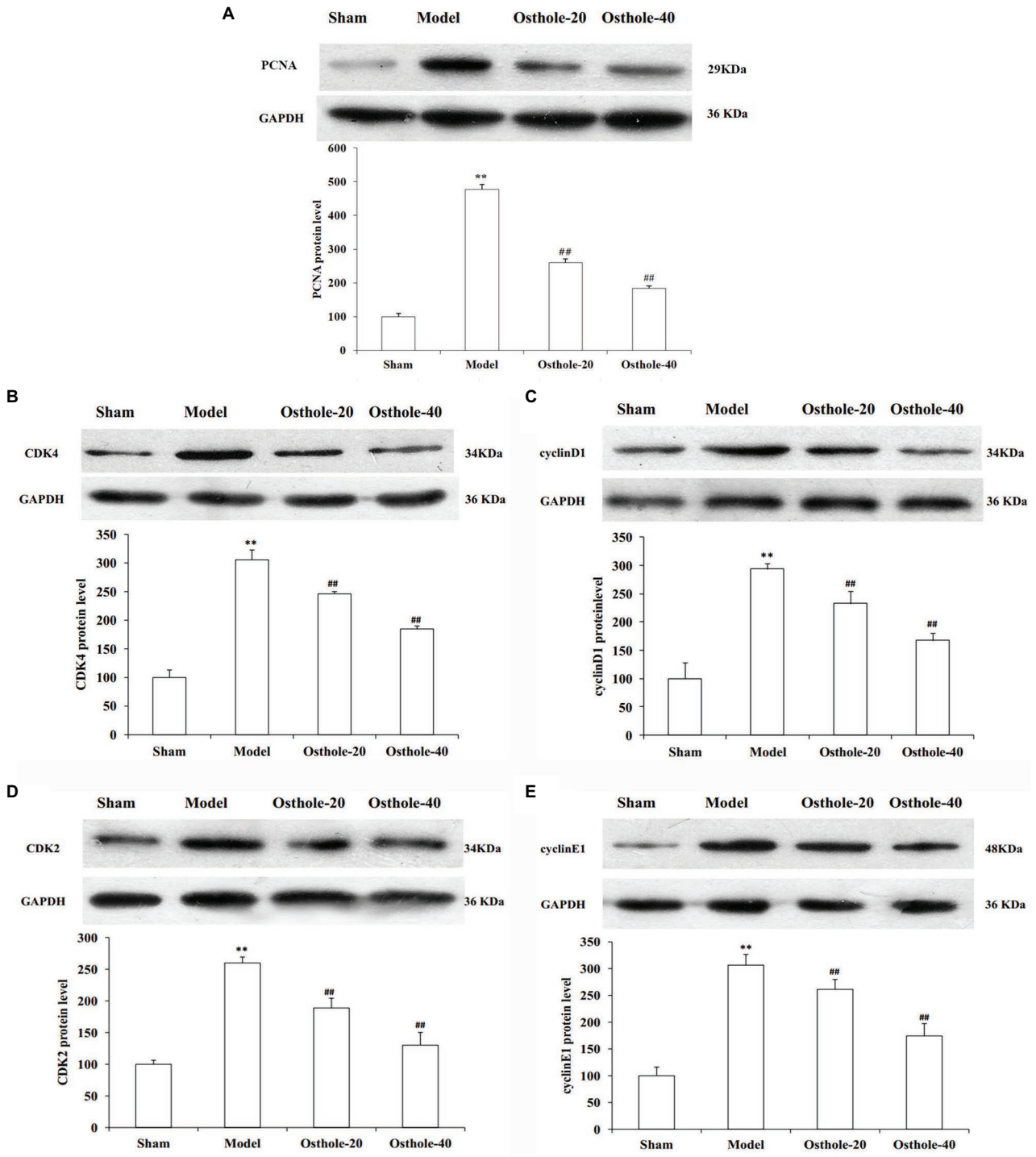

FIGURE 2 | Effects of osthole on PCNA, cyclinD1, CDK4, cyclin E1, and CDK2 protein expression in balloon-treated rat carotid arteries. **(A)** PCNA protein expression. **(B)** CDK4 protein expression. **(C)** Cyclin D1 protein expression. **(D)** CDK2 protein expression. **(E)** Cyclin E1 protein expression. Data are presented as the mean ± S.E.M. $n = 4$. **Significant difference compared with the sham group at $p < 0.01$, ##Significant difference compared with the model group at $p < 0.01$.

Antiproliferative Effect of Osthole on PDGF-BB-Stimulated VSMCs

To investigate the growth inhibition effect of osthole, cell proliferation was determined by MTT and EdU staining after treatment with osthole at different concentrations. According to images of the EdU assay (**Figures 3A,B**), the proliferation and viability of VSMCs cultured with PDGF-BB were increased compared with those of the control group ($p < 0.01$), while the proliferation and viability of VSMCs in the 20, 40, and 80 μM osthole-treated groups were decreased ($p < 0.01$). As shown in **Figure 3C**, when VSMCs were treated with DMSO for 24 h in the absence of PDGF-BB or osthole, no significant difference was observed in MTT absorbance ($p > 0.05$), suggesting that DMSO was not toxic to the cells. However, the addition of PDGF-BB (25 ng/ml) caused a strong increase in VSMC proliferation compared to that of the control group ($p < 0.01$); this increase was inhibited by the addition of osthole at 40 and 80 μM ($p < 0.01$).

Effect of Osthole on VSMC Cell Cycle Progression in the Presence of PDGF-BB

To determine whether osthole influences the cell cycle machinery, we examined cell cycle progression using flow cytometry. As shown in **Figures 4A,B,F**, cells subjected to a 24-h exposure to PDGF-BB had a significantly higher percentage of cells in and past S phase ($p < 0.01$). After treatment with osthole, most of the VSMCs were arrested at G_0/G_1 phase (**Figures 4C–F**). The PDGF-BB-stimulated VSMCs treated with osthole (20, 40, and 80 μM) showed that cell

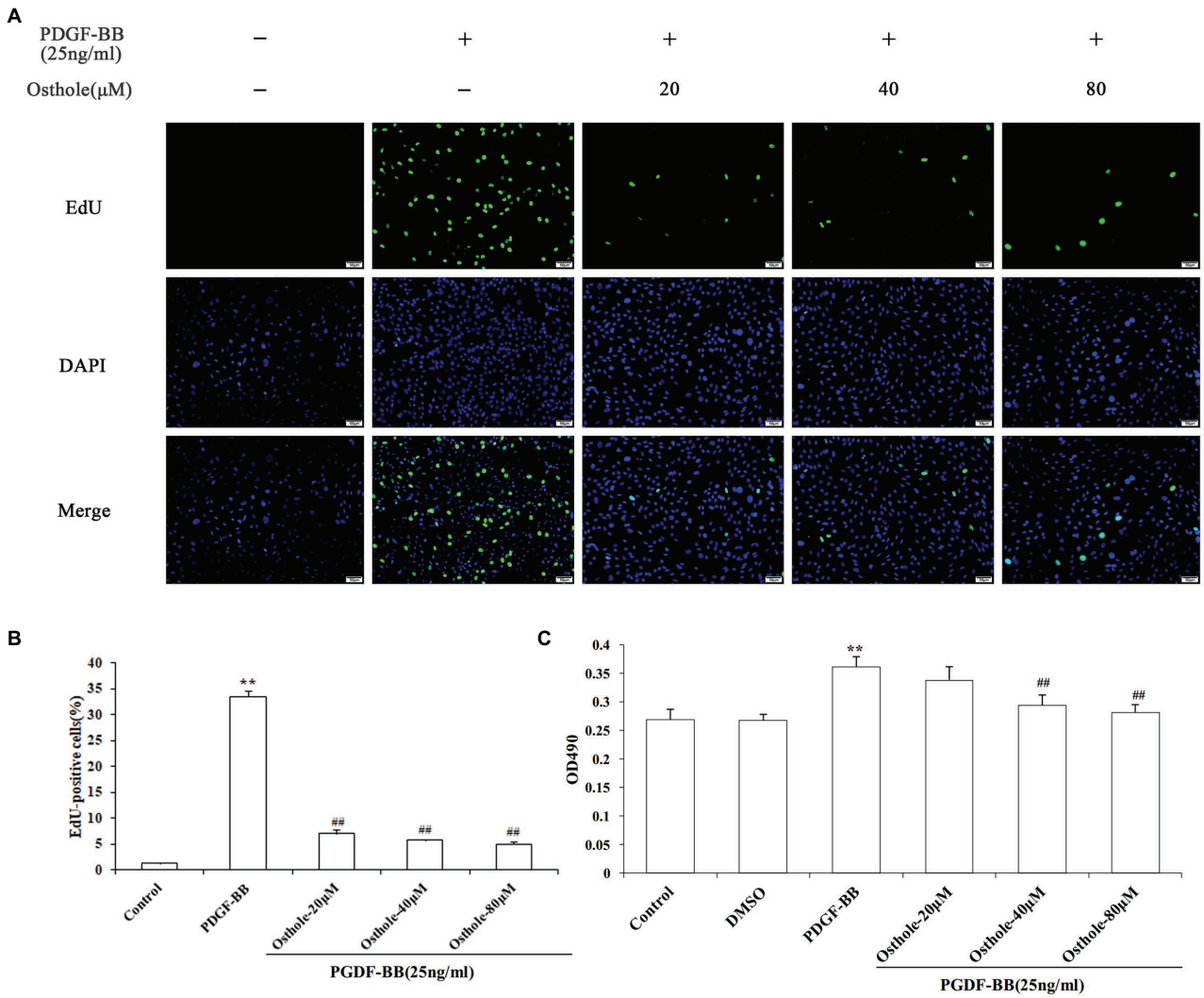

FIGURE 3 | Cells were rendered quiescent and treated with PDGF-BB, after which osthole (20, 40, and 80 μM) was added and incubated for 24 h. **(A)** Fluorescence images of EdU in staining are VSMCs. **(B)** Histograms showing the ratio of EdU-positive cells to total cells. **(C)** The MTT assay was used to evaluate the viability of VSMCs. Data are presented as the mean ± S.E.M. **Significant difference compared to the control group at $p < 0.01$, ##Significant difference compared to the PDGF-BB group at $p < 0.01$.

cycle progression was halted at G_0/G_1 phase (20 μM osthole: G_0/G_1 = 73.97%, $p > 0.05$; 40 μM osthole: G_0/G_1 = 78.9%, $p < 0.01$; 80 μM osthole: G_0/G_1 = 83.41%, $p < 0.01$).

Effect of Osthole on the mRNA and Protein Expression of Cyclin D1/CDK4 in VSMCs

Previous studies have demonstrated that cell cycle progression is tightly regulated by cyclin-CDK complexes during G1 phase. The cyclin D1/CDK4 complex, one such complex, plays a vital role in this process. To determine whether the antiproliferative effect of osthole was associated with the activity of the cyclin D1/CDK4 complex, we analyzed the cyclin D1/CDK4 mRNA and protein expression levels in cultured rat VSMCs using real-time RT-PCR and western blotting, respectively. As expected, our data showed that PDGF-BB (25 ng/ml) could elevate the cyclin D1 mRNA and

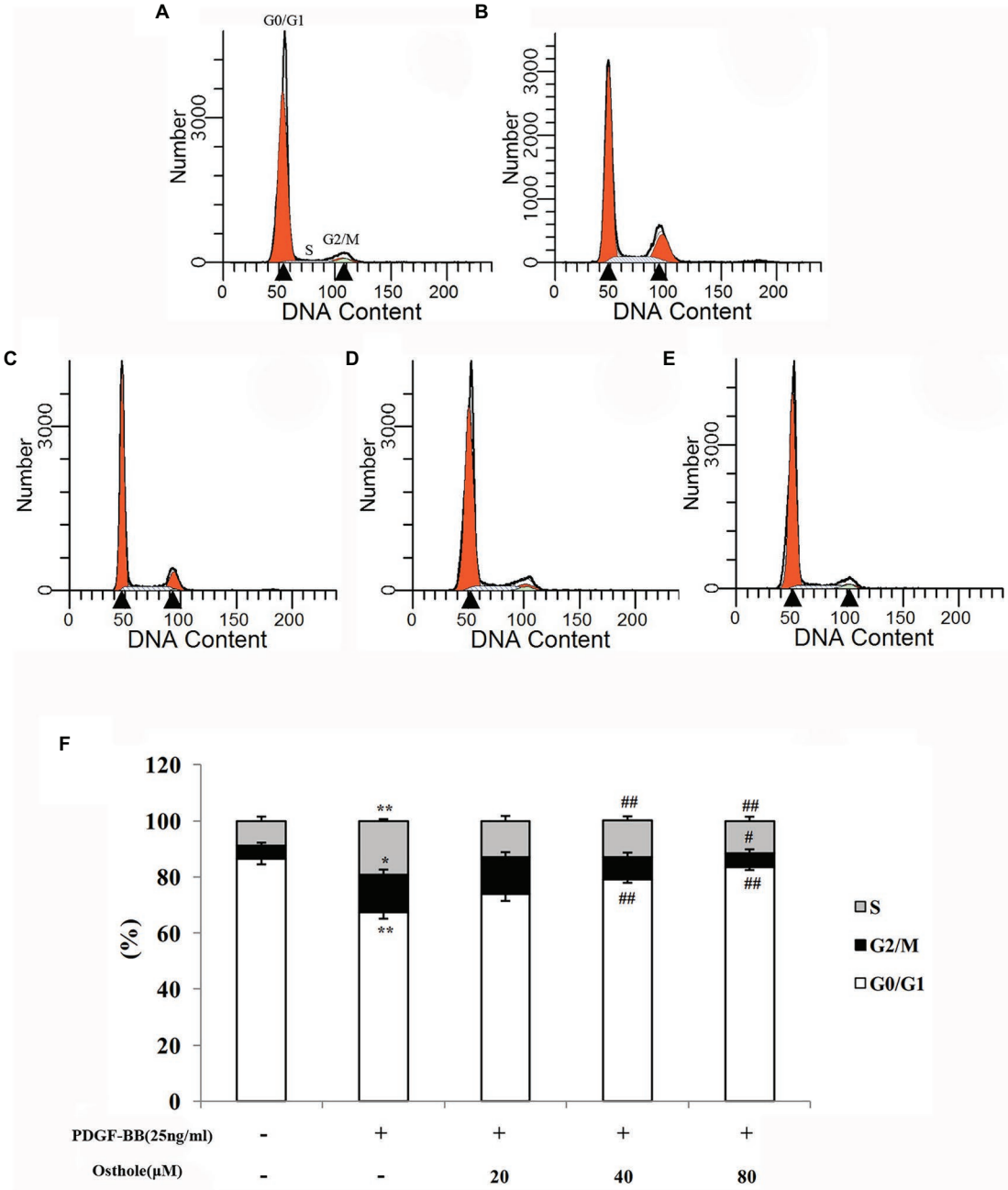

FIGURE 4 | Distribution of cell cycle stages of VSMCs as determined by flow cytometry. Representative images of **(A)** the control group, **(B)** the PDGF-BB group, **(C)** the Osthole-20 group, **(D)** the Osthole-40 group, and **(E)** the Osthole-80 group. **(F)** Percentage of cells in each phase of the cell cycle. Data are expressed as the mean ± S.E.M. n = 5~7. In **(F)**, $^{*}p < 0.05$, $^{**}p < 0.01$ vs. the control group; $^{\#}p < 0.05$, $^{\#\#}p < 0.01$ vs. the PDGF-BB group.

protein expression levels by approximately 4.1-fold and 2.3-fold compared to the levels in the control group, respectively ($p < 0.01$), and osthole could significantly blunt the increases in cyclin D1 mRNA and protein expression (**Figure 5A**). Meanwhile, cells stimulated with PDGF-BB showed a profound increase in CDK4 mRNA and protein expression compared to the respective levels in the control group ($p < 0.01$). However, treatment with osthole (40 and 80 μM) significantly decreased the mRNA and protein expression of CDK4 in PDGF-BB-stimulated VSMCs ($p < 0.01$; **Figure 5B**).

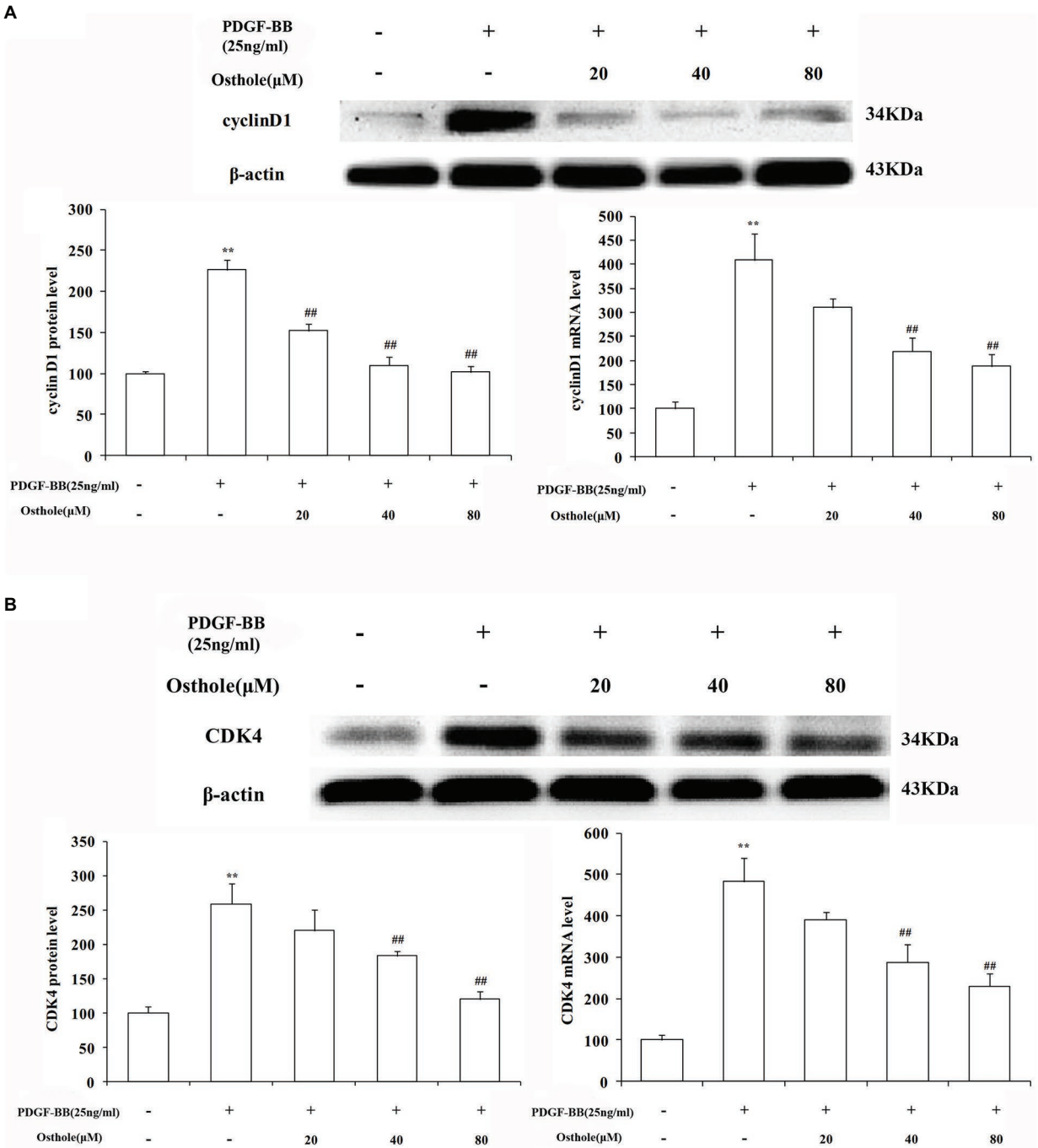

FIGURE 5 | Effect of osthole on cyclin D1/CDK4 mRNA and protein expression in VSMCs. **(A)** Relative mRNA and protein expression of cyclin D1 in VSMCs. **(B)** Relative mRNA and protein expression of CDK4 in VSMCs. Data are expressed as the mean ± S.E.M. $n = 5$. **Significant difference compared to the control group at $p < 0.01$, $^{\#\#}$Significant difference compared to the PDGF-BB group at $p < 0.01$.

Effect of Osthole on the mRNA and Protein Expression of Cyclin E1/CDK2 in VSMCs

To further verify our results, we sequentially applied real-time RT-PCR and western blotting to examine the expression levels of cyclin E1/CDK2 mRNA and protein in VSMCs. The results showed that after stimulation with PDGF-BB (25 ng/ml), the expression levels of cyclin E1/CDK2 mRNA and protein in VSMCs were markedly increased ($p < 0.01$). After treatment

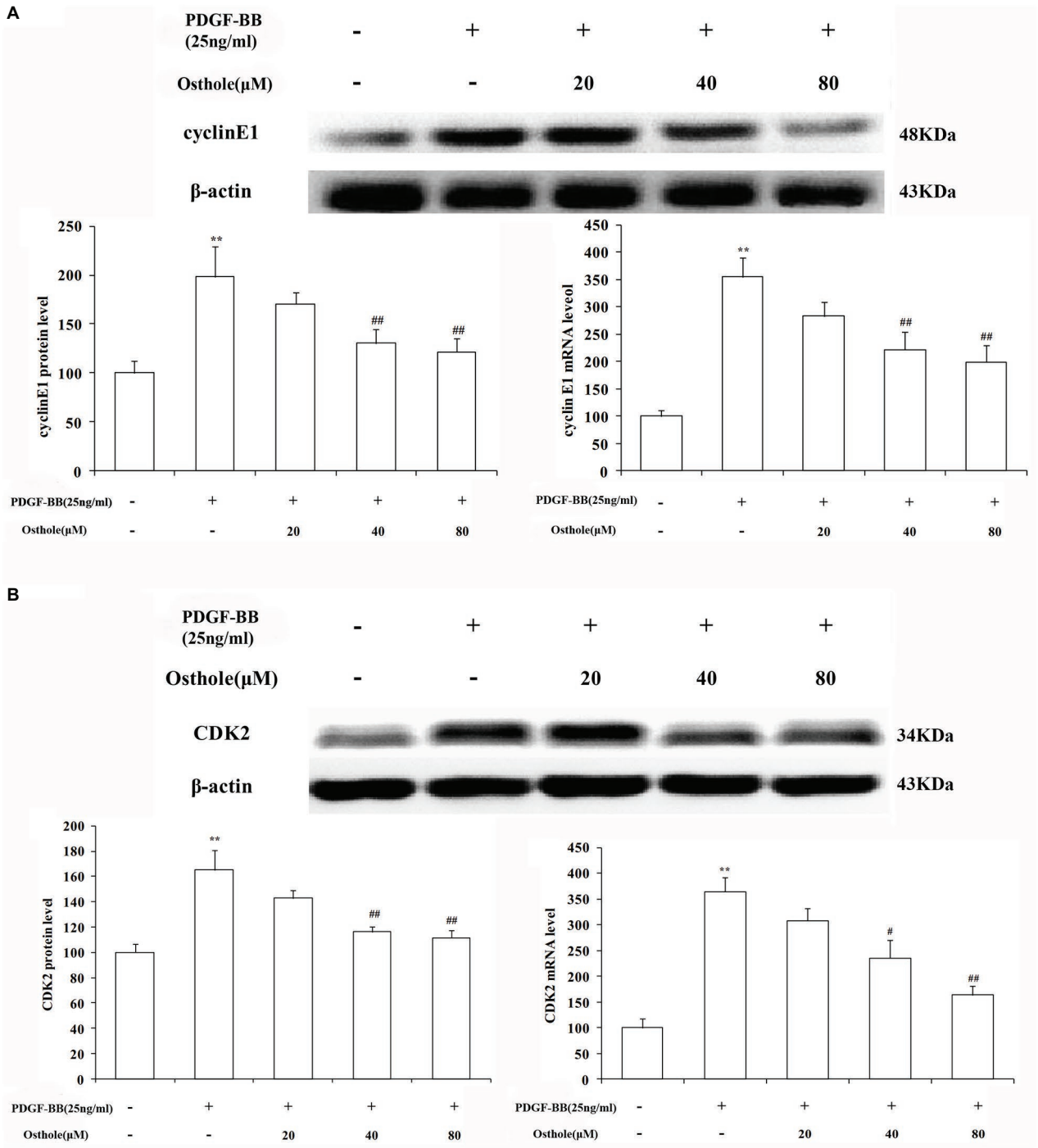

FIGURE 6 | Effect of osthole on cyclin E1/CDK2 mRNA and protein expression in VSMCs. **(A)** Relative mRNA and protein expression of cyclin E1 in VSMCs. **(B)** Relative mRNA and protein expression of CDK2 in VSMCs. Data are expressed as the mean ± S.E.M. $n = 5$. **Significant difference from the control group at $p < 0.01$, #Significant difference from the PDGF-BB group at $p < 0.05$, ##Significant difference from the PDGF-BB group at $p < 0.01$.

with osthole, we observed an expected decrease in cyclin E1/CDK2 mRNA and protein expression, especially at doses of 40 and 80 μM ($p < 0.01$; **Figures 6A,B**).

DISCUSSION

Osthole, a traditional Chinese medicine, is now being manufactured in many countries on a large scale with standardized quality. Previous studies have shown that osthole exerts cardiovascular protective activities. Abnormal VSMC proliferation is a major component of cardiovascular disease including atherosclerosis, vein graft occlusion, and restenosis after angioplasty, our *in vivo* experiment suggests that osthole treatment selectively inhibits the proliferation of those VSMC by suppressing inflammation (Wang et al., 2013; Li et al., 2017), Guh's studies indicated that the antiproliferative effect of osthole occurs early in G1 phase of the VSMC cell cycle and is due to increases in cyclic AMP and cyclic GMP levels (Guh et al., 1996; PMID: 8867108). In this research, we intend to explore whether the molecular mechanisms of osthole on vascular stenosis and VSMC proliferation are related to cell cycle and cell cycle regulatory proteins cyclin D1/CDK4 and cyclin E1/CDK2. We first established the balloon-induced carotid artery injury model in male Sprague-Dawley rats and observed the expression of PCNA, which is used as a marker of DNA synthesis or proliferation, in balloon-treated rat carotid arteries using western blotting, which further confirmed the protective effect of osthole on injured artery walls. We found that VSMC proliferation was proportional to the degree of intimal hyperplasia and that osthole significantly alleviated neointimal hyperplasia in balloon-injured artery walls by inhibiting the proliferation of VSMCs. The results indicated that the changes in PCNA protein expression were very consistent with the histomorphometric changes in the carotid artery walls.

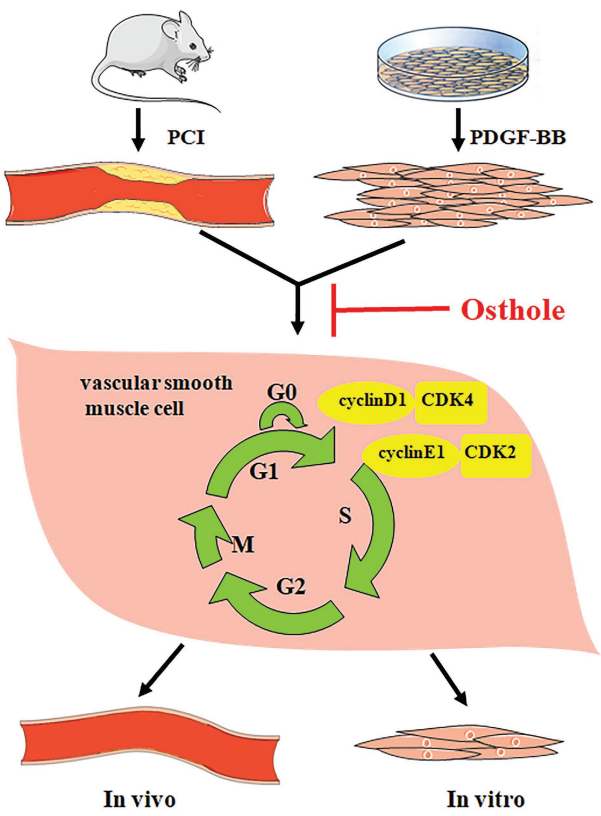

FIGURE 7 | Osthole alleviates neointimal hyperplasia in balloon-induced arterial wall injury and inhibits PDGF-BB-induced VSMC proliferation, and the mechanisms are related to the downregulation of cyclin D1/CDK4 and cyclin E1/CDK2 expression as well as the prevention of cell cycle progression from G0/G1 phase to S phase.

In vivo, this dynamic and cyclic process generally begins with a primary regulator such as interleukins (Alexander and Khalil, 2009), interferons (Boshuizen and Winther, 2015), platelet-derived growth factor (PDGF)-BB (Williams et al., 2012), and basic fibroblast growth factor (bFGF; Kesavan et al., 2013), among which PDGF-BB has been considered as the most potent chemoattractant and a strong mitogen present in serum that stimulates DNA synthesis. PDGF-BB can bind to all PDGF receptors, phosphorylate receptors, activate downstream signaling molecules and promotes phenotypic transformation, proliferation, and migration of VSMCs. The importance of PDGF-BB in the development of neointima formation has been established in models of arterial injury (Raines, 2004; Huang et al., 2012; Zhang et al., 2014; Zhao et al., 2014; Fang et al., 2020). Here, we used 25% PDGF-BB as a prototypical mitogen to establish a VSMC proliferation system, we then further examined the role of the osthole on VSMC proliferation *in vitro* experiments. Our data confirmed PDGF-BB induced significant increases in VSMC proliferation, while osthole exhibited a marked antiproliferative effect in VSMCs based on the results of the MTT assay and EdU staining.

Several observations have shown that regulating the cell cycle is an important mechanism for controlling cell proliferation (Liu et al., 2009; Yoo et al., 2013), as entry and the progression of cells through different stages of the cell cycle is an ordered, tightly regulated process involving a complex cascade of events, and cell cycle arrest can trigger the inhibition of proliferation (Eymin and Gazzeri, 2010; Yan et al., 2015). In the present study, cell cycle progression in each group was investigated by flow cytometry, and our results revealed that osthole suppressed PDGF-BB-induced VSMC proliferation and blocked PDGF-BB-induced cell cycle progression of VSMCs from G1 to S phase, which was exhibited by a significant accumulation of VSMCs in G0/G1 phase and a reduction of cells in G2/M+S phases, indicating that osthole-mediated inhibition of VSMC proliferation was attributed to apparent cell cycle arrest quite early during G0/G1 phase.

Cell cycle progression requires different signaling molecules to function at the right time, and the cyclin/CDK complexes play a prominent role because their expression is responsible for the transition from G1 to S phase (Bond et al., 2006; Dong et al., 2016). Both damaged and activated VSMCs induce cyclin D1 expression and thus facilitate the formation of the cyclin D1-CDK4 complex, which is essential for the entry of cells from G0 to G1 phase and prepares cells for the G1/S phase

transition. The cyclin D1/CDK4 complex is required to promote the phosphorylation of retinoblastoma (Rb) protein and the exposure of the binding site of E2F1-3 (Liu et al., 2015). Because our studies demonstrated that the treatment of PDGF-BB-stimulated VSMCs with osthole resulted in cell cycle arrest at G1 phase (**Figure 4**), we then analyzed the expression of cyclin D1/CDK4 to determine whether its effect is due to the downregulation of operative regulatory molecules. Consistent with relevant reported literature (Ge et al., 2016; Chen et al., 2017), high mRNA and protein expression levels of cyclin D1 and CDK4 were found after treatment with PDGF-BB. However, administration of osthole reduced these increases, which were accompanied by inhibition of cell proliferation and cell cycle, suggesting that decreasing cyclin D1/CDK4 expression might be the molecular mechanism by which osthole inhibits VSMC proliferation and arrests the cell cycle.

Furthermore, a growing body of evidence has demonstrated that increased cyclin E1 1 levels are associated with malignancies, such as ovarian cancer (Guo et al., 2011), and elevated cyclin E1 expression is a poor prognostic factor in lung adenocarcinoma patients (Eymin and Gazzeri, 2010). Activated cyclin E1 can bind to CDK2 to form the cyclin E1/CDK2 complex, which also serves to promote DNA replication and further phosphorylates pRb, leading to the formation of a positive feedback loop and regulation of the onset of DNA-synthesis referred to as S-phase (Liu et al., 2015). Interestingly, our results indicate that osthole administration inhibited PDGF-BB-induced cyclin E1-CDK2 upregulation, providing the further evidence for the above studies.

Of note, there still remains a limitation in this study. Although osthole has been proved to prevent cell cycle progression, the target that osthole could bind to is unknown at present, and it is worth further exploration in our next research.

Taken together, our results demonstrate that osthole can significantly alleviate neointimal hyperplasia in balloon-induced arterial wall injury and inhibit PDGF-BB-induced VSMC proliferation, and its regulatory activities are related, at least partially, to downregulation of cyclin D1/CDK4 and cyclin E1/CDK2 expression as well as the prevention of cell cycle progression from G0/G1 phase to S phase (**Figure 7**).

DATA AVAILABILITY STATEMENT

All datasets generated for this study are included in the article/supplementary material.

ETHICS STATEMENT

The animal study was reviewed and approved by the Animal Use and Care Committee of Zunyi Medical University.

AUTHOR CONTRIBUTIONS

D-LY participated in the study design. D-LY, Y-QL, Y-LL, YG, W-NL, X-TL, and J-YL carried out the experiment *in vivo* and *in vitro*. Q-HG analyzed the results. D-LY and Y-QL prepared the manuscript. All authors contributed to the article and approved the submitted version.

FUNDING

This work was supported by the National Natural Science Foundation of China (no. 81360498 and no. 81860647), the Joint Research Program of Zunyi Science and Technology Bureau and Zunyi Medical University [no. (2018)19], and the Zhuhai Premier-Discipline Enhancement Scheme of Pharmacology, Zhuhai Campus of Zunyi Medical University.

REFERENCES

Alexander, H. S., and Khalil, R. A. (2009). Inflammatory cytokines in vascular dysfunction and vascular disease. *Biochem. Pharmacol.* 78, 539–552. doi: 10.1016/j.bcp.2009.04.029

Begum, N., Hockman, S., and Manganiello, V. C. (2011). Phosphodiesterase 3A (PDE3A) deletion suppresses proliferation of cultured murine vascular smooth muscle cells (VSMCs) via inhibition of mitogen-activated protein kinase (MAPK) signaling and alterations in critical cell cycle regulatory proteins. *J. Biol. Chem.* 2011, 26238–26249. doi: 10.1074/jbc.M110.214155

Bond, M., Sala-Newby, G. B., Wu, Y. J., and Newby, A. C. (2006). Biphasic effect of p21Cip1 on smooth muscle cell proliferation: role of PI 3-kinase and Skp2-mediated degradation. *Cardiovasc. Res.* 69, 198–206. doi: 10.1016/j.cardiores.2005.08.020

Boshuizen, M. C., and Winther, M. P. (2015). Interferons as essential modulators of atherosclerosis. *Arterioscler. Thromb. Vasc. Biol.* 35, 1579–1588. doi: 10.1161/ATVBAHA.115.305464

Chen, S., Dong, S., and Li, Z. (2017). Atorvastatin calcium inhibits PDGF-BB-induced proliferation and migration of VSMCs through the G0/G1 cell cycle arrest and suppression of activated PDGFRI^2-PI3K-Akt signaling cascade. *Cell. Physiol. Biochem.* 44, 215–228. doi: 10.1159/000484648

Direnzo, D. M., Chaudhary, M. A., Shi, X., Franco, S. R., Zent, J., Wang, K., et al. (2016). A crosstalk between TGF-β/Smad3 and Wnt/β-catenin pathways promotes vascular smooth muscle cell proliferation. *Cell. Signal.* 28, 498–505. doi: 10.1016/j.cellsig.2016.02.011

Dong, Y., Hai, L., and Lai, Z. (2016). ClC-3 chloride channel proteins regulate the cell cycle by up-regulating cyclin D1-CDK4/6 through suppressing p21/p27 expression in nasopharyngeal carcinoma cells. *Sci. Rep.* 6, 30276–30292. doi: 10.1038/srep30276

Duan, J., Yang, Y., Liu, H., Dou, P. C., and Tan, S. Y. (2016). Osthole ameliorates acute myocardial infarction in rats by decreasing the expression of inflammatory-related cytokines, diminishing MMP-2 expression and activating p-ERK. *Int. J. Mol. Med.* 37, 207–216. doi: 10.3892/ijmm.2015.2402

Eymin, B., and Gazzeri, S. (2010). Role of cell cycle regulators in lung carcinogenesis. *Cell Adh. Migr.* 4, 114–123. doi: 10.4161/cam.4.1.10977

Fang, L., Wang, K. K., Zhang, P. F., Li, T., Xiao, Z. L., Yang, M., et al. (2020). Nucleolin promotes Ang II-induced phenotypic transformation of vascular smooth muscle cells by regulating EGF and PDGF-BB. *J. Cell. Mol. Med.* 24, 1917–1933. doi: 10.1111/jcmm.14888

Fusia, F., Sgaragli, G., Ha, L. M., Cuong, N. M., and Saponara, S. (2012). Mechanism of osthole inhibition of vascular Ca1.2 current. *Eur. J. Pharmacol.* 680, 22–27. doi: 10.1016/j.ejphar.2012.01.038

Ge, X., Chen, S. Y., Liu, M., Liang, T. M., and Liu, C. (2016). Evodiamine inhibits PDGF-BB-induced proliferation of rat vascular smooth muscle cells through the suppression of cell cycle progression and oxidative stress. *Mol. Med. Rep.* 14, 4551–4558. doi: 10.3892/mmr.2016.5798

Guh, J. H., Yu, S. M., Ko, F. N., Wu, T. S., and Teng, C. M. (1996). Antiproliferative effect in rat vascular smooth muscle cells by osthole, isolated from *Angelica pubescens*. *Eur. J. Pharmacol.* 298, 191–197. doi: 10.1016/0014-2999(95)00812-8

Guo, Z. Y., Hao, X. H., Tan, F. F., Pei, X., Shang, L. M., Jiang, X. L., et al. (2011). The elements of human cyclin D1 promoter and regulation involved. *Clin. Epigenetics* 2, 63–76. doi: 10.1007/s13148-010-0018-y

Huang, J., Li, L. S., Yang, D. L., Gong, Q. H., Deng, J., and Huang, X. N. (2012). Inhibitory effect of ginsenoside Rg1 on vascular smooth muscle cell proliferation induced by PDGF-BB is involved in nitric oxide formation. *Evid. Based Complement. Alternat. Med.* 2012, 314395–314402. doi: 10.1155/2012/314395

Jarzab, A., Grabarska, A., and Kiełbus, M. (2014). Osthole induces apoptosis, suppresses cell-cycle progression and proliferation of cancer cells. *Anticancer Res.* 34, 6473–6480.

Jiang, D., Li, D., and Wu, W. (2013). Inhibitory effects and mechanisms of luteolin on proliferation and migration of vascular smooth muscle cells. *Nutrients* 5, 1648–1659. doi: 10.3390/nu5051648

Kesavan, R., Potunuru, U. R., and Nastasijević, B. (2013). Inhibition of vascular smooth muscle cell proliferation by Gentianalutea root extracts. *PLoS One* 8:e61393. doi: 10.1371/journal.pone.0061393

Li, Z., Ji, H., Song, X., Hu, J. F., Han, N., and Chen, N. H. (2014). Osthole attenuates the development of carrageenan-induced lung inflammation in rats. *Int. Immunopharmacol.* 20, 33–36. doi: 10.1016/j.intimp.2014.02.013

Li, Y. M., Jia, M., Li, H. Q., Zhang, N. D., Wen, X., Rahman, K., et al. (2015). *Cnidium monnieri*: a review of traditional uses, phytochemical and ethnopharmacological properties. *Am. J. Chin. Med.* 43, 835–877. doi: 10.1142/S0192415X15500500

Li, Y. Q., Wang, J. Y., Qian, Z. Q., Li, Y. L., Li, W. N., Gao, Y., et al. (2017). Osthole inhibits intimal hyperplasia by regulating the NF-κB and TGF-β1/Smad2 signalling pathways in the rat carotid artery after balloon injury. *Eur. J. Pharmacol.* 811, 232–239. doi: 10.1016/j.ejphar.2017.06.025

Liu, W. Z., Hua, S. H., Dai, Y., Yuan, Y. Y., Yang, J. H., Deng, J. L., et al. (2015). Roles of Cx43 and AKAP95 in ovarian cancer tissues in G1/S phase. *Int. J. Clin. Exp. Pathol.* 8, 14315–14324.

Liu, G., Li, X., Li, Y., Tang, X., Xu, J., Li, R., et al. (2013). PPARδ agonist GW501516 inhibits PDGF-stimulated pulmonary arterial smooth muscle cell function related to pathological vascular remodeling. *Biomed. Res. Int.* 2013, 903947–903955. doi: 10.1155/2013/903947

Liu, J. Z., Lyon, C. J., Hsueh, W. A., and Law, R. E. (2009). A dominant-negative PPARγ mutant promotes cell cycle progression and cell growth in vascular smooth muscle cells. *PPAR Res.* 2009, 438673–438683. doi: 10.1155/2009/438673

Qiu, J., Zheng, Y., Hu, J., Liao, D., Gregersen, H., Deng, X., et al. (2013). Biomechanical regulation of vascular smooth muscle cell functions: from in vitro to in vivo understanding. *J. R. Soc. Interface* 11, 20130852–20130865. doi: 10.1098/rsif.2013.0852

Raines, E. W. (2004). PDGF and cardiovascular disease. *Cytokine Growth Factor Rev.* 15, 237–254. doi: 10.1016/j.cytogfr.2004.03.004

Tang, D. D., and Gerlach, B. D. (2017). The roles and regulation of the actin cytoskeleton, intermediate filaments and microtubules in smooth muscle cell migration. *Respir. Res.* 18, 54–66. doi: 10.1186/s12931-017-0544-7

Urrego, D., Tomczak, A. P., Zahed, F., Walter, S., and Pardo, L. A. (2014). Potassium channels in cell cycle and cell proliferation. *Philos. Trans R Soc. Lond. Biol. Sci.* 369, 20130094–20130103. doi: 10.1098/rstb.2013.0094

Wang, X. Y., Dong, W. P., Bi, S. H., Pan, Z. G., Yu, H., Wang, X. W., et al. (2013). Protective effects of osthole against myocardial ischemia/reperfusion injury in rats. *Int. J. Mol. Med.* 32, 365–372. doi: 10.3892/ijmm.2013.1386

Williams, H. C., San, M. A., and Adamo, C. M. (2012). Role of Coronin 1B in PDGF-induced migration of vascular smooth muscle cells. *Circ. Res.* 111, 56–65. doi: 10.1161/CIRCRESAHA.111.255745

Xu, X., Yi, Z., Dan, Q., Jiang, T. S., and Li, S. Q. (2011). Osthole induces G2/M arrest and apoptosis in lung cancer A549 cells by modulating PI3K/Akt pathway. *J. Exp. Clin. Cancer Res.* 30, 1–7. doi: 10.1186/1756-9966-30-33

Yan, G., Wang, Q., Shengda, H. U., Wang, D., Qiao, Y., Ma, G. S., et al. (2015). Digoxin inhibits PDGF-BB-induced VSMC proliferation and migration through an increase in ILK signaling and attenuates neointima formation following carotid injury. *Int. J. Mol. Med.* 36, 1001–1011. doi: 10.3892/ijmm.2015.2320

Yoo, S. H., Lim, Y., Kim, S. J., Yoo, K. D., Yoo, H. S., Hong, J. T., et al. (2013). Sulforaphane inhibits PDGF-induced proliferation of rat aortic vascular smooth muscle cell by up-regulation of p53 leading to G1/S cell cycle arrest. *Vasc. Pharmacol.* 59, 44–51. doi: 10.1016/j.vph.2013.06.003

Yue, Y., Li, Y. Q., Fu, S., Wu, Y. T., Zhu, L., Hua, L., et al. (2020). Osthole inhibits cell proliferation by regulating the TGF-β1/Smad/p38 signaling pathways in pulmonary arterial smooth muscle cells. *Biomed. Pharmacother.* 121:109640. doi: 10.1016/j.biopha.2019.109640

Zhang, Z. R., Leung, W. N., Cheung, H. Y., and Chan, C. W. (2015). Osthole: a review on its bioactivities, pharmacological properties, and potential as alternative medicine. *Evid. Based Complement. Alternat. Med.* 2015, 919616–919626. doi: 10.1155/2015/919616

Zhang, L., Pu, Z., Wang, J., Zhang, Z. F., Hu, D. M., and Wang, J. J. (2014). Baicalin inhibits hypoxia-induced pulmonary artery smooth muscle cell proliferation via the AKT/HIF-1α/p27-associated pathway. *Int. J. Mol. Sci.* 15, 8153–8168. doi: 10.3390/ijms15058153

Zhao, N., Koenig, S. N., Trask, A. J., Lin, C. H., Hans, C. P., Garg, V., et al. (2014). mir145 regulates TGFBR2 expression and matrix synthesis in vascular smooth muscle cells. *Circ. Res.* 116, 23–34. doi: 10.1161/CIRCRESAHA.115.303970

Conflict of Interest: The authors declare that the research was conducted in the absence of any commercial or financial relationships that could be construed as a potential conflict of interest.

Advantages of publishing in Frontiers

OPEN ACCESS
Articles are free to read for greatest visibility and readership

FAST PUBLICATION
Around 90 days from submission to decision

HIGH QUALITY PEER-REVIEW
Rigorous, collaborative, and constructive peer-review

TRANSPARENT PEER-REVIEW
Editors and reviewers acknowledged by name on published articles

Frontiers
Avenue du Tribunal-Fédéral 34
1005 Lausanne | Switzerland

Visit us: www.frontiersin.org
Contact us: frontiersin.org/about/contact

REPRODUCIBILITY OF RESEARCH
Support open data and methods to enhance research reproducibility

DIGITAL PUBLISHING
Articles designed for optimal readership across devices

FOLLOW US
@frontiersin

IMPACT METRICS
Advanced article metrics track visibility across digital media

EXTENSIVE PROMOTION
Marketing and promotion of impactful research

LOOP RESEARCH NETWORK
Our network increases your article's readership